Stem Cell Features in Spheroids and Standard Culture of a Renal Cell Carcinoma Cell Line

Inaugural-Dissertation
to obtain the academic degree
Doctor rerum naturalium (Dr. rer. nat.)

submitted to the Department of Biology, Chemistry and Pharmacy
of Freie Universität Berlin

by

Janine Löhr

2018

The work for this dissertation was performed from May 2013 to August 2018 under the supervision of Prof. Dr. Burghardt Wittig at the Foundation Institute Molecular Biology and Bioinformatics at Freie Universität Berlin, Germany.

1st Reviewer:	Prof. Dr. Burghardt Wittig
2nd Reviewer:	Prof. Dr. Rupert Mutzel
Date of Disputation:	28 May 2019

Selbstständigkeitserklärung

Hierdurch versichere ich gem. § 7 Abs. 2a und Abs. 4 der Promotionsordnung des Fachbereichs Biologie, Chemie, Pharmazie, dass ich die vorliegende Arbeit mit dem Titel „Stem Cell Features in Spheroids and Standard Culture of a Renal Cell Carcinoma Cell Line“ selbstständig und ohne unerlaubte Hilfe verfasst und nur die von mir angegebene Literatur und Hilfsmittel verwendet habe.

Ich versichere ebenfalls, dass ich meine Dissertation (ganz oder in Teilen) nicht veröffentlicht habe, die Dissertation nicht auf meiner Diplomarbeit aufbaut bzw. nicht daraus erwachsen ist und ich die Disseration auch nicht schon einmal in einem anderen Promotionsverfahren eingereicht habe.

Datum Unterschrift

Table of Contents

Abbreviations

Abbreviations used throughout this work are listed in the following tables.

Besides these, official gene symbols, some of which are listed in the tables, are used.

Abbreviation (A-C)	Full Name (A-C)
7-AAD	7-Aminoactinomycin D
A_λ	Absorbance (lower case: at wavelength (nm))
A-CS	CS cells grown under standard adherent condtions
A-SP	SP cells grown under standard adherent condtions
ABCB1	ATP binding cassette subfamily B member 1 (MDR)
ABCB5	ATP binding cassette subfamily B member 5
ABCG2	ATP binding cassette subfamily G member 2
AC-Medium	Adherent culture medium
ACC	Adherent culture condition
ACS	Chemical grade: highest purity according to American Chemical Society
ADIPOQ	Adiponectin, C1Q and collagen domain containing
AF-647/488	AlexaFluor® 647/488
AKT (PKB)	V-AKT murine thymoma viral oncogene homolog (PKB-alpha)
ALCAM	Activated leukocyte cell adhesion molecule
ALDH	Aldehyde dehydrogenase
AM	Ambion Kit
AP	Alkaline phosphatase
APC	Allophycocyanin
APM (ADIPOQ)	Adiponectin
ARP	Adult (CD133+/CD24+ sorted) normal renal progenitors
AS	Sequencing sample A-SP cells
AsAP	Ascorbate 2-phosphate
AT-MSC	Adipose tissue-derived mesenchymal stem cells
BAA	BODIPY™ aminoacetate
BAAA	BODIPY™ aminoacetaldehyde
BAM	Binary alignment map (file format)
BAP1	BRCA1 associated protein 1
BDNF	Brain-derived neurotrophic factor
bFGF (FGF-2)	Basic fibroblast growth factor
BGLAP	Bone gamma-carboxyglutamate protein
BHD	Folliculin, Birt-Hogg-Dubé Syndrome
BIH	Berlin Institute of Health
BM	Bone marrow
BM-MSC	Bone marrow-derived mesenchymal stem cells
BMI-1	Polycomb group RING finger protein 4
BMP	Bone morphogenetic protein
bp	*base pairs*
BRCA1	Breast cancer type 1 susceptibility protein
BRCP (ABCG2)	Breast cancer resistance protein (ATP binding cassette subfamily G member 2)
BSA	Bovine serum albumin
CALLA	Common acute lymphoblastic leukemia antigen, (CD10/Neprilysin)
cAMP	Cyclic adenosine monophosphate
Card	Cardiac stem cells
ccRCC	Clear cell renal cell carcinoma
CD	Cluster of differentiation
CDH1	E-Cadherin (epithelial cadherin)
CDH2	N-Cadherin (neuronal cadherin)
cDNA	Complementary DNA (DNA sequence resulting from reverse transcription of RNA)
CFE	Colony-forming efficiency (soft agar assay)
CIFM	Confocal immunefluorescence microscopy
CK	Cytokeratin (KRT)
CLDN	Claudin
CM	Condensed/cap mesenchyme
cMET	Hepatocyte growth factor receptor
COL	Collagen
CRB	Crumbs, cell polarity complex component
CRC	Colorectal cancer
CREB	cAMP response element (transcription factor)
CS	Clonally expanded spheroid cells derived from PA
CSC	Cancer stem cells
CSFE	Clonal spheroid-forming efficiency
CTL	Cytotoxic T-lymphocytes
CTR2/SLC31A2	Copper transporter 2/solute carrier family 31 member 2
CXCL12	C-X-C motif chemokine ligand 12
CXCR4	C-X-C chemokine receptor type 4 (CD184)
CXCR7	C-X-C motif chemokine receptor 7

Table 1.1.1: Abbreviations A-C

Abbreviation (D-K)	Full Name (D-K)
DC	Dendritic cells
DCLK1	Doublecortin-like kinase 1
ddNTP	Didesoxyribonukleosid triphosphate
DEAB	Diethylaminobenzaldehyde
DEG	Differentially expressed genes
DGE	Differential gene expression
DMEM	Dulbecco´s modified Eagle´s medium
DMEM-LG	Dulbecco´s modified Eagle´s medium - low glucose
DMF	N,N-Dimethylformamide
DMSO	Dimethyl sulfoxide
DNA	Deoxyribonucleic acid
dNTP	Deoxyribonucleotide triphosphate
DP-MSC	Dental pulp-derived mesenchymal stem cells
DPBS	Dulbecco's phosphate-buffered saline
DSP	Desmoplakin
ECM	Extracellular matrix
EDTA	Ethylenediamine tetraacetic acid
EGF	Epidermal growth factor
EGFR	Epidermal growth factor receptor (ERBB, HER1)
EglN	Egl family hypoxia inducible factor
EMT	Epithelial-to-mesenchymal transition
EpCAM	Epithelial cellular adhesion molecule
EpICD	EpCAM intracellular domain
ERBB	Epidermal growth factor receptor (EGFR, HER1)
ERK	Extracellular signal–regulated kinase
ESA	Epithelial surface antigen
ESC	Embryonic stem cell
ESCC	Esophageal squamous cell carcinoma
EZH2	Enhancer of zeste homolog 2, Histone-lysine N-methyltransferase EZH2
F-PBS	Dulbecco's Phosphate-Buffered Saline for flow cytometry
FABP4	Fatty acid binding protein 4
FACS	Fluorescence activated cell sorting
FBS	Fetal bovine serum
FCS	Fetal calf serum
FGF	Fibroblast growth factor
FHL2	Four-and-a-half LIM domains protein 2
FITC	Fluorescein isothiocyanate
FL	Fluorescence (flow cytometry)
FN1	Fibronectin
FOX	Forkhead box transcription factor
FSC	Forward scatter (flow cytometry)
FTC	Fumitremorgin C (ABCG2 specific inhibitor)
FZD	Frizzled receptor
GAPDH	Glyceraldehyde-3-phosphate dehydrogenase
GCAP	Germ cell alkaline phosphatase
GLI	GLI family zinc finger
GM	Geometric mean (flow cytometry)
GO	Gene ontology
GSEA	Gene set enrichment analysis
GSK	Glycogen synthase kinase
GSK3β	Glycogen synthase kinase 3 beta
HCC	Hepatocellular carcinoma
HEPES	4-(2-hydroxyethyl)-1-piperazineethanesulfonic acid
HGF	Hepatocyte growth factor
HGFR	Hepatocyte growth factor receptor (cMet)
HH	Hedgehog
HIF	Hypoxia inducible factor
HLA-DR	Human leukocyte antigen – DR isotype (MHC-II receptor)
HMGA2	Highmobilitygroup A2
HNSCC	Head and neck squamous cell carcinoma
Hoechst	Hoechst33324 (dye)
HPLC	High-performance liquid chromatography
HPRT1	Hypoxanthine phosphoribosyltransferase 1
HPSE	Heparanase
HRE	Hypoxia response element
HSP	Hoechst33324 side population
IAP	Intestinal alkaline phosphatase
IBMX	3-Isobutyl-1-methylxanthine
IESC	Intestinal epithelial stem cells
IFC	Flow cytometric immunophenotyping
IFN	Interferon
IGF	Insulin like growth factor
IHC	Immunohistochemistry
IL	Interleukin
IL-R	Interleukin receptor
ILK	Integrin-linked kinase
iPSC	Induced pluripotent stem cells
Iso	Isotype control antibody (flow cytometry)
ITGA	Integrin alpha chain
ITGB	Integrin beta chain
ITS	Insulin-Transferrin-Selenium
JNK	c-Jun N-terminal kinases (MAPK8)
kb	*kilo bases*
KLF4	Kruppel-like factor 4
KRT	Keratin

Table 1.1.2: Abbreviations D-K

Abbreviation (L-P)	Full Name (J-P)
LAM	Laminin
LC	Lung cancer
LCA	Lymphocyte common antigen
LEF	Lymphoid enhancer binding factor (transcription factor)
LIF	Leukemia inhibitory factor (cytokine)
LIN28A	Protein lin-28 homolog A
MAPCs	Multipotent adult progenitor cells
MAPK	Mitogen-activated protein kinase
MCAM	Melanoma cell adhesion molecule
MCB	Master cell bank
MDCK	Madin-Darby canine kidney cells
MDR1 (ABCB1)	Multi drug resistance protein 1 (ATP binding cassette subfamily B member 1)
MEK (MAP2K)	Mitogen-activated protein kinase kinase (MAP2K)
MET	Mesenchymal-to-epithelial transition
MGN1601	Cell-based tumor vaccine (MOLOGEN AG)
MHC	Major histocompatibility complex
MIAMI	Marrow-isolated adult multilineage inducible
MilliQ	Ultrapure water
miRNA	Mircro RNA
MKK (MAP3K)	Mitogen-activated protein kinase kinase kinase (MAP3K)
MMP	Matrix metalloproteinase
MN	Machery und Nagel Kit
MNM	Metanephric mesoderm/mesenchym
MPP5 (PALS1)	Membrane palmitoylated protein 5 (PALS1)
MRP (ABCC)	Multi drug resistance protein related protein (ATP Binding Cassette Subfamily C)
MSC	Mesenchymal stem cells
MSCA-1	Mesenchymal stem cell antigen 1 = TNAP
mTOR	Mechanistic target of rapamycin
MUSE	Multi-lineage differentiating stress-enduring
mut	mutant
MYC	v-Myc myelocytomatosis viral oncogene homolog (transcription factor)
NA	Not available, not determined
NANOG	Homeobox transcription factor Nanog
NCAM	Neural cell adhesion molecule
NCFCA	Neural colony-forming cell assay
ND	Nephric ducts
NF-κB	Nuclear factor 'kappa-light-chain-enhancer' of activated B-cells
NGFR	Nerve growth factor receptor/low affinity nerve growth factor receptor
NGS	Next generation sequencing
NIC/NICD	Notch intracellular fragment of notch/ Notch intracellular domain
NK	Natural killer (cells)
NOD	Non-obese diabetic (mouse strain)
NOTCH	Homo sapiens notch
NSA	Neurosphere assay
NSC	Neural stem cells
NSG	NOD/SCID/Interferon γ knock out, NOD/SCID/IL2Rynull (mouse strain)
NSP	Non-side population
nt	Nucleotides
OC/BGLAP	Osteocalcin/Bone gamma-carboxyglutamate protein
OCLN	Occludin
Oct	Octamer biding transcription factor
ODN	Oligodesoxyribonucleotides
OvCa	Ovarian cancer
P	Passage number
p.a.	Chemical grade: pro analysis
p38	P38 mitogen activated protein kinase (MAPK14)
p53	Tumor protein P53 (TP53)
PA	Parental cell line derived from RCC tumor
PAK	p21 (RAC1) activated kinase
PanC	Pancreas carcinoma
PATJ	Homo sapiens PALS1-associated tight-junction protein
PBST	Dulbecco's phosphate-buffered saline with tween
PC	Prostate cancer
PCR	Polymerase chain reaction
PDK1 (PDPK1)	3-phosphoinositide-dependent protein kinase-1
PD-1	Programmed cell death protein 1
PE	Phycoerythrin
PI3K	Phosphoinositide-3-kinase–protein kinase
PIK3CA	Phosphatidylinositol-4,5-bisphosphate 3-kinase catalytic subunit alpha
PIP2	Phosphatidylinositol-4,5-bisphosphate
PIP3	Phosphatidylinositol-3,4,5-triphosphate
PKB	Protein kinase B (Akt)
PKP	Plakophilin
PL-MSC	Placenta-derived mesenchymal stem cells
PLAP	Placental alkaline phosphatase
PLCγ	Phospholipase C gamma
POU5F1	POU class 5 homeobox 1 (also OCT3/4)
PPAR	Peroxisome proliferator activated receptor
pRCC	Papillary renal cell carcinoma
PRX1	Paired-related homeobox 1
PSC	Prostate stem cells
PTE	Proximal tubular epithelia
PTECs	Proximal tubular epithelial cells
PTEN	Phosphatase and tensin homolog deleted on chromosome 10

Table 1.1.3: Abbreviations L-P

Abbreviation (R-Z)	Full Name (R-Z)
RA	Retinoic acid
RAC	Rac Family Small GTPase
RAF	Rapidly accelerated fibrosarcoma (Kinase)
RAS	Rat sarcoma (small GTPase)
RCC	Renal cell carcinoma
Rho	Rhodamine 123
RHOA	Ras homolog gene family member A
RIN	RNA integrity number
RL (TNFSF11)	RANK-ligand/Homo sapiens TNF superfamily member 11
RNA	Ribonucleic acid
RNA-Seq	RNA sequencing
ROS	Reactive oxygen species
RPKM	Reads per kilobase million
RPTEC	Renal proximal tubular epithelial cells
rRNA	Ribosomal RNA
RSP	Rhodamine 123 side population
RSPA	Rhodamine 123 side population assay
RT	Room temperature
RT-PCR	Reverse transcription polymerase chain reaction
RUNX2	Runt related transcription factor 2 (also Cbfa1)
SAA	Soft agar assay
SAM	Sequence alignment map (file format)
SC-Medium	Spheroid culture medium
SCC	Spheroid culture condition
SCID	Servere combined immunodeficiency (mouse strain)
SDC1	Syndecan-1
SDF-1 (CXCL12)	Stromal derived factor-1
SHH	Sonic hedgehog
SILAC	Stable isotope labeling by/with amino acids in cell culture
siRNA	Small interfering RNA
SIX2	Sine oculis homeobox homolog 2
α-SMA (ACTA2)	α-smooth muscle actin, homo sapiens actin alpha 2
SMAD	SMAD; Mothers against decapentaplegic homolog (transcription factor)
SMO	Smoothened, frizzled class receptor
SNAI1	Snail family transcriptional repressor 1
SNAI2 (Slug)	Snail family transcriptional repressor 2 (also SLUG)
SOX	SRY (sex determining region Y)-box
SP	Spheroid cells derived from PA
SREBF1	Sterol regulatory element binding transcription factor 1
SSC	Side scatter (flow cytometry)
SSEA	Stage-specific embryonic antigen
STAT	Signal transducer and activator of transcription
S1P	Sphingosine 1-phosphate
T	Temperature
T_A	Primer annealing temperature
TAE	Tris base/acetic acid/EDTA
TAK	TGF-beta activated kinase
TBE	Tris base/borate/EDTA
TCF	T cell factor (transcription factor)
TGF	Tumor growht factor
TGFR	Tumor growth factor receptor complex
TH1	T-helper cell 1
TIC	Tumor-initiating cells
T_m	Primer melting temperature
TMA	Tissue microarray
TNAP	Tissue nonspecific alkaline phosphatase (AP Liver/Bone/Kidney = ALPL)
TNF	Tumor necrosis factor
TNFR	Tumor necrosis factor receptor complex
TNFSF11	Tumor necrosis factor superfamily member 11
TP53	Tumor protein P53
TPM	Transcripts per million
TRAF	TNF receptor-associated factor
Tris	Tris(hydroxymethyl)aminomethane
tRNA	Transfer RNA
TSC	Tuberous sclerosis protein
TSE	Tris base/sodium chloride/EDTA
TWIST	Twist family basic helix-loop-helix transcription factor
UCB-MSC	Umbilical cord blood-derived mesenchymal stem cells
VCAM-1	Vascular cell adhesion molecule 1
VEGF	Vascular endothelial growth factor
Ver	Verapamil
VHL	Von Hippel-Lindau tumor suppressor
VIM	Vimentin
VSELs	Very small embryonic-like stem cells
VTN	Vitronectin
vWF	von Willebrand factor
w	weeks
WCB	Working cell bank
Wnt	Wingless family member
wt	wild type
WT1	Homo sapiens Wilms tumor 1
ZEB	Zinc finger E-box binding homeobox
ZO1	Zonula occludens 1

Table 1.1.4: Abbreviations R-Z

Abstract

It is increasingly recognized that features attributed to stem cells show striking parallels in certain cell populations within solid tumors and that cells with stem cell attributes appear to play a fundamental role in development, proliferation, metastasis, and therapy resistance. In the last decade, cancer stem cells (CSC), also termed tumor-inducing cells (TIC), have been identified in a variety of solid tumor entities. A deeper knowledge of CSC molecular, cellular and immunological properties would allow for the development of therapeutic approaches directly targeting this tumor cell population.

A broad spectrum of methods, addressing known embryonic stem cell characteristics, has been used to identify and enrich the mostly rare and seemingly heterogeneous tumor cell populations with tumor inducing features. Among the methods, the 3-dimensional culture of cells as floating „spheroids“ or „spheres“ has been found to be a valuable tool to enrich and propagate CSC. Compared to monolayer culture of adherent cells, spheroid growth conditions select for cells with high plasticity, and the spheroids themselves generate loci of low oxygen and nutrient supply, thereby mimicking the natural tumor environment closely.

In contrast to other tumor entities, little is known about CSC in the most common form of kidney cancer, the clear cell renal cell carcinoma (ccRCC). Metastatic ccRCC are mostly resistant to chemo- and radiotherapy, respond only moderately to tyrosine kinase inhibitors (TKI), and survival benefit through the variety of immunotherapeutic approaches, currently tested in clinical studies, is observed only in a minor fraction of patients treated. Therefore the identification, characterization, and targeting of CSC in ccRCC is not only of scientific interest, but may lead to valid oncological treatment targets.

In my thesis an established ccRCC cell line, certified for use in clinical trials, was the parent cell line (PA) to generate spheroids for CSC enrichment and cellular cloning. The two spheroid cultivation procedures applied yielded two phenotypically distinguishable cell lines, termed SP and CS.

Although the PA, SP, and CS have similar long-term proliferative potentials, both spheroid derived cell lines, SP and CS, profoundly increase their self-renewal ability, assayed by spheroid-forming efficiency (CSFE), in long-term culture. Conversely, CSFE of PA, the parental cell line, dropped to almost zero after only five weeks of culturing.

When *in vitro* tumorigenicity was assayed by colony formation in soft agar, SP cells displayed a more than ten-fold higher ability to form large colonies compared to PA and CS.

The property of generating differentiated progeny was assayed *in vitro* by the potential to generate mesenchymal lineages, namely adipogenic or osteogenic cells. SP cells showed the highest potential of differentiation into both adipogenic and osteogenic cells. PA cells have a much lower differentiation potential, similar to CS cells. Of two CS cell subtypes assayed, termed CS1 and CS7, one differentiates into adipogenic the other into osteogenic progeny.

Most importantly, the spheroid-derived cell lines, SP and CS, maintained their properties of self-renewal, colony formation, and differentiation, i.e. their stem cell characteristics, when cultured under non stem cell selecting conditions in monolayer cultures favoring adherent cell growth over a long time.

As functional markers for CSC, the enzymatic activity of aldehyde dehydrogenase (ALDH) and the transporter function for multiple drug resistance (MDR1) were measured. ALDH is active in PA, SP, and CS, but due to variability of measurements in PA results were not statistically significant. MDR1 activity, though, is clearly different, if the two spheroid-derived cell lines (SP, CS) are compared with the parent cell line (PA). High dye pumping activity of MDR1 in PA is contrasted by low activity in SP and CS.

A variety of cell surface markers, but also intracellular markers all reported as correlates of “stemness” or pluripotency, were assayed and detected by flow cytometric immunophenotyping (IFC). Also the process of epithelial-to-mesenchymal-transition (EMT) was determined through IFC of Cadherins, Snail1, vimentin, and cytokeratin.

Results are discussed extensively in great detail, because no simple explanatory algorithm could be derived. However, the general picture fits an interpretation where some cancer stem cell (CSC) characteristics are already present in the PA cell line, but broadly and stably established in qualitative and quantitative terms in the SP cell line. If compared to SP, the CS cell line exhibits slightly less “stemness” and less stability in its CSC characteristics.

All the above assays bioinformatically represent a trained or filtered set of tools for CSC characterization. Therefore, whole transcriptome shotgun sequencing of their mRNA (RNA-Seq) was performed for PA, SP, and A-SP. Differentially expressed genes (DEG) were identified in PA, SP, and A-SP, allowing for gene set enrichment analysis (GSEA). Results are discussed in detail, but in general the characterizations found with the filtered tool set nicely match the RNASeq-based GSEA. In the spheroid-derived cell lines (SP, A-SP) their cancer stem cell properties are elicited through up-regulated signaling by ERK and AKT, CREB, HIF-1α, Wnt/Hedgehog/Notch, EGFR (ERBB), and PAK. In the adherently growing parental cell line (PA) cell adhesion and angiogenic pathways as well as S1P and NF-κB signaling prevail. If SP cells are kept under non CSC-selecting conditions in monolayer cultures they retain their up-regulated CSC signaling, but re-activate cell adhesion pathways comparable to PA.

Zusammenfassung (German Abstract)

Es wird zunehmend anerkannt, dass Merkmale von Stammzellen auch bestimmte Zellpopulationen innerhalb solider Tumore auszeichnen. Diese Zellen mit Stammzellattributen spielen eine grundlegende Rolle bei Entwicklung, Proliferation, Metastasierung und Therapieresistenz von Tumoren. In den letzten zehn Jahren wurden solche Tumorstammzellen („cancer stem cells“: CSC), auch Tumor-induzierende Zellen („tumor-inducing cells“: TIC) genannt, in einer Vielzahl von soliden Tumor-Entitäten identifiziert. Um therapeutische Ansätze zu entwickeln, die direkt auf diese Zellen abzielen, ist ein tieferes Wissen über die molekularen, zellulären und immunologischen Eigenschaften von CSC erforderlich.

Zur Identifikation und Anreicherung der meist seltenen und heterogenen CSC Tumorzellpopulationen findet ein breites Spektrum von Methoden Anwendung, welche auf der Verwendung bekannter Stammzellmerkmale basieren. Dabei hat sich die dreidimensionale Kultur von Zellen als sogenannte "Sphäroide" als wertvolles Werkzeug zur Anreicherung und Vermehrung von CSC erwiesen. Im Vergleich zur adhärenten Monoschicht-Kultur werden durch Sphäroid-Kultur Zellen mit hoher Plastizität selektiert. Die Wachstumsbedingungen in Sphäroiden entsprechen durch die Anwesenheit von Regionen mit geringer Sauerstoff- und Nährstoffversorgung zudem eher der natürlichen Mikroumgebung von Tumoren („tumor microenvironment“: TME).

Im Gegensatz zu anderen Tumor-Entitäten ist über CSC bei der häufigsten Form von Nierenkrebs, dem klarzelligen Nierenzellkarzinom („clear cell renal cell carcinoma“: ccRCC), relativ wenig bekannt. Metastasierte ccRCC sind weitgehend resistent gegen Chemo- und Strahlentherapie, sprechen nur moderat auf Tyrosinkinase-Inhibitoren (TKI) an, und auch die vielfältigen immuntherapeutischen Ansätze, die derzeit in klinischen Studien getestet werden, führen nur bei einem kleineren Teil der behandelten Patienten zu signifikant verlängertem Überleben. Daher sind Identifizierung, Charakterisierung und Targeting von CSC in ccRCC nicht nur von wissenschaftlichem Interesse, sondern auch Voraussetzungen für valide onkologische Behandlungsstrategien.

In dieser Arbeit diente eine etablierte ccRCC-Zelllinie, die für den Einsatz in klinischen Studien zertifiziert ist, als Ausgangszelllinie (PA), um Sphäroide für die CSC-Anreicherung zu erzeugen. Die beiden angewandten Verfahren der Sphäroid-Kultivierung lieferten zwei phänotypisch unterscheidbare Zelllinien, SP und CS.

Obwohl PA, SP und CS ein ähnlich hohes Langzeitproliferationspotential aufweisen, zeigen beide Sphäroid-Zelllinien, SP und CS, einen erheblichen Anstieg in ihrer Selbsterneuerungsfähigkeit, welche durch die klonale Sphäroid-Bildungseffizienz („clonal spheroid-forming efficiency“: CSFE) in Langzeitkultur nachgewiesen wurde. Dagegen sinkt die CSFE der Ausgangszelllinie, PA, nach nur fünf Wochen Kulturzeit auf nahezu Null ab.

Im „Soft Agar Assay“ als quantitativem Test auf Tumorigenität *in vitro*, zeigen SP-Zellen eine mehr als zehnfach höhere Fähigkeit, große Kolonien zu bilden als PA und CS.

Die Eigenschaft, differenzierte Nachkommen zu erzeugen, wurde *in vitro* durch das Potential untersucht, in mesenchymale Linien zu differenzieren. SP-Zellen zeigten das höchste Differenzierungspotential sowohl für Adipozyten als auch für Osteoblasten. Das Differenzierungspotential von PA-Zellen war dagegen, ähnlich wie das von CS-Zellen, vermindert.

Die beiden untersuchten CS-Zelllinien (CS1 und CS7) differenzierten jeweils nur in eine der beiden Zelltypen, d.h. entweder zu Adipozyten oder zu Osteoblasten.
Bedeutsam ist, dass die aus Sphäroiden gewonnenen Zelllinien SP und CS ihre Eigenschaften zur Selbsterneuerung, Koloniebildung und Differenzierung, d. h. ihre Stammzelleneigenschaften, auch dann behalten, wenn sie unter Kulturbedingungen, die nicht für Stammzellen selektieren, also in adhärenten Monoschicht-Kulturen über einen langen Zeitraum kultiviert werden (A-SP, A-CS).
Als funktionelle Marker für CSC wurden die enzymatische Aktivität der Aldehyd-Dehydrogenase (ALDH) und die Transporterfunktion des Transporters für multiple Arzneimittelresistenz (MDR1) gemessen. Sowohl in SP und CS als auch in PA wurde ähnlich hohe ALDH-Aktivität nachgewiesen. Aufgrund der Variabilität der Messungen in PA waren die Ergebnisse jedoch statistisch nicht signifikant. Deutliche Unterschiede zwischen den beiden Sphäroid-Zelllinien (SP, CS) und der Ausgangszelllinie (PA) wurden hingegen in der MDR1 Transporter-Aktivität beobachtet, die durch die Fähigkeit zur Abreicherung des Farbstoffes Rhodamin 123 aus den Zellen gemessen wurde. PA-Zellen zeigen im Gegensatz zu SP- und CS-Zellen hohe MDR1-Aktivität.
Eine Vielzahl von Zelloberflächenmarkern, aber auch intrazelluläre Marker, welche als Korrelate von Stammzelleigenschaften oder Pluripotenz gelten, wurden mittels durchflusszytometrischer Immunphänotypisierung (IFC) untersucht und nachgewiesen. Auch der Prozess des Überganges von epithelialen zu mesenchymalen Zellen („epithelial-to-mesenchymal-transition“: EMT) wurde durch IFC von Cadherinen, Snail1, Vimentin und Zytokeratinen bestimmt. Die Ergebnisse werden ausführlich diskutiert, da kein einfaches erklärendes Schema abgeleitet werden konnte. Das allgemeine Bild passt jedoch zu einer Interpretation, bei der einige CSC-Eigenschaften bereits in der PA-Zelllinie vorhanden sind, aber in der SP-Zelllinie qualitativ und quantitativ stärker und stabiler etabliert sind. Im Vergleich zu SP weisen die CS-Zelllinien leicht reduzierte und weiniger stabile CSC-Eigenschaften auf.
Die oben genannten Assays stellen bioinformatisch einen trainierten oder gefilterten Satz von Werkzeugen für die CSC-Charakterisierung dar. Für eine neutrale Analyse wurde deshalb für PA, SP und A-SP eine Sequenzierung der gesamten transkribierten mRNA (RNA-Seq) durchgeführt. Dabei wurden differentiell exprimierte Gene (DEG) in PA, SP und A-SP identifiziert und eine Gen-Mengen-Anreicherungsanalyse („gene set enrichment analysis“: GSEA) durchgeführt. Die Ergebnisse werden im Detail diskutiert.
Insgesamt stehen die mit dem gefilterten Werkzeugsatz gefundenen Daten in gutem Einklang mit den RNASeq-basierten Datensätzen. In den aus Sphäroiden gewonnenen Zelllinien (SP, A-SP) sind die Aktivitäten der ERK und AKT, CREB, HIF-1α, Wnt/Hedgehog/Notch, EGFR (ERBB) und PAK Signalwege erhöht; allesamt Korrelate für Stammzell-Eigenschaften. In der adhärent wachsenden Ausgangszellen (PA) dominieren Zelladhäsion und angiogene Signalwege sowie S1P- und NFkB-vermittelte Signaltransduktion. Auch die RNA-Seq Daten zeigen, dass die Stammzell-typischen Signaturen in Sphäroiden, die unter nicht CSC-selektierenden Bedingungen in Monoschicht-Kulturen kultiviert werden (A-SP), erhalten bleiben. Unter diesen Bedingungen werden aber auch Zelladhäsionswege reaktiviert, die in den adhärent wachsenden PA-Zellen aktiv sind.

1 Introduction

1.1 Stem Cells

Stem cells represent the apex of the tightly regulated hierarchical system, which is the basis for creation and maintenance of an organism. They can be classified according to their differentiation potentials with descending hierarchical position: a totipotent stem cell (zygote, morula) is able to give rise to the whole organism including extra-embryonic tissues; pluripotent stem cells (embryonic stem cells, ESC) are able to generate all germ layers from which all tissues of the organism are derived; multipotent stem cells are able to differentiate into all cell types of their respective germ layer (e.g.: mesenchymal stem cells, MSC); oligopotent, organ specific stem cells stem cells are able to form several but not all cells of the respective germ layer (e.g.: hematopoietic stem cells, HSC, neuronal stem cells, NSC); epidermal stem cells, breast stem cells, intestinal stem cells) give rise only to organ specific cells; unipotent stem cells are merely able to differentiate into one cell type (e.g.: muscle stem cells). [1] [2] The latter terms are not used stringently in the literature, so the term „multipotent“ is frequently used for oligopotent, organ specific stem cells. Differentiated somatic cells, which finally form the most parts of an organism, represent the bottom level of the hierarchy (see figure 1.1.1 and 1.1.2).

1.1.1 Embryonic Stem Cells and Development

An overview of early events during embryonic development and of tissue types emerging from different germ layers is shown in figure 1.1.1. From the totipotent cells contained in the morula, which in human arises after several cell divisions from the zygote, two more restricted cell types can be distinguished in the blastocyst stage approximately at day 5 after fertilization. The outer cell layer of the blastocyst is composed of pluripotent trophoblast cells, which give rise to extra embryonic tissues of the placenta. The inner cell mass of the blastocyst contains the pluripotent ESC, which form the basis for generation of the organism. In a first series of differentiation events, ESC give rise to the four germ layer linages: ectoderm, endoderm, mesoderm, and primordial germ cells. Cells of the epidermis, neurons, and pigment cells are derived from the ectoderm (outer layer), inner organs such as lungs, intestine, pancreas, liver, thyroid and thymus are derived from the endoderm (inner layer), and blood cells, bones, kidneys, muscles, cartilage, tendon, ligaments and adipocytes are derived from the mesoderm (middle layer). Germ cells are derived from the primordial germ cell layer. The whole organism is formed from these four layers in a tightly regulated series of differentiation and patterning events. The developmental program also includes trans-differentiation events, which are characterized by the switch between germ layers. The (reversible) trans-differentiation processes which are involved for example in gastrulation and primitive streak formation are termed epithelial-to-mesenchymal transition (EMT) and mesenchymal-to-epithelial transition (MET) [3]. Also during kidney development, which is explained in more detail in chapter 1.2.2, cells of mesenchymal origin trans-differentiate to epithelial cells (MET). Most of the current knowledge of embryonic development was achieved by use of model organisms, of which for the mammalian system the mouse is the most extensively studied organism, while data for human development due to ethical considerations are limited and are based on several established embryonic stem cell or teratocarcinoma cell lines. [4] [5] [6] [7] [8]

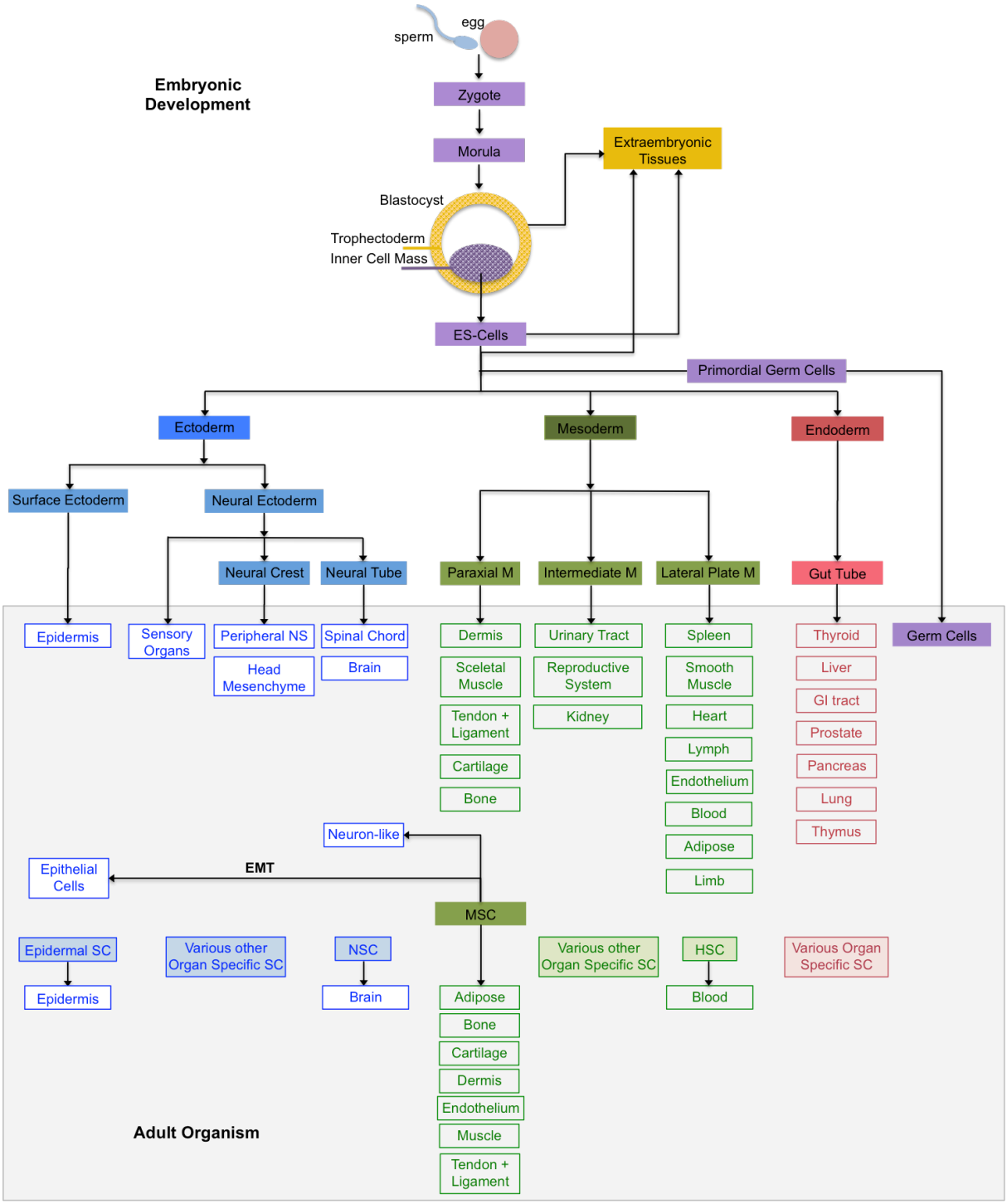

Figure 1.1.1: Stem Cell Hierarchy: Embryonic Development and Adult Stem Cells

Overview of ancestry of different adult organs (grey shaded) from the different germ layers arising during embryonic development (non-shaded) and stem cells in the adult organism. The germ layers are color-coded: Ectoderm (blue), Mesoderm (green), Endoderm (red), Germ Cell (violet). Totipotent and pluripotent stem cells are indicated in violet. Reduction of stem cell potency is indicated by lighter color, with non-shaded boxes representing fully differentiated, non-stem cells. Most of adult stem cells are able to differentiate into organ specific cells, whereas MSC are able to differentiate into a broad spectrum of mesoderm-derived cells but also to trans-differentiate into epithelial or neuron-like cells. The figure is not meant to be complete and is mainly based on information in LifeMap® „Embryonic Development & Stem Cell Compendium“ in the GeneCardsSuite.
EMT: epithelial to mesenchymal transition, HSC: hematopoietic stem cells, M: mesoderm, MSC: mesenchymal stem cells, NSC: neural stem cells, SC: stem cell.

1.1.2 Somatic or Adult Stem Cells - Mesenchymal Stem Cells

Adult stem cells have been found to reside in many organs (see figure 1.1.1). Especially in tissues with high cellular turnover rates like blood, skin and intestine they serve fundamentally in maintaining tissue homeostasis throughout the lifetime of an organism. But adult stem cells also serve for regeneration processes after injury in tissues with generally low cell turnover (e.g. NSC, kidney stem cells). Recent data indicate, that under stress conditions adult stem cells show remarkably high flexibility in order to regenerate the injured tissues. [9] [10] [11] [12] Besides adult stem cells, also pluripotent stem cells have been reported to reside in adult organs. They are termed “multipotent adult progenitor cells” (MAPC), “very small embryonic-like stem cells” (VSEL), “multi-lineage differentiating stress-enduring” (MUSE) cells or “marrow-isolated adult multilineage inducible” (MIAMI) cells. [13]

Since mesenchymal stem cells (MSC) have been found to reside in many organs including the kidney, and features of MSC have been found to correlate with tumor formation and metastasis (see 1.3.2), they are of special interest for this work.

Mesenchymal stem cells, also termed mesenchymal stromal cells (MSC) have first been described by Friedenstein [14] in 1970 as fibroblast colonies from bone marrow (BM) of guinea pigs with the ability to osteogenic differentiation. In 1994, the concept of MSC as a multipotent cell source for regeneration of mesenchymal tissues was introduced by Caplan. [15] In 1999 Pittenger et al [16] isolated and propagated MSC as fibroblast-like, plastic adherent, colony-forming cells from human BM with differentiation potential towards adipogenic, osteogenic and chondrogenic lineages. MSC have since been isolated from several other tissues including umbilical cord blood (UCB) [17], adipose tissue (AT) [18], synovial membrane (SV) [19], dental pulp (DP) [20] and placenta (PL) [21]. Besides differentiation into the three above mentioned mesenchymal lineages, also differentiation potential into muscle cells and endothelial cells as well as trans-differentiation potential into epithelial cells (EMT) and neuron-like cells has been reported for MSC. [18] [22] [23] [24] Due to their relatively high abundance and easy accessibility combined with their differentiative capacity to form osteoblasts, chondroblasts and muscle cells, MSC are central to regenerative medicine.

Minimal criteria for MSC were defined as adherently growing cells, which have the ability to differentiate into osteoblasts, adipocytes and chondroblasts and are positive for cluster of differentiation (CD) antigen CD105, CD73 and CD90 expression, but show now expression of hematopoietic lineage markers CD45, CD34, CD14, CD19 and HLA-DR. [25] Isolation of MSC from the various sources is mainly achieved by selecting for cells growing adherent to plastic in culture. Unfortunately, no single defining marker for prospective isolation of MSC from different sources has been identified, since MSC from different sources express a variable set of markers. Also many of the markers identified so far are expressed by other cell types and/or show differential expression in cultured MSC compared to freshly isolated cells. [26] [27] [28] Besides the defining markers CD105, CD90 and CD73 most cultured MSC express the surface markers CD9, CD13, CD10, CD29, CD44, CD49d, CD49e, CD54, CD106, CD146, CD166, and MHC-II (HLA-ABC). Also expression of CD56 and CD271 was found on subsets of MSC. The marker profile of MSC is almost identical to that of fibroblasts isolated from different sources with few exceptions (CD106, CD10, CD146). [29] [30] Whereas marker

expression of both cell types is very similar, fibroblasts differ from MSC in their potential to differentiate towards adipogenic or osteogenic lineages [29].

1.1.3 Stem Cell Features

Due to their outstanding status and function stem cells possess exceptional features, which are more pronounced the more prominent their hierarchical position. A hallmark feature of stem cells is their ability not only to self-renew by symmetric cell division but to create differentiated progeny by means of asymmetric cell division. This means they are able to generate two different daughter cells: one stem cell and one committed progenitor cell with reduced potency, which then further proliferates and gives rise to the finally differentiated cells of the organ or organism (see figure 1.1.2). These differentiated cells are able to self-renew only during their comparably rare cell divisions.

The two different modes of cell division are tightly regulated by extrinsic and intrinsic factors. Under steady-state conditions asymmetric cell divisions are predominant to maintain tissue homeostasis whereas after injury or during development of the organism the stem cell pool is expanded by an increase of symmetric division rate. The balance between the two modes is critical, since disturbances may lead to tissue degeneration (ageing) or hyperplasia/tumor formation. [31 32 33 34 35 36]

Another outstanding feature of stem cells is their high proliferative and replicative potential. In contrast to differentiated cells, which possess only a limited proliferative potential, i.e. the number of possible cell divisions is restricted to 20-100 generations before the cells enter into a senescent state or die [37 38], the proliferative potential of stem cells is not restricted. This is partially achieved by expression of the enzyme telomerase, which prevents the telomere shortening normally occurring during cell divisions. [39 40]

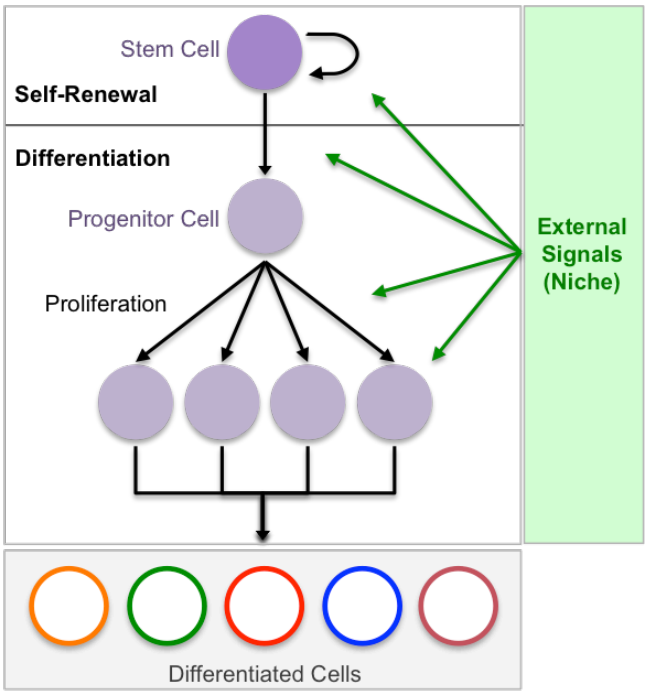

Figure 1.1.2: Stem Cell Self-Renewal and Differentiation

Stem cells are able to divide by two different mechanisms, resulting either in self-renewal of stem cells, thereby maintaining the stem cell pool, or in progenitor cells which after further rounds of proliferation are able to form various differentiated cells of an organ or organism. The processes are influenced by external signals, mostly derived of the stem cell niche.

1.1.3.1 Stem Cell Plasticity and Stem Cell Niche

Attributed with these features, stem cells are enabled to generate either a whole organism, as in case of ESC, or the different cell types of their respective tissues or organs in case of adult stem cells.

To fulfill their function, stem cells, in contrast to the functional terminally differentiated cells of the organism, show a high degree of plasticity, including trans-differentiation potential. This is regulated by external signals such as soluble factors (growth factors and cytokines) acting via their receptors or by cell-cell as well as cell-matrix interacting molecules (cellular adhesion molecules, Ig-like molecules, cell-junction molecules), which exert signal transduction pathways within the cell. Expression of the respective molecules in stem cells, and thereby the cellular plasticity of the cells, is regulated on epigenetic level, with chromatin modifying enzymes being fundamentally involved in this process.

Adult stem cells receive critical signaling (as described above) from their immediate microenvironment, a domain that is distinct from the rest of the organ and is termed the stem cell "niche". The niche, which is often characterized by a hypoxic status, provides signals for quiescence, or activation. These are critical for maintenance of the stem cell pool and production of progenitor cells engaged in tissue differentiation. The stem cell niche is a dynamic microenvironment that responds to local and systemic cues, ultimately influencing stem cell fate. [41] [42] [43] [44]

1.1.3.2 Regulation of Pluripotency - iPSC

The balance between self-renewal and differentiation of ESC is regulated by a core transcription unit consisting of Oct4, Sox2 and Nanog transcription factors in combination with Klf4 and c-Myc [45]. Expression of these factors is modulated by extracellular signals, of which LIF, Wnt, BMP/Activin/Nodal and FGF signaling, via MAPK/ERK, STAT3, SMAD and GSK3β pathways are central in ESC. [46] [47] [48]

By artificial overexpression of the key factors (Oct4, Sox2, Klf4 and c-Myc = OSKM factors) it is possible to induce fibroblasts to an ESC-like state, which was first achieved in mouse cells in 2006 and human cells in 2007 by Takahashi and Yamanaka. [49] [50] The resulting cells are termed induced pluripotent stem cells (iPSC). It has been shown that Nanog and LIN28A, two downstream targets of Klf4 and c-Myc, may replace for the latter for successful reprogramming [46].

Several markers have been identified as indicators of pluripotency of ESC. For example staining for alkaline phosphatase activity is often used to mark pluripotent stem cells. [39] [51] [52] [53] Also the glyco-epitopes detected by antibodies against so termed stage-specific embryonic antigens (SSEA-1, -3, -4) as well as podocalyxin, which is detected by antibodies reacting against TRA-1-60 and TRA-1-81 [54] [55] are expressed on pluripotent stem cells, while expression of these antigens is lost upon differentiation of the cells. Of note is that SSEA-1 and SSEA-4 expression in ESC of mouse and human origin is regulated conversely. In mouse ESC SSEA-1 is expressed on pluripotent stem cells and decreases with differentiation of the cells, whereas expression in human ESC increases with differentiation of the cells and vice versa for SSEA-4. [56] [57] [55] [58] Some of these pluripotency markers are also expressed on adult stem cells. [28] [59] [60] Besides these extracellular markers, also expression of the master pluripotency transcription factors Oct4, Sox2 and Nanog may be used as indicators for stem cell pluripotency state. [61]

1.2 Kidney

1.2.1 Kidney Structure and Function

Kidneys represent one of the most complex multi-tissue, multi-cellular and multifunctional organs. The main function of the kidneys is excretion of metabolic waste as urine. They also have central functions in regulating blood pressure and -volume, electrolyte- and pH balance, as well as in erythrocyte, and calcium homeostasis.

In the kidney two main regions can be distinguished, the cortex (outer part) and the medulla (inner part). Within these regions about one million nephrons, surrounded by capillaries, constitute the functional units of the kidney. A single nephron is composed of the renal corpuscle, followed by the proximal convoluted tubule, the loop of Henle (descending and ascending limb), the distal convoluted tubule and finally the connecting tubule, ending up in the collecting duct in which the concentrated urine of several nephrons is collected and transported to the ureter.

The renal corpuscle is the main filtering unit of the blood. It is composed of the Bowman's capsule and the glomerulus. The glomerulus consists of bunch of multi-convoluted capillaries lined by fenestrated epithelial cells, accompanied by mesangial cells for anchoring. Blood vessels are entering into the glomerulus as thick afferent arterioles and leaving as thinner efferent arterioles, thereby creating hydrostatic pressure within the capillary system. The Bowman's capsule is a cup like structure enclosing the glomerulus. The cup is formed by a basement membrane lined with cells surrounding a lumen called Bowman's space into which the primary urine is passed before its further concentrated in the renal tubules. According to the lining cell type two continuous layers can be discriminated. The visceral layer close to the glomerulus is part of the filtering system. It is composed of podocytes or "visceral epithelial cells", which, separated by the three-layered glomerular basement membrane, enwrap the glomerular capillaries with their interdigitating foot processes, thereby forming slits. The slits are connected via a special intercellular junction called slit diaphragm, containing the trans-membrane protein nephrin as major component. The outer parietal layer mainly consists of squamous epithelial cells. Endothelial cells and podocytes at either side synthesize the glomerular basement membrane. Whereas mesangial cells in the glomerulus by degrading its components have a function in homeostasis of the membrane.

Fenestrated epithelial cells of the capillaries, basement membrane and podocytes together form the filtering barrier of the renal corpuscle. Due to the hydrostatic and oncotic pressure and the porous nature of capillary's endothelial cells and basal lamina and the special arrangement of podocytes, about 1/5 of the incoming blood liquid including small molecules, but no blood cells or negatively charged macromolecules, is pressed/filtered into the Bowman's space. [62 63 64]

In the proximal tubule water, sodium and other solutes are reabsorbed from the glomerular filtrate. Also remaining proteins in the filtrate are removed almost completely by endocytosis. From the blood compartment various organic compounds are secreted into the tubular lumen. Tubular epithelial cells are complexly folded and form a brush border at the apical pole resulting in a huge plasma membrane surface of the cells, which allows for efficient solute transport. The membrane contains various transport proteins such as aquaporin, sodium coupled transporters for inorganic phosphate, glucose

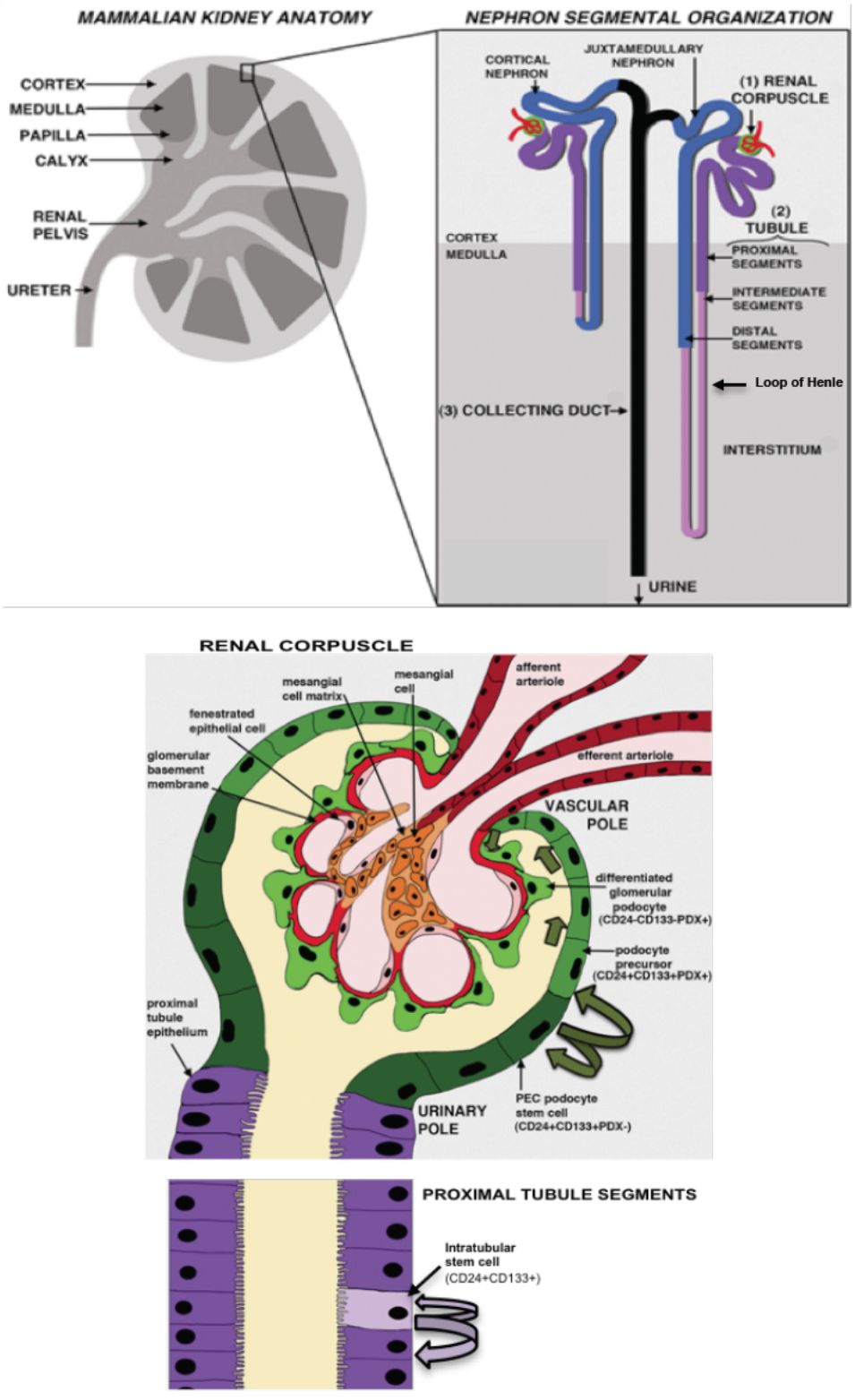

Figure 1.2.1: Kidney Structures

Schematic overview of kidney structures (not drawn to scale). Figure top left: anatomic overview of kidney structural organization. Figure top right: enlarged view of kidney region with overview of nephron segmental organization (short and long-looped nephrons) with renal corpuscle, proximal convoluted tubule, proximal straight tubule, loop of Henley (comprising: descending thin limb, ascending thin limb, thick ascending limb, distal convoluted tubule), connecting tubule, and collecting duct. Figure middle: Enlarged schematic view of renal corpuscle including the Bowman's capsule and the glomerulus. The different cell types (structures) are indicated as well as podocyte generating precursor cells (chapter 1.2.3). Figure bottom: enlarged schematic representation of proximal tubular segment with indication of tubular stem cells. The figures were slightly adapted from McCampbell and Wingert [65]

and multi-specific organic anion and cation transporters as well as Na/K-ATPase, Na/H exchangers and chloride channels. In the thick ascending limb of Henle's Loop (TAL) sodium is absorbed in excess of water by Na/K/Cl symporters and Na/K-ATPase, thus rendering the surrounding interstitium hypotonic, which allows the concentration of urine by osmotic pressure. This segment also has a prominent role in reabsorption of Ca and Mg ions as well as in acid-base homeostasis. In the distal convoluted tube (DCT), connecting tubules (CNT) and collecting duct (CD) final sodium reabsorption via amiloride and aldosterone-sensitive sodium channel EnaC takes place. Similar to TAL, DCT and CNT have a function in Ca and Mg homeostasis. In the CD also vasopressin regulated water and urea transporters are expressed for vasopressin-regulated reabsorption of water and urea. [63]

1.2.2 Kidney Development

In mammalian embryonic development the kidneys are derived from the intermediate mesoderm.
In mice at the 6-8 somite-stage the nephric ducts (ND/Wolffian duct) arise in a process of bilateral epithelialization and elongate, before they fuse with the cloak, which is the precursor of bladder and urethra. An overview of the stages of kidney formation starting about day 11 is depicted in figure 1.2.2.

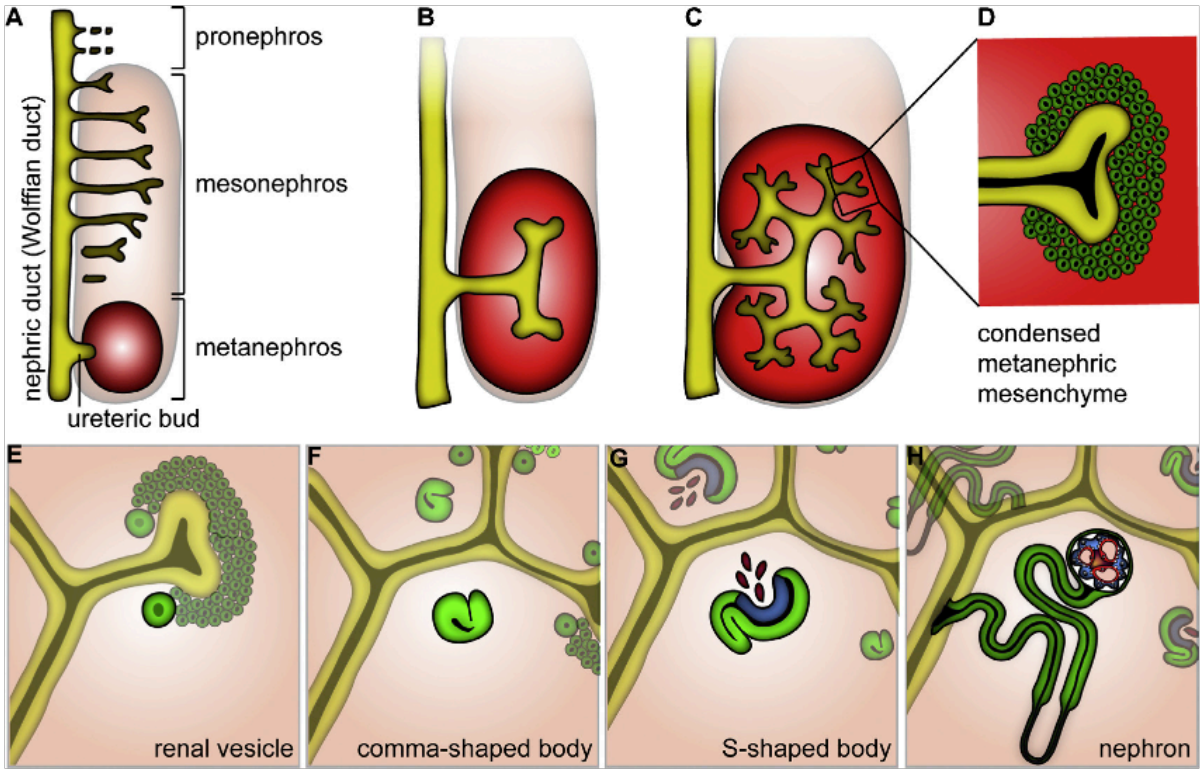

Figure 1.2.2: Kidney Development

Schematic representation of stages in mammalian kidney development. (A) Nephric duct compartments with invading ureteric into metanephric mesenchyme. (B), (C) Branching of ureteric bud. (D) Formation of condensed/cap mesenchyme at ureteric bud tip. (E) Formation of renal vesicles from condensed/cap mesenchyme. (F) Formation of a cleft to form the comma-shaped bodies. (G) Podocyte precursors (blue) attract angioblasts (red) in the S-shaped body. (H) Developing nephron connects with the nephric duct.
The figure was created by Schell, Wanner and Huber [64]

At the ND, by induction of neighboring metanephric mesoderm, three structures arise: pronephros, mesonephros and metanephros. In the further developmental stages pronephros and mesonephros become part of the male genital system or degenerate in females. The metanephros finally becomes

the kidney. The process of kidney formation is induced at the posterior end of the ND by interaction with the metanephric mesoderm/mesenchyme (MNM), by outgrowth of the ureteric bud (UB), which invades into the MNM and starts branching. At the tip of the UB the surrounding MNM condenses, thereby forming the condensed/cap mesenchyme (CM). CM is characterized by expression of a unique gene set composed of SIX2, OSR1, PAX2, SALL1, WT1, CITED1, GNDF, and the mesenchymal marker vimentin. Epithelialization of these cells via UB induced MET with concomitant repression of the CM specific genes and expression of E-Cadherin is induced by autocrine WNT4 signaling. Renal vesicles start forming from the CM. From the intermediate comma shaped bodies, the S shaped bodies, containing podocyte progenitors and parietal epithelial cells, evolve by forming a cleft. Podocytes attract endothelial cells by secretion of VEGF-A, which invade into the cleft and later form the capillaries. By secretion of PDGF from angioblasts/endothelial cells, mesangial cells are attracted and, by attaching to the endothelial cells, cause looping of the glomerulus. Already at the renal vesicle stage a proximal/distal polarity is established, in which WT1 and notch signaling are involved. This polarity is retained throughout further steps, with the distal segment of the S shaped body finally forming the distal tubule, which connects to the connecting segment on the collecting duct. The intermediate segment develops to the Loop of Henle' and the proximal segment finally gives rise to the glomerulus and the S1-3 segments of the proximal tubule. Whereas the nephron is formed from the ureteric bud and CM, another mesenchymal subset, which is characterized by expression of FoxD1, gives rise to several supporting cell types of the kidney such as interstitial fibroblast, pericytes and vascular smooth muscle cells (VSMC), but also to mesangial cells, which are characterized by expression of α-SMA and seem to be a specialized VSMC and angioblasts. [66] [64] [67] [68]

1.2.3 Adult Stem Cells in the Kidney

In the adult kidney two mechanisms have been shown to be probable sources for cellular regeneration. One mechanism for recovery after injury is the de-differentiation of surviving tubular epithelial cells by EMT, but also adult stem cells may be involved in this process. [69] [66] [70]

In human adult kidney several renal progenitor cell populations have been identified in the cortical, medullary and papillary regions of the kidney. These progenitor cells were all characterized by co-expression of CD24 and CD133 molecules. [71] [72] [73] [74] [75] [76]

In the Bowman's capsule different subsets of adult regenerating cells could be discriminated by their expression of the podocyte marker PDX, with $C133^{+}/CD24^{+}/PDX^{-}$ localized to the urinary pole are able to differentiate to tubular cells and podocytes, whereas cell with additional expression of the podocyte marker PDX, localized between urinary and vascular pole are able of podocyte generation only. Differentiation potential is restricted to $C133^{+}/CD24^{+}$ subsets, whereas $C133^{-}/CD24^{-}$ cells display phenotypic features of podocytes [77] [73] (see figure 1.2.1). These precursors might be used to treat glomerular disorders characterized by podocyte injury, proteinuria, and progressive glomerulo-sclerosis. Renal progenitors isolated from the parietal layer of the Bowman's capsule have been shown to possess differentiating potential not only into functional renal tubules but also into adipocytes, osteoblasts and into neuron-like cells. [73] In contrast, progenitors isolated from the tubular fraction of human kidneys were found to differentiate into tubular lineages only and were marked in contrast to glomerular derived podocyte precursors by lacking expression of CD106. [75]

Additionally, from adult human decapsulated glomeruli, resident renal progenitor cells of mesenchymal-like phenotype have been isolated. The cells are marked by their specific expression of CD146 and also expressed further MSC markers (CD73, CD90, vimentin) as well as the renal stem cell markers CD24 and Pax2, which are not expressed by MSC. This progenitor cell fraction, in contrast to the other progenitor subsets was identified to be negative for CD133 expression. Besides MSC specific differentiation capabilities into adipogenic, osteogenic, and chondrogenic lineages, they were also able to differentiate into endothelial, tubular epithelial and mesangial cells. [78]

The identification of renal stem cells or cells with renogenic potential is of urgent therapeutic interest for treatment of glomerular disorders and kidney failure. [66 79]

1.3 Tumor Formation and Tumor Cell Features

Tumor formation is the result of imbalanced homeostasis mechanisms due to genetic (mutations, copy number variations, deletions, amplifications, translocations) and/or epigenetic alterations (DNA methylation status and histone modifications) which provide the resulting tumor cells with the capability to proliferate extensively and potentially disseminate to other regions of the body as metastases. The process is referred to as transformation, and the resulting cells are termed transformed cells. Several key or driver genes have been identified with frequently altered expression in tumor cells. According to their function, they are either termed „oncogenes“ (aberrantly high expression or gain-of-function in tumor cells) or tumor suppressor genes (aberrantly low expression or loss-of-function in tumor cells). These genes often fulfill central functions in signaling pathways regulating cell proliferation (e.g. growth factor signaling, cell cycle control), stress response (e.g. DNA damage, hypoxia) or apoptosis.

The altered gene expression results in acquisition of the so termed “hallmarks of cancer” (see table 1.3.1) described originally in 2000 and revisited 2011 by Hanahan and Weinberg [80 81], which in a deregulated intertwined circuit of signaling events provide the basis for the abnormal cell growth and survival of tumors.

Cancer Hallmark	Probable Target Molecules
Sustaining proliferative potential	Growth factor receptor (EGFR) inhibitors
Evading growth suppressors	Cell cycle (CdK) inhibitors
Activating invasion and metastasis	Inhibtior of HGF/c-Met
Enabling replicative immortality	Telomerase inhibitors
Inducing angiogenesis	Inhibitors of VEGF signaling
Resisting cell death	Proapoptotic mimetics
Reprogramming of energy metabolism	Anaerobic glycolysis inhibitors
Avoiding immune destruction	Immune activating anti-CTLA4 mAB
Tumor promoting inflammation	Anti-inflammatory drugs
Genome instability and mutation	PARP inibitors

Table 1.3.1: Hallmarks of Cancer

Distinctive and complementary capabilities that enable tumor growth and metastatic dissemination and probable therapeutic targets thereof as described by Hanahan and Weinberg [81]

Most tumors are not composed of a homogenous cell population; instead they show high heterogeneity with respect to mutational and epigenetic status as well as to their morphological appearance. Besides, many tumors also show remarkable plasticity, as can be seen for example in the steps needed during formation of metastases (transversal to another organ and adaptation to the different growth conditions there), but also in acquisition of therapy resistance. [82] [83] [84] [85] [86] [87] [88]

1.3.1 Cancer Stem Cells (CSC) or Tumor-Initiating Cells (TIC)

With emerging knowledge on stem cell biology and plasticity, the idea that similar mechanisms might be involved in tumor formation came into focus. But this idea was not new either, since a stem cell origin of tumors was already proposed by Rudolf Virchow in 1855 in his „Embryonic-rest hypothesis' of tumor formation", which was based on histological similarities between tumors and embryonic tissues [89]. According to the cancer stem cell (CSC) hypothesis, tumors are organized, similar to other organs, in a hierarchical manner, containing a small subset of cells with stem cell characteristics, which are capable of regenerating the tumor, whereas most of the tumor is composed of differentiated progeny of these cells, which show limited proliferative potential. [90] [91] [92] [93] [94] The cell population with stem cell characteristics, and assumed to be responsible for tumor expansion, is denominated either as CSC or tumor-initiating cells (TIC) in the literature. It is important to be aware, that the cancer stem cell hypothesis does not imply that the tumor initiating cell population necessarily descends from a stem cell. Rather, the stem cell characteristics might also be acquired by mutational and/or de-differentiation events of various cell types. [95] The first evidence, that a small subpopulation of cells in human ALL are able to recapitulate the original disease phenotype in immune-compromised mice was provided 1997 by Bonnet and Dick [96]. Later on the first evidence for TIC in solid tumors were provided by Al Hajj [97] et al for breast tumors. These reports were subsequently followed by similar reports for brain tumors [98], prostate [99] and ovarian [100] tumors, melanoma [101], colon [102], pancreatic [103], liver [104] and lung cancer [105] [106]. The first report on TIC in RCC was published 2008 by Bussolati et al [78].

By now, TIC populations have been reported also for other tumor types and several approaches, yielding different populations, have been used to isolate these cells (see chapter 1.4.1). Thereby, in different reports the identified TIC populations varied in several aspects (size of population, characteristics) not only between different tumor entities but also between different isolation approaches and experiments. This has led to controversial discussions on the validity of the hypothesis. However, the concept of involvement of stem cell characteristics in tumor formation and propagation is now well accepted. The idea leads to the description of a more complex tumorigenesis model, which combines the clonal evolution idea with the stem cell hypothesis (see figure 1.3.1). This model puts a further challenging layer of complexity on the efforts to refine methods for identification of CSC. [88] [107] [108] [109] [110] [111] [112] [113] [126]

This is important for clinical oncology, since the involvement of cells with stem cell characteristics in tumor formation and propagation has profound implications for development of effective tumor targeting strategies. Most conventional therapeutic approaches (radio or chemo-therapy) aim to target fast proliferating cells, thereby shrinking the tumor mass. Owed to their stem cell features (quiescence, high resistance to damaging agents) TIC may not be eliminated efficaciously by this strategy and surviving CSC after treatment are able to re-form the tumor and/or metastases. Therefore, targeting

the founding CSC is necessary for effective long-term elimination of the tumor. Several approaches are now being tested, such as e.g. differentiation therapy, inhibitors for stem cell specific signaling components or drug conjugates based on molecular markers. [114 115 116 117 118 119 120 121 122 123 124 125]

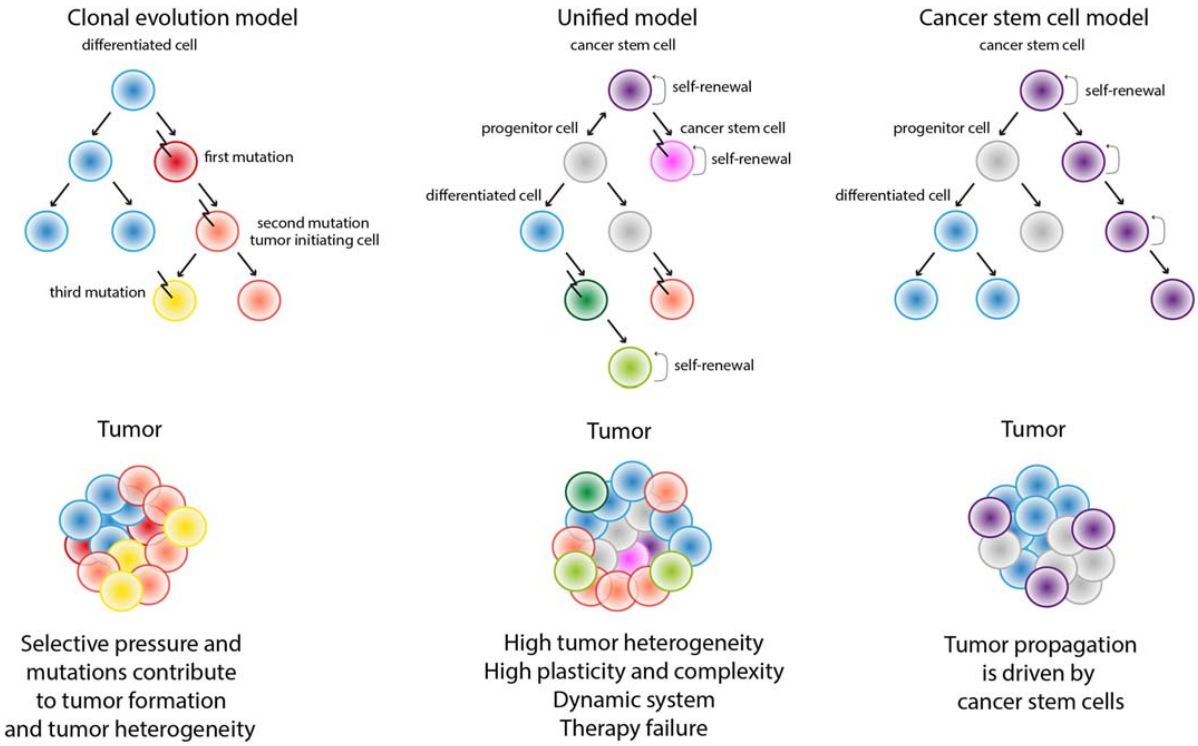

Figure 1.3.1: Models of Tumorigenesis

Three models for tumorigenesis are depicted, of which the "Unified" mode seems to be the most probable. Left: the clonal evolution model describes tumorigenesis as a stochastic process in which transformed tumor cell populations with growth and survival promoting advantageous mutations are selected by evolutional pressure and over time accumulate further mutations, which are similarly selected for growth and survival, resulting in tumor progression. Tumor heterogeneity according to this model is based on multiple different tumor growth promoting mutations. Right the cancer stem cell model implies that tumor growth is driven by a small subset of cells with stem cell features (acquired by mutation of stem, progenitor, differentiated or dedifferentiated cells). Tumor heterogeneity according to this model is established by the hierarchical organization based on stem cell intrinsic differentiating capacity. Middle: the unified, combined model is the most complex but most probable model for tumor genesis. It combines the stem cell characteristics depicted in the CSC model with the acquisition and selection of advantageous tumor promoting mutations over time at any stage of the differentiation hierarchy. Besides the heterogeneity, which is explained differently in both single models, this model also delineates the high plasticity and complexity of tumors. The figure was created by Corrò and Moch [110]

1.3.2 Epithelial-to-Mesenchymal Transition (EMT)

An aspect that has been recognized to be functionally involved in tumor dissemination but probably also in tumor formation is the process of trans-differentiation from epithelial to a mesenchymal (EMT) phenotype, which is known from embryonic developmental processes During this process polarized attached epithelial cells assume a stem ce l like mesenchymal motile phenotype The process is characterized by a number of molecular changes, of which the loss of expression of epithelial markers such as E-Cadherin (CDH1) and cytokeratins and gain of expression of mesenchymal markers N-Cadherin (CDH2) and vimentin are the most prominent indicators. EMT might be initiated by several external signals (e.g. TGF-β, cytokines, growth factors WNT, Notch ligands, SHH, integrin and hypoxia), which dependent on cellular signal integration, lead to epigenetic changes and subsequent

expression of the characteristic core transcription factors Snail, Zeb and Twist. [3] [88] [126] [127] [128] [129] [130] [131] [130] [132] [133] [134] [135] [136] [137] In figure 1.3.2 a model of EMT involvement in formation of tumor metastases is illustrated.

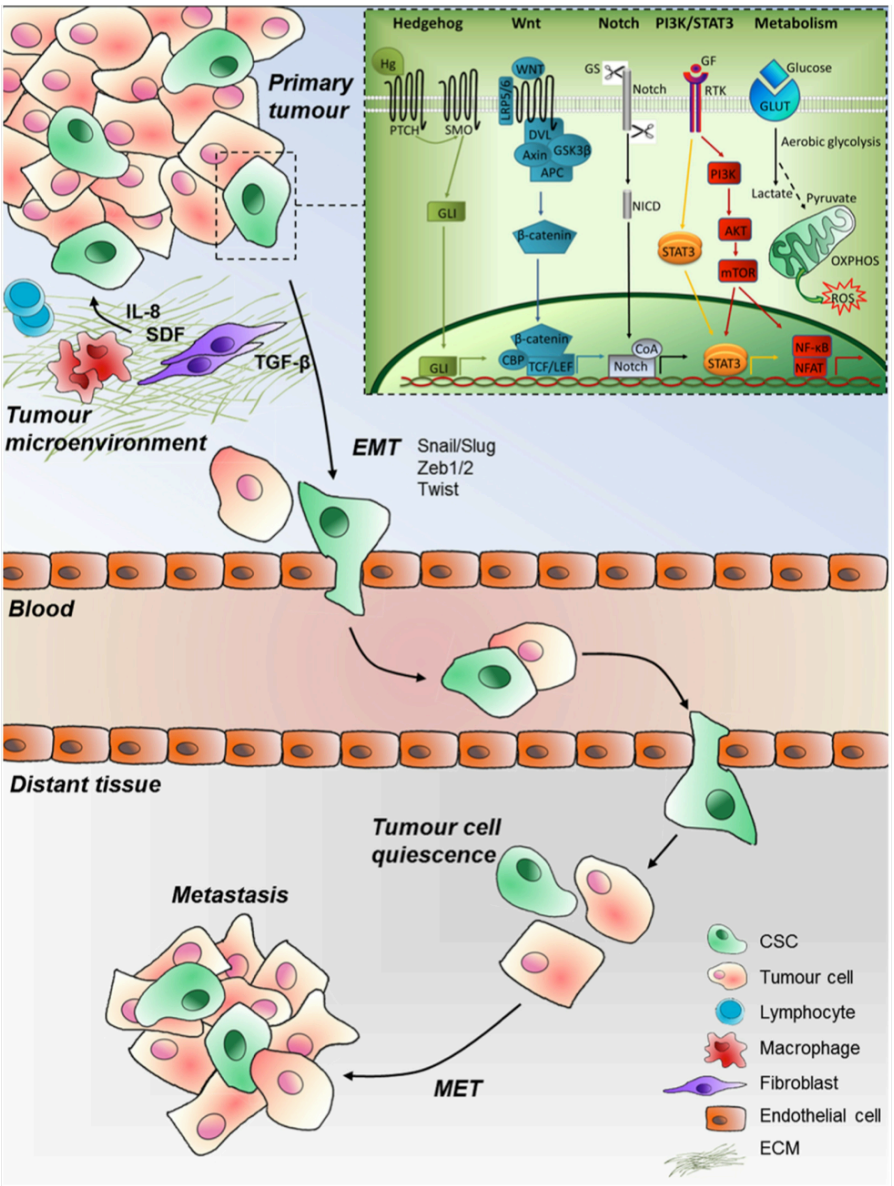

Figure 1.3.2: Trans-Differentiation in Metastasis Development and Pathways Active in CSC

Illustration of a model for metastasis formation by trans-differentiation processes induced by environmental signals. Signals from the tumor microenvironment (immune cells, stromal cells and ECM) may induce EMT in epithelial tumor cells by means of soluble factors or direct interaction. The resulting cells of mesenchymal phenotype are characterized by up-regulation of transcription factors Snail, Zeb and Twist, which induce expression of N-Cadherin and repress expression of E-Cadherin accompanied by induction of cytoskeletal changes. This changes result in a motile phenotype capable of intravasating into the blood vessel, survive in the blood stream and extravasating into distant organs. In the new environment cells might either stay in a dormant state or re-acquire epithelial properties and initiate growth of metastases. Inset top right: Growth and metastasis promoting developmental and PI3K/STAT3 pathways and deregulated metabolism in CSC.
CSC: cancer stem cell, ECM: extracellular matrix, EMT: epithelial-to-mesenchymal transition, IL-8: interleukin-8, MET: mesenchymal to epithelial transition, SDF: Stromal derived factor-1 or CXCL12. The figure was created a by Agliano, Calvo and Box [122]

1.4 Methods for the Analysis of CSC

For the investigation of tumor cells either primary tumor material derived from patient biopsies, tumors grown from this material in laboratory animals (xenograft tumors), or tumor cells grown *in vitro* may be used. The advantage of using primary tumor material is that the analysis of a "quasi" original state. The obvious disadvantage, though, is the limitation of available material. Primary tumors are therefore suitable for immune cytometric or immune cytochemical analyses as well as for gene expression, or genetic analyses, but only a small amount of functional tests can be performed.
To augment tumor material for further analyses, it can either be propagated *in vivo* by xeno-, allo-, or auto-transplantation into laboratory animals (mostly immune-compromised mouse strains) or using *in vitro* cell culture methods. Both methods suffer from the lack of original tumor environment and introduction of artificial conditions (xenogeneic/heterotopic environment of animals used for *in vivo* propagation, culture conditions used for *in vitro* propagation). Thus information obtained using propagated tumor cells contains effects that are artificially introduced by the artificial environment and effects that depend on the missing tumor environment, such as immune-interactions of the tumor. Thus, a clear advantage of *in vivo* models over *in vitro* propagation is the provision of complex interactive structures (microenvironment, immune-interactions). [138] [139] [140] [141] Expansion *in vitro*, though, allows for the definition and monitoring of growth- and other conditions to a much greater extent. In addition, also ethical considerations make *in vitro* cultivation and investigation of tumor cells a valuable tool to study tumors, with culture techniques steadily improving (3D-, co-culture). [142] [143] [144] [145] [146]

The gold standard to verify CSC features (self-renewal, differentiation and high replicative and proliferative potential) of a cell population is successful *in vivo* generation of a tumor resembling the tumor of origin. Self-renewal capacity and unlimited proliferative potential are confirmed by repeated growth of tumors after serial transplantation.
Besides this final proof for CSC, also *in vitro* methods can be used to analyze the defining characteristics of stem cells in the cell population investigated. The high replicative and proliferative potential can be shown by long-term *in vitro* growth of the cells without loss of these features over time. To test for self-renewal ability *in vitro*, the serial sphere-forming ability, assayed according to the so termed "Neurosphere Assay" (NSA) is frequently used. The multipotency of cells can be assayed by *in vitro* differentiation of the cells, when cultured under differentiation-inducing growth conditions. These are well established for ESC or adult SC.

1.4.1 Strategies for Isolation or Enrichment of CSC

1.4.1.1 Marker Expression

A straightforward method for isolation of distinctive cell populations is cell sorting according to expression of defining markers for the cells of interest. Cell sorting is accomplished either by fluorescence-activated cell sorting (FACS) or magnetic activated cell sorting (MACS). A pre-requisite for the use of these methods is the availability of suitable selection markers. For the isolation or enrichment of TIC from primary tumors and tumor cell lines, several markers have been identified. The difficulties in using these markers lie in their variable expression depending on tumor type, and their

non-selective character, i.e. expression also in other cell types (see table 4.6.1). Therefore often a combination of markers has to be used for successful enrichment of TIC. In table 1.4.1 an overview of the most commonly applied markers for isolation of CSC from different tumors is shown. Whereas some of the identified markers are typically expressed by stem or progenitor cells (CD133/AC133, EpCAM, CD90), others display no functional connection to stem cells (CD29, CD44). As seen for CD24, which serves as a marker for CSC from several tumors (mostly in combination with CD44), either high or low expression of this protein marks the CSC population in different tumors. Additionally, it has also been found that CSC isolated with a given marker do not necessarily show overlap in marker expression with CSC isolated with other methods. Therefore, by using these markers only a subset of the phenotypically heterogeneous TIC population becomes enriched. [60 107 113 147 148 147]

Tumor Type	Marker
Brain	CD44+, CD133+, CD90+, CD49f+
Breast	CD44+/CD24−, CD90+, CD49f+
Colon	CD44+, CD133+, CD166+, CD24+, EpCAM+, ESA+
Esophagus	CD44+, CD24+, CD133+, ABCG2+, CXCR4+
Gastric	CD44+, CD133+, CD24+, CD54+, CD90+, CD49f+, CD71+, EpCAM+
HNSCC	CD44+, CD133+, ALDH+, CD271+
Liver	CD44+, CD133+, CD90+, CD13+, EpCAM+
Lung	CD44+, CD133+, CD166+, CD90+, ABCG2+
Melanoma	CD20+, CD133+, CD271+, ABCB5+
Ovarian	CD44+, CD133+, CD24+, CD117+, EpCAM+
Pancreatic	CD44+/CD24+, CD133+, ESA+, CXCR4+, ABCG2+
Prostate	CD44+/CD24−, CD133+, Integrin α2β1high , CD166+, CD49f+

Table 1.4.1: Overview of Frequently Used Markers for Isolation of CSC from Solid Tumors

The table was modified from [113 148] and only the most frequently used markers and tumor entities are listed. Many other markers have been applied for CSC enrichment from various tumor types, also from tumor entities not listed in the table.
ABCG2: ABC subfamily G member 2, ABCB5: ABC subfamily B member 5, CD: cluster of differentiation, CXCR4: C-X-C chemokine receptor type 4, EpCAM: epithelial cellular adhesion molecule, ESA: epithelial surface antigen, HNSCC: head and neck squamous cell carcinoma

1.4.1.2 ALDH Activity

A method, originally developed for isolation of adult stem cells from bone marrow [149] and brain, utilizes the high expression of aldehyde dehydrogenase (ALDH) to discriminate stem cells or CSC from other cell types. ALDH comprise a family of 19 isoenzymes, converting aldehydes to their corresponding carboxylic acids. ALDH are involved in detoxification, but also in other cellular processes, such as differentiation, proliferation, and mobility. High ALDH expression is found in liver, pancreas and kidney, heart and skeletal muscle. The ALDH1 isoform, which is involved in retinoic acid (RA) metabolism and signaling, is highly expressed in stem cells. For identification of cells with high ALDH

activity the ALDEFLUOR™ assay is a widely used method. The non-toxic enzymatic assay converts the substrate into a fluorescent form that accumulates intracellularly. Adult stem cells from a variety of tissues (HSC, NSC, mammary, prostate, intestinal, myogenic) and CSC from a number of tumor entities, including breast, colon, pancreas, lung, liver, prostate and bladder have been isolated by combining the ALDEFLUOR™ assay with flow cytometric cell sorting. Similar to isolation strategies using other markers, the applicability of this assay for CSC enrichment is not without scientific debate, especially for isolation of CSC from tissue types with high expression of ALDH enzymes such as pancreas, liver and kidney. [69] [150] [151] [152]

1.4.1.3 Side Population Assay

A characteristic feature of stem cells and drug-resistant tumor cells is the high expression of detoxifying efflux transporters of the ABC-family. This characteristic is used in the side population assay to discriminate and enrich cells by flow cytometry based on their ability to transport or "pump out" the fluorescent DNA-binding dye Hoechst33342 or the mitochondrial binding dye Rhodamine 123 from dye-loaded cells. The name of the assay is derived from the small non-stained cell fraction seen in the flow chart, which represents the cells that pump out the dye, and is termed the "Side Population". The method was first used for enrichment of hematopoietic stem cells (HSC) [153] and later became a valuable tool to enrich stem cells from other tissues as well as CSC from different tumor origins [154]. ABC-transporters ABCB1 (MDR1/P-Glycoprotein), ABCC-members (MRP), and ABCG2 (BRCP) have been identified to be responsible for drug resistance, of which ABCB1 and ABCG2 have been assigned to be the responsible transporters for the SP-phenotype in mice. [155] [156] [157] The expression and contribution to the side population-phenotype varies between different tissues, tumor entities, and species. Similar to other methods applied for CSC enrichment, also the applicability of the side population assay for detection of CSC populations in different tumor types, not only in combination with methodological variations, are controversially discussed in the literature. [154] [155] [158] [159] [160] [161] [162] [163]

1.4.1.4 Sphere Formation Assay

An assay that has widely been used to isolate, propagate and characterize cells with stem cell features is the "Neurosphere Assay" (NSA), which was developed by Reynolds and Weis [164] for neuronal stem cells. In this assay selection of stem and progenitor cells is achieved by use of rigorous cell culture conditions. Adherence of cells is hampered by use of culture vessels not allowing attachment of the cells so that cells grow as non-adherent spheroids. The medium contains only defined growth factors (EGF, bFGF and insulin) known to promote stem cell growth. As a result only cells that are able to survive these conditions (stem and progenitor cells) are enriched, whereas differentiated cells die, due to improper signaling. By use of this assay CSC from several tumor types have been identified. [165] [166] [101] [167] [168] [169] The method is also applied to verify the self-renewal ability of assumed TIC *in vitro*. Repeated application of the assay with concomitant growth of spheroids is, similar to serial tumor formation *in vivo*, considered a proof of self-renewal ability of stem cells. [170]

By the spheroid assay, CSC are selected according to characteristic stem cell features and further markers for direct enrichment or targeting of TIC can be identified. This is an important advantage of

CSC isolation through spheroids. Even more important, compared to direct enrichment using specific markers, the phenotypic heterogeneity of the tumor's CSC is conserved. The probability of progenitor cells enrichment in addition to or instead of stem cells and phenotypic changes mediated by culture conditions are disadvantages of the assay. [171] [170] In the literature the terms "sphere" and "spheroid" are used synonymously as well as throughout this work.

1.5 Renal Cell Carcinoma (RCC)

1.5.1 Incidence and Classification

Renal cell carcinomas (RCC) are a heterogeneous class of urological tumors mostly derived of renal tubular epithelium. They comprise about 3-5% of all human cancers. Three main histological subtypes of RCC are discriminated according to the Heidelberg classification of renal cell tumors, which differ in their clinical outcome and molecular features. Clear cell adenocarcinoma (ccRCC) or "conventional" RCC is the most common form of RCC accounting for 70-80% of renal tumors, followed by papillary carcinoma (pRCC) type 1 and 2, which account for about 10–15% of RCCs, and chromophobe collecting duct carcinomas with an incidence of 5% are less frequent. Some rare renal tumors do not meet the classifications of these subtypes, such as medullary and collecting duct RCC. These are grouped into unclassified carcinomas. ccRCC and pRCC arise from proximal tubule cells showing specific hepatocyte nuclear factor (HNF) regulated gene expression profiles, whereas chromophobe RCC originate from intercalated cells of the collecting duct and show a characteristic forkhead box I1 transcription factor (FOXI1) driven-gene signature. [172] [173] [174] [175] [176] [177]

1.5.2 Therapy

Since RCC do not cause symptoms in early stages, most tumors are detected incidentally and upon presentation up to 30% of patients with RCC already have metastatic disease. For localized RCC, radical nephrectomy is the standard, often curative therapy. In contrast, about half of RCC patients, who present or develop metastatic disease are faced with a high cancer-specific mortality rate with an average survival of 4 months and a 5-year survival rate of 12%. Radiation and chemotherapy, due to high resistance of this tumor entity, are not efficacious in RCC therapy. RCC show low response rates to IFN-α and IL-2 immunotherapy (≈15% partial response rate, 2-5% complete response rates). The application of therapies targeting VEGF and mTOR pathways, which include tyrosine kinase inhibitors (sunitinib, sorafenib), monoclonal antibodies targeting VEGF (bevacizumab) and mTOR inhibitors (temsirolimus, everolimus), also in combination with interferon-based immunotherapies, offer improved progression-free and overall survival. Nonetheless, RCC is still a tumor of poor clinical outcome and more effective therapies are urgently needed. [172] [173] [174] [175] [176] [177]

Latest developments in the treatment of RCC are the anti-PD-1 antibodies (pembrolizumab, nivolumab) therapies [178] [179] which target regulatory T-cells, or various cell-based immunotherapeutic strategies, where autologous or allogeneic tumor cells are applied as therapeutic vaccines either directly or for priming of Dendritic cells, T-, or NK cells. [180] [181] The approach established in Prof. Wittig's group, to apply an allogeneic, fourfold gene-modified RCC tumor cell line in combination with a potent immunomodulator as therapeutic vaccine, successfully passed a clinical phase II trial. [182] [183]

1.5.3 Molecular Characteristics of RCC

Recent detailed molecular characterization of RCCs revealed a high heterogeneity of the tumors and lead to an ongoing revision and further elaboration of histological classification of RCC subtypes.

Most (60-80%) ccRCC are characterized by a defective von Hippel-Lindau (VHL) tumor suppressor gene, which is located on chromosome 3p25. A consequence of inactivation or loss of the E3 ubiquitin protein ligase, which under normoxic conditions targets oxygen-dependent posttranslational modified HIFα transcription factors for degradation, is a deregulation of HIF axis. Stabilization of HIF proteins results in expression of a variety of cell type specific HIF target genes, including VEGF, PDGF, TGF-α and EGFR, c-Myc, Oct4, Sox2 and p53. Also a number of histone demethylases as well as erythropoietin are up-regulated in some kidney cells, to promote tumor growth, angiogenesis and therapy resistance. Though the picture is still incomplete, an important role of HIF1α in tumorigenesis of RCC can be assumed. [184]

Besides VHL, also chromatin modifying components such as the chromatin-remodeling complex components PBRM1 and ARID1A, the histone methyltransferases SETD2 and JARID1C (also known as KDM5C) and the histone de-ubiquitinating enzyme BAP1 have been found to be mutated in ccRCC cancer cells of patients. TP53 and ATM, both involved in DNA-damage response, were found to be mutated in 40% and 10% of cases, respectively, in some tumor regions.

Also components of the PI3K/mTOR pathway (PTEN, MTOR, PIK3CA, TSC2), which has a key function in controlling cellular metabolism, cell growth, proliferation, and apoptosis, were identified as mutated in up to 20% of patients, with 60 % of patients harboring at least one mutation in this pathway. The mTOR pathway is also connected to the HIF pathway, since mRNA expression of HIF1α is governed by mTORC1, and the translation of HIF2α mRNA is regulated by mTORC2. Also the PI3K/AKT pathway has been found to be activated by different genomic mechanisms in all three different histological types of RCC (clear cell, papillary, and chromophobe). Activation of c-MET proto-oncogene, coding for hepatocyte growth factor (HGF) receptor, localized on chromosome 7q31-3, is frequently associated with papillary RCC. Chromophobe RCC has been associated with the BHD/Folliculin gene, which maps to the 17p11.2 locus in hereditary forms of the tumor. It is involved in AMPK and mTOR signaling. Also p53 mutation and up-regulated expression of the c-kit oncogene has been reported in this histological subtype. [86 184 185 186 187 188 189 190 191 192]

1.5.4 RCC Cell Lines

For *in vitro* investigation of RCC, many established cell lines for various histological subtypes are available, which differ in their mutational status as well as in their origin from primary or metastatic sites. A list of the most frequently used cell lines is shown in table 1.5.1.

Cell Line Name	Histo Subtype	Prim/Met	VHL status	Tumorigen in Mice
769-P	ccRCC	Prim	VHL *m* -/+#	T
786-O	ccRCC	Prim	VHL *m* t -/+#	T
A-498	ccRCC	Prim	VHL *m/wt#* t -	T
A-704	ccRCC	Prim	VHL *m* -	NT
ACHN	cc/papRCC#	Met	VHL *wt* +	T
Caki-1	ccRCC	Met	VHL *wt* +	T
Caki-2	cc/papRCC#	Prim	VHL *wt/m#* -	T
KRC/Y	ccRCC	Prim	VHL *wt* +	T
RCC various	various	various	various	T/ND
SKRC various	various	various	various	T/NT
SN12-C	ccRCC	Prim	VHL *wt* +	T
TK 10/164	cc/papRCC	Prim	various	NT
UM-RC various	ccRCC	Prim	various	T/NT
UOK various	various	Prim	various	T/NT

Table 1.5.1: Overview of Frequently Used RCC Cell Lines

Several frequently used RCC cell lines are listed. In column 1 the names are indicated. Some of the cell lines names are used for cell line collections of different institutions (names are extended by numbers). This is indicated by the term "various". The histological subtype is indicated in column 2 (cc: clear cell, pap: papillary RCC). For some of the cell line this feature is described inconsistently in the literature (#). In column 3 is indicated whether the cell line was derived from primary (Prim) or metastatic (Met) tumor. The VHL status of the cell lines are depicted in column 4 with the following abbreviations used: wt- wild-type gene, m- mutated, t- mRNA (transcript) detected, + protein expression, - no protein expression, # inconsistent data). In column 5 the tumorigenicity in mice is indicated; T: tumorigenic, NT: non-tumorigenic. The information contained in this table are adapted from Brodaczewska et al [193]

1.6 Cancer Stem Cells (CSC) in Renal Cell Carcinoma (RCC)

In 2008 Bussolati et al [78] identified a subpopulation of cells expressing the mesenchymal stem cell marker CD105 as possible CSC in RCC. They isolated $CD105^+$ cells (5-11% of tumor cells) from primary tumors, clonally amplified the cells in adherent monolayer culture, and tested their tumor-inducing ability in SCID mice. The cells were able to induce tumors in five of six mice already with low amounts of 10^2 injected $CD105^+$ cells, whereas after injection of 10^6 $CD105^-$ cells, tumor formation was observed in one of ten mice, only. The fraction of 9-13% of $CD105^+$ cells in the formed tumors was comparable to that seen in the primary tumors they were derived of. These cells were also capable to serially induce tumors in SCID mice, which can be seen as a proof for their self-renewing ability. The isolated cells showed a mesenchymal phenotype, indicated by their expression of further mesenchymal markers CD29, CD44, CD73, CD90, CD146 and vimentin (VIM), but lacking expression of epithelial marker Pan-CK and endothelial markers CD31 and vWF. Also differentiation into endothelial and epithelial linages, but not into osteogenic or adipogenic lineages, which are typical for mesenchymal stem cells, was observed. Expression of stem cell markers Nestin, Nanog, Oct4 (POU5F1) und Musashi, as well as of the renal stem cell marker Pax2 were also reported for the

$CD105^+$ selected cells. In serum free medium, approximately 40% of the cells were able to grow as spheroids over ten passages with a doubling time of 30 h.

Following this first report on possible CSC in RCC, further studies using CD105 as CSC marker were published, showing release of angiogenic microvesicles from the cells. [194] Therapeutic strategies, such as differentiation therapy using IL-15 [119 195 196] or c-Met inhibition to block bone metastases of RCC were tested. [197]

CD105 was subsequently also used as marker for sorting of CSC from the RCC cell lines Caki-2 [198 199], ACHN [199 200], A498 and SKRC-39 [201]. $CD105^+$-sorted SKRC-39 and A498 cells have been used for dendritic cell (DC)-based immunotherapy in a mouse model and were found to generate a cytotoxic T lymphocytes (CTL) as well as TH1-shifted humoral immune responses against $CD105^+$ cells more effectively. Compared to unsorted cells, the $CD105^+$-sorted fraction lead to further reduction of tumor growth. [201]

Recently another CSC sub-population was identified in tumor tissue from RCC patients by Galleggiante et al [202], which was marked by co-expression of $CD133^+$ and $CD24^+$. Similar to normal renal progenitor cells isolated in parallel, the cells were able to differentiate towards adipogenic, osteogenic, and epithelial lineages. But in contrast to normal renal progenitors, these cells were able to form colonies in soft agar assays and were marked by expression of the copper transporter CTR2 (SLC31A2). This marker was not expressed in normal progenitor cells, and seemed to be involved in cisplatin resistance of the tumor-derived cells. The cells were found to be positive for CD73 expression, but lacked expression of CD105 and CD90 mesenchymal markers. Sorting for $CD133^+/CD24^+$ cells from ACHN and Caki-1 cell lines was also shown to enrich for cells with CSC characteristics. [203]

In RCC cell lines putative CSC have also been identified based on chemokine receptor CXCR4 expression [204], aldehyde dehydrogenase activity [205 206 207], or side population enrichment using Hoechst 33342 dye [208] or Rhodamine 123. [209 210] ALDH sorted TIC from Caki-2 and ACHN cell lines were used to test a promising new differentiation therapy in mouse models using BMP-2. [207]

Besides marker expression and other functional assays, also their spheroid-forming ability was used to enrich for CSC from RCC cell lines SKRC-42 [211], ACHN [212], 786-O [213 210], Caki-1[212 213], RCC-26/-53 [204] but also from human embryonic cell line HEK293 [214]. Recently, spheroid growth was also used to isolate CSC in cell lines from primary RCC tissues by Song et al [210]. Spheroid-derived cells showed higher tumorigenicity and expression of CD73, compared to adherently grown cells. [110 201 215]

1.7 Objective of this Work

Rare tumor cells with stem cell characteristics, termed cancer stem cells (CSC) or tumor-initiating cells (TIC) have been found to play a major role in tumor formation and metastasis. The aim of my work was to enrich and further characterize such cells from a parental clear cell renal cell carcinoma (ccRCC) cell line, termed PA, by using the spheroid culture method.

Two slightly different methods for spheroid generation, resulting in two morphologically different spheroid subtypes, termed SP and CS, were to be evaluated with respect to their stem cell and cancer stem cell (CSC) properties.

Growth characteristics, such as long-term proliferative potential, growth in „soft agar assay“ (SAA) and spheroid-forming efficacy in the „Neurosphere Assay“ (NSA) over long-term passaging should be evaluated to assess and confirm stem cell features *in vitro*.

The hallmark of stem cells, namely their ability to generate differentiated progeny, should be evaluated by using *in vitro* differentiation assays for adipogenic and osteogenic lineages. Additionally, the expression of known stem cell markers was to be examined.

To finally probe for the naming and essential CSC characteristic, the tumorigenicity of cells from the parental cell line (PA) and from the two spheroid-derived cell lines (SP and CS) should be assayed *in vivo* for tumor generation in immunodeficient (NSG) mice.

Another important goal was the identification of possible markers for enrichment and quantification of CSC in the parental RCC cell line. For this purpose, surface expression of different known CSC markers should be determined through immunophenotyping by flow cytometry (IFC); in addition functional assays were to be evaluated for suitability.

Since the cellular reprogramming process known as epithelial-to-mesenchymal transition (EMT) appears to be involved in the generation of CSC, the expression of EMT markers in the cells lines obtained (SP, CS) should be determined. Also the role of EMT in gaining of stem cell characteristics in long-term cultures under spheroid conditions was to be tested.

Most importantly, the stability as well as the plasticity of spheroid-derived CSC cell lines compared to adherently grown cells should be investigated. For this purpose, spheroids were to be re-cultured long-term under conditions of adherent growth and assayed for retention of characteristics.

Besides such functional assays and analyses of known markers, a comprehensive characterization of spheroid-derived and adherently grown cells should be established by whole transcriptome shotgun sequencing of their respective mRNA populations (RNA-Seq).

2 Material

2.1 Equipment and Consumables

Consumable materials and technical equipment used for experiments are listed in the following tables. All devices were used and maintained according to instructions given in the manuals.

Equipment	Manufacturer/Supplier
Agilent 2200 TapeStation System	Agilent
Agilent-2100-Bioanalyzer	Agilent
Beaker, Schott DURAN®	Carl Roth
Bio-Rad Gel Doc 2000 Imaging System	BioRad
Biofuge Fresco	Heraeus Instruments
Biofuge Pico	Heraeus Instruments
Cary 1E UV-Visible Spektrophotometer	Varian
CASY® Cell Counter + Analyser System Model TT	Innovatis
cBot Clonal Amplification System	Illumina
Coulter Counter(R) Z1™	Beckman Coulter
Cryo 1°C freezing container Nalgene® "Mr. Frosty"	Thermo Fisher Scientific
Digital camera for microscope DCM 130E	Müller Germany
Digital camera Sony Cyber-shot	Sony
Digital pH meter	Knick
EasyPhor horizontal gel electrophoresis system	Biozym
Flow cytometer FACSCalibur™	BD Biosciences
Forma™ Steri-Cult™ CO_2 incubator	Forma Scientific
Forma™ Steri-Cult™ incubator	Thermo Fisher Scientific
Freezer (−20 °C storage)	Liebherr
Fridge (4 °C storage)	Liebherr
Glas bottles, Schott DURAN®	Carl Roth
HiSeq® 2500 System	Illumina
Inverted phase-contrast microscope Labovert	Leitz
Laminar flow cleanbench	Heraeus Instruments
Liquid nitrogen tank (−196 °C storage)	Taylor Wharton
Megafuge 1.0R	Heraeus Instruments
MilliQ Plus Ultra Pure Water System	Merck Millipore
Mithras Multimode Reader LB940	Berthold Technologies
NextSeq® 500 System	Illumina
Nikon D40	Nikon
Nikon Micro-Nikkor 55 mm F/2.8 AI-S Objektiv	Nikon
Pipettboy Accu Jet	Brand
Pipettes (2.5; 10; 20; 200; 1000)	Eppendorf
Power-Supply PowerPac 200	Bio-Rad Laboratories GmbH
Precision balance	Satorius
Qubit 2.0 Fluorometer	Thermo Fisher Scientific
Shaker Vortex Genie™	Bender & Hobein
Thermocycler Mastercycler® Gradient	Eppendorf
Thermocycler T1	Biometra
TrayCell ultra-microlitre cuvette	AnalytikJena
Ultra low freezer (−80 °C storage)	Thermo Fisher Scientific
Vaccuum pump	Vacuubrand
VARIOKLAV® laboratory autoclave	HP-Medizintechnik
Vertical laminar flow hood, clean bench	BDK Luft- und Reinraumtechnik
Water bath	Köttermann

Table 2.1.1: List of Equipment

Material	Sizes	Manufacturer/Supplier
Cell scrapers, sterile	various	Corning
Conical centrifuge tubes, sterile	15; 50 mL	Corning, Nunc
Cryo tubes	1.8 mL	Nunc
PCR soft tubes	0.2 mL	Biozym
PCR tube strips with lids	8 strip, 0.2 mL	Sarsted
Pipette tips, standard	0,1-20;1-200;100-1000	Nerbe
Pipette tips, standard, sterile	0,1-20;1-200;100-1000	Corning
Pipette tips, with filter, sterile	0,1-20;1-200;100-1000	Nerbe
Safe lock reaction tubes	0.5 mL, 1.5 mL, 2.0 mL	Eppendorf
Serological pipettes stipettes, sterile	1; 2; 5 ;10 ; 25 mL	Corning
Aspiration pipettes, sterile	2 mL	Corning
Syringe filter, sterile	0.2; 0.45 µm pore size	Corning
Syringes, sterile	1; 10 ;30 ; 50 mL	Various
Syring needles, sterile	20 gauge	Various
Tissue culture flasks, tissue culture treated	25 cm², 75 cm², 150 cm²	Corning, SPL Life Science
Tissue culture flasks; non tissue culture treated	25 cm², 75 cm², 150 cm²	Corning
Tissue culture plates; non tissue culture treated	6; 12; 24; 96 wells	Corning
Tissue culture plates; tissue culture treated	6; 12; 24; 96 wells	Corning, SPL Life Science
Sample tubes without caps	1.4; 5 mL	VWR
BD Falcon™ Round-bottom tubes, polystyrene	12 × 75 mm	Thermo Fisher Scientific
BD Falcon™ round bottom 96 well plates	96 wells	Thermo Fisher Scientific
Bottles, sterile	125; 250 mL	Corning
Gloves, microtouch, nitrile, powder-free	S	Ansell

Table 2.1.2: List of Consumables

2.1.1 Chemicals and Kits

Reagents and kits used for experiments are listed in the following tables. All reagents were stored and handled according to the manufacturer's recommendations.

Kit	Provider
ALDEFLUOR™ Kit	STEMCELL Technologies
Biozym Taq DNA Polymerase Kit	Biozym
DNA 500 LabChip kit	Agilent
EpiScript™ Reverse Transcriptase Kit	Biozym
Foxp3 / Transcription Factor Staining Buffer Kit	eBioscience
High Sensitivity RNA ScreenTape® Kit	Agilent
HiSeq Rapid Cluster Kit v2	Illumina
HiSeq Rapid SBS Kit v2	Illumina
HiSeq® 2500 System	Illumina
HiSeq® Sequencing Kit (200 Cycles)	Illumina
HiSeq® Single-Read Cluster Generation Kit	Illumina
mirVana™ miRNA Isolation Kit, with phenol	Thermo Fisher Scientific
NEBNext® Multiplex Oligos for Illumina® (Dual Index Primers Set 1)	NEB
NEBNext® Ultra™ RNA Library Prep Kit for Illumina® NEB (#E7530+#E7490)	NEB
NextSeq® 500 System	Illumina
NextSeq® 500/550 High Output Kit v2 (75 cycles)	Illumina
NextSeq® 500/550 Mid Output Kit v2	Illumina
NucleoSpin® RNA II	Macherey-Nagel
Qubit™ dsDNA High Sensitivity Assay Kit	Thermo Fisher Scientific
Qubit™ RNA High Sensitivity Assay Kit	Thermo Fisher Scientific
RNA-6000-Nano-LabChip-Kit	Agilent
SuperScript™ II Reverse Transcriptase Kit	Thermo Fisher Scientific
TURBO DNA-*free*™ Kit	Thermo Fisher Scientific
Venor®GeM OneStep, Mycoplasma Detection Kit for conventional PCR	Minerva Biolabs

Table 2.1.3: List of Kits

Name of Substance or Solution	Provider
(±)-Verapamil hydrochloride, ≥99% (titration), powder	Sigma
0.5-10 kb RNA ladder, 1 µg/µl	Invitrogen
100 bp DNA Ladder Invitrogen™	Thermo Fisher Scientific
2-Propanol, ROTIPURAN® ≥99.8 %, p.a., ACS, ISO	Carl Roth
3-Isobutyl-1-methylxanthine (IBMX), BioUltra, ≥99%	Sigma
Accumax™ - cell aggregate dissociation medium	PAA/eBioscience/Thermo Fisher Scientific
Agarose NEEO-Ultra	Carl Roth
AGENCOURT® AMPURE® XP Beads	Beckman Coulter
Albumin Fraction V, ≥98 %, powdered, for molecular biology	Carl Roth
Albumin Fraction V, very low endotoxin, CELLPURE® >98 %, very low endotoxin	Carl Roth
Alizarin red S, Alizarin sulphonic acid sodium salt, Alizarin carmine	Carl Roth
Ammonium hydroxide solution: Ammonia solution ROTIPURAN® 30 %, p.a., ACS	Carl Roth
Boric acid, ≥99.8 %, p.a., ACS, ISO	Carl Roth
Bromophenol blue sodium salt	Carl Roth
Calcium chloride, ≥98 %, dehydrated, powder	Carl Roth
CASYton	OLS Omni Life Science
Corning® Matrigel® basement membrane matrix, *LDEV-Free,	Corning
Crystal violet p.a., ACS	Carl Roth
D-(+)-Glucose solution, 45% in H_2O, sterile-filtered, BioXtra, suitable for cell culture	Sigma
Dexamethasone, powder, BioReagent, suitable for cell culture, ≥97%	Sigma
Dimethyl sulfoxide (DMSO), Hybri-Max™, sterile-filtered, BioReagent, suitable for hybridoma, ≥99.7%	Sigma
DMEM/F-12, HEPES, powder	Invitrogen
DMEM:F12, 1:1 mixture with 3.151 g/L glucose HEPES and L-glutamine	Lonza/Biozym (BE12-719F/12)
dNTP Mix 10 mM each	Biozym
DreamTaq DNA polymerase (5 U/µL)	Thermo Fisher Scientific
Dulbecco's phosphate-buffered saline (DPBS) 1X w/o Ca++, Mg++ 500 ml	Lonza/Biozym (17-512F)
Dulbecco´s modified Eagle´s medium (DMEM-LG), with 1.0 g/L glucose without L-glutamine	Lonza/Biozym (BE12-707F/12)
Dulbecco´s modified Eagle´s medium (DMEM) with 4.5 g/L glucose with L-glutamine	Lonza/Biozym (BE12-604F)
eBioscience™ 7-AAD viability staining solution	Thermo Fisher Scientific
Ethanol ROTIPURAN® ≥99.8 %, p.a.	Carl Roth
Ethidium bromide solution, BioReagent, for molecular biology, 10 mg/mL in H_2O	Sigma
Ethylenediamine tetraacetic acid disodium salt dihydrate, ≥99 %, p.a., ACS, $Na_2EDTA \times 2\ H_2O$	Carl Roth
FACS cleaning solution BD FACSClean™	BD Biosciences
FACS cleaning solution BD FACSRinse™	BD Biosciences
FACS sheath fluid, BD FACSFlow™	BD Biosciences
Fast Red Violet LB Salt	Sigma
Fast Ruler UltraLow DNA Ladder	MBI Fermentas
Fetal bovine serum (FBS)	Biochrom
Ficoll 400	Sigma
Formamide ≥99.5% (GC), BioReagent, for molecular biology	Sigma
GeneRuler™ 100 bp Plus DNA ladder	Thermo Fisher Scientific
GlutaMAX™ Supplement (200 mM)	Thermo Fisher Scientific
Glycerol, ≥98 %, Ph.Eur., anhydrous	Carl Roth
Ham's F12 medium with L-glutamine (BE12-615F)	Lonza/Biozym
Hemalun solution acid acc. to Mayer	Carl Roth
HEPES buffer (1M) in normal saline (BE17-737E)	Lonza/Biozym
Horse serum, Donor Herd, USA origin, Heat inactivated, sterile-filtered, suitable for cell culture	Sigma
Human Serum, from human male AB plasma	Sigma
Indomethacin, ≥99%	Sigma
Insulin-Transferrin-Selenium-G (ITS) Supplement (100X)	Thermo Fisher Scientific
KaryoMAX® Colcemid™ solution in PBS	Thermo Fisher Scientific
Kohrsolin® FF, Surface disinfectant	Carl Roth
L-15 (Leibovitz) w/o L-Glutamine, 500ml (BE12-700F)	Lonza/Biozym
L-Ascorbic acid, BioXtra, ≥99.0%, crystalline	Sigma
L-glutamine (200 mM) (BE17-605E)	Lonza/Biozym
LE-Agarose	Biozym

Table 2.1.4: List of Chemicals and Reagents (A-L)

Name of Substance or Solution	Provider
Magnesium chloride hexahydrate, CELLPURE® ≥99 %	Carl Roth
MEM essential vitamin mixture (100x) (13-607C)	Lonza/Biozym
N,N-Dimethylformamide (DMF), ROTIPURAN® ≥99.8 %, p.a., ACS, ISO	Carl Roth
Naphthol AS-MX phosphate, powder, ≥99% (HPLC)	Sigma
Oil Red O	Sigma
Orange DNA loading dye (6X)	Thermo Fisher Scientific
Penicillin-streptomycin mixtur, 10,000 U/ml each (DE17-602E/12)	Lonza/Biozym
poly $d(T)_{12-18}$ primer	Carl Roth
Random primer	Thermo Fisher Scientific
Recombinant human EGF	Peprotech
Recombinant human FGF-basic	Peprotech
Resazurin sodium salt , powder, BioReagent, suitable for cell culture	Sigma
Rhodamine 123, BioReagent, for fluorescence, ≥85% (HPLC)	Sigma
Riboflavin Cell Culture Tested	Sigma
RNase AWAY®	Carl Roth
RNase out	Life Technologies
RNAseA 10 mg/ml	Thermo Fisher Scientific
Roti®-CELL Leibovitz`s L15	Carl Roth
Rotihistofix 10%	Carl Roth
RPMI 1640 medium with UltraGlutamine (BE12-702F)	Lonza/Biozym
Sodium azide (NaN_3), ReagentPlus®, ≥99.5%,	Sigma
Sodium bicarbonate solution 7.5% (BE17-613E)	Lonza/Biozym
Sodium pyruvate solution Cell Culture Tested	Sigma
StemPro® Accutase® cell dissociation reagent	Thermo Fisher Scientific
Sterile Water Ampuwa®	Fresenius Kabi
TRIS hydrochloride PUFFERAN® ≥99 %, p.a.	Carl Roth
TRIS PUFFERAN® ≥99.9 %, p.a.	Carl Roth
Trypsin/EDTA Solution 100 ml (CC-5012)	Lonza/Biozym
UltraPure™ Agarose-1000	Invitrogen
β-Glycerophosphate disodium salt hydrate, BioUltra ≥99.0% (titration)	Sigma

Table 2.1.5: List of Chemicals and Reagents (M-Z)

2.1.2 Buffer and Solutions

In tables 2.6-2.8 the components of buffers and solutions made in-house are listed. Prepared buffers and solutions are listed in tables 2.4 and 2.5.

Name	Composition	Concentration	Comment
Solutions for Flow Cytometric Immunophenotyping			
Sodium azide	Sodium azide (NaN3)	0.1% (w/v)	toxic, filter sterilize, store RT
	MilliQ		
TSE buffer	TRIS-HCl pH 7.5	40 mM	filter sterilize, store RT
	EDTA	1 mM	
	Sodium chloride (NaCl)	150 mM	
F-PBS	DPBS w/o Ca++, Mg++	1x	store 4°C
	FBS	2% (v/v)	
	Sodium azid	0.001% (w/v)	
Block buffer (flow cytometry)	FACS-PBS	1x	store 4°C
	Human serum A/B	10% (v/v)	
DPBS with 1% BSA for FoxP3-Kit	PBS	1x	prepare fresh
	BSA	1%	
1X Fix/Perm Solution Foxp3-Kit	Foxp3-Kit Fixation and Permeabilization Buffer B	3 parts	prepare fresh
	Foxp3-Kit Fixation and Permeabilization Buffer A	1 part	
1X Wash Buffer Foxp3-Kit	Foxp3-Kit Wash Buffer	9 parts	prepare fresh
	PBS with 1% BSA	1 part	

Table 2.1.6: List of Solutions (IFC)

Name	Composition	Concentration	Comment
Solutions for Histological Staining			
DPBS with Ca/Mg	DPBS w/o Ca++, Mg++	1x	store RT
	Calcium chloride ($CaCl_2$) (anhyd.)	0.9 mM	
	Magnesium chloride hexahydrate ($MgCl_2x6H_2O$)	0.49 mM	
Oil Red O stock solution	Oil Red O	0.3 g	store RT
	2-Propanol	100 mL	
Oil Red O working solution	Oil Red O stock solution	3 parts	prepare fresh, let sit for 10 min
	MilliQ	2 parts	filter before use
60% Isopropanol	2-Propanol	60 mL	store RT
	MilliQ	40 mL	
Alizarin red S solution (22.5 mg/mL, pH 4.15)	Alizarin red S	0.9 g	adjust pH to 4,15 with NH_3OH
	MilliQ	40 mL	store RT, filter before use
Naphthol-AS-MX-Phosphate solution	Naphthol-AS-MX-Phosphate	20 mg	prepare fresh, according to volume needed
	DMF	1 mL	
AP-staining solution	Fast Red Violet LB Salt	0.6 mg/mL	prepare fresh, according to volume needed
	50 mM Tris-HCl, pH 8.7	1 part	
	MilliQ	1 part	
	Naphthol-AS-MX-Phosphate solution (20 mg/mL)	6 µL/mL	
PBST for AP-staining	DPBS with Ca/Mg	200 mL	store RT
	Tween 20	100 µL	
Tris-HCl for AP-staining	Tris base/HCl	50 mM	pH 8,7
Storage buffer for AP-staining	Glycerol	4 mL	store RT
	DPBS	21 mL	
Formaldehyde solution 4%	Rotihistofix 10%	20 mL	store RT
	MilliQ	30 mL	
Crystal violet solution 1%	Crystal violet	0.1 g	store RT
	sterile Water Ampuwa®	10 mL	filter sterilize
Solutions for Molecular Biology			
RNA sample buffer TBE 10x	Ficoll 400	7.5% (w/v)	dissolve by warming
	TBE buffer	5x	store RT
	Bromphenol blue	0.025% (w/v)	
Bromphenol blue solution	Bromphenol blue	2.5% w/v	
TBE buffer 5x	Tris base	54 g	store RT
	Boric acid	27.5 g	
	Na_2EDTA x 2 H_2O	3.72 g	
	MilliQ	1 L	
Ethidium bromide working solution (0,5 mg/mL)	Ethidium bromide solution (10 mg/mL)	50 µL	
	MilliQ	950 µL	
Tris-HCl buffers	Tris base	50 mM - 1 M	pH 7-8,5
	HCl	variing	variing
TE buffer 10x	1 M Tris HCl buffer pH 7.5	100 mM	store RT
	0.5 M NaEDTA, pH 8	10 mM	prepare desired streght by dilution
0.5 M NaEDTA, pH 8	Na_2EDTA x 2 H_2O	7.44 g	dissolve by stirring
	MilliQ	40 mL	pH 8 with NaOH
1.25% 0,5xTBE agarose gel for RNA	Agarose NEEO-Ultra	2.5 g	
	DEPC-H_2O	180 mL	dissolve
	5xTBE-Puffer	20 mL	boil, chill to 60°C
	Ethidium bromide working solution	0.25 µg/mL	add to final concentration when preparing the gel
1.5% 0,5xTBE agarose gel for DNA	Biozym LE-Agarose	6 g	
	MilliQ	360 mL	dissolve
	5xTBE-Puffer	40 mL	boil, chill to 60°C
	Ethidium bromide working solution	0.125 µg/mL	add to final concentration when preparing the gel
DEPC-H_2O	MilliQ	2 L	stirr, autoclave 121°C 20 min
	DEPC	800 µl	

Table 2.1.7: List of Solutions Continued (Histological Staining and Molecular Biology)

Name	Composition	Concentration	Comment
Solutions for Aldefluor Assay			
Aldefluor working solution (300 µM)	Dry ALDEFLUOR™ Reagent	50 µg	
	Dimethylsulphoxide (DMSO)	25 µL	dissolve, mix, let standt 1 min
	Hydrochloric Acid (HCl), 2N	25 µL	mix, incubate RT 15 min
	ALDEFLUOR™ Assay Buffer	360 µL	mix, aliquot, sotre -20°C
AF buffer	ALDEFLUOR™ Assay Buffer	V needed	prepare fresh, according to volume needed
	Aldeflour working solution	5 µL/mL	
DEAB-control buffer	AF buffer	V needed	prepare fresh, according to volume needed
	ALDEFLUOR™ (DEAB) Reagent 1.5 mM	5 µL/mL	
Solutions for Side Population Assay			
F-PBS without Azid	DPBS w/o Ca++, Mg++	1x	store 4°C
	FBS	2% (v/v)	
Rhodamine 123 stock solution	Rhodamine 123	2 mg	store dark 4°C
	Ethanol pA	1 mL	
Verapamil stock solution	Verapamil	12.5 mg	store 4°C
	Ethanol pA	500 µL	
	sterile Water Ampuwa®	500 µL	
Rho staining solution	AC-Medium (SC-Medium)	V needed	prepare fresh, according to volume needed
	Rhodamin 123 stock solution	10 µL/mL	
PBS-Ver	F-PBS without Azid	V needed	prepare fresh, according to volume needed
	Verapamil stock solution	2 µL/mL	
Medium-Ver	AC-Medium (SC-Medium)	V needed	prepare fresh, according to volume needed
	Verapamil stock solution	2 µL/mL	
Solutions for Growth Assay			
Resazurin stock solution	Resazurin	1 mM	filter sterilize, store RT, dark
	DPBS	1x	
Resazurin working solution	Resazurin stock solution (1 mM)	1 part	prepare fresh, according to volume needed
	Medium (same as for assay)	1 part	

Table 2.1.8: List of Solutions Continued (ALDEFLUOR™, Side Population, and Growth Assay)

Water used for preparation of solutions and buffers was ultrapure water (MilliQ). Buffers were prepared by dissolving the components for the desired concentration, adjusting pH when necessary, and finally adjusting the desired volume.

2.1.3 Cell Culture Media and Solutions

The composition of media for cell culture is listed in the following table. For all solutions to be used in cell culture, sterile water (Ampuwa®) was used. All sera were heat-inactivated for 20 min at 56°C, aliquoted and stored at -20°C. In tests for medium composition, the component to be tested was omitted, and was added separately in the respective concentrations to be tested.

Medium	Components	Volume or Mass	Concentration	Comment
Media and Solutions for Adherent and Spheroid Cell Culture of RCC Cells				
AC-Medium	L-15 (Leibovitz) w/o L-Glutamine	500 mL		store 4°C
	FBS	50 mL	10% (v/v)	
	Sodium bicarbonate solution 7.5%	7.5 mL	1.5% (v/v)	
	MEM essential vitamin mixture (100x)	5 mL	1x	
	Penicillin/streptomycin mixture, 10.000 U/mL each	5 mL	100 U/ml	
	L-glutamine (200 mM)	2.5 mL	1 mM	
	D-(+)-Glucose solution, 45% in H_2O	1.2 mL	1 g/L	
DMEM:F12-Medium	DMEM:F12, 1:1 mixture	500 mL		store 4°C
	BSA solution (20%)	6.3 mL	0.25% (w/v)	
	Penicillin/streptomycin mixture, 10.000 U/mL each	5 mL	100 U/ml	
	Sodium bicarbonate solution 7.5%	5 mL	1% (v/v)	
	ITS Supplement (100X)	2.5 mL	0.5 x	
	HEPES buffer (1M)	2 mL	4 mM	
SC-Medium	DMEM:F12-Medium or DMEM:F12-Medium-Mix	V needed		prepare fresh by adding growht factors according to volume needed
	bFGF solution (10 µg/mL)	1 µL/mL	10 ng/mL	
	EGF solution (20 µg/mL)	1 µL/mL	20 ng/mL	
DPBS w/o Ca++, Mg++	Potassium chloride (KCl)	2.67 mM		purchased as 1x solution
	Potassium phosphate monobasic (KH_2PO_4)	1.47 mM		
	Sodium Chloride (NaCl)	137.93 mM		
	Sodium Phosphate dibasic heptahydrate ($Na_2HPO_4x7H_2O$)	8.06 mM		
Trypsin/EDTA solution	Trypsin/EDTA Solution 10x	1x		aliquot, store -20°C
	DPBS	45 mL		add after thawing
BSA solution for cell culture	Albumin Fraction V, very low endotoxin	10 g	20% (w/v)	dissolve by warming
	DMEM:F12	50 mL		aliquot, store -20°C
DMEM/F12 (1:1) with BSA	DMEM:F12	20 mL		store 4°C
	BSA solution 20%	252 µL	0.25% (w/v)	
bFGF solution (10 µg/mL)	Recombinant human FGF-basic (50 µg)		10 µg/mL	aliquot, store -20°C
	5 mM Tris buffer, pH 7, filter sterilized	100 µl		
	DMEM/F12 (1:1) with BSA	4.9 mL		
EGF solution (20 µg/mL)	Recombinant human EGF (100 µg)		20 µg/mL	aliquot, store -20°C
	sterile Water Ampuwa®	200 µl		
	DMEM/F12 (1:1) with BSA	4.8 mL		
Freeze-Media				
AC-Freeze-Medium	AC-Medium	4 mL		
	FBS	500 µL	10% (v/v)	
	DMSO	500 µL	10% (v/v)	
SC-Freeze-Medium	SC-Medium	4 mL		
	BSA solution (20%)	500 µL	10% (v/v)	
	DMSO	500 µL	10% (v/v)	

Table 2.1.9: List of Cell Culture Media (Adherent and Spheroid Cell Culture, Freeze-Media)

Medium	Components	Volume or Mass	Concentration	Comment
Solutions and Media for Soft Agar Assay				
Soft agar assay-Medium 2x	DMEM/F-12 (1:1), HEPES, powder (1L)	1 Package (1 L)	2x	dissolve, filter sterilize
	sterile Water Ampuwa®	475 mL		
	Penicillin/streptomycin mixture, 10,000 U/mL each	10 mL	2x	store 4°C
	Sodium bicarbonate solution 7.5%	15 mL	2x	
Agarose for soft agar assay	UltraPure™ Agarose-1000	2 g	1.7% (w/v)	dissolve, autoclave, store RT
	sterile water Ampuwa®	120 mL		boil before use, chill to 42°C
Soft agar bottom layer-Serum (one 6-well plate)	Soft Agar-Medium 2x	5 mL	1x	pre-warm to 42°C
	FBS	1 mL	9 % (v/v)	
	Agarose for soft agar assay	4 mL	0.6% (w/v)	1.5 mL/well
Soft agar bottom layer-SC (one 6-well plate)	Soft Agar-Medium 2x	5 mL	1x	pre-warm to 42°C
	BSA solution (20%)	150 µL	0.25% (w/v)	
	ITS Supplement (100X)	100 µL	0.5 x	
	bFGF solution (10 µg/mL)	11 µL	10 ng/mL	
	EGF solution (20 µg/mL)	11 µL	20 ng/mL	
	Agarose for soft agar assay	4 mL	0.6% (w/v)	1.5 mL/well
Soft agar cell layer-Serum for triplicate	Soft Agar-Medium 2x	2.5 mL	1x	pre-warm to 42°C
	FBS	0.5 mL	10% (v/v)	
	Cell suspension of desired concentration	300 µL		1.5 mL/well
	Agarose for soft agar assay	2.5 mL		
Soft agar cell layer-SC for triplicate	Soft Agar-Medium 2x	2.5 mL	1x	pre-warm to 42°C
	BSA solution (20%)	75 µL	0.25% (w/v)	
	ITS Supplement (100X)	50 µL	0.5 x	
	bFGF solution (10 µg/mL)	5.5 µL	10 ng/mL	
	EGF solution (20 µg/mL)	5.5 µL	20 ng/mL	
	Cell suspension of desired concentration	300 µL		1.5 mL/well
	Agarose for soft agar assay	2.5 mL	0.78% (w/v)	
DMEM:F12-Medium for soft agar	DMEM:F12, 1:1 mixture	100 mL		store 4°C
	Penicillin/streptomycin mixture, 10.000 U/mL each	1 mL	100 U/ml	
	Sodium bicarbonate solution 7.5%	1 mL	1% (v/v)	
	HEPES buffer (1M)	400 µL	4 mM	
Soft agar assay maintenance medium-Serum	DMEM:F12-Medium for soft agar	50 mL		store 4°C
	FBS	5 mL	10% (v/v)	
Soft agar assay maintenance medium-SC	DMEM:F12-Medium for soft agar	50 mL		store 4°C
	BSA solution (20%)	630 µL	0.25% (w/v)	
	ITS Supplement (100X)	250 µL	0.5 x	
	bFGF solution (10 µg/mL)	1 µL/mL	10 ng/mL	add just prior to use according to volume needed
	EGF solution (20 µg/mL)	1 µL/mL	20 ng/mL	
Staining solution for soft agar assay	Crystal violet solution 1%	500 µL	0.01%	
	DPBS	50 mL		

Table 2.1.10: List of Solutions and Media for Soft Agar Assay

Medium	Components	Volume or Mass	Concentration	Comment
Solutions and Media for *in vitro* Differentiation				
Dexamethasone stock solution	Dexamethasone	4 mg	10 mM	store 4°C
	DMSO	1 mL		thaw before use
Dexamethasone working solution	Dexamethasone stock solution 10 mM	10 µL	0.1 mM	prepare fresh
	DMEM-LG-Medium	990 µL		
β-Glycerophosphate solution	β-Glycerophosphate disodium salt hydrate	550 mg	100 mM	prepare fresh with medium, filter sterilize
	DMEM-LG-Medium	25 mL		
IBMX stock solution	IBMX	111 mg	500 mM	
	DMSO	1 mL		
Indomethacin stock solution	Indomethacin	71.6 mg	200 mM	
	DMSO	1 mL		
LG-Medium	DMEM with 1.0 g/L glucose without L-glutamine	500 mL		
	FBS	50 mL	10% (v/v)	store 4°C
	GlutaMAX™ Supplement (200 mM)	5 mL	2 mM	
	Penicillin/streptomycin mixture, 10,000 U/mL each	5 mL	100 U/ml	
Osteo-Medium	LG-Medium	100 mL		store 4°C
	β-Glycerophosphate stock solution (100 mM)	25 mL	20 mM	
Osteo-Induction-Medium	Osteo-Medium	V needed		prepare fresh according to volume needed
	Dexamethasone working solution (100 µM)	1 µl/mL	0.1 µM	
Adipo-Induction-Medium	LG-Medium	V needed		prepare fresh according to volume needed
	Dexamethasone 10 mM	0.1 µl/mL	1 µM	
	IBMX stock solution 500 mM	0.1 µl/mL	50 µM	
	Indomethacin stock solution 200 mM	0.5 µl/mL	100 µM	
	ITS Supplement (100X)	2.5 µl/mL	0.25 x	
	Insulin (1 g/L)		2.5 mg/L	
	Transferrin (0.55 g/L)		1.375 mg/L	
	Sodium Selenite (anhydrous) (67 µg/L)		167.5 ng/L	

Table 2.1.11: List of Solutions and Media for Differentiation

2.1.4 Antibodies

Antibodies used for immune cytometric analyses are listed in the following table. Antibodies were stored at 4°C and diluted to working concentrations as indicated in the respective data-sheets. For handling, antibodies were placed in a cooling block at 4°C and protected from bright light.

Antigen	Conjugate	Isotype	Epitop/Clone	Supplier
Isotype control IgG1	FITC	IgG1	X40	BD
Isotype control IgG1	APC	IgG1	X40	BD
Isotype control IgG1	PE	IgG1	X40	eBioscience
Isotype control IgG2a	APC	IgG2a	eBR2a	eBioscience
Isotype control IgG2b	PE	IgG2b	eBMG2b	eBioscience
Isotype control IgM	FITC	IgM	G155-228	eBioscience
Isotype control IgM	APC	IgM	G155-228	eBioscience
Isotype control Rat IgG2a	AF488	Rat IgG2a	eBR2a	eBioscience
Isotype control Rat IgG2a	PE	Rat IgG2a	eBR2a	eBioscience
Anti-mouse	AF647	Goat anti Mouse	Poly	BD
Anti-rat	AF647	Goat anti Rat	Poly	BD
CD10 (Nephrilysin)	FITC	IgG1	HI10a	BioLegend
CD15 (SSEA-1)	APC	IgM	HI98	BD
CD15 (SSEA-1)	FITC	IgM	HI98	eBioscience
CD19	PE	IgG1	171B19	BD
CD24	FITC	IgG1	eBioSN3	eBioscience
CD29 (ITGB1)	PE	IgG1	TS2/16	eBioscience
CD44 (Hyaluronate receptor)	FITC	IgG1	Bu52	ABD
CD45 (LCA)	FITC	IgG1	HI30	BD
CD56 (NCAM)	FITC	IgG1	HCD56	BioLegend
CD56 (NCAM)	PE	IgG1	CMSB	eBioscience
CD73 (5'Ectonucleotidase)	APC	IgG1	AD2	eBioscience
CD90 (Thy-1)	PE	IgG1	DG3	Miltenyi
CD90 (Thy-1)	APC	IgG1	eBio5E10	eBioscience
CD105 (Endoglin)	PE	IgG1	SN6	eBioscience
CD106 (VCAM-1)	PE	IgG1	STA	BioLegend
CD133 (Prominin 1)	APC	IgG1	AC133	Miltenyi
CD133 (Prominin 1)	PE	IgG1	AC133	Miltenyi
CD133 (Prominin 1)	PE	IgG1	TMP4	ABD
CD146 (MCAM)	FITC	IgG1	P1H12	eBioscience
CD184 (CXCR4)	PE	IgG2a	12G5	eBioscience
CD184 (CXCR4)	APC	IgG2a	12G5	eBioscience
CD243 (MDR)	APC	IgG2a	UIC2	eBioscience
CD271 (NGFR)	APC	IgG1	ME20.4	BioLegend
CD271 (NGFR)	VB-FITC	IgG1	ME20.4	Miltenyi
CD324 (E-Cad)	PE	IgG1	67A4	BioLegend
CD325 (N-Cad)	APC	IgG1	8C11	BioLegend
CD326 (EpCAM)	APC	IgG1	EBA-1	BioLegend
CD326 (EpCAM)	FITC	IgG1	VU-1D9	ABD
CD49e (ITGA5)	PE	IgG2b	NKI-SAM1	BioLegend
CD49f (ITGA6)	FITC	Rat IgG2a	GoH3	eBioscience
CK19	FITC	IgG1	BA17	eBioscience
CK8	FITC	IgG1	LP3K	eBioscience
CXCR7	PE	IgG2b	8F11-M16	BioLegend
HLA-DR	PE	IgG2a	L243	BD
Oct3/4A	no	IgG2b	C-10	Santa Cruz
panCK	no	IgG1k	C11	BioLegend
Snail1	AF488	IgG2a	20C8	eBioscience
Sox2	AF488	Rat IgG2a	Btjce	eBioscience
SSEA-3	AF488	Rat IgM	MC631	BioLegend
SSEA-4	PE	IgG3	MC-813-70	BioLegend
TNAP	PE	IgG1	W8B2	BioLegend
TRA-1-81	PE	IgM	TRA-1-81	eBioscience
Vimentin	FITC	IgG1	V9	eBioscience

Table 2.1.12: List of Antibodies

2.1.5 Primer

Primer used for PCR reactions are listed in the following table. Primer sequences were chosen from the literature as indicated or designed using the Software OligoPerfect2 or Primer3 and checked with PrimerBlast with the default parameters. Primer oligodesoxynucleotides (ODN) were purchased GSF cleaned and lyophilized from TIB Molbiol Syntheselabor GmbH. ODN were resuspended in sterile water to yield a final concentration of 10 µM. Aliquots were stored at -20°C.

Primer Name	Sequence (5' – 3')	Product Size (bp)	Gene	GenBank Accession No.	T_m	T_A	Expected Product Length (bp)
H-v	GTTGTAGGATATGCCCTTGAC	313	HPRT1	NM_000194.2	56	50	313
H-r	GCCCAAAGGGAACTGATAGT				57		
R-v	CTCACTACCACACCTACCTG	320	RUNX2	NM_001024630.3 (Var 1), NM_001015051.3 (Var 2), NM_004348.3 (Var 3)	51	50	320 (all variants)
R-r	TCAATATGGTCGCCAAACAGATTC				53		
A-v	CAACATTCCTGGGCTGTACT	252	ADIPOQ	NM_001177800 (Var 1), NM_004797 (Var 2)	51	50	252 (both transcripts)
A-r	CCTGTGAAGGTGGAGTCATT				52		
S-v	TGTCTACGGTGAGCCAGTCA	200	SREBF1	NM_004176.4 (Var 1), NM_001005291.2 (Var 2)	60	52	200
S-r	TGAGGTTCCAGAGGAGGCTA				60		
RL-v	ACCAGCATCAAAATCCCAAG	196	TNFSF11	NM_003701.3 (Var 1), NM_033012.3 (Var 2)	57	52	196
RL-r	CCCCAAAGTATGTTGCATCC				57		
OC-v	GGCAGCGAGGTAGTGAAGAG	194	BGLAP	NM_199173.5	60	52	194
OC-r	AGCAGAGCGACACCCTAGAC				61		

Table 2.1.13: List of Primers for PCR

ADIPOQ: adiponectin, BGLAP: bone gamma-carboxyglutamate protein/Osteocalcin, bp: base pairs, HPRT: hypoxanthine phosphoribosyltransferase 1, r: reverse primer, Runx2: runt related transcription factor 2, Seq: sequence, SREBF1: sterol regulatory element binding transcription factor 1, TA: primer annealing temperature used in PCR reactions, Tm: primer melting temperature, TNFSF11: tumor necrosis factor superfamily member 11/Rank-ligand, v: forward primer
Primer Sequence Origin: HPRT [216], RUNX2 [18], ADIPOQ [217], other: Primer 3

2.2 Software and Databases

Software and databases used for data analysis are listed in the following table.

Software	Company	Description	Ref.
2200 TapeStation Analysis software	Agilent	TapeStation analysis software	
2200 TapeStation Controller Software	Agilent	TapeStation controller software	
Agilent Expert software	Agilent	Bioanalyzer software	
CellQuest Pro	Becton Dickinson	Flow cytometer software	
Cutadapt	freeware: Marcel Martin, code.google.com/p/cutadapt	Tool for adapter sequence removal	a
Cutadapt-1.16	code.google.com/p/cutadapt/downloads/list	Tool for trimming of NGS reads	
DESeq2 (Implemented in SeqMonk)	http://www. bioconductor.org/packages/release	Statistical tool for analysis of DGE	b
ExcelVersion 14.1.0	Microsoft Corporation	Data management, spreadsheet software	
fastqc_v0.11.7	freeware: http://www.bioinformatics.babraham.ac.uk	Quality control tool for sequencing data	c
FlowJo® Version 8.7	BD Biosciences	Flow Cytometer Software	
GeneAnalytics	LifeMap Sciences, Inc.	Tool for gene set analysis	
Gimp 2.8.22	www.gimp.org, Free Software Foundation, Inc. freeware	Image editing software	
HISAT2 2.1.0 release	https://ccb.jhu.edu/software/hisat2/index.shtml	Tool for alignment of NGS data	d
ImageJ	imagej.nih.gov, public domain open source software	Scientific image processing software	
IrvanView	Irfan Skiljan, www.irfanview.com, freeware	Image viewing software	
Java SE Development Kit v-8u171	Oracle Technology Network, http://www.oracle.com	Developer environment	
Mendeley Desktop 1.17.13	Elsevier, www.mendeley.com	Reference management software	
MikroWin, Version 4.41	Berthold Technologies	Microplate reader software	
miniconda 3	Anaconda, Inc.	Collection of open source software packages	
PathVisio 3.3.0	www.pathvisio.org	Tool for drawing of pathways	
PowerPoint Version 14.1.0	Microsoft Corporation	Presentation Software	
Python 3.6.5	Anaconda, Inc.	Programming language package	
R 3.5.0	https://www.r-project.org/, Free Software Foundation	Language environment	
R Studio Version 1.1.447	www.rstudio.com, RStudio, Inc., Open Source Edition	Integrated developer environment	
SAM tools 1.8	http://www.htslib.org/	Tool for conversion of SAM and BAM files	e
ScopePhoto	Müller Germany	Image aquisition software	
SeqMonk_v1.41.0	freeware: http://www.bioinformatics.babraham.ac.uk	Tool for analysing of NGS data	f
Text Edit v1.9	Apple	Text editing software	
Venny	bioinfogp.cnb.csic.es/tools/venny/index.html	Tool for comparing lists with Venn's diagrams	g
Vorschau Version 7.0	Apple	pdf viewer	
Word Version 14.1.0	Microsoft Corporation	Text editing software	
Xcode_7.3.1	Apple Distribution International	Integrated developer environment	

Table 2.2.1: List of Software

References:

a) Martin [218],
b) Love et al [219],
c) S. Andrews,
d) Kim et al [220] [221]
e) Li et al [222],
f) S. Andrews,
g) Oliveros, J.C. (2007-2015)

Name of Database/Tool	Description	URL	Ref.
Cancer Genome Anatomy Pathways	Pathway information provieded by Biocarta	cgap.nci.nih.gov/Pathways	a
cBioPortal for Cancer Genomics	Provides visualization, analysis and download of large-scale cancer genomics data sets	www.cbioportal.org	
ConsensusPathDB-human	Interaction networks in Homo sapiens including binary and complex protein-protein, genetic, metabolic, signaling, gene regulatory and drug-target interactions, as well as biochemical pathways.	cpdb.molgen.mpg.de	b
DAVID v6.8,	Database for Annotation, Visualization and Integrated Discovery	david.ncifcrf.gov	c
Ensembl	Various ressources incl. genome data	www.ensembl.org	
GeneCards®: The Human Gene Database	A searchable, integrative database that provides comprehensive, user-friendly information on all annotated and predicted human genes	www.genecards.org	
GEO (Gene Expression Omnibus)	Genomics data repository	www.ncbi.nlm.nih.gov/geo	
Harmonizome	A collection of information about genes and proteins from 114 datasets provided by 66 online resources.	amp.pharm.mssm.edu/Harmonizome	d
KEGG PATHWAY	Database collection of manually drawn pathway maps representing our knowledge on the molecular interaction, reaction and relation networks,reference database for Pathway Mapping	www.genome.jp/kegg/pathway.html	
NCBI	Various ressources incl. literature search, genome data, primer design	www.ncbi.nlm.nih.gov	
NCBI BioSystems Database	BioSystems database facilitates access to, and provides the ability to compute on, a wide range of biosystems data. Detailed diagrams and annotations for individual biosystems are then available on the web sites of the source databases.	www.ncbi.nlm.nih.gov/Structure/biosystems	
OligoPerfect™ Designer	Primer designing tool	tools.thermofisher.com	
Primer3web version 4	Primer designing tool	primer3.ut.ee/biotools.umassmed.edu	e
REACTOME	Pathway database		
SAGE Anatomy Viewer	Displays gene expression in human normal and malignant tissues by shading each organ in one of ten colors, each representing a different level of gene expression	cgap.nci.nih.gov/SAGE	f
TRRUST version 2	Transcriptional Regulatory Relationships Unraveled by Sentence-based Text mining, a manually curated database of human and mouse transcriptional regulatory networks	www.grnpedia.org/trrust	

Table 2.2.2: List of Databases

References:

a) Cancer Genome Anatomy Project,
b) Kamburov et al [223] [224],
c) Huang et al [225] [226],
d) Rouillard et al [227] [228],
e) Koressaar et al [229], Untergasser et al [230],
f) Cancer Genome Anatomy Project

2.3 Cell Lines

2.3.1 RCC Cell Line

The **parental cell line (PA)** used for all experiments was established from a primary clear cell renal cell carcinoma (ccRCC) tumor biopsy from a 52 year-old caucasian female patient. The cell line was established by Tomislav Dorbic and Burghardt Wittig and is a property of Mologen AG, where it is used as a starting material to produce the cell-based therapeutic tumor vaccine MGN1601. [182]

For cell line generation, cells were prepared from the tumor material without enzymatic disaggregation and cultured in AC-Medium for 7 passages (for 119 days) before freezing in the vaporous phase of liquid nitrogen. The cells were subsequently expanded to yield a master cell bank (MCB - MOL/0410/MCB1/POBE/1), which was further expanded into working cell banks (WCB). No cloning step was included during generation of the cell line; rather the cell line was selected for the tumor vaccine because of its morphological heterogeneity.

The starting cell aliquots used in this work originated from one WCB (980921/POBE-1 p26 08/03/06 native) and were at passage 26, with one exception, which originated from a different WCB in passage 23 (POBE-MEO, p23, 25/12/09).

2.3.2 Spheroid RCC Cell Lines

All spheroid derivatives of this cell line were established by sub culturing PA-cells in passage 28-30 under spheroid culture conditions. Two different starting conditions were applied yielding two morphologically distinct cell types:

Spheroid cells (SP) were cultured directly from PA cells with regular disaggregation of spheroids and sub culturing every 3-4 days.

Clonally expanded spheroid cells (CS) were derived from NSA experiments. They were generated by starting the spheroid culture from PA cells at a clonal cell density of 2-6x10^2 cells/mL in 96-well plates for 24-34 days without disaggregation of spheroids. Subsequent subculturing and regular disaggregation of these spheroids was performed in longer intervals of 8-10 days for the first 10-15 passages and 4-6 days in later passages.

2.3.3 Spheroid Cell Lines Re-Grown under Adherent Culture Conditions (ACC)

Spheroid cell lines at different passages were re-grown under ACC for various periods. The resulting cell lines are termed **A-SP** or **A-CS** depending on the spheroid cell line used.

2.3.4 A-SP Cells Re-Grown under Spheroid Culture Conditions (SCC)

A-SP cells at different passages were re-grown under SCC for various periods. The resulting cell lines are termed **A-SP-CS**.

3 Methods

3.1 Cell Culture Methods

To expand cells *ex vivo* they are cultured under sterile conditions in media, which contain the nutrients and growth-promoting factors needed for cell growth, and serve as pH-buffers. Many different media formulations, containing chemically defined concentrations of nutrients and trace elements, are available. To supply the complex mixture of growth factors required for cell proliferation, fetal bovine serum (FBS) is added to the medium, since it has been proven to be a suitable source in cell culture routine. This component is less well defined. Due to its biological origin and complexity, batch variations occur. Beside nutrients and growth factors, most cells are dependent on a proper substrate or surface to grow on, which is supplied by the culture vessel, a polystyrene flask or plate with a chemically treated surface designed to support attachment of cells or coated with biological materials such as ECM molecules. [231] [232] Optimal culture conditions vary for different cell types. To expand cells of interest, they are seeded under specified optimal conditions to proliferate. Upon cells are grown dense, the process is repeated, which is termed passaging. For passaging, cells have to be detached from the matrix and separated from each other. Enzymes, like trypsin, that cleave cell contacts are used for this purpose. Alternatively, cells can be mechanically dissociated, which is less sensitive and causes a high proportion of cell damage, or buffers containing calcium-chelating agents, that impair cell attachment by reducing calcium concentration, may be used. A limiting factor for cell expansion is the replicative potential of the cells of interest. Normal somatic cells have only a limited life span of 20-100 generations and gain a senescent phenotype or die after a defined number of cell divisions. [37] Therefore, only transformed cells or cells with intrinsic unlimited replicative potential can be expanded quasi indefinitely in culture. [233]

Cell culture work was done under aseptic conditions inside a laminar flow clean bench. All reagents, solutions, and material were either purchased sterile, sterilized by autoclaving, or filter-sterilized. The composition of media and solutions used for cell culture is listed in tables 2.1.9.-2.1.11. Media were stored at 4°C and warmed to 37°C before use. DBPS used in cell culture was the formulation without Ca^{2+} and Mg^{2+}. All cells were incubated at a temperature of 37°C in a humidified, CO_2-enriched (5%) atmosphere in a tissue culture incubator. A summary-overview of culture conditions used for different cells and *in vitro* differentiation is given in table 3.1.1.

3.1.1 Culture Conditions for Adherent PA Cells (ACC)

PA cells were cultured under standard conditions (ACC) as monolayer cultures in tissue culture treated flasks in serum containing AC-Medium on the basis of “Leibovitz’s L15” medium, which is the standard medium for this cell line, though cells grow well in other media tested. Cells were seeded at a density of 1.5-3x10^4 cells/cm^2 and passaged upon near confluence every 3-4 days. Passaging at earlier time-points led to impaired growth of the cells.

Name	Cells	Cell Culture Condition	
Adherent Culture Condition (ACC)	PA	Seeding density	1.5 x 10^4 to 3 x 10^4 cells per cm^2 growth area
		Morphology	adherent monolayer (2D)
		Culture vessel	tissue-culture treated cell culture flasks
		Medium	**AC-Medium:** "Leibowitz's L-15" containing 10% (v/v) serum (FBS)
		Passage	every 3-4 days; dissociation with Trypsin/EDTA
Sphere Culture Condition (SCC)	SP CS	Seeding density	4 x 10^4 to 7 x 10^4 cells per mL medium
		Morphology	non-adherent spheroids (3D)
		Culture vessel	non-treated cell culture flasks
		Medium	**SC-Medium:** „DMEM:F12, 1:1 Mixture", serum-free, containing insulin (5 µg/mL), EGF (20 ng/mL), bFGF (10 ng/mL), 0.25% (w/v) bovine serum albumin (BSA)
		Passage	every 4-5 days; dissociation with AccuMax™
CS-Generating Condition (CGC)	CS	Seeding density	3 x 10^2 to 8 x 10^2 cells per mL medium in 96-well plates; then 4 x 10^4 to 6 x 10^4 cells per mL medium
		Morphology	non-adherent spheroids (3D)
		Culture vessel	non-treated cell culture plates and flasks
		Medium	SC-Medium
		Maintenance Passage	medium change every 3-4 days; no dissociation for 21-34 days; then dissociation with AccuMax™ every 7-10 days for 10-15 passages; partial medium change every 3-4 days
Adherent Culture Condition for Spheres (ACC)	A-SP	Seeding density	2 x 10^4 to 4 x 10^4 cells per cm^2 growth area
		Morphology	adherent monolayer (2D)
		Culture vessel	tissue culture-treated cell culture flasks
		Medium	AC-Medium
		Passage Maintenance	every 4-7 days; dissociation with AccuMax™ or Accutase™; alternatively medium change every 3-4 days
	A-CS	Seeding density	4 x 10^4 to 6 x 10^4 cells per cm^2 growth area
		Morphology	adherent monolayer (2D)
		Culture vessel	tissue culture-treated cell culture flasks
		Medium	AC-Medium
		Passage Maintenance	every 4-9 days; dissociation with AccuMax™ or Accutase™; alternatively medium change every 3-4 days
Differentiation Conditions (AI/OI)	PA SP CS	Seeding density	2.5 x 10^4 to 5 x 10^4 cells per cm^2 growth area
		Morphology	adherent monolayer (2D)
		Culture vessel	tissue-culture treated 6- or 12-well cell culture plates
		Medium	"DMEM-LG" (1g/L Glucose) containing 10% (v/v) serum (FBS) and additives
		Additives for osteogenic induction (OI)	β-glycerophosphate (20 mM), dexamethasone (0.1 µM)
		Additives for adipogenic induction (AI)	insulin (2.5 µg/mL), indomethacin (100 µM), 3–Isobutyl–1–Methyl–Xanthin (IBMX) (50 µM), dexamethasone (1 µM)
		Maintenance	continuous growth for 15-37 days without passaging; medium change every 3-4 days

Table 3.1.1: Summary of Cell Culture Conditions

3.1.2 Passaging of PA Cells

For passaging, the medium was aspirated and the cells were washed quickly by rinsing with DPBS to remove traces of remaining medium. 0.05 % trypsin-EDTA solution was added in a sufficient volume to cover the cells, followed by incubation at 37°C for 3−5 min, to detach cells from the substrate. Once the cells were completely dissociated, the trypsin solution was diluted 1:10 by adding AC-Medium (containing FBS to stop trypsin activity). A single cell suspension was created by pipetting several times up and down with a serological pipette, thereby dispersing the cells. Cell count was performed as described (chapter 3.1.2) and an appropriate volume of cell suspension to yield the desired cell concentration was seeded into new tissue culture flasks containing AC-Medium.

3.1.3 Spheroid Culture - „Neurosphere Assay“ (NSA)

The „Neurosphere Assay“ (NSA) was initially developed by Reynolds and Weis [164] for the isolation of neuronal stem cells from adult mouse striatic brain tissue, and later on optimized and modified for a broader cell range. [234 235 236 237 238 239] Today the assay is widely used as a standard assay in stem cell and cancer research to asses the self-renewal ability of potential stem cells. [101 165 166 167 168 169 171 240]

The principle of the assay is based on cell selection by applying rigorous culture conditions, allowing only the desired cells to survive. For the NSA, cells are seeded at very low cell densities in serum-free medium containing epidermal growth factor (EGF), fibroblast growth factor (FGF), and insulin as sole growth factors in culture vessels, which do not support attachment of the cells. The basic assumption of the assay is, that only stem cells are able to grow under these rigorous conditions as floating cell clusters, so called „spheres“ or „spheroids“, whereas differentiated cells rapidly die due to the lack of proper adhesion- and growth-signals. Therefore, in applying the NSA it should be possible to select for stem cells according to their unique ability to be able to grow under these conditions. Repeated application of the assay with concomitant growth of spheroids is considered a proof of self-renewal ability of stem cells. In addition, long-term bulk culture should be used as a means to test for stem cell specific high proliferative potential. [170]

With some limitations, the assay can also be used to roughly estimate the quantity of stem cells contained in the starting preparation by counting the resulting spheres and determine the relative number of cells that were able to give rise to them (clonal spheroid-forming efficiency = CSFE). A critical parameter here is the cell density seeded, since aggregation and fusion events may distort the results. [241 242 243] Additional constraints in quantification of stem cells using the NSA are that (i) beside stem cells also committed progenitor cells may be able to grow as spheres [170], and on the other hand (ii) silent stem cells may not grow, an thus may be missed. [171] For quantification purposes the assay was therefore accordingly refined. In the so-called „Neural Colony-Forming Cell Assay“ (NCFCA) cells are seeded in a semi-solid matrix not allowing fusion or aggregation of cells. [244] For discrimination of stem cells from committed progenitor cells, colony size is used as a criterion, assuming that large colonies are derived from stem cells, whereas smaller colonies grow from progenitor cells with limited proliferative potential.

3.1.4 NSA Culture Conditions and Determination of Clonal Spheroid-Forming Efficiency (CSFE)

To determine and quantitate sphere-forming ability of cells, they were assayed in the NSA. For NSA, cells were seeded in 96-well flat bottom cell culture plates in a culture volume of 200 µl sphere culture medium (SC-Medium) on the basis of serum-free DMEM:F12 (1:1) containing the growth factors insulin, bFGF, and EGF. The medium composition used, was adapted from the one used by Ponti et al [166] and Bussolatti et al [78] for generation of mammospheres and RCC-derived spheres, respectively, albeit slightly reduced BSA concentration of 0.25% instead of 0.4% was used. Corning® not treated cell culture plates were used for the assay in order to reduce the tendency of cells to adhere to the surface of the culture plate. The use of “ultra-low attachment grade” plates for this purpose was not necessary, since cells rarely attached to the plates used. Cells were seeded at a concentration of 30-100 cells per well. At this cell number, cells were clearly discernible as dispersed single cells and

visual single-cell counting of cells and resulting spheroids could be performed. At least 15 wells per cell type were used for calculations of clonal spheroid-forming efficiency (CSFE).

For seeding cells in the NSA, 24 mL SC-Medium were prepared by addition of growth factors EGF and bFGF (1 µL/mL) to DMEM:F12-Medium and 100 µl per well were applied to 96-well plates. Single cell suspensions of the cells to be tested were prepared and cell number was determined as described for passaging (see chapter 3.1.8). Serial dilution of the cells was performed in SC-Medium to yield cell concentrations of $6x10^2$ cells/mL in a volume of 12 mL for one plate, or respectively less if 1/2, 1/3, or 1/4 plate per cell type were intended to be used. 100 µL of the resulting cell suspension was added to each well, and plates were incubated overnight. The next day, cell count was performed by microscopic inspection of the plates, thereby counting only obviously viable cells. The plates were incubated for 16-24 days, with regular medium replacement. Medium replacement was performed every 3-4 day by careful aspiration of 50 µL of the growth-medium per well and adding 50 µL of freshly prepared SC-Medium containing a 4 x growth factor concentration. When they had grown to a size of about 50-100 µm, healthy looking spheroids were counted by microscopic inspection of the plates. The outermost wells of the plate were not counted, since growth conditions were less optimal there. The in CSFE in per cent (%) of each cell type was calculated by dividing the mean of number of spheroids counted in 15-60 wells of one plate by the mean of number of cells seeded in respective wells, multiplied with 100. Standard deviations were calculated as described (chapter 3.17).

3.1.5 NSA Replating

To determine the secondary and tertiary CSFE for spheroids generated in the NSA, all spheroids grown from one cell type in one plate after 3-5 weeks were transferred to a 50 mL centrifuge tube and the wells were washed with 100 µL DPBS to remove all cells. The DPBS from the washing step was added to the tube containing the cells. Cells were pelleted by centrifugation at 400 x g for 3 min. The supernatant was aspirated and the cell pellet was resuspended in 0.5-1.5 mL DPBS and transferred to a 1.5 mL reaction tube. Cells were again pelleted by centrifugation at 260 g for 3 min and supernatant was removed. To disaggregate spheroids, they were resuspended in 200 µL Accumax™ solution and incubated for 15-20 min at 37°C in the cell incubator. Volume was added to 1 mL with DPBS and cells were pelleted again by centrifugation. After aspiration of the supernatant, pellet was resuspended in 100 µl of SC-Medium, and the suspension was pipetted several times up and down to fully disaggregate cells by additional mechanic disruption of aggregates. The volume was filled to 200 µl to 1 mL, depending on pellet size, and the cells were counted. Cells were seeded and assayed in the NSA as described (chapter 3.1.4).

3.1.6 Generation Spheroid Cells in Bulk-Culture - SP Cells

Since general growth of PA cells in the NSA was observed, but resulting cell numbers were very low, PA cells were directly cultured as bulk-culture under SC-conditions. For generation of spheroid bulk-culture, single cell suspensions of PA cells in passage 28 were pelleted by centrifugation and remaining serum-containing medium was aspirated. The cells were resuspended in SC-Medium and seeded at a density of 8×10^4 cells/mL in non-treated tissue culture flasks containing SC-Medium. At the very beginning of culture, cells adhered to the flask, starting to form a monolayer, which was later followed by progressive loss of adherence and formation spheroids, accompanied by accumulation of

dead cells. After 4 days of culture, the medium, containing the spheroids and 10 ml of PBS, which was used to for washing the flask, were transferred to a centrifuge tube, leaving adherent cells in the flask. The following steps were performed as described for passaging of spheroid cells (chapter 3.1.8).

3.1.7 Culture Conditions for Spheroid Cells (SCC)

Conditions used for culturing of spheroids (SCC) resembled conditions used for NSA and differed from ACC in several aspects. Besides the use of serum-free SC-Medium on the basis of "DMEM:F12 (1:1)", which has to be completed just prior to use by addition of EGF and bFGF growth factor solution (1 µL/mL, each), spheroids were cultured in Corning® not-treated tissue culture flasks to avoid unwanted adherence of the cells to the culture vessel. The use of "ultra-low attachment grade" flasks was not necessary, since cells rarely attached to the used flasks. To obtain single cells from the spheroids without too harsh mechanical disruption, the enzymatic cell aggregate dissociation solution Accumax™ was used, since Trypsin did not yield satisfactory results for this purpose. Seeding density of cells for optimal cell growth was adjusted according to the different growth rates of the spheroids, starting with 7 x 10^4 cells/mL for slowly growing cells at the beginning of spheroid culture lowering to 4 x 10^4 cells/mL for faster growing later passages. Spheroids were passaged every 4-5 days (SP cells) or 4-7 days (CS cells). In case of passaging intervals longer than 4-5 days, medium was replaced as described for generation of CS cells (chapter 3.1.6).

3.1.8 Passaging of Spheroid Cells

For passaging of spheroid cells, the medium containing the spheroids was transferred to a centrifuge tube, the cells were pelleted by centrifugation at 272 x g for 3 min and supernatant was aspirated. The culture flask was washed with DPBS (1/2 the volume of medium used for the flask), to remove all cells. DPBS from the washing step was added to the cells, followed by brief vortexing of the tube and centrifugation. For disaggregation of spheroids, the cell pellet was resuspended in 500 µL-750 µL Accumax™ solution using a 1 mL-blue tipped pipette. The cell suspension was incubated at 37°C for 12-15 min. Then, DPBS was added (1/2 the volume of medium used for the flask) and cells were vortexed. Cells were again centrifuged and supernatant was aspirated. The resulting cell pellet was resuspended in SC-Medium. To disaggregate cells additionally by mechanic force, the cells were resuspended first in 100 µl using a pipette, followed by addition of 900 µl using a blue tipped pipette, thereby pipetting the suspension several time up an down. The Volume was added up with SC-Medium to 2.5-6 mL, depending on the size of the pellet. Cells number was determined (see chapter 3.1.12) and cells were seeded in new flasks in SC-Medium, which was prepared beforehand by adding growth factors to 1x concentration.

3.1.9 Generation of Clonally Expanded Spheroid Cells - CS Cells

CS cells were obtained from spheroids grown in the NSA from PA cells in passage 28-31. For generation of a new cell line, spheroids grown in the wells of one 96-well plate (30-400) were harvested, disaggregated and counted as described for replating of cells in the NSA (chapter 3.1.5). Cells were seeded as described for passaging of spheroid cells (chapter 3.1.8). At the beginning of the culture (first 10-15 passages), cell number and growth rate were very low and cells were grown for 8-14 days without disaggregation of the spheroids. Every 3-4 days 1/5-1/3 of the growth-medium was

replaced. This was done by placing the flask upright, to let cells sediment, and aspirating 1/5-1/3 of medium with a serological pipette carefully, in order to not remove the cells. Then, the same amount of fresh medium, prepared to yield respective final 1 x concentration of growth factors, was added. Cells were passaged upon reaching adequate number as described for passaging of spheroid cells.

3.1.10 Culture of Spheroid Cells under ACC - A-SP and A-CS Cells

For re-culturing spheroid cells under standard AC-conditions, cells were seeded in tissue culture-treated flasks in AC-Medium at a seeding density of 2-4x10^4/cm for SP cells and 4-6x10^4/cm for CS cells, respectively. Cells were passaged when nearly confluent (at varying time points depending on cell growth 4-9 days). Alternatively, medium was changed every 3-4 days by aspiration and addition of fresh medium. Passaging was performed as described for PA cells with the exception that Accumax™ was used as dissociation reagent instead of trypsin. At the beginning of adherent culture, cells grew as adherent cell-islands and spheroids in parallel. Washing and aspiration steps were performed very carefully to not remove too many loose cells.

3.1.11 Culture of A-SP/A-CS Cells Under SC-Conditions

To assay the ability of spheroids grown for different periods as adherent monolayers to re-grow as spheroids, single cell suspensions of A-SP and A-CS cells obtained as described (chapter 3.1.10) were re-seeded under SC-conditions and passaged at least once as described for spheroid cells (chapter 3.1.8).

3.1.12 Cell Counting

Cell counts were performed using the Coulter Counter® Z1™. The instrument uses the principle of measuring the short-term resistance change, which occurs upon passage of low conductive particles (cells) through a small aperture/orifice in electrolyte solution (due to displacement of electrolyte by the particle). The resulting current pulse is recorded, whereby change of current is proportional to the particle size. By pulse-counting particle number can be determined.

For cell counting, a 75 µL aliquot of single cell suspension was diluted 1:100 in a 10 mL sample beaker with BD FACSFlow™ solution. Cell count was performed thrice per sample at a particle size range of 5-20 µm (12 µm). With dilution factor set to 100, cell concentration was the direct readout of the instrument. Mean of three measurements was calculated.

3.1.13 Cell Size Determination Using *CASY*® Modell TT

The "*CASY*® Modell TT" (Casy) instrument uses a similar, but more sophisticated principle to count cells and measure cell size then the "Coulter Counter® Z1™". Additional features are that also dead cells can be discriminated and the readout contains information on cell size distribution of the measured sample. Measurement was performed according to the manual: cell aliquots were diluted (usually 1:201) in the isotonic electrolyte solution CASYton and counted. Instrument settings were set according to the cell line characteristics to exclude dead cells and debris, which was for SP cells and adherent cells 7-12 µm, and for CS cells 4-9 µm.

3.1.14 Harvesting cells for molecular biologic analysis

For cell harvesting, single cell suspensions were prepared and cells were counted as described for passaging. Cells were washed with DPBS once by pelleting and aspirating supernatant to remove residual medium. Cells were resuspended in the desired volume of DPBS and aliquoted to 1 mL tubes yielding a cell number of 1-4x10^6, and again pelleted by centrifugation. Supernatant was removed and the pellet was shock-frozen in liquid nitrogen. Frozen cells were immediately placed in a freezer at -80°C.

3.1.15 Cryopreservation of Cells

For cryopreservation, single cell suspensions were prepared and cells were counted as described for passaging. Cells were pelleted by centrifugation at 272 x g and supernatant was aspirated. The cell pellet was resuspended in an appropriate volume of respective freeze medium containing 10% dimethyl sulphoxide (DMSO) as a cryoprotectant to yield a concentration of 5x10^6 cells/mL. Aliquots of 0.25 mL or 0.5 mL were transferred into cryo freezing tubes, which were immediately put in a cryo freezing container filled with isopropanol. The container was directly placed in a freezer at −80 °C to let the cells slowly cool down at a rate of −1°C/min. For long-term storage the cryopreserved cells were transferred into a liquid nitrogen tank (−196°C).

3.1.16 Thawing of Cryopreserved Cells

Tubes containing cryopreserved cells were warmed quickly by placing in a 37°C water bath. As soon as the ice inside the tubes had disappeared, 1 mL of respective growth medium was added drop wise. Cells were transferred to a centrifuge tube containing 9 mL medium and centrifuged at 272 × g for 3 min. Supernatant was aspirated and pellets were resuspended in fresh medium to decrease the cytotoxic effect of DMSO. Cells were seeded as described for passaging (chapters 3.1.2, 3.1.8), with the exceptions that AC-Medium for PA cells was supplemented with additional 10% FBS to ease recovery of the cells, and 24 h after thawing the medium was replaced to remove death cells and debris.

3.1.17 Testing for Mycoplasma Contamination

Since contamination with mycoplasmas is a constant peril in cell culture work, which may impair cell growth and behavior, cells were checked for mycoplasmas using the Venor®GeM OneStep Kit according to the kit instructions. The detection method is based on PCR detection of mycoplasma DNA from several strains in cell culture supernatants. In brief, cell culture 100 µL supernatant was taken from cells grown for at least 3 days, transferred to a reaction tube and incubated in a thermo cycler at 95°C for 5 min. The tube was shortly centrifuged at maximum speed to pellet all insoluble material and 2 µl of the supernatant were used for PCR reaction. Fresh medium was used as negative control, the positive control was provided with the kit. PCR was performed and 5 µL of PCR products were separated on an agarose gel (see chapter 3.13). Criteria for exclusion of mycoplasma contamination were: visibility of control bands in each lane, visibility of positive control band in positive control and no staining in the area of positive control band in the sample and negative control lanes. All cell lines tested were judged negative for mycoplasma contamination.

3.2 Cell Growth Assay (Resazurin Assay)

To test influences of different culturing conditions on cell growth, the relative number of viable cells grown under these conditions was determined using the fluorescent substrate resazurin. Resazurin is a cell permeable, non toxic blue dye with an absorption maximum at 605 nm, which is reduced in living cells to the pink molecule resorufin, which is highly fluorescent ($579_{Ex}/584_{Em}$) and has an absorption maximum at 573 nm. When the dye is added to living cells, the gradual increase of resorufin concentration owing to the cells' reducing activity is proportional to the number of cells, with a linear correlation between cell number and dye concentration within a defined concentration and time range. The rate at which the substrate is metabolized varies for different cell types. The change of dye concentration can be measured either by change (increase) of fluorescence excited at 530-560 nm and measured at 590 nm, or by change of absorption at 600 nm (decrease) and 570 nm (increase). [245] [246]

For the assay, cells were seeded in 96-well plates. According to the assay to be performed, cell concentration, media composition, or time of growth, were varied. Each condition to be tested was represented by 3-6 wells of the plate. Desired cell concentration was adjusted by performing serial dilutions of single cell suspensions, which were prepared as described in passaging of cells (chapters 3.1.2, 3.1.8). When medium variations were the intention of the assay, cells were centrifuged, the supernatant was aspirated, and the pellet was resuspended in the respective assay medium, which was prepared for the assay with omission of the substance to be tested. This medium was also used for serial dilutions. The test substance was added to an appropriate volume of the medium in 2x concentration and 75 µL/well were applied to respective sample wells. The outermost wells of the plate served as blank wells, containing only the medium used for the assay. Finally, 75 µl of cell suspension/well were added and the plates were incubated for 2-5 days in the incubator to allow cells to proliferate. On the day the assay was performed, resazurin solution (1 mM) was diluted 1:1 with DPBS in a 2 mL tube and 15 µl/well were applied to the test plate. The plate was incubated in the cell incubator and fluorescence of 578 nm emission for 535 nm excitation was measured at regular time intervals (1-2 h for 6-8 h) using the Mithras micro plate reader. The acquired raw data containing the measured fluorescence intensities of the samples were imported to Microsoft Excel software for evaluation. For comparison of different samples the following procedure was applied: a single measurement (time point) was chosen for further analysis by viewing a fluorescence/incubation time plot. The selection criteria were linearity of the measurement and maximal fluorescence difference of the samples. Mean values of the replicate wells were calculated and the blank value was subtracted from test values. For inter-assay comparison and comparison of different cell lines, values were normalized by calculating relative values to a standard condition.

3.3 Soft Agar Assay (SAA)

Soft agar assay is an assay for anchorage-independent growth of cells. Single cells are cultured in a semi-solid matrix consisting of agar, thus not allowing cell contacts. Growth of colonies after several weeks is an indicator for tumorigenic potential of the cells, since anchorage-independent growth is a hallmark of tumor cells. Therefore the assay may be used to estimate tumorigenic potential and

chemo sensitivity of cells *in vitro.* [247] [248] Albeit in many cases a correlation between growth of cells in the assay and tumorigenicity of cells *in vivo* is seen, the assay can not substitute for *in vivo* xenograft assays. [249] The basic principle of the assay is related to that used for NSA, allowing only cells to grow, which are able to do so as single cells without proper environmental signals. [247] In contrast to the NSA, in the standard soft agar assay additional constraints concerning medium composition are missing. Applying these constraints yields the conditions used for the NCFCA, with the exception that collagen is used there as matrix instead of agar. [244]

Soft agar assay was performed in two variants: the standard assay using serum-containing medium and an assay in which medium composition was the same as for NSA (SC-Medium).

Soft agar assay was performed in 6-well cell culture plates (well area = 34.8 mm^2). Usually three wells per sample were used. Agarose was boiled before use to liquefy and had to be cooled in a water bath to 42°C to not damage the cells. The medium used for the assay was also kept in a water bath at 42°C to avoid solidifying of agarose during preparation of the plate. Bottom layer was prepared one day before cell seeding by mixing 4 mL agarose with the respective 2 x soft agar medium, which was prepared beforehand in a 15 mL centrifuge tube. 1.5 mL of the mixture was applied to each well of a 6-well plate, dispersed and let sit on a plane surface to solidify. Plates were stored at 4°C over night and let warm to room temperature before use. For pouring the cell layer, agarose and medium were prepared as described for bottom layer. Single cell suspensions for seeding in the assay were prepared as described for passaging of the cells (chapters 3.1.2, 3.1.8). Cells were diluted to a concentration of $5.9x10^5$ cells/mL with DMEM:F12 (1:1)-Medium for a desired final concentration of $5x10^4$ cells per well. Cell count was performed to verify the cell concentration. For lower intended cell densities, cells were further diluted in DMEM:F12 (1:1)-Medium (1:5, 1:10, 1:25). 300 µL of cell suspension was mixed by vortexing with 2.5 ml respective medium prepared as described in a 15 mL centrifuge tube, and 2.5 mL agarose was added. The suspension was mixed again by pipetting and 1.5 mL per well was put onto the bottom layer and distributed equally by panning the plate. The plates were placed onto a plane surface to solidify. When the agar was steady, 400 µL maintenance medium was added per well. The plates were incubated for 28-36 days to allow growth of colonies. Every 3-4 days 400 µL of the respective medium was added. When colonies had grown to sufficient size, plates were stored at 4°C until analysis. For better visibility of the colonies, the plates were stained with 1.5 mL per well of 0.01% crystal violet solution for 2 days at 4°C. The staining solution was removed and the plates were washed several times with 4 mL MilliQ water overnight at 4°C until background staining was reduced sufficiently to count colonies. Plates were photographed on a light box with a Nikon D40 using a 55 mm/2.8 AI-S objective. Colony count was performed using the particle analysis tool of the ImageJ software. To do so a defined section of the original picture was analyzed by setting the threshold appropriately to detect stained colonies. For calculation of colony forming efficiency, which is the number of cells seeded to the number of colonies counted in %, the difference between area analyzed and total area of the well was taken into account (see chapter 3.17.4).

3.4 *In vitro* Differentiation

For evaluation of differentiation potential of the cells, adipogenic and osteogenic differentiation potential were assayed. The two were chosen since MSC have been shown and are defined to possess differentiation potential toward both lineages. [16 27]

Green and Meuth have described adipocyte differentiation for 3T3-L1 cell line already in 1974 and since, the cell line has been extensively used as a model for this process. For *in vitro* adipogenic differentiation of MSC various protocols are described, most of which use insulin, dexamethasone, indomethacin and IBMX at various concentrations. The optimal medium composition varies for cells from different origin and may contain also other components. The synthetic glucocorticoid dexamethasone is used to induce expression of C/EBP and PPARγ, which is the early master regulator of adipocyte differentiation. IMBX is a cAMP inhibitor, which serves to enhance PKA activity and thereby reduction of proliferation. IBMX also enhances expression of C/EBP, which is required for PPARγ expression. Indomethacin is a PPARγ ligand and similarly to the other factors induces expression of PPARγ via up-regulation of C/EBP. Insulin, depending on cell type and culture system is either necessary for the differentiation process and/or increases the lipid accumulation of the cells. [52 250 251 252 253]

Similarly, various compositions of media for osteogenic differentiation have been described, which mostly contain dexamethasone, β-glycerophosphate and ascorbic acid. Dexamethasone serves to induce expression of the osteogenic master regulator transcription factor Runx2. β-glycerophosphate on the one hand serves as phosphate source for mineralization by forming the hydroxyl apatite mineral ($Ca_{10}(PO_4)_6(OH)_2$) but also a role of inorganic phosphate as signaling molecule regulating the expression of osteogenic genes including BMP2 and osteopontin has been described. Ascorbic acid is needed for synthesis of proper collagen helices since it serves as a cofactor for prolin/lysine-hydroxylases. Ascorbate-2-phosphate instead of ascorbate is used, since it has been shown to be more stable in *in vitro* culture conditions. For osteogenic differentiation at least a 3 weeks period of treatment with the differentiation inducing components is needed. [254 255]

Marker for adipogenic differentiation are enhanced expression of PPARγ, adiponectin (ADIPOQ/ApM-1), fatty acid binding protein 4 (FABP4), leptin (LEP), fatty acid synthase (FASN), perilipin (PLIN1), lipo-proteinlipase (LPL), apolipoprotein E (APOE) and stearyl-CoA-desaturase (SCD). Osteogenic differentiation is marked by expression of Runx2, alkaline phosphatase (AP), osteocalcin (BGLAP/OC), collagen type I (COL1A1), osteopontin (OPN), dentin matrix acidic phosphoprotein (DMP), integrin binding sialoprotein (IBSP) and RANK-L (TNFSF11). [18 167 217 256 257 258 259]

3.4.1 Culture Conditions for Adipogenic Differentiation

For adipogenic differentiation, cells were seeded in 6-well or 12-well tissue culture plates at a seeding density of 2-5x10^4/cm in 2.5/1.5 mL adipogenic differentiation medium. The medium was prepared by addition of ITS, IBMX, dexamethasone and indomethacin to the yield the desired concentration in an appropriate volume of LG-Medium for the respective number of wells. For wells supposed to be negative control samples only the respective volume of DMSO instead of the supplements was added to the basal medium. The cells were incubated over a period of 12-35 days with regular medium change every 2-4 days by aspiration and addition of fresh medium. When necessary, cells were

washed with PBS once to remove dead cells and debris. Cells were monitored regularly for formation of characteristic lipid vacuoles and were fixed when they showed adipocyte morphology. Cells for RNA extraction were treated accordingly, with the exception that cells were seeded in 25 cm² tissue treated culture flasks in accordingly higher cell number and medium volume.

3.4.2 Culture Conditions for Osteogenic Differentiation

For osteogenic differentiation, cells were seeded in 12-well tissue culture plates at a seeding density of 2.5-5x10^4/cm in 1.5 mL osteogenic differentiation medium. The medium was prepared by addition of dexamethasone to the yield the desired concentration in an appropriate volume of Osteo-Medium for the respective number of wells. Addition of AsAP or ascorbic acid was omitted in most experiments since in former experiments addressing medium composition for osteogenic differentiation both substances had been shown to impair differentiation of the cells. Negative controls were seeded in LG-Medium instead of osteogenic differentiation medium. The cells were incubated over a period of 16-44 days with regular medium change every 2-4 days by aspiration and addition of fresh medium. When necessary, cells were washed with PBS once to remove dead cells and debris. Cells were monitored regularly for formation of characteristic calcium phosphate deposits and were fixed when deposits were clearly seen. Cells for RNA extraction were treated accordingly, with the exception that cells were seeded in 25 cm² tissue treated culture flasks in accordingly higher cell number and medium volume.

3.5 Histological Staining

To provide evidence for *in vitro* differentiation, histological staining for typical structures formed by adipocytes and osteoblasts was performed. To stain lipid droplets, which are typical intracellular structures of adipocytes, the lipid staining dye Oil Red O was used [260]. Mineralization, i.e. calcium phosphate depositions, which are typically seen after extended culture periods in osteoblast cultures, were visualized either with the dye Alizarin Red S, which forms a red chelate complex with the calcium ions present in the depositions or with the van Kossa staining method, whereby silver ions replace for calcium ions in the deposited phosphates, which become visible as metallic silver precipitates after photochemical degradation of the generated silver phosphate. [261] [25]

Staining for alkaline phosphatase (AP) activity, which is an early marker for osteoblast differentiation [262] [263], but also for embryonic stem cells and is also induced during adipogenesis [264] [265], was assayed using Naphthol-AS-MX-phosphate as a chromogenic substrate for the enzyme, which after cleavage by AP reacts with Fast Red Violet LB salt to form a red insoluble azo dye, thereby changing the color from yellow to red.

For histological staining cells were fixed using formalin, a relative mild fixing agent, containing formaldehyde as the active ingredient, which crosslinks proteins by reaction with amino groups. [266]

Medium was aspirated and cells were washed twice with DPBS containing Ca^{2+}/Mg^{2+} to prevent cells from detaching. Cells were fixed by addition 4% formalin solution and incubation for 30-60 min. Then, the individual staining procedure was executed. For washing steps 2 mL/well for 12-well plates or 4 mL/well for 6-well plates were used. The volumes used for all other solutions were 0.5 mL/well for

12-well plates or 1 mL/well for 6-well plates. The composition of solutions used for the staining procedures is listed in table 2.1.7.

3.5.1 Alizarin Red S Staining (Calcium Phosphate Deposition)

Alizarin red S staining solution was filtered before use. Fixed cells were washed 3 times with water before staining solution was applied. The incubation time for staining was 30-60 min. Staining solution was removed, wells were washed with water several times, and the plate was photographed.

3.5.2 Van Kossa Staining (Calcium Phosphate Deposition)

Fixed cells were washed 3 times with water before silver-staining solution was applied. The plate was set into the gel doc station and incubated for 20 min with UV-light. Staining solution was removed and wells were washed 3 times with water before addition of sodium thiosulfate solution for removal of access silver ions (fixation). After further washes the plate was photographed.

3.5.3 Oil Red O Staining (Lipid Droplet Accumulation)

Oil Red O working solution had to be prepared just prior to use by diluting 3 parts of stock solution with 2 parts of water and mix. The solution had to stand for at least 10 min and then be filtered, to remove aggregates. Fixed cells were washed with water once and then incubated for 2-3 min with 60% isopropanol. After removal of isopropanol, staining solution was added and the plates were incubated for 30-60 min. The plates were washed with water several times and stored at 4°C. In cases were nuclear counterstaining using hematoxylin was performed, this was done at earliest the next day by adding hematoxylin solution and incubation for 15-30 min. Wells were incubated with tap water to be blued. Tap water was replaced by MiliQ water and plates were stored at 4°C until pictures were taken using a microscope camera placed on an inverted phase contrast microscope.

3.5.4 Alkaline Phosphatase (AP) Activity Staining

The staining solution for AP activity had to be prepared just prior to use according to the volume needed. Medium was aspirated from the wells and cells were washed twice with DPBS containing Ca^{2+}/Mg^{2+} to prevent cells from detaching. Cells were fixed by addition 4% formalin solution. To avoid impairment of the enzyme activity formalin solution was left on the cells for 2-3 min, only. Cells were washed and permeabilized by addition of PBST twice. The staining solution was applied to the wells and the plates were incubated at room temperature for 15-30 min in the dark with regular inspection. The reaction was stopped by removing the staining solution, and washing twice with DPBS, when staining was visible. Storage buffer containing glycerol was added and the plates were stored at 4°C until pictures were taken using a microscope camera placed on an inverted phase contrast microscope.

3.6 Flow Cytometry

Flow cytometry is a method to measure light scattering characteristics and intrinsic or artificially introduced fluorescence of single cells. For this purpose a cell suspension is passed through a nozzle to yield a single cell stream. Light created by the laser(s) in the instrument is focused to pass the single cell stream. Several photomultiplier detectors are arranged to perceive the scattered and emitted light from one cell at a time. The recorded signals are proportional to the intensity of the scattered or emitted light.

Scattered light is measured with two detectors. One detector is set in the path of the laser so that measured intensity, resulting from light diffraction around the cell, is proportional to the cell size. This parameter is termed forward scatter (FSC). The second detector is set at an angle of 90° to the laser path, and the measured parameter is termed side scatter (SSC). SSC is influenced by the cell's inner structure, since the detected signal results from refraction and reflection of the light. Therefore cells with many granular structures show higher side scatter intensities than less complex cells. Different wavelengths of emitted fluorescence are measured with different detectors. The setup for fluorescence (FL) detection may vary for different instruments. By setting appropriate filters into the optical path, measured wavelengths are adjusted. The FACSCalibur™ flow cytometer used was equipped with a blue laser (488 nm), and a red diode laser (635 nm) and four fluorescence detectors, allowing parallel measurement of six different parameters of a cell. The wavelength parameter for the different fluorescence detectors (1 to 4) were as follows: FL1 (530 nm/30), FL2 (585 nm/42), FL3 (670 nm/LP), and FL4 (661 nm/16). Fluorescence is the characteristic feature of some molecules to be electromagnetically excited by light of a specific wavelength and, by energy absorption, emit light at a longer wavelength. Intrinsic cellular fluorescence is due to the presence of such molecules (e.g. riboflavin); it is usually low. By artificial addition of fluorescent molecules (fluorescent substrates, dyes or proteins) or fluorescently labeled antibodies these can be used to monitor cellular features of interest. [267]

Cells used for flow cytometric analyses were grown as described above and were used when reaching cell densities similar to passaging time points.

3.6.1 Immunophenotyping by Flow Cytometry (IFC)

For flow cytometric immunophenotyping applications a fluorescent molecule is covalently linked to antibodies, which recognize specific molecular epitopes (antigens), thus allowing their detection upon binding to the cell. The detected signal is proportional to the amount of antibody bound. But, since the measured signal is dependent on several factors such as labeling efficiency of antibody, emission characteristics of the fluorochrome used and staining efficiency, a semi-quantitative comparison is possible only within narrow ranges (same antibody with same fluorochrome and same staining procedure). [268]

3.6.1.1 Immunostaining of Cell Surface Antigens

Single cell suspensions were prepared from adherent cells and spheroid cells as described for their respective passaging using Accumax™ as a dissociation reagent for most purposes. Since some antigens proved to be sensitive to Accumax™ treatment, cells were incubated in TSE buffer instead of dissociation reagent and dissociated by pipetting the cell suspensions more vigorously. Cell count was performed, and 2-5x10^5 cells per sample were pelleted by centrifugation at 272 x g. Supernatant was aspirated and cell pellet was resuspended in appropriate volumes of F-PBS to yield 100 µL per sample. The following steps were performed protected from light on ice or 4°C, respectively. Individual antibody-containing staining solutions were prepared by diluting antibodies in block buffer according to the manufacturer's instruction to yield a final volume of 50 µL per sample. Cells were applied to 96-well round bottom plates, centrifuged at 400 x g for 4 min, and supernatant was decanted. Individual samples were resuspended in the respective antibody staining solution and incubated for 30-60 min. Cells were washed twice by adding FACS-PBS to a final volume of 200 µL followed by centrifugation and decanting supernatant. Cells stained with respective isotype control antibodies (non-specific antibodies with same isotype and fluorochrome conjugation as the test antibody) and/or unstained cells were used as controls and were prepared accordingly.

For staining of unstained mouse-derived antibodies with the compatible fluorescently labeled secondary antibody (AlexaFluor® 647 goat anti-mouse Ig), samples pre-incubated with primary antibody as described above, were resuspended in 50 µl secondary antibody staining solution each. The solution was prepared by diluting an appropriate volume of secondary antibody in block buffer to yield a concentration of 5 µL/mL. Samples were incubated for additional 30 min and washing steps were repeated as described above.

Antibody-stained cell pellets were resuspended in 100 µL FACS-PBS containing 25 µL (1.25 µg) 7-AAD viability staining solution/mL to stain dead cells, and incubated for at least 10 min before further dilution in FACS-PBS to a concentration of 1-2x10^6 cells/mL.

All steps were performed at 4°C or on ice and protected from bright light.

3.6.1.2 Immunostaining of Intracellular Antigens

For intracellular immonostaining, single cell suspensions were prepared as described for staining of surface antigens. Cells were fixed and permeabilized using the „Foxp3 Transcription Factor Staining Buffer Kit„ according to the manual. Antibody staining and final preparation of cell suspension was performed as described for staining of surface antigens in 96-well round bottom plates using 5x10^5 cells per sample with the exceptions, that for dilution of antibody and washing steps 1 x wash buffer from the kit was used, and addition of viability dye was omitted.

3.6.1.3 Data Acquisition and Analysis

FACSCalibur™ flow cytometer equipped with the acquisition software CellQuest™Pro was used for data acquisition. Individual instrument settings had to be applied to the different cell lines due to their varying sizes and auto fluorescence characteristics. Parameter were set as such that control samples were in the range of geometric mean (GM) 5 in the fluorescence channels and the populations were equally distributed in the forward/side scatter plot. Compensation settings for overlapping fluorescence

were set when needed using appropriate controls. $1x10^4$-$1x10^5$ total events were counted for each sample. Raw data were processed using the software FlowJo® (Version 8.7). An example of the gating strategy is given in figure 3 6 1 For comparison of fluorescence intensities of different samples, the fold change of geo mean values of the sample relative to the respective isotype control sample was calculated (see chapter 3.17.6).

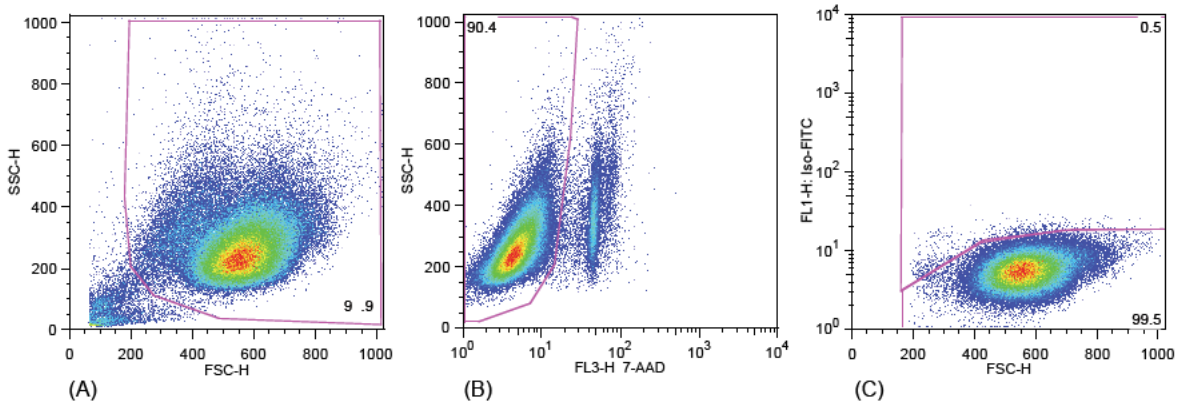

Figure 3.6.1: Gating Strategy for Analysis of Flow Cytometric Immunophenotyping

(A) The first gate was set in the SSC/FSC plot to exclude debris. (B) Dead cells were excluded by gating for the 7-AAD-negative population of the resulting population using SSC/FL3 plot = "live cell" population. The "live cell" population was used for further analysis. (C) Fluorescence thresholds for positive/negative gating were set according to respective isotype control samples in the respective fluorescence channel (FL1, FL2, FL4) using FL/FSC plot.
FITC: fluorescein isothiocyanate, FL: fluorescence, FSC: forward scatter, Iso: isotype control, SSC: side scatter

3.7 ALDEFLUOR™ Assay

Aldehyde dehydrogenases (ALDH) are cytosolic enzymes involved in dehydrogenation of aldehydes to their corresponding carboxylic acids. High expression of ALDH has been found in adult stem cells and subsequently has been used to mark TIC from several tumors. [151] [150] For assessment of ALDH activity an enzymatic assay, the ALDEFLUOR™ assay is widely used. For the assay the non-toxic fluorescent substrate BODIPY™ amino acetaldehyde (BAAA), which can freely diffuse into viable cells, is used. In the presence of active ALDH the substrate is converted by the enzyme to cell impermeable fluorescent BODIPY™ amino acetate (BAA), which accumulates in the cells. An efflux inhibitor is present in the solution, to avoid active efflux of the dye. The amount of BAA is proportional to ALDH activity in the cells and can be measured using a flow cytometer. As negative control for determination of background fluorescence a sample containing diethylaminobenzyldehyde (DEAB), a specific inhibitor of ALDH, is used. Cell concentration and incubation time have to be determined for the specific cell type assayed to achieve optimal signal to background ratios.

ALDEFLUOR™ Assay was performed using the ALDEFLUOR™ Kit according to the manual. AF buffer and DEAB-control buffer were prepared according to the number of samples to be analyzed.

For the Assay, single cell suspensions were prepared from adherent cells and spheroid cells as described for their respective passaging using Accumax™ as a dissociation reagent. Cell count was performed and an equivalent volume of cells to obtain $1x10^5$-$1x10^6$ cells per sample (representing $2x10^5$-$2x10^6$ cells/mL) were transferred to a 1.5 mL reaction tube and pelleted by centrifugation at 600 x g. Supernatant was aspirated and cell pellet was resuspended in 500 µL AF buffer or DEAB-

control buffer respectively. Samples were incubated for 30-40 min in the tissue culture incubator. After incubation, cells were pelleted by centrifugation at 600 x g for 3 min and supernatant was aspirated. Cells were resuspended in 100 µL ALDEFLUOR™ Assay Buffer containing 2.5 µL (1.25 µg) 7-AAD viability staining solution/mL to stain dead cells, and incubated for at least 10 min before further addition of 150 µL ALDEFLUOR™ Assay Buffer. Measurement was performed on FACSCalibur™ flow cytometer equipped with the acquisition software CellQuest™Pro. Parameter were set as such that populations were equally distributed in the forward/side scatter plot and control samples were clearly visible but in the low range of fluorescence channel 1 (about GM 10). Raw data were processed using the software FlowJo® (Version 8.7). Live cell gating was done as described for IFC (chapter 3.6.1.3). Fluorescence thresholds for positive/negative gating were set according to respective DEAB-control samples.

3.8 Rhodamine 123 Side Population Assay (RSPA)

It has been shown that a small cell population with stem cell characteristics can be discriminated by their ability to efflux foreign substances such as the fluorescence dyes Hoechst33342 or Rhodamine 123 (Rho). Those cells appear as a small dislocated population, in the respective plots obtained by flow cytometric measurements when using Hoechst33342 and are termed the “side population”. The accordingly named “side population” assay has successfully been used for isolation of progenitor cells from adult tissues as well as of TIC from tumor material or cell lines. [158] The molecular foundations of this characteristic behavior have been found to be the high expression of various ABC transporters, of which ABCB1 (MDR1/P-Glycoprotein) and ABCG2 (BCRP1) have been shown to be the main responsible transporters for efflux of the dyes used in the assay, with ABCG2 showing higher affinity for Hoechst33342 transport and ABCB1 seems to be the main responsible transporter for Rhodamine 123 efflux [155 269], but these characteristics seem to be species and tissue dependent [157] and ABCB1 was shown to be the responsible transporter for Hoechst33342 in 786-P renal carcinoma cell line, which do not express ABCG2. [208]

Both dyes have different fluorescence characteristics with Hoechst33342 fluorescence has to be excited with a UV-laser (350 nm), which is not standardly found in most flow cytometers, and emission is seen in the red and blue range [270], while Rhodamine 123 can be excited with the standard 488 nm laser and fluorescence is seen in the green/yellow range (FL1 channel). Besides this, both dyes have affinities to different cellular structures. While Hoechst33342 preferably binds to nucleic acids and is used as nucleic acid stain in other assays, Rhodamine 123 accumulates the mitochondria following the electrochemical gradient. After removal, the stain is preferentially retained in the mitochondria in an amount proportional to the mitochondrial membrane potential, therefore it is used as a probe for mitochondrial membrane potential [271] or for staining of mitochondria in other assays. [272] The side population assay was first described using the Hoechst33342 stain, but due to the special requirements on instruments and the cytotoxic nature of the molecule owed to its DNA-binding affinity, the alternative use of Rhodamine 123 was introduced and subsequently used, though not necessarily marking the same population like Hoechst33342 staining.[273 274 275]

The general principles of the assay comprise the following steps: the cells are incubated with a dye containing solution to achieve staining, then the solution is removed and residual dye is removed by

washing steps. To allow for dye efflux, the cells are incubated in unstained medium for a defined period, and the resulting staining characteristics are measured on a flow cytometer. Dye concentration and incubation times are critical, influencing parameters of the test. To discriminate staining characteristics of dye pumping cells from the non-pumping cells, a control sample, in which the dye efflux is inhibited is needed. Inhibition of dye efflux is achieved by addition of the respective membrane pumps using different pharmacological inhibitors, which often selectively inhibit different transporters. Since the nature of transporters responsible for the dye efflux is often not known and varies in different tissues, the use of the right inhibitor or inhibitor cocktail might influence the results. For example verapamil, by a yet unclear mechanism, targets preferably ABCB1, whereas Fumitremorgin C (FTC) is an ABCG2-specific inhibitor. [276]

The Rhodamine 123 side population assay (RSPA) in combination with ABCB1-inhibior verapamil was chosen to characterize individual dye efflux abilities of the different cell lines. In some experiments expression of ABCB1 (MDR1, CD243) was assayed in parallel by immunostaining of the cells to address the role of this transporter for the observed dye-efflux.

Single cell suspensions for RSPA were prepared from adherent cells and spheroid cells as described for their respective passaging using Accumax™ as a dissociation reagent. Cell count was performed and an equivalent volume of cells to obtain $1x10^6$ cells per sample was transferred to 15 mL reaction tubes. All washing steps were performed by pelleting cells at 400 x g for 4 min and aspiration of supernatant. The following samples were prepared for each cell line tested: unstained control sample (U), Rho-stained sample (Rho) and Rho-stained sample containing the efflux inhibitor verapamil (Ver). Cells were pelleted by centrifugation and resuspended in 2 mL of the Rho staining solution (Rho, Ver), which were prepared beforehand according to volume needed for the number of cell lines tested in the experiment. The unstained control sample was resuspended in medium without further supplements. All samples were incubated in the in the tissue culture incubator for 60 min to allow staining of the cells. Following staining, the solutions were removed and samples were washed three times with 4 ml F-PBS without Azid (Rho, U) or PBS-Ver (Ver). To assay the dye efflux capacity, the samples were resuspended in 12 mL AC-Medium without further supplements (Rho, U) or medium-Ver (Ver) and incubated for 90 min in the tissue culture incubator with occasional agitation. After incubation, cells were pelleted by centrifugation at 400 x g for 4 min and supernatant was aspirated. During the further procedure, the samples were placed on ice and protected from bright light to avoid further dye efflux and bleaching. Cells were resuspended in 100 µL PBS-Ver containing 2.5 µL (1.25 µg) 7-AAD viability staining solution/mL to stain dead cells, and incubated for at least 10 min before further addition of 150 µL PBS-Ver. In some experiments additional staining with CD243-APC antibody or respective isotype control was performed. In these experiments the cell number and volumes of all used solutions for the Rho samples was doubled and after the second incubation step the antibody staining was performed as described for immunostaining of cell surface antigens using half of the sample for staining with antibody or isotype control, respectively. During this procedure all samples were kept on ice and centrifugation steps were performed at 4°C. In one series of experiments SC-Medium instead of AC-Medium, which was routinely used for SP assay, was used to test for possible differences. In some experiments the Rho staining intensity was measured directly after staining, to evaluate the effectively

of the inhibitor and possible bleaching effects during the procedure. For this purpose, the cell number and volumes of Rho samples were doubled and one aliquot of the cells was prepared for measurement and assayed immediately after incubation in the staining solution.

The samples were measured on FACSCalibur™ flow cytometer equipped with the acquisition software CellQuest™Pro with instrument settings resulting in equally distributed populations in the forward/side scatter plot and unstained control samples being clearly visible in the low range of fluorescence channel 1 (about GM 5). Raw data were processed using the software FlowJo® (Version 8.7). Live cell gating was done as described for IFC (chapter 3.6.1.3). The general gating strategy used was identical to that used for IFC (see figure 3.6.1), but to set thresholds for positive/negative gating of the cells the respective Ver sample was used.

3.9 Tumor Formation by Xenotransplantation Assay

The final proof of stem cell central features, namely self-renewal and differentiation, can reliably be provided only *in vivo* by their ability to give rise to the respective organs/tumors. [92] Therefore, xenotransplantation assay using NSG mice was performed. The NSG (NOD.Cg-Prkdc^{scid} Il2rg^{tm1Wjl}/SzJ, also termed NOD/SCID/IL2Rγnull) mouse strain is the strain with the most heavily impaired immune functions. It is derived from the NOD/SCID strain with lacking T- and B-cells and impaired innate immune functions due to defects in complement, dendritic cells, macrophages and NK cells. In addition, the NSG strain also lacks NK-cells completely due to IL-2R γ-chain deficiency. Since NK cell residual activity has shown to compromise engraftment of xenogeneic material, this strain is superior over NOD/SCID mice for engraftment of xenotransplanted cells. [277] Cells were injected in Matrigel™ basement membrane matrix, which contains structural proteins and growth factors to facilitate engraftment of the cells. [278]

PA cells in passage 37 (same passage as used for preparation of MGN1601) and SP cells in passage 80 were used for the experiment. SP cells in this passage were chosen because of their growth characteristics seen in *in vitro* tests. The cells were cultured and harvested as described for culturing and passaging of the cells. PA cells for the experiment were provided by MOLOGEN AG.

Transplantation experiments were performed at “EPO GmbH, Berlin”. Cells were transported to the animal facility at room temperature in their respective growth medium (transport time 2 h). For application, the cells were pelleted and resuspended in in PBS: Matrigel™ 1:1 to yield the desired cell concentrations. $1x10^4$ (5 animals), $1x10^5$ (4 animals), and $1x10^6$ (3 animals) PA- and SP-cells respectively, were injected subcutaneously in a volume of 100 µL. Cell viability, which was checked in an aliquot after injection, was > 90% for all cell concentrations. Mice were maintained in the pathogen-free animal facility following institutional guidelines and with approval from the responsible authorities. Body weight and tumor formation were monitored and documented twice per week for 70 days. After this period mice were sacrificed and necropsies were performed.

3.10 RNA Isolation

RNA was isolated from cells using either "NucleoSpin® RNA II" kit (MN) or "mirVana™ miRNA Isolation Kit" (AM). MN is based on solid-phase silica membrane purification of RNA. AM uses a combination of chemical extraction of nucleic acids and solid-phase silica membrane purification to also retain small RNAs, which when using standard procedures get lost during the purification steps (either by not binding to the solid-phase or by not being recovered in ethanol precipitation after chemical extraction). The chemical extraction of RNA is based on the use of high concentrations of chaotropic salts in conjunction with phenol- or phenol-chloroform solutions to inactivate RNAses, precipitate proteins and extract nucleic acids from the aqueous phase. The solid-phase extraction is based on alterations of binding affinities of nucleic acids to the silica membrane, which are dependent on salt and alcohol concentration of the solution.

For isolation of nucleic acids, cells are homogenized by mechanical force (by passing suspension through a syringe needle) in a lysis buffer containing the chaotrophic salt guanidinium hydrochloride and β-mercaptoethanol to denature proteins, including RNAses, which is important to avoid RNA degradation during the process. The cell lysate is either filtered (MN) or nucleic acids are chemically extracted using acid phenol/chloroform (AM) before application to the membrane. For optimal binding of nucleic acids to the silica membrane, the ethanol concentration is adjusted by addition of ethanol to the filtered lysate (MN) or aqueous phase of the extract (AM). For retention of small RNAs in AM the ethanol concentration has to be adjusted to 55%, whereas only larger molecules (>200 nt) bind to the membrane when an ethanol concentration of 25% is used. In both methods the membrane is washed to several times with ethanolic buffer to remove unwanted molecules. Finally the RNA can be eluted in water. To minimize the risk of RNA degradation by RNAse contamination, all materials used for RNA preparation and handling were either sterile/RNAse-free, heated for 2 h at 220°C or cleaned with RNAse AWAY® to inactivate RNAses. All steps (except phenol/chloroform-extraction) were performed at a separate RNA-working space (clean bench). Either sterile water (Ampuwa), DEPC-treaded or RNAse-free water supplied with the kits was used.

3.10.1 mirVana™ miRNA Isolation Kit (Ambion: AM)

RNA extraction was performed according to the kit manual using 2-3x10^6 frozen cells. For cell lysis 600 µL Lysis/Binding Buffer were used and the solution was passed through a syringe needle several times. After addition of 60 µL miRNA Homogenate the solution was incubated for 10 min on ice before Acid-Phenol:Chloroform extraction was performed using 600 µL of the solution. The aqueous phase was recovered, comprising about 500 µL. An equivalent amount of ethanol was added and the solution was placed on the silica membrane containing filter unit. Washing steps were performed as described in the kit manual and RNA was eluted by addition of 120 µL and 100 µL respectively in two steps, yielding a total volume of RNA solution of about 200 µL, which was placed immediately on ice. RNA concentration was measured and the solution was aliquoted and stored at -20°C over night. DNAse digestion was performed the next day.

3.10.2 DNAse Digestion using Ambion® TURBO DNA-free™ Kit

DNAse digestion of RNA containing solutions obtained using AM-kit were performed with Ambion® TURBO DNA-free™ kit according to kit instructions using 30 µg of nucleic acid. The solution was diluted to a final concentration of 0.3 µg/µL by addition of RNAse free water. 11 µL 10xTURBO DNAse Buffer and 2 µL TURBO DNAse were added and the samples were incubated at 37°C for 30 min in a thermoblock. 23 µL of DNAse Inactivation reagent was added and the reaction mixture after thorough mixing was incubated for 5-7 min at room temperature. The tubes were centrifuged to pellet DNAse Inactivation beads and RNA containing supernatant was carefully removed and transferred to a fresh tube. The solution was placed on ice and RNA concentration was measured before aliquoting and storing at -80°C.

3.10.3 NucleoSpin® RNA II Kit (Macherey und Nagel: MN) and DNAse Digestion

RNA extraction was performed according to the kit manual using 2-3x10^6 frozen cells. For cell lysis 350 µL RA1 Buffer supplemented with 3.5 µL β-mercaptoethanol were used and the solution was passed to a syringe needle several times before application onto the filter unit. The lysate was filtered by centrifugation and 350 µL ethanol were added to the flow-through to adjust binding conditions for membrane binding of nucleic acids. The solution was placed on the silica membrane filter unit and loaded by centrifugation. The membrane was desalted by addition of 350 µL Membrane Desalting Buffer. On-column DNAse digestion was performed by addition of 100 µl DNAse reaction mixture and incubation for 15 min at room temperature. Washing steps were performed as described in the kit manual and the RNA was eluted by addition of 60 µL respectively in two steps, yielding a total volume of RNA solution of about 100 µL. The solution was placed on ice and RNA concentration was measured before aliquoting and storing at -80°C.

3.11 Reverse Transcription (RT) of RNA

For PCR, RNA was reverse transcribed to cDNA by using a reverse transcriptase enzyme in an appropriate buffer solution containing the four desoxyribose-nucleoside triphosphates (dNTPs). The primer needed for the reaction, were either random hexamer primer for random transcription of all RNA species or oligo-dT primer, to specifically transcribe mRNA. [279]

Reverse transcription was performed using “EpiScript™ Reverse Transcriptase Kit“ according to the kit instruction. 1 µg RNA was used for the reaction in a volume of 10 µL. Denaturation of RNA and primer annealing was done by incubation at 65°C for 2 min in a thermo cycler. After chilling on ice, the reaction mixture was completed by addition of 10 µL of a master mix containing 10x buffer, dNTPs, water and enzyme in appropriate concentration. Reaction was mixed by pipetting and incubated at 60°C for 37 min in a thermo cycler for reverse transcription, followed by 5 min incubation at 85°C to terminate reaction. Samples were chilled on ice and stored at -20°C until further use. To avoid contamination of the samples during pipetting steps, filter tips were used.

For RNA isolated from differentiated cells reverse transcription was performed using SuperScript™ II Reverse Transcriptase Kit according to the kit instruction. 1 µg RNA was used for the reaction in a final volume of 20 µL. Primer, RNA and dNTP were mixed and the volume was added to 10 µl with RNAse-free water. Denaturation of RNA and primer annealing was done by incubation at 65°C for

1 min in a thermo cycler. After chilling on ice, the reaction mixture was completed by addition of 9 µL of a master mix containing 10x buffer, $MgCl_2$, DTT, and RNAseOUT in appropriate concentrations. Reaction was mixed by pipetting and incubated at 42°C for 2.5 min in a thermo cycler, then the enzyme was added. The reaction mixture was incubated for 50 min at 42°C for reverse transcription, followed by 15 min incubation at 70°C to terminate reaction. Samples were chilled on ice and stored at -20°C until further use. To avoid contamination of the samples during pipetting steps, filter tips were used.

3.12 Standard PCR

PCR is a method to amplify DNA fragments of interest *in vitro*. DNA oligonucleotide primer sequences are selected as to bind specifically on the flanks of the DNA sequence of interest and thereby meet criteria to optimally bind at the used reaction temperatures and do not form secondary structures. The DNA sequence flanked by the primers is amplified using a DNA polymerase enzyme in a buffer solution containing the four desoxyribose-nucleoside triphosphates (dNTPs) and magnesium ions, by several cycles of thermal denaturation, primer annealing, and amplification. Primer annealing temperature varies according to the characteristics of the used primer. The amplified DNA can be visualized and evaluated qualitatively and semi-quantitatively by using agarose gel electrophoresis (see chapter 3.14.2). [279] Since PCR is a very sensitive method, for pipetting of the components filter tips were used to avoid contamination of the samples. Biozym Taq DNA Polymerase Kit was used for PCR reactions according to the manual. 2 µL of first strand cDNA were used in a reaction volume of 50 µL in PCR soft tubes or PCR 8-tube strips. The volumes used for one reaction are listed in table 3.12.1. Master mixes were prepared and either primer or template was added separately. PCR reaction was performed in a thermo cycler using the protocol as described in table 3.12.2. The annealing temperature was chosen according to the primer used (see table 2.1.13).

Component	Volume (µL)	Final concentration
10X PCR Buffer	5	1x
Sterile Water Ampuwa® to 50 µL	37.5	
40 mM dNTP Mix (10 mM each)	1.25	1 mM each
cDNA from first-strand reaction	2	variable
Forward primer (10 µM)	2	400 nM
Reverse primer (10 µM)	2	400 nM
Taq DNA polymerase (5 U/µL)	0.25	1.25 U

Table 3.12.1: PCR-Mix for one Reaction

Step	Process	Cycles	Time	Temperature in °C
1	Initial denaturation	1	2 min	95
2	Denaturation	25-37	15 s	95
3	Primer annealing		15 s	depending on primer used
4	Amplification		15 s	72
5	Repeat step 2-4 for an additional 24-36 times			
6	Final Extension	1	2 min	72
7	Cooling	1	∞	4

Table 3.12.2: Cycler Program for PCR

3.13 Agarose Gel Electrophoresis of PCR Products

The principle of separating charged molecules like RNA and DNA with a constant charge to mass ratio in gel electrophoresis is based on the different electrophoretic motilities of different sized molecules driven by a voltage gradient in a sieving like matrix. Smaller molecules migrate faster than big ones whereby the migration distance in gel (cm) is proportional to the log10 of the molecular size (bp/nt) of the molecule. Nucleic acids were visualized by staining with the fluorescent nucleic acid intercalating dye ethidium bromide, which in the intercalated state emits visible light (590 nm) after excitation with light in the UV spectrum range (254-366 nm).

To separate and visualize PCR products a 1.5% 0.5 x TBE agarose gel was prepared by dissolving 6 g Biozym LE-Agarose in 360 mL MilliQ and 40 ml 5 x TBE buffer, boiling and chilling to 60°C before casting the gel. Ethidium bromide was added to the liquid needed for one gel (40-100 mL) at a final concentration of 0.125 µg/mL. Gel mixture was immediately poured into the gel tray of a horizontal electrophoresis system with a comb attached to generate the pockets for sample loading. After the gel had polymerized, the tray was placed into the electrophoresis chamber, filled with buffer and the comb was removed. 1.5-10.5 µL of PCR product was applied per lane, diluted in a final concentration of 1x Orange DNA loading dye and water. Electrophoresis was run at 6 V/cm for 60 to 90 min. Finally ethidium bromide-stained DNA bands were visualized under UV light and photographed using the Gel Doc 2000 Imaging System.

3.14 RNA Quality Control

RNA quality is a critical requirement for obtaining reliable gene expression data. RNA degradation, DNA contamination or impurities influencing downstream enzymatic reactions may introduce unwanted biases such as loss of sequencing library complexity which compromise downstream analyses, especially differential gene expression analysis. [280] [281]

3.14.1 Photometric Measurement

Photometric measurement was used to determine the concentration and quality of RNA.

Nucleic acids show strong absorption of light with a wavelength of 260 nm, which is according to Beer-Lambert's law proportional to their concentration: $A_\lambda = \varepsilon \times c \times d$. ($A_\lambda$= absorption$_{wavelength}$, ε = molar extinction coefficient, d = pathlenght of the cuvette). The molar extinction coefficient is a molecule specific constant. For RNA it is equal to 0.025 $(\mu g/mL/cm)^{-1}$. By photometric measurement also contaminations of the sample with protein (280 nm) or organic substances like phenol (270 nm) or guanidine thiocyanate (220-230 nm) may be detected since they also show specific absorption maxima in the measured spectrum range. An indicator for „pure RNA" in TE buffer is an absorption ratio of >1.8 for 260/280 nm and 2 for 260/230 nm (varies according to the buffer system used). Only samples meeting these criteria were selected for further analyses. [282]

For absorption measurement RNA sample was mixed with 20 mM TE buffer 1:1. 10 mM TE buffer was used as blank value. 3 µl were applied to the cuvette (TrayCell with path length 0.1 cm) and absorption spectrum was measured from 220-320 nm in 0.5 nm steps. Blank spectrum values were subtracted from the respective values. From the resulting A_{260} value the background value at A_{320}

representing fluctuations of individual measurement was subtracted. RNA concentration was calculated according to the formula: c µg/mL = $(A_{260}-A_{320}) \times 2 \times (0.025\ (\mu g/mL/cm)^{-1} \times 0.1\ cm)^{-1}$.

3.14.2 Agarose Gel Electrophoresis of RNA

To estimate the integrity of RNA and select appropriate samples for sequencing respective samples were separated by agarose gel electrophoresis.

Cellular RNA is a mixture of different RNA-species. The major RNA-species of a cell is ribosomal RNA (rRNA) accounting for about 80-90% of cellular RNA. rRNA can be subdivided according to their size into 28S-, 18S-, and 5S/5.8S-rRNA. 28S- and 18S-rRNA are clearly visible on agarose gels as distinctive bands with a size of 5 kb and 2 kb, respectively. In contrast, mRNAs representing about 1-10% of total RNA (depending on cell type) are visible as a diffuse smear, due to their varying sizes between 0.3 and 100 kb (average length of 2.2 kb). The smaller 5/5.8S-rRNAs with a size of about 0.15 kb can be seen as diffuse band together with transfer RNAs (tRNAs). tRNAs with a size of about 100 nt account for about 15% of total cellular RNA content. The smallest functional RNAs are micro RNAs (miRNAs) and small interfering RNAs (siRNAs) with sizes of 15-30 bp/nt. Residual genomic DNA-contamination may be visible at the uppermost part of the gel since due to its size, genomic DNA does not migrate far in the gel. The band-distribution and resolution of different bands depends on the gel system used. An example of typical intact RNA is shown in figure 3.14.1. When RNA is degraded the characteristic band-distribution is accordingly changed. To assess RNA integrity, the ratio of peak intensities of the 28S- and 18S-rRNA band can be used as criterion. A ratio of 28S:18S > 2:1 is considered an indicator for intact RNA (although varying in different tissues). [282]

1.25% 0.5 x TBE agarose gels were prepared by dissolving 2.5 g Agarose NEEO-Ultra in 180 mL DEPC-water and 20 mL 5 x TBE-Puffer, boiling, and chilling to 60°C before casting the gel. Ethidium bromide was added to yield a final concentration of 0.25 µg/mL. For agarose gel electrophoresis RNA was dissolved at a final concentration of 0.3 µg RNA/mm lane (0.4 µg marker/mm lane) in a final concentration of 0.5 x TBE loading buffer (adjusted by addition of sterile water). To monitor gel electrophoresis, the tracking dye bromphenol blue was added at a concentration 0.15 µg/mL. A low concentration of the dye was used since its migration is equivalent to the small RNA fraction and therefore it may mask respective bands at higher concentrations. To disturb/prevent the secondary structure formation inherent to RNA, the samples had to be denatured before separation. This was done by addition of formamide to a final concentration of 60% (v/v) and heating the samples to 70°C for 10 min followed by immediate chilling on ice just before loading onto the gel. This step is critical since higher temperatures or too long incubation times lead to degradation of the RNA. Samples were applied to the gel, which was submerged in in 0.5 x TBE buffer and electrophoresis was run at 5 V/cm for 80-100 min. Bands were visualized by UV-light and the gel was photographed using the Gel Doc 2000 Imaging System.

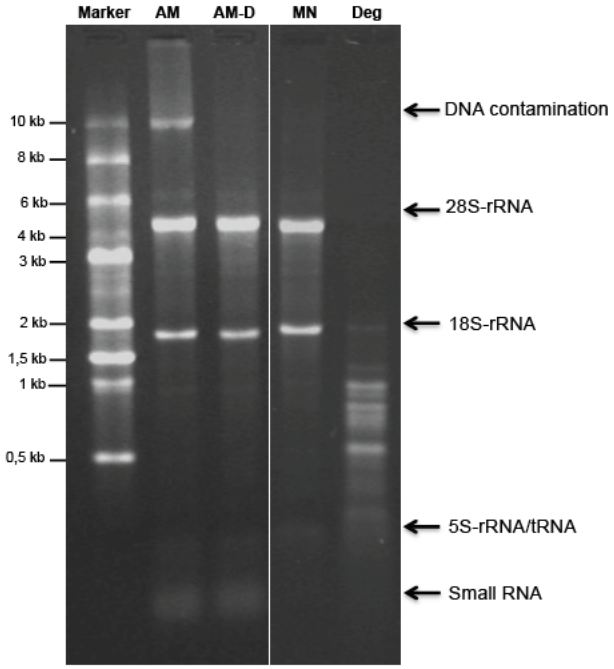

Figure 3.14.1: RNA Integrity on Agarose Gel

Agarose gel lanes with RNA samples AM: RNA isolated with "mirVana™ miRNA Isolation Kit" prior to DNAse digestion, AM-D: RNA isolated with "mirVana™ miRNA Isolation Kit" after DNAse digestion of contaminating DNA, MN: RNA isolated with "NucleoSpin® RNA II" and on column DNAse digestion, Deg: degraded RNA sample. In AM, AM-D and MN samples 28S/18S-rRNA and 5S-rRNA/tRNA bands are visible, in contrast to degraded RNA where only fragmented RNA is present; DNA contamination is clearly visible in AM sample before DNAse treatment; AM and AM-D samples contain small RNAs in contrast to MN sample.
AM: "mirVana™ miRNA Isolation Kit", D: DNAse digestion, Deg: degradation, MN: "NucleoSpin® RNA II"

3.14.3 Bioanalyzer and Tape Station Measurement

To assess RNA integrity, selected samples for sequencing were additionally analyzed with an Agilent-2100-Bioanalyzer or with the Agilent 2200 TapeStation System at the "Berlin Institute of Health (BIH) Core Facility Genomics at the Charité Campus Rudolf-Virchow" just prior the to sequencing.

The Bioanalyzer technology uses chip-based capillary electrophoresis to separate samples (chips for DNA, RNA and Protein analysis are available). The principle is the same as for traditional gel electrophoresis. The chip consists of a glass slide with micro capillaries, which are interconnected to different wells for samples, marker ladder and gel. Small electrodes are arranged on the chip to supply current flow to each sample separately when set into the chip-cartridge. A sieving polymer pre-mixed with an intercalating fluorescent dye is applied to the chip just before usage. By applying the sieving polymer an electrical circuit is created. After the chip is primed the samples are pre-mixed with an internal standard comprising a single marker fragment, and as well as the marker ladder are applied to the respective wells. The chip is set into the cartridge and analysis is started. Samples are separated by their electrophoretic mobility in the gel. Detection is achieved by laser-induced fluorescence measurement. Results can be displayed as electropherograms or as a densitometry plots (creating gel-like images). Bioanalyzer data analysis is done by Agilent Expert software, which quantitates and sizes RNA samples according to the applied standards and assigns a RIN (**R**NA **I**ntegrity **N**umber) to each trace. The RIN was developed for the assessment of RNA quality in Bioanalyzer measurements. The algorithm is not only based on the ratio of ribosomal subunits but also takes into account how

much signal is found between the 5S and 18S band, between the 18S and 28S bands, and after the 28S band (see figure 3.14.2 (A)). The RIN scale reaches from RIN 10 equivalent of perfect score or excellent RNA to RIN 1 representing totally degraded RNA. [283] [284] [285] Examples are depicted in figure 3.14.2.

The 2200 TapeStation System is an automatic gel electrophoresis system which uses credit-card-sized „ScreenTape"s composed of three layers of polymers: the protective layer, the electrode layer and the bioprocessing layer containing the gel matrix with individual separation channels (lanes) and buffer chambers for electrophoresis. Samples and marker are added to the instrument either in tube strips or 96-well plates and are automatically loaded onto the „ScreenTape" when the run is started. Analysis of TapeStation data is done by *2200 TapeStation Analysis software* which analogous to Bioanalyzer automatically determines size, quantity, and RIN^{e} (different RIN algorithm for TapeStation). [286]

For RNA quality control using the two systems all steps were performed according to „Agilent RNA 6000 Nano Kit Guide" or „Agilent High Sensitivity RNA ScreenTape System Quick Guide". For Bioanalyzer measurement 1 µL and for TapeStation measurements 2 µL RNA sample volume was used. Analysis was run in „Eucaryote Total RNA Nano" (Bioanalyzer) or „Eukaryotic RNA" (TapeStation) mode. The RIN values of all samples used for RNA-Sequencing were determined to be between 9 and 10 (see table 3.15.1).

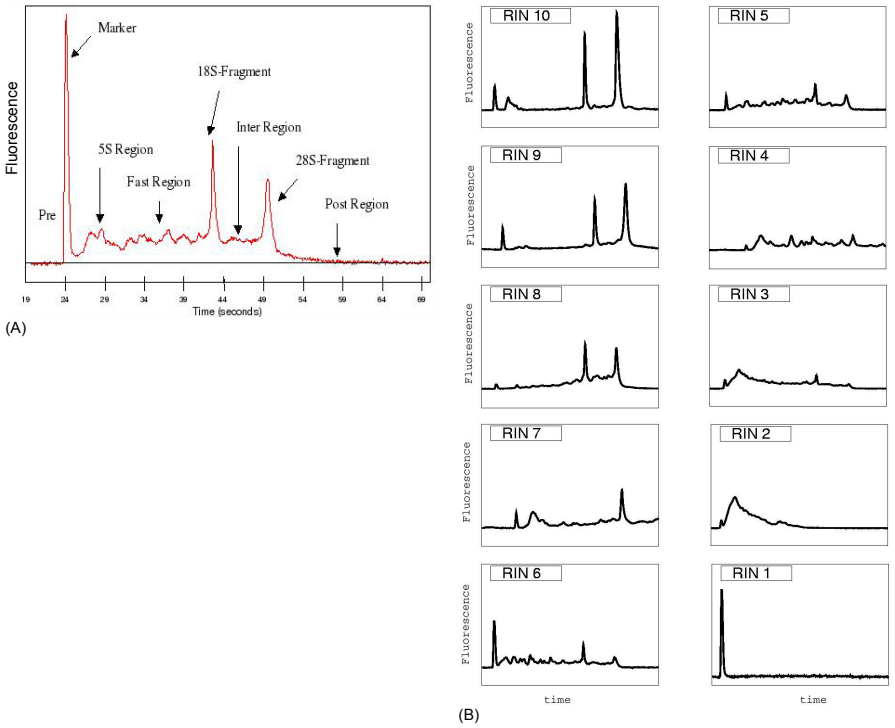

Figure 3.14.2: Example of Bioanalyzer Result for Different RIN Values

Electropherograms (fluorescence intensities over time) as measured on a Bioanalyzer or TapeStation System. (A) Regions defined and used for calculation of RIN values, containing the following RNA species: Marker (Marker fragment); 5S Region (5S, 5.8S and tRNA); Fast-Region (small RNAs, degraded RNA, mRNA); 18S-Region/28S-Region (18/28S rRNA); Inter-Region (mRNA, degraded ribosomal RNA); Region preceding 28S-Region (precursor RNA); Post-Region (DNA contamination). (B) RIN values for RNA samples with ascending amount of degradation starting from RIN 10 corresponding to excellent RNA to RIN 1 representing fully degraded RNA (from [285]).

3.15 RNA-Sequencing

Among the different techniques available to sequence whole transcriptomes in a high-throughput manner, RNA-sequencing on the Illumina platform was chosen. The sequencing principle of the Illumina platform is similar to the Sanger sequencing method in that it is based on cyclic reversible termination of DNA amplification. The four differently fluorescently marked 3'-blocked dNTPs are used to detect the complementary base in each cycle of elongation. The sequencing process is started by a primer, which is complementary to an adapter region, present in the sequencing template. After incorporation of one base the fluorescent signal is measured and unbound dNTPs as well as the blocking group are removed. The next cycle is started and the process is repeated for 50-300 cycles thus obtaining sequence information for 50 to 300 nt.

Single stranded fragments with a size of 200-1000 nt of the DNA of interest, or in case of RNA-sequencing of the respective cDNA, serve as templates for the reaction. These fragments, which are prepared from the starting material in several steps including fragmentation and adapter ligation, are termed the sequencing library. The library is immobilized on a glass slide, named the flow cell, which contains several lanes for different samples. On the flow cell's surface two universal ODN-adapters, which serve as primers and are complementary to adapters ligated to both ends of the sequencing library, are immobilized. By using sequence-tagged adapters/primers for library preparation, several samples can be applied to one lane and can be sequenced in parallel, being discriminable after sequencing according to the sequence tag used. Before the actual sequencing step, the single fragments have to be clonally amplified to yield local clusters of fluorescent molecules in order to gain a strong enough fluorescent signal for detection and discrimination of fragments. This is done by so-called bridge amplification of the fragments using the dense lawn of the two ODN on the flow cell as primers. A single stranded fragment from the library hybridizes randomly to a slide-bound primer/ODN. By adding unlabeled nucleotides and enzyme, the reverse strand is amplified, thus the fragment is immobilized on the slide. After denaturation and washing away the original fragment, a nearby second ODN, complementary to the opposite end of the fragment's complement, serves for priming a next round of amplification. The binding occurs through bending of the fragment in a bridge like manner. The process of denaturation and elongation is repeated several times, thereby amplifying each bound fragment locally. The process is illustrated in figure 3.15.1. Cluster density is critical for the quality of results, as too dense clustering impairs proper detection of the signal whereas a too small number of clustered fragments will reduce the coverage of the library.

After bridge amplification, the sequencing reactions can be started. The reverse stands are cleaved and the 3' ends are blocked with ddNTP to prevent unwanted priming. The sequencing begins with extension of the sequencing primer using fluorescently labeled nucleotides. Only one nucleotide is incorporated per cycle and the fluorescence signal is read by the instrument for the different clusters on the flow cell in parallel. The steps are repeated for up to 150 cycles to obtain sequence information of this length. [287] [288] [289] [290]

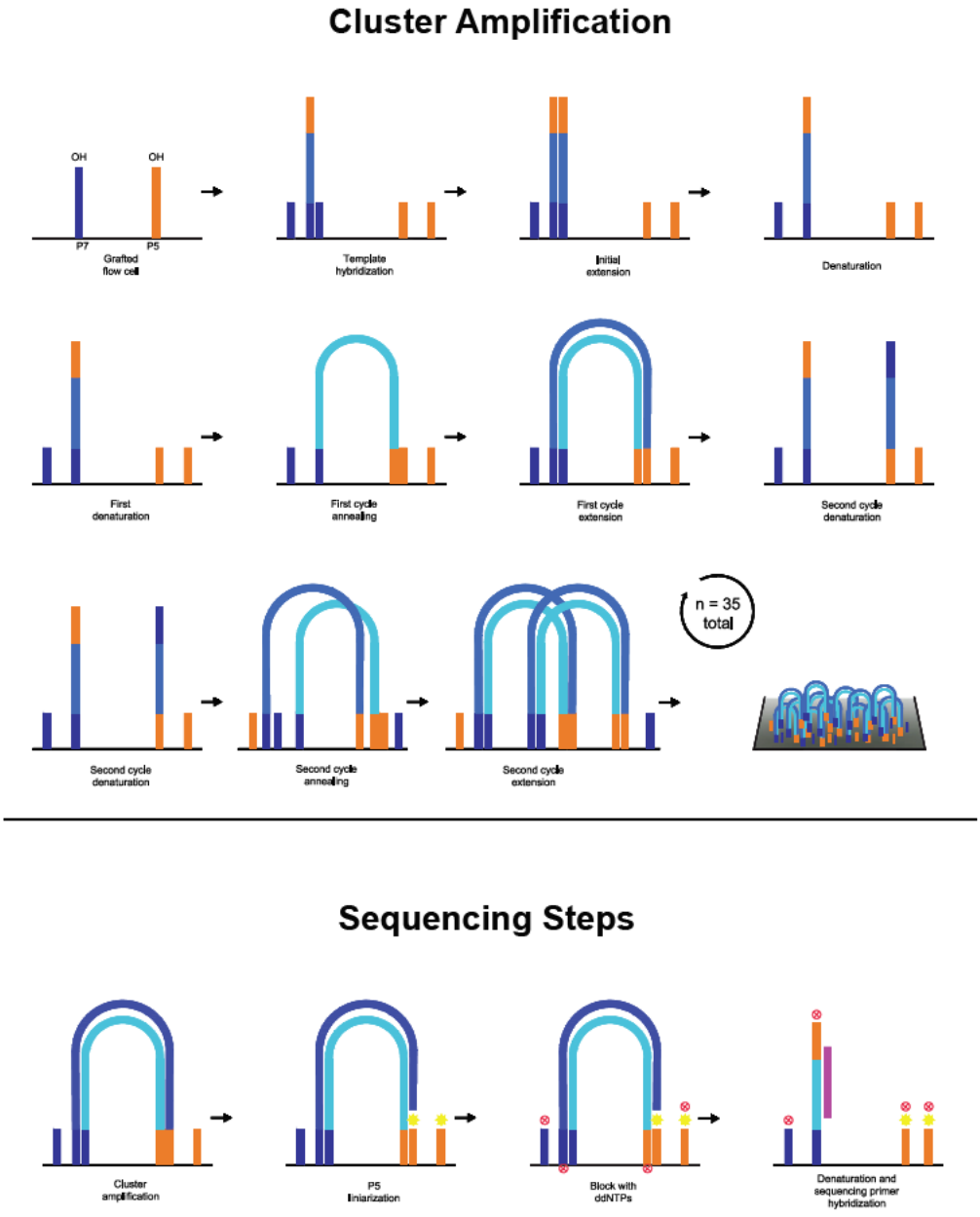

Figure 3.15.1: Illumina Sequencing Principle: Bridge Amplification and Sequencing

Illustration of cluster amplification process (figure top) and overview of sequencing steps (figure bottom). The figure was drawn according to Mardis [288].

The following steps required for RNA-sequencing, including quality control of RNA using Bioanalyzer/TapeStation instruments, were done at the "Berlin Institute of Health (BIH) Core Facility Genomics at the Charité Campus Rudolf-Virchow".

3.15.1 RNA Sequencing Library Preparation

Samples have to be prepared for sequencing in a process named library preparation, which includes selection of the sequences of interest (mRNA, removal of rRNA, specific selection of sequences), fragmentation, transcription to cDNA, sequencing adapter ligation and amplification steps. The resulting pool of cDNA is called the RNA-sequencing library. The process of library preparation is illustrated in figure 3.15.2.

Since rRNA is the most abundant but in most cases not relevant RNA species, it has to be removed from the sequencing pool of RNAs. This can be done either by depletion of rRNA using respective methods or by enriching for the RNA species of interest, in most cases mRNA by poly-A selection. mRNA depletion or poly-A selection methods differ in their results, whereby libraries prepared with the mRNA depletion method contain a higher fraction of non-protein coding sequences located in intergenic and intronic regions as well as non-polyA transcripts (e.g. histones). [291] When preparing the library according to the standard protocol it contains sequences in the sense and antisense orientation at random (50%), this means that strand information is lost during the process. To preserve information on strand orientation, which might be of importance for identifying antisense or overlapping transcripts, several methods exist. They are based either on addition of different adapters to both ends of the RNA or marking the strands chemically for example by incorporation of dUTP during second strand cDNA synthesis and subsequent removal of this strand. [292]

The use of paired-end (PE) cDNA libraries, which are created by using respective adapters/primers, provides additional information and allows isoform discrimination or detection of gene-fusion events. This is achieved by sequencing fragments from both ends, and thus producing a sense and antisense read for each fragment. The library preparation method depends on the intended aim of the study and the cost effectiveness. For transcriptome profiling a stranded, PE library would be the best selection. For differential expression studies a single-end (SE), non-strand specific library is sufficient.

The cells used for evaluation of gene expression by RNA-sequencing were maintained and harvested as described in sections 3.1.12 and 3.1.8. Sequencing samples were named according to the cell line. Biological triplicates were used for sequencing. [293] [294] Individual samples are discriminated by addition of A, B, C to the name of the cell line. An overview of specifications of cell lines and respective RNA used for library preparation and subsequent sequencing is given in table 3.15.1.

Prior to library preparation, RNA concentration was measured with the Qubit™ 2.0 Fluorometer, which relies on the highly sensitive and accurate fluorescence-based Qubit™ quantitation of RNA, using the "Qubit™ RNA HS Assay Kit", according to the kit instructions, since the use of exact quantities of input RNA is important for all later steps.

Sample	Name	Cells	Passage	ACC	RIN	Sequencing Sample No.	Number of Raw Reads
PA	PA-A	PA (Mo)	37		10	6017	4.82E+07
	PA-B	PA (Mo)	37		10	6018	4.71E+07
	PA-C	PA (Mo)	37		10	6019	4.06E+07
SP	SP-A	SP1P35-3	39		10	6020	4.38E+07
	SP-B	SP1P35.7	39		10	6021	4.29E+07
	SP-C	SP1P35.7	43		10	6022	4.25E+07
AS	A-SP-A	A-SP1P35.7-P36	57	14 weeks	9.6	180	6.36E+07
	A-SP-B	A-SP1P53.7-P54	75	14 weeks	9.6	181	7.08E+07
	A-SP-B	A-SP1P35.7-P36	56	14 weeks	9	182	6.16E+07

Table 3.15.1: Specifications of Cell Lines Used for RNA-Sequencing Library Preparation

For RNA sequencing 3 biological replicates (A-C) representing one sample were used. The names, passage numbers and time of culture under ACC are indicated in column 1-4. RIN values and numbers used in sequencing are shown in column 5-6. The numbers of raw read obtained are indicated in column 7.
ACC: adherent culture conditions, AS; adherently grown spheroids; A-SP: SP cells grown under ACC for 2 weeks, Mo: cells cultured at GMP facility of Mologen AG, P: passage number, PA: parental cell line, SP: spheroid cells derived from PA

For library preparation „NEBNext®Ultra™RNA Library Prep Kit for Illumina® (NEB #E7530+#E7490)“ was used according to kit instructions. 500 ng mRNA of each sample served as starting material for library preparation in a volume of 50 µL. Poly-A RNA was enriched using oligo(dT) magnetic beads according to kit instructions. The binding procedure was repeated for better removal of traces of rRNA. mRNA was eluted from beads in a volume of 17 µL buffer for first strand cDNA synthesis containing random hexamer primers and was incubated for 15 min at 94°C for denaturation and fragmentation of RNA. 15 µL of eluate were used for first strand cDNA synthesis reaction in final volume of 20 µL.
Reaction was performed on a thermocycler with the following protocol: 10 min 25°C; 15 min 42°C; 15 min 70°C; hold 4°C. Second strand cDNA synthesis was performed immediately by adding the components to the tube yielding a final volume of 80 µL. The reaction was incubated for 1 h at 16°C in a thermo cycler with 40°C heated lid. The reaction mixture was cleaned from PCR components using “AMPure XP Beads” according to instructions. 144 µL beads per reaction were used and elution was performed in 60 µL 0.1 x TE buffer pH 8. 55.5 µL of supernatant were transferred to a fresh tube. End repair, respectively 3’-adenylation, was performed by addition of buffer and enzyme yielding a final volume of 65 µl and incubation in a thermocycler with the following protocol: 30 min 20°C; 30 min 70°C; hold 4°C. Adapters for ligation were diluted in a freshly prepared 1:9 dilution of 10 mM Tris buffer and 10 mM NaCl and Blunt/TA Ligase mix, water and 1 µL of adapter were added to the tube yielding a final volume of 83.5 µL. The mixture was incubated at 20°C in a thermo cycler for 15 min to ligate adapters before addition of 3 µL USER enzyme and additional incubation at 37°C for 15 min to remove unpaired bases. The reaction mixture was cleaned using “AMPure XP Beads” according to instructions, using a final volume of reaction mixture adjusted by addition of water of 100 µL and 100 µL beads. DNA was eluted using 22 µL 0.1 x TE. 20 µL eluate were transferred to a fresh tube. The adapter ligated cDNA amplified in a PCR reaction in a thermo cycler using the following protocol:

Step	Process	Cycles	Time	Temperature in °C
1	Initial denaturation	1	30 sec	98
2	Denaturation	25-37	10 s	98
3	Primer annealing		15 s	65
4	Amplification		15 s	65
5	Repeat step 2-4 for an additional 12 times			
6	Final Extension	1	5 min	65
7	Cooling	1	∞	4

Table 3.15.2: Cycler Program for PCR in RNA-Sequencing Library Preparation

For PCR reactions master mix was added to the eluate and index primer (i7/i5) were chosen and added to each sample separately to allow multiplexing of 8 samples per lane in the sequencing step. The amplified library was cleaned from PCR components with “AMPure XP Beads” and eluted in a volume of 23 µL 0.1xTE buffer. 20 µL of the cleaned amplified library were transferred to a fresh tube.

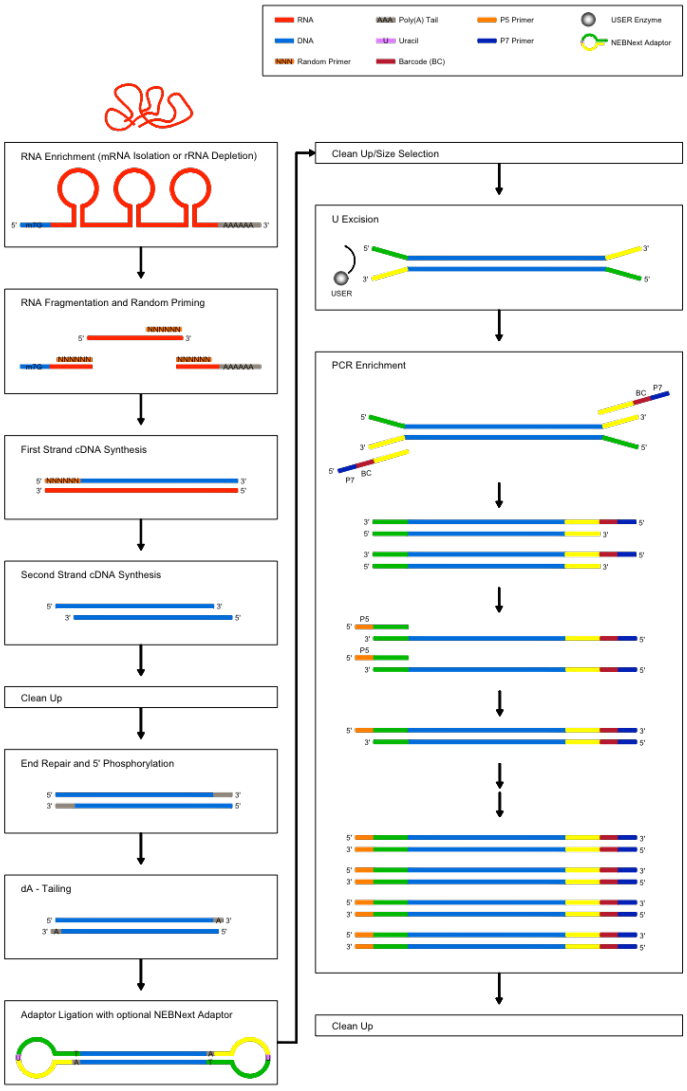

Figure 3.15.2: Schematic Overview of RNA-Sequencing Library Preparation Steps

Steps for preparation of RNA-Sequencing library with „NEBNext®Ultra™RNA Library Prep Kit for Illumina® as described in the text. mRNA was enriched using oligo(dT) magnetic beads. Clean up steps were performed using “AMPure XP Beads”.

3.15.2 RNA Sequencing Library Quality Control

Size distribution of cDNA library was checked by applying an aliquot of 1 µL to the "DNA 500 LabChip Kit" according to kit instructions and measuring on a 2100-Bioanalyzer. Analysis was run in „High Sensitivity DNA" mode. The size-distribution of sequencing libraries from all samples was in the desired range of 500-1000 nt with a medium size of 450 nt. An example of Bioanalyzer results is shown in figure 3.15.3. Prior to library pooling for sequencing, DNA concentration was measured with the Qubit 2.0 Fluorometer with the "Qubit™ dsDNA HS Assay Kit", according to the kit instructions. The use of an exact quantitation method is important to gain a good clustering density on the flow cell and equal amounts of single libraries in the sequencing pool.

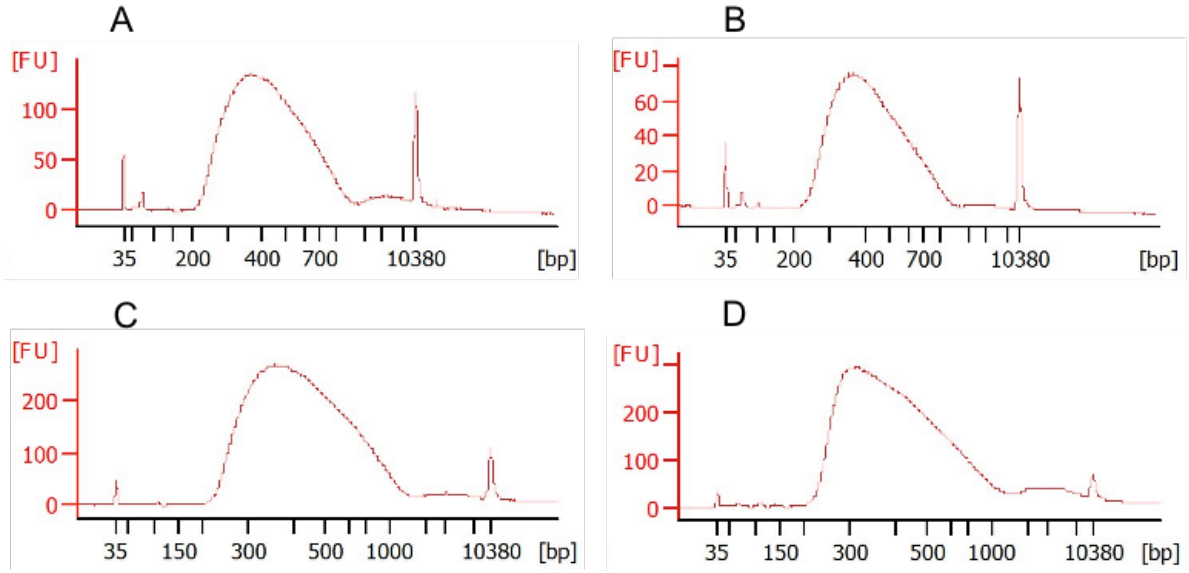

Figure 3.15.3: Example of Bioanalyzer Results for RNA-Sequencing Library Quality Control

Representative examples of Bioanalyzer results of RNA-sequencing libraries from samples
A: PA; B: SP; C: A-SP; D: A-SP

3.15.3 Next Generation Sequencing (NGS)

The samples were sequenced on Illumina "NextSeq® 500" and "HiSeq® 2500" systems, respectively. For sequencing on the NextSeq® system libraries and instrument were prepared according to the manual using the "NextSeq® 500/550 Mid Output Kit v2". The kit contains the flow cell and a cartridge containing all reagents needed for the run and clustering of the flow cell. Before loading, the samples were pooled (8 samples per lane) according to respective DNA concentration, using equal amounts of each sample to yield a final concentration of 4 nM cDNA in the pooled library. The concentration was again checked by "Qubit™ dsDNA HS Assay Kit" and pooled libraries were denatured by 5 min incubation in freshly prepared 0.2 N NaOH. An equal amount of Tris-HCl buffer pH 7 was added to prevent a too high concentration of NaOH in the sequencing reaction and the library was further diluted in a two step procedure to the final loading concentration of 1.8 pM with HT1 buffer. A volume of 1.3 mL was applied to the respective chamber of the cartridge. Flow cell, after thorough cleaning, cartridge and, buffers for the run were loaded onto the instrument and the run was started as „Single Read" for 50 cycles.

For sequencing on the "HiSeq® 2500 system" "HiSeq® Sequencing Kit" was used. The instrument was prepared according to the manual, by inserting sequencing reagents and performing the priming

procedure. The flow cell was inserted and the run was started as „Single Read“ for 50 in cycles in the „Rapid Run“ mode. In contrast to the NextSeq® system, the first step of flow cell clustering was performed according to the manual on a “cBot Clonal Amplification System“ using the „HiSeq Rapid Cluster Kit v2“, which contains the flow cell and reagents for clustering of the flow cell. Pooling and denaturation of the libraries to be sequenced was done as described for the NextSeq® system.
After the run, data were demultiplexed by the instruments software and raw reads obtained in the FASTQ file format [295], which besides the fragments’ sequences contains information on sequencing quality, were used for bioinformatic analyses.

3.16 NGS Data Analysis

3.16.1 Quality Control and Processing of Raw Reads

The quality of raw sequence reads was determined by using the software FastQC. All samples had similar profiles. The overall base quality was between a Phred quality score of 32 and 40. Phred quality score represents the probability that a base call is incorrect (see chapter 3.17.10). The values are Illumina encoded values, which means that the probability for correct base-call was between 99.9 to 99.99%. [296] The per base sequence content at the 5’ end of the read was not random, which is a known bias due to the usage of random hexamer primers for library preparation. [297] This bias can not be fixed by trimming since it is caused by non-random selection for amplified fragments, but it should not seriously affect analysis for differentially expressed genes. In the sequence duplication level plot two peaks were visible, which in DNA sequencing experiments is an indicator for PCR artifacts during library preparation. In contrast, sequence duplication is normal for RNA sequencing since there it is due to the presence of fragments that originate from transcripts with high expression levels. [298] The GC content per read exhibited relatively equal distribution around 50%. This is in the range of the average GC content of human genes (≈ 50%), which is higher compared to average GC content of the whole genome (≈ 40%). A slight shift of the sample curve towards lower GC content compared to the theoretical curve indicates the presence poly-A selected RNA. A shift toward higher GC content would be an indicator of rRNA contamination of the sample. In all samples overrepresented sequences, identified as Illumina adapter sequences, were detected. This is a sequencing artifact, due to sequencing of adapters or sequencing into the adapter at 3’ position of the read. [299] The overrepresented sequences were removed from the datasets with the software Cutadapt 1.16 [218] using the respective primer sequence for each sample and trimming mode for 3’ adapter with an error rate of 5%. Reads shorter than 20 bp after trimming were removed from the datasets. 1 to 2% of all reads were affected by trimming. Trimmed datasets were again analyzed with FastQC. An example of FastQC results is shown in figure 3.16.1.

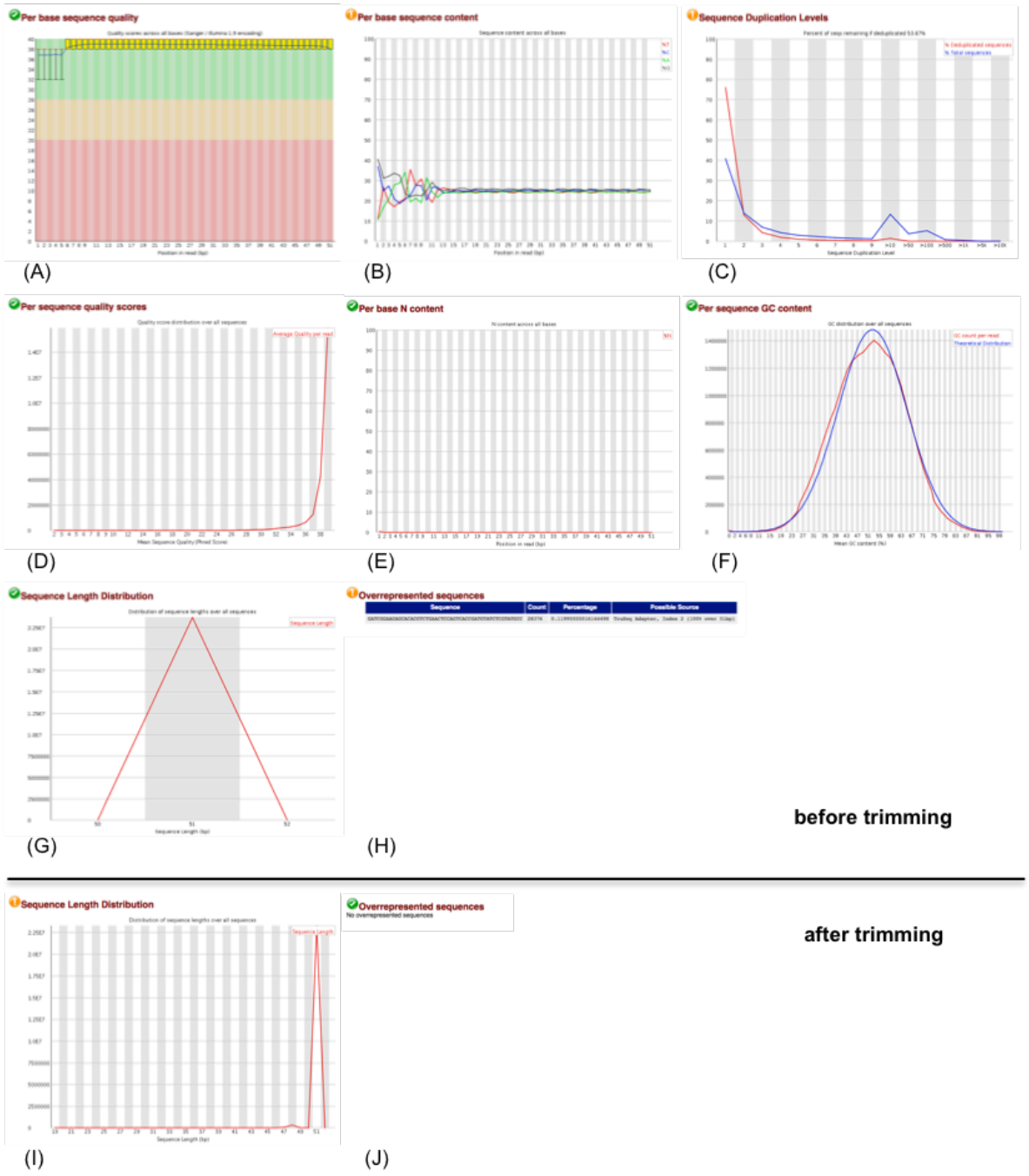

Figure 3.16.1: Example of FastQC results (Sample PA-A-Lane 1)

(A) Phred quality scores across all bases (Illumina 1.5 encoding), (B) Per base sequence content, (C) Sequence duplication levels, (D) GC distribution over all sequences (E) Per sequence quality scores (F) Per base N content (G) Sequence length distribution before trimming (H) Overrepresented sequences before trimming (I) Sequence length distribution after trimming (J) Overrepresented sequences after trimming. All other parameters were not affected by trimming.

3.16.2 Alignment

The sequence alignment on H. sapiens, GRCh38 transcriptome was done using the software HISAT2 version 2.1.0 using the standard settings for unpaired reads [221]. For conversion of the text encoded SAM files to binary encoded BAM files the software SAMtools version 1.8 was used [222].

3.16.3 Quantitation and Differential Gene Expression Analysis (DGE)

Further analysis of the aligned reads was performed using SeqMonk Package.

Aligned reads with a mapping quality score (Q_{MAP}) of 30 (representing a 0.01 probability for wrong mapping position, see chapter 3.17.10) were chosen for analysis of differential gene expression and SAM files containing the data were imported to SeqMonk accordingly. Homo sapiens genome release GRCH38_v90 was used for the analysis. Quality control of data was performed using the RNA-Seq QC plot option. The data were quantitated as raw counts using the RNA-Seq quantitation pipeline for mRNA Non-strand specific libraries and the „merge transcript isoform“ option. Homo sapiens CRch38_v90 was used for annotation and alignment.

The data were further processed by removing data for genes that had a number below 10 raw counts per gene in at least 3 of the 3 replicate stets of one sample (Expressed Genes), also genes with no description as well as probes resulting from read-through of genes and mitochondrial and rRNA genes were removed from the datasets before analysis (Expressed-C).

To obtain differentially expressed genes, the three datasets PA, SP and A-SP (AS) containing the three biological replicates (A-C) were compared pairwise (see table 3.16.1) using the R-based DESeq2 filter implemented in SeqMonk with a significance limit set below 0.01 after Benjamini and Hochberg correction. The biostatistics tool DESeq2 applies algorithms that assume a negative binomial distribution of data as a natural extension of Poisson distribution to account for biological variability of replicates, as well as flexible data-driven relationships between mean and variance for detection genes that are significantly differentially expressed. [300] [301]

After DESeq comparison the data were re-quantified to log transformed length corrected values. In this step also corrections for DNA contaminations were performed.

The resulting number of data (differentially expressed gene numbers in the range of 5100-9300) was still too high for further analyses. Therefore a refinement was done using two options:

- data were selected for “Intensity Difference“ (ID) with a minimum p-value when comparing two datasets to be below 0.05 with multiple testing correction applied with a sample size of 100-1000 when constructing the control distributions. The resulting differentially expressed gene numbers ranged from 59-82.
- genes with differences in expression value of 2-20 RPM between both samples were chosen manually from the scatter plot view (DESeq+Man) for further analysis. The resulting differentially expressed gene numbers ranged from 242 to 823.

To obtain genes, which are specifically expressed in each of the cell lines, the obtained gene lists from the two comparisons of the cell lines (see table 3.16.1) were combined using the logical combination AND. In this way also spheroid-specific and serum-specific genes were extracted by combining gene lists from respective samples. To remove genes that were expressed in a cell type specifically, these were subtracted using the logical list combination BUTNOT.

DESeq	(Man/ID/GSEA)	(Man/ID/GSEA)	(Man/ID/GSEA)
PA-SP	PA up (SP)	SP up (PA)	
PA-AS	PA up (AS)		AS up (PA)
SP-AS		SP up (AS)	AS up (SP)
Combination	PA+PA	SP+SP	AS+AS

Combination	Result	Combination	Result
SP up (PA) AND AS up (PA)	SP+AS	BUTNOT AS+AS, SP+SP	Spheroid
PA up (SP) AND AS up (SP)	PA+AS	BUTNOT AS+AS, PA+PA	Serum

Table 3.16.1: Diagram of Dataset Comparison Combinations

Upper Table: data were compared pairwise using the DESeq algorithm resulting in lists of differentially expressed genes (column 1). Up-regulated gens in respective cell line datasets were extracted using manual expression difference filtering (Man) or statistical intensity difference (ID) filtering of the data. Column 2: lists of genes up-regulated in PA. Column 3: lists of genes up-regulated in SP. Column 4: lists of genes up-regulated in SP. These data were used for GSEA. Line 5: Cell line specific genes were extracted by combining the lists using the logical combination AND (PA+PA, SP+SP, AS+AS). Lower table: up-regulated genes in serum or spheroid-derived cells were obtained by combination of lists for respective cell lines (column 1) and subtraction of cell line specific genes using the logical combination BUTNOT (column 3).
ACC: adherent culture conditions, AS adherently grown spheroids, A-SP: SP cells grown under ACC for 2 weeks, GSEA: gene set enrichment analysis, PA: parental cell line, SP: spheroid cells derived from PA, Cell line specific gene lists: for PA = PA+PA, for SP = SP+SP, for AS = AS+AS.

3.16.4 Gene Set Enrichment Analysis (GSEA) using GeneAnalytics™

Gene set enrichment analysis (GSEA) is a statistic based method, which determines if a gene set contains a signature similar to pre-defined gene modules comprising known gene sets of various numbers and phenotypes (molecular functions, biological processes, diseases, tissues or cells, signal transduction pathways). The gene modules are derived from different databases (e.g. Gene Ontology (GO), KEGG-Pathways, Reactome Pathways, WiKi-Pathways), which provide respective gene classifications.

The obtained gene lists from DGE analysis were tested for enriched gene sets using the GeneAnalytics™ software. A maximum of 409 genes was submitted for analysis. For samples with more than this number, the lists were sorted according to fold change of expression and the 370-409 genes (depending on expression levels) with highest difference in expression were submitted for analysis. The resulting Data were manually inspected for relevant information. The scores provided by the program are (-log2) transformed p-values, derived of a binomial distribution-based test for over-representation of the investigated genes in any compound from SuperPath or GO-terms databases. Three categories are indicated: high: corrected p-value smaller or equal to 0.001, medium: corrected p-value higher than 0.001 but less than 0.05, and low: corrected p-value higher than 0.05.

3.17 Calculations and Statistical Methods

3.17.1 Calculation of Growth Rate

$$\text{Growth rate per day} = \frac{\text{Total number of cells at passage}}{\text{Number of cells seeded} \times \text{Time of culture to passage (days)}}$$

3.17.2 Calculation of Accumulated Cell Number

$$\text{ACN } (P_n) = \sum_{n=0}^{n} \text{SCN } (P_{n-1}) \times \text{GRD } (P_n) \times t\ (P_n)$$

ACN = Accumulated cell number

SCN = Starting cell number

GRD = Growth rate per day

t = Time of culture (days)

(P_n) = Passage number n

$\text{SCN } (P_{n=0}) = 10^5$

Starting cell number for frozen aliquots was cell number obtained in passage of freezing of the cells

3.17.3 Calculation of Clonal Spheroid-Forming Efficiency (CSFE)

$$\text{CSFE \%} = \frac{\text{Mean (number of live cells seeded in 15 to 60 wells)}}{\text{Mean (number of spheroids in respective wells)}} \times 100$$

3.17.4 Calculation of Colony-Forming Efficiency (CFE) in Soft Agar Assay

$$\text{CFE \%} = \frac{\text{Number of cells seeded/well}}{\text{Number of colonies/well}} \times 100$$

$$\text{Number of colonies per well} = \frac{\text{Area}_{\text{well total}}}{\text{Area}_{\text{section analyzed}}} \times \text{Number of counted colonies}$$

3.17.5 Calculation of RNA Concentration

Beer-Lambert-Law: $A_\lambda = \varepsilon \times c \times d$

A_λ = $\text{absorption}_{\text{wavelength}}$

ε = molar extinction coefficient

d = path length of cuvette

$c\ \mu g/mL = (A_{260}\text{-}A_{320}) \times 2 \times (0.025\ (\mu g/mL/cm)^{-1} \times 0.1\ cm)^{-1}$

3.17.6 Calculation of Fold Change Expression Level in Flow Cytometric Immunophenotyping

$$\text{Fold change expression} = \frac{\text{Geo mean of antibody stained sample}}{\text{Geo mean of isotype control stained sample}}$$

3.17.7 Calculation of (Arithmetic) Mean, Geometric Mean, Median

$$\frac{1}{n}\left(\sum_{i=1}^{n} x_i\right) = \bar{x} = \text{(arithmetic) Mean}$$

$$\left(\prod_{i=1}^{n} x_i\right)^{\frac{1}{n}} = \text{Geometric Mean (GM)}$$

The median is the middle value of a numerically ordered dataset in case of an odd number of data or the mean of the two middle values of a numerically ordered dataset in case of an even number of data.

The values were calculated using Excel software.

x_i = observed value

n = number of values

3.17.8 Calculation of Standard Deviation

$$\sqrt{\frac{\sum_{i=1}^{n}(x_i \times \overline{x})^2}{(n-1)}} = \text{Standard Deviation (STD)}$$

x_i = observed value

$\overline{x}$ = (arithmetric) Mean

n = number of values

3.17.9 Determining Significance of Differences between Mean Values

Two-tailed Student's t-test using the Welch's correction for unequal variance was carried out to determine statistically significant difference between mean values. P <0.05 was considered as significant. Calculations were done using Excel software.

3.17.10 Phred Quality Scores (Q)

3.17.10.1 Sequencing Quality score (QSanger) [296]

$$Q_{Sanger} = -10 \times \log_{10} p$$

p = probability for incorrect base call (method of calculation differs for different instruments)

3.17.10.2 Mapping Quality score (Q_{MAP})

$$Q_{MAP} = -10 \times \log_{10} p$$

p = probability for wrong mapping position (method of calculation differs for different aligners)

(a value 255 indicates that the mapping quality is not available)

3.17.11 RNA Sequencing Quantification

The output data from RNA sequencing are sequence reads from fragments, which have to be subsequently aligned to a genome or transcriptome sequence. The number of reads that align to a specific gene then can be counted, obtaining a quantitative measure. The resulting information represents a relative measure of molar concentration of an individual mRNA to total mRNA analyzed. It does not represent an absolute measure for the abundance of an individual mRNA in a cell, since individual information on the measured cells (cell number, cell size, cell volume, cellular composition) is missing. For comparison of different genes or different samples, values have to be normalized for transcript length and sequencing depth by calculating RPKM or TPM values. [302] [303]

3.17.11.1 RPKM (Reads per Kilobase per Million Reads)

For quantitative comparison of different genes within the same dataset RPKM values, which correct for different transcript length and total library coverage, can be used. [302] These are calculated:

$$\mathrm{RPKM_g} = \frac{\frac{\mathrm{r_g} \times 10^3}{\mathrm{fl_g}}}{\frac{\mathrm{R}}{10^6}} = \frac{\mathrm{r_g} \times 10^9}{\mathrm{fl_g} \times \mathrm{R}}$$

$\mathrm{g} = \text{gene of interest}$

$\mathrm{G} = \text{all genes determined at experiment}$

$\mathrm{r_g} = \text{reads mapped to particular gene region}$

$\mathrm{fl_g} = \text{feature length (number of nucleotides in gene, i.e. total length of exonic region)}$

$\mathrm{R} = \text{sequencing depth} = \text{total number of reads from sequencing run} = \sum_{\mathrm{g} \in \mathrm{G}} \mathrm{r_g}$

Normalization for transcript length: $\frac{\mathrm{r_g} \times 10^3}{\mathrm{fl_g}}$

Normalization for sequencing depth: $\frac{\mathrm{R}}{10^6}$

3.17.11.2 TPM (Transcripts per Million)

For quantitative comparison of genes from different samples TPM values are calculated. TPM values are proportional to RPKM within one sample. For calculation of TPM normalization is done to transcript copies instead of reads so that the values are more consistent across different samples. [303]

$$TPM = \frac{r_g \times rl \times 10^6}{fl_g \times T}$$

$\mathrm{r_g} = \text{reads mapped to particular region}$

$\mathrm{fl_g} = \text{feature length (number of nucleotides in gene, i.e. total length of exonic region)}$

$\mathrm{rl} = \text{read length (average number of nucleotides mapped per read)}$

$\mathrm{T} = \text{total number of transcripts sampled in sequencing run} = \sum_{\mathrm{g} \in \mathrm{G}} \frac{\mathrm{r_g} \times \mathrm{rl}}{\mathrm{fl_g}}$

3.18 Copyright Statement

4 Results

4.1 Generation of Different Cell Lines

The aim of this work was to investigate cells with cancer stem cell (CSC) characteristics in a clear cell renal cell carcinoma (ccRCC) cell line, which was derived from the primary tumor material of a female patient with ccRCC. This cell line, which is certified for clinical use in humans and has already been employed in a four-fold gene-modified version in clinical trials, is termed parental cell line (PA) throughout this thesis. Central to all experimentation was the enrichment as well as the induction of stem cell, respectively cancer stem cell, characteristics by using the spheroid cell culture method. Spheroid cell cultures were first described for isolation of neuronal stem cells and subsequently used for isolation of stem cells from other sources, namely solid tumors, to gain CSC.

Several aliquots (A-O) of the parental ccRCC cell line (PA) were grown separately under standard conditions in serum-containing medium as adherent monolayers (ACC) for various periods, ranging up to more than 60 weeks. Spheroid cell lines were derived from PA by using two different starting conditions.

Firstly, spheroid cell lines were generated by culturing PA cells at passage 28 as “bulk” culture under serum-free, non-adherent spheroid culture conditions (SCC) with regular passaging. The resulting cell lines were termed SP (spheroid) cells. Three SP cell lines were independently established in this way (SP1-3), of which SP1 and SP3 were cultured for more than 60 weeks continuously. Aliquots of the cells were frozen at different passage numbers and later assayed either in parallel or at different time points.

Secondly, spheroid cell lines were also generated from spheroids derived from the “Neurosphere Assay” (NSA, see chapter 3.1.3), since it had been observed that these were morphologically distinct from SP spheroids. In contrast to starting conditions used for SP cells, in the NSA cells were plated at very low (clonal) densities and were grown without disaggregation of spheroids for 3-5 weeks. Additionally, at start of “bulk” culture of these cells, the passaging and thus disaggregation intervals were longer than those used for SP cells. The resulting cell lines were termed CS (clonally amplified spheroids). Seven cell lines were established in this way (CS1-7), of which CS1 and CS7, which slightly differed in cell size and spheroid morphology (see figure 4.1.4), were further characterized. Aliquots derived of frozen cells of CS1 and CS7 cell lines at passage 6 and 5 respectively were grown for periods of more than 60 weeks continuously.

To discriminate spheroid cell lines frozen at different passage numbers from continuously cultured cell lines, these cells were named according to the passage number of freezing, e.g. SP1.7, SP1.35, SP3.13. When several aliquots from frozen cells were cultured separately, these were discriminated by additional numbers, e.g. SP1.80-2, SP1.35-3. And cells obtained by freezing of thawed aliquots again were termed by subsequent numbering of both freezing passage numbers, e.g. SP1.35.7.

To investigate whether the differences seen in SP and CS cell lines compared to the PA cell line were immanent or simply induced by the different growth conditions, spheroid cell lines were also re-cultured under ACC. The resulting cell lines were named A-SP or A-CS according to their parental spheroid cell line. The passage number of spheroid cell line used to start adherent culture is indicated in the name, e.g. A-SP-P14, A-SP-P30. A-SP-P30, A-CS1-P7, and A-CS7-P6 were cultured

continuously under adherent conditions for more than 35 weeks. A-SP cells were also assayed for their ability to re-grow as spheroids after various culturing periods under ACC. These cells were termed A-SP-SC. In figures 4.1.1 and 4.1.2 the genealogy of cell lines used in this work is depicted.

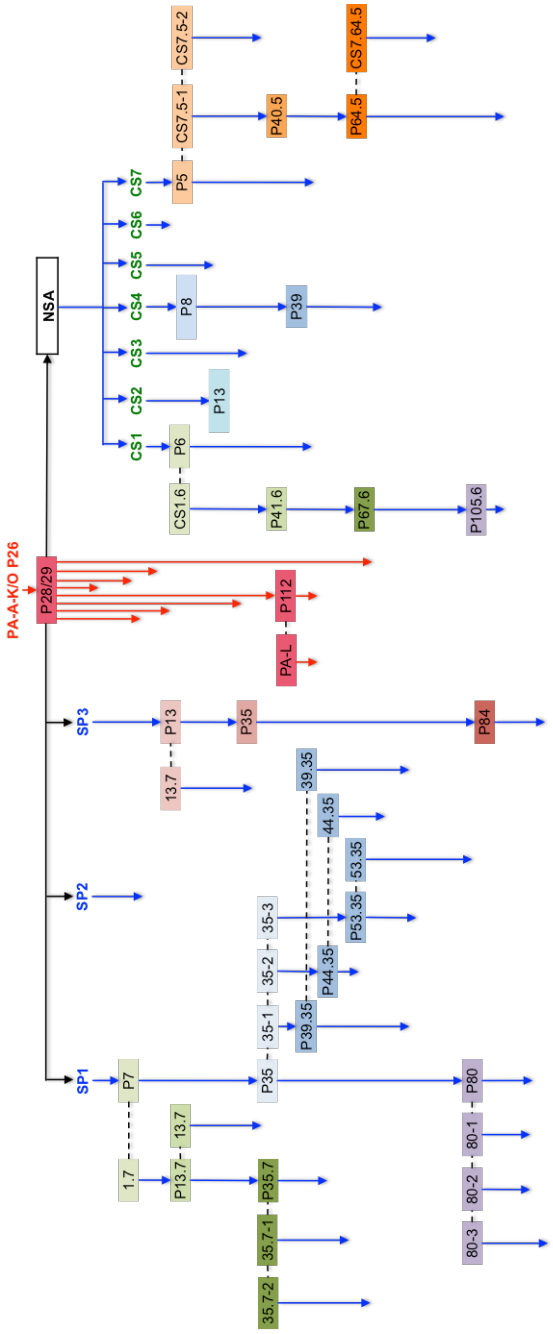

Figure 4.1.1: Genealogy of Cell Lines Used

Two distinctive spheroid cell lines SP and CS were derived from PA ccRCC cell line at passage 28/29 (middle, red). Several aliquots of PA cells were cultured separately (PA-A-O) for different periods. Three separate SP cell lines were generated (SP1-3), of which two were cultured for long time under SCC. Seven separate CS cell lines were obtained from NSA of PA cells, of which three were grown for long time under SCC, and two were characterized in more detail. At different passages (indicated) aliquots of the cell lines were frozen and later re-grown (dashed line). Cell lines were named after number of freezing passage (indicated). Blue arrows indicate continuous culture under SCC, red arrows indicated continuous culture under ACC.
ACC: adherent culture conditions, CS: clonally expanded spheroid cells derived from PA, NSA: „Neurosphere Assay“, P: passage number, PA: parental cell line, SCC: spheroid culture conditions, SP: spheroid cells derived from PA.

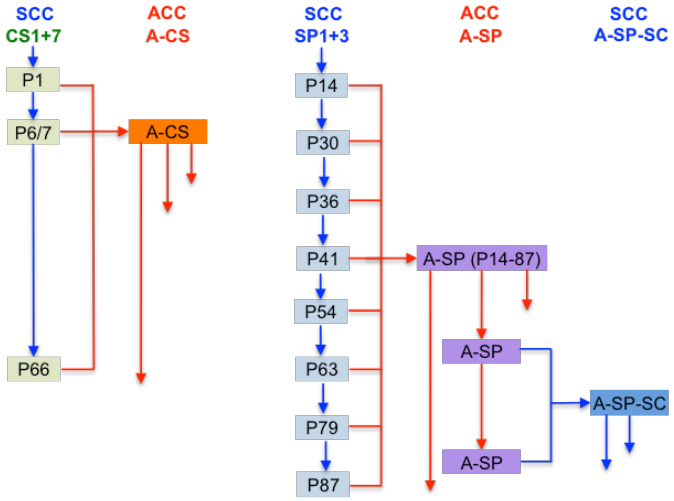

Figure 4.1.2: Genealogy of A-CS, A-SP, and A-SP-SC Cell Lines

Left: A-CS cell lines were generated from CS1 or CS7 cell lines in different passages (as indicated) and cultured for various time under ACC.
Right: A-SP cell lines were generated from SP1 or SP3 cell lines in different passages (as indicated) and cultured for various time under ACC. Some of the cells were re-grown under SCC for various periods.
Blue arrows indicate continuous culture under SCC; red arrows indicated continuous culture under ACC.
ACC: adherent culture conditions, A-CS: CS cells grown under ACC, A-SP: SP cells grown under ACC, A-SP-SC: A-SP cells re-cultured under SCC, CS: clonally expanded spheroid cells derived from PA, P: passage number, PA: parental cell line, SCC: spheroid culture conditions, SP: spheroid cells derived from PA.

4.1.1 Morphology of Cells under Adherent Culture Conditions (ACC)

The morphology of PA cell line and spheroid cell lines grown under adherent culture conditions in serum-containing medium (ACC) at almost confluence is shown in figure 4.1.3. No remarkable morphological differences were observed between PA cells and A-SP or A-CS1 cells, only A-CS7 morphology was slightly more homogenous when compared to other cell lines.

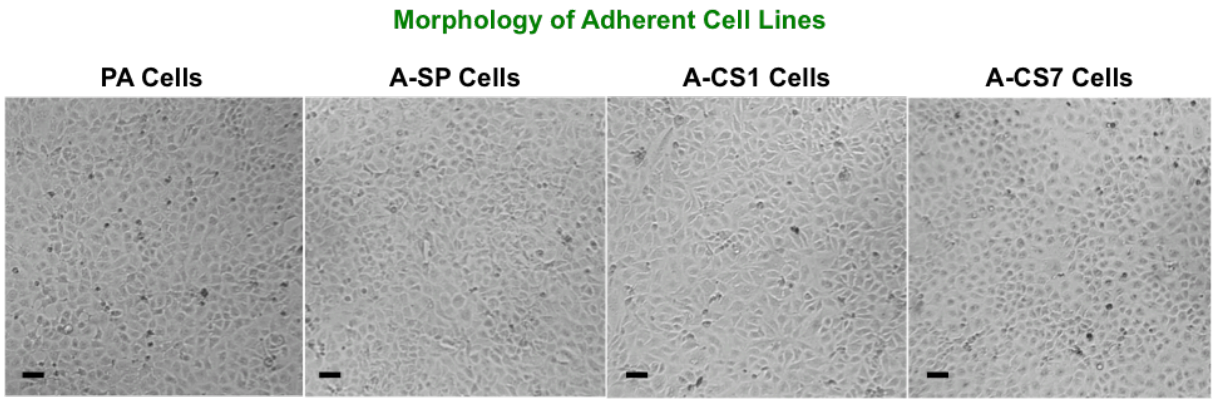

Figure 4.1.3: Morphology of Adherently Grown Cell Lines PA, A-SP, and A-CS

Microscopic pictures showing representative morphologies of PA cells and spheroid cell lines SP, CS1, CS7 grown for at least 3 passages under ACC (A-SP-P54, A-CS1-P6 and A-CS7-P7). Scale bars: 100 µm.
ACC: adherent culture conditions, A-CS: cells grown under ACC, A-SP: SP cells grown under ACC, CS: clonally expanded spheroid cells derived from PA, PA: parental cell line, SP: spheroid cells derived from PA

4.1.2 Spheroid Morphology

The cells and respective spheroids generated from bulk culture (SP) or from clonally expanded cells (CS) were found to be clearly distinctive by their different morphology. SP cells were larger and formed spheroids in which single cells could clearly be discriminated in enlarged view. CS cells in contrast were smaller and formed very compact spheroids, albeit the size and compactness of spheroids varied slightly between different CS cell lines. Representative microscopic pictures of disaggregated spheroid cells from SP, CS1 and CS7 cell lines and spheroids grown thereof within the passaging period of 3-5 days are shown in figure 4.1.4.

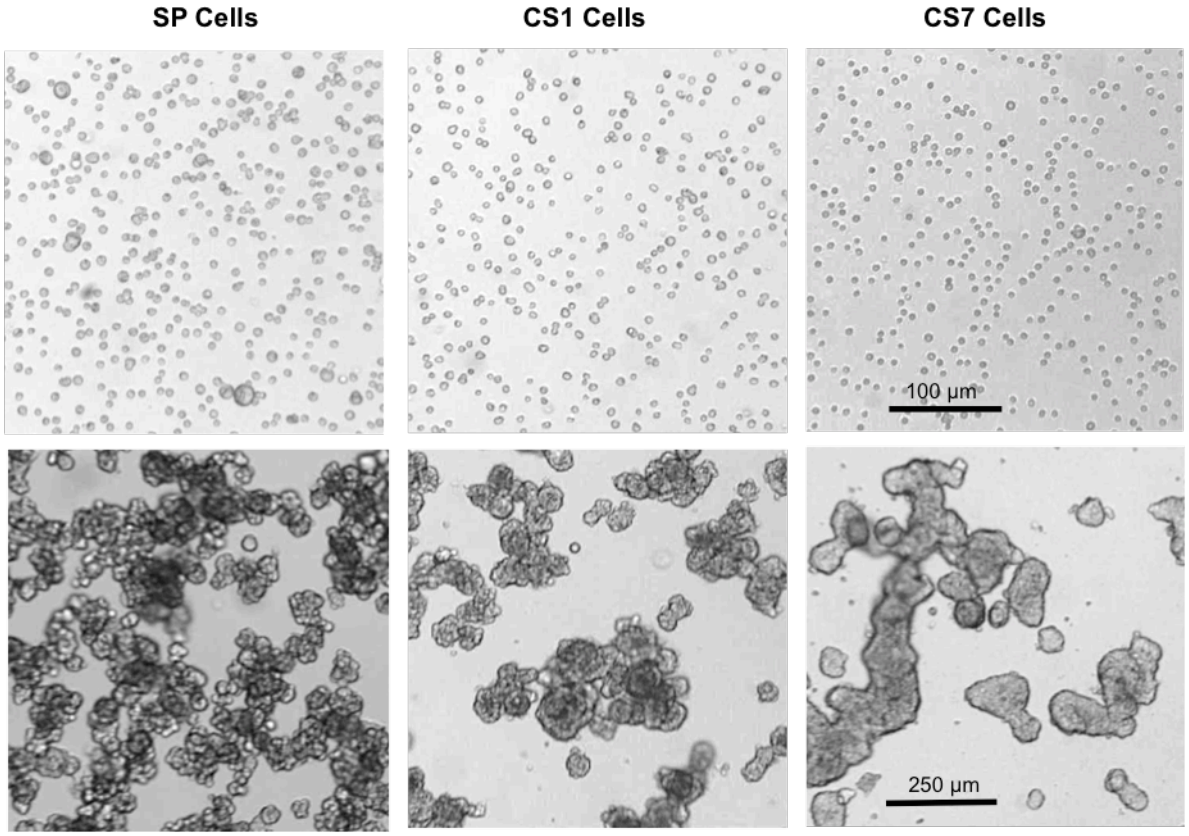

Figure 4.1.4: Different Morphology of Spheroids and Cells from Spheroid SP and CS Cell Lines

Spheroid cell lines show differences in spheroid compactness and cell size, with large cells forming loose spheroids seen in SP cell line, smaller cells forming more compact spheroids in CS1 cell line and very small cells forming highly compact spheroids in CS7 cell line.
Microscopic pictures of SP, CS1, and CS7 cells after dissociation with AccuMax™ (upper row) and following growth for 4 days under SCC (lower row). Scale bars indicated are valid for the respective rows.
CS: clonally expanded spheroid cells derived from PA, PA: parental cell line, SP: spheroid cells derived from PA

4.1.3 Cell Size and Viability

The cell size for PA, SP and CS7 cell lines was determined in single cell suspensions at every passage over a period of 4 weeks using the "CASY®" cell counter for cell lines in different passage numbers, obtained by thawing cells that were cultured before freezing for different periods. Similarly, the mean diameter of A-SP cells derived from different passages of SP cells (P14, P36, and P54) and A-CS7-P66 cells, which were all grown for 12 weeks under ACC at start of measurements, was determined.

The results are shown in figure 4.1.5. Thereby a reduction of cell size with time of culture was observed in PA, SP and CS7 cell lines. The average cell diameter of PA cells decreased slightly from 21.2 µm ± 0.5 µm in early passages (P24-29) over 20.8± 0.5 µm diameter (P46-56) to 19.8 ± 0.5 µm in high passage cells (P112-119). The mean diameter of SP cells assayed in P33-40 was determined to be 21.1 ± 0.2 µm, whereas in later passages (P55-62) the cell size decreased to 18.9 ± 0.2 µm and was further reduced (18. 6 ± 0. 2 µm) in cells in P73-80. Compared to PA and SP cell lines, CS7 cells were markedly smaller with a mean diameter of 15.0 ± 0.2 µm in P25-31, which further decreased to 13.7 ± 0.3 µm in cells at P60-66. CS7-P64 cells cultured under ACC with a mean diameter of 17.1 ± 0.7 µm were larger than their parental spheroids. The determined mean diameter of A-SP cells was found to be in the range of 20 µm and was only slightly reduced in cells derived from higher passage spheroids (mean diameters: 20.1/20.2/19.6 ± 0.5 µm for A-SP-P14/P36/P54).

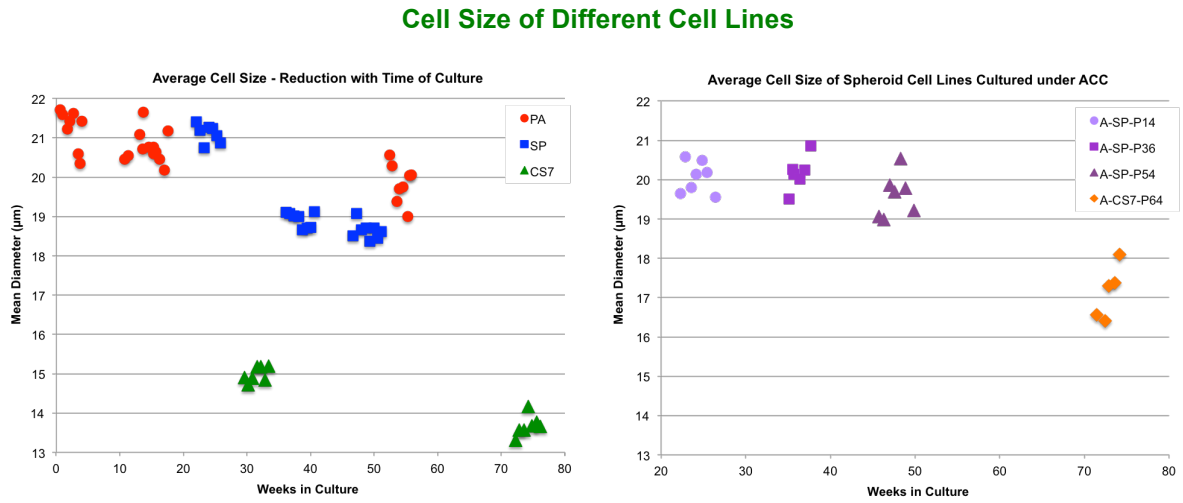

Figure 4.1.5: Variation of Cell Size in Different Cell Lines and with Time of Culture

Cell size differs between PA, SP and CS7 cell lines and decreases with time of culture for these cell lines.
A-SP cells show only low variations in cell size despite different time of culture as spheroids before ACC. The diameter of A-CS7 cells is markedly increased compared to parental spheroid cell line.
Cell size of cells cultured for different periods under their respective conditions was determined using "CASY®" cell counter at every passage over a period of 4-5 weeks. Each value depicted represents the mean diameter of single cell suspensions determined in three measurements of one sample.
Left diagram: Mean diameters of PA, SP, and CS7 cells after different time in culture, obtained by thawing cells that were frozen at different passage numbers. Right diagram: Mean diameters of A-SP-P14, -P36, -P54, and A-CS7-P66 cells. All cells were cultured for 12 weeks under ACC at start of measurements.
ACC: adherent culture conditions, A-CS7: CS7 cells grown under ACC, A-SP: SP cells grown under ACC, CS7: clonally expanded spheroid cells derived from PA, P: passage number, PA: parental cell line, SP: spheroid cells derived from PA

Besides the cell size also the viability of cells was assayed in the "CASY®" measurements. The viable cell fraction was determined to be relatively constant at 91±2% in all assayed cell lines. SP cells in lower passage numbers (P33-39) were the only exception, with a reduced viable cell fraction of 85±3%. This was not surprising, since during the first passages of SP cells, a considerable number of dead cells was observed, which decreased continuously but slowly with further passaging.

4.1.4 Growth Rate and Proliferative Potential of Different Cell Lines

For all cell lines at each passage, the total cell number obtained was determined and the growth rate per day was calculated (see chapter 3.17.1). In figures 4.1.6 and 4.1.7 the resulting values for all investigated cell lines over long-term culturing of the cells are shown. The different cell lines were shown to possess individual growth rates, which within one cell line were relatively stable for different aliquots used, but increased in PA, as well as in spheroid cell lines SP and CS with time of culture (age) of the cells.

In the PA cell line a slight gradual increase of growth rates per day from 0.9 -1.3 over the first 300 days was observed, which was followed by a massive increase to growth rates up to 2.5-3 per day after this period.

In SP cell line during the first passages still many cells died and spheroid morphology was often irregular, but with further passages, the number of death cells was reduced and the spheroid morphology became more regular. This was reflected in the very low growth rates below 0.5 per day during the first passages of the cells. After the first 50 days of culture under SCC a constant but slow increase of growth rates was observed from about 0.5 per day at 100 days of culture to 0.8-1 in the period to 300 days in culture. After very long culturing periods a growth rate of 1.5 per day was reached. Compared to PA cells, the growth rates of SP cells, especially at the beginning of SCC, were strongly reduced and the normal growth rate range of PA cells was reached by this cell line after about 200 days of culture. Besides the higher number of dead cells, the lower growth rates may also reflect lower proliferation rates of spheroid cells.

Similar to SP cell lines, CS cell lines showed low growth rates per day at the beginning of bulk culture, which was started at about 30 days after start of spheroid culture, in which the cells were grown as spheroids in the NSA. In CS7 cell line at the beginning of the culturing period as bulk spheroids, high variations in growth rates were obtained, which are probably due to the variations in passaging periods of the cells, which were with 6-9 days longer than the those used for subsequent passaging. Starting at about 100 days under SCC, the cells showed relatively stable growth rates in the range of 0.8-0.9 per day. Interestingly, after about 300 days of culture for CS7 cell line a massive increase of growth rates was observed reaching values of about 2 per day after 350 days of culture. In CS1 cell line the increase after 300 days of culture was less pronounced and the mean maximal growth rates observed in this cell line were about 1.1 per day.

Of note is, that the changes in growth rates with culturing periods seemed to be inherent to the cells, since they were on the one hand seen in two different SP cell lines, cultured independently, but also from aliquots that were frozen at different time points and propagated later, showing similar growth rates and changes thereof as the original cell lines. Though repeatedly frozen cells seemed to possess slightly higher growth rates than their parental continuously grown cell line, which might indicate a positive selection process of more viable cells with higher proliferative capacity by the cell freezing procedure. Similar, CS7 cells frozen in P64 and re-seeded were shown to possess the high growth rate seen in the parental cell line at high passage numbers. Likewise, PA cells frozen at passage 112 (PA-L) proliferated with similar high growth rate as the continuously grown cells they were frozen of.

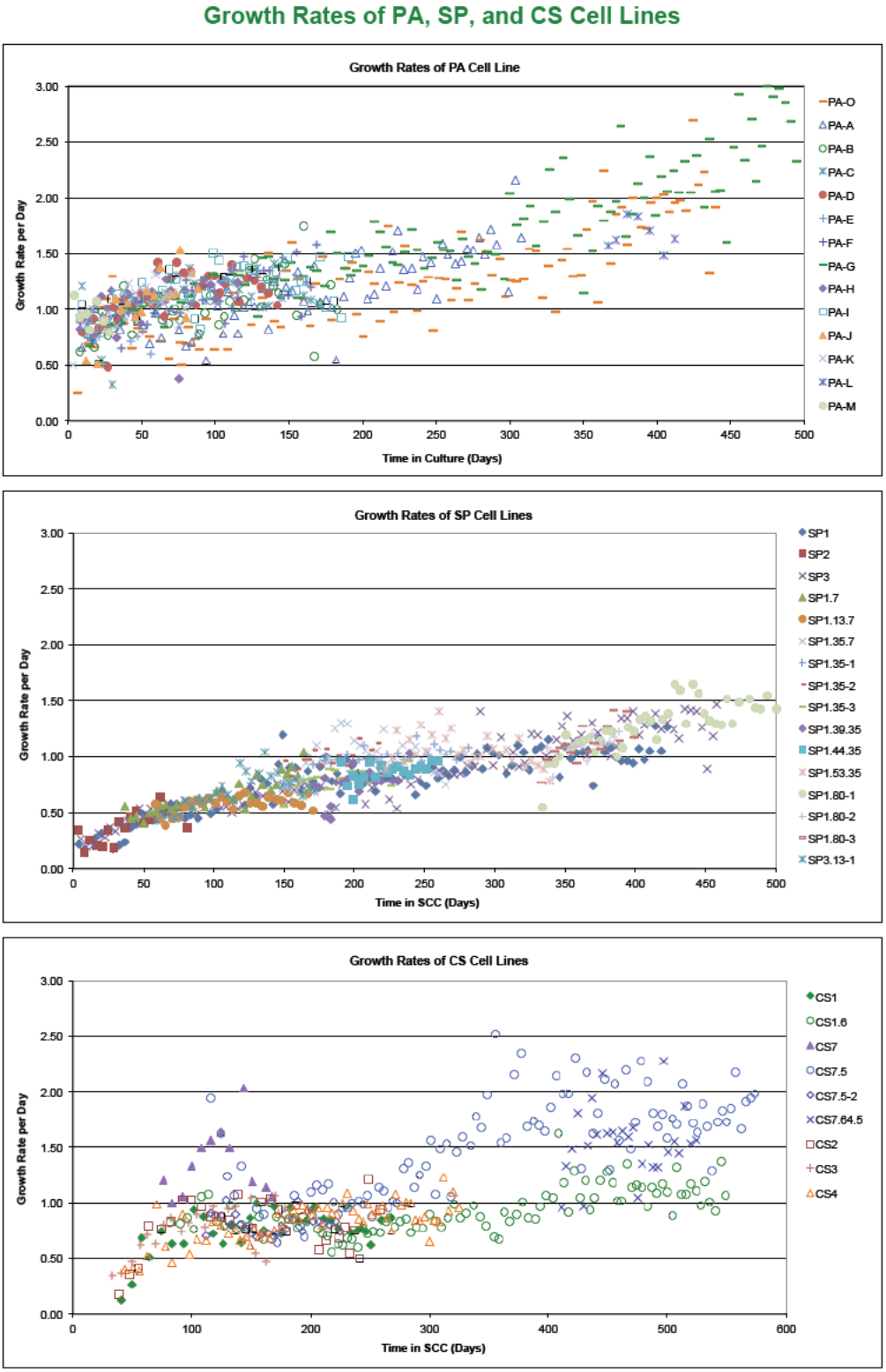

Figure 4.1.6: Growth Rates of PA, SP, and CS Cell Lines over Time in Culture

PA, SP and CS cell lines show different and cell line specific growth rates, which increase with time of culture of the cells.
Growth rate per day (PA upper panel, SP middle panel, and CS lower panel) is plotted vs. time in culture under the respective growth condition (ACC for PA cell line and SCC for SP and CS cell lines). Letters indicate different independently grown aliquots of PA cells (PA-L are PA-O cells frozen at passage 112). Numbers indicate the different SP or CS cell lines, which were independently generated from PA (SP: 1-3, CS: 1-7). Cells obtained from frozen cells are indicated by a dot, followed by the passage number(s) of freezing. Dash indicates different aliquots used. ACC: adherent culture conditions, CS: clonally expanded spheroid cells derived from PA, PA: parental cell line, SCC: spheroid culture conditions, SP: spheroid cells derived from PA

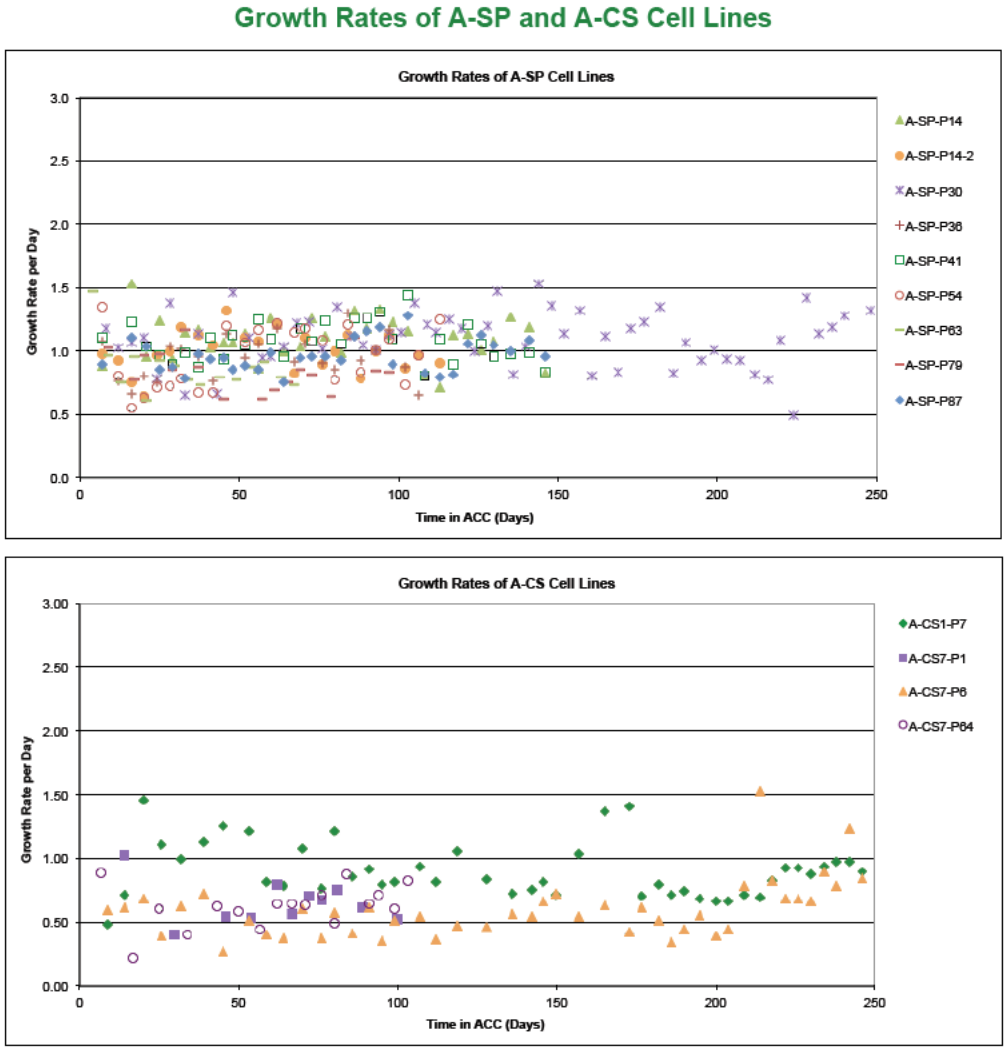

Figure 4.1.7: Growth Rates of A-SP and A-CS Cell Lines over Time under ACC

A-SP and A-CS show different and cell line specific growth rates, which are independent of passage number of spheroid cell lines, used at start of ACC and remain relatively constant over the investigated culturing periods.
Growth rate per day of A-SP and A-CS cell lines (A-SP upper panel, A-CS lower panel) is plotted vs. time in culture under ACC. The passage of spheroid cell line used for generation of A-SP or A-CS cell lines is indicated (-P14). A-CS14 was generated independently twice (-P14-2).
ACC: adherent culture conditions, A-CS: CS cells grown under ACC, A-SP: SP cells grown under ACC, CS: clonally expanded spheroid cells derived from PA, P: passage number, PA: parental cell line, SCC: spheroid culture conditions, SP: spheroid cells derived from PA

Also the growth rates of spheroid cell lines grown under ACC were determined (see figure 4.1.7) and found to be relatively constant over time in culture with values of about 1 per day for A-SP cell lines, which was in the range of growth rates seen for PA cells. Interestingly no correlation with passage number of spheroids was seen, when the cells were grown under ACC. For example the growth rate of P14 SP spheroids was below 0.5 per day, whereas the growth rates of A-SP-P14 cells were in the range of 1 per day right from the start of ACC. The growth rates of A-CS7 cells with about 0.5 per day were lower than those seen for A-SP or A-CS1 cells and did also not to be dependent on the passage number of spheroids used for start of ACC. Only one A-CS1 cell line was grown over longer periods under ACC, and the relatively high variation seen for the growth rates of these cells may be in part due to variations in passaging periods used for this cell line.

Proliferative Potential of PA, SP, and CS Cell Lines

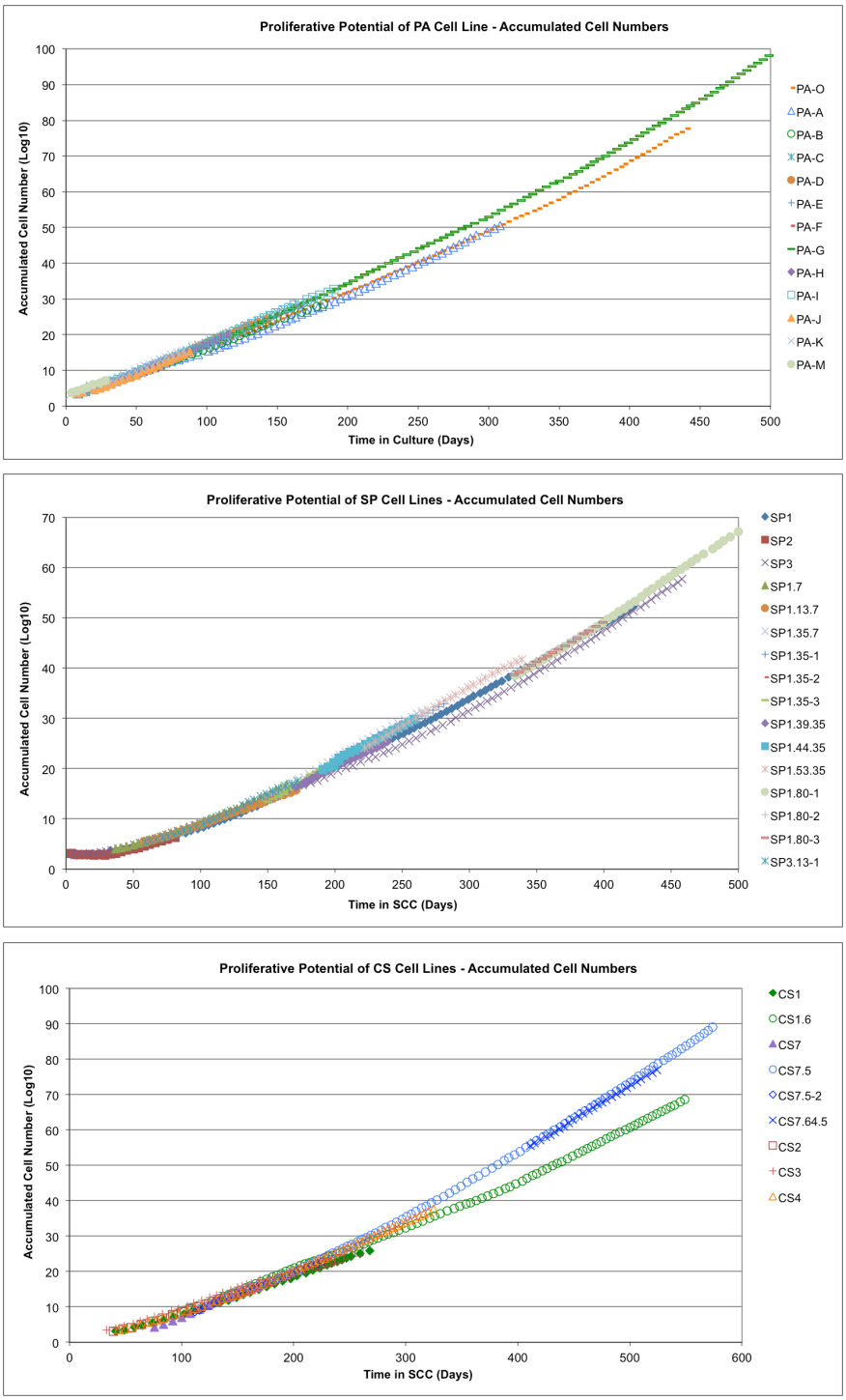

Figure 4.1.8: Proliferative Potential of PA, SP, and CS Cell Lines - Accumulated Cell Numbers

PA, SP and CS cell lines show high proliferative potential, as shown by constant increase of cell numbers, even after long-term culture of the cells.
Log10 of accumulated cell numbers of all investigated cell lines (PA upper panel, SP middle panel, and CS lower panel) is plotted vs. time in culture under the respective growth condition (ACC for PA cell line and SCC for SP and CS cell lines). Letters indicate different independently grown aliquots of PA cells. Numbers indicate the different SP or CS cell lines, which were independently generated from PA (SP: 1-3, CS: 1-7). Cells obtained from frozen aliquots of this cell lines are indicated by a dot, followed by the passage number(s) of freezing. Dash indicates separate culture of similar aliquots. For frozen cells, the cell numbers from passages of freezing were used as the starting numbers for calculation of accumulated cell numbers. ACC: adherent culture conditions, CS: clonally expanded spheroid cells derived from PA, PA: parental cell line, SCC: spheroid culture conditions, SP: spheroid cells derived from PA

Proliferative Potential of A-SP and A-CS Cell Lines

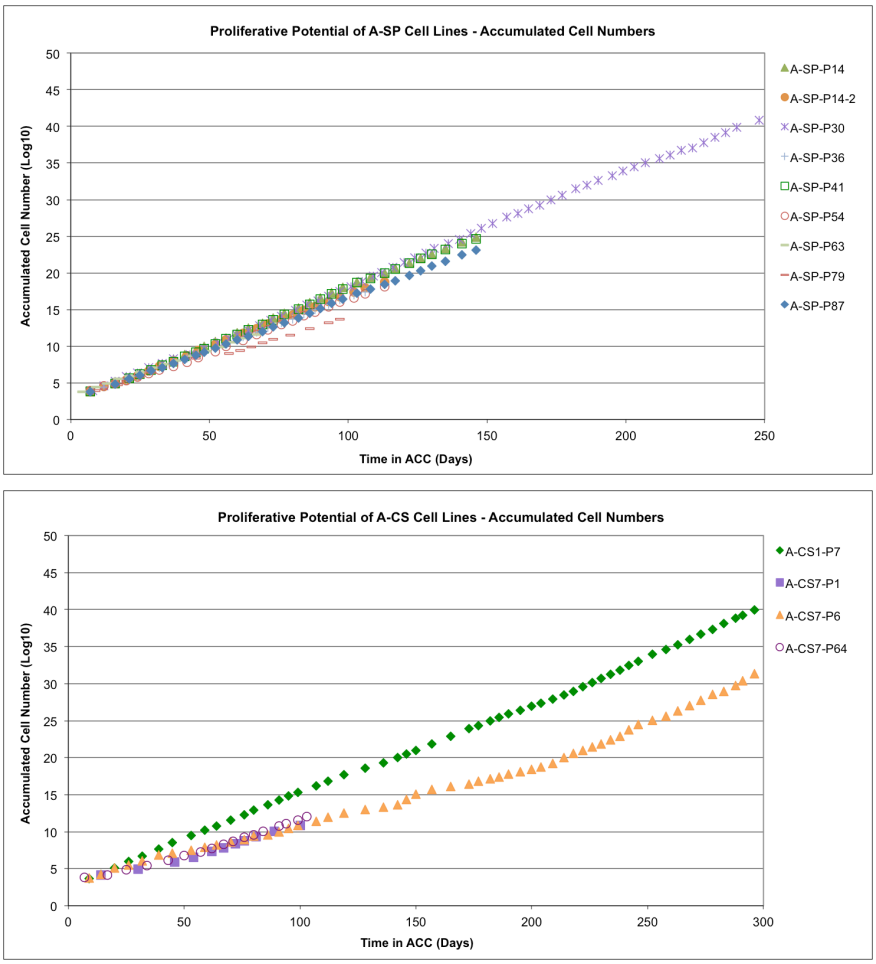

Figure 4.1.9: Proliferative Potential of SP and CS Cell Lines under ACC - Accumulated Cell Numbers

A-SP and A-CS do not loose proliferative potential when grown under ACC, as shown by constant increase of cell numbers, even after long-term culture of the cells.
Log10 of accumulated cell numbers of investigated A-SP and A-CS cell lines (A-SP upper panel, A-CS lower panel) is plotted vs. time in culture under ACC. The passage of spheroid cell line used for generation of A-SP or A-CS cell lines is indicated (-P14). A-CS14 was generated independently twice (-P14-2).
ACC: adherent culture conditions, A-CS: CS cells grown under ACC, A-SP: SP cells grown under ACC, CS: clonally expanded spheroid cells derived from PA, P: passage number, PA: parental cell line, SCC: spheroid culture conditions, SP: spheroid cells derived from PA

From the growth rates also the theoretical cell numbers, which would result from propagation of all cells (accumulated cell numbers) were calculated (see chapter 3.17.2) and are depicted in figures 4.1.8 and 4.1.9 for all cell lines assayed. From those figures the high growth potential of the cells becomes evident. The calculated cell numbers represent more than 350 population doublings (pds) in PA cells, more than 200 pds in CE1, almost 300 pds in CS7 and more than 190 pds in SP cell line. The high similarity of growth rates determined for SP cell lines, which were either obtained by separate generation or thawing of frozen aliquots, but also the slight increase of growth rates for multiply frozen cells are clearly visible in this diagram. But also similarities at the beginning of culture found for different CS cell lines (CS2, CS3, CS4), as well as the striking similar growth of different passages of SP and CS7 cell lines under ACC, with only one slightly slower growing cell line seen (A-SP-P79). The deviation of curves seen for long-term cultured PA cells is due to a short period of slightly reduced growth of the two cell lines at about passage 40.

4.2 Clonal Spheroid-Forming Efficiency (CSFE) in "Neurosphere Assay" (NSA)

The "Neurosphere Assay" (NSA) is a method, which was initially developed by Reynolds and Weis[164] for the evaluation and enrichment of neuronal stem cells from adult brain tissue and since has been refined and widely been used for enrichment of stem cells from other tissue sources, including tumor tissue. The assay principle is based on selection of cells, which are able to grow under non-adherent culture conditions as spheroids. Besides the lack of adequate substratum for adherence, a serum-free medium composition with defined growth factor content (EGF, FGF and insulin) is used for the assay. Since the conditions are very unfavorable for differentiated, "normal" cells, only stem cells and progenitor cells are able to grow, so that growth of spheroids in the assay is an indicator for the presence of cells with stem cell characteristics. The assay also allows a semi-quantification of stem cell content in a given sample by determining the clonal spheroid-forming efficiency, i.e. the percentage of starting cells, which are able to form spheroid colonies. By seeding cells at low density, aggregation of cells is omitted and spheroids can be counted.

The NSA was performed using non-tissue culture treated 96-well plates with seeding densities of 30-90 cells per well. PA, SP, CS, as well as A-SP and A-CS cells were seeded at different passage numbers for the assay and after culturing for 2-3 weeks, the resulting spheroids were counted. For each sample at least 15 single wells were counted and the mean value of spheroid forming efficiency was calculated. Although the standard deviations (depending on number of spheroids grown) ranged from 5-300% in single wells, the mean values reflected the obvious differences in growth potential quite well. The results obtained in the NSA for the different cell lines investigated are depicted in figures 4.2.1-4.2.4. As can be seen, the CSFE varied drastically between PA and spheroid cell lines, but also with different passage numbers/time of culture of cells.

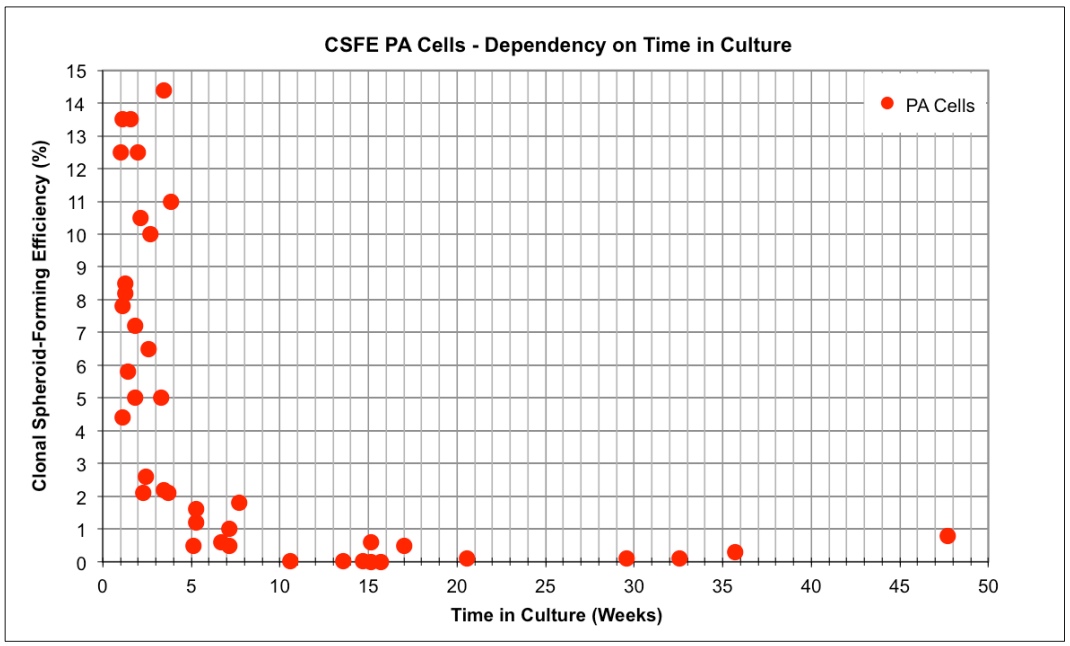

Figure 4.2.1: CSFE Determined for PA cells in NSA

The CSFE of PA cells is drastically reduced or even absent after 4 weeks of culture.
Results obtained from PA cells assayed in the NSA after different time of culture. Percentage of spheroid forming cells (CSFE) is plotted vs. culturing period of cells under ACC (weeks).
ACC: adherent culture conditions, CSFE: clonal spheroid-forming efficiency, NSA: „Neurosphere Assay", PA: parental cell line

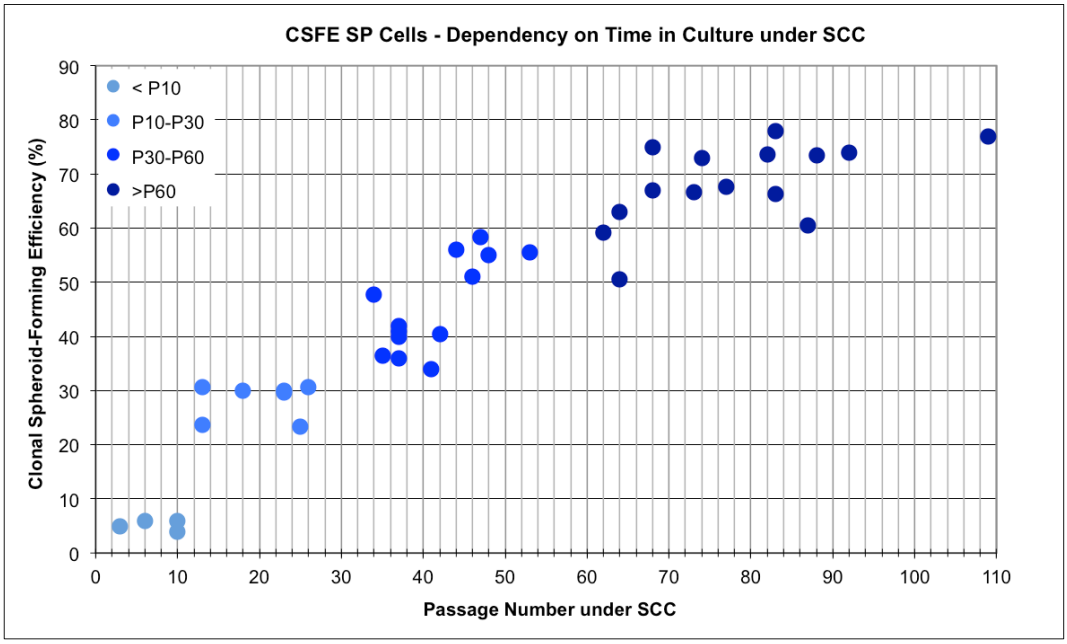

Figure 4.2.2: CSFE Determined for SP cells in NSA

The CSFE of SP cells increases over time in culture as spheroids.
Results obtained from SP cells assayed in different passage numbers of spheroid culture in the NSA. Percentage of spheroid forming cells (CSFE) is plotted vs. passage number of cells under SCC. The passage numbers represent < 50 days for passages <P10, 50-100 days for P10-P30, 100-200 days for P30-P60 and >200 days for passages >P60 under SCC.
SCC: spheroid culture conditions, CSFE: clonal spheroid-forming efficiency, NSA: „Neurosphere Assay“, PA: parental cell line, SP: spheroid cells derived from PA

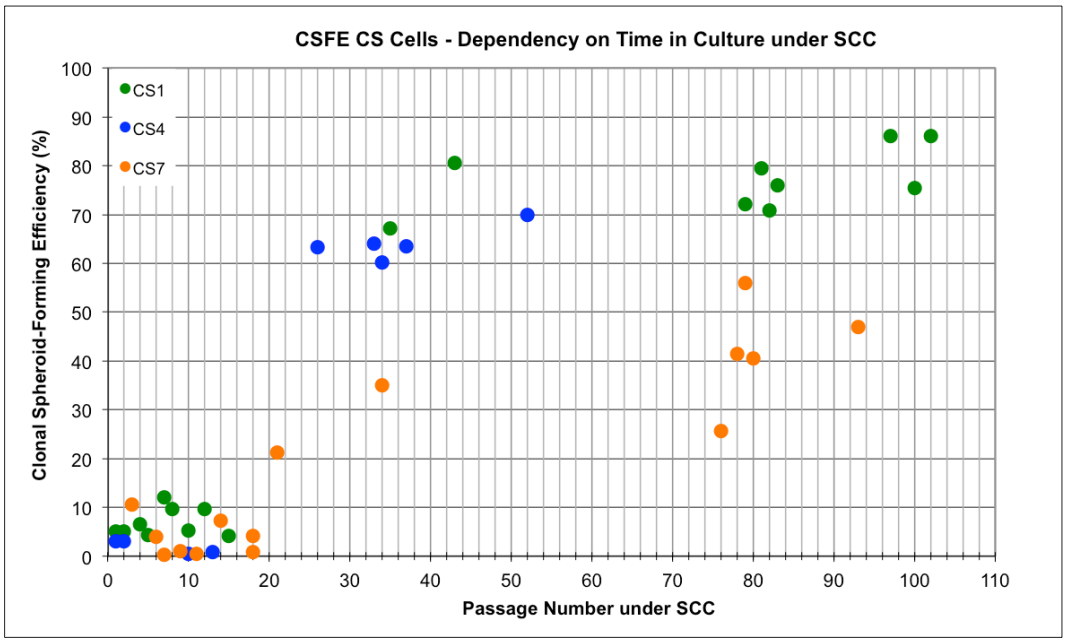

Figure 4.2.3: CSFE Determined for CS cells in NSA

The CSFE of CS cells increases over time in culture as spheroids and is slightly lower in CS7 cell line compared to CS1 and CS4 cell lines.
Results obtained from CS cell lines CS1, CS4 and CS7 assayed in different passage numbers of spheroid culture in the NSA. Percentage of spheroid forming cells (CSFE) is plotted vs. passage number of cells under SCC. The passage numbers represent < 200 days for passages <P20, >200 days for passage >P20 under SCC.
CS: clonally expanded spheroid cells derived from PA, CSFE: clonal spheroid-forming efficiency, NSA: „Neurosphere Assay“, SCC: spheroid culture conditions, PA: parental cell line

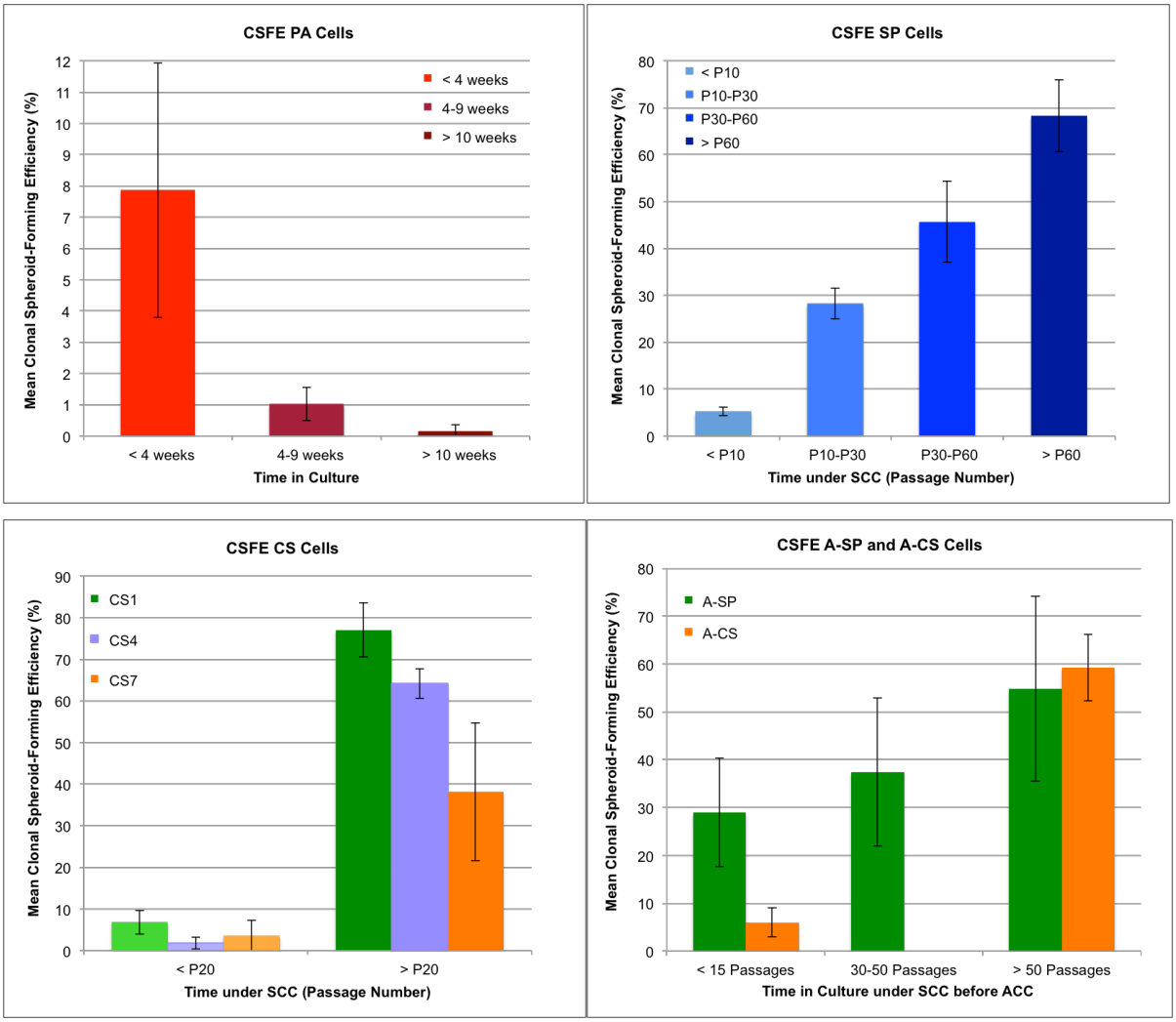

Figure 4.2.4: Mean CSFE Values of Different Cell Lines

Mean values of CSFE were calculated for all NSAs performed for groups with similar characteristics for all cell lines investigated. Groups were selected on the basis of obvious differences/similarities seen with passage of cells or time in culture. Cells used for the assays were either continuously grown (SP1/3, CS1, CS4) and/or obtained from cells frozen at different passage numbers. Error bars: standard deviation.
ACC: adherent culture conditions, A-CS: CS cells grown under ACC, A-SP: SP cells grown under ACC, CS: clonally expanded spheroid cells derived from PA, CSFE: clonal spheroid-forming efficiency, NSA: „Neurosphere Assay“, P: passage number, PA: parental cell line, SCC: spheroid culture conditions, SP: spheroid cells derived from PA.

The CSFE of PA cells was found to be in the range of 8±4% in the first 4 weeks of culture and dropped to below 1% after longer culturing periods, with almost no spheroid-forming ability being detectable (CSFE < 1%) after 10 weeks of standard culture of the cells.

In contrast to PA cells, the CSFE in SP cells increased continuously over passages as spheroids with starting numbers during the first 10 passages of 5±1%, then being relatively constant up to passage 30 at 28±3% and further increasing stepwise over 40-50% to values of 68±8% in passage numbers of more than 60. The CSFE in early passage number was quite similar to that of PA cells, and the gradual increase might indicate concomitant enrichment of cells with stem cell characteristics. But it cannot be excluded that the better growth of cells in later passages is due to better adaptation to the media conditions, which in the NSA are similar to normal growth conditions of the cells with the exceptions, that the seeding cell density in the assay is drastically reduced compared to bulk culturing.

Similar to standard culturing of the cells, also the morphology of the spheroids formed in the assay from later passages, was becoming more and more regular than spheroids grown from early passage cells.

Likewise to SP cells, the CSFE values obtained for CS cell lines increased with passage number of the cells under SCC. Thereby differences were seen between different CS cell lines. While CSFE in CS7 cell line seemed to increase similar gradually as that of SP cells, and was with maximal values in the range of 38%±10% lower than the values seen for other spheroid cell lines in high passage numbers, the increase of CSFE after about 200 days of culture seen for CS1 and CS4 cell lines was much more abrupt. All CS cell lines showed low and highly variable CSFEs in the first passages, which with 1.8±1.4% were lowest for CS4, slightly higher in CS7 4±4% and with 7±3% highest in CS1. CS1 cells reached very high CSFE values of 77±7% in high passage cells. The values obtained for CS4 cell lines did not include cells of very high passage numbers and with 64±4% were similar to the values obtained in SP cell line at passages >60. The number of data available for CS cell lines, compared to PA and CS cell lines is quite low, in the intermediate passage range, so that statements on these cell lines are less assured.

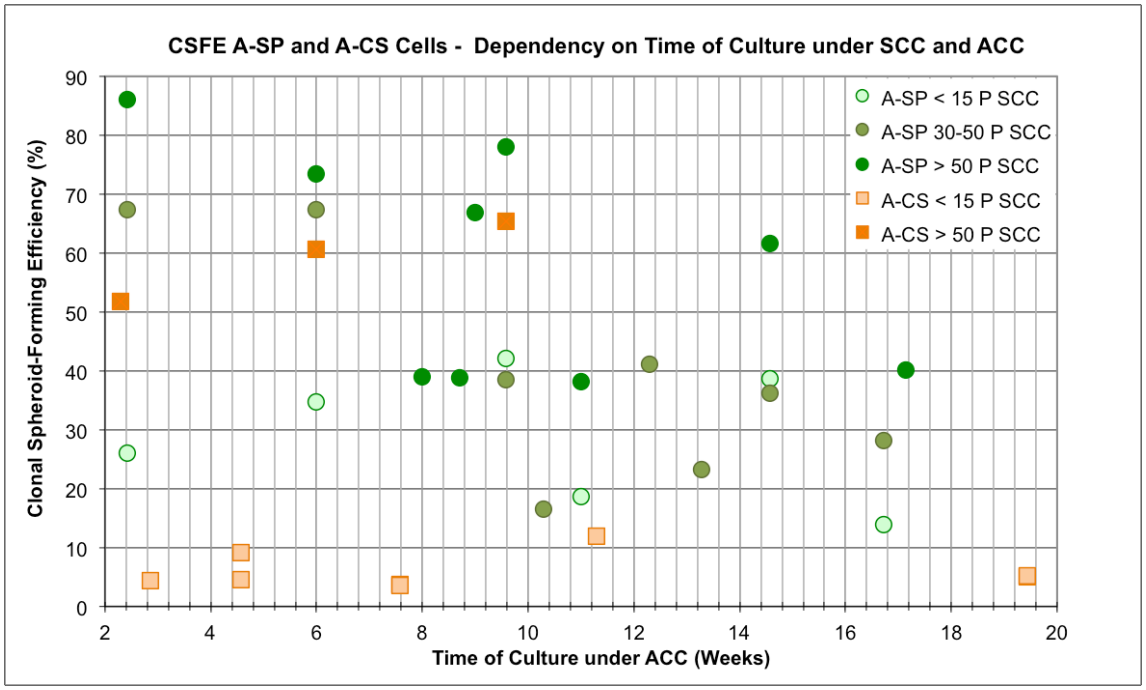

Figure 4.2.5: CSFE Determined for A-SP and A-CS Cells Cultured for Different Periods under ACC

The CSFE of A-SP and A-CS was dependent on passage number of spheroid cells used for starting adherent culture of the cells and was less depended on time in culture under ACC.
Results obtained from A-SP and A-CS cells assayed after different periods of ACC and derived of spheroid cell lines from different passages in SCC. Percentage of spheroid forming cells (CSFE) is plotted vs. time in culture under ACC (weeks). A-CS comprises values obtained from A-CS1 and A-CS7 respectively. Values shown for A-SP<P15 are from A-SP-P14 (n=6), A-SP P30-50 are from A-SP-P30 (n=7)/P36 (n=3)/P41 (n=3) and values for A-SP>P50 are from A-SP-P54 (n=3)/P63 (n=1)/P79 (n=2)/87 (n=3). Values shown for A-CS <P15 are from A-CS1-P7 (n=4) and A-CS-P6 (n=4), A-CS>P50 are from A-CS7-P66 (n=3).
ACC: adherent culture conditions, A-CS: CS cells grown under ACC, A-SP: SP cells grown under ACC, CS: clonally expanded spheroid cells derived from PA, CSFE: clonal spheroid-forming efficiency, NSA: „Neurosphere Assay“, P: passage number, PA: parental cell line, SCC: spheroid culture conditions, SP: spheroid cells derived from PA.

As can be seen from figure 4.2.5 and comparison of mean CSFE values depicted in figure 4.2.4, the CSFE of spheroid cells, which were cultured for different periods under ACC was quite similar to that seen in parental spheroid cell lines. High CSFEs were obtained from A-SP cells derived of high passage spheroids with mean values of 55±20% from A-SP-P54/63/79/87 and 59±7% from A-CS7-P66. In contrast, low CSFE values of 6±3% were obtained from A-CS1/C7-P6/P7. The values calculated from A-SP-P14 cells grown for different periods under ACC with 29%±11% are very similar to those seen for SP cells in this passage number range. In contrast to PA cells, where CSFE dropped dramatically after 5 weeks of culture, the CSFE of A-SP and A-CS cells derived from intermediate to high passage number spheroids was with percentages of about 40% relatively high, even after ACC culture of more than 10 weeks. This implies that immanent changes might have occurred during spheroid culture, either by enrichment or selection of cells with spheroid forming ability, which were not readily reversed when cells were cultured under serum-containing adherent conditions.

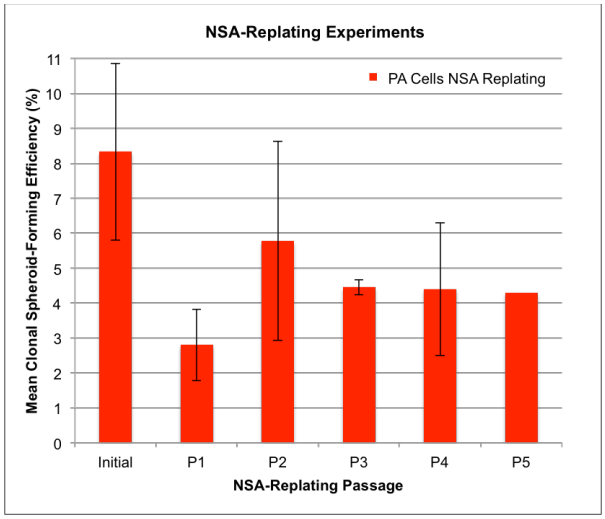

Figure 4.2.6: Mean CSFE Values for NSA Replating Experiments of PA Cells over five Passages

The CSFE values for direct replating of spheroids grown in the NSA are reduced compared to initial CSFE but relatively constant over 5 passages.
Mean values of CSFE were calculated for direct NSA replating of PA cells at passage 28-31 for 5 passages. The following numbers of values were used for calculations of mean: initial (n = 9), P1 (n=7), P2 (n=4), P3 (n=2), P4 (n=3), P5 (n=1). One experiment in passage 3 was not considered because of too high a number of cells seeded. Error bars: standard deviations.
CSFE: clonal spheroid-forming efficiency, NSA: „Neurosphere Assay“, P: passage number, PA: parental cell line.

Besides CSFEs determined for spheroids grown in bulk culture from the different cell lines, also the replating efficiency from spheroids grown in the NSA from PA cells was evaluated. The results of experiments comprising 5 passages of NSA-replating rounds are shown in figure 4.2.6. Compared to initial CSFEs with mean values of 8±3%, the replating efficiencies of PA cells were slightly reduced but relatively constant over the 5 passages investigated, resulting in a mean for all replating rounds of 4±2%. The values were quite similar to the values seen for spheroid cell lines at early passages, which indicates that NSA and bulk culture conditions were not quite different regarding quantity of selection/enrichment of stem like cells in the first passages, although the cell numbers seeded in the NSA were much lower than those used for bulk culture passaging.

4.3 Soft Agar Assay (SAA)

The soft agar assay (SAA) is a method to determine single cell growth under non-adherent culture conditions. Since the conditions of the assay allow only growth of cells with typical characteristics of tumor cells, namely high proliferative potential and insensitivity to improper cell-cell/cell-matrix contacts, the assay is frequently used as *in vitro* method for possible tumorigenic potential of cells. The standard SAA is performed in a semi-solid matrix of agarose polymer with serum-containing medium. By using serum-free medium with identical composition to that used for spheroid culture (SC-Medium), a further constraint on cell growth is added, and the assay conditions are similar to those used for the „Neural Colony-Forming Cell Assay“ (NCFCA)[244], which was proposed to be more suitable for calculation of stem cell content than the NSA. Thereby large colonies are assumed of being derived of stem cells, whereas small colonies are thought of being formed from progenitor cells.

To determine the growth capacity in SAA, the different cell lines (PA, SP, CS1, CS7, A-SP, A-CS1, A-CS7) were seeded at various starting numbers ($2x10^3$-$5x10^4$) per well in 6-well cell culture plates (at least in duplicate, usually in triplicate) in 0.6% (w/v) agarose in either serum-containing medium or SC-Medium and were allowed to grow for 4-5 weeks with regular medium exchange. To visualize the colonies, the plates were stained with crystal violet solution and magnified pictures were taken. Colony count was performed on defined sections of the plate using the particle count modus of the software ImageJ, with the size inclusion set to a colony diameter of >100 µm. From the program output the colony-forming efficiency (CFE) for every well and average particle sizes were calculated.

The results obtained are summarized using mean values of all experiments performed for one condition with one cell line in table 4.3.1 and depicted in figure 4.3.1. Since no significant difference was seen between the values obtained for CS1 and CS7 cell lines they were summarized to “CS” in these reports.

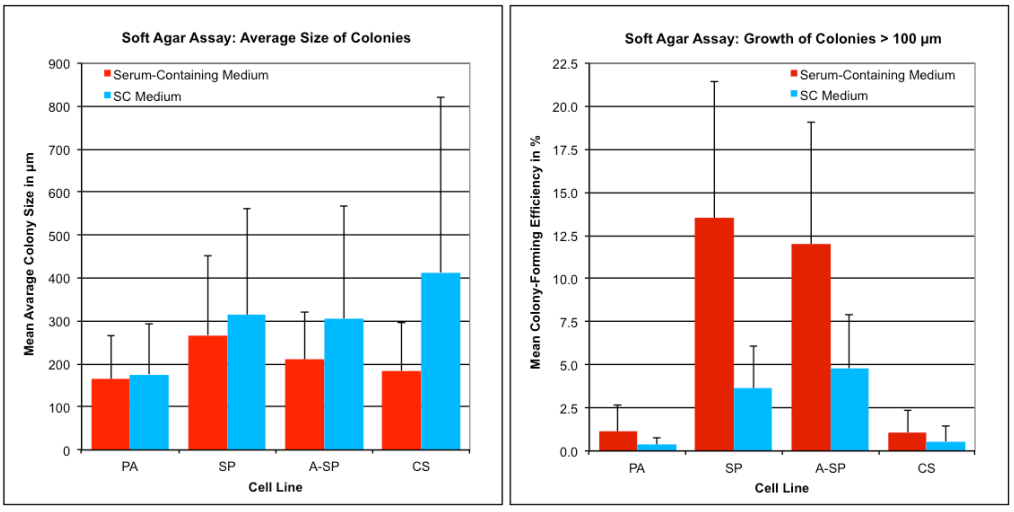

Figure 4.3.1: Comparison of CFEs and Colony Sizes of Different Cell Lines and Media in SAA

Mean values calculated for colony forming efficiencies (CFEs, left) and colony diameters (right) from all experiments for cell lines PA, SP, A-SP, and CS (CS1 and CS7) in different passages. The number of assays performed in duplicate or triplicate used for calculations and the range of passage numbers assayed for the different cell lines are specified in table 4.3.1, respectively. Only colonies >100 µm diameter were counted and used for further calculations. Values for SP and A-SP CFEs were significantly different from those of the other cell lines. Mean colony sizes of SP, A-SP and CS cell lines grown in SC-Medium were found to be significantly different from mean colony sizes of these cell lines grown in serum-containing medium. Error bars: standard deviation.

Condition	Cell Line	Mean Colony-Forming Efficiency (CFE) in %	CFE (StD)	Mean Colony Diameter (Dia) in µm	Dia (StD)	No. of Assays Perfomed	Passage Numbers Assayed (weeks under ACC)
Serum	PA	1	1.5	165	101	33	29-123
	SP	14	7.9	267	185	41	33-109
	A-SP	12	7.1	210	112	12	16-109 (2-38 w ACC)
	CS	1	1.3	184	113	13	6-101
SC	PA	0.4	0.4	176	118	35	29-123
	SP	3.6	2.4	315	245	41	33-109
	A-SP	4.8	3.1	306	261	12	16-109 (2-38 w ACC)
	CS	0.6	0.9	413	408	13	6-101

Table 4.3.1: Mean CFEs and Colony Sizes of Different Cell Lines and Conditions in SAA

ACC: adherent culture conditions, A-SP: SP cells grown under ACC, CFE: colony-forming efficiency, CS: clonally expanded spheroid cells derived from PA (CS1/CS7), P: passage number, PA: parental cell line, SAA: soft agar assay, SP: spheroid cells derived from PA, w: weeks

In the assay also no correlation of results with passage number of the cells was observed. Due to the method's inherent inaccuracy, the results obtained in different experiments showed relatively high variations, but these were within magnitudes to reliably detect differences between the investigated cell lines. Representative magnified sections of crystal violet stained SAA wells from different cell lines and culture conditions are shown in figure 4.3.2. There it can be seen clearly that the growth potential of different cell lines in the two media used in SAA varied considerably.

In serum-containing medium the growth potential of PA and CS cell lines was similar in the range of 1% of cells being able to grow and form small colonies with about 100-150 µm in diameter. In contrast, the SP cell line did show markedly (in the order of one magnitude) higher growth potential under these conditions, which was accompanied by significantly larger colony sizes seen in this cell line.

The number of cells being able to grow in SCC was reduced by the factor 2-3 in all cell lines. Whereas the size of colonies grown from PA cells did not change significantly under these conditions, the spheroid cell lines gave rise to considerably larger colonies, with highly variable sizes under SCC compared to serum-containing conditions.

Interestingly, similar to results obtained in NSA, the growth capacity of SP cells was retained even after long-term culture of the cells under ACC. A-SP cells derived of different passages of spheroids and grown for different periods (up to 38 weeks) under ACC showed almost identical growth potential than the parental spheroid cell line. A-CS cell lines (A-CS1 and A-CS7) were only assayed once in the SAA and results obtained were similar to that seen for respective CS spheroid cell lines.

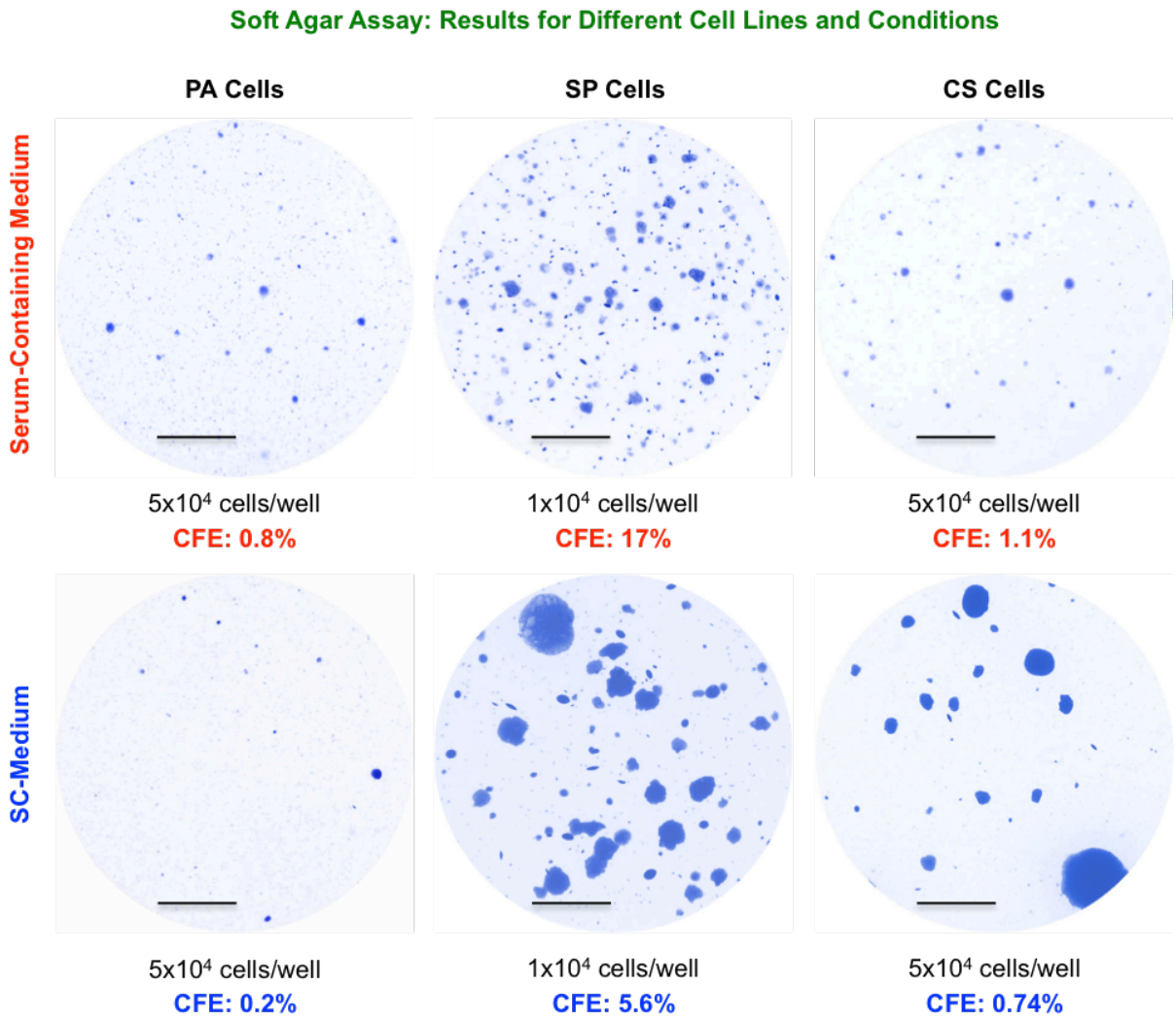

Figure 4.3.2: Results of Different Cell Lines in Serum-Containing and SC-Medium in SAA

Growth potential of SP cell line in soft agar assay was significantly higher than that of PA and CS cell lines and colonies grown from spheroid cell lines in SC-Medium were significantly larger than colonies grown in serum-containing medium.
Magnified sections of representative single soft agar wells stained with crystal violet. The respective numbers of cells seeded per well are indicated in black. Scale bar: 2.5 mm. Upper line: PA (P55), SP (P47), and CS7 (P41) cells grown for 4.5 weeks in soft agar with serum-containing medium. The calculated colony-forming efficiencies (CFE) are indicated in red. Lower line: PA (P55), SP (P50), and CS7 (P93) cells grown for 4.5 weeks in soft agar with SC medium. The calculated colony-forming efficiencies (CFE) are indicated in blue. Results shown are representative (within assay variations) for the respective cell lines PA (n = 35, P29-123), SP (n= 41, P10-109), and CS7 (n = 13, P6-101). Results for CS7 are representative also for CS1 cell line (n = 13, P14-100) and CS cell lines grown under ACC for 8 weeks: A-CS1 (P14), A-CS7 (P12). Results for SP are also representative for SP cell lines in different passages (P14, 30, 41, 79, 87) grown for 2-38 weeks under ACC: A-SP (n = 12, P16-109).
ACC: adherent culture conditions, A-CS: CS cells grown under ACC, A-SP SP cells grown under ACC, CFE: colony-forming efficiency, CS: clonally expanded spheroid cells derived from PA, P: passage number, PA: parental cell line, SAA: soft agar assay, SP: spheroid cells derived from PA, w: weeks

4.4 *In vitro* Differentiation

A hallmark feature of stem cells is their ability to generate differentiated cells with diverse functions.
To test for this ability, the different cell lines to be tested were cultured under cell culture conditions, which have been shown to induce adipogenesis or osteogenesis in MSC.

4.4.1 Osteogenic Differentiation

To assess osteogenic differentiation potential, the different cell lines were seeded in 12-well plates in osteogenic induction medium (2 wells per cell line and assay) or control medium (1-2 wells per cell line and assay), which lacked the osteogenic inducers dexamethasone and β-glycerophosphate. The cells were cultured with regular medium exchange until signs of calcium phosphate depositions became visible. The periods varied in different experiments and between different cell lines between 3-5 weeks. The cells were fixed and stained with Alizarin Red S to visualize the calcium phosphate depositions as red complexes. In two experiments also the van Kossa staining method was applied, in which silver deposits are indicative for calcium ions. Both methods resulted in similar staining qualities of the samples assayed in parallel. Representative results from different cell lines, as seen in microscopic inspection after Alizarin Red S staining are shown in figure 4.4.1.
The highest osteogenic potential was observed in the SP cell line, which showed strong staining intensities after Alizarin Red S staining in all experiments (n= 31, P5-91). Similar results were obtained for SP cells cultured for different time points under ACC (n=3: A-CS-P30, P50-P94, 7-30 weeks ACC, and A-SP-P36, P40, 3 weeks ACC). Of note is that the observed differentiation potential was similarly high in low and high passage number cells assayed.
For PA cell line the results varied between experiments. In half of the samples (n=17, P28-P125) calcium phosphate deposits were seen at least in some regions of the wells or filling the complete well similar to the pattern seen for SP cells, thereby indicating osteogenic induction, whereas in the other half (n=16, P28-P119) of the assays no considerable staining with Alizarin Red S was seen. In some experiments also one of the duplicate wells showed positive red staining parts, whereas in the other well no staining was seen. The reason for this is not clear, since for example no correlation of this behavior with passage number or with time of induction before staining was seen.
CS7 cell line (n = 4, P52-97), in all experiments showed positive staining of calcium phosphate deposits in some regions of the wells, with overall staining compared to SP cell line being obviously reduced. A similar staining pattern was seen in two experiments performed with A-CS7-P6 cell line (P53/P56), which were cultured for 37/40 weeks under ACC.
The results show that SP, PA and CS7 cell lines, albeit at various degrees, seem to possess osteogenic differentiation potential. In few experiments slight positive staining was seen also in control samples, which might indicate spontaneous differentiation of the cells toward osteogenic lineage.
In contrast, the CS1 cell line did not show signs for osteogenic differentiation under the applied conditions, indicated by lack of any red staining for Alizarin Red S calcium complexes in the experiments performed (n=11, P5-98). Similarly, also A-CS1-P7 cell line showed no staining when assayed in two experiments (P53/P58, 31/40 weeks ACC).

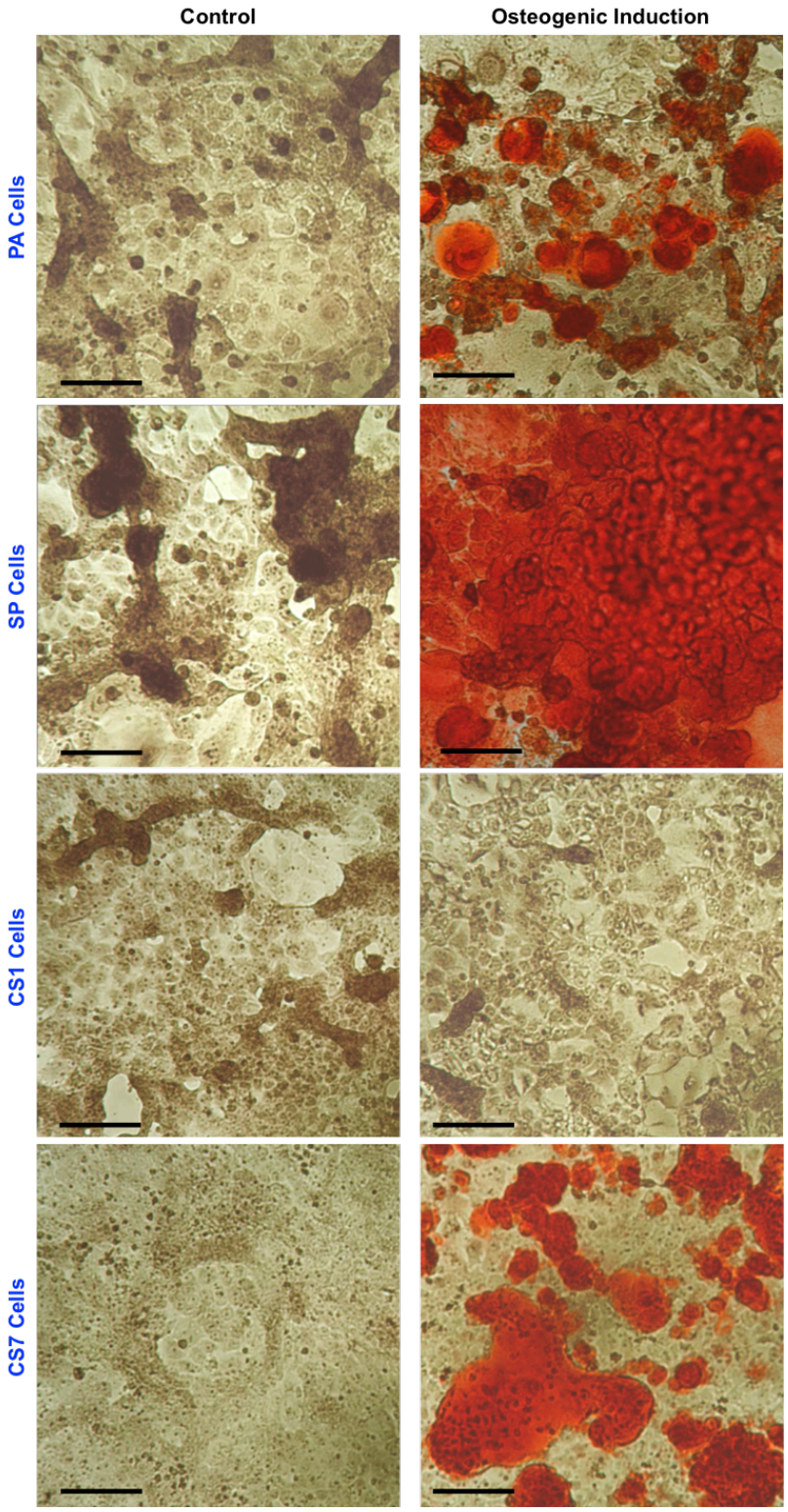

Figure 4.4.1: Osteogenic Differentiation of Different Cell Lines

SP, PA and CS7 cell lines show osteogenic differentiation potential.
Microscopic pictures of Alizarin Red S stained PA (P121), SP (P87), CS1 (P98), and CS7 (P97) cells grown for 3 weeks under osteogenic differentiation conditions (right panel) or control conditions (left panel). Red staining of calcium phosphate depositions indicates osteogenic differentiation. Scale bar: 100 µm. Results shown are representative for the respective spheroid cell lines SP, CS1, and CS7 as well as for these cell lines cultured under ACC. Results for PA cell line varied considerably and staining pattern as indicated above for CS1 or SP were also seen there.
ACC: adherent culture conditions, CS: clonally expanded spheroid cells derived from PA, PA: parental cell line, SP: spheroid cells derived from PA

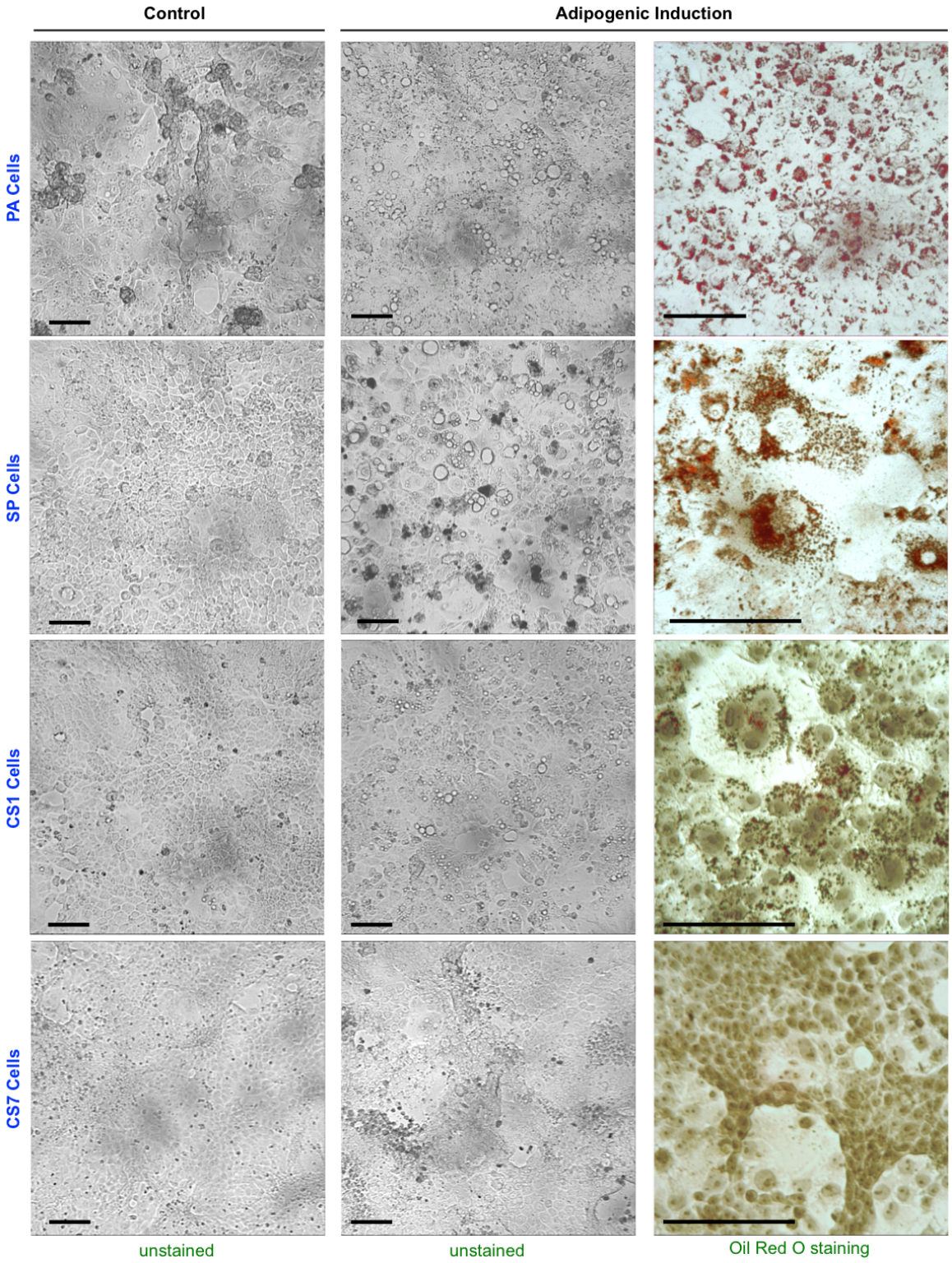

Figure 4.4.2: Adipogenic Differentiation of Different Cell Lines

SP, PA and CS1 cell lines show adipogenic differentiation potential.
Microscopic pictures of PA (P85), SP (P53), CS1 (P65), and CS7 (P65) cells grown for 3 weeks under adipogenic differentiation conditions (middle and right panel) or control conditions (left panel). Adipogenic differentiation is indicated by appearance of characteristic lipid vacuoles, which are visible in unstained cells and red staining of lipid droplets after staining with Oil Red O. Scale bar: 100 µm. Left panel: unstained control samples. Middle panel: unstained adipogenic induced samples. Right panel: adipogenic induced samples stained with Oil Red O and hematoxylin (CS1 and CS7). Results shown are representative for the respective cell lines.
ACC: adherent culture conditions, CS: clonally expanded spheroid cells derived from PA, PA: parental cell line, SP: spheroid cells derived from PA

4.4.2 Adipogenic Differentiation

Adipogenic differentiation potential was assayed by culturing the different cell lines in 6-well or 12-well plates in adipogenic induction medium (2 wells per cell line and assay), which contained insulin, dexamethasone, indomethacin and IBMX as adipogenesis inducing agents. Negative control samples (1-2 wells per cell line and assay) were seeded in control medium without the supplements. The cells were cultured with regular medium exchange until morphologic changes, namely the formation of lipid vacuoles, which are characteristic for adipocytes, were clearly visible. Then, the cells were fixed and stained with Oil Red O to visualize the lipid droplet accumulations in bright red color. The induction periods varied in different experiments and for different cell lines between 2 and 4 weeks. Cell lines and passages assayed for adipogenic differentiation potential were the same as described for osteogenic differentiation. A difficulty in experimental procedures was, that cells easily detached from the culture vessel in the staining procedure, also the lipid droplets were very sensitive for the washing procedures applied, so that often only a reduced number of cells was applicable for inspection and only small dispersed red staining drops were seen clearly only under high magnification in the microscope. Because of the high magnification needed, adequate acquisition of staining results with the equipment used was difficult due to the color and light sensitivity of the camera, especially, when counterstaining with hematoxylin was performed. Attempts to quantify the adipogenic process by using a fluorescent dye or extraction of Oil Red O after staining were shown to be very intricate and did not give satisfactory results without disproportional effort. In figure 4.4.2 representative microscopic views of different cell lines induced for adipogenic differentiation before and after oil red staining are shown.

The observed potential for adipogenic differentiation was quite dissimilar in the investigated cell lines.

When PA and CS1 cell lines were cultured under adipogenesis inducing conditions, formation of small lipid vacuoles was observed in some regions of the wells. After Oil Red O staining, lipid droplets were visible in some fractions of the cells. The amount of stained cells was higher in PA cell line when compared to CS1 cell line, but varied in different experiments.

The morphology of cells observed in SP cell line after adipogenic induction was different from PA and CS1 cell lines, in that large cells with high lipid vacuole content, resembling adipocyte morphology, were seen at varying numbers dispersed between normal epithelial cells. Single cells with similar adipocyte morphology as in differentiation experiments, were also seen in control experiments, indicating a tendency of spontaneous differentiation of SP cells into this line. As observed in osteogenic differentiation experiments, SP and CS1 cells that were cultured under ACC showed similar behavior like their parental spheroid cell lines also in adipogenic differentiation assays.

In CS7 cell line morphologic changes implying adipogenic differentiation and red stained lipid droplets were either not observed under the applied conditions or only in single cells in all experiments. Rather in some experiments with this cell line, signs of osteogenic differentiation were observed. Strikingly, when CS7 cells were cultured for long periods (31/40 weeks) under ACC, similar adipogenic potential to CS1 and PA cell lines was observed, implying, that lack of adipogenic differentiation in the parental spheroid cell line might be due to improper differentiation conditions for these cells.

In summary, the differentiation experiments showed that SP cells seemed to posses the highest differentiating capacity toward both lineages, whereas, although a differentiation capacity toward both

lineages was observed also in PA cells, this seemed to be reduced or impaired in this cell line, compared to SP. In contrast, for CS cell lines only reduced differentiation capacity was seen to either one of the two lineages respectively, with CS1 showing adipogenic potential only and CS7 showing preference of osteogenic differentiation. Since the results of differentiation experiments showed high overall variations, the number of experiments performed with CS cell lines was not sufficient to be regarded as significant. Since also no further optimization and quantitation experiments were performed, the results obtained here can be regarded as a rough estimation of differentiation potential of the cells, only.

4.4.3 Expression of Differentiation Markers

To substantiate differentiation results observed by histologic staining methods, also expression of genes, which are known to be preferentially expressed in adipocytes or osteoblasts, was assayed by semi-quantitative RT-PCR. Adiponectin (APM/ADIPOQ), and sterol regulatory element binding transcription factor 1 (SREBF1/SREBP1) were selected from the list of known adipocyte expressed genes; osteocalcin (OC), RANK-ligand/TNFSF11 (RL) and RUNX2 were selected from the known genes expressed in osteoblasts.

SP cells, which had shown to possess the highest differentiation potential toward both lineages, were used for this purpose. The cells were grown under adipogenic or osteogenic differentiation conditions for 3 weeks and RNA was extracted. Equal amounts of RNA were used for RT-PCR reactions and the resulting cDNA was used also at equal amounts for PCR reactions with primers specific for the transcripts of interest. HPRT served as housekeeping gene control. Equal amounts of the PCR reaction products were separated and visualized on 1.5% agarose gels, to allow a rough comparison of their expression.

A comparison of resulting bands of adipogenically induced (AI) and osteogenically induced (OI) samples, which were processed in parallel, is depicted in figure 4.4.3.

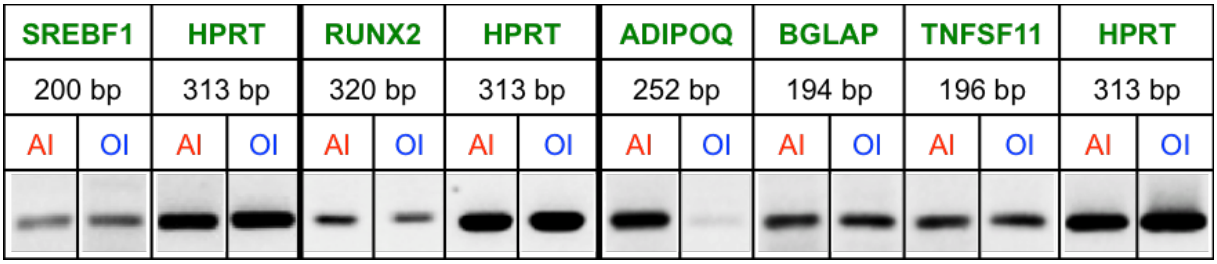

Figure 4.4.3: Evaluation of Expression of Differentiation Markers in Induced Cells by RT-PCR

Comparison of agarose gel lanes obtained for different transcripts amplified by RT-PCR in SP cells grown under adipogenic (AI) or osteogenic (OI) inducing conditions.
Column 1: gene name, column 2: length of PCR product, column 4: mode of induction, column 5: respective agarose gel bands. SREBF1 and RUNX2 were analyzed separately. For each separate analysis (discreted by thick lines) result for the housekeeping control gene (HPRT) are indicated at the rightmost columns.
ADIPOQ: adiponectin, AI: adipogenic induction, BGLAP: bone gamma-carboxyglutamate protein/osteocalcin, bp: base pairs, HPRT: hypoxanthine phosphoribosyltransferase 1, OI: osteogenic induction, RUNX2: runt related transcription factor 2, SREBF1: sterol regulatory element binding transcription factor 1, TNFSF11: tumor necrosis factor superfamily member 11 Rank-ligand

The only gene for which a clear difference in expression between both samples was observed is adiponectin (ADIPOQ), which was expressed, as expected, at markedly higher level in adipogenically

induced cells. Since expression of this molecule is relatively specific for adipocytes, this result seems to confirm adipogenic differentiation of the cells.

Expression of the other assayed genes was detected in both samples at low level, with no significant differences being observed between AI and OI cells, rather, contrary to expectations, slightly higher expression of osteogenic transcription factor RUNX2 was seen in AI cells, whereas adipogenic transcription factor SREBF1 seemed to be expressed at slightly higher amounts in OI cells. This might indicate osteogenic differentiation also in AI and/or low specificity of the chosen markers.

4.5 Alkaline Phosphatase Activity and Expression

4.5.1 Histological Staining for Alkaline Phosphatase Activity

High expression and activity of alkaline phosphatase is used as a marker for undifferentiated ESC. But activity of alkaline phosphatase is also observed in osteogenically differentiated cells and used as a marker for osteogenic differentiation potential. Activity of alkaline phosphatase was evaluated by histological staining, using Naphthol-AS-MX-phosphate as a chromogenous substrate for the enzyme.

SP, CS and PA cell lines, were grown for 2 weeks in 12 well plates as adherent cell layers in AC-Medium and assayed for alkaline phosphatase activity. Microscopic pictures showing results of AP staining are depicted in figure 4.5.1. In SP cell line on top of the monolayer spheroid like cells forming from the monolayer, showed high staining intensity when assayed for alkaline phosphatase activity, whereas in all other cell lines tested (PA, CS1, CS7) no staining was observed.

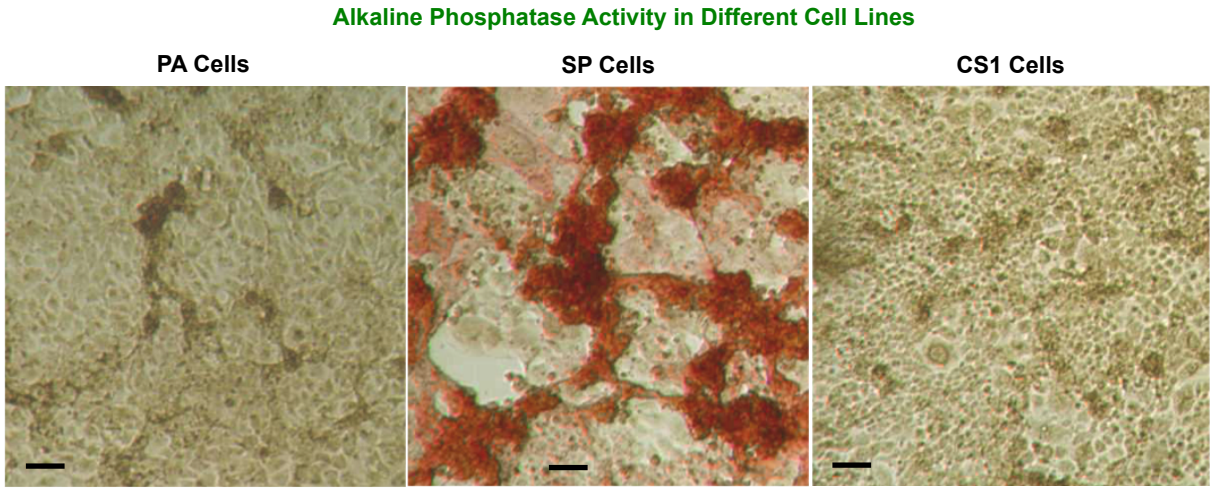

Figure 4.5.1: Alkaline Phosphatase Activity in Different Cell Lines

High alkaline phosphatase activity is detected in SP cells growing non-adherent on top of the monolayer under ACC, whereas no alkaline phosphatase activity is detected in PA or CS cell lines grown under the same conditions.
Microscopic pictures of PA (P66), SP (P59), CS1 (P70) cells grown for 4 weeks under ACC and assayed for alkaline phosphatase activity. Results shown for CS1 are also representative for CS7 (P69). Scale bar: 100 µm.
ACC: adherent culture conditions, CS: clonally expanded spheroid cells derived from PA, PA: parental cell line, SP: spheroid cells derived from PA

Alkaline phosphatase activity was also assayed in SP cells, which were grown for 2 weeks under conditions inducing osteogenic differentiation or under control conditions. Representative microscopic pictures showing the staining pattern of the cells are shown in figure 4.5.2. In cells grown under control conditions, again red stained, non-adherent cells were observed. In osteogenically induced samples

red staining of single adherent cells with osteoblast-like morphology was observed, which further substantiates the observed osteogenic differentiation potential of the cells.

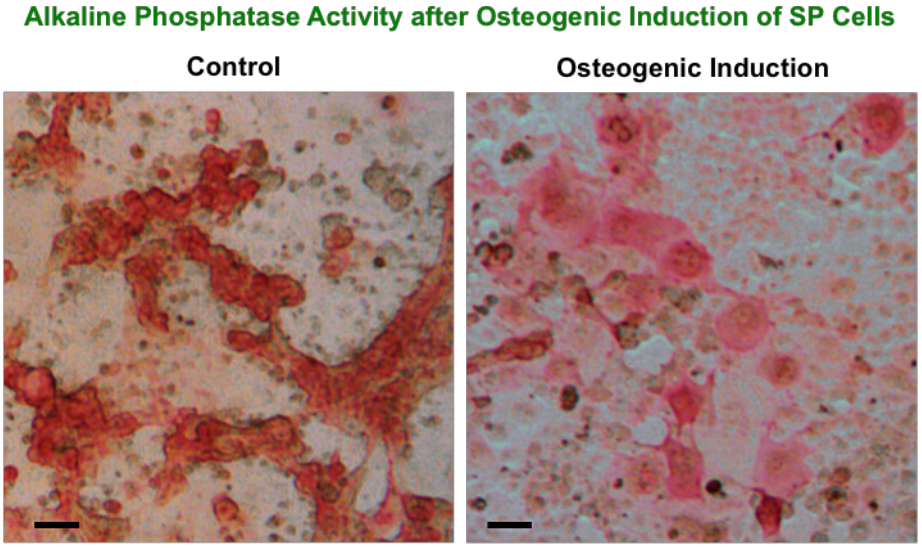

Figure 4.5.2: Alkaline Phosphatase Activity in SP Cells after Osteogenic Induction

After osteogenic induction of SP cell line, AP activity is detected in adherent cells with osteoblast-like morphology. Microscopic pictures of SP cells grown for 2 weeks under osteogenic differentiation conditions (right panel) or control conditions (left panel) assayed for alkaline phosphatase activity. Scale bar: 100 µm.
AP: alkaline phosphatase, PA: parental cell line, SP: spheroid cells derived from PA

4.5.2 Intracellular Expression of Tissue Nonspecific Alkaline Phosphatase (TNAP)

Intracellular expression of the tissue nonspecific alkaline phosphatase (TNAP), which is known to be expressed by stem cells (ESC, BM-MSC) was assayed once by intracellular IFC measurements on the four cell lines PA, SP, CS1 and CS7 as well as on A-CS1 and A-CS7 cells. For intracellular measurements cells were fixed and permeabilized using the „FOXP3 Transcription Factor staining Kit“ and subsequently stained with PE-conjugated antibody for detection of TNAP. No live cell discrimination using 7-AAD was applied. Results obtained are depicted in figure 4.5.3. Expression of the enzyme was detected in PA, CS and A-CS cell lines with similar low expression level. Compared to all other cell lines, TNAP seemed to be expressed at higher levels and with broader distribution in SP cells in this measurement.

4.5.3 Surface Expression of Tissue Nonspecific Alkaline Phosphatase (TNAP)

Also cell surface expression of TNAP on the four cell lines PA, SP, CS1 and CS7 was evaluated by standard flow cytometric measurements. On PA and CS cell lines no extracellular expression was detected, while on SP cells a slight shift in staining compared to isotype control sample was observed with a small number of cells seeming to express TNAP at low level on the surface. This is consistent to the higher expression level seen in intracellular measurements for this cell line. But the results varied between single measurements. About 10% TNAP positive cells were detected in 5 of 10 SP cell samples, whereas the other 5 samples showed similar staining pattern to PA or CS cells. No statistically significant correlation could be detected for this variation with the available number of data, although data hint to a lower expression in cells with very high passage numbers. In figure 4.5.4 examples of the two different staining patterns seen on SP cells from one measurement performed

with cells at different passage numbers are depicted, of which the negative staining pattern also exemplifies the staining pattern seen on PA and CS cells.

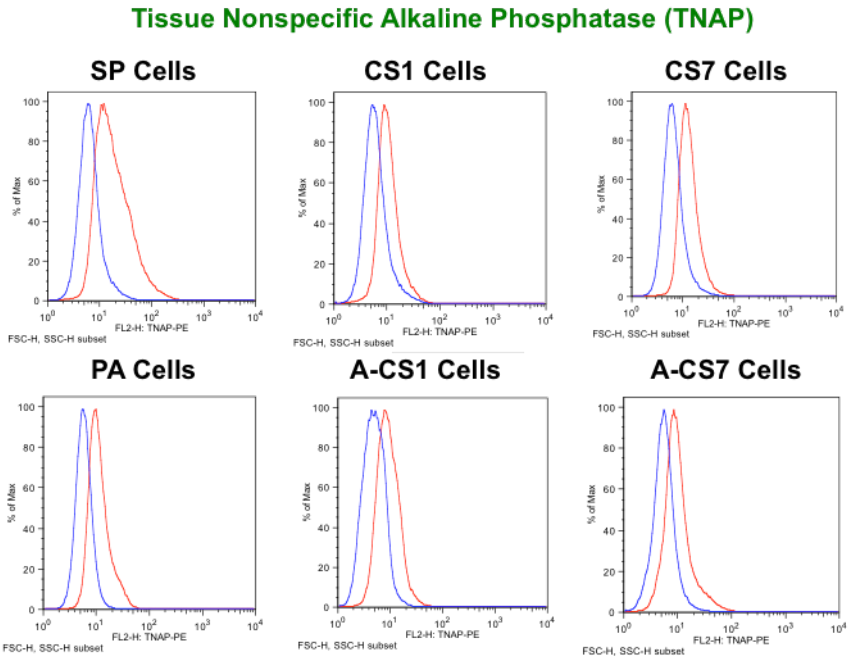

Figure 4.5.3: Intracellular IFC-Staining of Alkaline Phosphatase TNAP

PLAP is expressed in all investigated cell lines at similar intermediate level. TNAP expression is detected at low level in PA, CS and A-CS cell lines, whereas SP cells show higher expression of the enzyme.
Flow cytometric immunophenotyping (IFC) of cells stained with AF660 conjugated antibody for detection of PLAP and PE conjugated antibody for detection of TNAP. Comparison of PA, SP, CS1, CS7 and A-CS1, A-CS7 cells. Histogram of % Max (events) vs. fluorescence intensity, overlay of isotype control (blue) and sample (red).
ACC: adherent culture conditions, AF660: AlexaFluor® 660, A-CS: CS cells cultured under ACC, CS: clonally expanded spheroid cells derived from PA, FL2/4-H: fluorescence channel signal intensity, PA: parental cell line, PE: phycoerythrin, PLAP: placental alkaline phosphatase, SP: spheroid cells derived from PA, TNAP: tissue nonspecific alkaline phosphatase

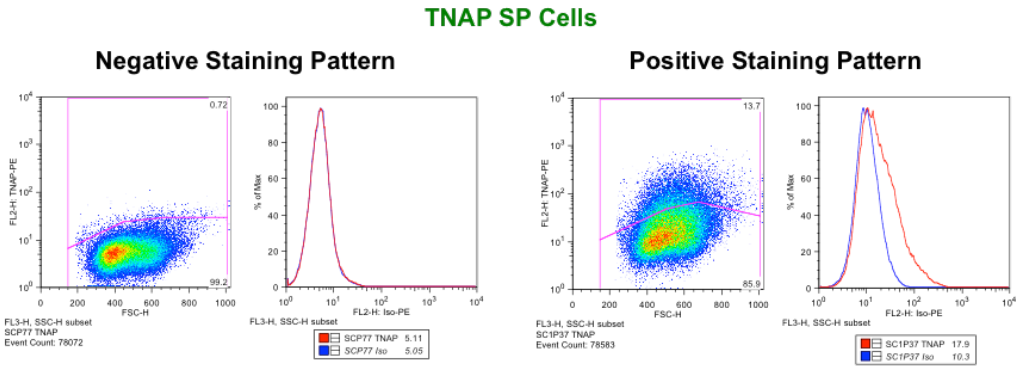

Figure 4.5.4: IFC-Staining Pattern for Cell Surface Expression of TNAP on SP Cells

Representative results of the two different staining patterns observed in flow cytometric immunophenotyping (IFC) of SP cells stained with PE conjugated antibody for detection of TNAP.
Example of negative staining pattern of SP in P77 representing also the staining pattern seen on PA and CS cells and different passage numbers of SP cells (P59, P70, P77, P102, P112)
Example of positive staining pattern of SP cells in P37 seen on 5 of 10 samples from SP cells from different passage numbers (P37 2x, P58, P70, P72).
Figure left: scatter plot of fluorescence intensity vs. forward scatter (cell size) of „live cell population“. Figure right: histogram of % Max (events) vs. fluorescence intensity, overlay of isotype control (blue) and sample (red), legend: geometric mean of fluorescence intensity.
CS: clonally expanded spheroid cells derived from PA, FL2-H: fluorescence channel signal intensity, IFC: flow cytometric immunophenotyping, PA: parental cell line, PE: phycoerythrin, SP: spheroid cells derived from PA, TNAP: tissue nonspecific alkaline phosphatase

4.6 Evaluation of Expression of CSC Markers by Flow Cytometric Immunophenotyping (IFC)

Surface expression of several antigens, which are known to be TIC markers for several solid tumors, was evaluated by flow cytometric immunophenotyping. In table 4.6.1 an overview of expression of the evaluated antigens on different types of cancer, stem cells and other cell types is given. Several of the molecules expressed by MSC, are also expressed by and used as markers for endothelial cells.

CD No.	Antigen Name	Marker				Tumor Type	Other Adult SC ★	Adult Tissue ★
		MSC	ESC	Endo	CSC			
CD10	Neprilysin	(+)				BC, HNSCC, RCC-Marker	Breast, Lung, HSC	rare (glandular, kidney, intestine, fat, lung)
CD29	Integrin β1	+	+	+	+	BC		ubiquitously
CD49e	Integrin α5	+	+	+		Upregulated in EMT, HIF		
CD49f	Integrin α6	(+)	+	+	+	BC, Gli, CRC	HSC	rare (urinary, rectum, bladder)
CD44	Hyaluronate receptor	+	O		+	BC, GC, CRC, HCC, OC, PanC, HNSCC	AT, HSC	most epithelia, lymph tissue
CD56	NCAM	(+)	O		+	LC	Renal, Muscle	rare (lymphoid)
CD73	Ecto-5-nucleotidase	+			+	RCC	Renal	lymphoid, smooth muscle, epi-, endothelial
CD90	Thy-1	+			+	Brain, HCC	Card	rare (neural, T-Cell, mesangial, endothelial)
CD105	Endoglin	+	O	+	+	RCC	Renal (some)	rare (endothelial)
CD106	VCAM-1	(+)		+			Muscle, Renal	
CD146	MCAM	+		+		Rhabdoid sarcoma	Renal	rare (endothelial)
CD326	EpCAM		+		+	CRC, PancC, HCC	IESC	rare (epithelial, intestinal, thyroid, kidney)
CD24	CD24 molecule		+		+/O	BC, GC, PancC, RCC	IESC, Renal	rare (B-Cell, neural, renal tubules)
CD133	Prominin-1				+	BC, CRC, Gli, PC, HCC, LC, OvC, RCC	HSC, NSC, PSC, Renal	rare (proliferative)
CD271	NGFR	(+)	O		+	Melanoma, HNSCC	NSC, Epidermal	rare (neural crest)
CD184	CXCR4		O	+	+	BC, Brain, PancC, RCC	NSC, Muscle	rare (lymphoid)
	CXCR7							
CD243	MDR1/ABCB1						diverse	intestine, liver, kidney, placenta, BBB
	SSEA-3	+	+			BC, TC		rare
	SSEA-4	+	+		+	LC, CRC, BC, TC	Card	rare
	TRA-1-81		+			BC, TC	Renal	rare
CD15	SSEA-1		O	+		RCC-Marker, Gli (mouse)		

+	positive
O	negative
+/O	variying
(+)	low expression

Table 4.6.1: Overview of Expression of Evaluated CSC Markers in Different Cells and Tissues

★ Expression of markers in adult SC and adult tissues predominantly based on Kim et al [60] and other literature cited in this work (not supposed to be complete).
AT: adipose tissue, BC: breast cancer, BBB: blood-brain barrier, Card: cardiac stem cells, CD: cluster of differentiation, CRC: colorectal carcinoma, CSC: cancer stem cells, CXCR: C-X-C chemokine receptor, EMT: epithelial-to-mesenchymal transition, Endo: endothelial cells, EpCAM: epithelial cellular adhesion molecule, ESC: embryonic stem cells, Gli: Glioma, HCC: hepatocellular carcinoma, HIF: hypoxia inducible factor, HNSCC: head and neck squamous cell carcinoma, HSC: hematopoietic stem cells, IESC: intestinal epithelial stem cells, LC: lung carcinoma, MCAM: melanoma cell adhesion molecule, MSC: mesenchymal stem cells, NCAM: neural cell adhesion molecule, NGFR: nerve growth factor receptor/low affinity nerve growth factor receptor, NSC: neural stem cells, PanC: pancreas carcinoma, PC: prostate cancer, PSC: prostate stem cells, RCC: renal cell carcinoma, SC: stem cell, SSEA: stage-specific embryonic antigen, TC: teratocarcinoma

All measurements were performed with single cell suspensions prepared with AccuMax™ cell dissociation reagent and 7-AAD staining prior to measurement, to exclude dead cells in the following analysis. The cell lines PA, CS1, CS7, SP and A-CS1, A-CS7, A-SP at different passages, were either obtained by continuous culture of the cells or by thawing cells, that were frozen at different time points. For the cell line CE1 for some of the antigens less data were available than for the other cell lines.

4.6.1 Marker with Low Variation in Expression on Different Cell Lines and Passages

Some of the assayed markers showed only slight variations in expression between different cell lines tested as well as over time in culture of the cells. Representative results for staining of these markers on PA cell line, which are also representative for SP and CS7 cells, and with exception of CD44 (hyaluronate receptor) and EpCAM (epithelial cellular adhesion molecule) for CS1 cells in high passage number (see chapter 4.6.5), are depicted in figure 4.6.1. Also no change in expression of these markers was seen in A-CS and A-SP cells.

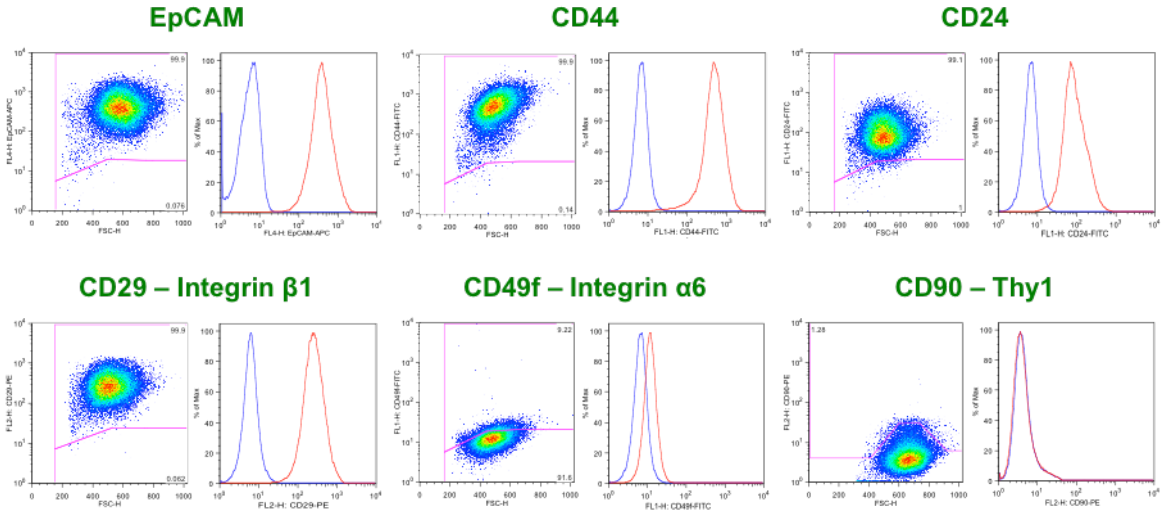

Figure 4.6.1: Representative Results for IFC-Staining of Markers Showing Low Variability

EpCAM, CD44, CD24 and CD29 showed similar low-varying high staining intensities on all cell lines. CD49f staining was low on all cell lines. No staining was detected for CD90 in all cell lines.
Flow cytometric immunophenotyping (IFC) of PA cells stained with different antibodies: EpCAM-APC (P62), CD29-PE (P38), CD44-FITC (P38), CD24-FITC (P38), CD29f-FITC (P38), CD90-APC (P33). Results are representative for all tested cell lines and passages (except CS1: CD44/EpCAM, see chapter 4.6.5).
Figure left: scatter plot of fluorescence intensity vs. forward scatter (cell size) of „live cell population". Figure right: histogram of % Max (events) vs. fluorescence intensity, overlay of isotype control (blue) and sample (red).
APC: allophycocyanin, CD: cluster of differentiation, CS: clonally expanded spheroid cells derived from PA, EpCAM: epithelial cellular adhesion molecule, FITC: fluorescein isothiocyanate, FL1/2/4-H: fluorescence channel, FSC-H: forward scatter, PA: parental cell line, PE: phycoerythrin

EpCAM expression was measured with two different antibodies. The APC conjugated antibody showed very high staining intensities on all cells, whereas the signal of FITC conjugated antibody gave much weaker signals. EpCAM was expressed at very similar levels (dependent on antibody used) on all cell lines and passages investigated. An exception was the CS1 cell line, on which reduced and variable EpCAM staining was observed over time in culture (see figure 4.6.25).

Similar results, also concerning expression on CS1 cell line (see figure 4.6.26), were obtained for CD44 staining, for which a FITC conjugated antibody with resulting high staining intensities was used.

For staining of CD24 with a FITC conjugated antibody a similar staining profile with intermediate staining intensities was seen in all cell lines and passages.

Expression of CD29 (integrin β1) was assayed with a PE conjugated antibody, which resulted in constantly high signal intensities in the different cell lines at various tested passages.

In contrast, CD49f (integrin α6) was detected only at low levels on all cell lines with the used FITC conjugated antibody.

No staining was observed in any of the tested cell lines for CD90 antigen, which is a defining marker for MSC, although 3 different antibodies were used and in addition also staining with secondary antibody was performed. To exclude possible degradation of the CD90 antigen by AccuMax™ treatment, cells were also detached and/or dissociated using TNE-buffer. But also these experiments did not show any staining of the cells with the CD90 antibodies.

4.6.2 Marker with Reduced Expression in Spheroid Cell Lines Compared to PA Cell Line

Some of the assayed markers showed reduced expression on spheroid cell lines compared to PA cell line. To test whether these changes were possibly induced by different culture conditions, these markers were also evaluated in spheroid cell lines grown under ACC. Since spheroid culture conditions have been shown to enrich for TIC and SC, markers that are expressed to a lesser extent on these cells do not seem to be suitable markers for direct enrichment of TIC from the PA cell line.

4.6.2.1 CD146 - Melanoma Cell Adhesion Molecule - (MCAM)

CD146 (MCAM), which is usually expressed on mesenchymal as well as on epithelial cells and has been found to be a marker for adult renal progenitor cells, was expressed at low level in the PA cell line with a mean of 25% low positive staining cells and a very slight shift of the cell population towards higher fluorescence intensity compared to isotype control samples seen with the FITC conjugated antibody used. Compared to PA cells, SP cells showed reduced expression of the marker with a mean of 5% positive cells, whereas on CS cells only single cells showed slight staining for the marker. Representative results for CD146 staining of the cell lines PA, SP and CS (CS1 and CS7) are shown in figure 4.6.2.

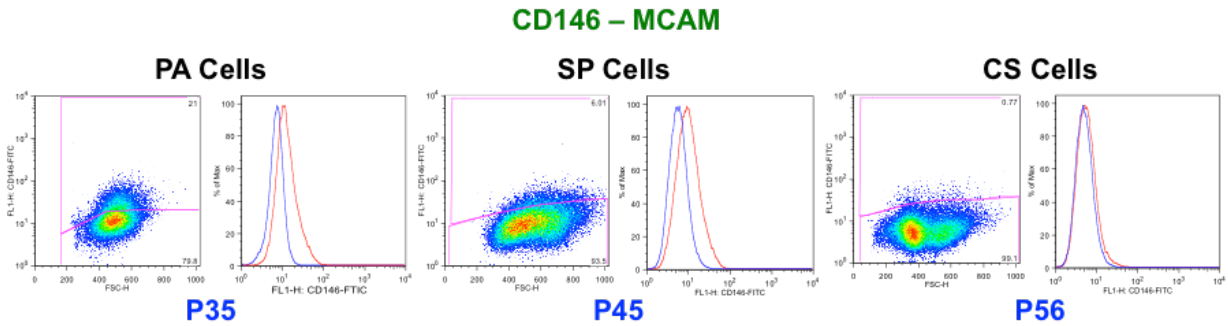

Figure 4.6.2: IFC-Staining of CD146 (MCAM) on Different Cell Lines

CD146 staining is observed on PA and SP cell lines with low staining intensity, but not on CS cell lines.
Flow cytometric immunophenotyping (IFC) of cells stained with FITC conjugated antibody for detection of CD146 antigen. Representative results for PA (n=23, P28-117), SP (n=11, P18-80), and CS cell lines CS1 (n=2, P18-P21) and CS7 (n=8, P10-P90). Passage of cells indicated in blue.
Figure left: scatter plot of fluorescence intensity vs. forward scatter (cell size) of „live cell population“. Figure right: histogram of % Max (events) vs. fluorescence intensity, overlay of isotype control (blue) and sample (red).
CD: cluster of differentiation, CS: clonally expanded spheroid cells derived from PA, FITC: fluorescein isothiocyanate, FL1-H: fluorescence channel 1, FSC-H: forward scatter, FITC: fluorescein isothiocyanate, MCAM: melanoma cell adhesion molecule, P: passage number, PA: parental cell line, SP: spheroid cells derived from PA

In contrast to the very low expression on spheroid cell lines, CD146 was rapidly and clearly induced, when spheroids were grown under ACC, as can be seen in figure 4.6.3. Thereby the CS cell lines, which under ACC show almost no staining for the antigen, express the molecule after long-term culture under ACC at even higher level (mean of both cell lines CS1 and CS7 was 40% positive cells) than PA cells. The markedly higher expression of CD146 in A-SP cells readily decreased after re-

culturing the cells under SCC in SP cells. This implies that CD146 expression is induced in spheroid cell lines either by serum or adherence of the cells. Another possibility of enhanced expression would be epithelial differentiation of the cells, when cultured under ACC. But the rapid decrease of expression points rather to a culture-condition dependent variation than to a differentiation process.

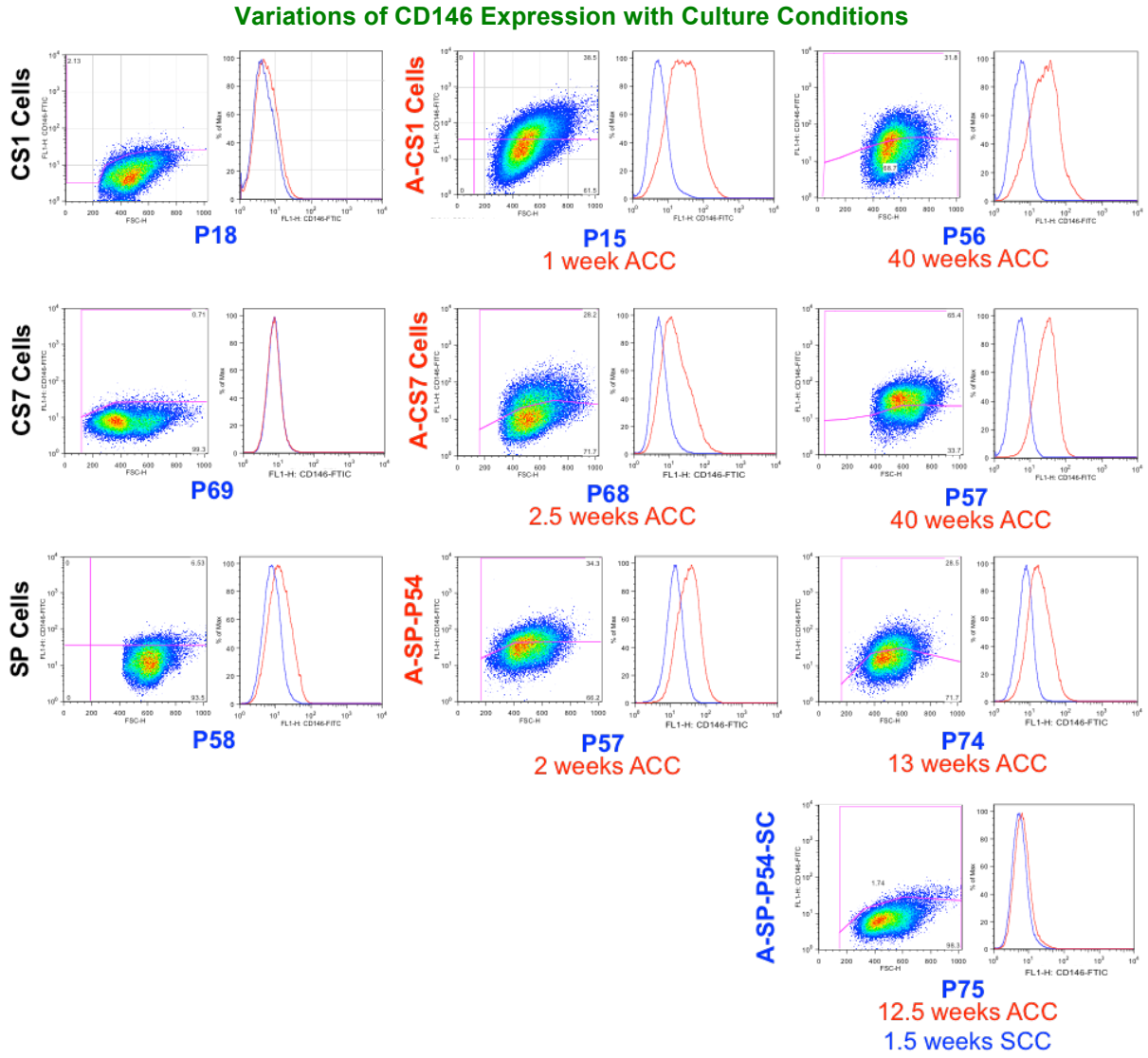

Figure 4.6.3: Comparison of CD146 Expression on Spheroid Cell Lines Grown under SCC or ACC

Expression of CD146 increases in spheroid cell lines under ACC and decreases after re-culturing under SCC. Flow cytometric immunophenotyping (IFC) of cells stained with FITC conjugated antibody for detection of CD146 antigen. Comparison of CS1, CS7 and SP cell lines in different passages (indicated in blue) representing parental spheroid cell lines at similar time point of measurement. Results are representative for A-CS7-P6/66 (n=3, P57-83, 2-40 w ACC), A-SP-SC (n=3, 1.5 w SCC, and A-CS7-SC n=1). For CS1 no further results are available. Figure left: scatter plot of fluorescence intensity vs. forward scatter (cell size) of „live cell population“. Figure right: histogram of % Max (events) vs. fluorescence intensity, overlay of isotype control (blue) and sample (red).
ACC: adherent culture conditions, A-CS: CS cells grown under ACC, A-SP: SP cells grown under ACC, CD: cluster of differentiation, CS: clonally expanded spheroid cells derived from PA, FITC: fluorescein isothiocyanate, FL1-H: fluorescence channel 1, FSC-H: forward scatter, MCAM: melanoma cell adhesion molecule, P: passage number, PA: parental cell line, SP: spheroid cells derived from PA, w: weeks

4.6.2.2 CD106 (Vascular Cell Adhesion Molecule 1 - VCAM-1)

CD106 (VCAM-1), which is similar to CD146 expressed on mesenchymal as well as on epithelial cells, was expressed at low level on a fraction of 10-50% of cells of the PA cell line with a mean of 22% positive staining cells seen with the PE conjugated antibody used. By contrast, no expression of this molecule was seen on the spheroid cell lines SP, CS1 and CS7. Representative results for CD106 staining of the cell lines are depicted in figure 4.6.4.

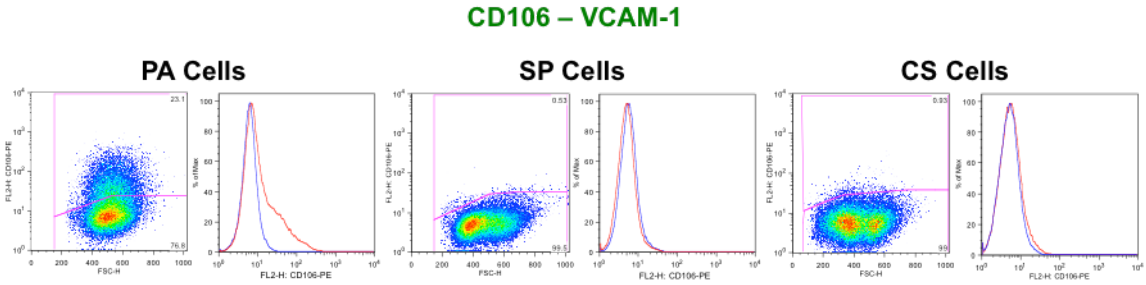

Figure 4.6.4: IFC-Staining of CD106 (VCAM-1) on Different Cell Lines

CD106 staining is seen in a subpopulation of PA cell line, whereas no staining is observed in spheroid cell lines. Flow cytometric immunophenotyping (IFC) of cells stained with PE conjugated antibody for detection of CD106 antigen. Representative results for PA (n=16, P29-130), SP (n=21, P17-115), and CS cell lines CS1 (n=6, P8-P96) and CS7 (n=13, P7-P95). Passage of cells indicated in blue.
Figure left: scatter plot of fluorescence intensity vs. forward scatter (cell size) of „live cell population“. Figure right: histogram of % Max (events) vs. fluorescence intensity, overlay of isotype control (blue) and sample (red).
CD: cluster of differentiation, CS: clonally expanded spheroid cells derived from PA, FL2-H: fluorescence channel 2, FSC-H: forward scatter, P: passage number, PA: parental cell line, PE: phycoerythrin, SP: spheroid cells derived from PA, VCAM: vascular cell adhesion molecule

Similar to CD146, CD106 expression increased when spheroids were grown under ACC. Three example experiments are shown in figure 4.6.5. As can be seen, the fraction of CD106 positive cells, as well as the time course of expression of the molecule after ACC culture varied highly between different assayed cell lines. Whereas the increase in low passage spheroid cells seemed to be faster and resulting in a higher portion of CD106 positive cells, in cells cultured at later passage under ACC, the increase in CD106 expression appeared at later time points and fewer cells stained positive for the marker. Upon re-culturing under SCC, the expression of CD106 was clearly reduced in all tested cell lines (n=4). Due to the high variability, the data obtained are not sufficient to gain a clear picture of CD106 expression on the tested cell lines.

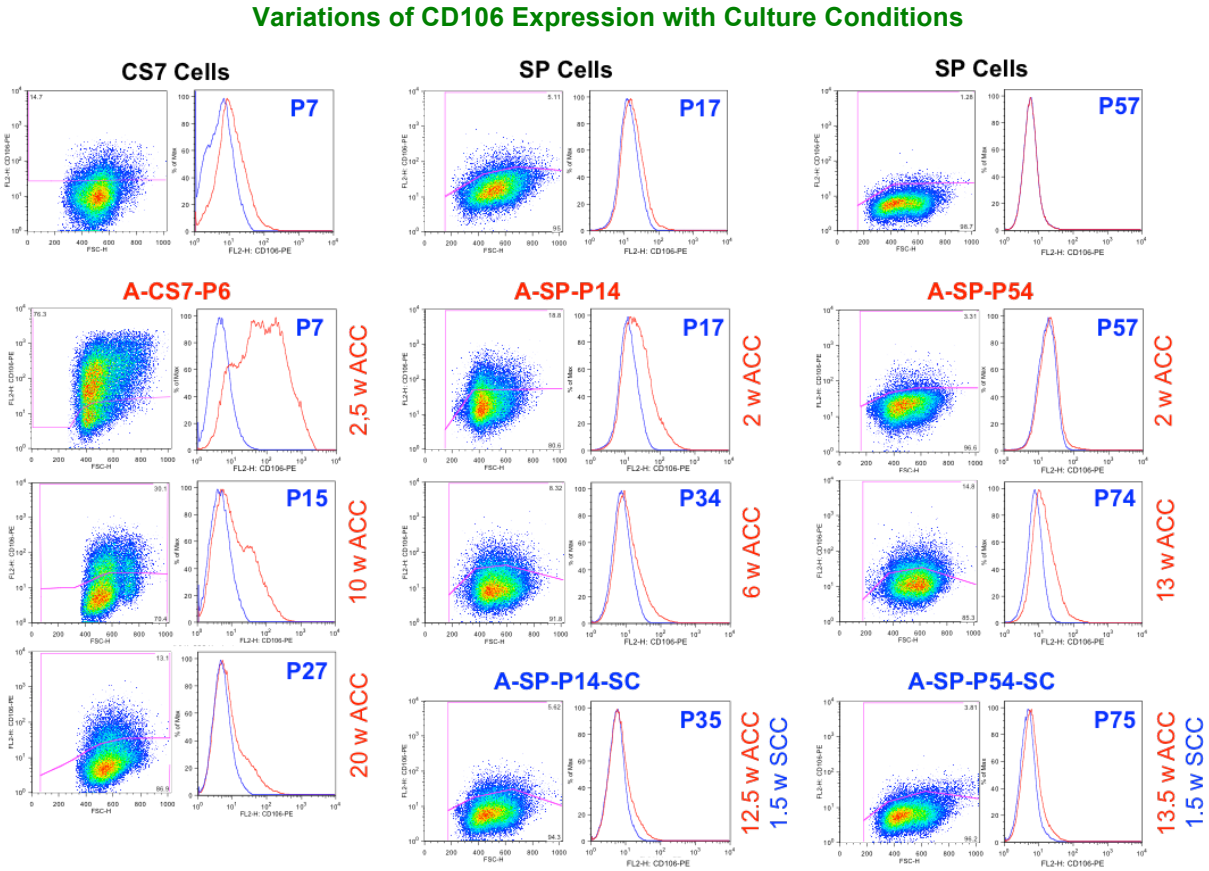

Figure 4.6.5: Comparison of CD106 Expression on Spheroid Cell Lines Grown under SCC or ACC

Expression of CD106 is observed at variable degrees in spheroid cell lines cultured under ACC and decreases after re-culture under SCC.
Flow cytometric immunophenotyping (IFC) of cells stained with PE conjugated antibody for detection of CD106 antigen. Comparison of CS7 and SP cell lines in different passages (indicated in blue) representing parental spheroid cell lines at similar time point of first measurement with A-CS7 and A-SP cells cultured for the indicated time under ACC. A-SP-SC cells were cultured for the indicated periods under ACC before re-cultivation under SCC for indicated periods before measurement. Results for A-SP-P54 are similar to results for A-SP-P63 and A-CS7-P66, and results for A-SP-P14 are similar to A-SP-P36.
Figure left: scatter plot of fluorescence intensity vs. forward scatter (cell size) of „live cell population“. Figure right: histogram of % Max (events) vs. fluorescence intensity, overlay of isotype control (blue) and sample (red).
CD: cluster of differentiation, CS: clonally expanded spheroid cells derived from PA, FL2-H: fluorescence channel 2, FSC-H: forward scatter, P: passage number, PA: parental cell line, PE: phycoerythrin, SP: spheroid cells derived from PA, VCAM: vascular cell adhesion molecule

4.6.2.3 CD105 (Endoglin)

CD105 (Endoglin) is a marker for MSC and has been found to be a suitable marker for CSC from RCC tumors and cell lines. Representative results for staining of the different cell lines PA, SP and CS (CS1 and CS7 in low to intermediate passage numbers) with PE-conjugated antibody against CD105 are shown in figure 4.6.6. In PA cells an intermediate staining pattern, showing equal distributions with almost all cells being positive for CD105 expression was observed, which in contrast to spheroid cell lines also did not show significant variation with time of culture of the cells. In spheroid cell lines variations in expression of CD105 were seen over time in culture, which is illustrated in figure 4.6.7.

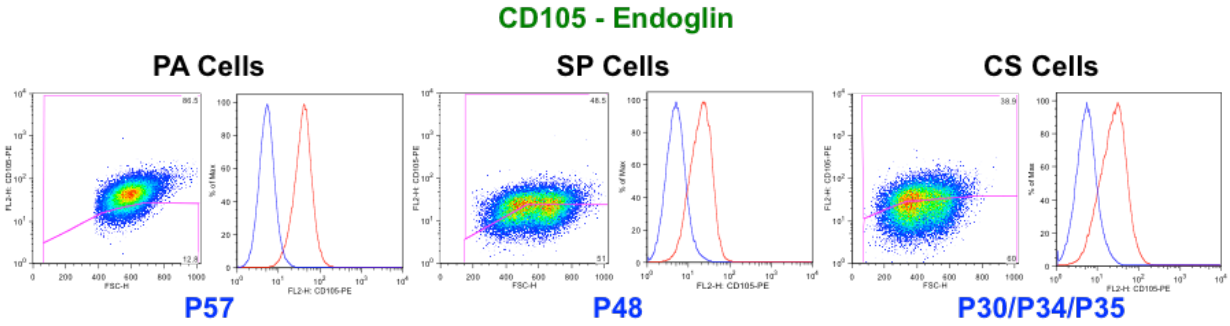

Figure 4.6.6: IFC-Staining of CD105 (Endoglin) on Different Cell Lines

Homogenous CD105 staining is seen on all cell lines, albeit with lower staining intensities in spheroid cell lines.
Flow cytometric immunophenotyping (IFC) of cells stained with PE conjugated antibody for detection of CD105 antigen. Representative results for PA (n=15, P28-130), SP (n=22, P17-P84), and CS cell lines CS1 (n=6, P18-P96) and CS7 (n=10, P10-P95) at low to intermediate passage numbers (see also figure 4.6.7).
Figure left: scatter plot of fluorescence intensity vs. forward scatter (cell size) of „live cell population". Figure right: histogram of % Max (events) vs. fluorescence intensity overlay of isotype control (blue) and sample (red).
CD: cluster of differentiation, CS: clonally expanded spheroid cells derived from PA, FL2-H: fluorescence channel 2, FSC-H: forward scatter, P: passage number, PA: parental cell line, PE: phycoerythrin, SP: spheroid cells derived from PA

In SP cell lines the expression level of CD105 was reduced, compared to PA cell line, although the staining pattern showed similar distribution as for PA cells, with a clear shift of the whole population to higher values compared to isotype control. Over time in culture the expression seemed to be slightly reduced (see figure 4.6.7) in SP cells, as indicated by reduced shifting of the population compared to isotype control, with some variation seen in different experiments.

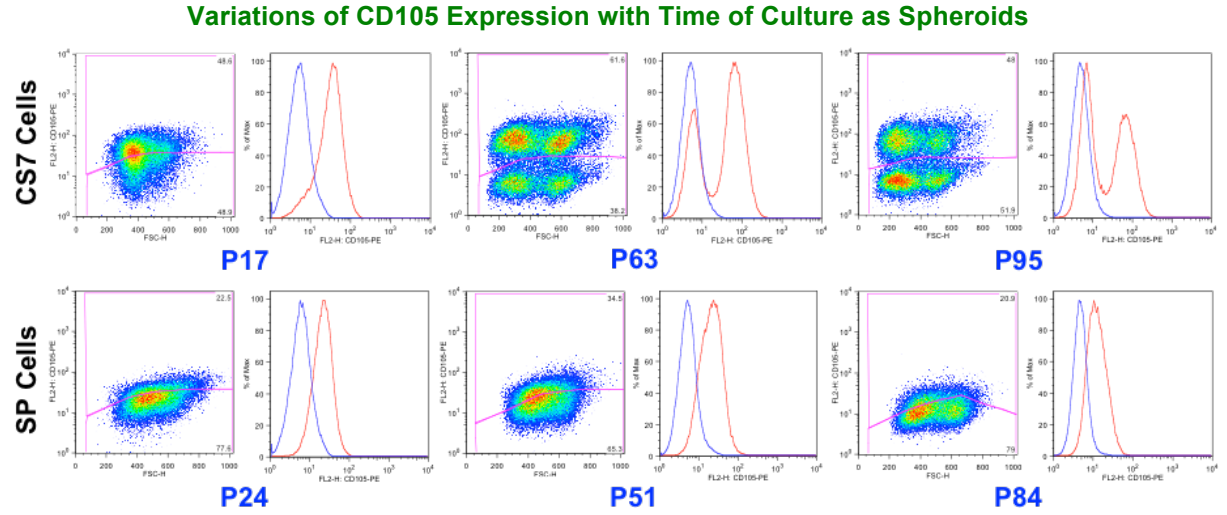

Figure 4.6.7: CD105 Variations in Expression with Time of Culture of Spheroid Cell Lines

CD105 expression is reduced on spheroid cell lines with time of culture under SCC and in CS cell lines a CD105 negative cell population evolves.
Flow cytometric immunophenotyping (IFC) of cells stained with PE conjugated antibody for detection of CD105 antigen on CS7 and SC cell lines in different passages (indicated in blue). Results are representative for cells at similar passage numbers.
Figure left: scatter plot of fluorescence intensity vs. forward scatter (cell size) of „live cell population". Figure right: histogram of % Max (events) vs. fluorescence intensity overlay of isotype control (blue) and sample (red).
CD: cluster of differentiation, CS7: clonally expanded spheroid cells derived from PA, FL2-H: fluorescence channel 2, FSC-H: forward scatter, P: passage number, PA: parental cell line, PE: phycoerythrin, SP: spheroid cells derived from PA

In contrast to the equal distribution of CD105 staining on PA and SP cell lines, CS cell lines, especially CS7, seemed to contain a CD105-high and a CD105-low/negative cell population, which were clearly discernible after long-term culture under SCC (see figure 4.6.8). The phenomenon was observed for cells grown continuously (CS7-B) as well as for cell lines frozen at different passages as shown in (CS7-A), where P16 and P30 were derived of cells frozen at P6 and P69 and P90 were derived from cells frozen at P66. For CS7 the evolvement of a CD105 negative cell population was also seen in cells cultured for long-term under ACC (A-CS7-P6, P57, 40 weeks ACC), although the expression of CD105 under this conditions seemed to be more constant than in cells cultured as spheroids. The seemingly more stable expression of CD105 under ACC can also be seen from results obtained for CS1 cells cultured under ACC (A-CS1), which are depicted in figure 4.6.8, showing that CD105 expression remained almost constant over 40 weeks under ACC, whereas the parental spheroid cell line showed marked reduction in CD105 expression. In this cell line the CD105-negative fraction was not as clearly visible and emerged at later passage (P64/96) than in CS7 cells.

Variations of CD105 Expression with Culture Conditions in CS Cell Lines

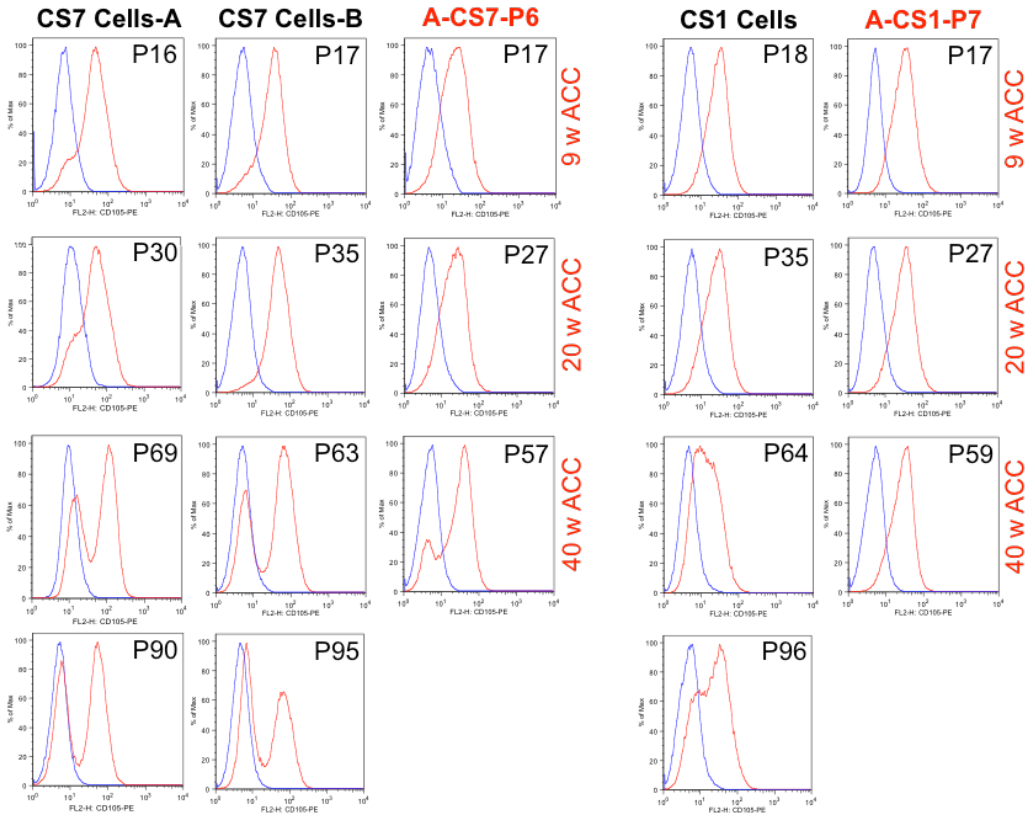

Figure 4.6.8: Comparison of CD105 Expression on CS Cell Lines Grown under SCC or ACC

In CS cell lines over time a CD105$^-$negative cell fraction evolves, which is more clearly visible in CS7 cell line. When cultured under ACC the expression of CD105 seems to be more stable than under SCC.
Flow cytometric immunophenotyping (IFC) of cells stained with PE conjugated antibody for detection of CD105 antigen on CS1 and CS7 cell lines in different passages (indicated on top right) grown continuously (CS1, CS7-B) or cells frozen at passage 8 (P16, P30) or 64 (P69, P90) and grown for several weeks (CS7-A). A-CS1-P7 and A-CS7-P6 cells were grown continuously under ACC for the indicated time from passage 7 and 6 respectively.
Figure left: scatter plot of fluorescence intensity vs. forward scatter (cell size) of „live cell population“. Figure right: histogram of % Max (events) vs. fluorescence intensity overlay of isotype control (blue) and sample (red).
ACC: adherent culture conditions, A-CS: CS cells grown under ACC, CD: cluster of differentiation, CS: clonally expanded spheroid cells derived from PA, FL2-H: fluorescence channel 2, FSC-H: forward scatter, P: passage number, PA: parental cell line, PE: phycoerythrin, w: weeks

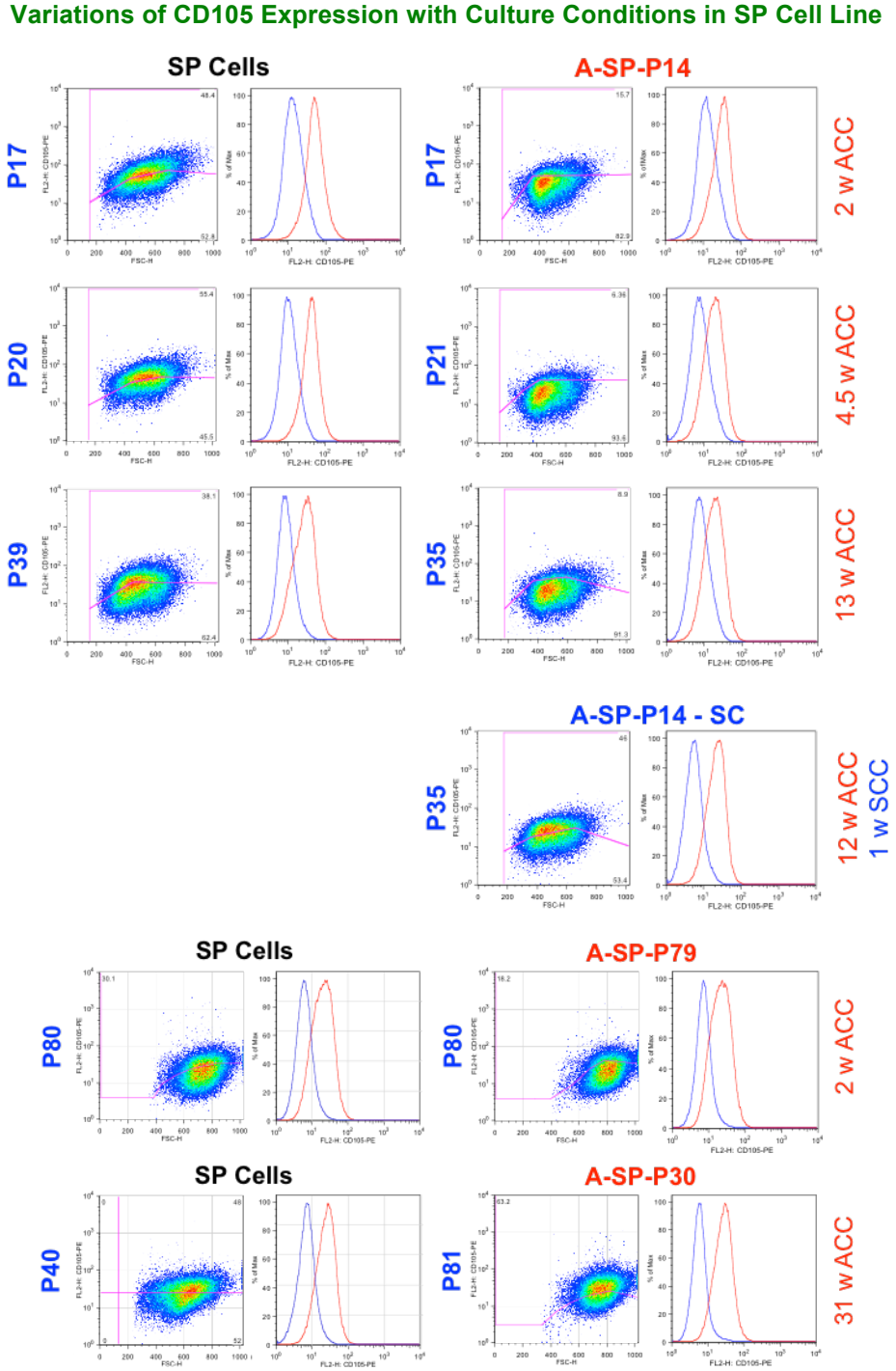

Figure 4.6.9: Comparison of CD105 Expression on SP Cell Lines Grown under SCC or AC

Expression of CD105 on SP cells was either reduced under ACC and re-induced under SCC or remained constant even after long-term culture.
Flow cytometric immunophenotyping (IFC) of cells stained with PE conjugated antibody for detection of CD105 antigen on Comparison of expression on SC cell lines in different passages (indicated in blue) representing either parental spheroid cell lines at start of ACC culture (P17, P40) or at similar time point of measurement (P39, P80, P20) and A-CS cells grown for the indicated time under ACC. Two sets of experiments with different results: A-SP-P14 also representative for A-SP-P36 and A-SP-P54 in one experiment performed on cell lines thawed at different passage numbers, and A-SP-P30 and A-SP-P79 experiments performed on continuously grown cells.
Figure left: scatter plot of fluorescence intensity vs. forward scatter (cell size) of „live cell population“. Figure right: histogram of % Max (events) vs. fluorescence intensity overlay of isotype control (blue) and sample (red).
ACC: adherent culture conditions, A-SP: SP cells grown under ACC, CD: cluster of differentiation, FL2-H: fluorescence channel 2, FSC-H: forward scatter, P: passage number, PA: parental cell line, PE: phycoerythrin, SP: spheroid cells derived from PA, w: weeks

For SP cell lines, data obtained varied between different experiments, not only concerning the reduction of CD105 expression level with time of culture of the cells but also concerning changes of expression under ACC (see figure 4.6.9). Whereas in one set of experiments no significant changes were seen regarding CD105 expression, even after long-term culture under ACC (A-SP-P79 and P30), which was similar to the staining profile seen in A-CS1 cell line, in another set of experiments CD105 expression was clearly reduced upon culturing the cells under ACC (A-SP-P14, also seen in A-SP-P54). In this set of experiments also an increase of CD105 expression was seen, after re-culturing A-SP cells under SCC for 9 days. The reason for these variations is not clear, which makes further experimental data necessary to understand the regulation of CD105 expression on these cells.

4.6.2.4 CD243 (MDR1/ABCB1)

Since CD243 (MDR1/ABCB1) seems do be the determining transporter for Rhodamine 123 in side population assay (see chapter 4.10), the expression of this molecule was measured by flow cytometry on cell lines PA, CS1, CS7, SP and A-CS1, A-CS7, A-SP in different passage numbers.

Clear but variable expression of CD243 was detected on PA cells, with a clear shift in staining of the whole cell population compared to isotype controls (mean fold change geo mean = 3±1) resulting 8-60% positive staining cells (mean 32%±14%). In SP cells the staining pattern was different in that only a fraction of cells stained positive (mean 8% positive cells), whereas most of the cells did not show expression of the marker. CS cell lines were negative for CD243 expression, with staining seen only on single cells (mean 1-2% positive cells). Representative results for staining with APC conjugated antibody against CD243 are shown in figure 4.6.10.

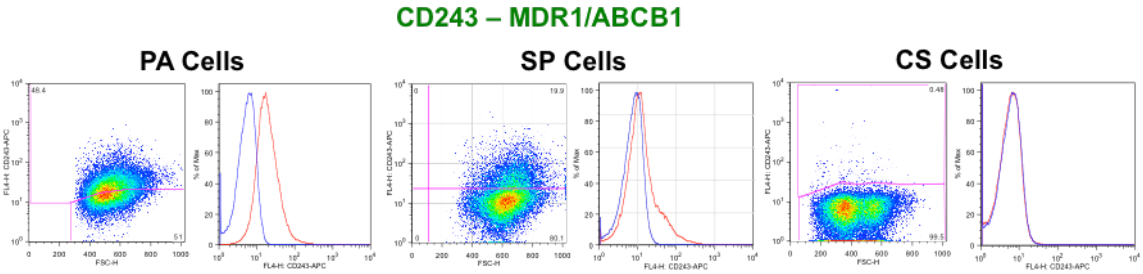

Figure 4.6.10: IFC-Staining of CD243 (MDR1/ABCB1) on Different Cell Lines

CD243 expression differs in PA and spheroid cell lines, with clear expression of CD243 in PA cells and reduced or lack of expression on SP and CS cells, respectively.
Flow cytometric immunophenotyping (IFC) of cells stained with APC conjugated antibody for detection of CD243 antigen on PA (P33), SP (P50) and CS - (CS1/7 -CS7 P36) cell lines. Representative results for PA (n=19, P28-117), SP (n=8, P26-96), and CS cell lines CS1 (n=3, P8-P37) and CS7 (n=2, P7-36).
Figure left: histogram of % Max (events) vs. fluorescence intensity overlay of isotype control (blue) and sample (red) for FITC conjugated antibody stained cells. Figure right: scatter plot of fluorescence intensity vs. forward scatter (cell size) of „live cell population“ for APC conjugated antibody stained cells.
APC: allophycocyanin, CD: cluster of differentiation, CS: clonally expanded spheroid cells derived from PA, FL4-H: fluorescence channel 4, FSC-H: forward scatter, P: passage number, PA: parental cell line, SP: spheroid cells derived from PA

Expression of CD243 was also evaluated on A-CS and A-SP cells. Under these conditions, CD243 expression was seen in a higher fraction of the A-SP cells (mean 20%) compared to SP cell line and the same was observed for A-CS cell lines, which showed positive staining in about 15% of the cells. Results obtained from an experiment comparing the expression of CD243 on parental spheroid cells with A-CS/SP cells after one to two weeks under ACC are shown in figure 4.6.11.

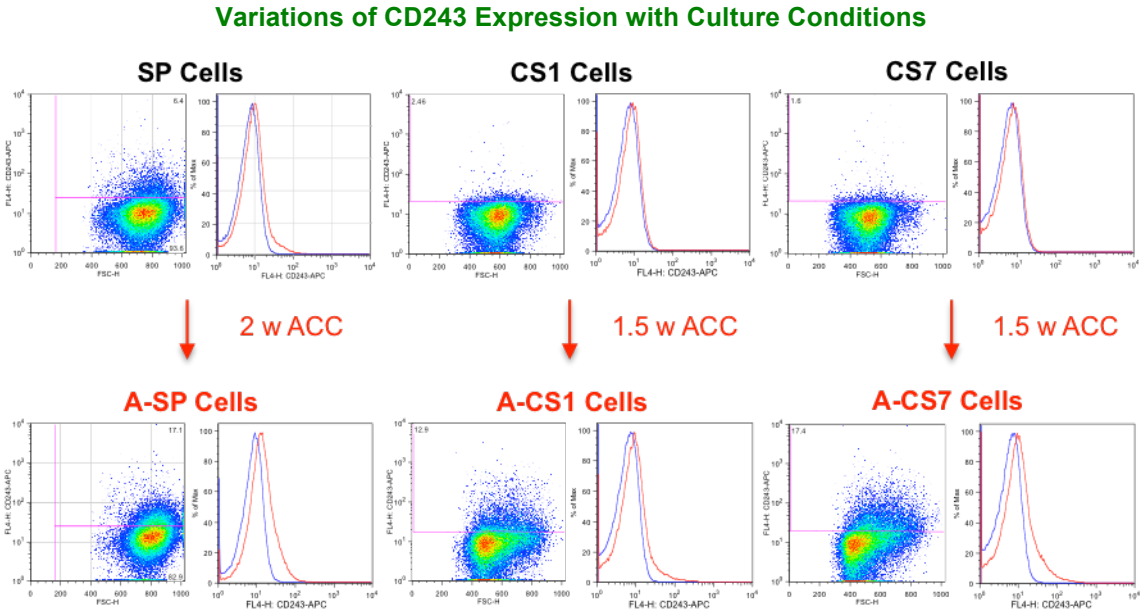

Figure 4.6.11: Comparison of CD243 (MDR1) on Spheroid Cell Lines Grown under SSC or ACC

Expression of CD243 is induced in spheroid cell lines under ACC.
Flow cytometric immunophenotyping (IFC) of cells stained with APC conjugated antibody for detection of CD243 antigen. Comparison of CS1, CS7 and SP cell lines representing parental spheroid cell lines at similar time point of measurement with A-CS1, A-CS7 and A-SP cell lines grown for indicated time under ACC. Results for A-SP are representative for A-SP (n=8, A-A-SP-P30-84, 1-38 w ACC). For CS cell lines no further results are available.
Figure left: scatter plot of fluorescence intensity vs. forward scatter (cell size) of „live cell population“. Figure right: histogram of % Max (events) vs. fluorescence intensity overlay of isotype control (blue) and sample (red).
ACC: adherent culture conditions, A-CS: CS cells grown under ACC, APC: allophycocyanin, A-SP: SP cells grown under ACC, CD: cluster of differentiation, CS: clonally expanded spheroid cells derived from PA, FL4-H: fluorescence channel 4, FSC-H: forward scatter, MDR1 (multi drug resistant protein 1), P: passage number, PA: parental cell line, SP: spheroid cells derived from PA, w: weeks

4.6.3 Marker Expressed with Higher Staining Intensity on Spheroid Cells

4.6.3.1 CD73 (Ecto-5-Nucleotidase)

The enzyme CD73 serves as a marker for MSC and has recently been identified to be a TIC marker in RCC[210] when expressed at high level. With the APC conjugated antibody used, CD73 was stained with high intensity on all cell lines. Though, the staining intensity was found to be significantly higher in SP cells compared to PA or CS cell lines. This as can be seen from the representative results obtained for CD73 staining shown in figure 4.6.12 and the diagram in figure 4.6.13 showing mean relative staining intensities for CD73. The staining pattern for CD73 of CS cell lines showed a broader distribution than those seen in PA and SP cells, ranging from CD73 low expressing cells to CD73 high expressing cells as were seen in SP cell line.

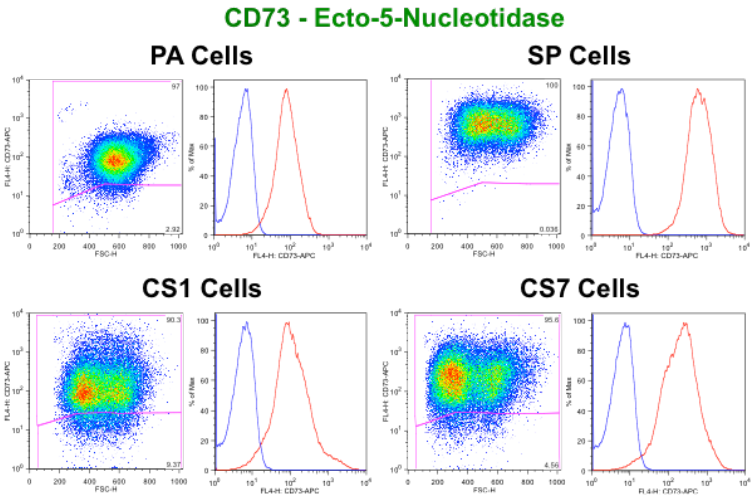

Figure 4.6.12: IFC-Staining of CD73 (Ecto-5-Nucleotidase) on Different Cell Lines

Flow cytometric immunophenotyping (IFC) of cells stained with APC conjugated antibody for detection of CD73 antigen. Representative results for PA (n=5, P59-129), SP (n=6, P44-84), and CS cell lines CS1 (n=2, P64, P96) and CS7 (n=2, P37, P53). Figure left: scatter plot of fluorescence intensity vs. forward scatter (cell size) of „live cell population". Figure right: histogram of % Max (events) vs. fluorescence intensity overlay of isotype control (blue) and sample (red). APC: allophycocyanin, CD: cluster of differentiation, CS: clonally expanded spheroid cells derived from PA, FL4-H: fluorescence channel 4, FSC-H: forward scatter, P: passage number, PA: parental cell line, SP: spheroid cells derived from PA

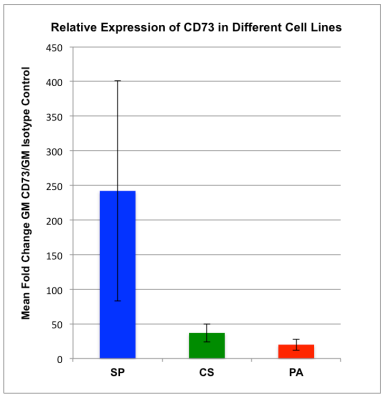

Figure 4.6.13: Relative IFC-Staining Intensity of CD73 (Ecto-5-Nucleotidase) in Different Cell Lines

Mean of fold change expression levels for CD73 stained samples. Number of samples: CS1 = 2, CS7 = 2, SP = 6, PA = 5. Fold change was calculated relative to respective isotype control: Fold change expression = GM CD73 stained sample/GM isotype control stained sample. Error bars: standard deviation.
APC: allophycocyanin, CD: cluster of differentiation, CS: clonally expanded spheroid cells derived from PA, IFC: flow cytometric immunophenotyping PA: parental cell line, SP: spheroid cells derived from PA

4.6.3.2 CD49e (Integrin α5)

Integrin α5 is expressed on MSC and epithelial cells and serves as MSC marker.

For detection of CD49e a PE conjugated antibody was used. The staining revealed a higher overall expression of CD49e on spheroid cell lines SP and CS7 compared to PA cell line. Additionally, in all cell lines an increase in CD49e staining intensity was observed with prolonged culturing of the cells. This is shown exemplary in figure 4.6.14.

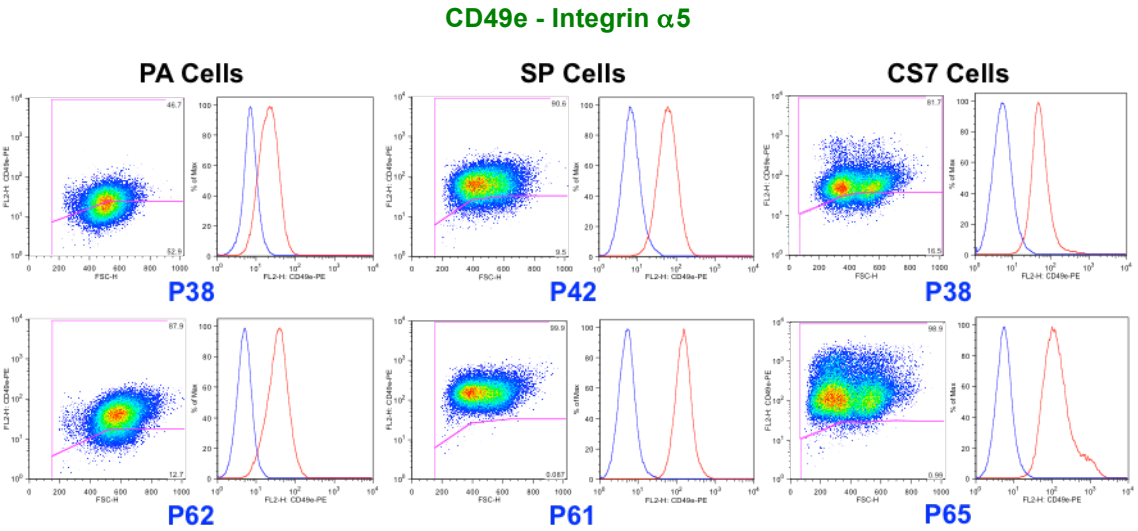

Figure 4.6.14: IFC-Staining of CD49e (Integrin α5) in Different Cell Lines

Flow cytometric immunophenotyping (IFC) of cells stained with PE conjugated antibody for detection of CD49 antigen. Representative results for PA (n=8, P34-129), SP (n= 12, P20-101), and CS7 (n=6, P14-90) cell lines. CS7 are also representative for CS1 (n=2, P40, P66)
Figure left: scatter plot of fluorescence intensity vs. forward scatter (cell size) of „live cell population". Figure right: histogram of % Max (events) vs. fluorescence intensity overlay of isotype control (blue) and sample (red).
CD: cluster of differentiation, CS: clonally expanded spheroid cells derived from PA, FL4-H: fluorescence channel 4, FSC-H: forward scatter, PA: parental cell line, PE: phycoerythrin, SP: spheroid cells derived from PA

CD49e staining was reduced in A-CS7 and A-SP cells compared to their parental spheroid cell lines, which is shown in figure 4.6.15. Also an increase in CD49e staining intensity after re-culturing adherently cultured spheroid cell lines under SCC was observed. Although the staining intensity was markedly reduced in A-CS7 and A-SP cell, the level measured after two weeks under ACC seemed to remain relatively constant over the assayed period of 13 weeks.

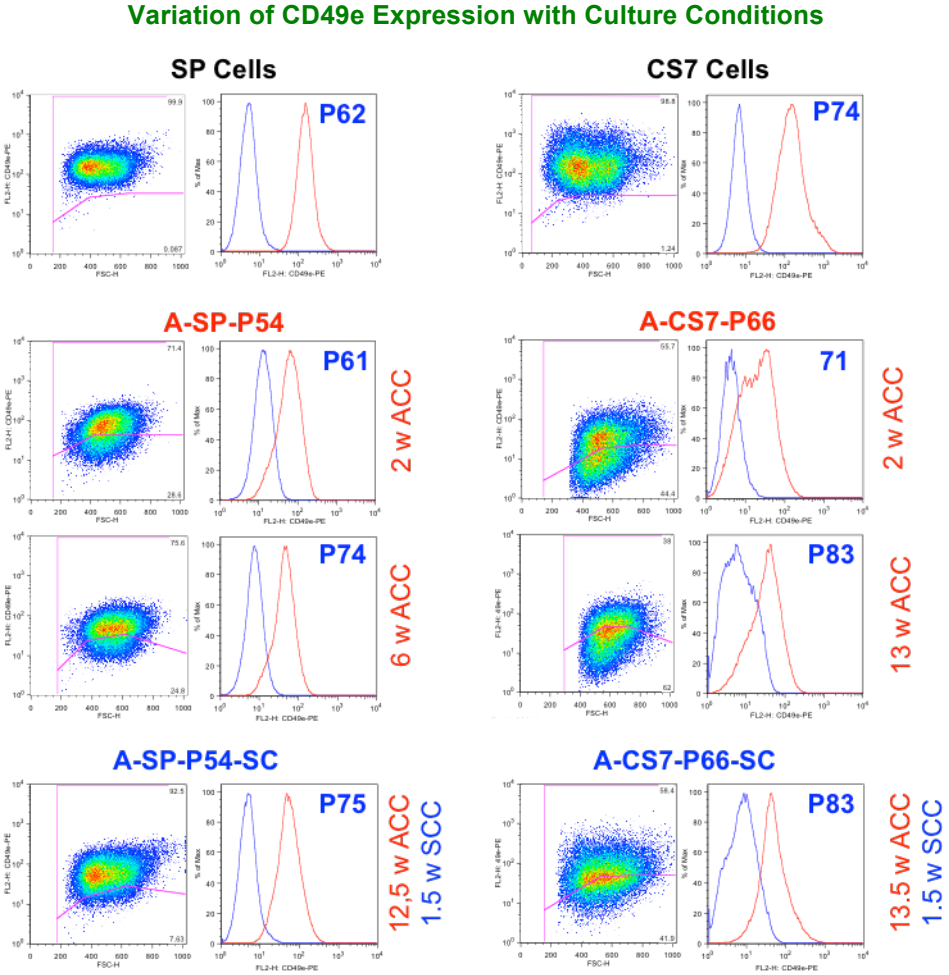

Figure 4.6.15: Comparison of CD49e Expression on Spheroid Cell Lines Grown under SCC or ACC

Flow cytometric immunophenotyping (IFC) of cells stained with PE conjugated antibody for detection of CD49 antigen. Comparison of CS7 and SP cell lines in different passages (indicated in blue) representing parental spheroid cell lines at comparable time point of first measurement with A-CS7 and A-SP cells cultured for the indicated time under ACC. A-SP-SC and A-CS7-SC cells were cultured for the indicated periods under ACC before re-cultivation under SCC for indicated periods. Results for A-SP-P54 are representative also for A-SP-P14/P36/P87 and results for A-SP-P54-SC are representative also for A-SP-P14/P36 -SC.
Figure left: scatter plot of fluorescence intensity vs. forward scatter (cell size) of „live cell population“. Figure right: histogram of % Max (events) vs. fluorescence intensity overlay of isotype control (blue) and sample (red).
ACC: adherent culture conditions, A-CS7: CS cells grown under ACC, A-SP: SP cells grown under ACC, A-CS7-SC: A-CS7 cells re-cultured under SCC, A-SP-SC: A-SP cells re-cultured under SCC, CD: cluster of differentiation, CS7: clonally expanded spheroid cells derived from PA, FL2-H: fluorescence channel 2, FSC-H: forward scatter, P: passage number, PA: parental cell line, PE: phycoerythrin, SCC: spheroid culture conditions, SP: spheroid cells derived from PA, w: weeks

4.6.4 Marker with Expression on Spheroid Cell Lines and Low or No Expression on PA Cells

Several CSC markers were identified to be expressed on spheroid cell lines, but they were very rarely detected on PA cells. To test whether these changes were possibly induced by different culture conditions, these markers were also evaluated in spheroid cell lines grown under ACC.

Since for direct enrichment of possible CSC from the PA cell line, markers have to be identified, which show only weak staining or staining of distinct cell populations on PA cell line and - assuming that sphere culture enriches for CSC - a more pronounced staining on spheroid cells, might render these markers possible candidates for enriching CSC directly from PA or RCC tissues.

4.6.4.1 CD271 (Nerve growth factor receptor - NGFR/LNGFR)

CD271 (Nerve growth factor receptor (NGFR)/low affinity nerve growth factor receptor (LNGFR)) has been shown to be an MSC marker as well as a promising CSC Marker for melanoma. For detection of CD271 three antibodies with different fluorochrome conjugation were used. With all three antibodies a very faint staining was observed with lowest levels seen with the FITC conjugated antibody. The same was true when staining was achieved by use of a secondary antibody against the primary mouse antibodies, which was done to exclude the possibility that the weak staining was due to problems with antibody conjugation. Although staining was very weak, in all experiments a slight shift of staining intensity compared to isotype control was seen in spheroid cell lines, indicating 5-15 % faintly positive cells. In the PA cell line only single positive cells (1-2%) were seen. No significant change of the staining pattern for CD271 was seen, when spheroid cell lines were cultured under ACC (A-CS, A-SP) for 2-16 weeks. Representative results for CD271 staining are shown in figure 4.6.16.

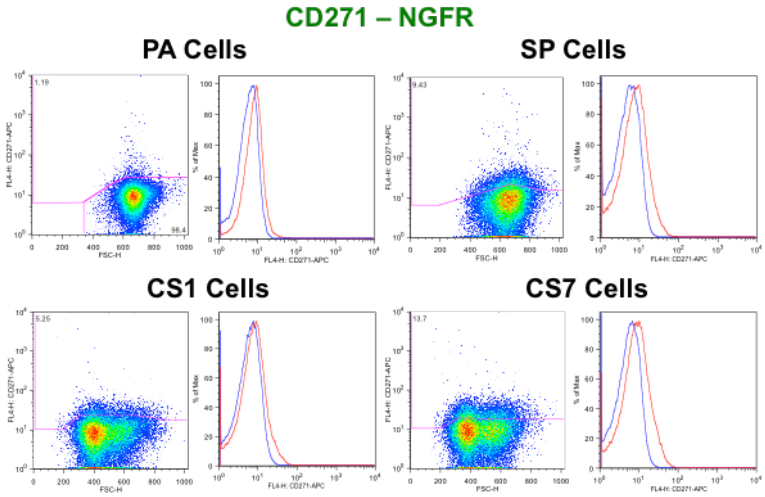

Figure 4.6.16: IFC-Staining of CD271 (NGFR) in Different Cell Lines

Flow cytometric immunophenotyping (IFC) of cells stained with APC conjugated antibody for detection of CD271 antigen. Representative results for PA (n=11, P29-127), SP (n= 25, P16-117), CS1 (n=2, P8, P57) and CS7 (n=8, P7-90) cell lines: PA P51, SP P39, CS1 P8, and CS7 P9. CS1/7 are also representative for A-CS1/7 cells (n=2, P8, 9 1-2 w ACC/n=7, P7-71, 1-10 w ACC) and SP is also representative for A-SP cells (n=19, P14-87, 2-16 w ACC).
Figure left: scatter plot of fluorescence intensity vs. forward scatter (cell size) of „live cell population“. Figure right: histogram of % Max (events) vs. fluorescence intensity overlay of isotype control (blue) and sample (red).
APC: allophycocyanin, CD: cluster of differentiation, CS: clonally expanded spheroid cells derived from PA, FL4-H: fluorescence channel 4, FSC-H: forward scatter, PA: parental cell line, SP: spheroid cells derived from PA

4.6.4.2 CD56 (Neural Cell Adhesion Molecule - NCAM)

CD56 (NCAM) expression has been shown on MSC subsets and the molecule seems to be correlated with more aggressive phenotypes in some tumors, including ccRCC.

For determination of CD56 expression two differently fluorochrome conjugated antibodies, recognizing different epitopes were used, of which the FITC conjugated antibody against HCD56 antigen showed very faint signals compared to PE conjugated antibody, which recognizes CMSSB antigen, while detection with secondary antibody against mouse IgG gave very similar results for both antibodies, indicating a problem with the fluorochrome conjugation of the FITC antibody and not a connection with the different epitope specificities of the antibodies.

CD56 expression was detected in subpopulations of cells from the cell lines SP and CS7 after some time of culture under SCC (about > passage 40-50), with increasing numbers of positive staining cells seen with prolonged culture periods. Although the number of positive staining cells varied between different cell lines and passages, a clear increase of $CD56^+$ cell fractions with age of the cells was visible. No staining with CD56 antibody was seen on PA and CS1 cell lines, as well as in SP cell lines of low passage numbers. Representative results are shown in figure 4.6.17.

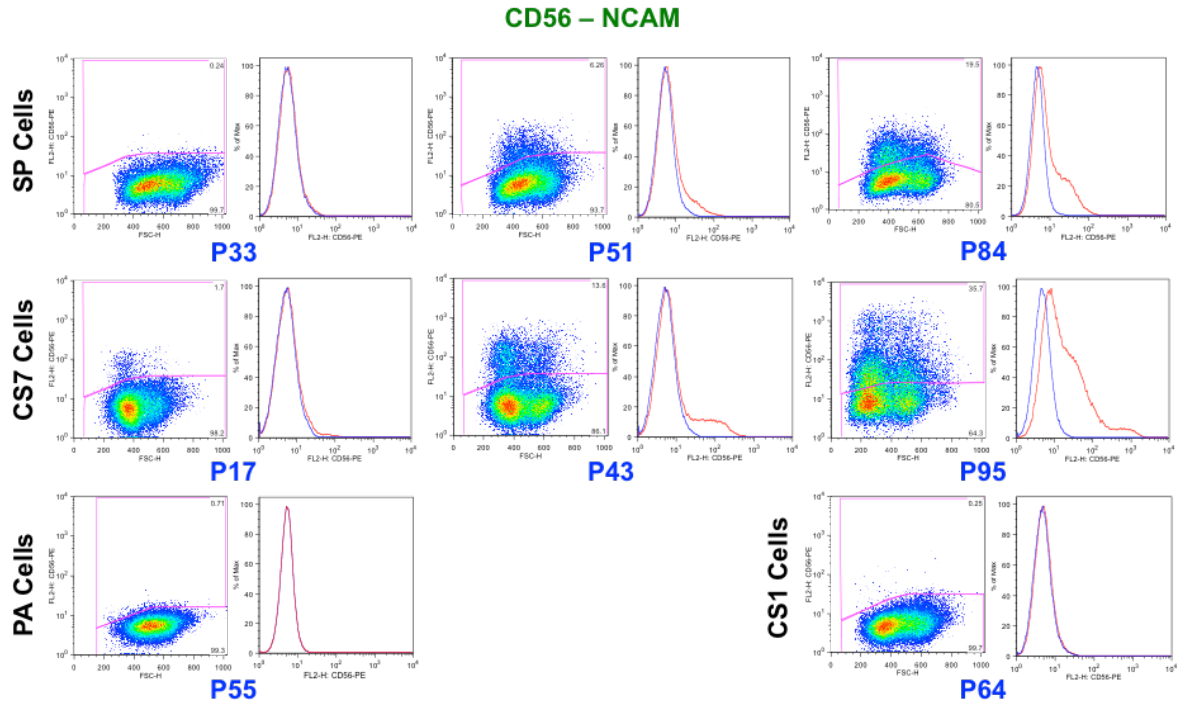

Figure 4.6.17: IFC-Staining of CD56 (NCAM) on Different Cell Lines

PA cells, CS1 and low-passage number SP and CS7 cells show now staining for CD56. Positive staining populations evolve in SP and CS7 cell lines with increased time of culture.
Flow cytometric immunophenotyping (IFC) of cells stained with PE conjugated antibody for detection of CD56 antigen. Results for PA, SP, CS1 and CS7 at different passage numbers (indicated in blue). Results are representative for cells at similar passage numbers of CS1 (n=11, P8-96) and CS7 (n=15, P7-95) cell lines and representative for PA (n=20, P28-130) and SP (n=37, P16-114) cell lines irrespective of passage number (indicated in blue).
Figure left: scatter plot of fluorescence intensity vs. forward scatter (cell size) of „live cell population“. Figure right: histogram of % Max (events) vs. fluorescence intensity overlay of isotype control (blue) and sample (red).
CD: cluster of differentiation, CS: clonally expanded spheroid cells derived from PA, FL2-H: fluorescence channel 2, FSC-H: forward scatter, NCAM: neural cell adhesion molecule, P: passage number, PA: parental cell line, PE: phycoerythrin, SP: spheroid cells derived from PA

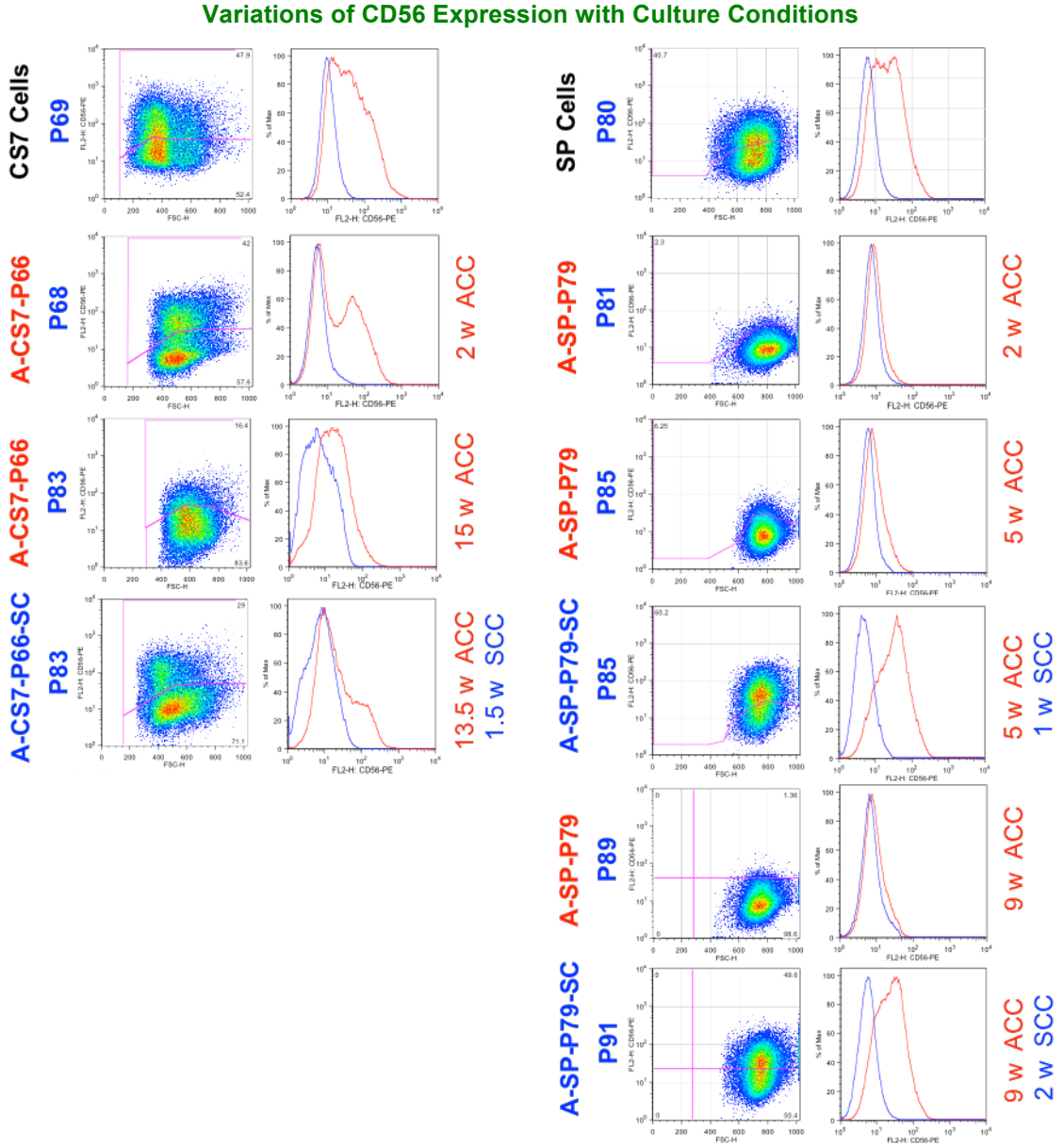

Figure 4.6.18: Comparison of CD56 (NCAM) on Spheroid Cell Lines Grown under SCC or ACC

Expression of CD56 decreases in spheroids cultured under ACC but is rapidly induced after re-culturing A-SP/A-CS cells under SCC, even after long-term culture under ACC.
Flow cytometric immunophenotyping (IFC) of cells stained with PE conjugated antibody for detection of CD56 antigen. Comparison of CS7 and SP cell lines in different passages (indicated in blue) representing parental spheroid cell lines at similar time point of first measurement with A-CS7 and A-SP cells cultured for the indicated time under ACC. A-SP-SC and A-CS7-SC cells were cultured for the indicated periods under ACC before re-cultivation under SCC for indicated periods. Results for A-SP-P79 are representative also for A-SP-P54/63/84/P87/P92 and results for A-SP-P79-SC are representative also for A-SP-P63-SC.
Figure left: scatter plot of fluorescence intensity vs. forward scatter (cell size) of „live cell population“. Figure right: histogram of % Max (events) vs. fluorescence intensity overlay of isotype control (blue) and sample (red).
ACC: adherent culture conditions, A-CS7: CS cells grown under ACC, ALCAM: Activated leukocyte cell adhesion molecule, A-SP: SP cells grown under ACC, A-CS7-SC: A-CS7 cells re-cultured under SCC, A-SP-SC: A-SP cells re-cultured under SCC, CD: cluster of differentiation, CS7: clonally expanded spheroid cells derived from PA, FL2-H: fluorescence channel 2, FSC-H: forward scatter, MCAM: melanoma cell adhesion molecule, P: passage number, PA: parental cell line, PE: phycoerythrin, SCC: spheroid culture conditions, SP: spheroid cells derived from PA, w: weeks

The CD56$^+$ cell population in both cell lines decreased, with a slightly more rapid kinetic in SP cells compared to CS7 cells, when cells were cultured under ACC. This is shown in figure 4.6.18. Very interestingly, CD56$^+$ cell populations quickly re-occurred when cells were re-cultured under SCC.

4.6.4.3 CD184 (CXCR4)

The chemokine receptor CXCR4 (CD184) which serves, together with CXCR7, as receptor for the proinflammatory cytokine CXCL12 has been used to isolate TIC from several tumors, including RCC. CD184 expression was measured with two different antibodies, of which the APC conjugated antibody showed slightly higher staining intensities compared to the PE conjugated antibody. On PA cell lines only a very small number (≈ 1%) of cells showed weak staining for the antigen. In the spheroid cell lines CS1 and SP a higher fraction of positive cells was observed (≈ 10%), which increased in SP cells with continuous culture of the cells to (30%), whereas in CS1 cell line over time in culture the fraction varied slightly depending on antibody used. In contrast, in CS7 cell line at low passages a clear CD184 positive cell population was seen, which increased over time in culture. Cells in high passage numbers showed high staining intensity for CD184 antigen, with the two populations still being discernible. Representative results for CD184 staining are shown in figure 4.6.19 and 4.6.20.

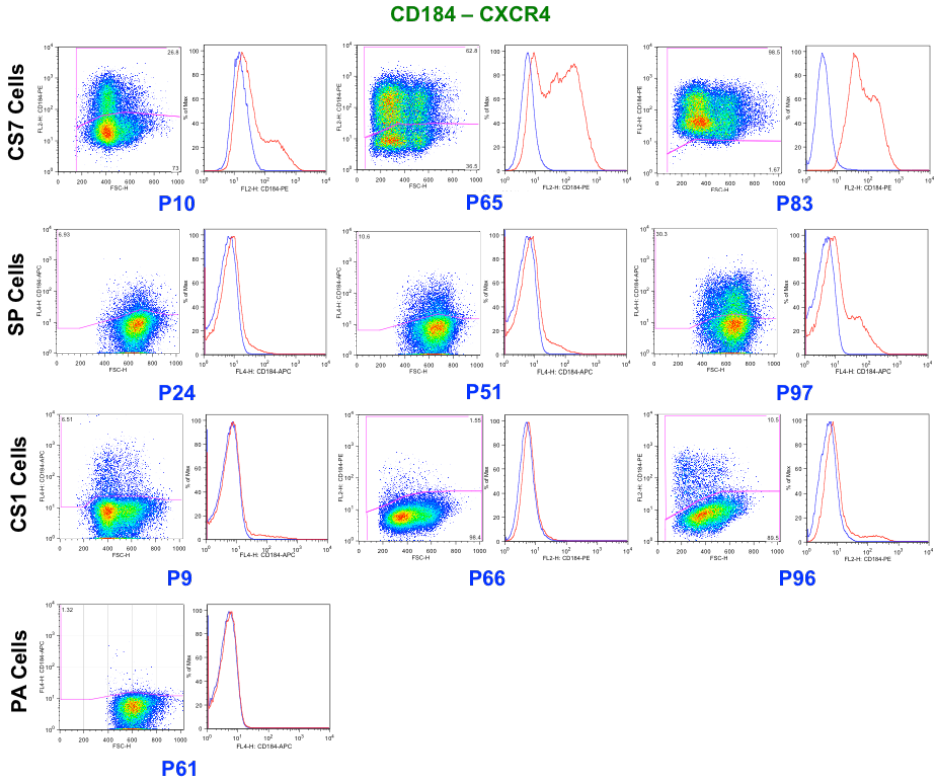

Figure 4.6.19: IFC-Staining of CD184 (CXCR4) on Different Cell Lines

Flow cytometric immunophenotyping (IFC) of cells stained with APC or PE conjugated antibody (as indicated) for detection of CD184 antigen. Results for different passage numbers (indicated in blue) of PA (n=24, P28-129), SP (n=24, P17-115), CS1 (n=5, P8-96) and CS7 (n=12, P2-95) cell lines. Results for CS1, CS7 and SP are representative for cells at similar passage numbers. Results for PA cells are representative irrespective of passage number.
Figure left: scatter plot of fluorescence intensity vs. forward scatter (cell size) of „live cell population“. Figure right: histogram of % Max (events) vs. fluorescence intensity overlay of isotype control (blue) and sample (red).
APC: allophycocyanin, CD: cluster of differentiation, CS: clonally expanded spheroid cells derived from PA, CXCR4: C-X-C chemokine receptor type 4, FL2/4-H: fluorescence channel 4, FSC-H: forward scatter, P: passage number, PA: parental cell line, PE: phycoerythrin, SP: spheroid cells derived from PA

Similar to CD56, the positive cell populations in CS7 and SP cell lines decreased when cells were cultured under ACC (see figure 4.6.20). In A-CS7 cell line at the time of measurement, after two weeks of culture the positive fraction comprised only 20% low to moderately positive cells and after 15 weeks of culture under ACC similar to PA cell line and A-SP cell lines only single cells were stained by CD184 antibody.

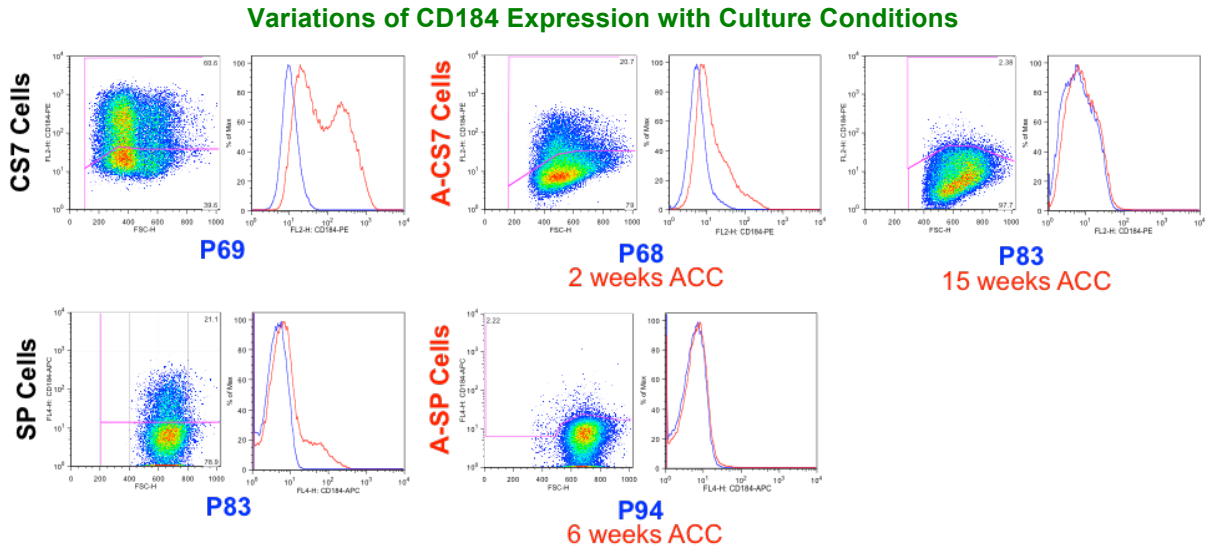

Figure 4.6.20: Comparison of CD184 (CXCR4) on Spheroid Cell Lines Grown under SCC or ACC

Flow cytometric immunophenotyping (IFC) of cells stained with APC or PE conjugated antibody (as indicated) for detection of CD184 antigen. Comparison of CS7 and SP cell lines in different passages (indicated in blue) representing parental spheroid cell lines at start of ACC culture with A-CS7 (P66) and A-SP (P87) cells cultured for the indicated time under ACC. A-CS7 cells are representative also for A-CS7-P6 and A-SP are representative also for A-SP-P14/36/41/54/63 evaluated after 2-16 weeks of culture under ACC.
Figure left: scatter plot of fluorescence intensity vs. forward scatter (cell size) of „live cell population“. Figure right: histogram of % Max (events) vs. fluorescence intensity overlay of isotype control (blue) and sample (red).
ACC: adherent culture conditions, A-CS7: CS cells grown under ACC, APC: allophycocyanin, A-SP: SP cells grown under ACC, CD: cluster of differentiation, CS7: clonally expanded spheroid cells derived from PA, CXCR4: C-X-C chemokine receptor type 4, FL2/4-H: fluorescence channel 2/4, FSC-H: forward scatter, P: passage number, PA: parental cell line, PE: phycoerythrin, SP: spheroid cells derived from PA

4.6.4.4 CXCR7

The chemokine receptor CXCR7 similar to CXCR4 serves as receptor CXCL12 and has been found to be highly expressed on several tumors. The expression pattern of CXCR7 on CS7 cell line was very similar to that seen for CXCR4. Also results for CXCR7 staining of CS7 cell grown under ACC were comparable to that of CXCR4 (see figure 4.6.20, results not shown). In contrast, on SP cells and CS1 cells, similar to PA cells, CXCR7 expression was rarely detected. A-SP cells were not assayed for CXCR7 expression. Representative results for CXCR7 staining with the PE conjugated antibody used are depicted in figure 4.6.21.

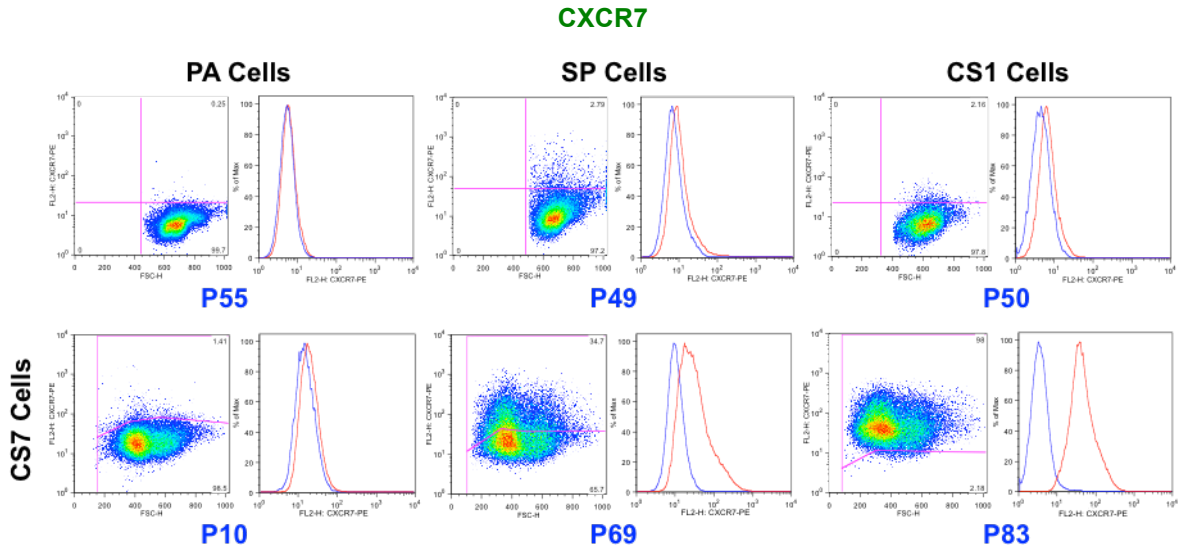

Figure 4.6.21: IFC-Staining of CXCR7 on Different Cell Lines

No expression of CXCR7 was detected in PA and CS1 cell lines, only single positive staining cells were seen in SP cell line, whereas CXCR7 expression strongly increased in CS7 cell line with time of culture under SCC.
Flow cytometric immunophenotyping (IFC) of cells stained with PE conjugated antibody for detection of CXCR7 antigen. Representative results for PA (n=8, P28-130), SP (n=13, P49-106), CS1 (n=4, P13-80) cell lines. Results for CS7 (n=15, P7-95) cell line for which an increase of expression over time in culture was observed are representative for cells at same passage numbers (passage numbers indicated in blue).
Figure left: scatter plot of fluorescence intensity vs. forward scatter (cell size) of „live cell population“. Figure right: histogram of % Max (events) vs. fluorescence intensity overlay of isotype control (blue) and sample (red).
ACC: adherent culture conditions, A-CS7: CS cells grown under ACC, APC: allophycocyanin, A-SP: SP cells grown under ACC, CD: cluster of differentiation, CS7: clonally expanded spheroid cells derived from PA, CXCR7: C-X-C chemokine receptor type 4, FL2/4-H: fluorescence channel 2/4, FSC-H: forward scatter, P: passage number, PA: parental cell line, PE: phycoerythrin, SP: spheroid cells derived from PA

4.6.4.5 CD133 (Prominin 1)

CD133 (Prominin 1) has been found to be a suitable TIC marker in marker in many tumor types and the molecule is expressed on several progenitor cells including renal progenitors, but in RCC seems to be of minor relevance as TIC marker. The AC133 antibody recognizes the TIC/stem cell specific isoform specifically, whereas epitopes detected by other antibodies are specific also to isoforms of the molecule, which are expressed on several normal tissues. CD133 expression was evaluated by using three different antibodies: one APC and PE conjugated AC133 specific antibody respectively, and one PE conjugated clone TMP4. Between the staining patterns of the cells using the two different antibody clones, no significant differences were observed, while use of APC conjugated antibody resulted in slightly higher staining intensities over that seen with the PE conjugated antibody.

The observed expression patterns for CS cell lines were comparable to those seen for CXCR4 staining in that a variable fraction of positive staining cells (1-30% positive cells) was seen in CS1 cell line, whereas the fraction of positive cells increased significantly with prolonged spheroid culture periods in CS7 cell line, from a mean value of 1-3% positive cells (mean 2%±1%) seen in passages numbers below 40 (passage number for calculation of mean values was chosen arbitrarily, according to obvious differences and data available) and 11-60% (mean 35%±18%) positive cells observed in CS7 cells with higher passage numbers. In contrast, SP cell line contained only single CD133 positive staining cells (2%±2%) and the number of positive staining cells in PA cell lines was even lower (0.5%±0.5%). Representative results for AC133 staining of the different cell lines are shown in figure 4.6.22. In A-CS cell lines the fraction of CD133 positive cells varied in different experiments with a tendency to higher expressing cell numbers seen after short term culture of the cells under ACC (assayed after 1 or 2 weeks of culture under ACC), whereas after long-term culture as adherent cell monolayer (assayed after 10,15 and 40 weeks) the number decreased significantly, as can be seen from figure 4.6.23. One experiment was performed in which A-CS7 cell line after 13.5 weeks ACC culture was re-cultured under SCC for 1.5 weeks. In this experiment no significant difference in the low number of CD133 positive staining cells was observed.

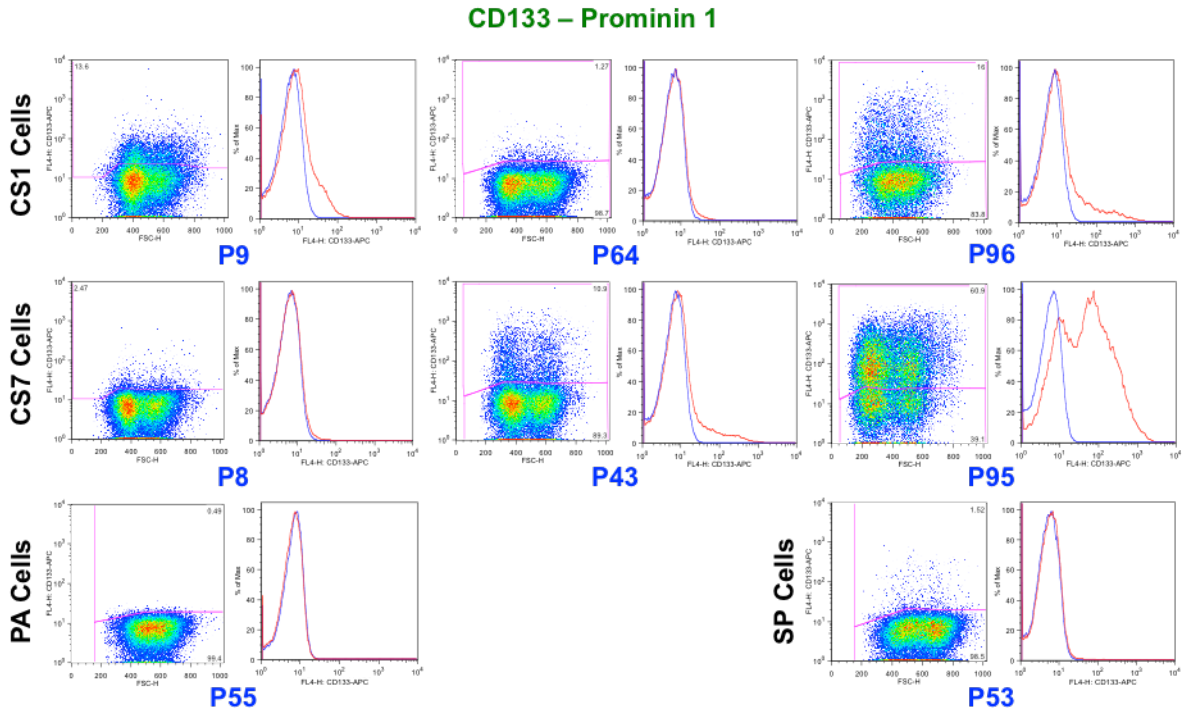

Figure 4.6.22: IFC-Staining of CD133 (Prominin 1) on Different Cell Lines

CD133 is expressed on CS cell lines on varying fractions of cells and only on very low cell numbers of SP cell line. No expression of CD133 is seen on PA cell line. Flow cytometric immunophenotyping (IFC) of cells stained with APC conjugated antibody for detection of AC133 antigen epitope. Representative results for PA (n=16, P28-127), SP (n=15, P20-98) and CS1 (n=10, P8-96) cell lines. Results for CS7 (n=14, P2-95) cell line are representative for cells at similar passage numbers (indicated in blue) Figure left: scatter plot of fluorescence intensity vs. forward scatter (cell size) of „live cell population“. Figure right: histogram of % Max (events) vs. fluorescence intensity overlay of isotype control (blue) and sample (red).
CD: cluster of differentiation, CS: clonally expanded spheroid cells derived from PA, FL4-H: fluorescence channel 4, FSC-H: forward scatter, P: passage number, PA: parental cell line, PE: phycoerythrin, SP: spheroid cells derived from PA

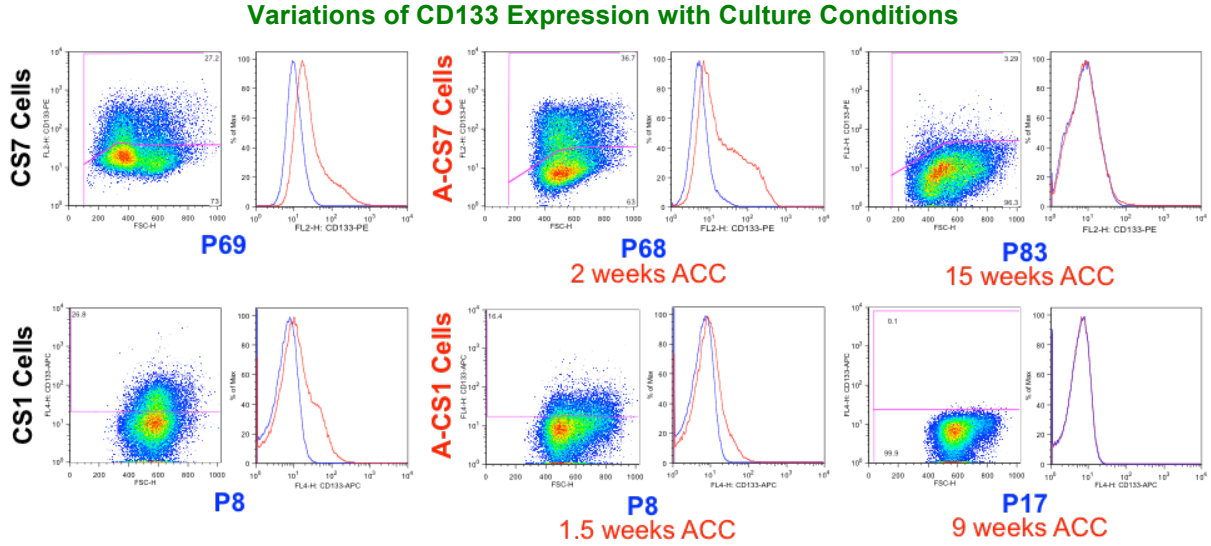

Figure 4.6.23: Comparison of CD133 (Prominin 1) on CS Cell Lines Grown under SCC or ACC

Expression of CD133 on CS cell lines is strongly reduced after long-term culture under ACC.
Flow cytometric immunophenotyping (IFC) of cells stained with APC or PE conjugated antibody (as indicated) for detection of AC133 antigen. Comparison of CS7 and CS1 cell lines in different passages (indicated in blue) representing parental spheroid cell lines at start of ACC culture with A-CS7-P66 and A-CS1-P6 cells cultured for the indicated time under ACC. A-CS7-P66 are also representative for A-CS7-P6.
Figure left: scatter plot of fluorescence intensity vs. forward scatter (cell size) of „live cell population". Figure right: histogram of % Max (events) vs. fluorescence intensity overlay of isotype control (blue) and sample (red).
ACC: adherent culture conditions, A-CS: CS cells grown under ACC, APC: allophycocyanin, CD: cluster of differentiation, CS: clonally expanded spheroid cells derived from PA, FL2/4-H: fluorescence channel 2/4, FSC-H: forward scatter, P: passage number, PA: parental cell line, PE: phycoerythrin

4.6.4.6 CD10 (Neprilysin)

CD10 (Neprilysin) is a membrane metallo-endopeptidase expressed in a variety of tissues, with high abundance in kidney and lung. CD10 serves as differential marker for ccRCC, where it was found to be highly expressed.

Expression of CD10, investigated by using a FITC conjugated antibody, was exclusively found on SP cell line, whereas no expression of the antigen was detected on either PA or CS cell lines. The fraction and staining pattern seen for CD10 staining of SP cells at different passages varied considerably between 12 and 63 % positive staining cells with a mean of 29% and a standard deviation of 17%. No correlation between passage number and expression of CD10 was observed. Representative results for CD10 staining are shown in figure 4.6.24, also showing variation of SP cell staining in cells with similar passage number. Expression of CD10 was also investigated on spheroid cell lines cultured under ACC, thereby no significant differences were observed compared to parental cell lines, though variations of expression in SP cell line complicate the detection of differences that might occur under ACC, a slight tendency to reduced expression of CD10 in A-SP cells might be present.

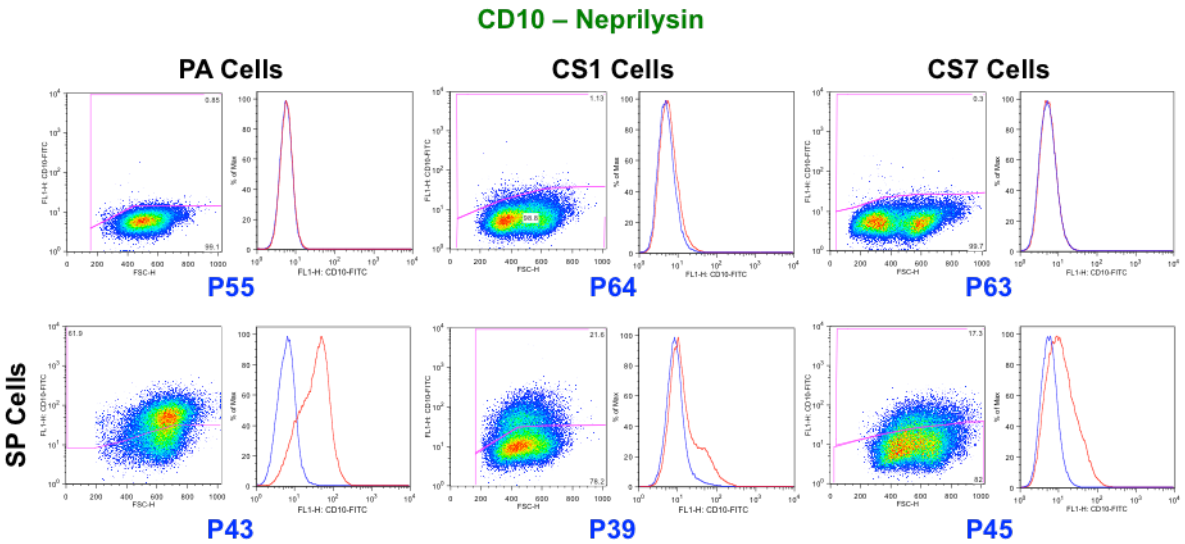

Figure 4.6.24: IFC-Staining of CD10 (Neprilysin) on Different Cell Lines

CD10 is expressed on varying fractions of SP cell line, but not in PA, or CS cell lines.
Flow cytometric immunophenotyping (IFC) of cells stained with FITC conjugated antibody for detection of CD10 antigen. Representative results for PA (n=15, P28-130), CS1 (n=6, P8-96) and CS7 (n=2, P10-95) cell lines and of variations seen in SP (n=29, P16-115) cell lines. Passage of cells indicated in blue.
Figure left: scatter plot of fluorescence intensity vs. forward scatter (cell size) of „live cell population". Figure right: histogram of % Max (events) vs. fluorescence intensity overlay of isotype control (blue) and sample (red).
CD: cluster of differentiation, CS: clonally expanded spheroid cells derived from PA, FITC: fluorescein isothiocyanate, FL1-H: fluorescence channel 1, FSC-H: forward scatter, FITC: fluorescein isothiocyanate, P: passage number, PA: parental cell line, SP: spheroid cells derived from PA

4.6.5 Variations in EpCAM and CD44 Expression on CS1 Cell Line

CS1 cell line in contrast to all other tested cell lines showed differences in expression of EpCAM and CD44 antigens. The cell line was frozen at passage 6 (6 weeks culture under SCC) and the thawed cells were continuously passaged for a total of 74 weeks (P107). From the latter also A-CS1 cell line was derived, which was continuously grown under ACC for 47 weeks, starting at P7. For both antigens besides the positive cell population, which was also seen in the other cell lines, several fractions with less staining were observed in the starting cell line (P21) and were confirmed after re-growth. Results obtained for EpCAM expression of the cell line are depicted in figure 4.6.25. As can be seen, EpCAM staining was reduced in CS1 cells and over long-term culture an EpCAM negative cell fraction, which finally comprised most of the cells, and an EpCAM high fraction could be discriminated. Compared to the spheroid cell line grown under SCC, the continuously grown cell line from passage 7 under ACC showed higher and constant expression of EpCAM in the same period, with only a minor fraction showing less staining of the antibody after 40 weeks of culture. Similar results were seen for expression of CD44 on this cell line as shown in figure 4.6.26, where the staining more rapidly decreased to most of the cells showing no expression of CD44 in passage 65. Interestingly, after further culturing of the cells a CD44 high cell fraction evolved, which mostly comprised smaller cells, as was also seen for the EpCAM positive cell fraction.

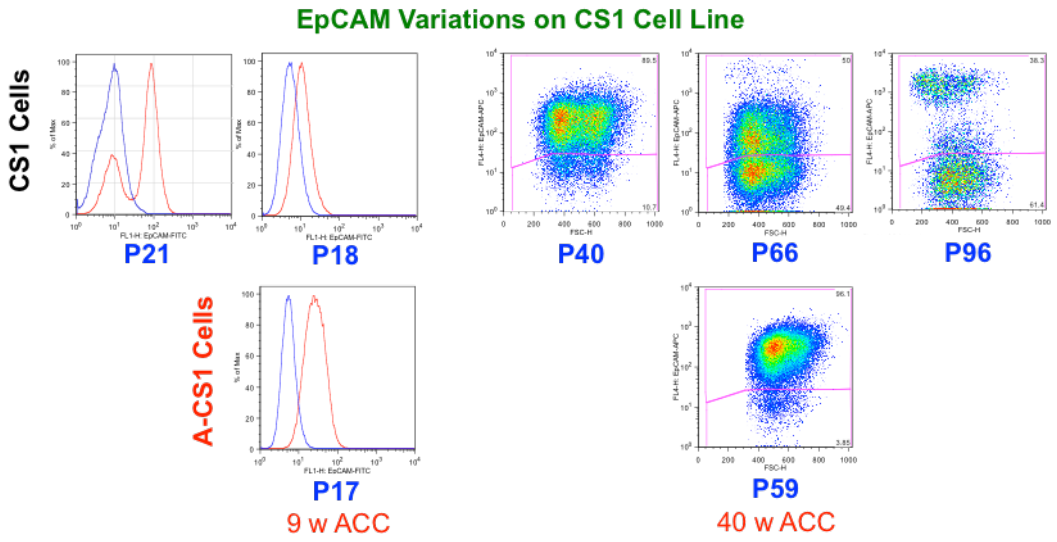

Figure 4.6.25: EpCAM on CS1 Cell Line - Change over Time in Culture and Comparison to A-CS1

EpCAM expression is drastically reduced over time in culture on CS1 cell line.
Flow cytometric immunophenotyping (IFC) of cells stained with APC (right) or FITC (left) conjugated antibody for detection of EpCAM antigen on CS1 cell lines in different passages (indicated in blue) and A-CS1 cells grown from passage 7 under ACC for indicated time (red). P21 cells from starting culture of the cell line (4 weeks), P9-P107 (8-74 weeks) continuously grown cells from cells frozen at P6.
Figure left: histogram of % Max (events) vs. fluorescence intensity overlay of isotype control (blue) and sample (red) for FITC conjugated antibody stained cells. Figure right: scatter plot of fluorescence intensity vs. forward scatter (cell size) of „live cell population“ for APC conjugated antibody stained cells.
ACC: adherent culture conditions, A-CS1: CS cells grown under ACC, APC: allophycocyanin, CS1: clonally expanded spheroid cells derived from PA, FL1-H: fluorescence channel 1, FSC-H: forward scatter, P: passage number, FITC: fluorescein isothiocyanate, PA: parental cell line, w: weeks

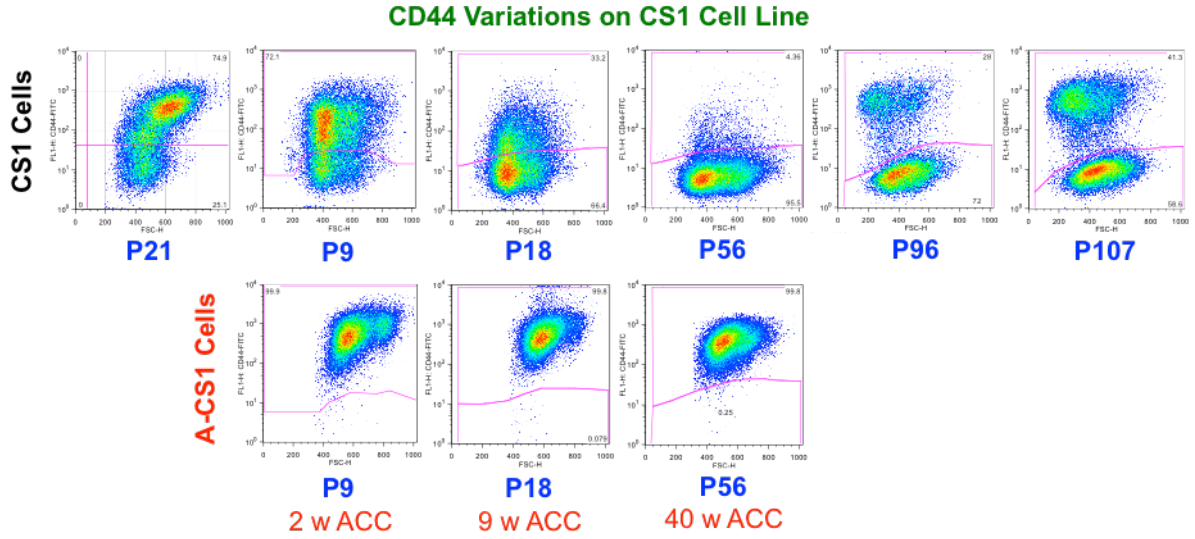

Figure 4.6.26: CD44 on CS1 Cell Line - Change over Time in Culture and Comparison to A-CS1

CD44 expression on CS1 cells varies dramatically over time in SCC culture and seems to be more stable under ACC.
Flow cytometric immunophenotyping (IFC) of cells stained with FITC conjugated antibody for detection of CD44 antigen on CS1 cell lines in different passages (indicated in blue) and A-CS1 cells grown from passage 7 under ACC for indicated time (red). P21 cells from starting culture of the cell line (4 weeks), P9-P107 (8-74 weeks) continuously grown cells from cells frozen at P6.
Scatter plots of fluorescence intensity vs. forward scatter (cell size) of „live cell population“.
ACC: adherent culture conditions, A-CS1: CS cells grown under ACC, CD: cluster of differentiation, CS1: clonally expanded spheroid cells derived from PA, FL1-H: fluorescence channel 1, FSC-H: forward scatter, P: passage number, FITC: fluorescein isothiocyanate, PA: parental cell line, w: weeks

4.6.6 Expression of MSC Negative Markers

Besides expression of markers that are used as positive markers for MSC or TIC, also markers used as negative markers for MSC were evaluated on PA, SP and CS cell lines. The cell lines did not show any staining, when antibodies against CD19, CD45, or HLA-DR were used (results are not shown, but were comparable to that seen for CD90 staining as shown in figure 4.6.1).

4.7 Evaluation of Expression of Stem Cell Markers by Flow Cytometric Immunophenotyping (IFC)

4.7.1 Expression of Stem Cell Markers SSEA-1 (CD15), SSEA-3, SSEA-4, TRA-1-81

For evaluation of pluripotency of embryonic stem cells (ESCs), antibodies detecting the stage-specific embryonic antigens (SSEA)-1, -3, and -4 as well as TRA-1-81 carbohydrate epitopes are widely used. These antibodies detect different glycosylated structures, which are highly expressed in undifferentiated, pluripotent stem cells, whereas expression is lost upon differentiation of the cells.

The staining pattern of the four antigens was evaluated by standard flow cytometric measurements on PA, SP, CS1 and CS7 cell lines, as well as on A-SP and A-CS cells.

Of the four glyco-antigens, SSEA-4 showed a staining pattern, which was very similar on all cell lines tested, with slightly broader staining distribution towards lower antigen expression in spheroid cell lines compared to PA cells. Representative results for SSEA-4 staining are shown in figure 4.7.1. The staining pattern for SSEA-3 antigen of PA and SP cells was very similar, showing moderate expression with normal distribution among cells, whereas in CS cell lines a very broad distribution of staining was observed, ranging from very dim to high expressing cell populations. Results, representative for the different cell lines for SSEA-3 staining are shown in figure 4.7.2. For both antigens the staining pattern of A-CS and A-SP cells was very similar to that of the CS or SP cells they were derived of. Also within the variations of experiments no significant differences in staining pattern for cells in different passage numbers was observed.

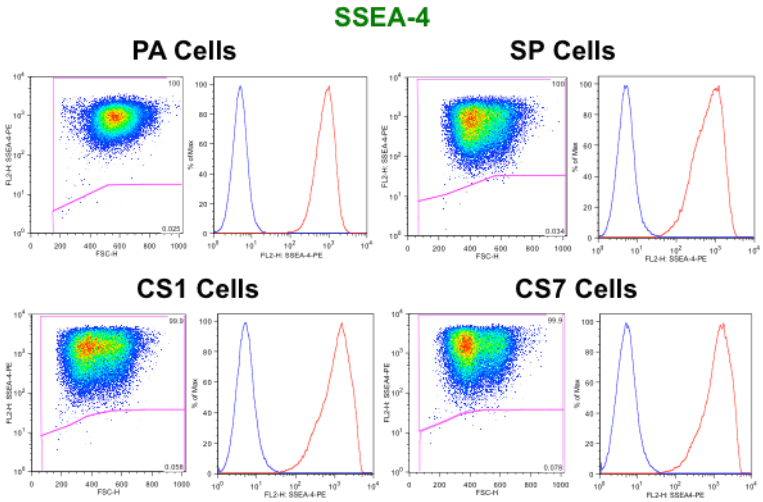

Figure 4.7.1: IFC-Staining of SSEA-4 on Different Cell Lines

All assayed cell lines show strong staining of SSEA-4, which is slightly more heterogeneous in spheroid cell lines (SP, CS1, CS7) compared to PA cell line.
Flow cytometric immunophenotyping (IFC) of cells stained with PE conjugated antibody for detection of SSEA-4 antigen. Representative results for PA (n=13, P29-129), SP (n= 17, P20-84), CS1 (n=5, P35-96) and CS7 (n=8, P14-95) cell lines: PA P62, SP P54, CS1 P66, CS7 P65. CS1/7 are also representative for A-CS1/7 cells (n=2, 20-40 w ACC/n=5, 6-40 w ACC) and SP is also representative for A-SP cells (n=7, 2-13 w ACC).
Figure left: scatter plot of fluorescence intensity vs. forward scatter (cell size) of „live cell population“. Figure right: histogram of % Max (events) vs. fluorescence intensity overlay of isotype control (blue) and sample (red).
ACC: adherent culture conditions, A-CS: CS cells cultured under ACC, A-SP= SP cells cultured under ACC, CS: clonally expanded spheroid cells derived from PA, FL1-H: fluorescence channel, FSC-H: forward scatter, PA: parental cell line, PE: phycoerythrin, SSEA: stage-specific embryonic antigen, SP: spheroid cells derived from PA, w: weeks

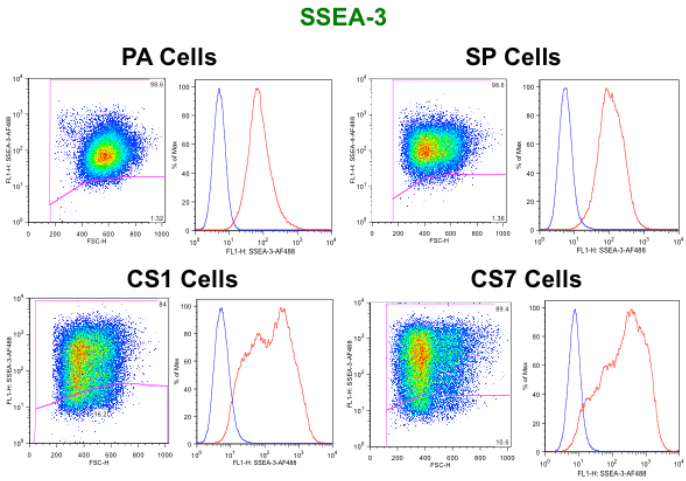

Figure 4.7.2: IFC-Staining of SSEA-3 on Different Cell Lines

Intermediate level staining pattern for SSEA-3 is similar in PA and SP cell line, whereas in CS cell lines several populations ranging from high to low staining cells can be discriminated.
Flow cytometric immunophenotyping (IFC) of cells stained with AF488 conjugated antibody for detection of SSEA-3 antigen. Representative results for PA (n=15, P29-130), SP (n=9, P17-101), CS1 (n=3, P40-66) and CS7 (n=6, P10-83) cell lines: PA P62, SP P57, CS1 P66, and SC7 P69. CS1/7 are also representative for A-CS1/7 cells (n=1, 40 w ACC/n=4, 2-40 w ACC) and SP is also representative for A-SP cells (n=8, 2-13 w ACC). Figure left: scatter plot of fluorescence intensity vs. forward scatter (cell size) of „live cell population“. Figure right: histogram of % Max (events) vs. fluorescence intensity, overlay of isotype control (blue) and sample (red).
ACC: adherent culture conditions, A-CS: CS cells cultured under ACC, AF: AlexaFluor®, A-SP: SP cells cultured under ACC, CS: clonally expanded spheroid cells derived from PA, FL1-H: fluorescence channel, FSC-H: forward scatter, PA: parental cell line, SSEA: stage-specific embryonic antigen, SP: spheroid cells derived from PA, w: weeks

The staining pattern for TRA-1-81 antigen with the PE conjugated antibody used, showed a broad distribution, ranging from low to high expressing cell fractions, in all cell lines tested. Exemplary results for TRA-1-81 staining at comparable passage number of the four tested cell lines are shown in figure 4.7.3. Similar results were obtained for A-CS and A-SP cell lines.

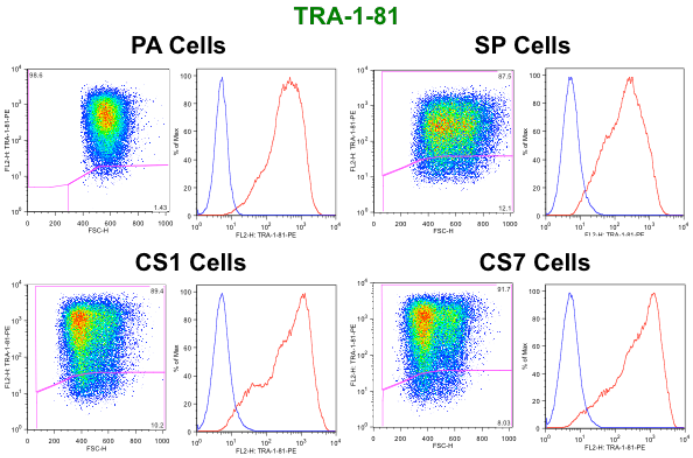

Figure 4.7.3: IFC-Staining of TRA-1-81 on Different Cell Lines

TRA-1-81 staining pattern is relatively heterogeneous on all tested cell lines.
Flow cytometric immunophenotyping (IFC) of cells stained with PE conjugated antibody for detection of TRA-1-81 antigen. Representative results for PA (n=13, P29-129), SP (n=20, P33-77), CS1 (n=4, P18-96) and CS7 (n=8, P14-95) cell lines: PA P33, SP P33, CS1 P43, and CS7 P43. CS1/7 are also representative for A-CS1/7 cells (n=2, 9-40 w ACC/n=4, 6-40 w ACC) and SP is also representative for A-SP cells (n=6, 2-13 w ACC). Figure left: scatter plot of fluorescence intensity vs. forward scatter (cell size) of „live cell population“. Figure right: histogram of % Max (events) vs. fluorescence intensity, overlay of isotype control (blue) and sample (red).
CS: clonally expanded spheroid cells derived from PA, FL2-H: fluorescence channel 2, FSC-H: forward scatter, P: passage number, PA: parental cell line, PE: phycoerythrin, SP: spheroid cells derived from PA

A striking feature of TRA-1-81 staining was the high variation of staining patterns seen for cell lines in different passages and experiments. This is illustrated in figure 4.7.4, where representative results for three different passage numbers of the cell lines are shown. In this figure also a tendency of change in expression over time of culture, which was observed, can be seen, showing a higher fraction of low staining cells at low passage numbers, with a shift towards higher TRA-1-81 expression level with almost exclusively positive staining cells at intermediate passage numbers, to the development of low to negative staining cell fractions in very high passage cells. But du to the high variation in staining, the number of measurements is not sufficient to draw this conclusion at a significant level.

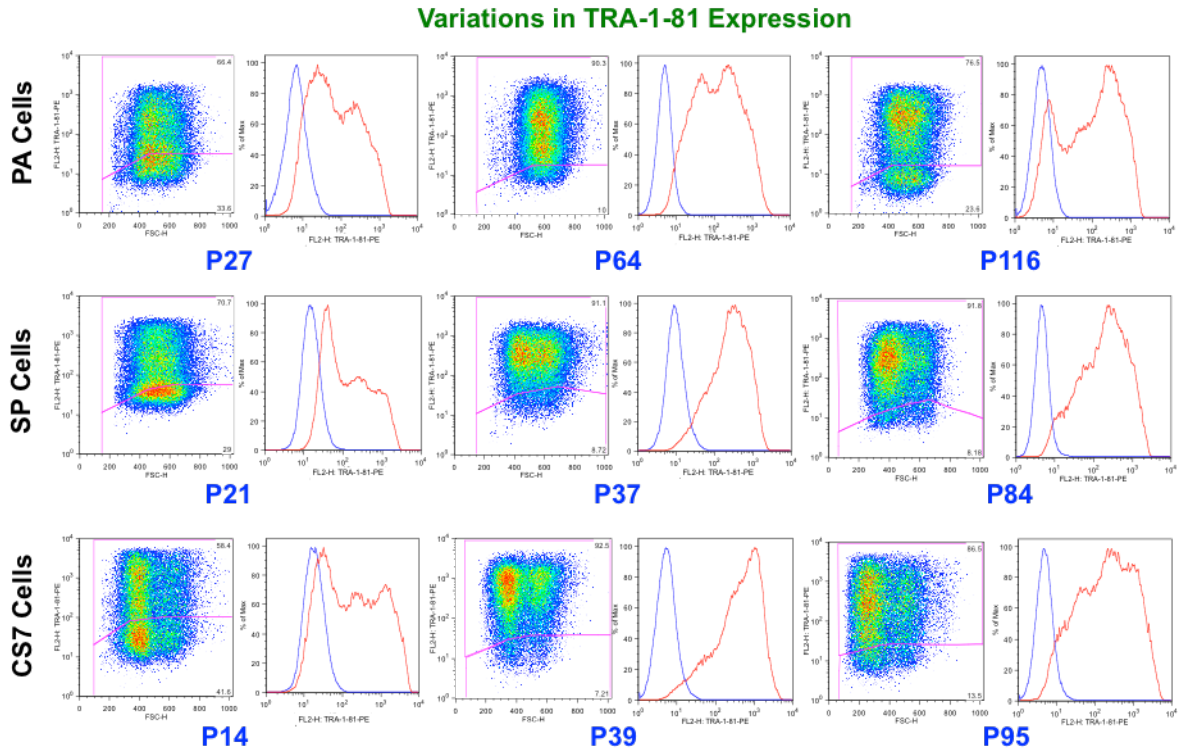

Figure 4.7.4: Variation in IFC-Staining of TRA-1-81 on Different Cell Lines at Different Passages

TRA-1-81 staining pattern is highly variable in all tested cell lines, with different populations being discernible.
Flow cytometric immunophenotyping (IFC) of cells stained with PE conjugated antibody for detection of TRA-1-81 antigen. Results for PA, SP and CS7 at different passage numbers (indicated in blue).
Figure left: scatter plot of fluorescence intensity vs. forward scatter (cell size) of „live cell population“. Figure right: histogram of % Max (events) vs. fluorescence intensity overlay of isotype control (blue) and sample (red).
CS: clonally expanded spheroid cells derived from PA, FL2-H: fluorescence channel 2, FSC-H: forward scatter, IFC: flow cytometric immunophenotyping, P: passage number, PA: parental cell line, PE: phycoerythrin, SP: spheroid cells derived from PA

For detection of SSEA-1 two differently fluorochrome conjugated antibodies were used. The staining pattern seen with both antibodies were comparable, although the staining intensity was lower when FITC conjugated antibody was used. In contrast to SSEA3/4 and TRA-1-81, SSEA-1 was expressed only by a fraction of the cells, whereas most cells were not or in case of PA cells, weakly stained. Representative results for SSEA-1 staining are shown in figure 4.7.5. The staining pattern varied for PA and spheroid cell lines. For PA cells a clear tendency to increased expression of SSEA-1, which in high passage numbers was indicated additionally by a shift of the whole cell population towards higher staining intensities was observed. CS cells, in contrast, showed a relatively high expression of CD15 on cells at low passage numbers with a mean of 30% positive cells, which was lost upon long-term

culture of the cells. In SP cells, SSEA-1 expression was detected on single cells only at very low passage numbers, whereas intermediate and high passage cells were not stained. A-CS cell line did not show significant differences to their parental cells lines, whereas A-SP cell lines showed slightly higher numbers of positive staining cells than SP cells they were derived of.

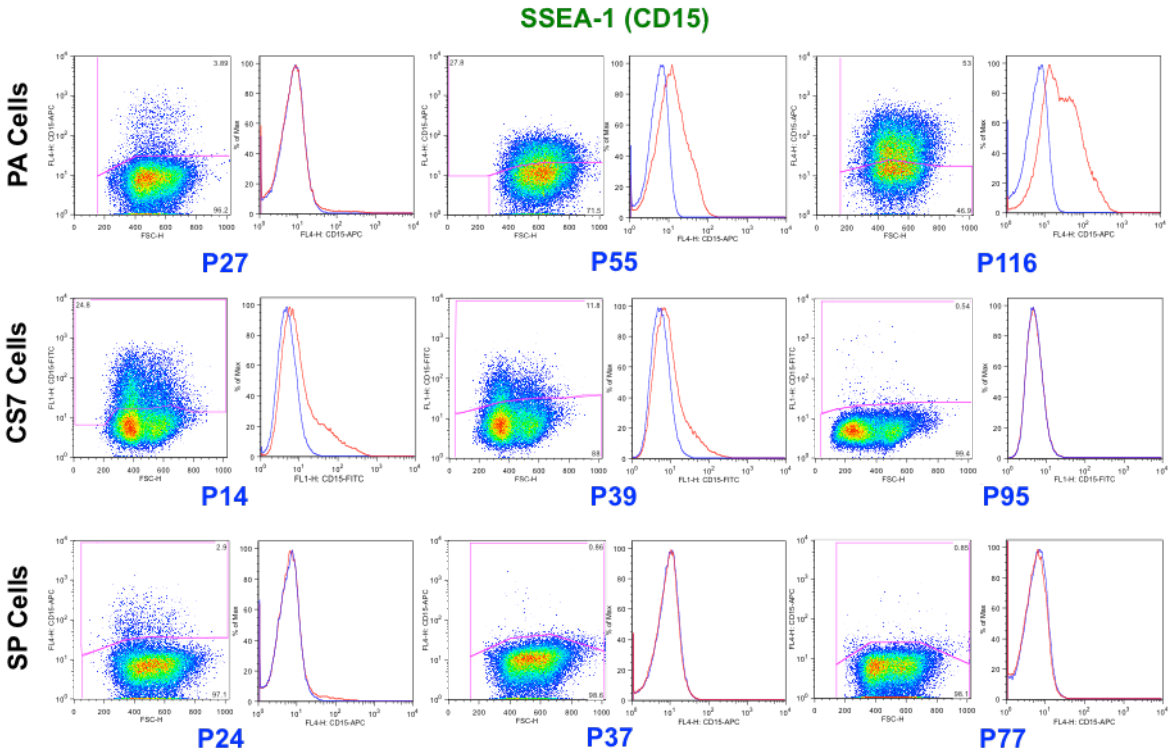

Figure 4.7.5: IFC-Staining of SSEA-1 on Different Cell Lines at Different Passages

In PA cell line SSEA-1 expression increases with time of culture, whereas expression in spheroid cell lines (SP, CS) decreases with time of culture and is lowest in SP cell line.
Flow cytometric immunophenotyping (IFC) of cells stained with APC (PA, SP cells) or FITC (CS7 cells) conjugated antibody for detection of SSEA-1 antigen. Representative results low, intermediate and high passage numbers of PA (n=37, P28-129), SP (n=36, P17-1115), and CS7 (n=18, P2-95) cell lines (passage numbers indicated in blue) CS7 results are also representative for CS1 (n=12, P8-61) and A-CS1/7 cells (n=12, 1-40 w ACC/n=18, 2-40 w ACC) and SP P24 is also representative for A-SP cells (n=32, 2-38 w ACC).
Figure left: scatter plot of fluorescence intensity vs. forward scatter (cell size) of „live cell population“. Figure right: histogram of % Max (events) vs. fluorescence intensity overlay of isotype control (blue) and sample (red).
ACC: adherent culture conditions, A-CS: CS cells cultured under ACC, AF: AlexaFluor®, A-SP: SP cells cultured under ACC, CS: clonally expanded spheroid cells derived from PA, FL1-H: fluorescence channel, FSC-H: forward scatter, IFC: flow cytometric immunophenotyping, PA: parental cell line, SSEA: stage-specific embryonic antigen, SP: spheroid cells derived from PA, w: weeks

4.7.2 Expression of Stem Cell Pluripotency Markers Oct4 and Sox2

Expression of the two core stem cell specific transcription factors Oct4 and Sox2 was determined by intracellular flow cytometric measurements. For this purpose, cells were fixed and permeabilized using „FOXP3 Transcription Factor staining Kit“. Discrimination of dead cells by 7-AAD was thus not applicable. AF488 conjugated antibody was used for Sox2 detection and isoform-specific Oct4A antibody was used for detection of Oct4/POU5F1. Since Oct4A antibody was not fluorochrome conjugated, for detection of this antigen the use of secondary antibody was necessary. No live/dead cell discrimination using 7-AAD was applied.

PA, SP cells and the two CS-cell lines CS1 and CS7 in different passage numbers (PA: P25-114, SP: P33-76, CS1: P19-62, CS7: P5-88) were used for experiments. To summarize results, mean of fold change of fluorescence geo mean values of antibody stained cells relative to isotype control stained cells of all analyzed samples of one cell type were calculated for the two antigens respectively. Since no significant differences were observed between CS1 and CS7 cells, the two cell lines were grouped as CS for calculation of the values. The number of samples used for calculation of mean values is given in the figure legend. The values are depicted in figure 4.7.6.

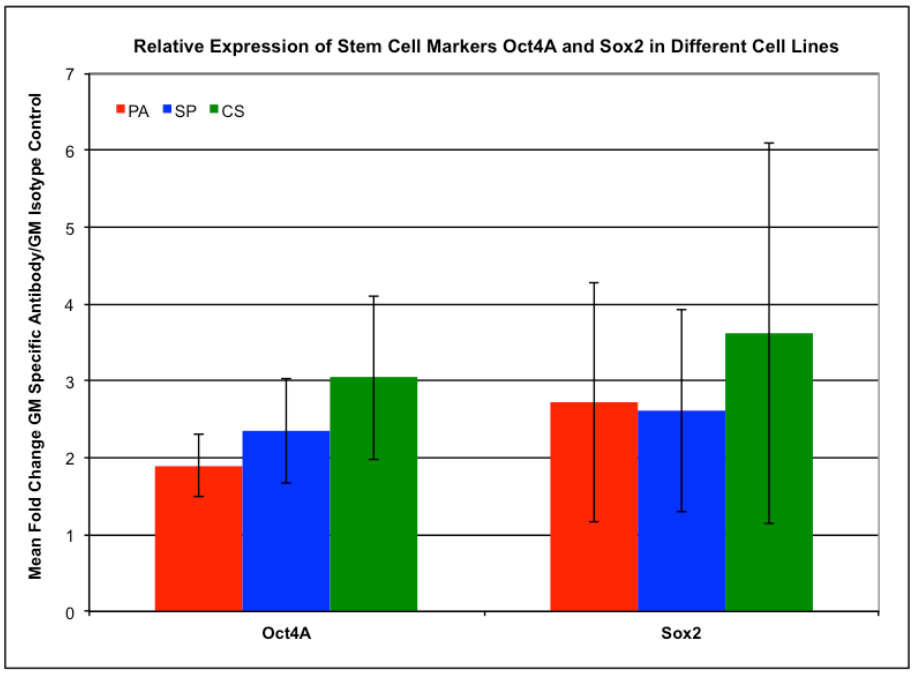

Figure 4.7.6: Relative Staining Intensity of Intracellular Stem Cell Markers in Different Cell Lines

Intracellular stem cell markers within the high variations seen, show similar low (Oct) to intermediate (Sox2) staining in all cell lines tested.
Mean of fold change staining intensities for antibody stained samples of all experiments. Staining was performed with antibodies against Sox2 and using a secondary antibody in for detection of Oct4. Number of samples for Oct4A: PA = 3, SP = 4, CS = 4 (CS1 = 2 CS7 = 2). Number of samples for Sox2: PA = 5, SP = 5, CS = 4 (CS1 = 1 CS7 = 3). Error bar: standard deviation.
CS: clonally expanded spheroid cells derived from PA, GM: geo mean of fluorescence intensity, Oct: Octamer biding transcription factor, PA: parental cell line, Sox: SRY (sex determining region Y)-box transcription factor, SP: spheroid cells derived from PA

Expression of the two transcription factors Oct4A and Sox2 was detected on all cell lines at low levels (see figure 4.7.7). No significant differences in expression of the antigens between different cell types were observed, although slight differences were seen between single experiments. Compared to Oct staining, signals obtained with Sox2 antibody were slightly higher, but still low compared to those measured for Snail1 (see figure 4.8.7).

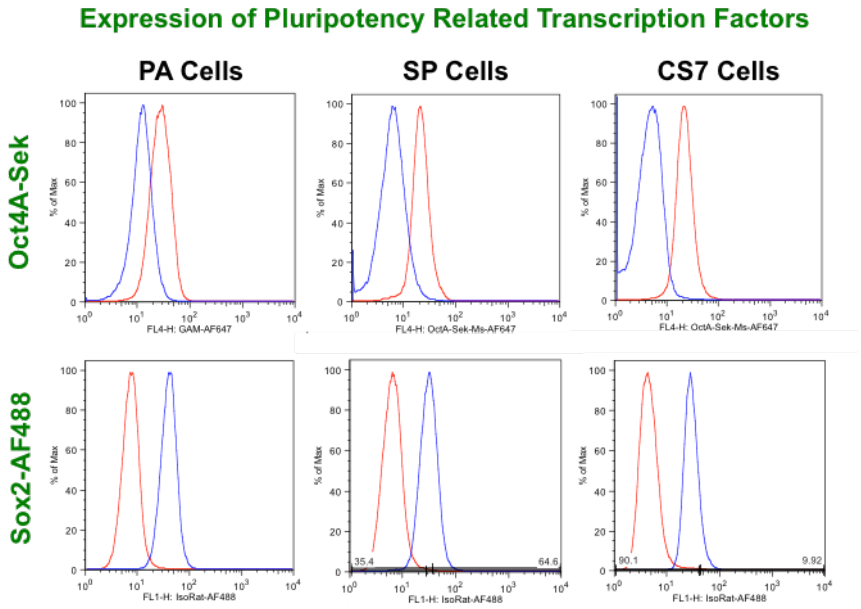

Figure 4.7.7: IFC-Staining of Oct4A and Sox2

Similar low staining of Oct4A and Sox2 was detected in all cell lines, with low staining intensities seen for Oct4A and slightly higher staining intensities seen for Sox2.
Flow cytometric immunophenotyping (IFC) of cells stained either with AF647 conjugated goat anti-mouse antibody for detection of mouse antibody against Oct4A (Oct4A-Sek) or AF488 conjugated antibody for detection of Sox2 (indicated in green). Upper line: histogram of % Max (events) vs. fluorescence intensity stained with secondary antibody against Oct4A, overlay of isotype control (blue) and sample (red). PA (P114), SP (P33), CS7 (P42). Lower line: histogram of % Max (events) vs. fluorescence intensity stained with primary antibody against Sox2, overlay of isotype control (red) and sample (blue). PA (40), SP (P48), CS7 (P5).
AF: AlexaFluor®, CS7: clonally expanded spheroid cells derived from PA, FL2/4-H: fluorescence channel, Oct: Octamer binding transcription factor, P: passage number, PA: parental cell line, SP: spheroid cells derived from PA, Sox: SRY (sex determining region Y)-box transcription factor

4.8 Evaluation of EMT Signature by Flow Cytometric Immunophenotyping (IFC)

4.8.1 Expression of Marker Antigens E-Cadherin (CDH1) and N-Cadherin (CDH2)

The process of epithelial to mesenchymal transition (EMT), this means the acquisition of stem cell features by endothelial cells, has been proposed as a critical mechanism in TIC emergence as well as during cancer progression and metastasis. To define the nature of the cell lines in respect to their epithelial or mesenchymal characteristics, expression of the two complementary cell-adhesion protein markers E-Cadherin (epithelial phenotype) and N-Cadherin (mesenchymal phenotype) was analyzed by flow cytometric immunophenotyping. Since the antigens detected by the antibodies for both molecules proofed to be highly sensitive to degradation by different tested cell dissociation reagents, single cell suspensions for measurement had to be prepared by using TSE-Buffer and mechanical disaggregation. This resulted in a higher proportion of dead cells in the samples to be analyzed compared to standard dissociation methods. The cell lines PA, SP, CS1, and CS7 were tested for marker expression at different time points, i.e. at different passages of continuously grown cell lines, as well as by using cells at different passage numbers obtained from thawing and culturing of cells that were frozen at different time points.

Representative results obtained for PA and SP cells and the two CS cell lines CS1 and CS7 are shown in figure 4.8.1 and figure 4.8.2 respectively. Expression of E-Cadherin as well as N-Cadherin expression was detected on all cells in the four cell lines, indicating an intermediate EMT-phenotype of these cells. At low passage numbers no significant difference in expression was observed between all cell lines, albeit slightly higher measured GM values for both markers in cell lines grown as spheroids compared to parental cell line. The signal detected for N-Cadherin staining was relatively high in all cell lines (probably due to the APC-staining of the antibody used). Fluorescence intensity was higher in SP and CS cells than in PA cells, with a slight tendency to increasing values in SP cells with age. Although direct comparison of fluorescence intensity values between measurements due to the limited accuracy of the method, especially when comparing separate measurements and instrument settings, which differed between SP/PA and CS cells, must be done with utmost caution, to illustrate the differences observed, mean of fold change of fluorescence geo mean values of N-Cadherin antibody stained cells relative to isotype control stained cells of all analyzed samples were calculated and depicted in figure 4.8.3. The passage numbers used to divide high and low expressing cell subsets for calculation of mean values were chosen arbitrarily, according to obvious differences and data available. For CS1 cell line only a limited number of data for EMT marker expression is available. The respective number of measurements used for calculations is indicated in the figure legends.

Interestingly, with exception of CS7 cell line, who expressed both markers relatively consistent over time, a continuous decrease of E-Cadherin expression with increasing duration of culture was observed in the other three cell lines, up to the evolvement of E-Cadherin negative cell fractions in cells with high passage numbers, indicating a transition from intermediate to mesenchymal phenotype during long-term culture of the cells. Mean fraction of E-Cadherin negative (mesenchymal) cells was calculated for all measurements and values are shown in figure 4.8.4. When directly comparing cells with the same or very similar passage number, the characteristics observed were not equal but the

same tendency over time was observed in all cell lines tested, with frozen cells seeming to reach the more mesenchymal status at earlier time points, although results are not statistically significant.

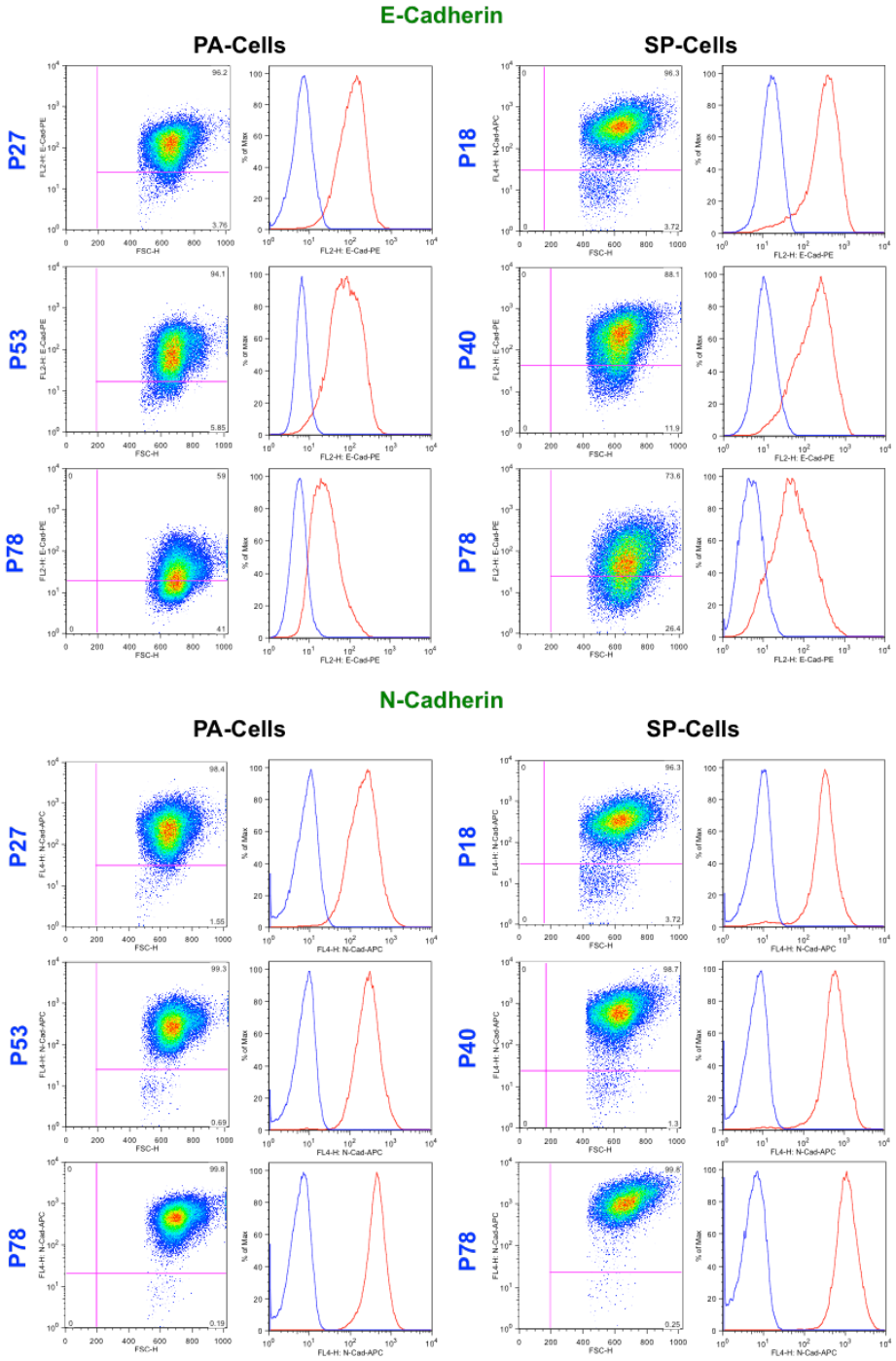

Figure 4.8.1: Expression of EMT Markers of E-Cadherin and N-Cadherin on PA and SP cells

E-Cadherin is expressed on PA and SP cells at similar high levels and is reduced over time in culture. Also N-Cadherin expression is observed at similar high levels on PA and SP cell lines and increases slightly over time in culture in both cell lines.
Representative results of flow cytometric immunophenotyping (IFC) of cells stained with PE and APC conjugated antibodies against E-Cadherin (top) and N-Cadherin (bottom). Comparison of PA cells left and SP cells right at different time points (respective passage indicated in blue left). Figure left: scatter plot of fluorescence intensity vs. forward scatter (cell size) of „live cell population“. Figure right: histogram of % Max (events) vs. fluorescence intensity overlay of isotype control (blue) and sample (red).
APC: allophycocyanin, E-Cad: E-Cadherin, EMT: epithelial to mesenchymal transition, FSC-H: forward scatter, FL2/4-H: fluorescence channel signal intensity, N-Cad: N-Cadherin, P: passage number, PA: parental cell line, PE: phycoerythrin, SP: spheroid cells derived from PA

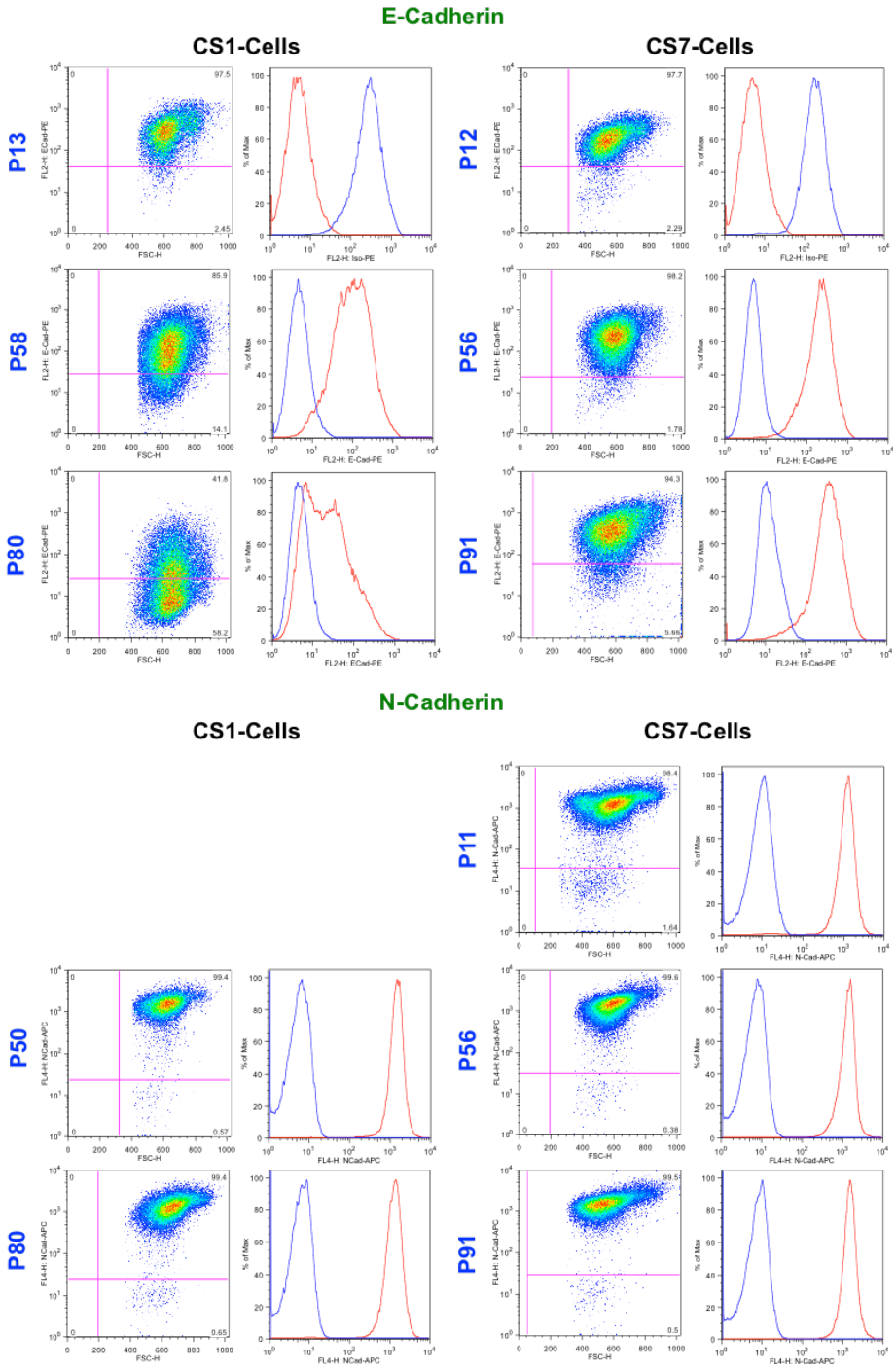

Figure 4.8.2: Expression of EMT markers E-Cadherin and N-Cadherin on CS-cell lines

E-Cadherin is expressed on CS1 and CS7 cells at similar high levels in early passage cells, which are comparable to that of SP and PA cell lines. Reduction of E-Cadherin expression over time in culture, similar to PA and SP cell lines, is only seen in CS1 cell line, whereas in CS7 cell line, high expression is remained over long-term culture. N-Cadherin expression is observed at similar high levels in both cell lines and does not seem to change markedly over time in culture.

Representative results of flow cytometric immunophenotyping (IFC) of cells stained with PE and APC conjugated antibodies against E-Cadherin (top) and N-Cadherin (bottom). Comparison of CS1 cells left and CS7 cells right at different time points (respective passage indicated in blue left). For CS1 cells no measurement in early passage was performed. Figure left: scatter plot of fluorescence intensity vs. forward scatter (cell size) of „live cell population“. Figure right: histogram of % Max (events) vs. fluorescence intensity overlay of isotype control (blue) and sample (red).

APC: allophycocyanin, CS: clonally expanded spheroid cells derived from PA, E-Cad: E-Cadherin, EMT: epithelial to mesenchymal transition, FSC-H: forward scatter, FL2/4-H: fluorescence channel signal intensity, N-Cad: N-Cadherin, P: passage number, PA: parental cell line, PE: phycoerythrin

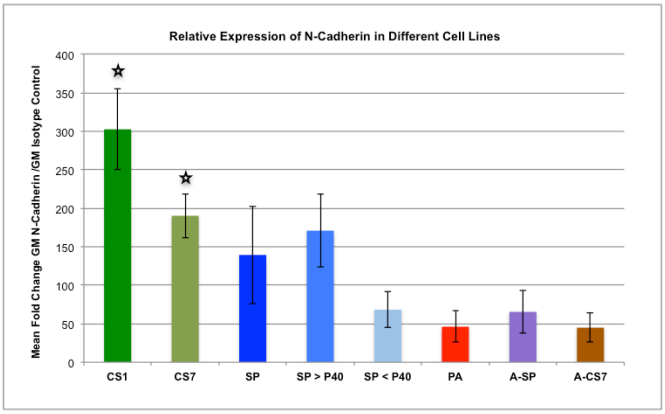

Figure 4.8.3: Relative Staining Intensity of N-Cadherin in Different Cell Lines

N-Cadherin expression level is higher in spheroid cell lines. In SP cell lines, expression level increases with passage. A-CS and A-SP cells show similar N-Cadherin expression levels to PA cells.
Mean of fold change expression levels for N-Cadherin stained samples. Number of samples: A-SP = 7 (+3), A-CS7 = 2 (+1), CS1 = 4, CS7 = 11, SP = 26, SP<P40 = 8, SP>P40 = 18, PA = 13 (+2). Fold change was calculated relative to respective isotype control: Fold change expression = GM N-Cadherin stained sample/GM isotype control stained sample. Error bars: standard deviation. In SP cell lines significant variation of GM values with prolonged culturing of the cells was observed, therefore separate values for cells analyzed in low (< P40) and high (>P40) passage numbers were calculated. * Instrument settings for CS cell lines differed significantly from instrument settings for the other samples. Since this influences GM values in a non-linear fashion, direct comparison values to the other samples is not applicable.
ACC: adherent culture conditions, A-SP: SP cells cultured under ACC, A-CS7: CS7 cells cultured under ACC, CS: clonally expanded spheroid cells derived from PA, GM: geo mean of fluorescence intensity, P: passage number, PA: parental cell line, SP: spheroid cells derived from PA

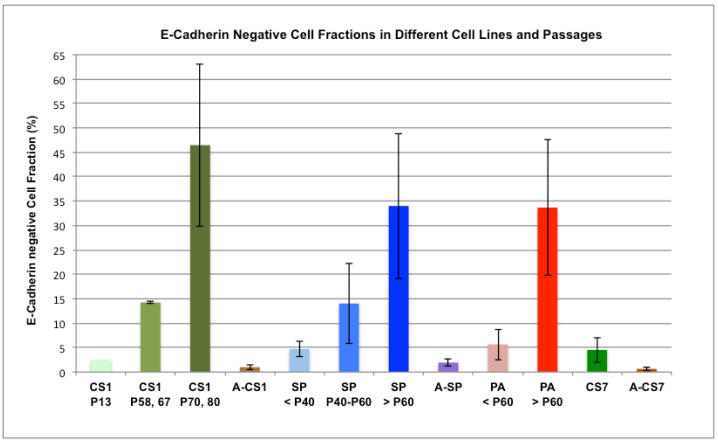

Figure 4.8.4: E-Cadherin Negative Cell Fractions in Different Cell Lines and Passages

E-Cadherin negative cell fraction increases significantly in CS1, SP and PA cells with time of culture. A-SP, A-CS and CS7 cell lines show only small numbers of E-Cadherin negative cells.
Mean of percentage of E-Cadherin negative stained cells as determined by gating cells according to respective samples stained with isotype control antibody. Number of samples: A-SP = 7, A-CS7 = 2, A-CS1 = 2 (P53, 64), CS1: passage numbers of 1/2 measurements indicated, CS7 = 11 (P11-P91), SP<P40 = 7, SP P40-P60 = 11, SP>P60 = 7, PA <P60 = 9, PA >P60 = 6. Error bars: standard deviation.
ACC: adherent culture conditions, A-SP: SP cells cultured under ACC, A-CS7: CS7 cells cultured under ACC, CS: clonally expanded spheroid cells derived from PA, GM: geo mean of fluorescence intensity, P: passage number, PA: parental cell line, SP: spheroid cells derived from PA

Results from one experiment in which cells were stained with both antigens in parallel are shown in figure 4.8.5. PA and SP cells at different passage numbers (obtained from thawing cells that were frozen at different time points), as well as of A-SP cells, that were derived from these SP cells in passage 63 or 36 and cultured for 12 or 15 weeks under ACC were analyzed with the same instrument settings. The gradual evolvement of E-Cadherin negative cells is clearly visible. Also an

increase of N-Cadherin fluorescence intensity with increasing age of the cells is observed. The small cell fraction of N-Cadherin negative cells (≈ 1%), which was seen in all experiments, was also negative for E-Cadherin staining, indicating that these were not epithelial cells.

Parallel Staining for E-Cadherin and N-Cadherin on Different Cell Lines and Passages

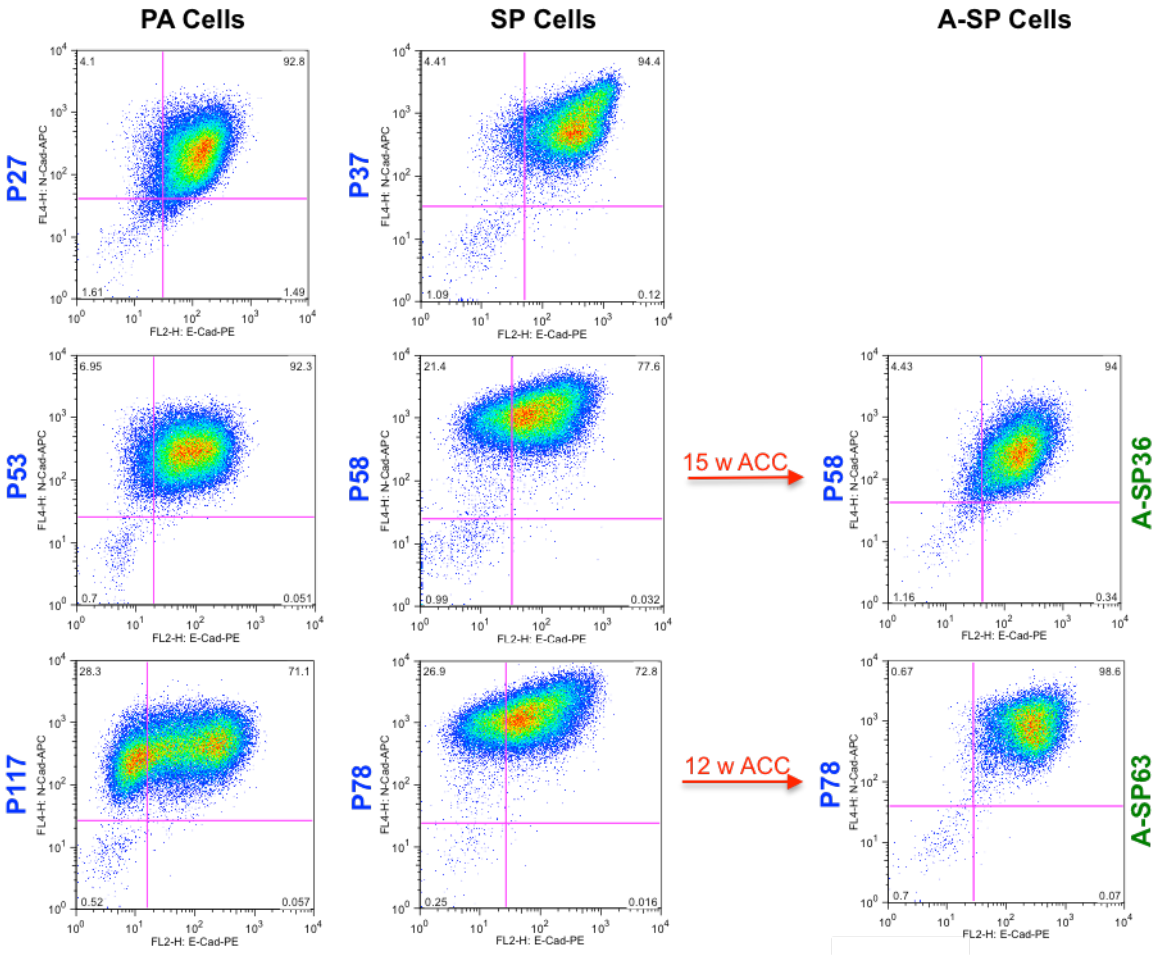

Figure 4.8.5: Double Staining of EMT markers E-Cadherin and N-Cadherin

Reduction of E-Cadherin positive staining cells and increase of N-Cadherin expression level is seen with time of culture of PA and SP cells. After culturing SP cells 12-15 weeks under ACC, expression levels of both markers resemble those of early passage PA cells.
Results of flow cytometric immunophenotyping (IFC) of PA and SP cells from different passage numbers and A-SP cells derived from these SP cells in passage 36 or 63 (respective passage indicated in green left) and cultured for 12 or 15 weeks under ACC. Staining was performed with PE and APC conjugated antibodies against E-Cadherin and N-Cadherin in parallel. Passage numbers are indicated in blue. Scatter plot of fluorescence intensity N-Cadherin staining vs. E-Cadherin staining of „live cell population". Gates set according to fluorescence intensity of isotype control antibodies of respective samples.
ACC: adherent culture conditions, APC: allophycocyanin, A-SP: SP cells cultured under ACC, CS: clonally expanded spheroid cells derived from PA, E-Cad: E-Cadherin, EMT: epithelial to mesenchymal transition, FL2/4-H: fluorescence channel signal intensity, N-Cad: N-Cadherin, P: passage number, PA: parental cell line, PE: phycoerythrin, SP: Spheroid cells derived from PA, w: weeks

In figure 4.8.5 also another important aspect that was observed regarding EMT marker expression can be seen: A-SP-P36 cells derived from SP cells in passage 36 after 12 weeks of cultivation under ACC show an expression level of the two markers, which is similar to that of PA cells in early passage, namely an intermediate phenotype, with expression of both markers similarly and missing the mesenchymal population indicated by low or lost E-Cadherin expression, that was seen in the SP cells

they were derived of (see also figure 4.8.6). A-SP-P63 cells, which were cultured under ACC at later passage also did not contain the mesenchymal population, but compared to A-SP36 showed higher N-Cadherin expression.

When spheroid cell lines were cultured under ACC the E-Cadherin negative cell fraction was lost and expression levels of N-Cadherin were reduced. This reduction of N-Cadherin expression also was present in the CS7 cell line, which under SCC showed stable expression of the markers over time. Interestingly, N-Cadherin expression although reduced, was not lost completely, even after 44 weeks under ACC, which is not consistent with the assumption that cells differentiate to epithelial cells under standard culture conditions. A-CS1 cells were analyzed only once for EMT marker expression and the results were similar to that obtained for A-CS7 cells. In figure 4.8.6 results for A-SP and A-CS7 cell lines are shown in comparison to measurements representing cells at equal passage numbers as the respective parental spheroid cell lines at start of ACC culture, as well as parental spheroid cell lines measured at the same time (after 10/44 weeks of culture). The time course of these changes is not very well resolved by experimental data.

Variations of E- and N-Cadherin Expression with Culture Conditions

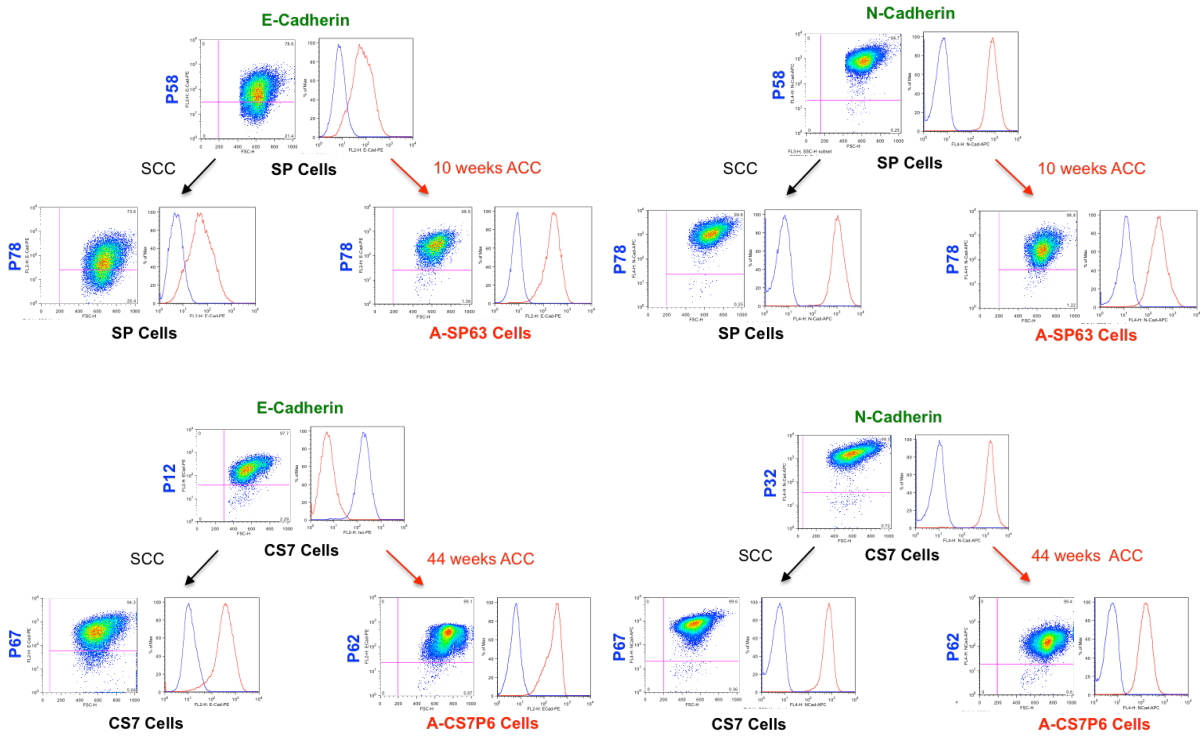

Figure 4.8.6: EMT Marker Expression in A-SP and A-CS Cells Compared to SP and CS Cells

E-Cadherin expression increases on spheroid cell lines when cultured under ACC, whereas N-Cadherin expression is reduced.

Flow cytometric immunophenotyping (IFC) of cells stained with PE and APC conjugated antibodies against E-Cadherin (left) and N-Cadherin (right). Top: SP/CS7 cells in passage similar to founding cells for A-SP/CS cell lines, bottom: comparison of founding SP/CS7 cells (left) to A-SP/CS7 cells (right) after indicated culture period (red) under ACC (respective passage indicated in blue left). Figure left: scatter plot of fluorescence intensity vs. forward scatter (cell size) of „live cell population". Figure right: histogram of % Max (events) vs. fluorescence intensity, overlay of isotype control (blue) and sample (red), legend: geometric mean of fluorescence intensity.

ACC: adherent culture conditions, APC: allophycocyanin, A-SP: SP cells cultured under ACC, CS: clonally expanded spheroid cells derived from PA, EMT: epithelial to mesenchymal transition, FL2/4-H: fluorescence channel signal intensity, P: passage number, PA: parental cell line, PE: phycoerythrin, SP: Spheroid cells derived from PA, w: weeks

4.8.2 Expression of Intracellular EMT-Markers Cytokeratin, Vimentin, and Snail1

Besides expression of defining adhesion-molecule markers for EMT, E-Cadherin and N-Cadherin, also expression of intracellular localized intermediate filament markers cytokeratin (CK, epithelial phenotype) and vimentin (mesenchymal phenotype) as well as the EMT inducing core transcription factor Snail1 was evaluated by IFC measurements. For this purpose, cells were fixed and permeabilized using „FOXP3 Transcription Factor staining Kit“. Discrimination of dead cells by 7-AAD was thus not applicable. For detection of the two CKs, known to be usually expressed on ccRCC, CK8 and CK19, specific monoclonal antibodies were used. Additionally, a mix of two monoclonal antibodies (Pan-CK), which bind to a broad spectrum of other cytokeratin, was applied to test for CK expression. Since some antibodies used were not fluorochrome conjugated staining was achieved by use of AF647 conjugated secondary antibodies.

Representative results for the three cell lines are shown in figures 4.8.7 and 4.8.8. Expression of each antigen was measured at least twice (CS7/CS1) and/or in cells with different passage numbers (PA: P25-114, SP P36-76, CS7: P5-88, CS1: 19-62) with similar results. Results obtained for CS1 cells were similar to those of CS7 cells. Mesenchymal marker antigens as well as cytokeratin antigens were stained in all cell lines at very similar, equally narrow distributed levels and no distinct subpopulations were detectable, with very high measured GM values for vimentin and intermediate GM values for Snail1 and cytokeratin. The GM values for Snail1 and vimentin staining in CS cells were slightly higher than for PA and SP cells, but this might also be attributable to the different instrument settings applied. No variations were seen when cells in different passage numbers were assayed.

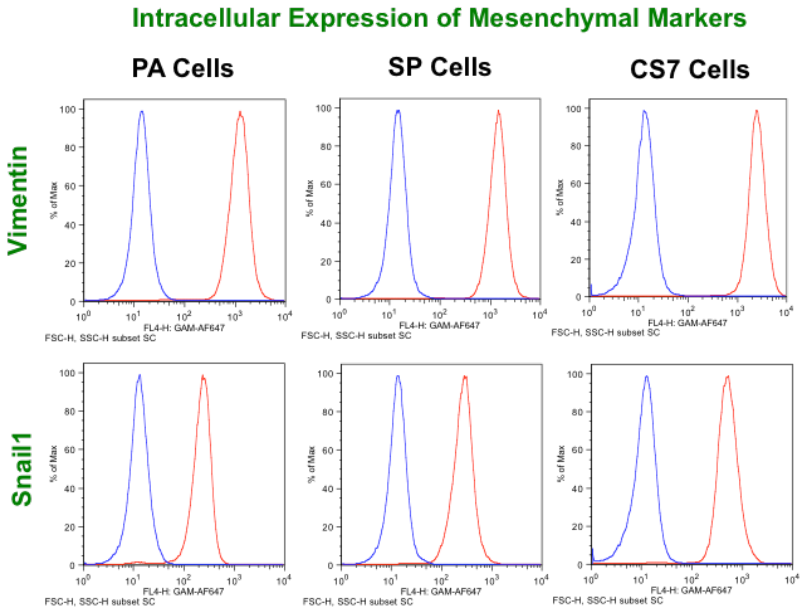

Figure 4.8.7: Expression of Intracellular Mesenchymal Markers Vimentin and Snail1

Intracellular mesenchymal markers antigens are expressed in PA, SP, and CS cell lines at similar levels.
Flow cytometric immunophenotyping (IFC) of cells stained with AF647 conjugated goat anti-mouse antibody for detection of mouse antibodies against Snail1 and vimentin. Comparison of representative results for PA (P25-114), SP (P36-76) and CS cell lines (CS7: P5-88, CS1: 19-62).
Histogram of % Max (events) vs. fluorescence intensity overlay of isotype control (blue) and sample (red), legend: geometric mean of fluorescence intensity.
AF647: AlexaFluor® 647, CS7: clonally expanded spheroid cells derived from PA, FL4-H: fluorescence channel 4 signal intensity, P: passage number, PA: parental cell line, SP: spheroid cells derived from PA

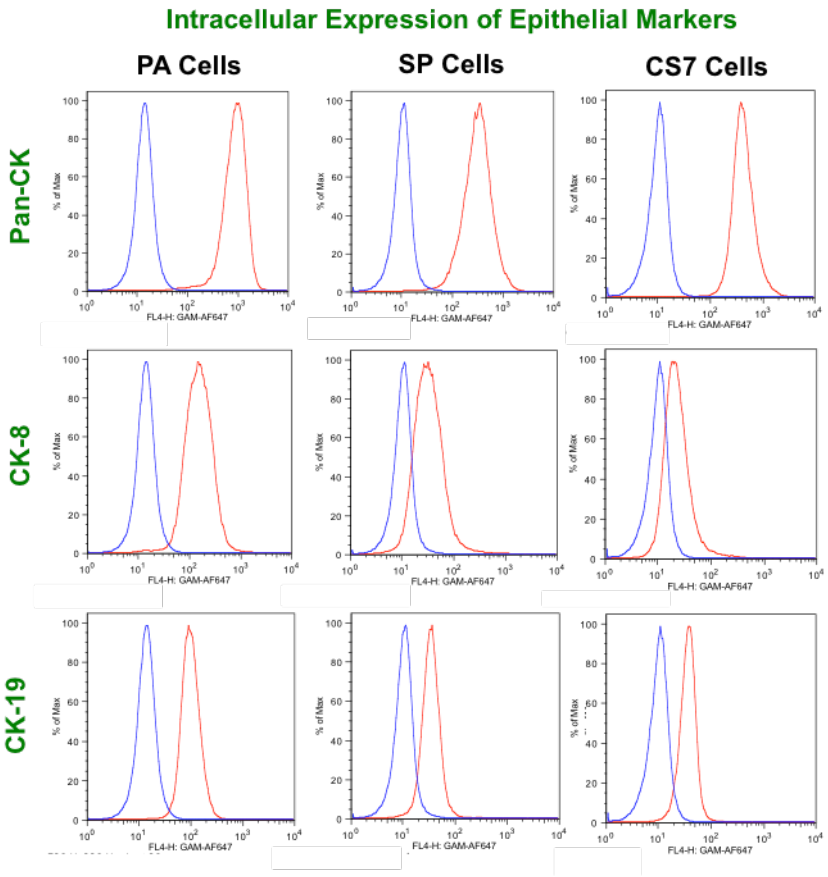

Figure 4.8.8: Intracellular IFC-Staining of Cytokeratin

Cytokeratin antigens are expressed in all cell liens and detected with slightly higher staining intensities in PA cell line compared to SP and CS cell lines.
Flow cytometric immunophenotyping (IFC) of cells stained with AF647 conjugated goat anti-mouse antibody for detection of mouse antibodies against CK8, CK18 and Pan-CK.
Comparison of PA, SP and CS7 cells. Histogram of % Max (events) vs. fluorescence intensity overlay of isotype control (blue) and sample (red), legend: geometric mean of fluorescence intensity.
AF647: AlexaFluor® 647, CS7: clonally expanded spheroid cells derived from PA, FL4-H: fluorescence channel 4 signal intensity, P: passage number, PA: parental cell line, SP: spheroid cells derived from PA

Staining with Pan-CK antibody, which detects a mixture of different cytokeratin, did not yield big differences between the three cell lines but in contrast to mesenchymal markers, CK19, and especially CK8 expression seemed to be higher in PA than in SP and CS cells, with lowest expression level in CS cells. But since the number of data for this antigen is limited, this variation cannot be considered significant. For PA and SP cells, results also did not vary significantly between different passage numbers measured in the same experiment. Similar to E-Cadherin and N-Cadherin, intracellular markers for epithelial and mesenchymal cells were expressed in parallel at similar levels, further confirming the intermediate EMT phenotype of the cell lines. Interestingly, the observed E-Cadherin negative cell fraction, which was observed in late passage PA and SP cells was not reflected in the results for intracellular antigens.

4.9 ALDEFLUOR™ Assay

High expression of the enzyme ALDH has been shown to mark adult stem cell populations and TIC from several tumors. [304] For evaluation of the possible use of ALDH activity for discrimination of stem-like cells in the cell lines investigated, the ALDEFLUOR™ assay was performed. The principle of the assay is measuring the enzyme activity by accumulation of a fluorescent substrate in the cells by flow cytometry. The nature of enzymatic assays is their dependency on concentrations of substrate and enzyme and time. By keeping the incubation time and concentration of substrate constant, the variable assayed was the enzyme concentration by using different cell concentrations. A sample containing the ALDH inhibitor diethylaminobenzaldehyde (DEAB) was used as negative control for background staining. In a first set of experiments PA and SP cells were assayed twice at different cell concentrations ranging from $2x10^5$-$2x10^6$ cells/mL and incubation times of 30-40 min. Results for the experiment in which 3 cell concentrations were tested are shown in figure 4.9.1. As expected, the staining intensity increased with reduced cell concentrations used for the assay. Both cell lines showed quite similar staining patterns at the respective cell concentrations. As can also be seen from figure 4.9.2 the cell concentration dependent variations were slightly higher for PA cells than for SP cells, with control samples showing only low variation between different concentrations and cell type. Also geo mean values were slightly higher for PA cells compared to SP cells, which might indicate a slightly higher ALDH activity in PA cells. But when comparing the positive cell fractions (determined by using a positive gate as such that less than 1 % of control cells were found in the region), the difference was less pronounced. At low cell concentrations, with optimal signal to background ratios, both cell lines showed positive staining of the whole cell population. Therefore, ALDH activity was excluded as a suitable marker for enrichment of cells with stem cell characteristics from the PA cell line and the test was put aside.

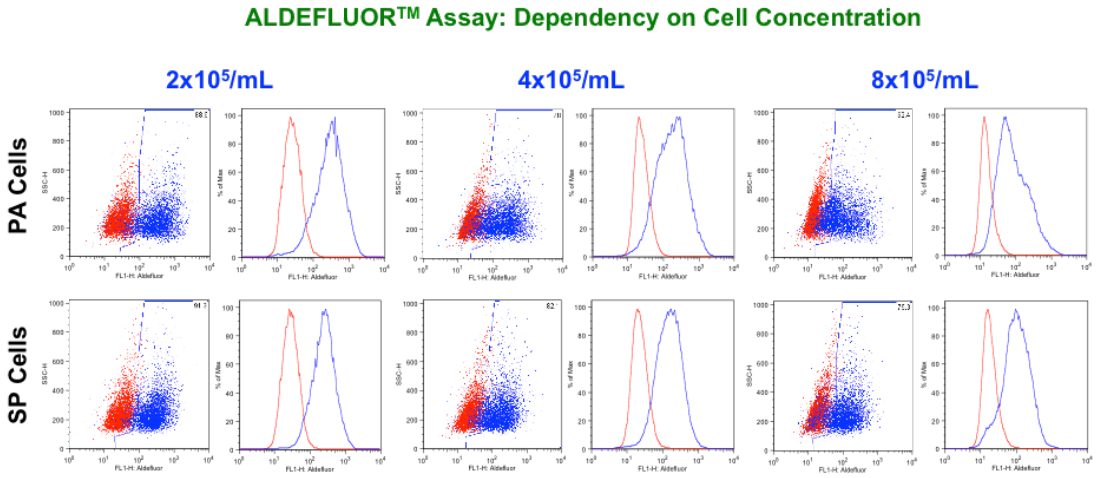

Figure 4.9.1: ALDEFLUOR™ Assay: Variations with Cell Concentration Used

Staining for ALDEFLUOR™ activity is dependent on cell concentration used for the assay. Values decrease with increasing cell concentrations and are similar for PA and SP cell lines.
Flow cytometric measurements of cells assayed for ALDEFLUOR™ activity in PA (P33) and SP (P88) cell lines at different cell concentrations (indicated in blue). Results of $2x10^5$ cells/mL are representative also for measurements of PA P28 and SP P82. Figure left: scatter plot of fluorescence intensity vs. side scatter (SSC) of „live cell population". Figure right: histogram of % Max (events) vs. fluorescence intensity, overlay of DEAB control (red) and sample (blue).
DEAB: diethylaminobenzaldehyde, FL1-H: fluorescence channel 1 signal intensity, SSC-H: side scatter, P: passage number PA: parental cell line, SP: spheroid cells derived from PA

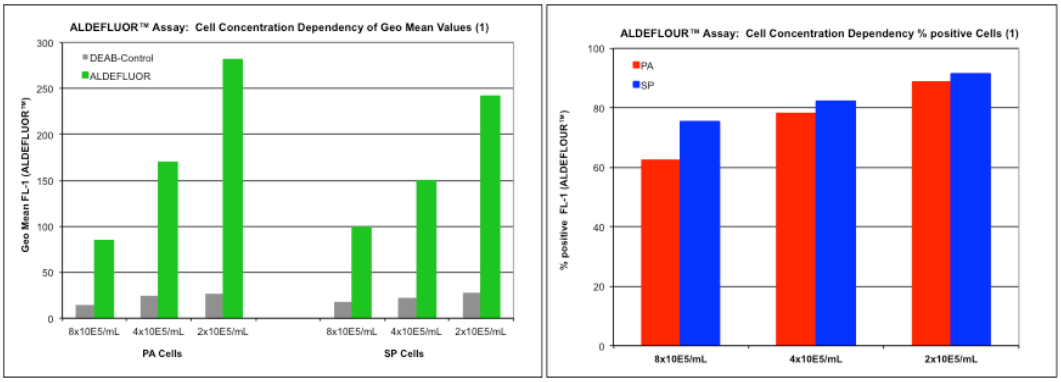

Figure 4.9.2: ALDEFLUOR™ Assay: Variations with Cell Concentration Used - Quantitation (1)

Fluorescence intensity values as well as positive staining cell numbers for ALDH activity depends on cell concentration used for the assay with similar results obtained for PA and SP cell lines.
Geo mean values and number of positive staining cells for ALDEFLUOR™ activity are dependent on cell concentration used for the assay, with decreasing values at increasing cell concentrations. Results are similarly high for PA and SP cell lines. Geo mean values and percent positive staining cells obtained in flow cytometric measurements of cells assayed for ALDEFLUOR™ activity in PA (P28), SP (P88) cell lines at different cell concentrations as shown in figure 4.9.1.
DEAB: diethylaminobenzaldehyde, FL1-H: fluorescence channel 1 signal intensity, P: passage number, PA: parental cell line, SP: spheroid cells derived from PA

A second set of experiments was done to assure the first results and to evaluate possible differences in ALDH activity between the two spheroid cell lines SP and CS7. Surprisingly, results from this test series obtained for PA cell line varied dramatically from the results obtained in the first experiments, as can be seen from figure 4.9.2. and 4.9.3. The staining intensity of the cells was strongly reduced compared to SP cells and also the concentration dependent increase was less pronounced. The number of ALDH positive staining cells was reduced to half of the values obtained in the first experiments, with a high portion of negative staining cells. For the experiments, two separately cultured PA lines at passage numbers between 37-42 were used and concentrations of 2, 4 and 8 x 10^5 cells/mL were tested in the assay. The results for the experiments illustrated in figure 4.9.3 are representative for all measurements (n=8).

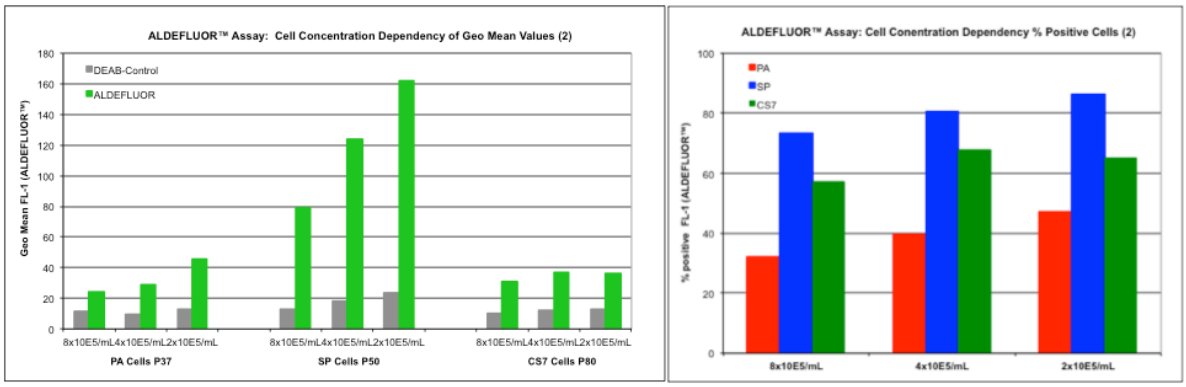

Figure 4.9.3: ALDEFLUOR™ Assay: Variations with Cell Concentration Used - Quantitation (2)

Results for PA cell line in second set of experiments are different from first set of experiments, in being strongly reduced, whereas results for SP cell line show no significant differences. CS7 cell line shows lower staining intensities than SP for ALDH activity and no strong correlation with cell concentrations but high numbers of positive staining cells. Geo mean values obtained for CS7 cell line are markedly lower, and number of positive staining cells is slightly lower than those obtained for SP cell line.
Geo mean values and percent positive staining of PA (P37), SP (P50) and CS7 P80 cell lines obtained in flow cytometric measurements of cells assayed for ALDEFLUOR™ activity in at different cell concentrations.
CS7: clonally expanded spheroid cells derived from PA, DEAB: diethylaminobenzaldehyde, FL1-H: fluorescence channel 1 signal intensity, P: passage number, PA: parental cell line, SP: spheroid cells derived from PA

Whereas, results obtained for SP cell line, investigated at different passages numbers (P28-P72), were very similar to that seen in the first experiments, with the exception that overall staining intensities were slightly reduced (probably due to the use of frozen substrate or variations in instrument settings). No variations with passage number of the cells were observed in the 15 measurements performed, comprising different cell concentrations of 2, 4 and 8 x 10^5 cells/mL. The reason for the high variation of results seen for PA cell line in the two sets of experiments is not clear. Since for SP cell line no remarkable differences were observed, they are less likely attributed to differences in experimental procedures. One explanation might be the very low passage number of cells used in the first assays (P28 and P33), which was in the low range of passage numbers determined to be able grow as spheroids. To address this possibility, a lot more experiments with cells in low passage numbers are needed. Another possible reason for the differences seen might be the higher activity of efflux pumps in the PA cell line (see chapter 4.10), which in the second set of experiments might not have been sufficiently inactivated. To exclude this possibility, tests with different concentrations of efflux inhibitors would be needed.

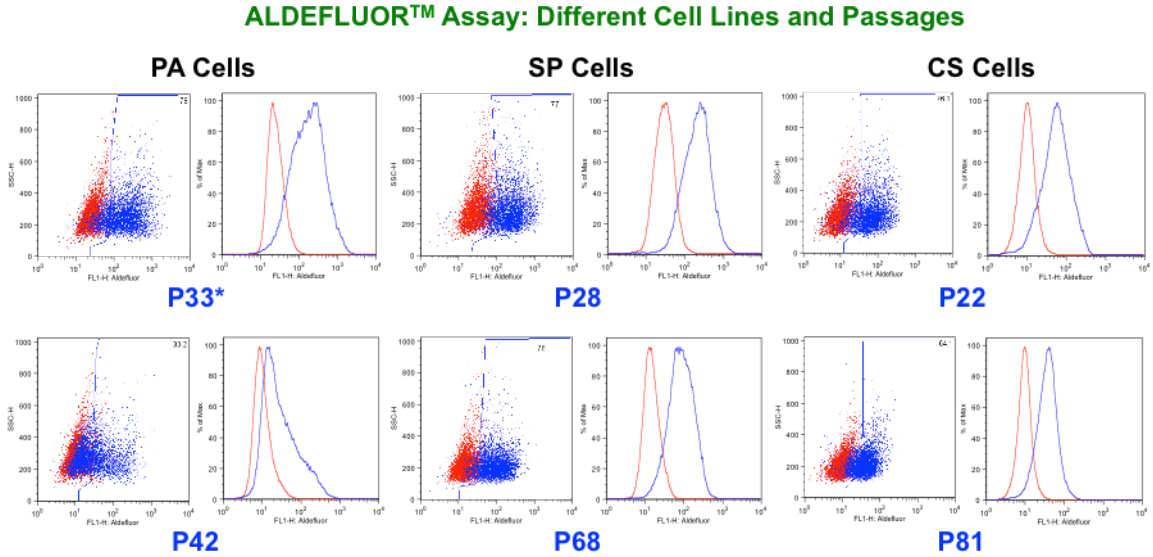

Figure 4.9.4: ALDEFLUOR™ Assay: Variations in Different Cell Lines, Passages, and Experiments

ALDH activity varies between experiments (passage numbers) for PA cells, with low activity seen in high passage (exp 2) cells and high activity seen in low passage number cells (exp1). ALDH activity of SP cells is constantly high, independent of passage number of cells. CS7 cells show high ALDH activity with slight but not statistically significant decrease with passage number of cells.
Representative results for flow cytometric measurements of 4x10^5 cells/mL assayed for ALDEFLUOR™ activity in PA, SP and CS7 cell lines at different passages (indicated in blue). Results are representative for at least two measurements of cells incubated at the same cell concentration and similar passage numbers for CS7 (n=2 P22/23, n=3 P80/81/84), SP (n=3 P28/30/32, n=4 P68/70/72/88), PA (n=4 P37/39/40/42). *PA P33: result from first experiments, comparable results were seen for PA P28. Figure left: scatter plot of fluorescence intensity vs. side scatter (SSC) of „live cell population“. Figure right: histogram of % Max (events) vs. fluorescence intensity, overlay of DEAB control (red) and sample (blue).
CS7: clonally expanded spheroid cells derived from PA, DEAB: diethylaminobenzaldehyde, exp: experiments, FL1-H: fluorescence channel 1 signal intensity, SSC-H: side scatter, P: passage number, PA: parental cell line, SP: spheroid cells derived from PA

CS7 cell line was assayed in high (P80-84) and low (P22-23) passage cells in parallel, which were obtained by thawing cells frozen at different time points. Thereby a slight difference was seen in ALDH staining intensity and number of positive staining cells between cells at low and high passage numbers, with the latter showing less intense staining. But the number of measurements for this cell

line is too low to regard these differences as statistically significant. The same is true for the low variation seen in one experiment performed with different cell concentrations on CS7 P88 (illustrated in figure 4.9.4). Though the substrate staining intensity of CS7 cell line was reduced compared to SP cells, most of the cells showed positive staining, with no distinct populations discernible, similar to that seen for SP cell line, indicating a uniform expression of the enzyme. The lower staining intensity as well as the reduced cell concentration dependency of staining might be due to the reduced size of cells compared to SP cells.

To allow a rough comparison of the three cell lines, mean values of experiments, in which a comparable cell concentration was used, were calculated and are depicted in Figure 4.9.5. For better comparability of results from different cell lines and experiments the fold change of GM test sample/GM control sample were calculated. Since PA and CS7 cell lines showed variations with passage number and/or set of experiments, the same number of experiments of either condition was used for calculation of mean values. For CS7 this was possible only with a concentration of $4x10^5$ cells/mL, since only one experiment with a cell concentration of $2x10^5$ cells/mL was performed with this cell line. In this experiment low variation to the sample using $4x10^5$ cells/mL was observed (see figure 4.9.3).

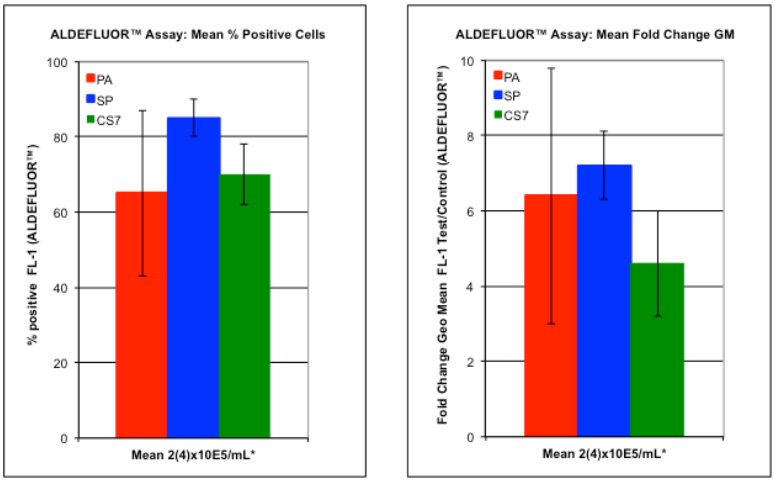

Figure 4.9.5: ALDEFLUOR™ Assay: Mean Values for Different Cell Lines

ALDH activity is high in all cell lines tested with high experimental variation seen for PA cell line and slightly lower staining intensities seen in CS7 cell line.
Mean of percent positive staining cells and fold change GM test sample/GM control sample obtained in flow cytometric measurements of cells assayed at comparable cell concentrations ($2x10^5$ cells/mL for PA and SP and $4x10^5$ cells/mL for CS7) for ALDEFLUOR™ activity in PA, SP and CS7 cell lines. Error bar: standard deviation of 4 representative experiments (CS7, PA) and 5 experiments (SP), respectively.
CS7: clonally expanded spheroid cells derived from PA, DEAB: diethylaminobenzaldehyde, FL1-H: fluorescence channel 1 signal intensity, GM: geo mean, P: passage number, PA: parental cell line, SP: spheroid cells derived from PA

4.10 Rhodamine 123 Side Population Assay (RSPA)

The side population assay is a functional assay, which tests for the dye efflux capacity of cells, using flow cytometry. The assay has been successfully used to identify and isolate adult stem cells as well as TIC from several tumor entities. The molecular basis for dye efflux is the high expression of detoxifying ABC-transporters in stem cells and drug-resistant tumor cells. The test was originally introduced using the fluorescent DNA-binding dye Hoechst33342, which has to be excited by a UV-laser. In a variant of the assay, the fluorescent mitochondrial stain Rhodamine 123 is used as an alternative, since it can be excited with standardly equipped flow cytometers and is not genotoxic. The transporter found to be mainly responsible for Rhodamine 123 efflux is MDR1/ABCB1/P-Glycoprotein. For the assay, cells are stained with the respective dye, and after removal of the dye and washing, the cells are incubated in medium for a defined period to allow for dye efflux. In a control sample, the dye efflux is inhibited by addition of transport inhibitors.

The ability to efflux the mitochondrial stain Rhodamine 123 (Rho) was assayed on PA, CS1, CS7, SP and A-CS7, A-SP cells at different passage numbers. The cells were stained for 60 min in dye-containing solution or control solution containing the efflux inhibitor verapamil. Dye efflux was allowed for 90 min. 7-ADD was added before flow cytometric measurement to be able to exclude dead cells in the analysis. To determine the cell fraction with dye efflux ability, the gate was set according to the verapamil control sample, defining cells below this region as dye pumping cells (RSP).

As can be seen from figure 4.10.1, the dye efflux characteristics of PA cells and cells grown as spheroids (SP, CS1, CS7) varied considerably. After the 90 min incubation period, most PA cells had pumped out the dye with a mean fraction of dye pumping cells of 71%±15% (n = 7, P28-P116). Results were quite similar for all samples measured (P36-P116) with a slight tendency to increased efflux capacity in cells with higher passage numbers, when measured in parallel, though in one experiment, using cells at very low passage number (P28), the efflux capacity was found to be reduced. In contrast, only a very small number of cells were able to efflux the dye in SP cell line, with a mean fraction of cells pumping out dye of 2%±2% (n = 9, P30-P83). CS1 (n=1) and CS7 (n=2) were unable to efflux the dye. The difference seen between spheroid cell lines and PA was not caused by the AC-Medium used for the RSPA, since similar results were obtained with SC-Medium used as basis for the assay. When SP or CS7 cells were cultured under ACC, a fraction of cells pumping out dye was observed, even in A-CS7 cells, but which were measured only once. A-SP cells derived of several passages of SP cells and cultured for different periods under ACC were used for RSPA. Thereby only slight variations in the fractions of cells pumping out dye were seen, with two extreme results of 9% and 65%, resulting in a mean value of 26%±16% RSP (see figure 4.10.1 and 4.10.2 for three examples). No correlation with time of culture under ACC or passage number of spheroids seeded under ACC was detectable. Interestingly, even after 40 weeks under ACC, a huge fraction of cells did not efflux the dye, which might be indicative for retention of SP-like characteristics instead of reverting to PA-like phenotype of the cells.

Besides the differences seen in transport activity, also the overall staining intensity was observed to be different between PA and spheroid cell lines. Though this feature was not addressed directly, the fold change of geo mean values of Ver control samples/unstained samples were markedly lower

(factor 5-10) in PA cells compared to SP and CS cell lines. Though comparison of different staining experiments due to intrinsic experimental variations and variations in instrument setting are not

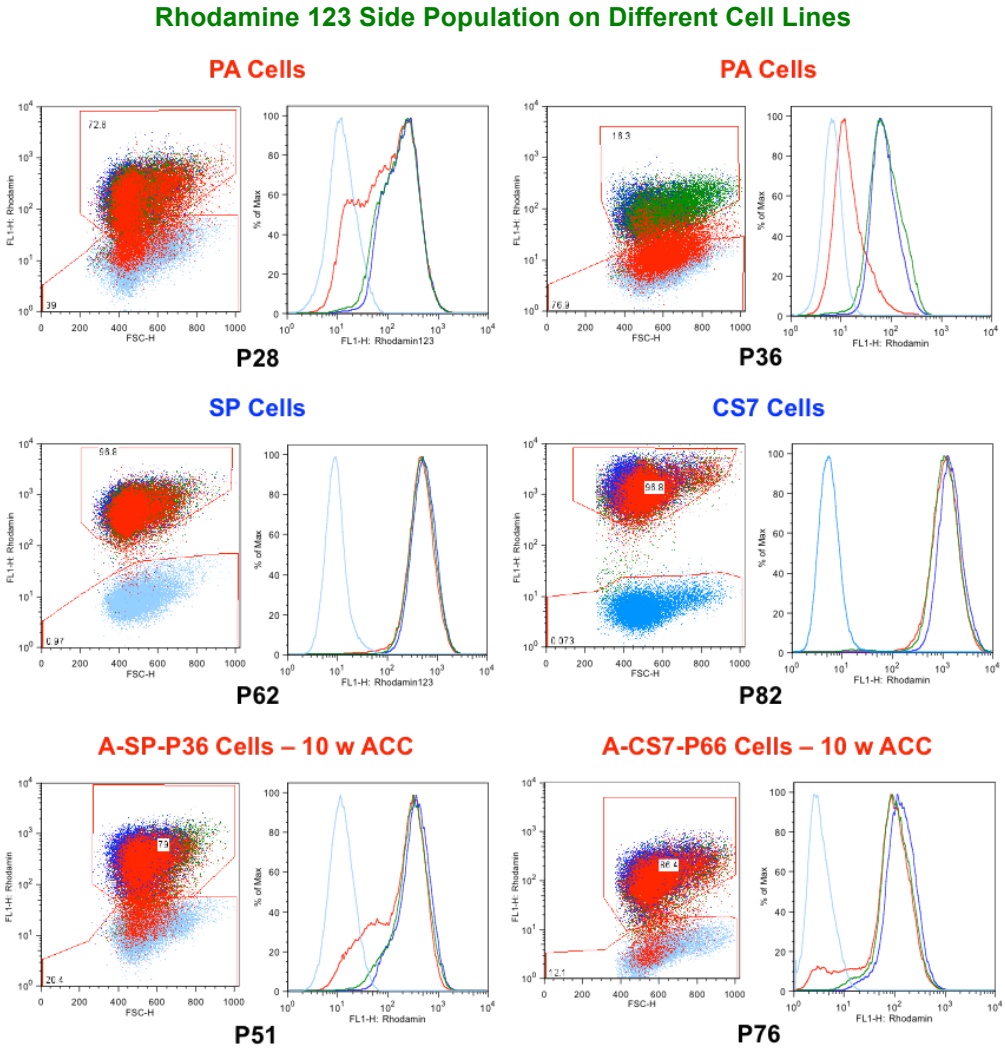

Figure 4.10.1: Representative Results of RSPA from Different Cell Lines

Dye efflux capacity of cells varies between spheroid and adherently grown cell lines. PA cell line shows high efflux capacity, which is slightly reduced in low passage number cells. CS and SP cell lines do not efflux the dye and show higher staining intensity for Rho 123. In A-SP and A-CS cell lines populations pumping out dye are present.
Flow cytometric measurements of cells assayed in RSPA. Comparison of results for different cells lines. With exception of PA P28, results are representative for other measurements PA P36 for PA (n = 6, P36-P116), SP P62 for SP (n = 9, P30-P83), CS7 P82 for CS1 (n=1, P51) and CS7 (n=2, P51), A-SP-P36 for A-SP (n=10, A-SP-P14-P94, P29-P97, 2w-41 w ACC) cell lines. For A-CS7 no further results are available.
Overlays of unstained cells (light blue), Rho-stained cells measured directly after staining (dark blue), Rho-stained cells after 90 min incubation in medium (red) and Rho-stained cells after 90 min incubation in the presence of verapamil (green). Passage number of cells is indicated in black. Figure left: scatter plot of fluorescence intensity vs. forward scatter (cell size) of „live cell population“. Figure right: histogram of % Max (events) vs. fluorescence intensity.
ACC: adherent culture conditions, A-CS7: CS cells grown under ACC, A-SP: SP cells grown under ACC, CS7: clonally expanded spheroid cells derived from PA, FL1-H: fluorescence channel 1 signal intensity, FSC-H: forward scatter, P: passage number, PA: parental cell line, Rho: Rhodamine 123, RSPA: Rhodamine 123 side population assay SP: spheroid cells derived from PA, w: weeks

generally applicable, the overall picture reflected the results seen also in single experiments performed with the cell lines in parallel. To exclude the possibility that ineffective transport inhibition in PA cells might be responsible for this observation, Rho-stained samples were measured directly after

the staining procedure (dark blue lines in figure 4.10.1). The staining pattern of these samples was almost identical to that seen in Verapamil containing control samples, which indicates effective inhibition of dye efflux by Verapamil.

The dye efflux capacity of different cell lines was quite similar to the immune flow cytometrically observed surface expression of CD243 (MDR1). To test whether MDR1 expression is responsible for the RSP phenotype, resulting cells from RSPA were additionally stained with APC conjugated CD243 antibody. Exemplary results of these experiments are shown in figure 4.10.2. Experiments revealed a clear correlation of RSP phenotype and MDR1 expression, indicated by CD243-staining of dye pumping cells.

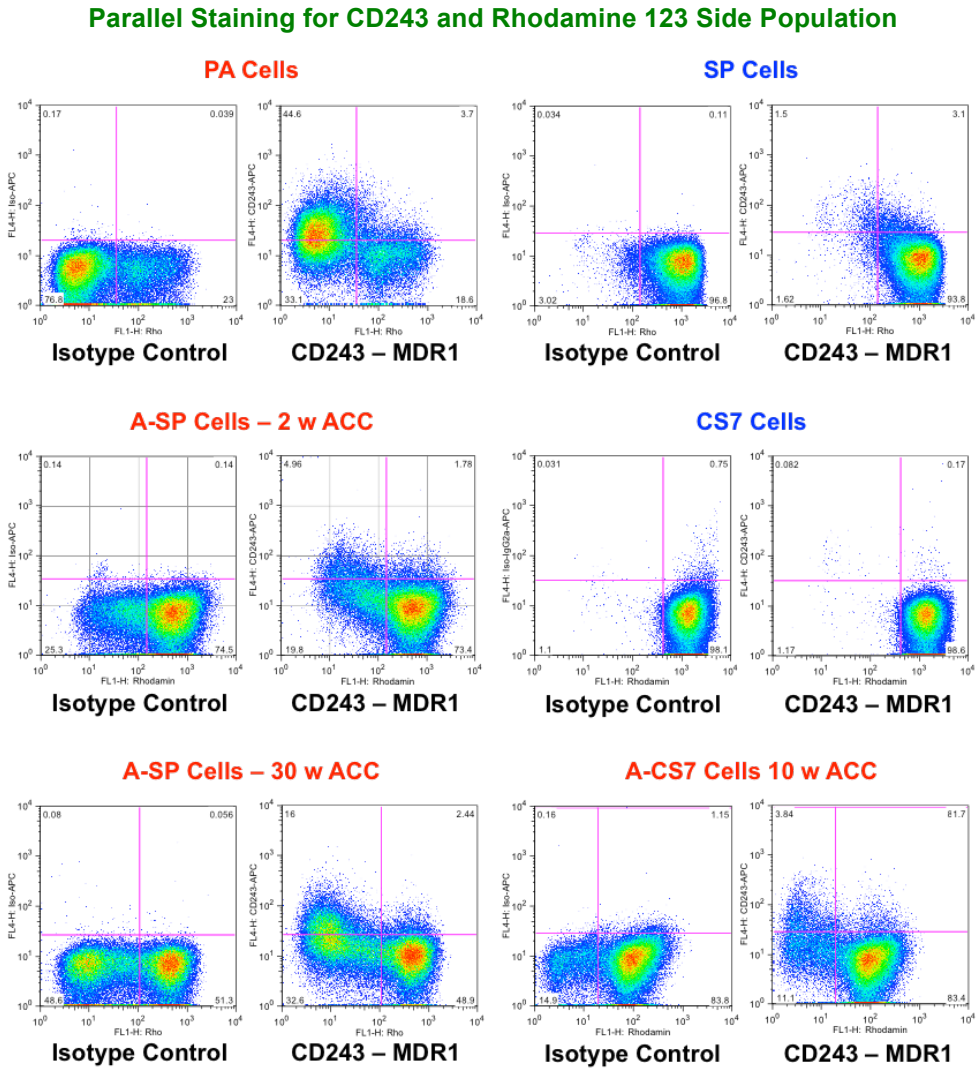

Figure 4.10.2: RSPA with Parallel IFC-Staining of CD243 (MDR1/ABCB1) on Different Cell Lines

Dye efflux capacity of cells correlates with expression of CD243 in all cell lines.
Flow cytometric immunophenotyping (IFC) of cells stained with APC conjugated antibody for detection of CD243 antigen on cells assayed in RHSPA. Comparison of Rho aliquots stained with APC conjugated isotype control antibody (figure left) with CD243 specific antibody stained aliquots (figure right).
Scatter plot of fluorescence intensity of FL4 (CD243/Isotype-APC) vs. fluorescence intensity of FL1 (Rho) of „live cell population“ for APC conjugated antibody stained cells.
ACC: adherent culture conditions, A-CS7: CS cells grown under ACC, APC: allophycocyanin, A-SP: SP cells grown under ACC, CS7: clonally expanded spheroid cells derived from PA, CD: cluster of differentiation, CS: clonally expanded spheroid cells derived from PA, FL1/4-H: fluorescence channel 1/4 signal intensities, IFC: flow cytometric immunophenotyping, MDR1 (multi drug resistant protein 1), P: passage number, PA: parental cell line, Rho: Rhodamine 123, SP: spheroid cells derived from PA, w: weeks

4.11 Tumor Formation Assay - Xenotransplantation

The central stem cell features, i.e. self-renewal ability and the capability to regenerate the tumor of origin, can only reliably proven *in vivo*. For this purpose, different amounts of PA and SP cells were injected in Matrigel™ into the flanks of strongly immuno-compromised NSG mice kept by "EPO GmbH, Berlin". The mice were monitored regularly for tumor growth over a period of 70 days. During this period no tumor growth was observed and all mice were healthy. Necropsies were performed by "EPO GmbH", after the observation time passed and mice did not show any signs of tumor growth at the injection sites. The results of the xenotransplantation assay are summarized in Table 4.11.1.

	Tumor bearing mice / Mice injected		
Injected Cells	**$1x10^4$**	**$1x10^5$**	**$1x10^6$**
PA cells at passage 37	0/5	0/4	0/3
SP cells at passage 80	0/5	0/4	0/3

Table 4.11.1: Results of Tumor Formation Assay

PA: parental cell line, SP: spheroid cells derived from PA

4.12 Whole Transcriptome Shotgun Sequencing of mRNA (RNA-Seq)

To obtain a more comprehensive view into gene expression differences between spheroid cells (SP) and parental cell line (PA), but also into changes or similarities of spheroids grown under ACC (AS) with SP and PA cell lines, mRNA of three biological replicates of PA cell line (P37), SP cell line (P39 and 43), as well as from A-SP cell line (derived of SP cells in passages P36 and P54) after 14 weeks of culture under ACC were analyzed using the next generation sequencing (NGS) technique. The raw data were processed and aligned to the human genome version GRCH38_v90 using HISAT2 alignment software. The overall alignment rate for all samples was 97% of processed reads. Analysis of aligned data was performed using the SeqMonk application.

Results obtained after hierarchical cluster analysis of the 9 datasets are shown in figure 4.12.1. Separate clustering of PA cells and SP and A-SP cells, respectively, reveals a clear difference between PA and spheroid-derived cells. This indicates, that differences in spheroid cell lines are partially retained, even after culturing under ACC.

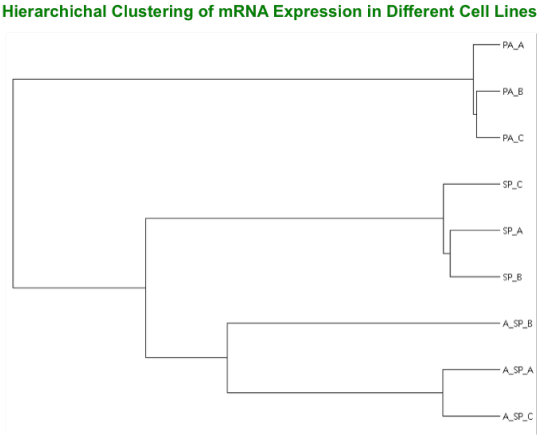

Figure 4.12.1: Hierarchical Clustering of Different Cell Lines

mRNA expression of spheroid derived cells (SP and A-SP) clusters separately from that of PA cells.
SeqMonk result for hierarchical cluster analysis of mRNA-Sequencing data from all analyzed samples.
ACC: adherent culture conditions, A-SP: SP cells grown under ACC for 14 weeks, PA: parental cell line, SP: spheroid cells derived from PA

4.12.1 Differential Gene Expression

For analysis of differential gene expression, the data were filtered for genes with significant expression levels (represented by a raw read number of more than 10 reads per gene). Also the gene list was confined to annotated genes. This refinement resulted in a number of 13955 expressed, annotated genes (Expressed-C), which were used for further analyses.

In figure 4.12.2 the overlap of genes with expression levels log2 TPM > 0, representing in the order of about 500-1000 raw reads per gene (depending on gene length), are depicted. Most genes above this value were expressed in all samples. A low percentage of genes were expressed differentially at lower levels in the different samples. Thereby the percentage of overlap between spheroid-derived cell lines (SP and A-SP) was in the same range as that for the samples grown in serum-containing medium (PA and A-SP), whereas the percentage of overlap between SP and PA cells was slightly lower. Also, the percentage of genes expressed in one of the cell lines only below this cut-off value was in the same range.

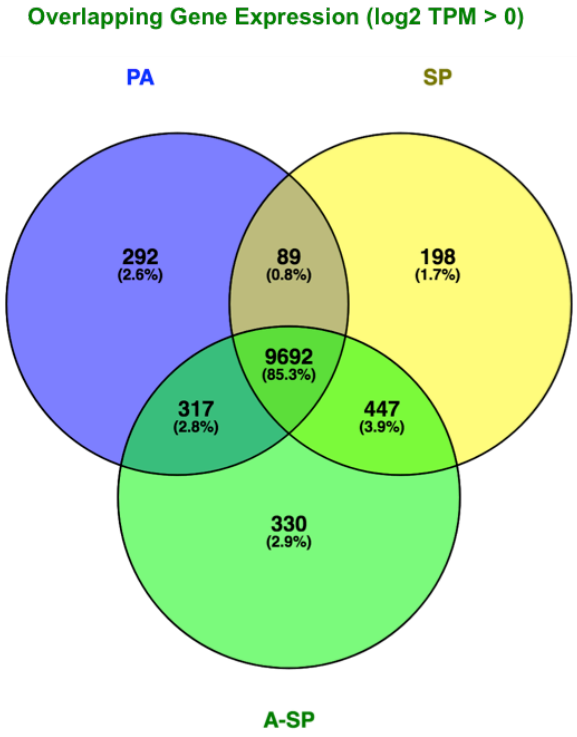

Figure 4.12.2: Genes Expressed at log2 TPM Values >0 in Different Cell Lines

Genes with detected expression levels of log2 TPM > 0 of each cell line dataset (PA, SP, A-SP) were compared logically to show the relation of different gene sets to each other.
ACC: adherent culture conditions, A-SP: SP cells grown under ACC for 14 weeks, PA: parental cell line, SP: spheroid cells derived from PA

Differentially expressed genes (DEG) between PA, SP and A-SP cell lines in pairwise comparisons (PA vs. SP, PA vs. A-SP and SP vs. A-SP) were filtered using the DESeq algorithm. Further narrowing of the results was performed using a filter based on expression differences between 2 and 20 log2 TPM (Man) or the „Intensity Difference“ filter implemented in SeqMonk (ID). In figures 4.12.3-5 the respective expression levels of genes for the three comparisons made are depicted and the respectively filtered datasets are indicated. The resulting numbers of DGE for the pairwise comparisons, which were up-regulated in respective cell line, are indicated in table 4.12.1. This table also contains the number of genes which were obtained by logical combinations of the lists, resulting in genes with up-regulated expression in one of the respective cell lines only or in genes, that were up-regulated in both spheroid-derived datasets (SP and A-SP) or in both datasets obtained form cells grown under ACC (PA and A-SP). The number of DGEs was highest in comparison of PA with SP cells, slightly lower in comparison of PA with A-SP cells, and lowest in comparison of SP with A-SP cells. In figures 4.12.6-9 exemplary results for differentially expressed genes, that were found to be up-regulated in the different samples (PA, SP and A-SP) in the pairwise comparisons (PA vs. SP, PA vs. A-SP, and SP vs. A-SP), as well as results obtained for logical filtering of genes, that were found to be up-regulated in spheroid cell lines (SP and A-SP) compared to PA cell line, and in cell lines grown under ACC (PA, A-SP) compared to non-adherently, serum-free cultured spheroids (SP) are shown. The genes for these figures were chosen from the list of DEGs according to high differences in expression level.

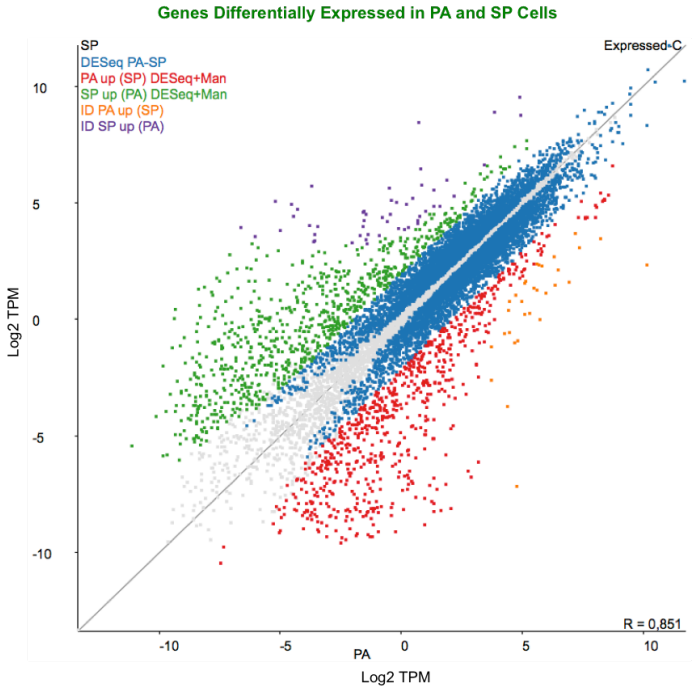

Figure 4.12.3: mRNA Expression Levels and Filters Applied for PA and SP Cells

Expression levels of SP vs. PA cells. Differentially expressed genes detected by different filtering strategies are color-coded.
PA: parental cell line, SP: spheroid cells derived from PA, Filters applied: DESeq (blue), DESeq and expression difference of 2-20 log2 TPM = DESeq+Man (red/green), DESeq and „Intensity Difference“ = ID (orange/violet), non-differentially expressed genes (grey).

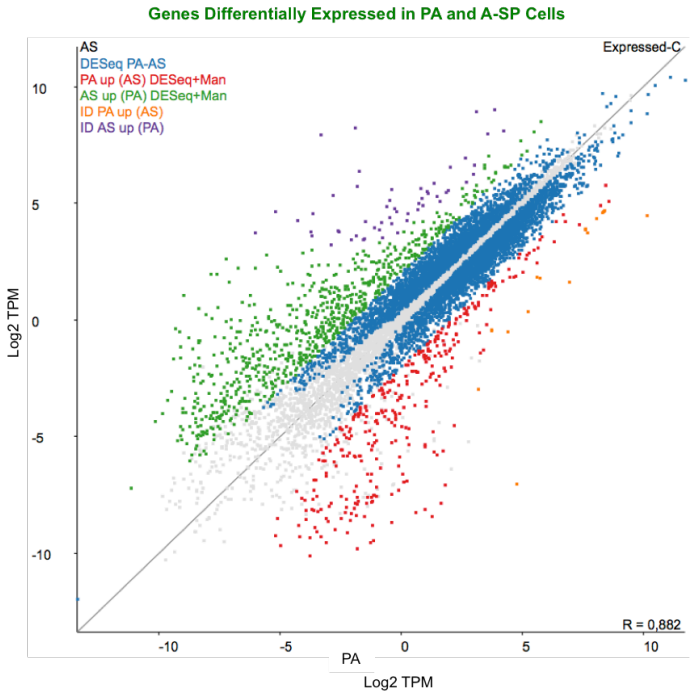

Figure 4.12.4: mRNA Expression Levels and Filters Applied for PA and A-SP Cells

Expression levels of PA vs. A-SP cells. Differentially expressed genes detected by different filtering strategies are color-coded.
ACC: adherent culture conditions, AS: adherently grown spheroids, A-SP: SP cells grown under ACC for 14 weeks, PA: parental cell line, SP: spheroid cells derived from PA, Filters applied: DESeq (blue), DESeq and expression difference of 2-20 log2 TPM = DESeq+Man (red/green), DESeq and „Intensity Difference“ = ID (orange/violet), non-differentially expressed genes (grey).

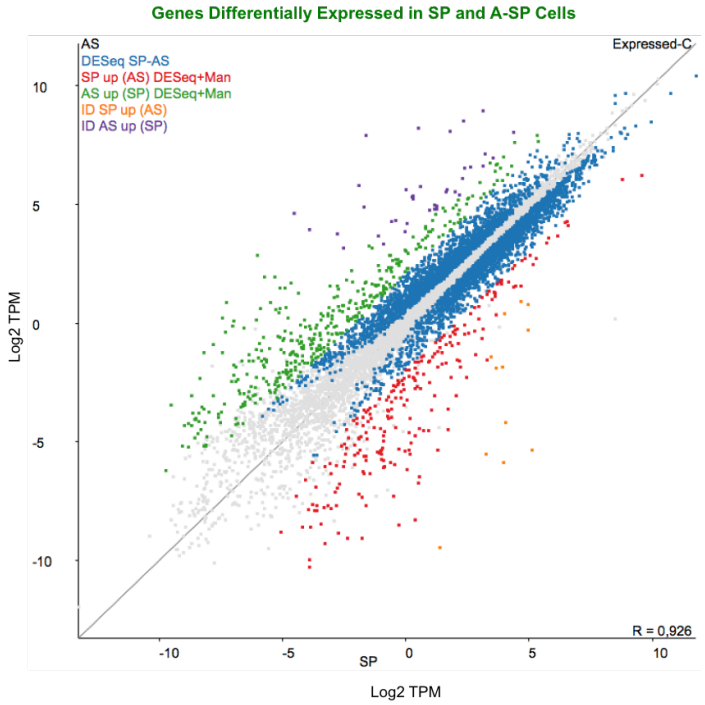

Figure 4.12.5: mRNA Expression Levels and Filters Applied for SP and A-SP Cells

Expression levels of SP vs. A-SP cells. Differentially expressed genes detected by different filtering strategies are color-coded.
ACC: adherent culture conditions, AS: adherently grown spheroids, A-SP: SP cells grown under ACC for 14 weeks, PA: parental cell line, SP: spheroid cells derived from PA, Filters applied: DESeq (blue), DESeq and expression difference of 2-20 log2 TPM = DESeq+Man (red/green), DESeq and „Intensity Difference“ = ID (orange/violet), non-differentially expressed genes (grey).

DESeq Result	Results (Man/ID/GSEA)	Results (Man/ID/GSEA)	Results (Man/ID/GSEA)
PA-SP (9327)	PA up (SP) (698/31/367)	SP up (PA) (823/51/368)	
PA-AS (7522)	PA up (AS) (346/18/343)		AS up (PA) (799/54/404)
SP-AS (5138)		SP up (AS) (242/29/241)	AS up (SP) (428/30/427)
Combination	PA+PA (251)	SP+SP (178)	AS+AS (147)

Combination	Result	Combination	Result
SP up (PA) AND AS up (PA)	SP+AS (461)	BUTNOT AS+AS, SP+SP	Spheroid (409)
PA up (SP) AND AS up (SP)	PA+AS (200)	BUTNOT AS+AS, PA+PA	Serum (168)

Table 4.12.1: Number of DEG Obtained for Different Comparisons and Filtering

Upper table: Results of differentially expressed genes in pairwise comparison of data using the DESeq algorithm (column 1). Numbers of up-regulated gens in respective cell line datasets after extraction using manual expression difference filtering (Man) or statistical intensity difference (ID) filtering of the data as well as number of genes submitted for GSEA (indicated in brackets, respectively). Column 2: genes up-regulated in PA. Column 3: genes up-regulated in SP. Column 4: genes up-regulated in SP. Line 5: number of cell line specific genes obtained by combining the lists using the logical combination AND (PA+PA, SP+SP, AS+AS).
Lower table: number of up-regulated genes in serum or spheroid-derived cells obtained by combination of lists for respective cell lines (column 1) and subtraction of cell line specific genes using the logical combination BUTNOT (column 3).
ACC: adherent culture conditions, AS: adherently grown spheroids, A-SP: SP cells grown under ACC for 14 weeks, DEG: differentially expressed genes, GSEA: gene set enrichment analysis, PA: parental cell line, SP: spheroid cells derived from PA, Cell line specific gene lists: for PA = PA+PA, for SP = SP+SP, for AS = AS+AS

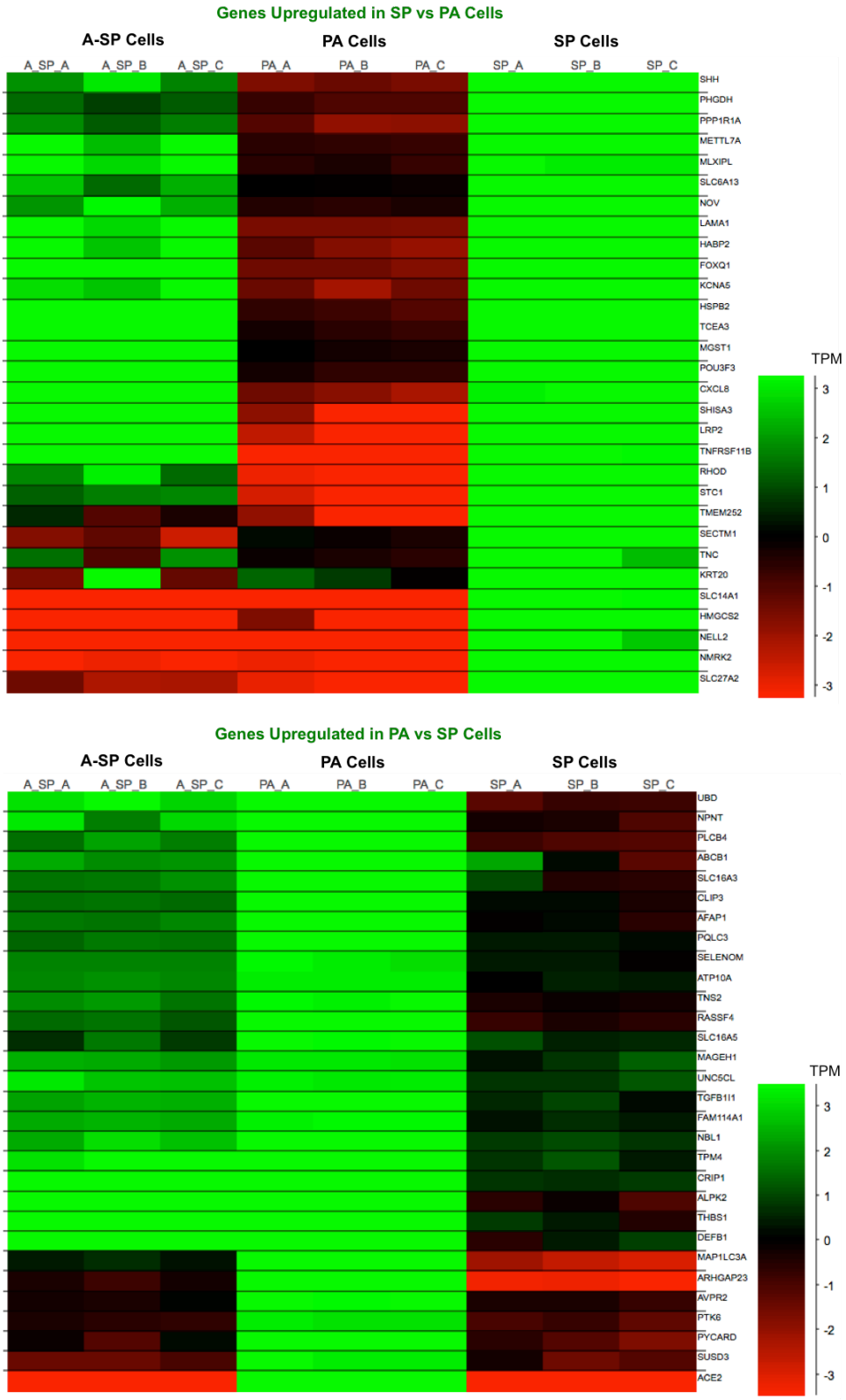

Figure 4.12.6: Heat Maps of Up-regulated Genes in Comparison of SP Cells to PA Cells

Figure top: Differentially expressed genes found to be up-regulated in SP cell line datasets.
Figure bottom: Differentially expressed genes found to be up-regulated in PA cell line datasets.
Examples of up-regulated genes after SP vs. PA comparison with highest differences in expression level between SP and PA datasets. Expression level is color-coded (see open scale on the right). Data are depicted for all datasets (indicated on top). Official gene symbols are indicated on the right.
PA: parental cell line, SP: spheroid cells derived from PA, TPM: transcripts per million

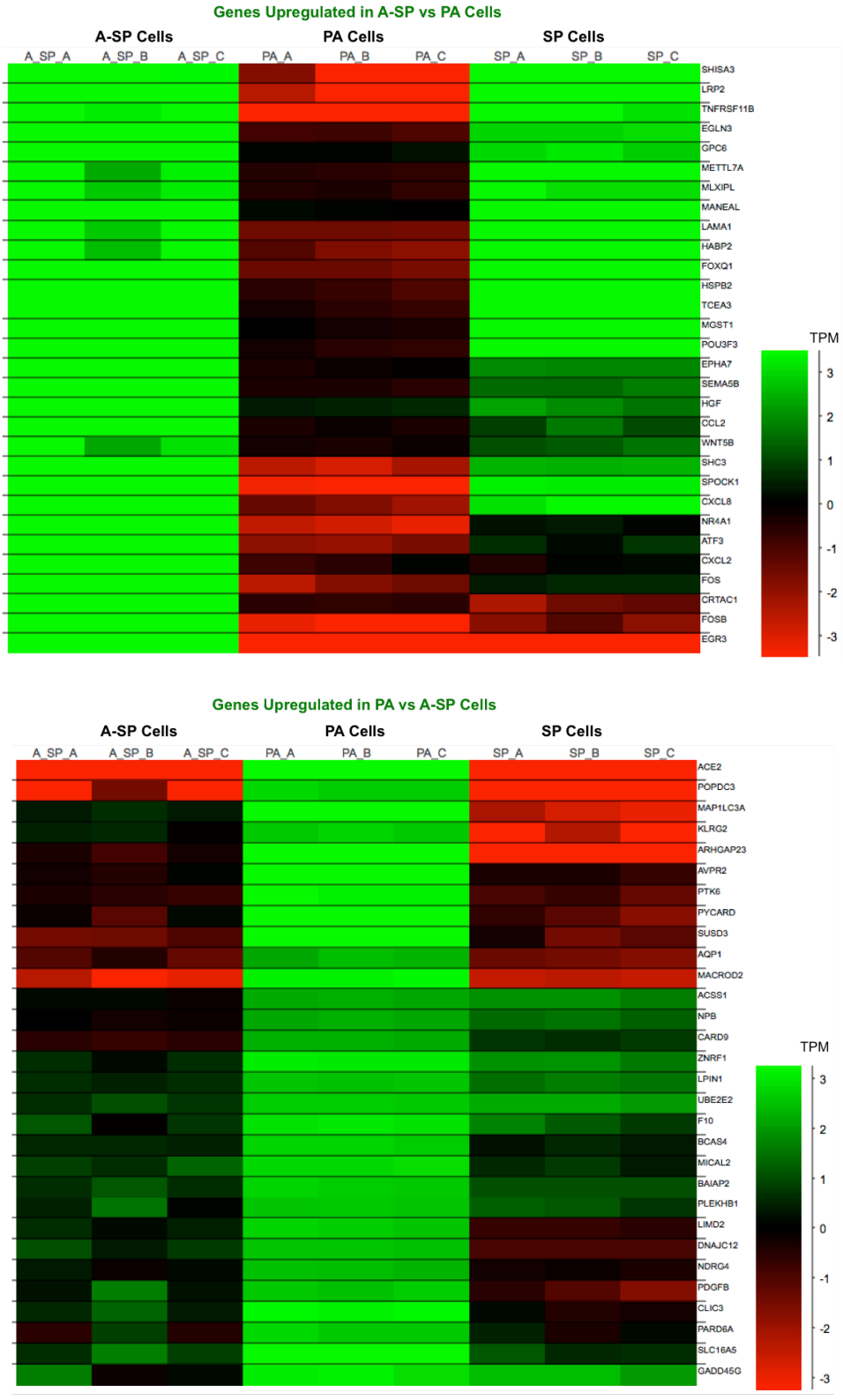

Figure 4.12.7: Heat Maps of Up- regulated Genes in Comparison of A-SP Cells to PA Cells

Figure top: Differentially expressed genes found to be up-regulated in A-SP cell line datasets.
Figure bottom: Differentially expressed genes found to be up-regulated in PA cell line datasets.
Examples of up-regulated genes after A-SP vs. PA comparison with highest differences in expression level between A-SP and PA datasets. Expression level is color-coded (see open scale on the right). Data are depicted for all datasets (indicated on top). Official gene symbols are indicated on the right.
ACC: adherent culture conditions, A-SP: SP cells grown under ACC for 14 weeks, PA: parental cell line, SP: spheroid cells derived from PA, TPM: transcripts per million

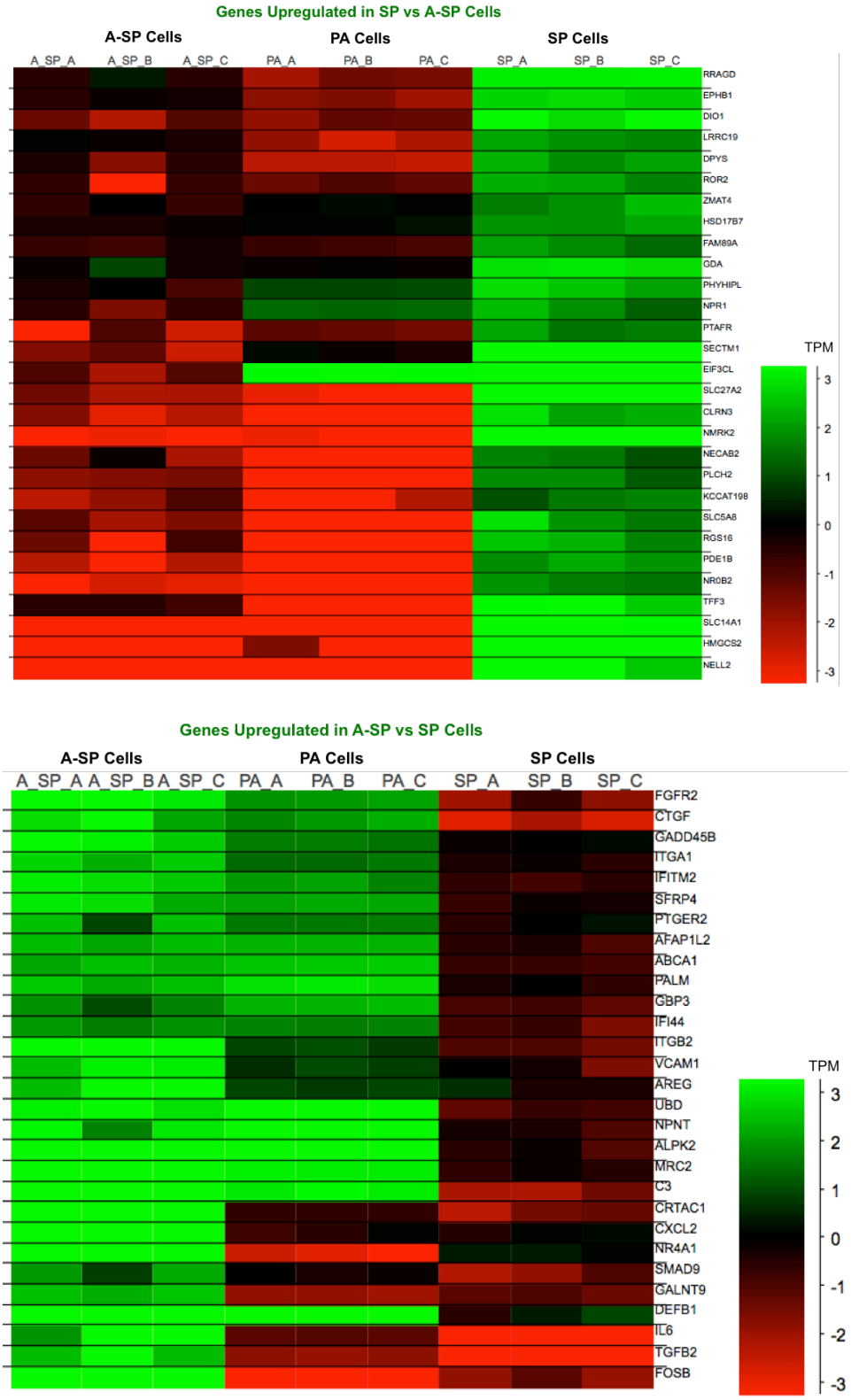

Figure 4.12.8: Heat Maps of Up-regulated Genes in Comparison of SP Cells to A-SP Cells

Figure top: Differentially expressed genes found to be up-regulated in SP cell line datasets.
Figure bottom: Differentially expressed genes found to be up-regulated in A-SP cell line datasets.
Examples of up-regulated genes after SP vs. A-SP comparison with highest differences in expression level between SP and A-SP datasets. Expression level is color-coded (see open scale on the right). Data are depicted for all datasets (indicated on top). Official gene symbols are indicated on the right.
ACC: adherent culture conditions, A-SP: SP cells grown under ACC for 14 weeks, PA: parental cell line, SP: spheroid cells derived from PA, TPM: transcripts per million

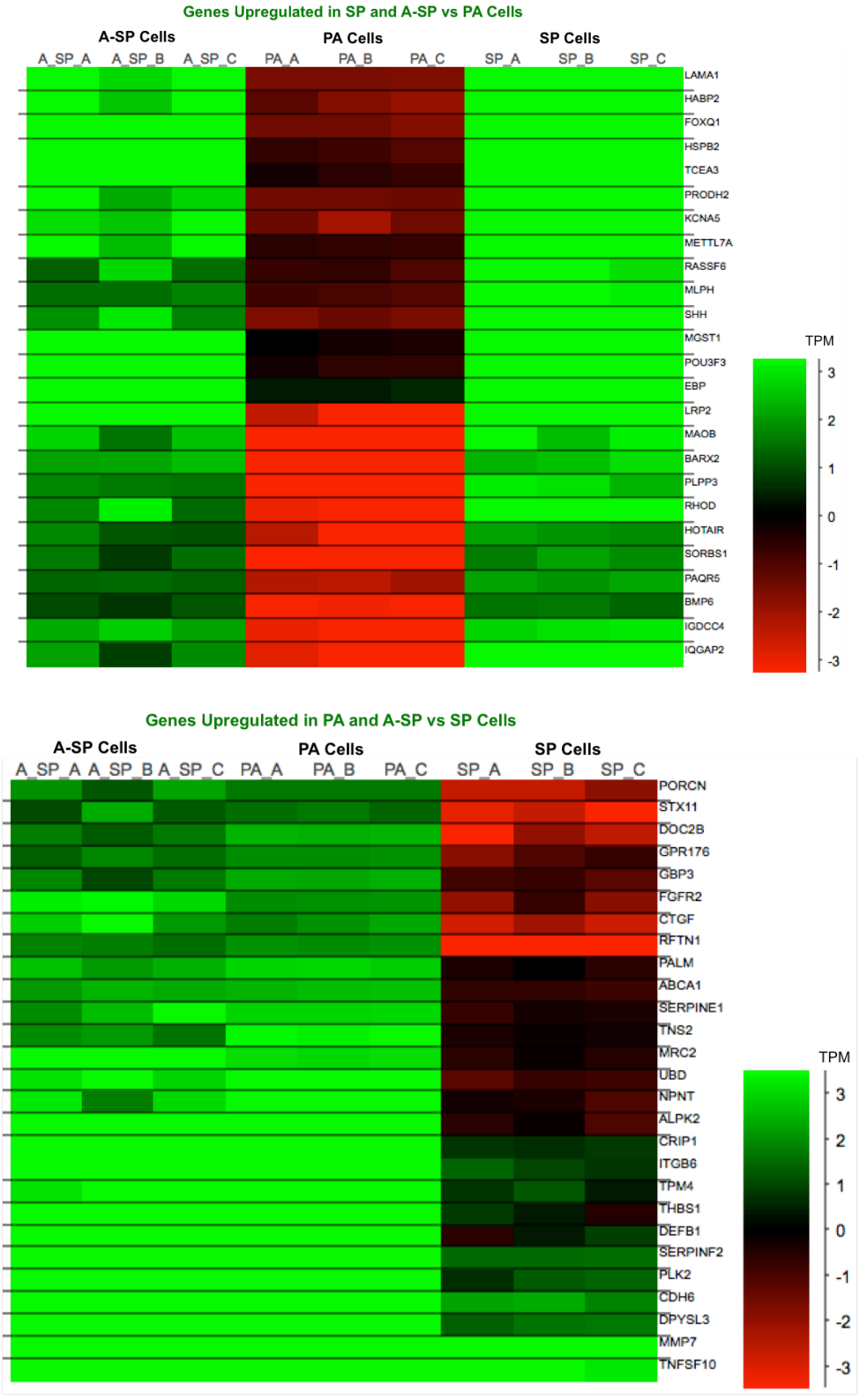

Figure 4.12.9: Heat Maps of Up-regulated Genes in Spheroid and ACC-Cultured Cell Lines

Figure top: Differentially expressed genes found to be up-regulated in spheroid cell line datasets (SP, A-SP).
Figure bottom: Differentially expressed genes found to be up-regulated in ACC-cultured cell line datasets (PA, A-SP). Examples of up-regulated genes with highest differences in expression level between spheroid and serum datasets (see table 4.12.1). Expression level is color-coded (see open scale on the right). Data are depicted for all datasets (indicated on top). Official gene symbols are indicated on the right.
ACC: adherent culture conditions, A-SP: SP cells grown under ACC for 14 weeks, PA: parental cell line, SP: spheroid cells derived from PA, TPM: transcripts per million

As can be seen from figures 4.12.6.-4.12.9, some variation in expression levels for several of the genes could be observed between replicate sets, especially the A-SP-B sample, which was derived from spheroids seeded at higher passage number (P54) into ACC, showed variations when compared to both other samples descending form spheroids at earlier passage (P36). It can also be seen, that some of the genes were either similarly up-regulated in A-SP and SP cells (spheroid-derived cell lines) compared to PA cells or in A-SP and PA cells (cells grown under ACC) compared to SP cells, whereas some genes were differentially expressed in only one of the cell lines. For example high expression of ACE2 is found in PA cells only, FOS/FOSB and EGR3 are up-regulated in A-SP cells and SLC14A1 and NMRK2 are up-regulated in SP cells specifically, when compared to both other cell lines. Also genes with relatively high expression levels in all cell lines were differentially expressed e.g. MMP7 and TNFSF10.

4.12.2 Gene Set Enrichment Analysis (GSEA)

The differentially expressed genes (DEGs) obtained from the analyses were submitted for gene set enrichment analysis (GSEA) to the GeneAnalytics™ application to identify significantly up-regulated signatures in the different cell lines. Genes with high expression differences were chosen for this analysis. Since the methods applied for GSEA are statistics-based the manually filtered data were chosen for this purpose. In cases, where the number was too high (more than 400), those genes with highest difference in expression values were selected.

In general a high number of brain- or neuron-associated terms were among the top listed entities for all datasets. The top-ranked disease terms were various cancerous diseases, especially different histological subtypes of RCC. Comparison of spheroid-derived cell line up-regulated datasets in comparison to PA cell line datasets with gene expression data from *in vitro* cell lines revealed the “Human embryonic stem cells (family)“ among the top ranked results for, with 44 and 46 gene matches (e.g. CXCR4, LRP2, RARRES2, STC1, METTL7A, EMX1, SHISA9, DCLK1, ALPL) representing a score value of 5.

An overview of pathways found to be enriched in the investigated datasets is given in tables 4.12.2.-14.12.6. Thereby in spheroid-derived cell line datasets Akt / Erk signaling, CREB pathway, HIF-1α transcription factor network, Wnt/Hedgehog/Notch signaling, EGFR (ErbB) signaling, and p21-activated kinases (PAK) pathway, but also differentiation-related pathways were found to up-regulated compared to PA cell line dataset. Whereas, genes up-regulated in cell lines grown in serum-containing medium (PA and A-SP) derived datasets were predominantly involved in immune-regulatory pathways, but also in adhesion and angiogenesis, as well as sphingosine-1-phosphate (S1P) stimulated signaling, and NF-κB signaling.

Comparison of SP cell line dataset with A-SP and PA cell line datasets showed up-regulation of metabolic pathways, especially in lipid metabolism, but also a tendency to neuronal differentiation. When compared to both other cell lines for A-SP cell line dataset a high number of pathways was detected to be changed, among which were e.g. adipogenesis, TNF and TGF-β pathway, and ATF-2 transcription factor network. Pathways detected specifically up-regulated in PA cell line dataset compared to other cell line datasets were integrin signaling and phagocytic activity. The up-regulated

DGEs in this dataset also contained several genes associated to aryl hydrocarbon receptor (AHR) pathway involved in xenobiotic-metabolism.

In tables 4.12.7-4.12.10 biological processes, identified to be enriched in the up-regulated DEG datasets from different cell lines are shown. Enriched processes in spheroid-derived cell line datasets were glucose metabolism, response to oxidative stress and cellular (osteogenic) differentiation. The datasets obtained from cell lines grown under ACC were enriched in inflammatory response, adhesion, and ECM related functions. In PA cell line a high number of protocadherin genes (PCDHA) was found to be up-regulated compared to spheroid-derived cell lines. In A-SP cell line dataset an up-regulation of chemokine-mediated signaling pathways and pathways involved in muscle cell differentiation was detected.

Up-regulated Genes in SP Cell Line Dataset vs. PA Cell Line Dataset				
Score	**Pathway Name**	**Total Genes**	**Matched Genes**	**Matched Genes (Symbols)**
29.43	Metabolism	2547	88	KMO, G0S2, GALNT18, ACOT6, ACMSD, GAMT, ADA2, SLC27A2, LRP2, SLC27A3, ADCY5, CPNE7, SLC5A8, SLC6A12, SLC5A3, NMRK2, AGMAT, AGT, CSGALNACT1, AK5, AK7, PLA1A, MAN1A1, MAOB, MAOA, PLCH2, PLEKHA1, ALOX5, ALPL, PLPP3, GDA, PNPLA3, NT5E, POLE2, UPP1, ANPEP, APOC1, APOE, GNB3, APOM, DDC, MGAT5, MGST1, GPC6, PPM1L, PRKAA2, DIO1, ASNS, PRODH2, GYG2, SQLE, DPYS, B3GALT5, PTGS1, DSEL, HK2, OXCT1, EBP, HMGCS1, HMGCS2, LIPG, PCSK5, PCSK6, RDH10, ELOVL6, PDK4, ENO2, RGL1, TCN2, PHGDH, MLXIPL, CA12, FABP7, FAH, MSMO1, MT1A, IL4I1, INSIG1, FDPS, FFAR1, ITPR1, KCNJ11, FMOD, SERINC2, CHST2, NAGS, NAPRT, CKB
12.36	ERK Signaling	1178	39	COL23A1, ADCY5, LAMA1, TUBA8, PLCB1, PLPP3, CXCL14, CXCL6, CXCL8, NRG3, CXCR4, ANGPT4, DDR2, PPP1R1A, PRG2, PRKAA2, WNT5A, SPOCK1, BMP2, BMP4, BMP6, HNF4A, PDGFRA, RHOD, EPHB1, EPHB3, EPHA3, ERBB4, TGFBR3, THPO, CACNA1A, TNC, CCL15, IL3RA, FBLIM1, ITGAD, MYH15, MYH13, FRAS1
13.40	PEDF (SERPINF1) Induced Signaling	743	29	ACKR3, CNTFR, NFATC4, PLCB1, ALOX5, CXCL14, CXCL6, CXCL8, CXCR4, ANGPT4, DDR2, PPP1R1A, PRKAA2, PRLR, PTGS1, BMP2, BMP4, BMP6, PDGFRA, EPHB1, EPHB3, EPHA3, ERBB4, THPO, CACNA1A, TNFRSF11B, CCL15, IL3RA, FCER1G
17.70	CREB Pathway	528	26	NFATC4, ADCY5, SLC8A1, PLCB1, PLPP3, NRG3, DDR2, GRIA3, GRM1, GRM8, GUCY1A2, BMP2, BMP4, BMP6, PDE1B, PDE3B, PDGFRA, RHOD, HTR1D, EPHB1, EPHB3, EPHA3, ERBB4, TGFBR3, THPO, CACNA1A
13.52	Activation of cAMP-Dependent PKA	628	26	CLCNKA, CLCNKB, NFATC4, ADCY5, PLCB1, PLPP3, NRG3, DDR2, PPP1R1A, PTPRB, BMP2, BMP4, BMP6, PDE1B, PDE3B, PDGFRA, RGS16, EPHB1, EPHB3, EPHA3, ERBB4, TGFBR3, THPO, CACNA1A, KCNK2, KCTD15
11.72	Akt Signaling	681	26	GABRD, PLCB1, PLPP3, CXCL14, CXCL6, CXCL8, NRG3, CXCR4, ANGPT4, DDR2, BMP2, BMP4, BMP6, PDE3B, PDGFRA, RHOD, EPHB1, EPHB3, EPHA3, ERBB4, THPO, ETV1, CCL15, IL3RA, FCER1G, ITGAD
11.68	PAK Pathway	682	26	SLC2A5, TUBA8, PLCB1, PLPP3, CXCL14, CXCL6, CXCL8, NRG3, CXCR4, ANGPT4, SORBS1, DLL1, PTPRB, PTPRR, BMP2, BMP4, BMP6, HNF4A, PDGFRA, RHOD, TGFBR3, THPO, CCL15, IL3RA, MYH15, MYH13
11.66	Nanog in Mammalian ESC Pluripotency	533	22	ADCY5, TUBA8, NOSTRIN, PLCB1, PLPP3, NRG3, AQP4, DDR2, PRKAA2, WNT5A, GUCY1A2, BDKRB1, BDKRB2, BMP2, BMP4, BMP6, PDGFRA, EPHB1, EPHB3, EPHA3, ERBB4, THPO
10.29	Phospholipase-C Pathway	498	20	COL23A1, NFATC4, ADCY5, LAMA1, PLCB1, PLCH2, PLPP3, NRG3, PRG2, SPOCK1, BMP2, BMP4, BMP6, PDGFRA, RHOD, TGFBR3, THPO, TNC, ITGAD, FRAS1
10.51	G-Beta Gamma Signaling	349	16	CNR1, ADCY5, TUBA8, NOV, PLCB1, GJA1, GRM1, GRM8, WNT5A, GUCY1A2, BMP2, BMP4, BMP6, PDE1B, PDE3B, CACNA1A
9.25	Glucose / Energy Metabolism	307	14	SLC47A1, ME2, APOE, PRDX2, PRKAA2, ATF3, HK2, HMGCS1, HMGCS2, HNF4A, ENO2, PHGDH, IGFBP3, CA12
12.82	Calcium Signaling Pathway	182	12	SLC8A1, PLCB1, GRM1, AVPR1B, BDKRB1, BDKRB2, PDE1B, PDGFRA, ERBB4, CACNA1A, ITPKB, CHRM3
10.68	Phospholipase D Signaling Pathway	185	11	ADCY5, PLCB1, PLPP3, CXCL8, GRM1, GRM8, AVPR1B, PDGFRA, FCER1G, SHC2, SHC3
12.47	ESC and iPSC Diff Pathways + Lin-specific Markers	133	10	NCAM1, NOG, CXCR4, GJA1, ONECUT2, PROM1, WNT5A, BMP4, THPO, SHH
8.96	Wnt / Hedgehog / Notch	182	10	TRIB2, NDRG1, NKD2, ALPL, GDF15, DLL1, BMP6, TLE3, KLF4, SHH
18.02	HIF-1-alpha Transcription Factor Network	65	9	NDRG1, ADM, CXCR4, NT5E, HK2, HNF4A, EGLN3, TFF3, FOS
15.89	NSC Diff. Pathways and Lin-spec. Markers	79	9	NCAM1, GAD1, CXCR4, PROM1, BMP2, BMP4, PDGFRA, FABP7, SHH
9.54	ErbB Signaling Pathway	143	9	EGLN3, ERBB3, CAMK1, CAMK1D, CCND1, CDKN1A, FOS, SHC2, SHC3
11.80	Oxidative Stress	31	5	MAOA, MGST1, GPX3, SOD3, FOS

Up-regulated Genes in SP Cell Line Dataset vs. A-SP Cell Line Dataset				
Score	**Pathway Name**	**Total Genes**	**Matched Genes**	**Matched Genes (Symbols)**
18.71	Metabolism	2547	56	ACAT2, ACOT1, ACSS2, ADA2, SLC27A2, SLC5A8, LSS, NMRK2, AK5, NOSTRIN, PKLR, UAP1L1, NPC1L1, NPAS2, PLB1, PLCG2, PLCH2, GCNT4, GDA, PNPLA3, ANPEP, APOA2, APOE, MGAT4A, PPP1R3C, DHCR7, ASPA, DIO1, PRODH, XDH, DPYS, BBOX1, BDH1, HMGCS1, HMGCS2, LIPT2, PCSK9, HS3ST5, HSD17B7, RGN, PGAM4, PHGDH, CA4, MOGAT3, MOGAT1, FADS2, FAH, MSMO1, MT1X, INSIG1, FDFT1, FFAR1, KCNB1, CHRM3, CHST2, NAGS
7.90	CREB Pathway	528	14	TRPM8, PLCG2, NPR1, NRG3, GRIA3, GRM8, ROR2, GUCY1A2, SPON1, PDE1B, PDE3B, HTR1D, EPHB1, TGFBR3
10.89	Regulation of Cholesterol Biosynthesis By SREBP	55	5	LSS, DHCR7, HMGCS1, INSIG1, FDFT1, APOA2, APOE, PCSK9, FDFT1
9.02	FOXA2 and FOXA3 Transcription Factor Networks	44	4	PKLR, BDH1, HMGCS1, PDX1
7.70	ECM Proteoglycans	57	4	NCAM1, COL9A3, LAMA2, ITGAX

Table 4.12.2 Pathways Up-regulated in SP Cell Line Dataset Comparisons

Upper part: relevant pathways detected for datasets from DEG up-regulated in SP cell line dataset compared to PA cell line dataset. Lower part: relevant pathways detected for datasets from DEG up-regulated in SP cell line dataset compared to A-SP cell line dataset. Score in Column 1 represents (-log2) transformed p-values.
ACC: adherent culture conditions, A-SP: SP cells grown under ACC for 2 weeks, DEG: differentially expressed genes, PA: parental cell line, SP: spheroid cells derived from PA

Up-regulated Genes in PA Cell Line Dataset vs. SP Cell Line Dataset				
Score	**Pathway Name**	**Total Genes**	**Matched Genes**	**Matched Genes (Symbols)**
26.92	Degradation of The Extracellular Matrix	298	23	COL5A1, COL9A1, LRP4, ADAMTS2, CTSS, MATN3, DMD, BGN, PDGFB, TGFB2, THBS1, MMP16, MMP7, MMP9, TLL2, TNN, FBN1, ITGB6, FGB, JAM3, FGG, FN1, SERPINE1
16.26	ECM Proteoglycans	57	8	LRP4, LAMA5, MATN3, BGN, ITGB3, ITGB6, ITGAV, SERPINE1
15.51	Adhesion	123	11	CTGF, CYR61, ST14, TGFB1I1, MMP2, MMP9, TNS2, ITGB3, ITGAV, CDH6, SERPINE1
15.11	Interferon Gamma Signaling	202	14	TRIM38, GBP3, GBP1, UBA7, UBE2L6, OAS1, SOCS3, XAF1, STAT1, IFITM2, IFITM1, MX1, TRIM2, TRIM34
14.80	Amb2 Integrin Signaling	48	7	LRP1, CTGF, CYR61, MMP2, MMP9, JAM3, FN1
14.36	Angiogenesis (CST)	89	9	NDRG4, VEGFC, THBS1, MMP7, MMP2, MMP9, ITGB3, ITGAV, FGFR2
13.44	Toll-like Receptor Signaling Pathway	322	17	ACE, GBP4, GBP3, GBP2, GBP1, LBP, PLCB4, MEFV, OAS2, PYCARD, C3, TGFB2, TLR2, TLR6, CASP4, CASP1, SERPINE1
12.71	Collagen Chain Trimerization	184	12	ACE2, SLC15A1, COL5A1, COL9A1, ADAMTS2, CTSS, MMP7, MMP9, TLL2, FGB, FGG, KCNJ13
12.28	Phagocytosis of Microbes	85	8	PLCD3, PLCB4, C3, MRC2, ITGB3, ITGB6, ITGAV, FN1
12.13	ECM-receptor Interaction	112	9	COL9A1, THBS1, TNN, FBN1, ITGB6, FGB, JAM3, FGG, FN1
12.08	Non-integrin Membrane-ECM Interactions	46	6	LAMA5, NTN4, PDGFB, THBS1, ITGB3, ITGAV
11.63	Immune Response IFN Alpha/beta Signaling Pathway	91	8	OAS1, SOCS3, XAF1, STAT1, IFITM2, IFITM1, IL15, MX1
11.42	S-1P Stimulated Signaling	95	8	PLCB4, PDGFB, PDGFRB, CASP4, CASP1, S1PR1, CDH18, CDH6
11.23	Cytokine Signaling in Immune System	760	28	TRIM38, GBP3, GBP1, LAMA5, UBA7, UBE2L6, OAS1, APBB1IP, SOCS3, XAF1, DUSP1, STAT1, PDGFB, IFITM2, IFITM1, MMP2, MMP9, IL15, IL1RAP, TNFRSF6B, IL34, CD40, ITGB3, FGFR2, FN1, MX1, TRIM2, TRIM34
11.12	Osteopontin-mediated Events	34	5	GSN, MMP2, MMP9, ITGB3, ITGAV
10.41	Integrin AlphaIIb Beta3 Signaling	38	5	ADRA2C, APBB1IP, RAPGEF3, ITGB3, FN1
10.34	TGF-beta Receptor Signaling (WikiPathways)	58	6	SMAD6, BAMBI, STAT1, THBS1, ITGB6, SERPINE1
10.20	Focal Adhesion	283	14	LAMA5, VEGFC, PTK6, STYK1, PDGFB, THBS1, CAPN5, TNK2, ITGB3, ITGB6, ITGAV, FLNA, FN1, MYL9
9.05	Phagosome	152	9	TUBB3, CTSS, HLA-DPA1, RAB7B, C3, THBS1, TLR2, TLR6, MRC2
7.64	NRF2 Pathway	145	8	SLC2A9, SLC6A15, SLC2A10, UGT1A6, UGT1A9, PDGFB, TGFB2, CES4A
7.61	Cell Adhesion_ECM Remodeling	61	5	MMP16, MMP7, MMP9, FN1, SERPINE1
Up-regulated Genes in PA Cell Line Dataset vs. A-SP Cell Line Dataset				
Score	**Pathway Name**	**Total Genes**	**Matched Genes**	**Matched Genes (Symbols)**
10.98	Integrin AlphaIIb Beta3 Signaling	38	5	APBB1IP, RAPGEF3, FGB, FGG, FN1
12.44	Aryl Hydrocarbon Receptor Pathway	48	6	UGT1A7, UGT1A3, UGT1A4, UGT1A1, UGT1A6, UGT1A9
10.18	NRF2-Antioxidant Response Pathway	145	9	SLC2A9, UGT1A7, UGT1A3, UGT1A4, UGT1A1, UGT1A6, UGT1A9, GGT2, CES4A
11.59	Collagen Chain Trimerization	184	11	ACE2, SLC15A1, COL9A1, CTSS, PROC, MMP9, TLL2, F10, FGB, FGG, KCNJ13
34.43	Steroid Hormone Biosynthesis	59	13	AKR1C2, AKR1C1, AKR1D1, UGT1A7, UGT1A3, UGT1A4, UGT1A1, UGT1A8, UGT1A6, UGT1A10, UGT1A5, UGT1A9, UGT2B4

Table 4.12.3: Pathways Up-regulated in PA Cell Line Dataset Comparisons

Upper part: relevant pathways detected for datasets from DEG up-regulated in PA cell line dataset compared to SP cell line dataset. Lower part: relevant pathways detected for datasets from DEG up-regulated in PA cell line dataset compared to A-SP cell line dataset. Score in Column 1 represents (-log2) transformed p-values.
ACC: adherent culture conditions, A-SP: SP cells grown under ACC for 2 weeks, DEG: differentially expressed genes, PA: parental cell line, SP: spheroid cells derived from PA

Up-regulated Genes in A-SP Cell Line Dataset vs. PA Cell Line Dataset				
Score	**Pathway Name**	**Total Genes**	**Matched Genes**	**Matched Genes (Symbols)**
13.82	Signaling By GPCR	2599	18	LRP2, ADM, LAMA1, NR4A1, CXCL1, CXCL2, CXCL8, GFRA1, OPN3, GPC6, HES1, DUSP1, DUSP5, PCSK6, HPN, IL6, JUN, SHC3
13.66	Innate Immune System	2129	16	NR4A1, CXCL1, CXCL2, CXCL8, GFRA1, MGST1, DUSP1, DUSP5, EGR1, TNFRSF11B, CCL2, IL6, JUN, FOS, SERPINA1, SHC3
21.99	ERK Signaling	1178	15	LAMA1, CXCL1, CXCL2, CXCL8, GPC6, ATF3, SPOCK1, DUSP1, EPHA7, CCL2, IL6, JUN, FOSB, FOS, FRAS1
20.87	Cytokine Signaling in Immune System	760	12	CXCL1, CXCL2, CXCL8, GFRA1, DUSP1, DUSP5, EGR1, TNFRSF11B, CCL2, IL6, FOS, SHC3
15.53	PEDF Induced Signaling	743	10	CXCL1, CXCL2, CXCL8, PTGS1, EPHA7, TNFRSF11B, CCL2, IL6, JUN, FOS
22.58	Toll-like Receptor Signaling Pathway	322	9	CXCL1, CXCL2, CXCL8, CCL2, IL6, JUN, FOSB, FOS, TRIP6
15.92	Integrin Pathway	568	9	LAMA1, CXCL1, CXCL2, CXCL8, SPOCK1, CCL2, JUN, FOS, FRAS1
10.11	RET Signaling	972	9	NR4A1, GFRA1, DUSP1, DUSP5, PCSK6, IL6, JUN, FOS, SHC3
11.76	TGF-Beta Pathway	652	8	CXCL8, GPC6, DUSP1, EPHA7, CCL2, IL6, JUN, FOS
11.34	Akt Signaling	681	8	CXCL1, CXCL2, CXCL8, GPC6, EPHA7, CCL2, IL6, FOS
23.43	Glucocorticoid Receptor Regulatory Network	82	6	NR4A1, CXCL8, EGR1, IL6, JUN, FOS
21.12	TNF Signaling Pathway	108	6	CXCL1, CXCL2, CCL2, IL6, JUN, FOS
19.78	C-type Lectin Receptor Signaling Pathway	127	6	EGR3, EGR2, IL6, JUN, FOSB, FOS
19.46	Direct P53 Effectors	132	6	ATF3, DUSP1, DUSP5, BTG2, IGFBP3, JUN
15.78	TNFR1 Pathway	207	6	ATF3, TNFRSF11B, CCL2, IL6, JUN, FOS
12.31	MAPK Signaling Pathway	321	6	NR4A1, DUSP1, DUSP5, HSPB2, JUN, FOS
16.97	ErbB1 Downstream Signaling	102	5	DUSP1, ZFP36, EGR1, JUN, FOS
14.61	Brain-Derived Neurotrophic Factor (BDNF) Signaling P	144	5	EGR1, EGR2, JUN, FOS, SHC3
10.63	Regulation of Lipid Metabolism Insulin Signaling	262	5	EGR1, IGFBP3, JUN, FOS, SHC3
9.21	NF-kappaB Signaling	327	5	NR4A1, PTGS1, EGR1, RIPK4, CCL2

Table 4.12.4: Pathways Up-regulated in A-SP Cell Line Dataset Comparisons

Relevant pathways detected for datasets from DEG up-regulated in A-SP cell line dataset compared to PA cell line dataset. Score in Column 1 represents (-log2) transformed p-values.
ACC: adherent culture conditions, A-SP: SP cells grown under ACC for 2 weeks, DEG: differentially expressed genes, PA: parental cell line, SP: spheroid cells derived from PA

Up-regulated Genes in A-SP Cell Line Dataset vs. SP Cell Line Dataset				
Score	**Pathway Name**	**Total Genes**	**Matched Genes**	**Matched Genes (Symbols)**
38.26	ERK Signaling	1178	64	COL11A1, COL12A1, COL1A1, ACTG2, SMAD9, NOTCH3, LIMS2, CTGF, PLCB4, CXCL2, CXCL3, CXCL8, NRP1, NTF4, DCHS1, AREG, PPP1R15A, PPP2R2C, PRKCG, SOX18, ATF3, AXL, PTGS2, HGF, DUSP1, STAT4, BMPR1B, PAK3, PDGFRB, TCF4, TGFB2, CACNA1G, CACNG6, CACNG8, CACNG5, CACNA1H, IL18R1, IL1R1, TNFAIP6, CCL2, TNFSF10, TNF, IL6, CCL5, FBN1, CCL20, IRS4, ITGB2, ITGA1, ITGB4, ITGB6, CDH22, CDH23, FGF5, CDH6, FGFR2, JUNB, JUN, FLNC, FN1, FOSB, FOS, MYH14, KLF10
35.68	Toll-like Receptor Signaling Pathway	322	30	GABARAPL1, ACE, GBP3, GBP2, GBP1, NLRP1, LBP, PLCB4, CXCL2, CXCL3, CXCL8, PPP2R2C, P2RX7, C3, TGFB2, TLR1, TLR5, TLR6, TLR3, CASP4, CASP1, CCL2, TNF, IL6, CCL5, JUNB, JUN, FOSB, FOS, SERPINE1
27.24	Akt Signaling	681	40	GABRB3, ACTG2, CTGF, PLCB4, CXCL2, CXCL3, CXCL8, NTF4, AREG, PPP2R2C, PRKCG, AXL, HGF, STAT4, BMPR1B, PAK3, PDGFRB, TGFB2, TLR1, TLR5, TLR6, TLR3, IL18R1, IL1R1, TNFAIP6, CCL2, TNFSF10, TNF, IL6, CCL5, CCL20, ITGB2, ITGA1, ITGB4, ITGB6, FGF5, FGFR2, JUNB, FOS, KLF10
25.58	PAK Pathway	682	39	ACTG2, SLC2A3, NOTCH3, CTGF, PLCB4, CXCL2, CXCL3, CXCL8, NRP1, NTF4, AREG, PRKCG, PTPRB, PTPRD, PTPRO, HGF, BMPR1B, PAK3, PDGFRB, TCF4, TGFB2, CASP4, CASP1, IL18R1, IL1R1, TNFAIP6, CCL2, TNFSF10, TNF, IL6, CCL5, CCL20, FGF5, FGFR2, JUN, FLNC, FOS, MYH14, KLF10
23.25	TNF Signaling Pathway	108	14	CXCL2, CXCL3, VCAM1, SOCS3, PTGS2, IL18R1, CCL2, TNF, IL6, CCL5, CCL20, JUNB, JUN, FOS
22.94	Degradation of The Extracellular Matrix	298	23	COL11A1, COL12A1, COL1A1, COL26A1, LOX, LOXL4, ADAMTS8, CTSS, MATN3, NTN4, VCAM1, BGN, ELANE, TGFB2, THBS1, MMP7, FBN1, ITGB2, ITGA1, ITGB4, ITGB6, FN1, SERPINE1
22.40	Integrin Pathway	568	33	COL11A1, COL12A1, COL1A1, ACTG2, PLCB4, CXCL2, CXCL3, CXCL8, VCAM1, PRKCG, STAT4, PAK3, TGFB2, THBS1, MMP7, CACNA1G, CACNG6, CACNG8, CACNG5, CACNA1H, CCL2, CCL5, FBN1, CCL20, ITGB2, ITGA1, ITGB4, ITGB6, JUN, FN1, FOS, SERPINE1, MYH14
21.10	MAPK Signaling Pathway	321	23	GADD45B, NR4A1, NTF4, AREG, PRKCG, HGF, DUSP1, PDGFRB, EREG, TGFB2, CACNA1G, CACNG6, CACNG8, CACNG5, CACNA1H, CASP1, IL1R1, TNF, FGF5, FGFR2, JUN, FLNC, FOS
20.20	Cytokine Signaling in Immune System	760	38	TRIM22, GBP3, GBP2, GBP1, LBP, CXCL2, CXCL8, GFRA1, OASL, VCAM1, SOCS3, PRTN3, XAF1, PTGS2, HGF, DUSP1, EGR1, PDGFRB, EREG, IFITM2, IFITM1, CASP1, IL18R1, IL1R1, CCL2, IL34, TNF, IL6, CCL5, SAA1, CCL20, IRF1, ITGB2, FGF5, FGFR2, JUNB, FN1, FOS
19.55	TGF-Beta Pathway	652	34	SMAD9, UBD, CTGF, CXCL8, NTF4, AREG, PPP2R2C, SOCS3, AXL, HGF, DUSP1, STAT4, PAK3, PDGFRB, TCF4, TGFB2, IL18R1, IL1R1, CCL2, TNFSF10, TNF, IL6, CCL5, CCL20, IRS4, ITGB2, ITGA1, ITGB4, ITGB6, FGF5, FGFR2, JUN, FOS, KLF10
18.81	NF-kappaB Signaling	327	22	NFKBIZ, NLRP1, UBD, NR4A1, VCAM1, VSIR, SOCS3, PTGS2, STAT4, EGR1, RIPK4, ID3, TLR1, TLR6, TLR3, CARD11, CCL2, TNF, CCL5, IRF1, ITGB2, JUNB
18.21	PEDF (SERPINF1) Induced Signaling	743	36	UBD, PLCB4, CXCL2, CXCL3, CXCL8, ARC, PPP1R15A, PPP2R2C, PRKCG, SOCS3, AXL, PTGS2, HGF, BMPR1B, PDGFRB, TGFB2, CACNA1G, CACNG6, CACNG8, CACNG5, CACNA1H, CASP4, CASP1, IL18R1, IL1R1, TNFAIP6, CCL2, TNFSF10, IL34, TNF, IL6, CCL5, CCL20, FGFR2, JUN, FOS
17.82	Innate Immune System	2129	75	KLRD1, KLRK1, TRIM22, GBP3, GBP2, GBP1, LRG1, SLC2A3, NLRP1, LBP, CRISPLD2, CTSS, NR4A1, CXCL2, CXCL8, GFRA1, OASL, VCAM1, DEFB1, PRKCG, SOCS3, PRTN3, XAF1, PTGS2, DTX4, PTPRB, HGF, DUSP1, P2RX7, PAK3, EGR1, ELANE, HPSE, PDGFRB, C1R, C1S, EREG, C3, C4BPA, C4B, IER3, IFITM2, IFITM1, TLR1, TLR5, TLR6, TLR3, MRC2, CARD11, CASP4, CASP1, IL18R1, IL1R1, TNFAIP6, CCL2, IL34, TNF, IL6, CCL5, SAA1, CCL20, FCGR2A, IRF1, ITGB2, FGF5, FGFR2, JUNB, JUN, FN1, FOS, CFB, CFH, CFHR3, CFI, MYLIP
17.76	Immune Response IFN Alpha/beta Signaling Pathway	91	11	GBP2, CXCL8, OASL, SOCS3, XAF1, EGR1, IFITM2, IFITM1, TNF, IL6, IRF1
15.13	Adipogenesis	132	12	GADD45B, SOCS3, PTGIS, EGR2, ID3, TNF, IL6, IRS4, SERPINE1, SFRP4, KLF6, KLF7
14.88	P70S6K Signaling	391	22	ACE, CTGF, NRP1, NTF4, VCAM1, AREG, PPP1R15A, PPP2R2C, PRKCG, AXL, PTGS2, HGF, PAK3, PDGFRB, TGFB2, CCL2, IL6, FGF5, FGFR2, JUN, FOS, KLF10
14.70	Wnt / Hedgehog / Notch	182	14	NKX2-5, SMAD9, NOTCH3, CTGF, DKK1, AXIN2, HES1, RIPK4, ID3, TGFB2, TGFBI, TLE4, RUNX3, SERPINE1
13.99	Phospholipase-C Pathway	498	25	COL11A1, COL12A1, COL1A1, ACTG2, CTGF, PLCB4, NRP1, NTF4, AREG, PRKCG, HGF, PDGFRB, TGFB2, TGM2, IL6, FBN1, FCGR2A, ITGB2, ITGA1, ITGB4, ITGB6, FGF5, FGFR2, FN1, KLF10
13.84	Apoptotic Pathways in Synovial Fibroblasts	725	32	ACTG2, CTGF, NRP1, NTF4, AREG, PPP1R15A, PPP2R2C, PRKCG, HGF, BCL2A1, PAK3, PDGFRB, TGFB2, CACNA1G, CACNG6, CACNG8, CACNG5, CACNA1H, CASP4, CASP1, TNFSF10, TNF, IL6, ITGB2, ITGA1, ITGB4, ITGB6, FGF5, FGFR2, JUN, FOS, KLF10
13.37	PI3K-Akt Signaling Pathway	512	25	COL1A1, NOTCH3, NR4A1, NTF4, OASL, AREG, PPP2R2C, PTGER4, AXIN2, PTGS2, HES1, HGF, PDGFRB, EREG, THBS1, TLR3, TNF, IL6, IRF1, ITGA1, ITGB4, ITGB6, FGF5, FGFR2, FN1
13.36	Senescence and Autophagy in Cancer	106	10	GABARAPL1, COL1A1, MAP1LC3A, CXCL8, THBS1, IL6, IRF1, JUN, FN1, SERPINE1
13.04	Hippo Signaling Pathway	154	12	FRMD6, CRB1, SMAD7, CTGF, AREG, PPP2R2C, AXIN2, BMPR1B, ID1, TGFB2, ITGB2, SERPINE1
12.95	Angiogenesis (CST)	89	9	NOTCH3, PTGS2, HGF, PDGFRB, TGFB2, THBS1, MMP7, CCL2, FGFR2
12.71	BMP Pathway	158	12	NKX2-5, SMAD9, BMPR1B, CACNA1G, CACNG6, CACNG8, CACNG5, CACNA1H, CASP1, TNF, JUN, FOS
12.49	Nanog in Mammalian ESC Pluripotency	533	25	ACTG2, CTGF, PLCB4, NTF4, DCHS1, AQP9, AREG, PPP2R2C, PRKCG, AXL, HGF, PDGFRB, TGFB2, TNF, IL6, S1PR3, CDH22, CDH23, FGF5, CDH6, FGFR2, JUN, FOS, FRAT1, KLF10
12.26	S-1P Stimulated Signaling	95	9	PLCB4, DCHS1, PDGFRB, CASP4, CASP1, S1PR3, CDH22, CDH23, CDH6
12.09	GPCR Pathway	708	30	ACTG2, CTGF, PLCB4, NRP1, NTF4, AREG, PPP1R15A, PPP2R2C, PRKCG, AXL, PTGS2, HGF, STAT4, P2RY6, PAK3, RCAN3, PDGFRB, TGFB2, MMP7, IL6, FCGR2A, ITGB2, ITGA1, ITGB4, ITGB6, FGF5, FGFR2, JUN, FOS, KLF10
11.66	Adhesion	123	10	COL1A1, CTGF, CYR61, VCAM1, TGFBI, TNS2, ITGB2, ITGB4, CDH6, SERPINE1
10.88	Direct P53 Effectors	132	10	DKK1, ATF3, HGF, DUSP1, BCL2A1, EDN2, BTG2, CASP1, JUN, SERPINE1
10.56	ECM-receptor Interaction	112	9	COL1A1, VCAM1, THBS1, FBN1, ITGB2, ITGA1, ITGB4, ITGB6, FN1
10.56	Beta-Catenin-dependent Wnt Signaling	112	9	GADD45B, NOTUM, GLI3, DKK1, AXIN2, HHIP, TLE4, RSPO3, SFRP4
10.30	Wnt Signaling Pathway and Pluripotency	191	12	NOTUM, PLCB4, PORCN, PPP2R2C, PRKCG, DKK1, AXIN2, BAMBI, MMP7, JUN, FRAT1, SFRP4
10.08	Presenilin-Mediated Signaling	142	10	NOTCH3, UBD, CACNA1G, CACNG6, CACNG8, CACNG5, CACNA1H, CASP4, CASP1, CDH6

Table 4.12.5: Pathways Up-regulated in A-SP Cell Line Dataset Comparisons

Relevant pathways detected for datasets from DEG up-regulated in A-SP cell line dataset compared to SP cell line dataset. Score in Column 1 represents (-log2) transformed p-values.
ACC: adherent culture conditions, A-SP: SP cells grown under ACC for 2 weeks, DEG: differentially expressed genes, PA: parental cell line, SP: spheroid cells derived from PA

Up-regulated Genes in PA and A-SP Cell Line Dataset vs. SP Cell Line Dataset				
Score	**Pathway Name**	**Total Genes**	**Matched Genes**	**Matched Genes (Symbols)**
8.83	Innate Immune System	2129	30	KLRD1, KLRK1, TRIM22, GBP3, GBP2, GBP1, LRG1, LBP, CRISPLD2, OASL, DEFB1, SOCS3, XAF1, DTX4, P2RX7, PDGFRB, C1S, IFITM2, IFITM1, TLR1, TLR5, TLR6, MRC2, CARD11, CASP4, CASP1, TNFAIP6, CCL5, FGFR2, CFHR3
20.86	Toll-like Receptor Signaling Pathway	322	14	GABARAPL1, ACE, GBP3, GBP2, GBP1, LBP, P2RX7, TLR1, TLR5, TLR6, CASP4, CASP1, CCL5, SERPINE1
7.94	Cytokine Signaling in Immune System	760	14	TRIM22, GBP3, GBP2, GBP1, LBP, OASL, SOCS3, XAF1, PDGFRB, IFITM2, IFITM1, CASP1, CCL5, FGFR2
14.30	Interferon Gamma Signaling	202	9	TRIM22, GBP3, GBP2, GBP1, OASL, SOCS3, XAF1, IFITM2, IFITM1
12.45	TRAF Pathway	188	8	LBP, UBD, TLR1, TLR5, TLR6, CASP4, CASP1, TNFSF10
10.11	NF-KappaB Family Pathway	241	8	UBD, CTGF, NTF4, TLR1, TLR5, TLR6, CARD11, FGFR2
15.97	S-1P Stimulated Signaling	95	7	DCHS1, PDGFRB, CASP4, CASP1, S1PR3, CDH23, CDH6
12.38	Presenilin-Mediated Signaling	142	7	UBD, CACNA1G, CACNG8, CACNA1H, CASP4, CASP1, CDH6
10.26	Calcium Signaling Pathway	182	7	ADRB2, ATP2A3, P2RX7, P2RX6, PDGFRB, CACNA1G, CACNA1H
13.07	Immune Response IFN Alpha/beta Signaling Pathway	91	6	GBP2, OASL, SOCS3, XAF1, IFITM2, IFITM1
7.90	Apoptosis and Autophagy	183	6	XAF1, BCL2A1, TFAP2A, CASP4, CASP1, TNFSF10
8.42	P53 Signaling	117	5	UBD, THBS1, CASP4, CASP1, TNFSF10

Up-regulated Genes in SP Cell and A-SP Line Dataset vs. PA Cell Line Dataset				
Score	**Pathway Name**	**Total Genes**	**Matched Genes**	**Matched Genes (Symbols)**
20.45	ESC and iPSC Dif Pathways and Lin.-spec. Markers	133	14	LRIG1, NEUROD1, NOG, ALB, CXCR4, GJA1, SOX7, WNT5A, BMP4, IL11, SERPINA1, KLF4, KLF2, SHH
13.13	ERK Signaling	1178	43	COL23A1, ACVRL1, ADCY5, LAMA1, LTBP1, TUBA8, CSF2, PLCB1, MAPK8IP2, PLPP3, CXCL14, CXCL1, PMAIP1, CXCR4, GPC6, ARHGEF6, PRG2, PRKAA2, SOX7, DIRAS3, WNT5A, SPOCK1, BMP2, BMP4, BMP6, RASGRP2, HNF4A, PDGFRA, RHOD, EPHA7, EPHA3, ERBB4, ERBB3, CACNA1A, CACNA2D4, IL11, TNFRSF13C, IL3RA, CCR6, INSR, ITGB7, MYH13, FRAS1
12.90	Akt Signaling	681	29	GABRD, ACVRL1, LTBP1, CSF2, TXK, PLCB1, MAPK8IP2, PLPP3, CXCL14, CXCL1, CXCR4, GPC6, DIRAS3, BMP2, BMP4, BMP6, PDGFRA, RHOD, EPHA7, EPHA3, ERBB4, ERBB3, ETV1, IL11, TNFRSF13C, IL3RA, CCR6, INSR, ITGB7
12.14	NSC Diff. Pathways and Lin-spec. Markers	79	8	GAD1, NEUROD1, CXCR4, BMP2, BMP4, PDGFRA, FABP7, SHH
11.44	NSC Diff. Pathways and Lin-spec. Markers	182	12	ADORA2A, SLC8A1, PLCB1, AVPR1B, BDKRB1, BDKRB2, PDGFRA, ERBB4, ERBB3, CACNA1A, ITPKB, ITPR1
11.37	HIF-1-alpha Transcription Factor Network	65	7	NDRG1, ADM, CXCR4, HNF4A, EGLN3, TF, IGFBP1
11.10	Differentiation Pathway	48	6	NOG, WNT5A, BMP4, TF, IL11, SHH
9.83	CREB Pathway	528	22	NFATC1, ADCY5, LTBP1, SLC8A1, PLCB1, PLPP3, GPC6, ARHGEF6, DIRAS3, BMP2, BMP4, BMP6, PDGFRA, RHOD, EPHA7, EPHA3, ERBB4, ERBB3, CACNA1A, CACNA2D4, INSR, ITPR1
9.66	Nanog in Mammalian ESC Pluripotency	533	22	ADCY5, LTBP1, TUBA8, PLCB1, PLPP3, AQP4, GPC6, PRKAA2, WNT5A, BDKRB1, BDKRB2, BMP2, BMP4, BMP6, PDGFRA, PDK4, EPHA7, EPHA3, ERBB4, ERBB3, INSR, ITPR1
9.64	Wnt / Hedgehog / Notch	182	11	TRIB2, NDRG1, NKD2, ALPL, WNT5A, DLL1, BMP4, BMP6, PAX5, KLF4, SHH
9.46	PAK Pathway	682	26	ACVRL1, SLC2A5, LTBP1, TUBA8, CSF2, PLCB1, PLPP3, CXCL14, CXCL1, CXCR4, GPC6, SORBS1, DIRAS3, DLL1, PTPRN, BMP2, BMP4, BMP6, HNF4A, PDGFRA, RHOD, IL11, TNFRSF13C, IL3RA, CCR6, MYH13

Table 4.12.6: Pathways Up-regulated in Spheroid-Derived and ACC-Cultured Cell Line Datasets

Upper part: relevant pathways detected for datasets from DEG up-regulated in PA and A-SP cell line datasets compared to SP cell line dataset. Lower part: Relevant pathways detected for datasets from DEG up-regulated in SP and A-SP cell line datasets compared to PA cell line dataset. Score in Column 1 represents (-log2) transformed p-values. ACC: adherent culture conditions, A-SP: SP cells grown under ACC for 2 weeks, DEG: differentially expressed genes, PA: parental cell line, SP: spheroid cells derived from PA

Up-regulated Genes in SP Cell Line Dataset vs. PA Cell Line Dataset				
Score	**Biological Process**	**Total Genes**	**Matched Genes**	**Matched Genes (Symbols)**
20.31	Glucose Homeostasis	107	12	CNR1, ACSM2A, VGF, PRKAA2, SSTR5, HNF4A, RBP4, TFAP2B, MLXIPL, CACNA1A, FFAR1, KCNB1
16.61	Regulation of Signaling Receptor Activity	452	23	ADA2, NOV, CXCL14, CXCL6, CXCL8, NRG3, VGF, WNT5A, SST, STC1, STC2, BMP2, BMP4, BMP6, PCSK9, ERFE, TG, THPO, TNFRSF11B, CCL15, INSL3, SECTM1, SHH
15.65	Negative Regulation of Cell Proliferation	435	22	NDRG1, ADM, CXCL1, CXCL8, GJA1, VDR, ROR2, DLL1, SPRY2, ZBTB7C, SST, SSTR5, P3H3, HNF4A, BTG1, RERG, IGFBP3, FABP7, CDKN1A, CDKN3, CGREF1, KLF4
14.59	Positive Regulation of Bone Mineralization	34	6	SLC8A1, OSR2, BMP2, BMP4, BMP6, FAM20C
13.28	Cell Differentiation	1020	36	NDRG2, NFATC4, NOG, LGALS3, ANKS4B, ANPEP, DDR2, ONECUT2, ARX, WNT5A, DLL1, SPDEF, OSR2, BMP2, BMP4, BMP6, PAQR5, RARRES2, PAX5, EHF, PDGFRA, TENM4, EPHB1, EPHB3, EPHA3, ERBB4, ETV1, ETV4, TLL1, CATSPERG, ILDR2, SCUBE2, FOXF2, FOXQ1, SH2D2A, MYO7B
12.82	Response to Oxidative Stress	128	10	APOE, PRDX2, GPX3, SOD3, PTGS1, STC2, BTG1, PDLIM1, MMP14, NAPRT
11.77	Neurogenesis	69	7	WNT5A, SPOCK1, BCL11B, PCSK9, EPHB1, PHGDH, FABP7
11.34	Positive Regulation of Cytosolic Ca Ion Concentration	147	10	ADCY5, SLC8A1, CXCR4, GJA1, AVPR1B, BDKRB1, BDKRB2, PDGFRA, CACNA1A, CALCR
10.91	Positive Regulation of ERK1 and ERK2 Cascade	242	13	ACKR3, NECAB2, DDR2, BMP2, BMP4, PDGFRA, EPHB1, EPHB3, EPHA3, ERBB4, THPO, CALCR, CCL15
10.66	Cellular Oxidant Detoxification	78	7	APOE, APOM, MGST1, PRDX2, GPX3, SOD3, PTGS1

Up-regulated Genes in SP Cell Line Dataset vs. A-SP Cell Line Dataset				
Score	**Biological Process**	**Total Genes**	**Matched Genes**	**Matched Genes (Symbols)**
17.33	Lipid Metabolic Process	532	20	ACAT2, SLC27A2, LSS, NPC1L1, PLB1, PLCG2, PLCH2, PNPLA3, APOE, DHCR7, HMGCS1, HMGCS2, PCSK9, HSD17B7, MOGAT3, MOGAT1, FADS2, MSMO1, INSIG1, FDFT1
12.08	Cellular Calcium Ion Homeostasis	102	7	TRPM8, APOE, ATP13A4, STC1, SYPL2, RGN, CCL15
10.70	Insulin Secretion	32	4	CPLX1, PDX1, ILDR2, FFAR1
10.38	Regulation of Cholesterol Biosynthetic Process	34	4	LSS, DHCR7, HMGCS1, FDFT1

Table 4.12.7: Enriched Biological Processes in SP Cell Line Dataset Comparisons

Upper part: relevant biological processes detected for datasets from DEG up-regulated in SP cell line dataset compared to PA cell line dataset. Lower part: Relevant biological processes detected for datasets from DEG up-regulated in SP cell line dataset compared to A-SP cell line dataset. Score in Column 1 represents (-log2) transformed p-values. ACC: adherent culture conditions, A-SP: SP cells grown under ACC for 2 weeks, DEG: differentially expressed genes, PA: parental cell line, SP: spheroid cells derived from PA

Up-regulated Genes in PA Cell Line Dataset vs. SP Cell Line Dataset				
Score	**Biological Process**	**Total Genes**	**Matched Genes**	**Matched Genes (Symbols)**
45.57	Cell Adhesion	625	44	COL5A1, ADGRG1, L1CAM, CTGF, NPNT, CYR61, APBA1, DSC3, STYK1, PCDH20, PCDHA10, PCDHA1, PCDHA11, PCDHA12, PCDHA13, PCDHA2, PCDHA3, PCDHA4, PCDHA5, PCDHA6, PCDHA7, PCDHA8, PCDHA9, PCDHAC1, PCDHAC2, PCDHB12, PCDHB2, PCDHB4, PCDHB6, PCDHB8, PCDHB5, BVES, PDZD2, THBS1, MSLN, S1PR1, ITGB6, CDH18, CDHR1, CDH6, JAM3, SDK2, FN1, FREM1
29.28	Extracellular Matrix Organization	204	20	ABI3BP, COL5A1, COL9A1, CRISPLD2, NPNT, MATN3, CYR61, VWA1, BGN, PDGFB, THBS1, MMP9, CCDC80, FBN1, ITGB6, FGB, JAM3, FGG, FN1, SERPINE1
19.25	Cell-matrix Adhesion	95	11	L1CAM, CTGF, NPNT, MSLN, TNN, ITGB6, FGB, JAM3, FGG, FN1, FREM1
14.94	Kidney Development	108	10	ACE, LRP4, LHX1, GLI3, GLI2, WT1, TFAP2A, TGFB2, TNS2, FBN1
13.15	Metanephric S-shaped Body Morphogenesis	5	3	LHX1, WT1, PDGFRB
13.08	Extracellular Matrix Disassembly	80	8	LCP1, CTSS, MMP16, MMP7, MMP9, TLL2, FBN1, FN1
12.42	Toll-like Receptor Signaling Pathway	45	6	LBP, CTSS, TLR2, TLR6, FGB, FGG
11.55	IFN-gamma-mediated Signaling Pathway	71	7	TRIM22, GBP2, GBP1, OAS2, OASL, HLA-DPA1, IRF6
11.46	Cell Migration	233	13	COL5A1, ADGRG1, L1CAM, LCP1, CTGF, PTK6, BAMBI, STYK1, PDGFRB, TGFB2, THBS1, S1PR1, JAM3
11.17	Metanephric Mesenchyme Development	8	3	WT1, BASP1, PDGFRB

Up-regulated Genes in PA Cell Line Dataset vs. A-SP Cell Line Dataset				
Score	**Biological Process**	**Total Genes**	**Matched Genes**	**Matched Genes (Symbols)**
35.03	Calcium Ion Binding	707	40	CLGN, NCALD, LRP4, ADGRE2, LCP1, SLIT2, SLIT3, PLA2G4A, PLCB4, MCTP2, PROC, GSN, DSC3, SYT13, PCDHA1, PCDHA12, PCDHA13, PCDHA2, PCDHA3, PCDHA4, PCDHA7, PCDHA8, PCDHA9, PCDHAC2, PCDHB2, PCDHB6, PCDHB8, PCDHB5, ENPP2, RGN, TESC, THBS2, TLL2, F10, CAPSL, FAT2, CDH15, CDHR1, CDH4, MYL9
24.93	Transferase Activity, Transferring Glycosyl Groups	237	19	FUT9, GBGT1, UGT1A7, UGT1A3, UGT1A4, UGT1A1, UGT1A8, UGT1A6, UGT1A10, UGT1A5, UGT1A9, UGT2B4, UGT3A1, UGT3A2, B3GNT7, PYGB, ST6GALNAC2, ST8SIA4, QPRT
30.50	Retinoic Acid Binding	25	9	UGT1A7, UGT1A3, UGT1A4, UGT1A1, UGT1A8, UGT1A6, UGT1A10, UGT1A9, UGT2B4
11.90	Steroid Binding	33	5	AKR1C2, AKR1C1, AKR1D1, UGT1A1, UGT1A8

Table 4.12.8: Enriched Biological Processes in PA Cell Line Dataset Comparisons

Upper part: relevant biological processes detected for datasets from DEG up-regulated in PA cell line dataset compared to SP cell line dataset. Lower part: Relevant biological processes detected for datasets from DEG up-regulated in PA cell line dataset compared to A-SP cell line dataset. Score in Column 1 represents (-log2) transformed p-values. ACC: adherent culture conditions, A-SP: SP cells grown under ACC for 2 weeks, DEG: differentially expressed genes, PA: parental cell line, SP: spheroid cells derived from PA

Up-regulated Genes in PA and A-SP Cell Line Dataset vs. SP Cell Line Dataset				
Score	**Biological Process**	**Total Genes**	**Matched Genes**	**Matched Genes (Symbols)**
12.33	Innate Immune Response	551	14	KLRD1, KLRK1, LBP, OASL, DEFB1, STYK1, SUSD4, C1S, IFITM2, IFITM1, TLR1, TLR5, TLR6, CASP4
12.69	Inflammatory Response	408	12	AFAP1L2, APOL3, P2RX7, THBS1, TLR1, TLR5, TLR6, CASP4, TNFAIP6, CCL5, S1PR3, ITGB6
14.82	Calcium Ion Transport	148	8	ATP2A3, P2RX7, CACNA1G, CACNG8, CACNA1H, CCL5, CDH23, NALCN
13.50	Positive Reg of I-kBKin/NF-kB Signaling	169	8	TRIM22, UBD, PLK2, APOL3, TLR6, CARD11, CASP1, TNFSF10
11.67	Extracellular Matrix Organization	204	8	CRISPLD2, NPNT, MATN3, BGN, THBS1, FBN1, ITGB6, SERPINE1
11.75	Kidney Development	108	6	ACE, GLI3, DCHS1, TFAP2A, TNS2, FBN1
10.36	Cellular Response to Tumor Necrosis Factor	130	6	GBP3, GBP2, GBP1, NPNT, THBS1, CCL5
12.93	Positive Regulation of Smooth Muscle Cell Proliferation	58	5	PDGFRB, THBS1, CCL5, FGFR2, SERPINF2
16.18	Positive Regulation of Calcium Ion-dependent Exocytosis	17	4	DOC2B, SYT1, CACNA1G, CACNA1H
13.61	Positive Regulation of Interleukin-8 Production	27	4	AFAP1L2, LBP, TLR5, SERPINE1

Up-regulated Genes in SP Cell and A-SP Line Dataset vs. PA Cell Line Dataset				
Score	**Biological Process**	**Total Genes**	**Matched Genes**	**Matched Genes (Symbols)**
18.73	Glucose Homeostasis	107	12	CNR1, NEUROD1, VGF, PRKAA2, BHLHA15, HNF4A, PDK4, TFAP2B, MLXIPL, IGFBP5, CACNA1A, INSR
18.45	Skeletal System Development	150	14	AEBP1, NOG, PITX1, ALPL, VDR, PTHLH, EBP, BMP2, BMP4, BMP6, HOXC11, TLL1, FAM20C, TNFRSF11B
15.74	AC-activating GPCR Signaling Pathway	72	9	ADGRF1, ADCY5, ADM, ADORA2A, GPR3, GPR78, PTHLH, RAMP2, CALCR
14.49	Cell Differentiation	1020	40	NDRG2, LRMDA, NEUROD1, NOG, TXK, MECOM, DCLK1, VDR, PRAME, ARX, WIPF3, WNT5A, DLL1, SPDEF, SSPO, OSR2, BMP2, BMP4, BMP6, PAQR5, RARRES2, EFNB3, PAX5, PDGFRA, TENM4, EPHA7, EPHA3, ERBB4, ERBB3, ETV1, ETV4, TLL1, CCDC136, INSR, SEMA6B, FOXA3, FOXF2, FOXQ1, SH2D2A, KLF4
13.75	Positive Regulation of Bone Mineralization	34	6	SLC8A1, OSR2, BMP2, BMP4, BMP6, FAM20C
13.45	Cell Migration	233	15	GPC6, VTN, WNT5A, BDKRB1, STRIP2, BTG1, PDGFRA, EMP2, RHOD, RHOU, EPHA3, ERBB4, MMP14, CASS4, SBK2
11.66	Osteoblast Differentiation	105	9	LRRC17, NOG, ALPL, GJA1, BMP2, BMP4, BMP6, IGFBP5, IGFBP3
11.37	Kidney Development	108	9	AGT, POU3F3, BMP4, BMP6, PCSK5, TFAP2B, MME, SALL1, SHH

Table 4.12.9: Enriched Biological Processes in Sphere-Derived and ACC-Cultured Cell Line Datasets

Upper part: relevant biological processes detected for datasets from DEG up-regulated in PA and A-SP cell line datasets compared to SP cell line dataset. Lower part: Relevant biological processes detected for datasets from DEG up-regulated in SP and A-SP cell line datasets compared to PA cell line dataset. Score in Column 1 represents (-log2) transformed p-values. ACC: adherent culture conditions, A-SP: SP cells grown under ACC for 2 weeks, DEG: differentially expressed genes, PA: parental cell line, SP: spheroid cells derived from PA

Up-regulated Genes in A-SP Cell Line Dataset vs. PA Cell Line Dataset				
Score	**Biological Process**	**Total Genes**	**Matched Genes**	**Matched Genes (Symbols)**
39.96	Skeletal System Development	150	22	COL12A1, COL1A1, COL9A2, AEBP1, NOG, PITX1, ALPL, PTHLH, EBP, BMP2, BMP6, RASSF2, HOXC11, HOXD10, PHEX, TGFB2, ETS2, TLL1, FAM20C, TNFRSF11B, RUNX2, KLF10
22.18	Cytokine-mediated Signaling Pathway	321	23	LRRTM4, CSF2, ALOX5, CXCL1, CXCL2, CXCL8, MCL1, VCAM1, HGF, BCL6, EDN2, RHOU, CCL2, RTN4RL1, RTN4RL2, TNF, CCND1, IL6, SAA1, ITGB2, CDKN1A, JUNB, FOS
21.36	Positive Regulation of Osteoblast Differentiation	58	10	CTHRC1, GJA1, CYR61, HGF, BMP2, BMP6, ID4, FAM20C, IL6, RUNX2
21.30	Nervous System Development	555	31	NDRG2, LRP2, NLGN1, CSGALNACT1, NOG, NR2F1, NR4A2, CXCL1, NRP2, GFRA1, POU3F3, GLRB, VLDLR, ATOH8, SPOCK1, DOC2A, DSCAML1, ZC3H12A, HES1, BARX2, EFNB3, PCDH1, EPHA7, CAMK1, CAMK1D, FABP7, FGF5, SEMA5B, SEMA6B, FOS, KIAA0319
20.40	Skeletal Muscle Cell Differentiation	48	9	MAFF, ANKRD1, NUPR1, ATF3, HLF, EGR1, EGR2, BTG2, FOS
19.76	Extracellular Matrix Organization	204	17	COL1A1, LOX, COL9A2, NID2, LAMB3, LAMA1, CSGALNACT1, CYR61, VCAM1, VTN, PDGFRA, ICAM5, TGFBI, TNFRSF11B, TNF, ITGB2, ITGB7
18.85	Response to Hypoxia	168	15	ACVRL1, ADM, CRYAB, NR4A2, CXCR4, VCAM1, BMP2, EGR1, EGLN3, PDLIM1, TGFB2, TGFB3, MMP14, ITPR1, KCNA5
16.72	Response to Glucocorticoid	66	9	ADM, ALPL, AREG, DUSP1, BMP6, TNF, CCND1, IL6, CDKN1A
16.43	Osteoblast Differentiation	105	11	COL1A1, NOG, ALPL, CYP24A1, GJA1, CYR61, BMP2, BMP6, IGFBP3, RUNX2, JUNB
13.65	Kidney Development	108	10	AGT, PKHD1, POU3F3, BMP6, PCSK5, TGFB2, MME, SALL1, CENPF, SHH
13.38	Inflammatory Response	408	21	NFKBIZ, ALOX5, CXCL1, CXCL2, CXCL3, CXCL8, CXCR4, PTGS1, ZC3H12A, BCL6, BMP2, BMP6, RARRES2, C3, CAMK1D, TNFRSF11B, CCL2, TNF, IL6, ITGB2, FOS
13.12	Positive Regulation of Cell Migration	211	14	COL1A1, CYR61, ONECUT2, GTSE1, WNT5B, SPRY2, PTP4A1, HGF, BMP2, PDGFRA, RHOD, MMP14, INSR, TRIP6
12.97	Response to Hydrogen Peroxide	54	7	COL1A1, CRYAB, AREG, PPP1R15B, DUSP1, JUN, KCNA5
12.82	Cellular Response to Hypoxia	116	10	NDRG1, CPEB2, PMAIP1, ANKRD1, GNGT1, PTGIS, HILPDA, STC1, STC2, KCNK2
12.20	Negative Regulation of Wnt Signaling Pathway	59	7	NKD2, NOTUM, RNF43, DKK1, CCND1, TRABD2B, SHH
12.06	SMAD Protein Signal Transduction	60	7	ATOH8, BMP2, BMP6, TGFB2, TGFB3, JUN, FOS
12.04	in Utero Embryonic Development	200	13	ACVRL1, MAFF, NOG, GJA1, HES1, BMP2, RARRES2, RDH10, PDGFRA, EMX1, TGFB3, JUNB, KLF2
Up-regulated Genes in A-SP Cell Line Dataset vs. SP Cell Line Dataset				
Score	**Biological Process**	**Total Genes**	**Matched Genes**	**Matched Genes (Symbols)**
38.06	Inflammatory Response	408	35	TSPAN2, NFKBIZ, AFAP1L2, NLRP14, NLRP1, CXCL2, CXCL3, CXCL8, APOL3, PTGER4, AXL, PTGS2, ZC3H12A, P2RX7, BMPR1B, C3, C4B, THBS1, TLR1, TLR5, TLR6, TLR3, CASP4, TNFAIP6, CCL2, IL34, TNF, IL6, CCL5, S1PR3, CCL20, ITGB2, ITGB6, SCN9A, FOS
30.87	Positive Regulation of Smooth Muscle Cell Proliferation	58	13	NOTCH3, PTGS2, ELANE, PDGFRB, EREG, TGM2, THBS1, TNF, IL6, CCL5, FGFR2, JUN, SERPINF2
27.06	Cytokine-mediated Signaling Pathway	321	26	LBP, CXCL2, CXCL8, PODNL1, VCAM1, SOCS3, PRTN3, PTGS2, HGF, STAT4, BGN, EDN2, EREG, CASP1, IL1R1, CCL2, IL34, TNF, IL6, CCL5, SAA1, CCL20, ITGB2, JUNB, FN1, FOS
23.31	Extracellular Matrix Organization	204	19	COL11A1, COL1A1, LOX, CRISPLD2, NPNT, MATN3, CYR61, VCAM1, BGN, TGFBI, THBS1, TNF, FBN1, ITGB2, ITGA1, ITGB4, ITGB6, FN1, SERPINE1
17.67	Cellular Response to Tumor Necrosis Factor	130	13	COL1A1, GBP3, GBP2, GBP1, NPNT, CXCL8, VCAM1, ZC3H12A, ZFP36, THBS1, CCL2, CCL5, CCL20
15.43	Positive Regulation of Apoptotic Process	353	21	GADD45B, UBD, ALDH1A2, CYR61, APBB1, PTGS2, DUSP1, BCL2A1, P2RX7, BMF, RASSF2, HPGD, PDGFRB, ID3, TGM2, TLR3, TNFSF10, TNF, IL6, JUN, SFRP4
15.04	Skeletal System Morphogenesis	41	7	COL11A1, COL1A1, CSRNP1, ALX4, HHIP, P2RX7, FGFR2
14.75	Positive Regulation of Osteoblast Differentiation	58	8	NPNT, CYR61, GLI3, HGF, BMPR1B, ID4, IFITM1, IL6
14.65	Cell-matrix Adhesion	95	10	CTGF, NPNT, VCAM1, BCAM, HPSE, ITGB2, ITGA1, ITGB4, ITGB6, FN1
13.48	Positive Regulation of Angiogenesis	149	12	LRG1, CXCL8, NRP1, PTGIS, ZC3H12A, HGF, RLN2, C3, THBS1, TLR3, ITGB2, SERPINE1
13.14	Kidney Development	108	10	ACE, ALDH1A2, GLI3, DCHS1, WT1, HPGD, TFAP2A, TGFB2, TNS2, FBN1
11.31	Brown Fat Cell Differentiation	29	5	LRG1, ADRB2, MB, PTGS2, RGS2

Table 4.12.10: Enriched Biological Processes in A-SP Cell Line Dataset Comparisons

Upper part: relevant biological processes detected for datasets from DEG up-regulated in A-SP cell line dataset compared to PA cell line dataset. Lower part: Relevant biological processes detected for datasets from DEG up-regulated in A-SP cell line dataset compared to SP cell line dataset. Score in Column 1 represents (-log2) transformed p-values. ACC: adherent culture conditions, A-SP: SP cells grown under ACC for 2 weeks, DEG: differentially expressed genes, PA: parental cell line, SP: spheroid cells derived from PA

4.12.3 mRNA Expression Levels of Markers Investigated by IFC

The data obtained by mRNA sequencing allow a comparison of mRNA expression levels of PA, SP and A-SP cell lines with the results obtained in IFC measurements. Additionally, results allow identification of differences in mRNA expression levels of other relevant markers between the investigated cell lines. When comparing those results, it is important to keep in mind that mRNA expression levels represent the mean of the different cell populations seen in IFC.

4.12.3.1 mRNA Expression Levels of TIC Markers Investigated by IFC

Results for mRNA expression levels of the TIC marker genes investigated by IFC are depicted in figure 4.12.10. The mRNA expression levels in different cell lines were generally in good correlation with the data obtained in IFC measurements for the respective antigens (see table 5.6.1), including the relative high variations in expression of ABCB1 and TNAP expression seen in SP cell line. TNAP mRNA expression in A-SP cell line was similar to that seen in SP cell line. TNAP expression was not

investigated by other methods in this cell line. For CD90 (THY1) in contrast to results obtained in IFC, where no staining for CD90 was detected, low mRNA expression was seen in all cell lines. Also, CXCR7 mRNA was expressed at similar levels to CXCR4 mRNA in spheroid-derived cell lines (SP and A-SP), whereas in IFC CXCR7 was detected at lower level than CXCR4 on SP cells. Neither for CXCR4 nor for CXCR7 a difference in mRNA expression level was seen between spheroids and spheroids cultured under ACC, which contrasts results obtained by IFC. The high variation seen for CD271 expression in A-SP cells was due to higher expression level of the gene seen in the A-SP-P54 (P75) sample, which might indicate an increase in expression over time in culture as spheroids, as was seen for other markers.

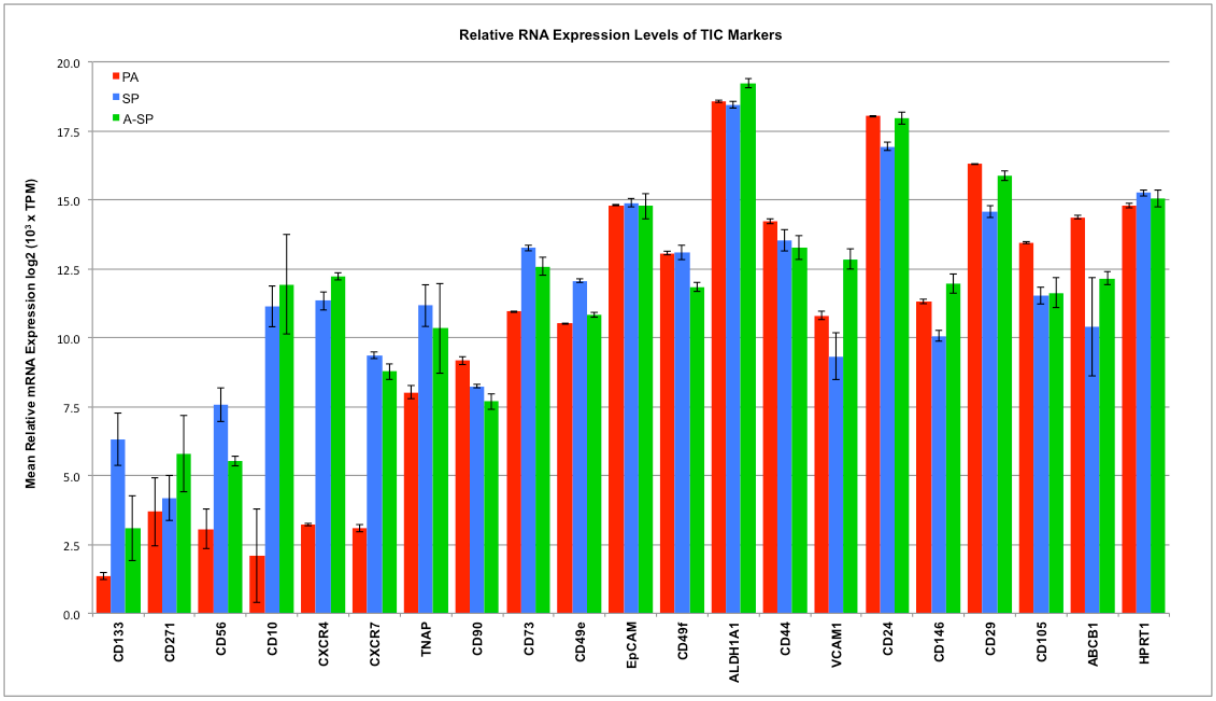

Figure 4.12.10: Relative mRNA Expression Levels of CSC Markers

Mean values of relative mRNA expression levels for different TIC markers obtained by RNA-Sequencing from three replicate samples of PA (P37), SP (P39/43) and A-SP (A-SP-P36/P54, P56, 57, 75) cell lines. Log2 transformed TPM values, which were multiplied by 10^3 to omit negative values, are indicated. Error bar: standard deviation. Expression level of the housekeeping gene HPRT1 is indicated for comparison.
ACC: adherent culture conditions, AS: adherently grown spheroids = A-SP: SP cells grown under ACC for 14 weeks, HPRT1: hypoxanthine phosphoribosyltransferase 1, P: passage number, PA: parental cell line, SP: spheroid cells derived from PA, TPM: transcripts per million

4.12.3.2 mRNA Expression Levels of EMT Markers

Results for mRNA expression levels of the mesenchyme specific EMC marker genes CDH2 (N-Cadherin), SNAI1, VIM, but also of the transcription factors TWIST1, SNAI2 (Slug), ZEB1 and ZEB2 for PA, SP and A-SP cell lines, as well as mRNA expression levels for epithelial marker antigens CDH1 and cytokeratin 8 and 19 (KRT8, KRT19) are shown in figure 4.12.11. Confirming the results obtained by IFC, similar high expression levels were seen for CDH1 and CDH2 and VIM in all cell lines investigated, as well as slightly lower expression levels of cytokeratin in SP and A-SP cell lines compared to PA cell line. mRNA expression levels for VIM, CDH1 and CDH2, ZEB1 and SNAI1 were slightly higher in A-SP cell line compared to PA and SP cell line, but also showed higher variations between replicate samples. Genes for transcription factors were expressed at lower levels than genes

coding for surface-expressed and intermediate filament proteins. Thereby the transcription factors TWIST1, ZEB2 and SNAI2 were expressed markedly lower levels than SNAI1 and ZEB1. Expression levels for ZEB1 were similar in PA and SP cell line. SNAI1, TWIST1 and ZEB2 mRNA expression was reduced in SP cell line compared to the cell lines grown under ACC, whereas SNAI2 expression levels were higher in PA cell line compared to spheroid-derived cell lines. TWIST1 expression, similar to CD271 expression, was markedly higher in the A-SP-P54 (P75) sample compared to the samples derived from spheroids in passage 36, which showed almost identical expression values of the gene.

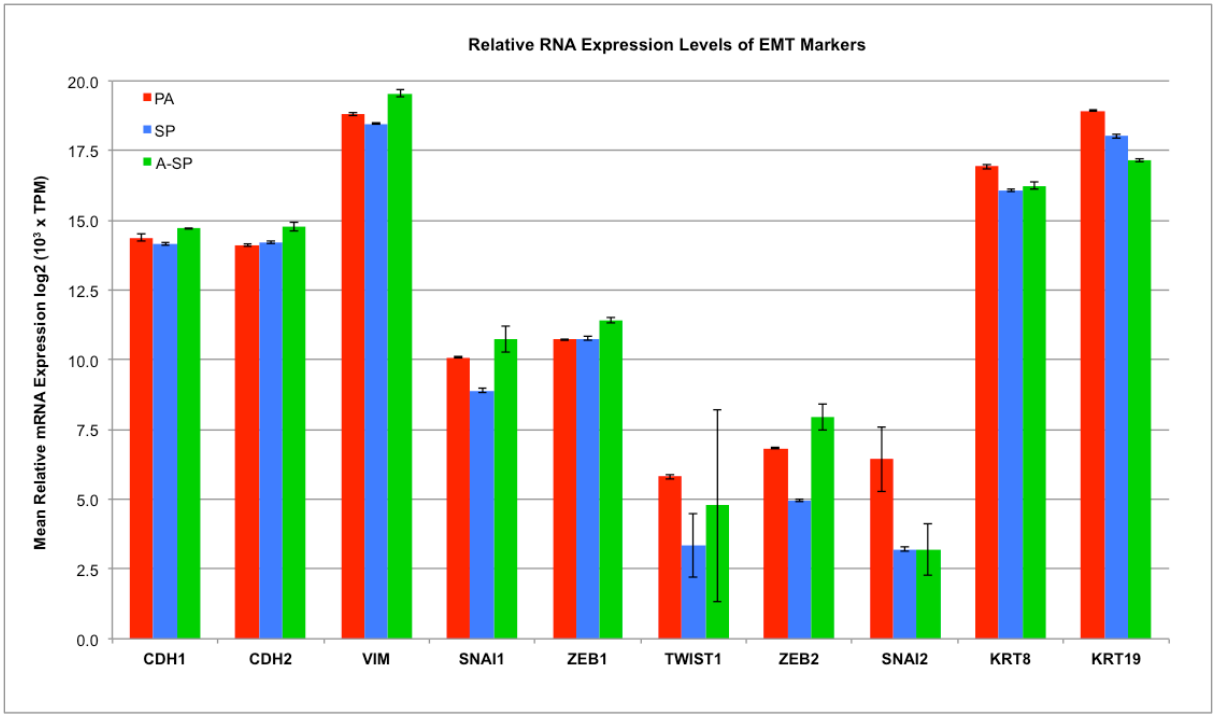

Figure 4.12.11: Relative mRNA Expression Levels of EMT Markers

Mean values of relative mRNA expression levels for different EMT markers obtained by RNA-Sequencing from three replicate samples of PA (P37), SP (P39/43) and A-SP (A-SP-P36/P54, P56, 57, 75) cell lines. Log2 transformed TPM values, which were multiplied by 10^3 to omit negative values, are indicated. Error bar: standard deviation.
ACC: adherent culture conditions, AS: adherently grown spheroids = A-SP: SP cells grown under ACC for 14 weeks, P: passage number, PA: parental cell line, SP: spheroid cells derived from PA, TPM: transcripts per million

4.12.3.3 mRNA Expression Levels of Pluripotency Markers Investigated by IFC

The expression levels of the transcription factors POU5F1/Oct4, SOX2, NANOG, KLF4 and MYC, which are involved in maintenance of pluripotency of stem cells, for the three cell lines used for RNA-Sequencing experiments are shown in figure 4.12.12. In contrast to results obtained by IFC, mRNA expression levels of Oct4 were found to be higher than SOX2 expression levels in all cell lines investigated. A slightly higher expression of Oct4 was observed in SP and A-SP cell lines compared to PA cell line, whereas expression levels of SOX2 were slightly higher in the latter and significantly reduced in A-SP cell line samples. In all cell lines NANOG was expressed at markedly lower level, whereas high expression of MYC was observed. The expression of KLF4 varied highly between the three investigated cell lines, with highest expression found in A-SP and lowest expression seen in PA cell line.

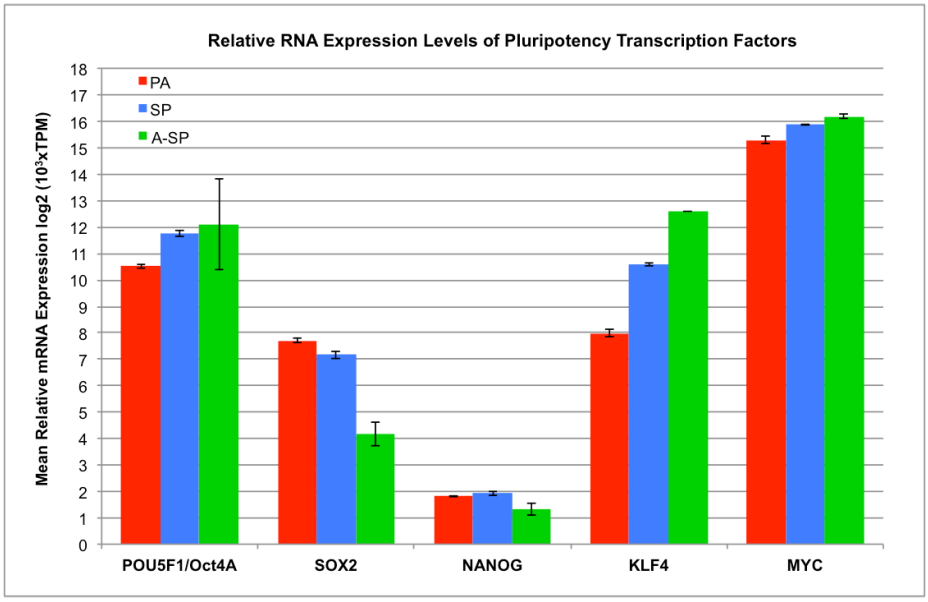

Figure 4.12.12: Relative mRNA Expression Levels of Pluripotency Associated Transcription Factors

Mean values of relative mRNA expression levels transcription factors involved in maintenance of pluripotency obtained by RNA-Sequencing from three replicate samples of PA (P37), SP (P39/43) and A-SP (A-SP-P36/P54, P56, 57, 75) cell lines. Log2 transformed TPM values, which were multiplied by 10^3 to omit negative values, are indicated. Error bar: standard deviation.
ACC: adherent culture conditions, AS: adherently grown spheroids = A-SP: SP cells grown under ACC for 14 weeks, P: passage number, PA: parental cell line, SP: spheroid cells derived from PA, TPM: transcripts per million

5 Discussion

5.1 Growth Characteristics

5.1.1 Growth Potential of Different Cell Lines

A fundamental feature of stem cells is their unrestricted replicative potential, whereas differentiated cells enter a senescent state or die after a defined number of cell divisions.

The replicative potential of cell lines investigated in this work was tested by long-term *in vitro* culture of the cells. All cell lines were shown to possess high replicative potentials, reaching from 190 population doubling in SP cell lines, 200 and 300 population doublings in CS1 and CS7 cell line to 350 population doublings in PA cell line during the observed periods. Also no reduction of growth rate over the investigated period of more than 60 weeks of continuous culture was observed, rather an increase of growth rate over time in culture was seen in all cell lines investigated, which might be a strong hint for enrichment of stem-like cells in the cell lines over long-term culture.

5.1.2 Cell Size as Indicator of Senescence or Stem Cell State

Long-term culture of a cell line always raises the question for enrichment of senescent cells with time of culture. This would on the one hand be indicated by a reduction of proliferation rate, and on the other hand by and increase in cell size, since irreversible growth arrest and an increase of cell size have been described as characteristics of senescent cells. [305] [306] For both factors, the opposite has been observed for the cell lines investigated: the growth rate increased and the cell size decreased with time of culture, for both, PA cells and spheroid cell lines. Also a marked reduction of cell size has been observed in the CS cell lines compared to PA but also to SP cells. Taken both of these facts together makes a scenario of accumulation of senescent cell over time in culture, though not directly analyzed, less likely.

The idea that small cell size might be linked to a quiescent stem cell phenotype is apparent, since the metabolic needs of quiescent cells are fundamentally different to those of proliferating progenitors or differentiated cells. Thus adult stem cells isolated from different tissues have been shown to be characterized by their small cell size. Also in keratinocytes cell size was shown to positively correlate with the expression of the differentiation markers. In contrast, an opposite correlation was reported for mouse mammary stem cells, implying tissue dependent variations. A causal link between cell size and CSC characteristics has not been addressed in quite detail. Few publications found that cells with CSC characteristics showed reduced size, when compared to their non-CSC counterparts. For example, sorting of the highly tumorigenic PC3 prostate cancer cell line according to size led to enrichment of CSC in the small cell size fraction. Also spheres generated from the A431 epidermoid carcinoma cell line were enriched in a small cell population with CSC features. In contrast CSC that were enriched by side population sorting of medulloblastoma cell line DAOY differed from the non-Side Population counterparts by increased cell size. The picture might be complicated by the fact that PI3K/AKT/mTOR signaling pathways, which are major regulators of cell growth, are frequently compromised in cancer cells. For example overexpression of Myc, which often found in cancer cells, has been shown to increase cell size. Also YAP, a component of the Hippo pathway, which is mainly

involved in cell size regulation, is frequently overexpressed in cancers. [307] For this reason a deduction of stem cell characteristic enrichment in the obviously smaller CS cell line would be misleading.

5.1.3 Spheroid Culture Method

Enrichment of CSC by spheroid culture has been shown for many tumor types. In most studies only a small fraction of the primary tumor cells or cell lines was able to grow under these conditions. And the surviving cells showed higher expression of stem cell markers and higher tumor formation efficiency when compared to cells grown under conventional monolayer growth conditions. Also it has been shown, that cells grown as spheroids better retain the characteristics of the original tumor than cells grown under conventional monolayer conditions. This might in part be due to the fact, that the 3-dimensional growth of cells may better resemble the natural tumor environment with regions of low oxygen and nutrient supply. Spheroid-formation assay therefore has become a standard method to assay stem cell characteristics, especially but not only in breast “mammospheres” and colon cancer “colonospheres”. [145 147 168 308 309 310 311 312]

The methods employed for spheroid-formation assays in the literature are highly variable, ranging from seeding of high cell numbers to clonal determination of spheroid growth. In this work spheroid-forming efficiency was determined at a single cell, albeit not clonal level, which was shown to be sufficient to avoid aggregation of the cells. Spheroid cell lines were generated in this work by to different methods. In the “bulk” culture method cells were seeded at normal densities under spheroid-promoting growth conditions, yielding the SC cell lines. There, aggregation as well as other interactions of the cells were present during cell growth and spheroid formation. Clonally amplified cell lines (CS) in contrast, were generated by plating and growth of cells at single cell level. There, no cellular interactions or paracrine signaling was present during the first period of spheroid growth and selection.

Both culture methods resulted in distinct cell types, which were shown to differ in some of the investigated characteristics in this work.

5.1.3.1 Spheroids from Kidney-Derived Cells and RCC

Buzhor et al [313] compared gene expression profiles of spheroids and adherently grown kidney epithelial cells derived of human nephrectomy tissue samples using microarray as well as flow cytometric immunophenotyping (IFC). In their study de-differentiation of the cells in serum containing medium was observed after a few passages, whereas cell propagation as spheroids in serum-free medium showed up-regulation of stemness markers compared to adherently grown cells. The spheroid phenotype was characterized as being $EpCAM^+/CD24^+/CD133^+/CD44^+$. The cells grown as spheroids were also able to reconstitute tubular epithelia when cultured on chorioallantoic membrane of chick embryos.

Zhong et al [211] investigated the sphere culture method for enrichment of CSC from SK-RC-42 RCC cell line. They found spheroid cells enriched in Hoechst side population (HSP) cells (10% vs. 2% in adherent counterparts) and being able to induce tumor growth in BALB/c nude mice at injected cell numbers of 2×10^5 compared to 3×10^6 adherent cells needed to form tumors. The spheroids showed also higher mRNA expression levels of stemness genes Oct3/4, BMI1, Nanog and β-Catenin in semi-quantitative RT-PCR compared to adherent cells. No difference was observed in expression of CD24

and CD44, which both were expressed on adherent and spheroid cell lines, whereas no expression was seen for CD133 on both cell lines. CD105 was also expressed on both cell lines, but with lower intensity on spheroid cell lines, compared to adherently grown cells. Assays for radiation and drug sensitivity to mitomycin C and 5-fluorouracil showed higher resistance of spheroid cells, compared to adherent counterparts. Differences in expression were seen for some immune-relevant molecules, which were expressed by spheroid cells in a manner resulting in a more immune-evading phenotype compared to adherently grown cells.

Micucci et al [213] investigated sphere-forming abilities of 786-O, Caki-1 and 786-P and Caki-2 RCC cell lines and found only the former two to be able to form spheroids in a magnitude of 0.3% in non-adherent culture conditions using DMEM/F12 growth factor supplemented medium, whereas the sphere forming ability of Caki-2 and 786-P cell line was reduced by a factor of >10. Only the spheroid derived cells of 786-O and Caki-1 cell lines, but not the adherently grown counterparts were able to differentiate into adipocytes. The spheroid-derived cells of both cell lines were also shown to possess higher tumorigenic potential in NOD/SCID mice ($5x10^4$ cells led to tumor formation in all mice tested) than the adherently propagated counterparts ($3x10^6$ cells led to tumor formation in all mice tested). No tumor formation was observed from spheroids obtained from Caki-2 cell line. The higher tumor-forming ability of the 786-O spheroid cells was shown to be related to the observed higher expression of HIF-2α. By means of shRNA dependent silencing of expression, reduced tumor-forming ability and size in adherent and spheroid-derived cells as well as sphere-forming ability in these cell lines were seen. Another factor, which was reported to be influencing spheroid growth, was the functionality of the chemokine receptor CXCR4, which when inhibited led to strongly reduced sphere-forming efficiency in this work. Reduced mRNA expression of CXCR4 was detected upon HIF-2α knockdown.

Similar to the results obtained in my work, the spheroid-forming efficiency of 786-O cell line increased with spheroid passage number. The sphere culture conditions used by Micucci et al [213] were a mix of the two methods used in my work, in that the cells were seeded at a relatively high density of $2x10^5$ cells/mL, similar to SP cells, but were passaged at long intervals, which was comparable to CS cells.

Gassenmaier et al [204] investigated sphere-forming ability in two RCC cell lines RCC-26, RCC-53 which, were derived from primary tumors of stage I and IV patients, respectively. They found sphere-forming abilities of 10% in RCC-53 cells and 2% in RCC-26 cell lines. Spheroid cells derived of RCC-53 were found to possess higher resistance to kinase inhibitors sorafenib, sunitinib, and pazopanib than adherent counterparts and showed increased expression of stemness markers Oct4, Nanog and Sox2 compared to adherent cells. Spheroids were also characterized by higher expression of CXCR4. $CXCR4^+$ sorted cells had a higher sphere-forming ability than $CXCR4^-$ cells. The authors, in accordance with results of Micucci et al[213], also showed that the receptor seemed to be functional for sphere-formation, since siRNA knockdown or inhibition lead to reduced spheroid-formation ability of the cells.

Spheroid formation was also investigated by Lichner et al [212] in ACHN and Caki-1 RCC cell lines. They found 4% of cells from both cell lines being able to grow as spheroids, and an increased sphere-forming ability of 12% in both cell lines for spheroid-derived cells. Spheroids derived from Caki-1 cell line were found to possess increased tumor-forming ability in NOD/SCID mice at injected cell numbers

of 10^4 and 10^6, with higher tumor masses compared to adherently grown cells of this cell line. Compared to adherently grown cells spheroids of both cell lines also showed increased expression of stem cell markers (Nanog, LIN28, KLF4), EMT markers (ZEB, Twist, Vimentin, N-Cadherin). Also CD24 expression was up-regulated in spheroids compared to adherent counterparts of the cell lines. The authors also investigated expression of miRNAs in spheroids and adherent cells and found several miRNAs differentially expressed, which were associated to TGF-β and BMP signaling components thereby favoring TGF-β TGFBR2-SMAD2/3-mediated branch of the TGF-β pathway over the BMPR-SMAD1/5/8-mediated branch of TGF-β pathway. Targeting of miR-17, which targets ACVR1 receptor and was found to be up-regulated in spheroids, by anti-miR-17 lead to increased sphere-forming ability, tumor growth. Treatment with TGF-β1 increased sphere-forming ability in ACHN cell line and induced higher expression of EMT transcription factors Twist, Snail and Zeb1.

CSFE of Caki-1 and ACHN cell lines was also determined by Xiao et al [203] and they report relative high values of 15-18% spheroid-forming cells in those cell lines, whereas $CD133^+/CD24^+$ sorted cells showed increased CSFE values of 40% in cells from ACHN and 60% in in cells from Caki-1 cell lines respectively. In contrast to Xioa et al [203], Hu et al [200] determined the sphere-formation efficiency for ACHN cell line to be in the range of 4% of the cells. The sphere-formation efficiency of $CD105^+$ sorted cells was found to be only slightly higher.

Song et al [210] used spheroid growth to enrich for CSC from primary RCC tissues and the 786-O RCC cell line. The found spheroid-derived cells showed higher tumorigenicity with 500 injected cells being able to form tumors compared to $1.5x10^4$ injected adherent cells needed for tumor growth in in NOD/SCID mice. Spheroids also expressed CD73, which was shown to be a marker for CSC in this work, at higher level, and were less sensitive to radiation and mitomycin C treatment than adherent counterparts. The spheroids could be propagated for more than 60 passages, demonstrating the self-renewal ability of the cells *in vitro*. Similar to results obtained with cells investigated in this work, the authors report, that spheroids were able to grow under adherent conditions as monolayer and retained their spheroid-forming ability under adherent culture conditions.

Debeb et al [214] investigated sphere-formation of human embryonic kidney cell line HEK293 and found primary sphere-forming ability of 2%, which increased to 8% in secondary spheroids. Compared to adherent cell line, spheroids showed higher expression of stemness markers Oct4, Sox2, Klf4, Nanog, survivin, β-Catenin and Rex1 as well as EMT markers N-Cadherin, Vimentin, Zeb1, Snail1 and Snail2, additionally microRNAs, known to target EMT-components were found to be down regulated. Also spheroids were found to be enriched in $ALDH^{high}$ cells (40%) compared to cells grown under adherent culture conditions (6%) and showed higher resistance to radiation and retinoic acid treatment. Expression of CD24, which was detected by IFC at high levels in HEK293 adherent cells, was reduced in fractions of spheroid cells.

Spheroid-formation of 786-O cell line was determined by Peng et al [314] and found to be in the range of 2% and similar values of 3% were reported by Yun et al [315]for this cell line.

For A498 and SK-RC-39 cell lines Zhang et al [201] reported sphere-forming ability being restricted to $CD105^+$ sorted cells, whereas $CD105^-$ cells were unable to form spheroids in serum-free medium. For unsorted A498 RCC cell line Li et al [316] report CSFE of 3%.

In Wilms' tumor (a pediatric tumor of the kidney with possible stem cell origin) derived primary cell cultures Pode-Shakked et al [317] investigated whether spheroid growth might enrich for stemness markers and found two of the tumors showed higher expression of markers in spheres while cells from one tumor overexpressed the stemness genes in the adherent culture and one cell line showed mostly comparable expression levels, indicating no correlation of stemness signature and sphere culturing method. Of note is that, in those experiments the medium composition for spheroid growth only slightly varied from the medium used for adherent culture: both media contained serum, EGF, FGF and stem cell factor, with the spheroid growth medium even containing a higher amount of serum (20% FBS) than the medium used for adherent culture (10% FBS), and sphere growth was thus induced solely by lack of attach ability of the cells to the ultra-low attachment plates used.

The clonal spheroid-forming efficiency observed in this work for PA cell line with 8±4% resembled those reported for other RCC cell lines. Direct assay for repeated sphere-formation form the cell line, revealed a slight decrease of CSFE to 4±2% over 5 passages. The repeated growth of spheroids over several passages is an indicator for the self-renewal ability of the cells. This ability was further substantiated by experiments performed with spheroid cell lines (SP and CS). The results obtained for these cell lines show a profound increase in spheroid-forming efficiency over long-time spheroid culture, which in high passage numbers of cells was found to reach values of 60-80%. This indicates, that over long-term spheroid culture, such cells could be enriched, albeit it is not clear whether this enrichment was achieved by selection of cells or reprogramming processes. Similar to observation by Song et al [210] the spheroid-forming efficiency of the SP and CS cell lines was retained under adherent culture conditions. The results obtained in my work show, that even after relative long culturing periods under ACC (up to 15 weeks), spheroid-forming efficiency of the cells was retained in similar ranges, as were seen for founding spheroid cells. This is an indicator for immanent changes of phenotype in spheroid culture (either by enrichment or reprograming of the cells). An interesting and important result of this work is that, in contrast to spheroid cell lines, the spheroid-forming efficiency of PA cell line is rapidly (within 5 weeks) lost upon ACC culture of the cells.

5.1.4 Soft Agar Assay: *in vitro* Tumorigenicity

Soft agar assay may be used as an *in vivo* test for possible tumorigenicity and drug sensitivity. [247] [248] For example Galleggiante et al [202] assayed $CD133^+/CD24^+$ putative CSC, healthy adult renal progenitors isolated from RCC patients and Caki-2 cell line in soft agar assay for their *in vitro* tumorigenic potential and found only tumor cells and Caki-2 cells to form small colonies after 21 days, whereas healthy progenitor cells did not grow in the assay. Another example are the growth potentials of $CD133^+/CD24^+$ sorted putative CSC from ACHN and Caki-1 cell line, which were assayed by Xiao et al [203] in soft agar assay, sphere-forming assay and *in vivo* compared to parental unsorted cells. Thereby results obtained in soft agar assay reflected the variance seen in growth potential of the tested cells *in vivo*.

But also several reports have shown that the growth potential in soft agar assay may not necessarily reflect *in vivo* growth characteristics nor may indicate a more mesenchymal state of cells. For example, two fractions of the sarcomatoid cell line RCC52, which were sorted by Hsieh et al [318] according to CD24 expression level, were shown to possess different growth potentials. The

epithelioid $CD24^{Low}$ fraction showed faster *in vitro* growth kinetics and higher growth potential in soft agar assay, whereas the fibroblastoid $CD24^{Hi}$ fraction showed increased tumor forming ability, indicated by higher tumor volume, in NOD/SCID mice. Also, Khan et al [319] tested the growth potential of the metastatic RCC cell line ACHN in soft agar assay and report a plating efficiency of 5% for unsorted cells, and a 5 fold reduction for sorted ($CD105^{+}$/$CD105^{-}$) cells, of which the $CD105^{+}$ sorted cells were shown to possess higher tumorigenicity *in vivo*. They also investigated colony-formation in soft agar assay for various other RCC cell lines (SMKR-R2/3, Caki-1/2, 786-O/P, RCC6, ACHN) and observed CFE values between 3 and 12%.

The colony-forming ability of cell lines investigated in this work was assayed by conventional soft agar assay using serum-containing medium. The obtained CFEs observed for PA and CS cell lines with 1% were in the lower range of reported colony-forming efficiencies in the assay for other RCC cell lines. In contrast, the colony forming efficiency observed in SP cell line with 14% was markedly higher and in the upper range of reported CFE values for RCC cell lines. This enhanced growth potential in soft agar assay of SP cell line was, with mean values of 12% CFE, was retained, when cells were cultured for up to 38 weeks under ACC, which is a further hint for permanent changes occurring during spheroid culture of the cell line.

5.1.5 Evaluation of CSC Content

The sphere-formation efficiency from primary material is usually low (1-10%) and since in the NSA also progenitor cells are able to survive, the sphere-formation efficiency cannot be used as a direct readout of stem cell content. Instead, the repeated formation of sub-spheres is used as a proof for the self-renewal ability of stem-like cells. In the literature some authors describe a reduced sub-sphere-forming efficiency of their tested cells, whereas others observed an increase of sphere-forming efficiency with passage of spheres. [311] The latter is an indicator for enrichment of stem like cells, but might also indicate the enrichment of progenitor cells. Soft agar assay, when used in conjunction with SC-Medium is very similar to the NCFCA proposed by Louis et al [244] for enumeration of stem cell content.

To estimate the content of stem cells from the NSA in “bulk” culture Deleyrolle [320] presented and tested a simple mathematical model of the assay. According to this model the slope of the growth curve of spheres cultured as bulk culture under steady state growth conditions is a representation of the stem cell population’s symmetric division rate and thus of stem cell content of the culture. They used the model to compare relative variation in stem cell frequencies for different neural stem cell cultures and conditions and the predicted values were in good correlation with results obtained from NCFCA.

A refined mathematical model developed for the growth kinetics of cancer stem cells by Liu et al [321] predicts a contrary outcome. According to this model, in which feedback regulations on stem cell symmetric division rate are considered, a decrease of stem cells in sphere culture after several passages is predicted. The reason for this is the disturbance of equilibrium between stem cell and non stem cell compartments during passaging. As a result of this model bulk culture of spheres should be enriched for committed progenitors instead of stem cells.

For the spheroid cell lines investigated here, a strong increase of sphere-forming efficiency was seen with prolonged culturing period as spheroids to values where almost 60-80% of spheroid cells were able re-from spheroids after plating. Also the growth rate of the cells increased over time in culture, which according to the model proposed by Deleyrolle [320] would be an indicator for enrichment of stem cells over long-term culture.

But when using NCFCA conditions (SCC) in soft agar assay, the growth potential was markedly reduced in all cell lines tested compared to serum-containing medium conditions and also to spheroid-formation efficiency seen in the NSA. But spheroid cell lines formed considerably larger colonies under these conditions, when compared to serum-containing conditions. The observation that the growth potential of all cell lines, including spheroid cell lines, was reduced in soft agar assays under SCC conditions, and only spheroid cell lines gave rise to considerably larger colonies, might be a hint, that these conditions indeed support the growth of cells with stem cell characteristics only and that such cells are present at low numbers in the cell lines cultured as spheroids. Compared to SP cell line, the frequency of such cells was much lower in CS cell lines and the fraction of cells being able to grow under SCC was still low in both cell lines (SP: ≈ 4%, CS: ≈ 0.6%). Also no correlation of the results with time of culture of the cells as spheroids was observed in the SAA experiments, which would be expected in either case: enrichment of stem cells over long-term culture or adaptation of cells to culture conditions. But since a relatively high variability was seen in assay results, and the too low number of assays at different time points of spheroid culture of the cells, probable differences might have been missed under the used experimental settings.

Interestingly, the growth potential and the size of colonies in of A-SP cells, which were grown for up to 38 weeks under ACC, was similar to that seen in SP cell line, which shows that this feature was conserved even after adherent monolayer growth of the cells.

In contrast to results obtained in soft agar assay under SCC, the growth rates of CS cell line in “bulk” culture was found to be higher after long-term spheroid culture than those seen for SP cell lines and also the colonies formed from CS cell lines under SCC in SAA were slightly bigger than those of SP cell lines. The higher growth rate of CS cells and their lower colony forming efficiency in SAA compared to SP cell lines, might be an indicator for a higher content of progenitor-like cells in this cell line. The reduced growth of cells in the SAA compared to NSA might also be a hint for cell interaction and/or autocrine stimulation dependency of the spheroid cell lines for optimal growth.

5.2 Differentiation Potential

One of the hallmarks of stem cells is their ability to give rise to several differentiated cell types. In this work adipogenic and osteogenic differentiation potential were assayed, since cells with progenitor or CSC characteristics isolated from primary tissues or RCC cell lines were described in the literature to show these potentials.

Differentiation potential into adipogenic and osteogenic lineages was shown for $CD133^+/CD24^+$ adult renal progenitors by Sagrinati et al [73]. Similar to normal renal progenitors, $CD133^+/CD24^+$ putative CSC isolated by Galleggiante et al [202] from RCC tumors, were shown to posses adipogenic and osteogenic differentiation potential at a clonal level, which was shown by alizarin red staining of calcium deposits and oil red staining of lipid droplets, respectively, and there results were comparable

to that seen from PA cell line in this work. Differentiation potential into mesenchymal lineages was also observed in $CD105^+$ sorted renal progenitors isolated by Bussolati et al [322], which are marked by lack of CD133 expression.

By comparative gene expression profiling of normal patient-matched renal tissue with ccRCC tumor tissue, Tun et al [323] found an adipogenic gene expression signature enriched in ccRCC, which indicates adipogenesis as an inherent process found in this tumor type. This is also in line with the typical lipid-laden morphology of these tumors. In differentiation experiments, the authors found similar differentiation potential as was seen for SP cell line, in A498 RCC cell line and two primary tumor cell lines, whereas no differentiation potential was observed in the patient-matched normal renal cells or MDCK cells. Micucci et al [213] investigated adipogenic differentiation potential of 786-O and Caki-1 RCC cell lines and found only the sphere-derived cells being able give rise to cells with the typical adipocyte morphology, when cultured under respective conditions.

Similar to the cell lines investigated in this work, differentiation potential into osteogenic and or adipogenic lineages was also observed in $ALDH^{br}$ fractions of Caki-2 and ACHN cells by use of BMP-2 treatment [207], and sorted HSP cells from embryonic and mouse kidney[324], which were shown to be able to differentiate into adipogenic and osteogenic lineages.

The differentiation potential of the investigated cell lines was assayed by culturing the cells under conditions that had been shown to induce adipogenesis or osteogenesis in MSC and subsequent staining of structures, which are specific for both lineages. Although some variation within the experimental results occurred, these histologic analyses revealed, that all cell lines seemed to be able to give rise to at least one of the investigated cell types.

Thereby SP cell line seemed to possess the highest differentiation capacity among the investigated cell lines into both assayed cell types. Adipogenic differentiation potential of this cell line was further supported by their expression of the adipocyte marker adiponectin, as assayed by RT-PCR, which was seen at marginal level in osteogenically induced cells of the same cell line. The osteogenic differentiation potential of SP cell line, could be further substantiated by staining for alkaline phosphatase activity in osteogenic induced cells, which revealed fractions of positive staining cell with morphologic similarities to osteoblasts.

Differentiation potential toward both lineages was also observed for PA cells, although the observed adipocyte morphology was less pronounced than that seen for SP cells and osteogenic differentiation potential was not observed in all experiments performed. Surprisingly, the differentiation potential of CS cell lines was further reduced, compared to SP cell line in that both cell lines showed differentiation potential mainly into one of the two assayed lineages. This might be a hint for different pathways active in these cell lines, for example Wnt/β-catenin signaling pathway is known to suppress adipogenesis in mesenchymal stem cells [325], whereas retinoic acid signaling via Smad3 is required for osteoblast differentiation of MSC, and inhibits adipogenic differentiation. [326] Taking into account the complex nature of the differentiation process and the relatively small number of experiments performed with these cell lines, the variations seen might therefore also simply be related to suboptimal differentiation conditions used for these cell lines.

It was also obvious from the experiments that differentiation occurred only in a fraction of cells seeded, since also cells with normal morphology were present in the induced samples. This, on the one hand might be a hint for the heterogeneous nature of the investigated cell lines, or on the other hand this may also simply reflect the sub-optimal differentiation conditions used.

Results obtained by RT-PCR analysis of genes typically expressed in adipocytes and osteoblasts, besides adiponectin expression in adipogenic induced cells, were not suited to proof differentiation of the cells, since markers were expressed at similar low levels in cells induced into either lineage. These results might further indicate sub-optimal differentiation conditions, lacking strong enough inhibition of the respective other lineage. For example the role of dexamethasone in osteogenic differentiation is the induction of RUNX2, the same might be true when dexamethasone is used in the adipocyte differentiation cocktail. Also it has been shown that for osteogenic induction of human BMSC cultures ECM proteins Col1 and vitronectin are sufficient. [254]

On the other hand, the results obtained are in line with a study performed by Köllner et al [256] who observed that frequently used markers for osteogenic differentiation are expressed also in adipogenic induced hMSCs and in control samples. For example, comparable to the results obtained here, BGLAP/Osteocalcin, but also OPN/Osteopontin and alkaline phosphatase expression, were seen at similar or even higher levels in basal and the adipogenic induction group than in the osteogenic induction group. Expression levels of these genes also varied highly between different time points of assessment. In contrast to osteogenic markers, the investigated adipogenic markers were shown to be clearly expressed at higher levels in the adipogenic induction group compared to basal or osteogenic group after 28 days of induction. But this also was strongly dependent on the time of assessment: for adiponectin for example no difference in expression was seen between groups assayed at day 14. SREBF1 has been shown to be a key regulator at early time points of adipogenesis[327], and also stimulates the expression of many of the genes necessary for lipogenesis including lipoprotein lipase, fatty acid synthase, and glycerol phosphate acyltransferase.[328] The fact that no difference in expression between osteogenic and adipogenic induction groups was found by RT-PCR, might be due on the one hand by the wrong time point of assessment and also may be caused by the basal adipogenic signature found in ccRCC.

An interesting fact observed in this work is, that the differentiation potential did not seem to be reduced over long-term culture of the cells, neither as spheroids nor under adherent culture conditions, since Gharibi and Hughes [329] observed a loss of osteogenic and adipogenic differentiation potential in MSC after long-term culture with bFGF supplemented medium and MSC differentiation potential has been shown to be reduced with increasing age of donors.

5.3 Side Population Assay for Enrichment of CSC

The expression of ABC-transporters confers cells with detoxifying abilities, which are of great importance for stem cell integrity as well as for tumor cell chemo-resistance. The so termed “side population" assay is a functional test using the ability of cells to pump out the DNA-binding dye Hoechst33342, which is mainly attributed to expression of ABCG2 (BCRP) and ABCB1 (MDR1). The assay has successfully been used to enrich for stem/progenitor cell fractions from several tissues and CSC from tumors of different origin. [158] [161] [276] Results reported in the literature for the two established

variants of the assay (Hoechst and Rhodamine side population) for kidney normal and tumor tissue are discussed below in more detail.

5.3.1 Hoechst Side Population (HSP)

Challen et al [324] used the Hoechst side population sorting strategy to enrich for stem cells residing in embryonic and adult mouse kidneys, which comprised 0.1% of the cells. The sorted cells (HSP) showed differentiation ability into osteocytes and adipocytes *in vitro*, which was not seen in the main cell population, they also showed enriched capacity for integration into developing metanephric ducts *in vivo*. Comparative gene expression analysis by microarray revealed relatively few differences between embryonic and adult HSP cells, indicating that this fraction might represent a renal resident stem cell population in adult kidney. By comparing differences between HSP and non-SP cells, the HSP was found to be enriched in genes expressed in proximal tubule segments indicating a possible spatial localization of the cells. Of note is, that the major membrane transporter ABCG2 (BCRP), which is known in other organs to convey the HSP-phenotype, by using riboprobes for mRNA detection, has been found to be expressed predominantly in collecting ducts but not in tubular cells and was not found to be expressed with significant difference between SP and non-SP in this study, which may suggest, that in the kidney other transporters may be responsible for dye efflux.

In contrast to this, protein and mRNA expression of ABCG2 has been demonstrated at the brush border membranes of proximal tubules at the apical membrane of proximal tubular cells in healthy human as well as in mouse and rat kidneys by Huls et al [160] using immunofluorescence microscopy. By using western blot analysis and RT-PCR, expression of ABCG2 (BCRP) was detected in the cortex and proximal tubule cell monolayers as well as in mixed cell fractions, but not in collecting ducts. It was also noted that ABCG2 in human tissue is expressed at relatively lower level than in rat and especially in mouse tissue. The reason for the controversial findings regarding ABCG2 expression compared to the report of Challen et al [324] is not clear and might be attributed to different methodologies used. By also using the Hoechst33324-SP assay in human primary proximal tubular cells and either the ABCG2 specific inhibitor fumitremorgin C (FTC) or nelfinavir, which is an inhibitor of ABCG2 and ABCB1, Huls et al [160] show that both transporters seem to contribute to the efflux of Hoechst at similar level in these cells.

Hoechst side population (HSP) and non-side population (NSP) fractions from tissues obtained from normal human kidney and RCC were characterized by Addla et al [330]. They found 4-6% of the cells in both entities were able to pump out the dye (HSP), and these had greater proliferative potential and colony- as well as sphere-forming ability compared to NSP cells, indicating that the HSP in both, the kidney and RCC, enriches for cells with stem-like features.

Zhong et al [211] investigated HSP characteristics of spheroids and adherent counterparts of SK-RC-42 RCC cell line. Thereby found 10% of spheroid cells being able to efflux the dye (HSP), whereas HSP of adherently grown cells was only 2%.

Ueda et al [205] also used the Hoechst side population sorting strategy to isolate HSP fractions from ACHN and KRC/Y RCC cell lines, which comprised 1.4% and 1.7%, respectively. The SP from ACHN cell line was shown to possess a higher sphere-forming ability (HSP: 0.8%, NSP: 0.4%), higher ALDH activity (HSP: 33%, NSP: 15%) as well as higher tumor forming ability compared to the NSP. No

significant differences between SP and NSP in regarding these characteristics were seen in the KRC/Y cell line. Both cell lines did not show significant differences in expression of several investigated genes related to EMT, apoptosis, hypoxia and self-renewal, with the exception of ALDH1A and ABCG2 expression, which was slightly higher in HSP of ACHN, whereas ABCB1 expression was slightly higher and ABCG2 expression slightly reduced in HSP of KRC/Y cell line. Li et al [316] used HSP assay to study the influence of honokiol on this characteristic in A-498 cell line and found a reduction of HSP cells from 3% to 1% after honokiol treatment.

Huang et al [331] isolated and characterized HSP and NSP cells isolated from the RCC cell line 786P and found 5% of the cells were able to efflux the dye (HSP). HSP cells possessed higher clone-forming ability and resistance to radiation and mithoxantrone and 5-fluorouracil treatment (but not to sutinib treatment) and were able to form tumors in NOD/SICD mice at lower injected cell-doses than NSP cells. Expression of ABC-transporters was assayed by RT-PCR and western-blot analyses, thereby the expression of ABCB1 but not ABCG2 or ABCC1 in HSP and only low level expression of the transporter in the NSP was detected, implying that ABCB1 in this cell line is the main responsible transporter for HSP-phenotype.

5.3.2 Rhodamine 123 Side Population (RSP)

Due to the special requirements for instrumentation and the toxicity of the Hoechst33342 dye, Liu et al [275] proposed the use of Rhodamine 123 as an alternative dye. By using the MHCC97 liver cancer cell line for sorting of cells pumping out Rhodamine 123 dye (RSP) in parallel with cells pumping out the Hoechste33342 dye (HSP), they obtained similar results for cell growth and tumor forming ability of HSP/RSP or H-NSP/R-NSP *in vitro* and *in vivo*. RSP was also used to enrich putative $CD34^+$ HSC from different sources [273] [274]. Though, the HSP and RSP might not necessarily mark the same population of cells, since it has been shown in mice, that different ABC-transporters have different affinities for the dyes. There, ABCG2 had higher affinity for Hoechst33342 stain and ABCB1 seemed to be involved in efflux of Rhodamine 123. Also the contribution of both transporters to the SP phenotype varies in different cell types and species [276]. Since Rhodamine 123 dye accumulates in mitochondria its retention may also reflect mitochondria number and activity [274].

RSP was assayed by Lu et al [209] in the 786-O RCC cell line. In contrast to results seen with HSP, where cells pumping out dye comprise the putative stem cell population, the authors found that instead cells with high staining intensity for the dye (Rho^{high}), which comprised a minor fraction of the cells, were enriched for stem cell characteristics such as tumor-forming ability in NOD/SCID mice, growth potential in soft agar assay, and higher resistance to radiation. Rho^{high} were also able to give rise to Rho^{low} cells, whereas Rho^{low} cells did not show a change of their phenotype in culture.

Similar results were obtained by Song et al [210] who used RSP to identify possible CSC in primary tumor cells derived from RCC tissues as well as in 786-O RCC cell line. The dye retaining cell fraction (Rho^{high}), which comprised 19±7% of primary cells, was found to be enriched for CSC characteristics such as higher tumor-forming ability in NOD/SCID mice and expression of CD73. Differential expression of several proteins between Rho^{high} cell and Rho^{low} cell fraction was analyzed and revealed, besides higher expression of CD73, also higher expression of ITGB5 and EGFR in Rho^{high}

cells. The Rho^{high} cells were, similar to results obtained in my work, characterized by reduced expression of CD243 (MDR1).

For my work, the Rhodamine 123 side population assay in combination with ABCB1-inhibior verapamil was chosen to characterize individual dye efflux abilities of the different cell lines. In some experiments expression of ABCB1 (MDR1, CD243) was assayed in parallel by immunostaining of the cells to address the role of this transporter for the observed dye efflux. Thereby, profound differences were seen between PA and spheroid cell lines (SP and CS). While PA cells were able to pump out the dye rapidly, the dye was almost completely retained in spheroid cell lines during the same period. Parallel staining with ABCB1 (CD243) antibody revealed, that the transporter appeared to be responsible for the dye-pumping capability of the cells. This was also confirmed by experiments performed with A-SP and A-CS cell lines, which in contrast to their parental spheroid cell lines expressed the transporter in sub-fractions of cells, and those were, similar to PA cells, able to pump out the dye. Additionally to dye retention of spheroid cells, they also showed higher staining intensities for the dye compared to PA cells, an indicator for differences in mitochondrial number and/or function in these cells, which might an interesting point for further evaluations.

Thus, spheroid cells resembled the Rho^{high} cell fractions, reported by Lu [209] and Song [210] to be enriched in CSC characteristics. Interestingly, in an experiment performed with low passage PA cells, these seemed to contain a similar Rho^{high} cell fraction, which was absent in later passage cells. Though this was seen in a single experiment only, sorting for Rho^{high} cells in early passage PA cells could be a means to enrich for a fraction of spheroid-forming cells that is drastically reduced in later passages of the PA cell line.

The results obtained in this work as well as the results obtained by Lu [209] and Song [210] using RSP assay contradict results obtained for other cell lines, as well as those seen for HSP [205 211 330] in RCC cell lines. Since the test is based on the general assumption that high expression of ABCB1 or ABCG2 and concomitant dye efflux are associated with a stem cell phenotype and confer resistance to chemotherapeutic agents, it would be interesting to test for chemo-sensitivity of Rho^{high} cells, to see whether probable other mechanisms are used by these cells to confer therapy resistance, or whether the observations made in the RSP assay are dye-specific.

5.4 ALDH Activity - ALDEFLUOR™ Assay for Enrichment of CSC

Aldehyde dehydrogenases (ALDH) are a huge family of iso-enzymes involved in the detoxification of a wide variety of aldehydes to their corresponding weak carboxylic acids, including xenobiotic aldehydes. They are also being involved in maintenance of low ROS levels and retinoic acid (RA) metabolism and signaling. According to their functions, expression of ALDH isoforms is found in a variety of tissues, especially in kidney, liver, heart and muscle. High expression, of the isoform ALDH1A1, which, together with ALDH1A2-3 and ALDH8A1, is involved in RA metabolism, has been found in stem cells and has been used to isolate adult stem cells (HSC, NSC, mammary, prostate, intestinal, myogenic) and CSC from several tumor entities, where ALDHs seem to be involved in the maintenance of stem cell phenotype. For this purpose the ALDEFLUOR™ assay is widely used, since it is a non-toxic enzymatic assay, which can easily performed and detects activity of the enzyme in a non-isoform specific manner. The assay was first used by Kastan et al [149] to isolate hematopoietic

progenitor cells, thereby starting a high number of reports on the use of this assay, with varying and partially conflicting results concerning suitability of the assay for different cell and tumor types. [150] [151] One possible reason for discrepancies of reports on ALDH expression was investigated by Opendaker et al [332] in different cell lines, who observed a decreased ALDH activity in most cell lines grown at high cell densities, which comprised more than 50% of the obtained values, whereas sphere-formation were not affected. Another obvious reason for variation of results may be attributed to the nature of the assay. Results highly depend on cell concentration and/or incubation time, which varies for different cell types. This was clearly seen from the experiments done here, using different cell concentrations.

ALDH activity has been assayed in several cancer cell lines and has been found to vary among them. For example Suzuki et al [333] investigated ALDH activity in several cells lines of colorectal carcinoma (CRC) and report high fraction of ALDH expressing cells only in HCT116, whereas Caco2 and SW480 cell lines only contained a small number of ALDH positive staining cells. Charafe-Jauffret [334] investigated ALDH activity in 33 breast cancer cell lines and found 23 of them to contain $ALDH^+$ staining cell fractions, ranging from 0.2% to 100% in SK-BR-3 and HCC38 cell lines. $ALDH^+$ fractions were found in all basal/mesenchymal breast cancer cell lines, whereas 7/12 luminal breast cancer cell lines did not express the enzyme. $ALDH^+$ sorted cells displayed a higher sphere-forming ability as well as tumorigenicity compared to $ALDH^-$ fractions. The same authors [335] had previously shown that $ALDH^+$ sorting of normal breast and breast tumor tissue, enriches for normal beast progenitor cells and, in combination with $CD44^+/CD24^-$ sorting, for CSC, respectively. The $ALDH^-/CD44^+/CD24-$ cell fraction did not show tumorigenicity in xenotransplantation assay.

Lindgren et al [74] used ALDH assay to isolate renal progenitors from cortical tissue deprived of glomeruli. Cells with high ALDH expression, which comprised about 7% of viable cells isolated from human cortical tissues, were able to form hollow epithelial spheres in Matrigel™ and compact spheroids in NSA, whereas $ALDH^{low}$ cells did not grow in the respective assays. Comparison of gene expression profiles of both fractions showed CD133 and CD24, both of which had previously been shown to mark renal progenitor cells in the Bowman's capsule, among the most up-regulated genes in $ALDH^{high}$ fractions compared to $ALDH^{low}$ cells. Also CK7, CK19 and vimentin were found to be up-regulated in $ALDH^{high}$ cells. Using IHC analysis with these markers, which are not normally expressed by proximal tubular cells, the authors found scattered cells, often localized to the apices of creases formed by the convolution of the proximal tubules, which stained positive for CK7, CK19, CD133 and vimentin. Similar staining was seen in pRCC TMA samples, suggesting a role of the identified cells as potential origin of this tumor type. By comparison with gene signature databases, $ALDH^{high}$ cells have also been found to be enriched in a meta-signature for stem cells, hypoxic response signatures, and several signatures associated with cellular stress. Although enrichment of progenitor cells from adult kidney seemed to be possible using the ALDEFLUOR™ assay, the same group (Axelson et al [69]) reports, that their efforts to isolate CSC from ccRCC were not successful due to the lack of distinct aldefluor positive populations.

ALDH1 expression in ccRCC was investigated by Wang et al [336] using IHC. The authors report high expression of the enzyme in 60% of cases, which was associated with tumor size and stage, recurrence rate, and vascular invasion, being an independent prognostic factor for ccRCC patients.

Similar results were obtained by Ozbek et al [337] also showing higher staining of ALDH1 in cancer tissue compared to normal renal tissue and a correlation with tumor stage. In contrast, a large TMA study performed by Abourbih et al [304] on primary and metastatic RCC tumor samples found no correlation of ALDH1 expression with tumor stage or grade.

Abdulrahman et al [338] investigated differential expression of genes in cell lines with different pVHL mutation status' by microarray analysis, RT-PCR and western blot. For this purpose the VHL negative cell line RCC4 was transfected with several vectors containing either the wild type variant or different mutations of the gene. Caki-1 pVHL-wt and pVHL-null SKRC18 cell line with low ALDH expression were used as control. ALDH1A1 and ALDH7 were among the down-regulated genes in cells bearing RCC-associated mutations. Expression of ALDH1A1, but not ALDH7, was shown to be repressed under hypoxic conditions. Involvement of HIF-1α but not HIF-2α was further verified by transfection with siRNA constructs targeting the two isoforms. No effect of restoration of ALDH activity on colony-formation efficiency in soft agar assay, which was assayed by transfection of SKRC18 cell line with respective vectors, was observed.

This is contrasted by results obtained for 786-O and A498 RCC pVHL-mutant cell lines, where ALDH1 protein expression was evaluated by Wang et al [336] and found to be higher in the latter. Knocking down of ALDH1 in A498 cell line by shRNA lead to reduced colony formation and migratory ability as well as higher chemo sensitivity *in vitro* compared to mock treated cells, indicating a possible involvement of this enzyme in these processes. An explanation for the discrepancy between the two reports might be that reports on genotype of A498 cell line are controversial on pVHL-mut status [193]. A pVHL-wt status of the cell line would be in line with higher expression of ALDH1 compared to 786-O cell line.

Despite the problems, that were reported by Axelson et al [69] regarding the use of ALDEFLOUR^{TM} assay for isolation of CSC from RCC, three reports have been published, in which this method was applied, of which two report successful enrichment of TIC from RCC cell lines by this method.

ALDEFLOUR^{TM} assay was used by Ueda et al [205] to isolate ALDH^{+} cells from ACHN and KRC/Y cell lines, which comprised 15% and 6%, respectively. Compared to ALDH^{-} cell fractions the ALDH^{+} expressing cells showed higher sphere-forming and tumor-forming abilities, which was absent in ALDH^{-} cell fractions, when $1x10^5$ cells were applied. Self-renewal ability was assayed by serial spheroid-formation assay in sorted ACHN cells, thereby sphere-forming ability was lost upon passage in ALDH^{-} cell fractions whereas ALDH^{+} cells were able to generated tertiary spheres, albeit reduction of sphere-forming ability was observed over passages. Gene expression analysis revealed higher expression of Twist, c-Myc, BMI-1, HIF-1α, and ABC-transporters ABCB1 and ABCG2 besides ALDH1A1 in ALDH^{+} cell fractions of ACHN cells. No change in expression level of Snail transcription factor was observed.

Chen et al [206] determined the influence of CBFA2T2 expression on the fraction of ALDH^{br} cells in 786-O and A498 cell lines using the ALDEFLUOR^{TM} assay. siRNA treatment against CBFA2T2 reduced the fraction of ALDH^{br} cell from 11 to 2% and 34 to 10% in 786-O and A498 cell line, respectively. The authors also investigated the association of ALDH1A3 expression and clinical outcome in RCC

patients in a database search and found higher levels of ALDH1A3 expression were associated with shorter survival of patients

Wang and Park et al [207] used ALDH expression (ALDEFLUOR™ assay) to isolate CSC from Caki-2 and ACHN cell lines and primary RCC tumor xenografts. The fraction of $ALDH^{br}$ cells ranged from 1% to 13% and was higher in ACHN compared to Caki-2 xenografts. The fraction of $ALDH^{br}$ was observed to be relatively constant over serial transplantation of the cells. For $ALDH^{br}$ and $ALDH^{low}$ fractions tumorigenic potential, growth potential in cell culture and soft agar assay, as well as expression of stemness markers Oct3/4, Nanog and Pax2 were determined and found to be higher in the $ALDH^{br}$ cell fraction of the xenografts. The authors also tested a differentiation therapy approach using BMP-2 to induce osteogenic differentiation of $ALDH^{br}$ fractions and found reduction of expression of stemness markers and up-regulation of osteogenic differentiation markers Runx2 and collagen type I upon BMP-2 treatment. In xenograft experiments they observed highly reduced tumor volume accompanied by bone formation in BMP-2 treated tumors. Showing that differentiation therapy using BMP-2 might be a promising new approach for RCC treatment.

The cell lines investigated in my work showed overall high activity of ALDH, comparable to that seen in the SK-BR-3 breast cancer cell line, which is used as a positive control for the assay. Also expression levels determined by mRNA-Sequencing of PA, SP and A-SP cells revealed similar high expression of the enzyme in all three cell lines. According to the high activity of the enzyme, a relatively low cell number was needed to achieve substrate saturation in the assay. The observed staining intensities in PA cells from first set of experiments and spheroid cell lines SP and CS7 were also high, when compared to ALDH activities reported for other RCC cell lines, being in the range of $ALDH^{br}$ cells of these reports. The differences seen between spheroid cell lines SP and CS7 were only marginal and probably mainly attributed to different cell sizes. The results obtained for PA cells showed high variations between experiments. Though higher observed activity of the enzyme in the first set of experiments might be attributed to the low passage number of cells, which would imply suitability of the assay to enrich for CSC from low passage number of PA cell line, due to the low number of experiments performed with cells at different passage numbers, this cannot be convincingly concluded from the results and further experiments are needed to confirm this hypothesis. Another fact, that has not been addressed in the experiments is dye efflux, which was seen for Rhodamine 123 in PA cells, and might be responsible for differences in results seen in PA cell lines, due to insufficient inhibition of transporters. Thus, further experiments would be needed to address those questions and come to a convincing conclusion regarding the suitability of the assay. From the results obtained so far, and taking also the similar high expression of ALDH1, which was observed in mRNA-Sequencing experiments into account, the assay does not seem to be a very promising method to enrich for CSC from the cell lines investigated.

5.5 AP-Staining and TNAP Expression as Marker for Stem Cells or Differentiated Cells

Alkaline phosphatase (AP) is used as a marker for several cell types. Among the four tissue-specific isoforms of the enzyme, namely intestinal (IAP), germ cell (GCAP), placental (PLAP), and tissue nonspecific alkaline phosphatase (TNAP), the latter is expressed at high levels in liver, bone, and kidney. PLAP and GCAP are expressed in embryonic stem cells. But especially TNAP serves as a

marker for the undifferentiated state of ES cells, and its expression is quickly up-regulated during the process of iPSC generation by transfection with Oct4, Sox2 and Klf4 transcription factors, with expression seeming directly regulated by Oct4/Sox2 transcription factor network. [53 4 46]

Additionally, TNAP serves as an osteoblast marker, where it plays an important role in the mineralization process by degrading pyrophosphate to phosphate, of which the first is an inhibitor and the latter an inductor of bone mineralization. [262 263] Expression during adipogenesis of mesenchymal stem cells, associated with a role in induction of cytoplasmic lipid storage has also been observed, together with characteristic expression of TNAP in lipid storing cell types. [264 265]

TNAP has been identified to be identical to the MSC marker MSCA-1 [339]. Its expression is restricted to the CD271^{high} population of BM-derived MSC and sorting for this marker in combination with CD56 enriches for multipotent cells. Within the MSCA-1-positive cells the CD56 positive subpopulation had no adipogenic differentiation potential, whereas chondrogenic differentiation potential was only seen in this subpopulation, suggesting that MSCA-1 is no suitable marker for immature highly self-renewing multipotent MSC, rather it seems to be expressed on subpopulations with more restricted differentiation potential. [340] A different group sorted cells from the same cell type for TNAP expression only. TNAP-positive cells exhibited low proliferation rates and differentiated predominantly into the osteogenic and adipogenic lineage, whereas TNAP-negative cells possessed 3-lineage differentiating potential, as well as higher expression of pluripotency genes. They found that TNAP expression is correlated with cell size, as well as with culture density and age, being higher in larger cells, at higher cell density and age, accompanied by higher expression of osteogenic markers. They also found no expression of TNAP in UCB-derived MSC, which posses multilineage and high proliferative potential. Also they could not observe a correlation of the varying TNAP expression levels in different donors with donor age or expression of other surface markers of MSC. These results suggest, that TNAP in BM-MSC, in contrast to ESC, is no suitable marker for immature cells, it rather indicates a more heterogeneous restricted progenitor cell type, or even osteogenic committed progenitors. [341]

Expression of TNAP is also observed in tumor cells. For example in prostate carcinoma TNAP expression is higher in mesenchymal than in epithelial cells, and high AP expression is associated with metastatic disease and decreased disease-free survival of patients. The authors found a correlation of AP expression and EMT marker expression (Snail1, E-Cadherin). Additionally, inhibition of AP in prostate cancer cell lines led to induction of MET as well as reduced viability and proliferative potential of the cells. [342]

In the kidney TNAP is expressed mainly in the proximal convoluted tubule (the S1 and S2 segments) but also in the S3 segment [343] and considered a marker for proximal tubular epithelial cell differentiation [73]. Taking into account the proposed origin of RCC from these structures [172], expression of the enzyme might be intrinsic to those cells.

Khan et al [319] tested several RCC cell lines for AP activity and found single AP-positive cells in all tested cell lines, but in CD105-positive sorted cells a higher AP staining pattern was seen, which might be an indicator of TNAP expression being not intrinsic to RCC but rather confined to stem like cells.

Intracellular and extracellular expression of TNAP was assayed by IFC on PA, CS1, CS7 and A-CS cell lines. Thereby low level intracellular, but no extracellular staining was detected on PA cell line and

CS cell lines and adherent counterparts. In contrast, SP cell line showed higher staining intensities for the enzyme in fractions of cells intracellular as well as on the surface, albeit with highly variable results. Histological staining for enzyme activity in adherently grown cells derived of PA, SP and CS cell lines revealed high staining intensities on non-adherent cells growing on top of the monolayer of SP cells, whereas no staining was observed in any of the other tested cell lines. So, alkaline phosphatase was found to be expressed exclusively on fractions of SP cell line. The results obtained by histological staining and IFC were also confirmed in mRNA-Sequencing experiments, where a higher but variable expression level of the enzyme in SP cell line compared to PA cell line was also seen. In these experiments also a higher and variable expression of the enzyme was seen for A-SP cell lines tested. Due to the described expression of alkaline phosphatase not only in ESC, where it serves as a marker for pluripotent state, but also on tubular epithelial cells in the kidney and osteogenic precursor cells it is not clear whether of this scenarios lays behind this observation. On the one hand it might indicate a stem-like phenotype of the cells or the contrary, indicating differentiation of the cells either to tubular or osteogenic lineages.

5.6 Evaluation of Surface Marker Expression

Surface expression of several antigens that are characteristically expressed on MSC, ESC or used as CSC markers was evaluated by flow cytometry on PA cells and three different spheroid cell lines derived thereof (SP, CS1, CS7). Thereby expression of many of the investigated markers was detected on all cell lines tested.

Some markers were only expressed on spheroid cells, whereas other markers showed reduced expression on spheroid cell lines compared to PA. For some of the antigens also changes in expression over long-term culture could be observed. The results are summarized in table 5.6.1 (see also table 4.6.1).

To test whether differences in expression were induced by the different culture conditions, spheroid cell lines were also cultured adherently (A-SP, A-CS) in serum-containing medium and marker expression was evaluated at different time points of adherent culture. For some markers, also changes upon re-culturing of A-SP or A-CS7 cells as spheroids was investigated, showing that many of the observed changes seen in A-SP/CS cells compared to their parental spheroid cells were reversible, when the cells were grown as spheroids again. An overview of these markers and their expression pattern seen in different culture conditions is given in table 5.6.2.

For direct enrichment of possible TIC from the PA cell line, markers have to be identified, which show only weak staining or staining of distinct cell populations on PA cell line and - assuming that spheroid culture enriches for CSC - a more pronounced staining on spheroid cells. As can be seen from table 5.6.1, this prerequisite was met satisfactorily by none of the investigated markers, since markers with higher expression on spheroid cell lines, namely CD10, CD56, CD133, CD184/CXCR7, and CD271, showed incoherent staining patterns on the three spheroid cell lines tested on the one hand, and very low or no expression on PA cells on the other hand.

Antigen	PA			SP			CS7			CS1		
	MW %	Rel GM	Age	MW %	Rel GM	Age	MW %	Rel GM	Age	MW %	Rel GM	Age
CD24	++++	+++	→	++++	+++	→	++++	+++	→	++++	+++	→
CD29	++++	++++	→	++++	++++	→	++++	++++	→	++++	++++	→
SSEA-4	++++	++++	→	++++	++++	→	++++	++++	→	++++	++++	→
SSEA-3	++++	+++	→	++++	+++	→	+++	+++	→	++++	+++	→
TRA-1-81	++++	++++	≈±	++++	++++	≈±	+++	++++	≈±	++++	++++	≈±
CD73	++++	+++	→	++++	++++	→	++++	++++	→	+++	+++	→
EpCAM	++++	++++	→	++++	++++	→	++++	++++	→	+++	++	↓
CD44	++++	++++	→	++++	++++	→	++++	++++	→	++	++	↓
CD49e	+++	++	↑	++++	++	↑	++++	+++	↑	NA	NA	
CD105	+++	++	↑	++	+	≈±	+++	++	≈±	++	+	≈±
CD106	++	(+)	≈±	O	O	↓	O	O		O	O	
CD243	++	+	≈±	(+)	O	≈±	O	O		O	O	
CD15	++	+	↑	O	O	↓	++	+	↓	++	(+)	↓
CD49f	(+)	(+)	→	(+)	(+)	→	++	+	→	(+)	(+)	→
CD56	O	O		(+)	O	↑	++	+	↑	O	O	→
CD184	O	O		(+)	O	↑	+++	++	↑	(+)	(+)	≈±
CD271	O	O		(+)	O	→	(+)	(+)	→	(+)	O	
CD133	O	O		O	O		+	+	↑	+	O	
CXCR7	O	O		O	O		++	+	↑	NA	NA	
CD10	O	O		++	(+)	≈±	O	O		O	O	
TNAP	O	O		(+)	O		O	O		NA	NA	

Symbol	% Positive
O	0-5
(+)	5-10
+	10-20
++	20-50
+++	50-80
++++	80-100
NA	not determined

Symbol	Relative GM
O	0-1.5
(+)	1.5-2.5
+	2.5-5
++	5-15
+++	15-30
++++	30-100
++++	>100

≈±	highly variable
↑	up
↓	down
→	no difference

Table 5.6.1: Overview of Expression Levels of All Investigated Extracellular Antigens

Summary of results obtained for IFC staining of different cell lines for expression of various surface expressed antigens. Expression level was graded according to criteria listed in the legend using mean values of all performed measurements.
CS: clonally expanded spheroid cells derived from PA (CS1 and CS7), IFC: flow cytometric immunophenotyping, MW: mean value, PA: parental cell line, Rel GM: relative fluorescence intensity = geo mean value sample/geo mean value isotype control, SP: spheroid cells derived from PA

CD No.	Antigen Name	Expression (% Positive)			SP/CS vs PA	Medium	
		PA	SP	CS		ACC	SCC
CD56	NCAM	O	(+)	+/O	↑	↓	↑
CD184	CXCR4	O	(+)	+	↑	↓	
CXCR7	CXCR7	O	O	+	↑ CS7	↓	
CD146	MCAM	+	O	O	↓	↑	↓
CD106	VCAM-1	+	O	O	↓	↑	↓
CD15	SSEA-1	+	O	+	↓SP	↑	↓
CD243	MDR1/ABCB1	+	(+)	O	↓SP	↑	↓

Symbol	
O	less than 5% positive cells
(+)	less than 10 % positive cells
+	more than 10% positive cells
+/O	variying
↑	up
↓	down

Table 5.6.2: Overview of Markers Showing Variations in Cells Cultured under ACC or SCC

Summary of results obtained for IFC staining of different cell lines for expression of surface markers, for which differences in staining pattern were seen in cells cultured under ACC or SCC conditions. Expression level was graded according to criteria listed in the legend using mean values of all performed measurements.
ACC: adherent culture conditions, CS: clonally expanded spheroid cells derived from PA (CS1 and CS7), IFC: flow cytometric immunophenotyping, PA: parental cell line, SCC: spheroid culture conditions, SP: spheroid cells derived from PA

The surface markers evaluated in this work are discussed in detail in the following sections.

5.6.1 Epithelial Cell Adhesion Molecule (EpCAM)

EpCAM (epithelial cell adhesion molecule) is a single span trans membrane glycoprotein, with no structural relationship to the four typical CAM-families and besides functioning as adhesion molecule it also functions in cell signaling, proliferation and migration. In most carcinomas of various origins (e.g. mesodermal, ectodermal, neurogenic, melanoma) EpCAM expression correlates with tumor aggressiveness and reduced survival, whereas in RCC and thyroid cancer EpCAM expression is correlated with increased life expectancy. EpCAM expression in the healthy adult is restricted to simple epithelial cells, whereas high expression of this molecule on rapidly proliferating tumors of epithelial origin has lead to its wide use as cancer marker.

During embryonic development EpCAM is expressed in embryonic stem cells and EpCAM expression is also induced during kidney development. EpCAM expression is reduced with further differentiation of the epithelia to their functional state, with epithelial progenitor cells in the intestine, liver or skin expressing EpCAM while differentiated cells such as hepatocytes or keratinocytes are EpCAM negative. EpCAM is typically present in tissues with a high number of proliferating cells, whereas EpCAM expression is low in differentiated cells, and absent in lymphoid or bone-marrow derived, as well as mesenchymal, muscular, and neuroendocrine tissues. Expression of EpCAM has been shown to be up-regulated during inflammatory response and contrary has been shown to be down regulated by TNF-α signaling via NF-κB mediated regulation of EpCAM promoter. Also p53 has been described as EpCAM repressor, whereas β-catenin activation via binding of TCF/Lef induces expression of EpCAM. EpCAM is involved in homophilic adhesion, but compared to E-Cadherin homophilic EpCAM adhesion is weaker. By disturbing the E-Cadherin cytoskeletal interactions, EpCAM when co-expressed with E-Cadherin also weakens intracellular adhesions. EpCAM signaling involves intracellular proteolytic cleavage of EpICD by TACE/γ-Secretase, and following association with β-catenin and FHL2 followed by LEF1-binding leading to transcriptional activation of target genes, resembling canonical wnt signaling pathway. The cell proliferation inducing genes c-Myc and cyclin D1 are known target genes of EpCAM. [344] [345] [346]

EpCAM expression has been found to be as suitable marker for CSC in colorectal carcinoma (CRC), hepatocellular carcinoma (HCC), pancreatic cancer (PanC) and gallbladder carcinoma (GBC). [147]

In normal breast tissue, EpCAM staining discriminates the stem cell ($EpCAM^-$) and luminal progenitor-like fractions ($EpCAM^+$) in $CD49f^+$ sorted progenitor-like cells. [347] [348] In a study performed by Keller et al [349] $EpCAM^+$ as a marker for the luminal cell fraction was confirmed, and the basal $EpCAM^{Low}$ cell fraction was shown to be marked by CD10 expression, which was not expressed on the luminal $EpCAM^+$ fraction. In this study $EpCAM^+$ cells showed higher sphere-forming ability than $EpCAM^-$ cells, which were observed to have a higher tendency to grow adherently and form lesser but more compact spheres. In contrast, in the study performed by Bachelard-Cascales et al [350] $EpCAM^+$ cells showed reduced sphere-forming efficiency compared to the $CD10^+/EpCAM^-$ subpopulation of $CD49f^+$ normal mammary cells.

Metsuyanim et al [351] evaluated expression of EpCAM in fetal and adult kidney and found EpCAM expression is absent from the metanephric mesenchyme (MM) and increases with nephron

differentiation, with 80% of the cells showing positive staining for EpCAM in IFC analysis in the adult kidney, therefore EpCAM$^{low/dim}$ cells may represent putative renal progenitor cells.

Expression of EpCAM in normal kidney and RCC using TMA was investigated by Seligson et al [352]. They report consistent EpCAM expression in the distal nephron on normal renal epithelium and a difference between ccRCC, which showed only minimal and infrequent EpCAM staining, with only 10% of ccRCC showed staining of EpCAM in >50% of the cells. In contrast, chromophobe and collecting duct RCC showed intense and frequent EpCAM staining patterns. In this study EpCAM expression has been found to be an independent predictor associated with improved patient survival. The results were confirmed by a more recent study performed by Zimpfer et al [353], who found ≈ 80% positive staining cases for papillary and chromophobe RCC, and ≈40% positive staining cases in ccRCC, oncocytomas and unclassified tumors. Additionally, they found EpCAM overexpression as independent marker for longer progression-free survival in all RCC entities. IHC analysis preformed by Liu et al [354], comparing expression of EpCAM on different RCC subtypes, also found high staining intensities in all cases of chromophobe RCC, whereas in oncocytomas a different staining pattern as well as lower overall staining was observed. In RCC 33% showed positive staining for EpCAM, which was almost equally distributed among low, moderate and high staining intensities.

In a comparison of mRNA expression of matched normal and RCC samples by NGS performed by Landolt et al [355], EpCAM mRNA was found to be expressed at lower levels in tumor tissue compared to normal tissues. In a study performed by Hasmin et al [356] xenograft propagation of primary tumor cells was used to evaluate stem cell characteristics by sorting xenograft tumors generated from a primary RCC cell line according to different criteria. Thereby EpCAM expression seemed to evolve over serial transplantation of tumors and was seen in CD133^{+} sorted xenograft cells at significantly higher level than in the CD133^{-} fraction, which showed growth advantage over CD133^{+} cells and higher tumor forming ability. EpCAM expression for RCC cell lines ACHN and KRC/Y has been shown by Ueda et al [205] by IFC, with both cell lines showing high uniform staining for EpCAM.

Expression of EpCAM was evaluated on all cell lines in my work by IFC and was found to be constantly and uniformly high in PA, SP, CS7 cell lines and adherent counterparts of these cell lines. The high expression of EpCAM in the investigated cell lines might be on the one hand an indicator for a less aggressive tumor variant of origin of the cell line, since in RCC EpCAM seems to be correlated with better patients prognosis in RCC. But on the other hand, due to the various factors influencing expression and function of EpCAM, and for example similar expression as seen on the cell lines investigated here also on the highly tumorigenic ACHN RCC cell line, might also indicate a more aggressive phenotype of the cells.

CS1 cell line differed from all other cell lines investigated here in EpCAM expression characteristic. The cell line showed a broader distribution of staining intensities and reduction of EpCAM positive staining cells over time in culture under SCC, whereas no changes in EpCAM expression were seen over long-term culture under ACC. It might be interesting to further investigate the mechanism responsible for this behavior, and whether the EpCAM^{-} cell fraction possesses different stem cell characteristics.

5.6.2 CD24

CD24 is a glycosylated single chain protein, which is bound by GPI anchor to the extracellular membrane. CD24 was primarily detected on B-Cells and used as a B-Cell marker, later expression was also found on keratinocytes and renal tubules and seems to be a P-selectin ligand expressed on activated endothelia, thus may be involved in transmigration of the cells and metastasis. In several cancers CD24 expression has been associated with a more aggressive behavior. [357]

CD24 is used as a positive marker for CSC from gastric cancer and colon cancer, whereas low or negative staining marks CSC from breast and prostate in combination with CD44 positive staining. [358] [359] Although, in breast cancer cell lines CD24 expression is used to distinguish mesenchymal ($CD44^{Hi}/CD24^{Lo}$) and the metastable hybrid EMT phenotypes ($CD44^{Hi}/CD24^{Hi}$) within different cell lines and it has been shown that the latter possesses higher CSC potential and drug tolerance. [360] Similar results were obtained by Hsieh et al [318] from a $CD44^{Hi}$/CD24 sorted sarcomatoid RCC cell line RCC52, where $CD24^{Dim}$ and $CD24^{Hi}$ cells showed different morphology, expression and growth characteristics. $CD24^{Dim}$ cells were of epithelioid morphology and expressed E-Cadherin. Compared to $CD24^{Hi}$ cells they showed faster *in vitro* growth kinetics and higher growth potential in soft agar assay. $CD24^{Hi}$ cells in contrast, were of fibroblastoid morphology and no expression of E-Cadherin was observed in this cell fraction. Additionally, the $CD24^{Hi}$ cell population showed increased expression of Notch1 and Oct4 as well as increased migration and invasion and tumor-forming ability, indicated by higher tumor volume, compared to unsorted and $CD24^{Dim}$ cells.

In the ovarian cancer cell line Caov-3 after induction of EMT via TGF-β treatment or hypoxic conditions, besides reduced expression of E-Cadherin and induction of Snail, also induction of CD24 expression was seen. Overexpression of CD24 in this cell lines resulted in similar changes as were seen after EMT-induction by TGF-β or hypoxia, further supporting the role of this molecule in EMT. The authors also report increased chemo-resistance and growth potential in normal culture, soft agar and tumor-formation assay of CD24 overexpressing cells. [358]

Grasz et al [361] investigated the role of CD24/CD44 expression on intestinal epithelial stem cells (IESC) based on $EpCAM^+$ sorting and found that $CD24^+/CD44^+$ and $CD24^-/CD44^+$ in contrast to $CD24^-/CD44^-$ and $CD24^+/CD44^-$ represent the stem cell fraction, albeit $CD24^+/CD44^+$ cells showed growth restrictions under normal culture conditions, but could be propagated in co-culture with myofibroblast, albeit at lower rates. Both populations possessed multipotent differentiating potential to enteroendocrine, goblet and Paneth cells as well as absorptive enterocytes. Although the $CD24^+$ stem cell fraction according to this report seemed to have reduced potential compared to $CD24^-$ cells, $CD24^+$ cells from CRC have been shown to possess CSC characteristics, when isolated in combination CD29 as $CD24^+/CD29^+$ co-expressing cell fraction. [147] Similar to results for ovarian cancer, also in CRC cell lines, a connection between CD24 expression and EMT has been shown by Okano et al [362]. Sorted $N\text{-Cadherin}^+/CD24^+$ EMT induced cells showed higher expression of Notch1 and other stemness markers and higher tumor-forming ability compared to $CD24^-$ cell fractions. Also $CD24^+$ cells were more prone than their negative counterparts to further TGF-β stimulation. In contrast in esophageal cancer, the CSC population seemed to be $CD44^+/CD24^-$ [147]

In the study performed by Metsuyanim et al [351] $CD24^+$ and $CD133^+$ as well as $CD24^+/CD133^+$ cells comprise more than 50% of human fetal kidney cells, which also show to be $EpCAM^{bright}$, indicating that these molecules do not mark progenitor cell-like phenotypes in the kidney but rather are markers of differentiation. In contrast to that finding, Challen et al [363] by investigating differential gene expression in metanephric mesenchyme and intermediate mesoderm using microarray analysis, found CD24 strongly and specifically expressed in the uninduced metanephric mesenchyme, implying that CD24 may be a useful marker for renal progenitor cell population.

In the Bowman's capsule different subsets of adult regenerating cells could be discriminated by their expression of CD133 and CD24, with $C133^+/CD24^+$ localized to the urinary pole are able to differentiate to tubular cells and podocytes, whereas cell with additional expression of the podocyte marker PDX, localized to between urinary and vascular pole are able of podocyte generation only. Differentiation potential is restricted to $C133^+/CD24^+$ subsets, whereas $C133^-/CD24^-$ cells display phenotypic features of podocytes. [77] Also renal progenitors isolated according to their characteristic expression of CD133 from tubular parts of the cortex and papillae showed positive staining for CD24. [351 73 75 74 76] But also $CD133^-$ mesenchymal like renal progenitor cells, which were isolated from the Bowman's capsule by Bussolati et al [322] were shown to express CD24, whereas BM-MSC did not show expression of the marker. Together with expression of the renal stem cell marker Pax2 this indicated a different origin of the renal progenitors, and implies that CD24 might be a more robust marker than CD133 for renal adult stem cells.

CD24 expression assayed by IHC showed positive staining in 786-O, SMKT-R2 and to a lesser extent in ACHN cell lines, whereas no staining was observed in 786-P, Caki-1 and -2 cell lines and $CD105^+$ sorted cells from ACHN and Caki-2. [319] In contrast to this in Caki-2 cell line Jaggupilli [357] found CD24 positive staining on 55% of cells using flow cytometry. Expression of CD24 by IFC was also evaluated by Xiao et al [203] in ACHN and Caki-1 cell lines, where they report high expression of the molecule on 12% and 6% of the cells, respectively. Sorting for $CD133^+/CD24^+$ cells from these cell lines enriched for cells with CSC characteristics, such as enhanced sphere-forming and tumor-inducing ability, chemo-resistance and increased expression of mRNA for stem cell markers Oct4 and Klf4 as well as ABCB1/MDR1 when compared to $CD133^-/CD24^-$ negative cell fractions.

IFC staining of six different cell lines representing histological RCC subtypes performed by Hsieh et al [318] showed moderate to high CD24 staining in clear cell RCC, chromophobe and papillary RCC, whereas only a small subset of cells stained positive in the sarcomatoid RCC52 cell line investigated.

Zhong et al [211] similar to experiments performed in my work did not detect any difference in CD24 expression between spheroids and adherent counterparts of SK-RC-42 RCC cell line.

CD24 expression was investigated using IFC also by Lichner et al [212] on ACHN and Caki-1 RCC cell lines grown either adherently or as spheroids. Thereby only low fractions of ACHN (2%) and Caki-1 (0.5%) adherently grown cells expressed the molecule at low level, whereas spheroids derived of this cell lines showed expression of the molecule in similar fractions of 10% of the cells.

The cell lines investigated in my work in contrast to most reports for other RCC cell lines, but in accordance with reports for the RCC cell lines from different origins investigated by Hsieh et al [318] showed similar high staining for CD24 in IFC experiments, thus resembling progenitor cells isolated

from adult human kidneys. Also no difference was observed in expression levels between adherently grown cells or spheroid cell lines. Although, a slight difference was seen in RNA-Sequencing experiments where SP cell line showed slightly reduced mRNA expression values compared to adherently grown cells (PA and A-SP), which might imply additional regulatory mechanisms involved at the post-transcriptional level for the surface expression of the molecule.

5.6.3 Hyaluronate Receptor (CD44)

CD44 (Hyaluronate Receptor) is a trans membrane glycoprotein of which several isoforms exist. Generally it acts as specific receptor of hyaluronic acid. By binding ECM components such as collagen, fibronectin, laminin and chondroitin sulfate, it functions in cell-matrix interactions. But it has also functional roles in cell-cell interactions and participates in lymphocyte activation, recirculation and homing. CD44 also binds osteopontin, which serves as cytokine inducing up-regulation of IFN-γ and IL-12 as well as in attachment of osteoclasts to mineralized bone matrix as well as in cancer cell migration. By interaction with neighboring receptors it is involved in various signaling cascades and also signaling via cleavage of ICD and transcriptional activation of genes that are involved in cell survival during stress, inflammation, oxidative glycolysis, tumor invasion (Notch1, MMP9, RANKL) has been described for CD44. CD44 in its different isoforms is expressed in almost all normal and on most cancer cells. [357] [364]

CD44 expression is a characteristic feature of many CSC from various tissue origins including breast, pancreas, gastric, prostate, head and neck, ovarian, and colon. [359]

In breast cancer, CD44 in combination with CD24 has been found a suitable marker for CSC. CD44 is expressed on mesenchymal and epithelial subsets respectively, which are distinguished by their expression of CD24. [360]

On intestinal epithelial stem cells (IESC) isolated based on $EpCAM^+$ sorting, Grasz et al [361] identified $CD24^+/CD44^+$ and $CD24^-/CD44^+$ in contrast to $CD24^-/CD44^-$ and $CD24^+/CD44^-$ as the fractions with stem cell characteristic, indicating CD44 as marker for progenitor cells in the gut.

In accordance with these findings, EpCAM and CD44 have been found to be the most robust markers for CSC in CRC. Similarly expression of CD44 in combination with other markers has been found to enrich CSC from gastric cancer ($CD44^+/CD54^+$), HCC ($CD90^+/CD44^+$) and esophageal cancer ($CD44^+/CD24^-$). [147]

A meta-analysis performed by Cheng et al [365] found CD44 over expression correlated with worse patient prognosis in RCC. The study by Hsieh et al [318] using IFC staining of six cell lines representing different histological RCC subtypes showed positive CD44 staining in all tested cell lines. And similar results were obtained by Khan et al [319] in $CD105^+$ sorted ACHN and Caki-2 cell lines. Also Zhong et al [211] found similar staining for CD44 in spheroids and adherent counterparts of SK-RC-42 RCC cell line. Expression of CD44 on ACHN and Caki-1 RCC was also investigated by Lichner et al [212] using IFC and was found to be expressed in both cell lines at similar high levels, also no difference in expression was observed when both cell lines were grown as spheroids.

In contrast to this, some studies call the use of CD44 as a suitable marker for pluripotent stem cells into question and imply that CD44 expression is correlated with a more mature progenitor like phenotype. For example during generation of iPSC from fibroblast cells, CD44 expression is gradually

lost resulting in CD44 absence in fully reprogrammed cells. CD44 expression in contrast to other pluripotency markers such as alkaline phosphatase or SSEA-3/4, TRA-1-60/-1-81 may serve as a differentiation marker between fully reprogrammed and partially reprogrammed cells. [366]

In a study on several cancer cell lines, CD44 was not co-expressed with the pluripotency marker SSEA-4 but enrichment of CD44 was seen in the SSEA-4$^-$ cell fraction. In sorted xenograft tumor cells of DU145 prostate cancer cell line, the highest tumorigenicity was seen in SSEA-4$^+$/CD44$^-$ cell fraction whereas SSEA-4$^-$/CD44$^+$ fraction showed lowest tumorigenic potential [367], further supporting the idea that CD44 is a negative marker for pluripotent stem cells.

CD44 expression is described for most cultured MSC. But Qian et al [368] found that CD44 was induced during *in vitro* culture of the cells, whereas primary multipotent high proliferative MSC from bone marrow reside in the CD44$^-$ cell population.

The cell lines investigated in my work similar to reports for other RCC cell lines, showed high staining in IFC experiments, and no differences were seen in expression levels between adherently grown cells and spheroid cell lines SP and CS7. Although, slight differences were seen in mRNA-Sequencing experiments, where SP and A-SP cells showed slightly reduced expression levels of CD44 mRNA compared to PA cell line, but these differences were within experimental errors. In contrast, the CS1 cell line showed variations of CD44 expression over long-term culture of the cell line under SCC, which were not observed when the cells were cultured for long-term under ACC. This is especially interesting in the light of reports by Quintanilla et al [366], who found reduction of CD44 expression during the reprogramming process of fibroblasts to fully reprogrammed iPSC and might indicate similar processes taking place in the CS1 cell line over long-term culture under SCC. Though, similar changes in this cell line were only observed for EpCAM expression but neither in expression of other pluripotency markers such as SSEA-3/4 or TRA-1-81. But since these markers showed a broad staining distribution in CS1 cell line, a sorting strategy for SSEA-4$^+$/CD44$^-$ as used by Sivasubramaniyan et al. [367] might be a possible and interesting approach for this cell line for enrichment of cells of a more immature phenotype.

5.6.4 Ecto-5'-Nucleotidase (CD73)

CD73 (Ecto-5'-Nucleotidase) serves as one of the defining markers for MSC. [25] The ecto-enzyme activity produces extracellular adenosine, which serves as ligand for adenosine receptor signaling. Besides its enzymatic functions, CD73 participates in invasive properties of cancer cells due to its adhesive quality, by which it regulates cell interactions with extracellular matrix components, such as laminin and fibronectin. Overexpression of CD73 has been reported for several tumor entities, accompanied by functional involvement of the molecule in angiogenesis, drug-resistance, and cell proliferation and survival. [369] Also CD73 enzyme activity was found to limit antitumor T cell immunity. [370] CD73 expression on tumor cells has been shown to be regulated by a variety of signals of which thyroid hormone signaling, hypoxic conditions and IFN-α and IFN-β have been shown to up-regulate CD73 expression, whereas estrogen receptor signaling, IFN-γ, and glutamate were found to down regulate CD73 expression [369].

CD73 expression has also been reported on renal progenitor cells, which were obtained from different portions of the human kidney by using CD133$^+$ and CD133$^+$/CD24$^+$ sorting strategy, respectively. [76] [72]

Also, expression of CD73, but not of the mesenchymal markers CD90 and CD105, was observed by Galleggiante et al [202] in cells with progenitor characteristics and differentiation potential toward adipogenic, osteogenic and epithelial lineage, enriched by a $CD133^+/CD24^+$ sorting strategy from healthy and tumorous tissue of resected kidneys from RCC patients.

In a study performed by Song et al [210] with CSC from primary RCC tissues and the 786-O RCC cell line, high expression of CD73 was found to be a marker for CSC. In this study higher expression of CD73 was observed on spheroids compared to their adherently grown counterparts. Sorting for CD73 expression resulted in enrichment of cells with sphere-forming ability, higher expression of Oct3/4, and higher resistance to radiation and mitomycin treatment. Tumor forming ability in NOD/SICD mice was restricted to cells with high expression levels of CD73 (tumor formation in 5 of 5 mice at injected doses of $5x10^2$ cells). The functional involvement of CD73 in this process was shown by shRNA knockdown of 73, which drastically reduced tumor formation of the cells, compared to control shRNA treated cells. The authors also found a correlation of CD73 expression with ccRCC progression using TMA staining of RCC and normal renal tissues.

Expression of CD73 was investigated by IFC on PA, SP and CS cell lines (CS1 and CS7). High uniform staining for CD73 was observed on all cell lines tested. Thereby a higher staining intensity was seen in SP cell line compared to all other assayed cell lines, with CS cell lines showing a broader distribution of staining compared to PA and SP cell lines, indicating a more heterogeneous nature of these cell lines with respect to CD73 expression, containing high and low staining fractions. The results for SP cell line are in the light of results obtained by Song et al [210] imply a higher CSC status of this cell line compared CS cell lines and especially to PA cell line.

5.6.5 Endoglin (CD105)

Endoglin (CD105) is a cell membrane glycoprotein, that is predominantly expressed on endothelial cells with elevated expression in activated endothelial cells [371]. Its expression in endothelial cells is up-regulated at low O_2 concentrations by HIF-1 in cooperation with TGF-β1 [372]. Endoglin is a co-receptor of TGF-β-Receptor I/II complexes, where it modulates TGF-β signaling. [373]

In addition, CD105 serves as one of the defining positive markers for MSC [25]. MSC are uniformly strongly positive for CD105 staining, regardless of passage number [374]. Gharibi et al [329] observed that CD105 expression was significantly reduced following osteogenic and adipogenic differentiation of the cells. They also investigated the influence of medium supplementation with several growth factors and found a slight reduction of CD105 expression upon addition bFGF. Qian et al [368] found higher expression of CD105 in *in vitro* cultured BM-MSC compared to freshly isolated cells.

Expression of CD105 was also found on progenitor cells isolated from human kidney by use of $CD133^+$ sorting strategy in the parietal epithelial layer of the Bowman's capsule [73]. But also $CD133^-$ mesenchymal like renal progenitor cells, which were isolated from the Bowman's capsule by Bussolati et al [322] were shown to express CD105.

In contrast, $CD133^+$ renal progenitor cells from the normal portion of human renal cortex lacked expression of CD105, but rather expression was induced under endothelial or epithelial differentiation conditions [72]. Also cells isolated from papillary region of renal pyramid by the same group [71] were reported to express CD105 at low level only on a subset of the cells.

Despite its varying expression on renal progenitor cells, Bussolati et al [78] identified CD105 as possible marker for isolation of CSC from primary RCC tumors (see chapter 1.6). Primary $CD105^+$ CSC were used to evaluate IL-15 differentiation therapy by Azzi et al [119], thereby confirming the results of Bussolati concerning CSC features of this subpopulation. Additionally, the authors investigated further functional stem cell characteristics, namely side population as well as ALDH expression. The sorted cells displayed uniform ALDH expression, and a side population was visible. Both features were lost after differentiation of the cells. No change in expression of stem cell markers was observed for more than 50 passages when cells were cultured in multipotent adult progenitor cell medium consisting of DMEM-LG containing 5% FCS medium supplemented with ITS, 10^9 M dexamethasone, and 10 ng/mL EGF. Transferring the cells to RPMI medium with higher glucose content and 10% FCS instead of the other supplements, induced epithelial differentiation, as marked by Pan-CK expression and expression of E-Cadherin, which were not detected in undifferentiated cells. Differentiation of the cells could also be induced by addition of IL-15 to the medium. This resulted in gradual loss of expression of CD105 and stem cell markers POU5F1/Oct4, Nestin and Nanog within 4 weeks. Sphere-forming efficiency of the sorted cells was reported to be 40% as observed already by Bussolati et al [78] and was reduced after differentiation of the cells.

Hu et al [200] observed similar changes in $CD105^+$ sorted xenograft tumors generated from ACHN $CD105^+$ sorted cells. When the cells were cultured in standard RMPI-1640 medium instead of the expansion medium used by Bussolati [78], positive immunohistochemical staining for CK7 was seen, which was week/absent in parental and $CD105^+$ sorted cells. In contrast, staining for the EMT marker vimentin was observed in $CD105^+$ sorted cells only but not in the parental cells. The expression of vimentin was lost upon standard culture of the cells. Similar results were obtained for Oct4, and Sox2, also CXCR4 and Nanog mRNA levels were down regulated under standard conditions.

The expression of CD105 in several RCC cell lines was investigated by Khan et al [319]. CD105 expression was detected by IHC and weak staining was observed in 786-O/P, ACHN, Caki-1 and SMKT-R2 cell lines, whereas Caki-2 cell line showed strong staining pattern for CD105. They sorted CD105-positive cells from ACHN (4% of total cells) and Caki-2 (3% of total cells) cell lines and investigated CSC characteristics as well as gene expression profiles of the cells. Of note is that they report a loss of CD105 expression in more than 50% of sorted cells upon standard culture conditions, being in accordance with a balance between stem cell self-renewal and differentiation. CD24 expression was not detected on $CD105^+$ sorted cells, but almost all cells expressed MSC markers CD90 and CD73. CD146 and CD44 were expressed only by subpopulations of the cells. CD105 expression on KRC/Y RCC cell line has been investigated by Ueda et al [205] using flow cytometry. The cells showed low expression of CD105 in 5% of non-side population cells, whereas the fraction of positive staining cells was found to be higher (25%) in cells sorted for the side population characteristic.

A study performed by Matak et al [199] on the expression of CD105 on different renal cancer cell lines confirmed high expression of CD105 on Caki-2 cell line, which was comparable to the expression seen on PA cells. Similar expression was seen on the cell line SMKT-R2. Other tested cell lines were either negative (769-P, RCC6) or showed only weak expression of CD105 (ACHN, 786-O). The

normal renal embryonic cell line ASE displayed a median expression level of CD105. Sphere-forming ability was tested and was only seen in Caki-2 and ACHN cell lines. The same was true for expression of Oct4 and Sox2 stem cell markers, which was higher in Caki-2 cells compared to ACHN cells. Thereby Sox2 expression of Caki-2 cell was comparable to that of ASE cell line, whereas Oct4 expression was about 40% of that seen in the embryonic cell line. In ACHN, the expression of stem cell markers as well as of CD105 could be induced under hypoxic conditions. In this study CD105 expression as well as Oct4 and Sox2 expression at mRNA level were shown to be up-regulated by hypoxic conditions in the ACHN cell line. Hsieh et al [318] investigated CD105 expression on the sarcomatoid cell line RCC52 in parental, $CD44^{Hi}/CD24^{Dim}$ and $CD44^{Hi}/CD24^{Hi}$ sorted cells, of which the latter showed increased tumorigenicity as well as a more mesenchymal phenotype compared to parental and $CD24^{Dim}$ cell fraction and found similar expression levels of CD105 in all three cell fractions comprising 3-5% positive staining cells.

Zhang et al [201] reported a frequency of 8.3 ± 1.3% $CD105^{+}$ cells in the A498 RCC cell line, and of 4.9 ± 1.7% in the SK-RC-39 cell line. They observed sphere-formation ability only in the $CD105^{+}$ cells while $CD105^{-}$ cells did not survive in the serum free medium. According to the proposed stem cell characteristics of $CD105^{+}$ cells, they formed tumors in BALB/c nude mice at lower cell concentrations compared to $CD105^{-}$ cells. Additionally, significantly higher expression of the established stem cell markers Sox2, Nanog, c-Myc, and Klf4 was observed in $CD105^{+}$ cells of both cell lines compared to $CD105^{-}$ cells using IHC staining.

In the ACHN cell line Hu et al [200] recently reported reduced sphere-formation ability, expression of stemness markers (Oct4, Sox2, Nanog, Klf4), CSC-marker CXCR4, accelerated senescence *in vitro* as well as reduced tumorigenicity of the cells upon knockdown of CD105. This is further supporting the evidence of CD105 being an important molecule and marker of CSC in RCC.

Another cell line which seems to express relatively high levels of CD105 was the SK-RC-42 cell line, which was analyzed by Addla et al [330] for sphere-forming ability and side population characteristics. Interestingly CD105 expression detected by IFC was lower in spheroids compared to adherently cultured cells, which has also been observed for SP and CS cells derived from PA in my experiments. Similar results were obtained by Zhong et al [211] on spheroids and adherent counterparts of SK-RC-42 RCC cell line and by Gassenmaier et al [204] with SK-RC-17 cell line, which both showed similar high expression of CD105 as PA cell line, and also similar reduction of CD105 expression in spheroid derivatives. The line RCC-26 investigated by this group [204] expressed CD105 in a minor fraction of cells and reduction of CD105 expression was also seen after spheroid culture. In both cell lines, CD105 expression was regained after adherent culture of the spheroids. In contrast, the RCC-56 cell line, also investigated by Gassenmaier et al [204], did not show expression of CD105. Since RCC-56 cell line compared to RCC-26 cell line seemed to contain a higher fraction of CSC, CD105 was not correlated with the stem cell characteristics of these cell lines.

In contrast to the conclusion that might be drawn from several of the above studies highlighting CD105 as an important molecule and marker of CSC in RCC, in a TMA screen of 210 patients performed by Sandlund et al [375] no up-regulation of CD105 in higher tumor stage or grade could be observed. In contrary, patients with high CD105 expression were found to have a more favorable prognosis than

patients with low CD105 expression. Although, in a more recent TMA-study performed by Zanjani et al [376] a correlation of tumor grade and stage as well as overall survival with higher tumor cytoplasmic and vascular CD105 expression was observed for clear cell type of RCC.

As can be seen from the above mentioned studies, although CD105 might mark CSC in some cell lines, it does not necessarily indicated CSC characteristics in others.

The PA cell line used for my experiments uniformly expressed CD105 on all cells resembling Caki-2 SK-RC-17 and SK-RC-42 cell lines in this respect. Therefore a similar sorting strategy for enrichment of possible CSC with this marker as was used in the cited studies from this cell line was not applicable. Remarkably, in contrast to reports from Azzi et al [119] and Hu et al [200], who found reduction or loss of CD105 expression upon culture of cells in standard serum containing medium instead of growth factor containing expansion medium, here a reduction of CD105 expression in spheroid cells grown in serum-free growth factor containing medium compared to cells cultured under standard ACC was seen, which was also observed by Addla et al [330] and Zhong et al [211] for SK-RC-42 cell line and Gassenmaier et al [204] for SK-RC-17 cell line. A reduced expression of CD105 mRNA on SP cells and also on A-SP cells compared to PA cell line was also detected by RNA-Sequencing. Interestingly, CS cell lines seemed both to contain cell populations with low or no expression of CD105, which under spheroid culture conditions increased over long-term culture. Since both cell lines showed evolvement of this populations repeatedly, this seems to be a functional characteristic of the cell lines, which might be interesting for further investigations of the mechanisms underlying this changes. Also the basis for variations seen in expression of CD105 on SP cell line under ACC or SCC culture conditions might be interesting for further understanding of the role of CD105 in RCC.

In their study Zhang et al [201] used $CD105^+$ sorted and unsorted cells to test a possible immunotherapeutic strategy against CSC by priming dendritic cells (DC) *in vitro* with cell lysates. When using $CD105^+$ cell lysates for priming of DC, activated specific T cells, as well as antibodies against $CD105^+$ CSC were observed. In cell lysis assays a specific lysis of $CD105^+$ cells was observed by cytotoxic T cells (CTL) that were activated by incubation with $CD105^+$-primed DC. For *in vivo* assay, differently activated CTL together with unsorted tumor cells were injected into nude mice. When using $CD105^+$ cell lysates for priming of CTL, a considerable reduction of tumor volume as well as a reduction of $CD105^+$ cell content of formed tumors compared to CTLs stimulated by DCs that were primed with unsorted or $CD105^-$ cell lysates, was observed for both cell lines. The study shows that targeting CSC directly in immunotherapeutic approaches is even more effective than using unsorted tumor cells, although the fraction of $CD105^+$ CSC in the formed tumors comprises only about 10% of the cells. Thus the expression pattern of CD105 on the cell line investigated might be an indicator of stem cell phenotype and may render the cell line especially useful for therapeutic vaccination as in the vaccine MGN1601. [182]

5.6.6 Multi Drug Resistance Protein 1 (MDR1/CD243/ABCB1/P-Glycoprotein)

The multi drug resistance protein 1 (MDR1), which is also named P-Glycoprotein, ABCB1 and CD243, is a member of the large and diverse ABC-family of ATP-driven membrane pumps. The endogenous substrates of the transporter are steroids, lipids, bilirubin, bile acids, and platelet activating factor, but it has also been found to be fundamentally involved in chemo resistance of cancer cells by its

detoxifying transport activity for several exogenous substances used for chemotherapy of cancer. MDR1 is normally expressed in small intestine, liver, kidney, placenta, and blood brain barrier but high expression is also found in stem cells of diverse origin. The detoxifying activity of MDR1 is one of the major components responsible for the side population assay (see chapter 5.3), which has been used to enrich for adult stem cells and CSC, respectively. Several pathways involved in stem cell and cancer signaling, including Hedgehog, PI3K/Akt, and NF-κB, as well as p53 and ERBB2 have been shown also to regulate expression of ABCB1 in different cancer cell lines. HIF-driven or pVHL-dependent up-regulation of ABCB1 expression has also been observed. [162] [163]

In kidney CSC PKCε was shown to directly regulate ABCB1 expression. [331] In rat proximal tubular epithelial cells ABCB1 expression has been shown to be up-regulated by exposure to TNF-α via TLR4 activation and NF-κB nuclear translocation [377].

Boysen et al [378] by investigating expression of glycoproteins using SILAC, identified ABCB1, among others, as important discriminator between pRCC and ccRCC, with ABCB1 expression marking ccRCC. Using ABCB1 expression for hierarchical clustering gave similar accurate results for identification of ccRCC to CD10.

As described in chapter 5.3 ABCB1 in human kidney cells and RCC cell lines seems to be fundamentally involved in conveying the HSP phenotype. [330] [331] [205]

In accordance with the described expression of MDR1 on ccRCC, expression of CD243 (MDR1) was detected in the PA cell line by flow cytometric immunophenotyping, though at low to moderate and varying level. The transporter was also found to be involved in the dye efflux, which was seen in this cell line in RSPA. Surprisingly, expression of CD243 assayed by flow cytometric immunophenotyping of spheroid cells was found only on a small subset of cells (SP) or was even absent (CS). Those cells did not show relevant functionality of the transporter in RSPA. After re-culturing spheroid cell lines in serum-containing medium, re-expression and functionality of the transporter were observed in fractions of the cells. It would be interesting to further evaluate the mechanisms responsible for this behavior. On the one hand, expression of MDR1 might have been induced by some of the undefined components of serum, on the other hand also metabolic variations or yet more basic changes might be responsible for the observed variations.

5.6.7 Melanoma Cell Adhesion Molecule (MCAM, CD146)

CD146 is an Ig member membrane glycoprotein which functions as a Ca^{2+} -independent cell adhesion molecule involved in heterophilic cell–cell interactions. Due to its expression and functional role in melanomas, the molecule is also termed Melanoma cell adhesion molecule (MCAM).[379]

CD146 is expressed on endothelial cells and is used as a marker for this cell type. Similarly, CD146 also serves as marker for MSC. Also, CD146 may be used to discriminate MSC from fibroblasts, since it was shown by Halfon et al [380] that only 5% of fibroblasts were CD146 positive compared with MSCs, where CD146 expression was markedly higher, but slightly decreased with time of culture from 92% in passage 2 to 80% in passage 6 cells. For CD146 expression on MSC besides passage dependent decrease, additional appearance of a second population has been described [26]. Also, CD146 expression has been shown to be markedly reduced, when MSC were cultured in the presence of bFGF, but returned to control level after one week cultivation in the absence of growth factor. In

contrast, no change in CD146 expression was seen when cells were induced to osteogenic or adipogenic differentiation. [329]

In the kidney, CD146 was found to be a marker for renal progenitor cells, which were isolated from adult human glomeruli. These cells expressed further MSC markers and the renal stem cell markers CD24 and Pax2 and, besides MSC specific differentiation capabilities into adipogenic, osteogenic, and chondrogenic lineages, they were also able to differentiate into endothelial, epithelial and mesangial cells. Expression of CD146 was unchanged upon endothelial and mesangial differentiation of the cells. In contrast to most progenitor cells isolated from human adult kidneys, the $CD146^+$ progenitors were characterized by lack of CD133 expression [78]. But also on $CD133^+$ sorted human adult kidney progenitors expression of CD146 has been observed. [71]

Expression of CD146 was investigated by Khan et al [319] on $CD105^+$ sorted CSC from Caki-2 and ACHN cell lines by IFC and weak staining for CD146, indicated by a shift in the whole cell population compared to isotype control, similar to that seen for PA cells in my experiments, was seen. The expression level of CD146 on SP cell line was reduced and even absent in CS cell lines. For the molecule a clear growth condition-dependent induction was seen in spheroid cell lines. The relatively fast reduction of expression after re-culturing A-SP cells under SCC in combination with other cellular charcteristics of adherently grown spheroids makes a possible szenario of epithelial differentiation of the cells under ACC less likely. The expression pattern of CD146 was quite similar as that described by Gharibi et al [329] for MSC cultured in bFGF containing or serum-containing conditions. According to this variable expression pattern, CD146 does not seem to be suited for sorting of probable CSC from RCC.

5.6.8 Vascular Cell Adhesion Molecule 1 (VCAM-1, CD106)

CD106 (Vascular Cell Adhesion Molecule 1) is a member of the Ig superfamily and is involved in leukocyte-endothelial cell adhesion and signal transduction during inflammation. It has been shown to be suitable marker for MSC, since CD106 is expressed on MSC and an up-regulation of CD106 expression by TNF-α was observed in this cell type, whereas expression of the molecule on fibroblasts is about 10-fold reduced with no changes seen upon TNF-α stimulation of the cells. [29 380] It has been shown that CD106 expression is reduced during *in vitro* culture of BM-MSC. [368]

Expression of CD106 has been reported on $CD133^+/CD24^+$ renal progenitor cells with multilineage differentiating potential isolated from the Bowman's capsule. [73] CD106 has also been found to mark a population with higher proliferative and differentiation potential compared to the $CD106^-$ cell fraction of renal progenitors derived from glomerular or tubular structures of the cortex. [75] The results obtained in my work, where in IFC staining variable fractions of $CD106^+$ staining cells were seen in PA cell line, whereas no expression was observed in spheroid cell lines and highly variable expression patterns were observed after ACC culture of spheroid cell lines, do not support expression of CD106 being a suitable CSC marker in RCC. Albeit, the mechanisms underlying the observed changes of CD106 expression observed in this work, might be interesting for further research on the role of this molecule.

5.6.9 CD90 (Thy-1)

CD90 is a GPI-anchored glycoprotein of the IgG-superfamily involved in cell-cell and cell-matrix interactions, which is mainly expressed in leukocytes. Expression has also been reported in neurons, activated endothelial cells, and mesangial cells. High levels of the protein are also expressed in subsets fibroblasts and MSC, where it serves as one of the defining markers.

In ovarian and nasopharyngeal cancer as well as in neuroblastoma CD90 has been found to act as tumor suppressor, whereas CD90 in hepatocellular carcinoma (HCC), gastric cancer, esophageal squamous cell carcinoma (ESCC) and brain cancer was found to mark CSC populations. [381] [382] [383] [147] [60]

CD90 expression in human fetal kidney was evaluated by Metsuyanim et al [351] using immunostaining. The authors found CD90 positive staining predominantly in renal tubular cells but not in the nephrogenic zone. The expression level of about 25% positive staining cells was also seen in IFC analysis of adult kidney. On renal progenitor cells derived from the renal cortex and medulla isolated by Bussolati et al [72] [71] and from healthy renal tissue of RCC patients by Galleggiante et al [202] also no staining of the cells for CD90 in IFC analysis was observed. These results indicate that CD90 in the kidney might be differently regulated and is no indicator of progenitor-like cells in contrast to MSC, where it is highly expressed and serves as one of the defining markers.

Primary tumors of the kidney as well as RCC cell lines have been shown to express CD90. [319] [78] [119] [205] In primary $CD105^+$ CSC investigated by Azzi et al [119] CD90 expression was lost upon differentiation of the cells. High expression of CD90 was also observed in in primary Wilms' tumor cell lines [317]. In contrast, RCC-26 and RCC-53 cell lines investigated by Gassenmaier et al [204] did not show expression of CD90.

The cell lines investigated here also did not show expression of CD90. Although, low level expression of CD90 mRNA was detected in RNA-Sequencing experiment. This indicates, that lack of CD90 expression is not due to probable deletion of the locus in the investigated cell lines.

5.6.10 Nerve Growth Factor Receptor (NGFR, CD271)

CD271 (Nerve growth factor receptor (NGFR)/low affinity nerve growth factor receptor (LNGFR)/$p75^{NTR}$/TNFRSF16) is a member of the TNF receptor superfamily and is expressed in embryonic stem cells and in adult stem cells of diverse origin including neuronal, epidermal and mesenchymal derived stem cells and seems to be involved in maintenance of the undifferentiated state of these cells. [384] The receptor has low affinity to several mature neurotrophins and high affinity for pro-neurotrophins. [385] Signal transduction of the receptor depends strongly on co-receptors and is diverse, depending on cell type types and context. CD271 has been shown to be a MSC marker [386] [340] as well as a promising CSC marker for melanoma, [387] [388] [389] and has also been found to mark CSC in neuroblastoma, squamous cell carcinoma (esophageal, oral). [147] [390] CD271 has been found to be a suitable marker for isolation of mutlipotent MSC form BM, but it's expression is rapidly down regulated upon culture of the cells. [59]

Expression of CD271 and its ligand pro-BDNF has been investigated by Cruz-Morcillo et al [385] in ccRCC. Both were found to be overexpressed in ccRCC tumor samples investigated by IHC. High expression of CD271 was also associated with higher Fuhrman grade of the tumors. Expression of

CD271 and pro-BDNF was also investigated in 786-O and ACHN RCC cell lines on mRNA and protein level. Thereby differences in expression between both cell lines were observed, with ACHN cell lines showing higher expression of pro-BDNF. The authors also investigated expression of the molecules in serum-containing and serum-free culture conditions and found CD271 protein expression up-regulated under serum-starving conditions in both cell lines and up-regulation of pro-BDNF under these conditions in ACHN cell line. In contrast to its pro-apoptotic function reported for neuronal cells, pro-BDNF was found to have a pro-survival role in both cell lines and activation of both, AKT and ERK1/2 pathways was detected after pro-BDNF addition to culture media of 786-O cell line. CD271 and pro-BDNF were also shown to be involved in cell migration of both cell lines using the wound-healing assay. siRNA silencing of CD271 led to reduced migratory ability as well as viability of the cells, highlighting that activation of p75NTR by pro-BDNF plays a major role in cell survival and migration of RCC cell lines.

Low-level expression of CD271 was detected on a small subset of spheroid cell lines SP and CS, whereas only single cells showed positive staining for CD271 in PA cell line in IFC experiments. Very low expression of CD271 mRNA was also observed in mRNA-Sequencing experiments, where also high variability was observed between single samples, which is in accordance with a small number of cells expressing the molecule. No variation of expression level was seen between different passages of spheroids or in spheroids grown under ACC. Though cells expressing the molecule are very rare in PA cell line, enrichment of CD271 expressing cells, might be a means to enrich for a probable CSC-containing cell sub-population from the cell line, especially in the light of results obtained by Cruz-Morcillo et al [385] in 786-O cell lines.

5.6.11 Chemokines and Receptors (CXCR4, CXCR7, CXCL12)

Chemokines, especially CXCL12 (SDF-1) and its receptors CXCR4 and CXCR7, have been found to be involved in cancer progression and metastasis. Chemokines have profound roles in the immune system, where they act as chemoattractants for several cell types with expression of the respective receptors and are involved in developmental processes. CXCR4 and CXCR7 have been found to be receptors for CXCL12, which upon binding of the ligand induce Gαi signal transduction pathways resulting in reduced cAMP production and intracellular calcium mobilization, and activation of multiple downstream targets and pathways, including ERK1/2, MAPK, JNK, and AKT. CXCR7 in contrast seems to act via different pathways than CXCR4, probably acting as a scavenger-receptor for the ligand but also through heterodimerization with CXCR4, thereby modulating signal transduction, but also by recruiting β-arrestin-2. In tumor cells, where up-regulation of CXCR4/CXCR7/CXCL12 by VEGF via HIF-1 signaling has been observed on various tumor entities, the chemokine-chemokine-receptor axis promotes tumor growth by promoting survival and dissemination of tumor cells, but also by acting on tumor microenvironment. Therefore these molecules seem to be suitable targets for therapeutic strategies. [391] [392] [393]

Comparison of gene expression profiles of normal kidney to RCC samples performed by Chen et al [394] found high expression of CXCR4 to serve as independent prognostic marker for poor survival of patients. Similarly, in a meta-analysis Cheng et al [365] found that high expression of CXCR4 correlated with worse prognosis for RCC patients. Similarly, CXCR4 was found among the significantly up-

regulated genes in comparative gene expression profiling of normal patient-matched renal tissue with ccRCC tumor tissue performed by Tun et al [323].

Struckmann et al [395] showed that CXCR4 as well as CXCL12 show increased expression in RCC, suggesting autocrine signaling route of this chemokine in RCC. Using the 786-O cell line (VHL-null) it was shown that expression of both molecules seems to be HIF-dependent, since expression of the molecules on mRNA and protein level detected by CIFM was strongly reduced in cells transfected either with pVHL19 or pVHL30.

Gassenmaier et al [204] investigated two RCC cell lines for sphere-forming ability and observed up-regulation of CXCR4 in the more tumorigenic RCC-53 cell line from 2% $CXCR4^+$ staining cells to a shift of the whole cell population in IFC staining, resulting in 38% $CXCR4^+$ cells after spheroid growth of the cell line. Whereas the less tumorigenic cell line RCC-26 did not show expression of CXCR4 in the parental cell line and only a small fraction of CXCR4 expressing cells (2%) in the spheroids derived thereof. Sorting for CXCR4 in the RCC-53 cell line increased sphere-forming as well as tumor-inducing ability. The functional involvement of CXCR4 in these processes was shown by siRNA mediated down regulation and pharmacological inhibition of CXCR4, which reduced sphere-formation, cell viability and chemo-sensitivity of the cells. Expression of CXCR4 on spheroid cells from both lines was reduced upon adherent standard culture of the cells.

In line with results of Struckmann et al [395] and Gassenmaier et al [204] Micucci et al [213] found CXCR4 and its ligand SDF-1 as highly up-regulated in spheroid cells derived from 786-O and Caki-1 RCC cell lines, when compared to their adherent counterparts. Also inhibition of CXCR4 led to reduction of sphere-forming efficiency in both cell lines and the connection of CXCR4 expression to HIF-2α was shown by reduced expression of CXCR4 mRNA in shRNA-HIF2α transfected cells.

Hu et al [200] observed down regulation of CXCR4 expression in $CD105^+$ sorted xenograft tumors generated from ACHN $CD105^+$ sorted cells after culturing the cells in standard medium conditions.

In line with the results obtained by other authors, expression of CXCR4 was seen in spheroid cell lines, whereas in PA cell line only very small numbers of cells stained positive for the receptor in IFC experiments. In SP and especially CS7 cell line an increase of CXCR4 expressing cell fraction over time in culture as spheroids was observed, whereas in CS1 cell line, the fractions of positive staining cells for the receptor were comparably lower and showed high variations in different experiments. The reduction of CXCR4 expression upon standard culture of spheroid cell lines, which was observed in my work also parallels the reports of Gassenmaier et al [204] Hu et al [200].

In contrast, Micucci et al [213], who found upregulation of CXCR4 in both investigated cell lines (786-O and Caki-1) at similiar level, the spheroid cell lines investigated in my work were found to express the molecule at different levels. The expression level on the investigated parental cell line PA thereby was similar to results obtained by Gassenmaier et al [204] for the less tumorigenic RCC-26 cell line and SK-RC-17 cell line, whereas expression pattern after long-term spheroid growth of CS7 cell line resembled the more tumorigenic RCC-53 cell line, and expression pattern of SP cell line in my work was similar to that reported for SK-RC-17 cell line.

In addition to surface expression of CXCR4 also CXCR7 expression on PA and spheroid cell lines derived thereof was investigated by IFC and the results were quite similar to that obtained for CXCR4

expression. But for this receptor the observed difference between spheroid cell lines was much more pronounced, with CS7 cell line showing similar expression pattern of the receptor as was seen for CXCR4, whereas on SP and CS1 cell lines the expression of CXCR7 compared to CXCR4 was markedly reduced. mRNA expression levels for CXCR7 determined for SP cell line, as well as for A-SP cell line were markedly enhanced compared to PA cell line, which is a further incidator for induction of expression of this molecule on spheroid cell lines. But also similar high expression of CXCR4 mRNA was seen in SP and A-SP cell lines, which contrasts the observed lower surface staining of the molecule on the latter by IFC. This might indicate that further mechanisms are involved in surface expression of the molecule.

5.6.12 Neural Cell Adhesion Molecule (NCAM, CD56)

Neural cell adhesion molecule (NCAM/CD56) of the immunoglobulin super family is a cell adhesion molecule, which is a marker for neural lineage cells and is expressed as well as on several blood lineage cells (NK-cells, γδT-cells, activated $CD8^+$ T-cells and dendritic cells). [396] [397] Besides mediating cell-cell contact by homophilic and heterophilic binding, it is also involved in FGF receptor signaling. [398] CD56 epitopes NCAM16.2 and E-39D5, of which the latter is not expressed on peripheral blood natural killer cells, are expressed on a small subpopulation of BM-derived MSC. Sorting for CD56 in combination with CD271 or MSCA-1 enriches for cells with high clonogenic, proliferative and differentiation potential, albeit lacking adipogenic differentiation potential. [340]

In hepatocellular carcinoma (HCC) NCAM expression, evaluated by IHC of tumor specimen, although present on a small number of tumors (3%) only, was found to be associated with worse prognosis of patients [399]. CD56 also expressed on a variety of other tumors. For example expression of CD56 ovarian carcinomas was correlated with high grade and advanced stage [400], also CD56 may serve as a differential marker for small cell lung carcinoma (SCLC). [401] Additionally in ovarian carcinomas, it has been shown that NCAM seems to be involved in tumor dissemination, which is based on NCAM/FGFR interaction as has been shown by use of antibodies that block this interaction in NCAM transfected cell lines and thereby reduce migratory ability of the cells. [402]

Metsuyanim et al [351] evaluated expression of NCAM in fetal and adult kidney and found expression of NCAM exclusively in the metanephric mesenchyme (MM) and its nephron progenitors as well as in stromal cells. They found elevated expression of renal progenitor genes SIX2, WT1, CITED1 and SALL1 in $NCAM^+/EpCAM^-$ sorted cell fractions, which seem to represent the putative MM stem cell fraction, whereas the $NCAM^+/EpCAM^+$ cell fractions seems to represent MM-derived progenitors, showing reduced expression of stem cell genes compared to the former. In adult kidney expression of NCAM was evaluated by IFC, thereby about 10% of the cells were $NCAM^+$. In human fetal kidneys NCAM expressing cell fraction evaluated by IFC was slightly higher than in adult kidneys [351] and NCAM staining in IHC has been observed in the nephrogenic mesenchyme .[317]

Buzhor et al [403] identified NCAM to mark a cell population in the range of 15±9% within cultured proliferative adult human kidney epithelial cells from adult human kidney specimen, which might represent a putative adult renal progenitor population (uniformly positive for CD24/CD133). Of note is that the molecule is not expressed *in situ* in renal epithelia. Comparison of $NCAM^+$ to $NCAM^-$ cell fractions revealed that early nephron progenitor markers PAX2, SALL1, SIX2, WT1 were over-

expressed and reduced expression of kidney differentiation markers as well as of CDH1 and vimentin indicated an EMT of the $NCAM^+$ cell fraction. The $NCAM^+$ cells also were shown to possess differentiating potential not only into tubular epithelial but also into osteogenic and adipogenic lineages. Similarly, in renal progenitors derived from the papillary region of human adult kidney by $CD133^+$ sorting strategy applied by Bussolati et al [71], CD56 was expressed on the main fraction of the cells, whereas also a CD56 negative cell fraction was seen.

In Wilms' Tumor, a pediatric tumor of the kidney with possible stem cell origin, NCAM, according to its expression pattern, which also correlated with expression of stemness genes and poor prognosis of patients, was proposed to be a suitable marker for enrichment of CSC [317].

In RCC, NCAM expression, investigated by immunohistochemical staining of 338 tumor samples, was detected in 15% of the tumors and expression was correlated with aggressiveness of the tumors, as indicated by tumor size, Fuhrman grading and patient survival rate. Also a strong correlation of NCAM expression with the occurrence of CNS metastases was observed [404]. Therefore NCAM expression might be a marker for more aggressive CSC like tumor cells.

In CRC cell lines NCAM expression has been shown to be up-regulated after treatment with TGF-β, which has been shown to induce EMT in these cell lines in a study performed by Okano et al [362].

Buzhor et al [403] detected NCAM expression of proliferating renal epithelial cells (putative adult renal stem cells) after culturing the cells but not *in situ*, and found $NCAM^+$ cells being enriched in stem cell characteristics.

In IFC experiments performed in my work NCAM expressing cells were only detected on spheroid cell lines SP and CS7, but not on PA cell line or CS1 cell line. Also it has been shown, that NCAM expression on the investigated cell lines is dependent on culture conditions. NCAM expression increased with extended culturing periods as spheres, but rapidly decreased after adherent standard culture of the cells. The lack of expression of the molecule on parental cell line is in agreement with the findings of Khan et al [319], that in different RCC cell lines, cultured as conventional monolayers, no expression of the NCAM gene has been detected.

For the above mentioned reasons, although differentially expressed in spheroid and PA cells and marking cells of more aggressive or CSC-like nature in other tumors, NCAM had to be excluded as possible enrichment marker for CSC from the investigated PA cell line. It might be interesting to further evaluate the mechanisms that underlie the observed variations in NCAM expression. One possibility is that a connection with the use of bFGF in the spheroid growth medium exists. The gradual evolvement of an NCAM positive cell fraction over time in culture, which was quickly lost upon serum culture of the cells but re-emerged after short-term re-culturing the cells as spheroids again, might be rather an indicator of reversible reprogramming of the cells.

5.6.13 Neprilysin (CD10)

CD10 (Neprilysin), also known as enkephalinase or common acute lymphoblastic leukemia antigen (CALLA), is a type II trans membrane glycoprotein with zinc-dependent neutral endopeptidase activity, which inactivates a number of signaling peptides (neural peptides: enkephalin, opioid peptide, substance P; immunogenic peptides: bradykinin, tachykinins, interleukins; growth factors: FGF-2). Independently of enzymatic function, by intracellular association with Lyn/p85 CD10 prevents activation of FAK indirectly by blocking PI3K activation by competitive binding and by association with PTEN and concomitant reduction of PIP3 leads to reduced activation of Akt pathway. Both signaling mechanisms lead to reduction of tumorigenic and metastatic potential, whereas expression of CD10 and the peptidase activity of the enzyme have been found to promote tumor progression and metastasis in some settings or reduce tumor progression in other setting. CD10 is expressed on several tissues including kidney, nervous system, lung, intestine, prostate and immune cells (B-cells and neutrophils) and it has been found to be a surface marker of stem cells in several tissues (bone marrow and adipose tissue (MSC), breast and lung). CD10 has first been identified as a marker for ALL (CALLA), and following its increased expression has been found on a variety of other tumor entities (carcinomas of various origins, neuroblastoma and melanoma). [405]

CD10 is also highly expressed on fibroblasts and due to its markedly lower expression on BM-MSCs may be used for discrimination of the two entities. [29] In MSC, clear expression of CD10 on primary and cultured MSC has been found on $CD271^+$ $CD56^{\pm}$ cell fractions. [340] But for CD10 expression in MSC also considerable donor-dependent variations in expressions have been observed. [26] CD10 expression has been shown to be up-regulated upon osteogenic differentiation of MSC. [406]

In normal breast tissue CD10 expression marks the basal progenitor cell fraction ($EpCAM^{low}/CD49f^+$). Bachelard-Cascales et al [350] found that sorting of $CD49f^+/CD10^+$ cells enriches for sphere-forming cells with high expression of CD29 and ALDH. EpCAM expression and CD10 expression on this cell subsets were shown to be mutually exclusive, with $EpCAM^+$ cells showing markedly reduced spheroid-forming efficiency, suggesting, that the $CD10^+$ subpopulation contains the stem like or early progenitor cell fraction in breast stem cell hierarchy and probably also in breast cancer. The authors found CD10 a suitable marker also for enrichment of spheroid-forming cells from adult brain, skin, adipose and mammary tissues as well as from MSC. In this work also dependency of stem cell phenotype on protease activity of CD10 in concert with CD29 interaction has been shown. This was confirmed by the study of Keller et al [349], who identified the $CD10^+/EpCAM^{low}$ cell fraction as basal like progenitor cell fraction, which in contrast to the luminal $EpCAM^+$ cell fraction, when transduced to form tumors, these were found to show a less differentiated gene signature, which is associated with the claudin-low breast tumor type. In this study a contradictory behavior to the study performed by Bachelard-Cascales [350] was seen regarding spheroid growth of $CD10^+$ and $EpCAM^+$ cells, in that the latter seemed to grow more readily as spheroids and the $CD10^+$ cell fraction had a higher tendency to grow adherently, showing less, but more compact spheroids, when assayed under non-adherent conditions. In contrast to the above findings, indicating CD10 as a marker for stem cell enrichment in breast tissue and cancer, $CD44^+/CD24^{-/low}/ESA^+$ CSC in human breast tumors initially identified by Al-Hajj et al [97] were characterized by lack of CD10 expression, which might be explained by the results obtained by

Keller et al [349], who found that probably most breast tumors ($ER^{+/-}$) might be derived from $EpCAM^{+}/CD10^{-}$ luminal progenitor like cells, whereas $CD10^{+}$ basal-like progenitors might give rise to rare undifferentiated claudin-low tumors.

Expression of CD10 in melanoma has been shown to be correlated with tumor progression and worse patient prognosis. Oba et al [407] investigated the role of CD10 in this tumor entity by overexpressing the molecule in a melanoma cell line. They observed alterations in gene expression profile of transformed cells, which comprised up-regulation of NCAM, CD133 (Prominin 1), FGFBP1, Neuropilin1, IGFBP3 among others in the microarray analysis, as well as higher tumorigenicity and drug resistance, but lower migratory abilities compared to mock transfected control cells.

In B cell lymphomas CD10 is expressed in germinal center subtypes, whereas CD10 expression is low or absent in the more aggressive activated B-Cell subtype. In esophageal squamous cell carcinoma (ESCC) cell lines and one gastric cancer cell line, CD10 has been shown to be transcriptionally up-regulated by lentivirally introduced EMT-promoting transcription factor Twist1. [408]

In the kidney CD10 expression, investigated by TMA, has been found in proximal tubules, glomerular epithelium and Bowman's capsule. [354] Immunohistochemical analysis of different RCC tumor samples revealed positive staining of CD10 on 85% of clear cell RCC and 23% of papillary RCC, in this study also 88% of ccRCC and 18% of pRCC showed positive staining for the renal embryonic marker Pax2. [409] Similar results were obtained by Liu et al [354], where CD10 staining was observed in 91% of ccRCC, 45% of chromophobe RCC and 29% of oncocytomas. Thus CD10 may be used for differential diagnosis of clear cell RCC but expression is also detected in many other primary or metastatic carcinomas. [410] Similarly, Boysen et al [378] in a screen for surface glycoproteins found CD10 as one of the discriminating surface molecules between pRCC and cRCC. By using the pVHL-negative cell line 786-O and a corresponding transfectant stably re-expressing pVHL, they could show a direct link between CD10 expression and pVHL dependent transcriptional regulation. Also they found CD10 to be a putative serum marker for ccRCC. In prostate cancer cell lines, CD10 expression has been shown to be negatively regulated by hypoxia on the transcriptional level by binding of HIF-1α to HRE in the CD10 promoter [411] and a correlation of CD10 expression with a more aggressive and metastatic potential of this tumor entity has been shown. [412]

In contrast to the high expression observed in ccRCC tumor samples, in the cell lines investigated in this work, expression of CD10 was found only on varying fractions of SP cells by IFC and the expression pattern of the molecule was retained after adherent culture of the cells. Neither PA nor CS cell lines showed positive staining for CD10. Results obtained in mRNA-Sequencing experiments confirmed the results seen in IFC, with similar high expression levels seen in SP and A-SP cell lines, whereas mRNA levels detected in PA cell line were very low. This implies that the molecule might be a marker for defined subsets of spheroid cells or CSC in RCC and SP cell line might be a suitable tool for further investigations of the basis for CD10 expression in ccRCC.

5.6.14 Prominin 1 (CD133)

The tetraspanin prominin 1 (CD133) is expressed by almost all cell types, especially on epithelial cells at apical membrane protrusions and it seems to be involved in plasma membrane remodeling and signaling. The expression of one differently glycosylated isoform which is detected by the AC133 (CD133/1) antibody has been shown to be more restricted to progenitor cells and this antibody has been used as marker for progenitor cells and CSC in a wide variety of tumors, especially of brain origin but also on other cancers e.g. CRC, HCC, lung cancer, ovarian cancer, and melanoma. [413]

In the kidney CD133 is expressed during embryonic development and in the adult kidney CD133 positive staining was observed in proximal tubule epithelial cells and the parietal layer of Bowman's capsule. [413]

A study performed by Metsuyanim et al [351] found that in the human fetal kidney $CD24^+$ and $CD133^+$ as well as $CD24^+/CD133^+$ cells were found to comprise more than 50% of the cells, which also show to be $EpCAM^{bright}$, indicating that these molecules do not mark progenitor cell like phenotypes but rather are markers of differentiation in the kidney. In human fetal kidneys CD133 expression evaluated by IHC showed positive staining in tubular epithelial cells, whereas in Wilms' tumor, CD133 predominantly stained the tumor vasculature. [317] Bussolati et al [71] evaluated AC133 staining in several regions of adult human kidneys using CIFM and found positive staining cells in the Bowman's capsule and some tubular cells in the cortex. In the outer medullary region CD133 staining was restricted to some small tubules, which also showed co-staining for CD24. In the inner medullary region CD133 positive staining cells were observed in some tubules and the Henle's loop, but not in the Bellini ducts. The CD133 positive staining cells did not show co-staining with several tested nephron specific markers, except for megalin in cortical tubuli.

CD133 was used to isolate renal progenitor cells from the normal portion of human renal cortex by Bussolati et al [72]. The $CD133^+$ cells, comprising ≈ 1% of the tissue, were shown to be able to differentiate into endothelial and epithelial cells *in vitro* and *in vivo*, but lacked adipogenic differentiation potential. Their renal lineage origin was confirmed by expression of renal embryonic marker Pax2 and the cells were positive for mesenchymal markers CD73, CD44 and CD29 and vimentin but lacked expression of CD90 and CD105. Expression of CD133 was lost upon differentiation of the cells, whereas CD44 expression as well as expression of Pax2 remained unchanged. Expression of CD105 and cytokeratin was seen in endothelial or epithelial differentiated cells respectively. The lifespan of the cells *in vitro* has been evaluated to comprise 20-25 doublings.

Sagrinati et al [73] identified a $CD133^+/CD24^+$ cell subpopulation with stem cell characteristics in the parietal epithelial layer of the Bowman's capsule, which comprised 0.5-4% of total cortical renal tissue. The cells showed high cloning efficiency and self-renewal potential and were able to differentiate *in vitro* into functional renal tubule cells, adipocytes, osteoblasts, and also into neuronal cells. The cells were shown to express additional surface markers CD105, CD106 and CD44, as well as vimentin and cytokeratin and stemness markers Oct4 and Bmi1, whereas no expression of either the podocyte markers synaptopodin and WT1, or endothelial markers CD31 and CD34 was detected. *In vitro* application of the cells into mice with acute renal failure resulted in reduction of kidney damage by regeneration of tubular structures. During further characterization of the cells by Ronconi et al [77]

different subsets of adult regenerating cells could be discriminated in the parietal layer of the Bowman's capsule by their expression of additional markers. $C133^+/CD24^+$ localized to the urinary pole are able to differentiate into tubular cells and podocytes, whereas cell with additional expression of the podocyte marker PDX, localized between urinary and vascular pole, are able of podocyte generation only. Differentiation potential is restricted to $C133^+/CD24^+$ subsets, whereas $C133^-/CD24^-$ cells display phenotypic features of podocytes.

From the cortical, glomeruli deprived region of adult human kidneys Lindgren et al [74] isolated a stem cell population according to high ALDH activity. By comparative gene expression analysis this population showed higher expression of CD133 and CD24 as well as CK7, CK19 and vimentin. By use of immunohistochemical analysis with these identified markers $CD133^+/CD24^+$ cells were identified, which were scattered mostly at the convolution of the proximal tubules, and stained also positive for CK7, CK19, CD133 and vimentin, resembling cells that were identified Challen et al [324] from mouse kidney by using Hoechst side population enrichment and were probably identical to the cells isolated by Angelotti et al [75] from the tubular fraction of human kidneys by use of $CD133^+/CD24^+$ sorting strategy. These cells were further characterized by the lack of expression of CD106 (VCAM), which was identified to be expressed on almost all cells isolated from human glomerular tissue portions using the same strategy. Both cell fractions, though being equally positive for CD133 and CD24 markers showed different characteristics, with $CD106^+$ glomerular derived cells showing higher proliferative potential and potential to differentiate into podocytes as well as into tubular cells, whereas the tubular region derived $CD106^-$ cells were able to differentiate toward tubular lineage only, suggesting that these cells represent more committed tubular progenitors.

CD133 also marked progenitor cell fraction, which was isolated by Ward et al [76] from renal papillary tissue. These cells also showed expression for stem cell markers Nestin, SSEA-4 and TRA-1-81 as well as increased expression of Sox2 and Nanog compared to unsorted cells and were able to integrate into developing mouse tubular structures. The same integrative capacity was seen in $CD133^+$ sorted cells from cortical tissue, whereas unsorted cells from both tissue types were seen primary in the interstitium. Similarly, Bussolati et al [71] isolated $CD133^+$ cells, which were found to comprise ≈ 6 % of the tissue, from the papillary region of renal pyramid. The $CD133^+$ isolated cells were investigated for expression of several other markers by flow cytometry and positive staining of the whole cell population for CD24, CD44, CD73, CD49f (integrins $\alpha 6$), CD29 (integrin $\beta 1$) and SSEA-4 antigens was observed. In contrast, the renal TIC marker CD105 was expressed at low level only on a subset of the cells and CD56 was expressed by most of the cells, but also a negative cell fraction was detected. Expression of vimentin, cytokeratin (Pan-CK), Nestin, Pax2, Six1/2, Oct4, Klf4 and c-Myc, which were evaluated by CIFM or RT-PCR, was also demonstrated in the $CD133^+$ sorted cells. The authors report that clonogenic potential of the $CD133^+$ cell fraction was markedly higher than that of unsorted or $CD133^-$ cell fraction. Also the cells possessed epithelial differentiation potential *in vitro* and *in vivo*, which was shown by the gain of expression of several tubular markers upon culturing cells under differentiation conditions and by tubular structure formation of cells subcutaneously injected in Matrigel™ into SCID mice. CD133 expression was lost and Oct4 expression was reduced in differentiated cells. Since the papillary region of the kidney is known to possess a relatively low

oxygen pressure, the influence of hypoxia was also investigated. The authors found constitutive expression of HIF2α in the $CD133^+$ sorted cells, which did not change under hypoxic conditions. In contrast, HIF1α, CD133 and Oct4a expression were quickly and clearly up-regulated under hypoxic conditions, and cell proliferation as well as clonogenic potential was increased.

In contrast, the MSC-like $CD146^+$ renal progenitor cells isolated from glomeruli deprived of the Bowman's capsule by Bussolati et al [322], contained two subpopulations regarding CD133 expression, of which the $CD133^-$ fraction exhibited stem cell features such as self-renewal ability and multipotency, whereas the $CD133^+$ fraction was $CD24^-$ and co-expressed endothelial markers CD31 and von Willebrand factor (vWF).

In contrast to other tumor entities, and the use as marker of adult renal progenitor cells, a study performed by Bruno et al [414] revealed that in RCC CD133 did not seem to bee a CSC marker, rather $CD133^+$ sorted cells seemed to represent a fraction of tumor cells, possibly representing normal renal progenitors, which support tumor vascularization and promoted tumor growth, when applied in combination with neoplastic cells.

But, using a double sorting strategy for $CD133^+/CD24^+$ to isolate progenitor cells from kidney specimen of RCC patients from tumor tissue and corresponding healthy tissue, Galleggiante et al [202] yielded an enrichment of CSC and renal progenitors in both tissues, respectively. Expression of other surface markers revealed, that both cell fractions were positive for CD73 expression, but lacked expression of CD105 and CD90 mesenchymal markers. Gene-expression analysis, as expected, revealed differences in expression of cancer associated gene signatures in tumor-derived and normal-tissue derived cell fractions, but these were more marked in comparison of tumor-derived cells to normal tubular epithelial cells. Differences were also observed in growth potential in soft agar assay, which was absent in the normal-derived cells, whereas both fractions showed similar differentiation potential toward adipogenic, osteogenic and epithelial lineages. The results imply that the $CD133^+/CD24^+$ may represent a cancer cell sub-population, which might co-exist and cooperate with the $CD105^+/CD133^-$ CSC population identified by Bussolati et al [78].

Xiao et al [203] used a sorting strategy for $CD133^+/CD24^+$ cells from ACHN and Caki-1 cell lines, and found sorted cells, which comprised a fraction of 12% in ACHN and 6% in Caki-1 cell line, showing enhanced sphere-forming and tumor-inducing ability, chemo-resistance and increased expression of mRNA for stem cell markers Oct4 and Klf4 as well as ABCB1/MDR1 when compared to $CD133^-/CD24^-$ negative cell fractions. They also found components of the Notch signaling pathway to be up-regulated in these cell fractions.

CD133 was evaluated in primary Wilms' tumor cell lines by Pode-Shakked et al [317] as marker for stemness signature of the cells, thereby no difference in cloning ability between $CD133^+$ and $CD133^-$ cell fractions was observed, also the stemness signature comprising components of the Wnt pathway (FZD7, β-catenin), polycomb group (BMI-1, EZH2) and nephric-progenitor (SIX2, WT1) genes as well as pluripotency marker Oct4, did not show significant differences between the two cell fractions, rather expression of most of the evaluated genes was slightly higher in the $CD133^-$ cell fractions with exception of β-catenin and BMI-1.

In a study performed by Hasmin et al [356] stem cell characteristics were evaluated by sorting and re-grafting xenograft tumors generated from a primary RCC cell line. They found significantly lower tumor forming ability in $CD133^+$ cells compared to the $CD133^-$ fraction. The latter also showed growth advantage over $CD133^+$ cells and markedly higher expression of ERBB4, whereas lower expression of several tumor suppressor genes was detected in this population compared to the $CD133^+$ fraction. Also the ability to form tumors serially was reduced in the $CD133^+$ fraction and time to tumor formation increased during serial transplantation for both fractions compared to unsorted cells. This further supports the view, that CD133 in ccRCC is expressed by a less aggressive subset of CSC.

In a meta-analysis done by Cheng et al [365] evaluating the relevance of several CSC markers for patient prognosis, the authors found CD133 an independent favorable factor for prognosis of RCC. Chen et al [206] investigated the association of CD133 with patient prognosis in a database search and found no significant correlation to survival rate of the RCC patients.

In a recent study performed by Zanjani et al [415] in ccRCC, but not in other RCC subtypes, CD133 cytoplasmic expression, but not membranous expression was found to be correlated with tumor aggressiveness and disease state.

Zhong et al [211] did not detect expression of CD133 on spheroids and adherent counterparts of SK-RC-42 RCC cell line, although spheroid cells possessed several CSC features.

Expression of CD133 on Caki-2 and ACHN RCC cell lines and the normal embryonic kidney cell line ASE by flow cytometry and RT-PCR was evaluated in the study performed by Matak et al [199]. They found weak expression of CD133 in Caki-2 and ACHN cell line and high expression on ASE cell line in IFC measurements, whereas mRNA expression level in Caki-2 seemed to be higher than in ASE cells. In contrast to this, Khan et al [319] did not detect staining of Caki-2 and ACHN cell lines with AC133 in flow cytometry, similarly 786-O, 786-P and Caki-1 cell lines did not show positive staining in the experiments, though week staining for CD133 was seen in 786-O and ACHN cell lines in IHC experiments, which might be an indicator for intracellular localization of the protein in this cell lines. In contrast, the cell lines SMKT-R2/3 and RCC-6 were shown to express CD133 at low level in a small subset of the cells. Though, results for IFC measurements in this report do not seem to have been measured with optimal instrument setting.

Expression of CD133 protein has been shown to be induced by hypoxia via down regulation of mTOR pathway as well as by TGF-β signaling and also seems to be up-regulated by NF-κB. [416]

An up-regulation of CD133 mRNA expression has been shown in spheroids derived from 786-O and Caki-1 cell lines by Micucci et al [213], which was accompanied by higher protein content of HIF-2α in the spheroid cell lines.

Expression of CD133 was observed predominantly in CS cell lines, whereas only small numbers of SP cells were found to stain positive for AC133 antigen in IFC experiments, and PA cell line did not seem to express the marker. Differential expression of CD133 mRNA at very low levels was also seen in mRNA-Sequencing experiments, with higher expression values observed on SP cell line compared to PA cell line, which is in accordance with expression of the molecule on small subsets of cells. Compared to PA cell line, expression level of CD133 mRNA was also elevated in A-SP samples.

From the two investigated CS cell lines CS7 cell line showed the highest number of CD133 expressing cells, which increased over time in culture as spheroids, whereas expression level in CS1 cell line was detected at varying and lower cell numbers. In both cell lines, CD133 expression was detected in variable fraction of cells after short-term culture under ACC but was lost after long-term culture under these conditions. Considering the growth characteristics of CS and SP cell lines, with high growth rates observed in CS7 cell line in high passage cells, CD133 seems to mark a cell population with high proliferative potential. Due to its expression characteristics of the marker, CS7 cell line seems to be a suitable tool for further studies of CD133 expression and function in ccRCC.

5.6.15 Integrins - CD29 (Integrin β1), CD49e (Integrin α5), CD49f (Integrin α6)

Integrins are single-pass type I trans membrane proteins, which form heterodimers composed of α and β subunits and serve as receptors for components of extracellular matrix (ECM) but also, especially in cells of the immune system, to receptors expressed on other cells. Integrins, depending on their α/β subunit-composition, are involved in various cellular processes including cell anchorage, angiogenesis, cell-cycle regulation, differentiation, chemotaxis, proliferation and survival. Via different adapter molecules, which interact with their short intracellular domain, integrins are linked to components of the cytoskeleton and thereby serve in anchoring of the cells but also serve as signaling scaffolds, by binding Src-kinases, focal adhesion kinase (FAK) or integrin-linked kinase (ILK) or growth factor receptors. [417] [418] [419]

Integrin α6 is a laminin receptor and combines with β1 or β4 subunits. α6β1 is the essential receptor for vascular laminins and is involved in platelet activation and thrombosis. α6β4 serves as laminin receptor of epithelial cells. α5 integrin belongs to the RGD-binding subunits of integrins, which recognize Arg-Gly-Asp (RGD) motif within their ligands, and bind to fibronectin (FN), fibrinogen, vitronectin, von Willebrand factor and many other large glycoproteins. The α5 subunit combines with the β1 subunit and α5β1 has been found to be involved in angiogenesis. [419]

In cultured MSC expression of various integrin subunits including α6 (CD49f) has been described [420] and integrins α4 (CD49d), α5 (CD49e), and β1 (CD29) serve as MSC positive markers. CD49e (ITGA5, Integrin α5) has been shown to be up-regulated upon osteogenic differentiation of MSC [406]. Also several integrins (CD49a, CD49c, CD49d, CD49f) have been shown to be up-regulated in *in vitro* culture compared to freshly isolated BM-MSC. [368]

In normal breast tissue, sorting of $CD49f^+$ (ITGA6, integrin α6) cells enriches for cell populations ($EpCAM^{+/-}$) with stem cell ($EpCAM^-$) and luminal progenitor like phenotype ($EpCAM^+$), whereas $CD49f^-$ cells comprise epithelial cells ($EpCAM^+$) and stromal cells ($EpCAM^-$). [350] [347] [348] $CD49f^+$ sorting in combination with CD24 or CD29 also lead to enrichment of CSC subpopulations in breast cancer cells in a mouse model system. [152] Under hypoxic conditions CD49e (ITGA5) and CD29 (ITGB1) are up-regulated in breast cancer. HIF-1 and HIF-2 have been found to be directly required for CD49e (ITGA5) induction in breast cancer cell lines, which leads to enhanced migration and invasion of single cells within a multicellular 3D tumor spheroid but did not affect migration in a 2D microenvironment, whereas CD29 (ITGB1) expression is dependent on HIF-1α only. The same study revealed that in

breast cancer biopsies CD49e (ITGA5) expression has been shown to be associated with an increased risk of mortality and seems to be required for metastases to lymph nodes and lungs. [421]

In prostate cancer, cells with high expression of CD49b (ITGA2) and CD29 (ITGB1) subunits have been shown to possess cancer stem cell properties. In CRC co-expression of CD29 (ITGB1) on $CD24^+$ cell fraction has to be used to mark the cell fraction for successful isolation of CSC [147]. In CRC, also CD49f (ITGA6) has been found to be a marker for CSC enrichment in combination with other markers. [422]

Integrin expression on four RCC cell lines (A498, ACHN, Caki-1, Caki-2) and respective mouse xenograft tumors was evaluated by Korhonen et al [423]. All cell lines expressed Integrin α1 (CD49a), α3 (CD49c), α7, β1 (CD29), β3 (CD61), β5. Integrin α6 (CD49f) chain was expressed on all cell lines except Caki-1. Caki cell lines also expressed α5 Integrin (ITGA5, CD49e), which is up-regulated during EMT. The same has been observed for ITGA1 (CD49a) [355], which was expressed on all cell lines. The α5 (CD49e) isoform was also seen in the xenograft tumors formed from A498, ACHN and Caki-1 cell line but not in tumors from Caki-2 cell line. Integrin α1 and β5 were not expressed on tumors formed from the cell lines. Strong laminin expression was detected surrounding cysts of Caki-2 and A498 tumors, which showed well to moderate differentiated morphology of clear cell RCC grade1/2 respectively, while staining pattern was diffuse or punctate in poorly differentiated tumors grown from ACHN and Caki-1 cell lines.

In this work, expression of ITGB1 (CD29), ITGA5 (CD49e) and ITAG6 (CD49f) on the different cell lines was investigated by IFC. Thereby, similarly high and constant expression of CD29 was observed in PA and spheroid cell lines, whereas only low staining was observed for CD49f in all cell lines. CD49e was found to be expressed at higher levels in spheroid cell lines, and staining intensity increased with long-term culture in all cell lines investigated. CD49e expression was also found to vary with culture conditions on spheroid cell lines. Since CD49e has been shown to be induced during EMT, the observed expression pattern might be a hint for a slow shift of EMT status of the cells over long-term culture.

Similar expression of CD49f mRNA was detected in SP and PA cell lines, but values were higher than those seen for CD49e mRNA, which might indicate a problem with the antibody used for CD49f staining. The higher expression of CD49e in SP cell line was confirmed by mRNA-Sequencing results. mRNA-Sequencing experiments also revealed lower expression levels of ITGA1, ITGB2 and ITGB6 in SP cell line compared to adherently grown PA and A-SP cells.

Though differential expression of CD49e on spheroid and PA cell line was observed, the expression pattern of the molecule excludes it as a suitable marker for CSC enrichment from PA cells.

5.6.16 Stem Cell Markers SSEA-1/3/4, TRA-1-81

Expression of stage-specific antigens SSEA-3 and -4 as well as TRA-1-81 are used as markers for undifferentiated state of mouse and human ESC. The TRA-1-81 antibody detects the high molecular weight isoform of podocalyxin, which was initially described as trans membrane glycoprotein on glomerular podocytes and is expressed on ESC and HSC, but has also been identified to be a marker for several cancers including Wilms' tumor of the kidney, breast cancer, hepatocellular carcinoma and ALL. [54 55].SSEA-3 and SSEA-4 have also been found to be markers for multipotent MSC from BM and

some other sources [28], whereas TRA-1-81 may be used as a marker for placental derived MSC. [59] SSEA-3 has been shown to select an adipocyte precursor cell fraction when used as marker to sort $CD271^+$ BM-derived MSC. Interestingly expression of SSEA-3 on primary cells is lost during culture of the cells. [59] In contrast SSEA-4 expression seems to gradually increase in BM culture over time. SSEA-3 expression has also been shown to mark a rare MSC subset termed MUSE (multilineage-differentiating stress enduring) cells, which also co-express other pluripotency markers such as Oct4, Sox2 and Nanog. [28]

IFC-staining of $CD133^+$ sorted renal progenitor cells isolated from human papillae performed by Ward et al [76], showed high staining intensities for SSEA-4 and TRA-1-81 in sorted papillary cells, whereas in immortalized normal renal cortical tubular epithelial cells no staining for these antigens was observed. SSEA-4 expression was also reported on similar cells ($CD133^+$ sorted cells from human papillary region of the kidney) obtained by Bussolati et al [71], which were also shown to express renal stem cell marker Pax2 and pluripotency marker Oct4A.

In colorectal cancer (CRC) cell lines SSEA-3 was markedly expressed in the HCT116 cell line and SSEA-3 expression was correlated with increased tumorigenicity and higher proliferative ability but reduced sphere-forming ability of the cells. The authors conclude that SSEA-3 may mark a subset of transit amplifying CSC. [333] In human cancer cell lines DU145 (prostate cancer) and HCT116 (CRC) and MCF-7 (breast cancer) investigated by Sivasubramaniyan et al [367] $SSEA\text{-}4^+$ sorted cells were also enriched for expression of TRA-1-60/81 and N-Cadherin. In contrast, E-Cadherin and CD44 were not co-expressed with SSEA-4, but enrichment of these markers was seen in $SSEA\text{-}4^-$ cell fractions. Also higher tumorigenicity of $SSEA\text{-}4^+$ DU145 cells was observed compared to the $SSEA\text{-}4^-$ cell fraction.

Expression of these antigens has also been reported on teratocarcinomas and CSC from breast and prostate cancers. [60]

Expression of SSEA-1 (CD15) on human ESC is up-regulated during differentiation of the cells and the antigen, in contrast to mouse ESC is not expressed on pluripotent ESC [56]. CD15 is known to be expressed on several subtypes of RCC as shown by TMA staining of tumor samples and may be used for differential diagnosis of RCCs, with high expression being found on ccRCC, pRCC, and Oncocytoma, and low staining on chromophobe RCCs. [424]

Expression of SSEA-3, SSEA-4 as well as of TRA-1-81 and SSEA1 was investigated by IFC staining of parental cell lines and spheroid cell lines SP and CS. Thereby expression of the pluripotency markers SSEA-3, SSEA-4 and TRA-1-81 was observed on all cell lines at relatively high levels. Whereas SSEA-4 showed relatively similar staining pattern in all cell lines investigated, with a slightly broader distribution of staining on spheroid cell lines, SSEA-3 was found to be expressed at similar high levels in PA and SP cells, whereas CS cell lines showed higher heterogeneity in expression of the epitope, indicated by several differently stained fractions being discernible. TRA-1-81 expression was found to be highly heterogeneous and variable in all investigated cell lines. Thus further investigations and cell sorting using these markers might be suitable for discrimination of various cell fractions probably being enriched in cells with stem cell characteristics contained in the cell lines. The expression of these markers is a strong indicator for stem cell characteristics of the investigated cell lines.

In contrast to pluripotency markers, the expression pattern observed for SSEA-1, which in humans marks more differentiated subsets of ESC, was found to differ profoundly between PA and spheroid cell lines, as well as between SP and CS cell lines. Whereas expression of SSEA-1 was detected on PA cell line and increased with time of culture, indicating enrichment of a more mature phenotype over long-term culture of the cells, the expression of SSEA-1 was lost upon long-term culture of spheroid cell lines under SCC, which might indicate a loss of more mature cells during this mode of cultivation. Compared to expression on CS cell lines, SP cell line showed very reduced staining for the marker even at low passage of spheroid cells, which might be an indicator that bulk culture is superior over single cell culture in enrichment of progenitor cells.

5.7 Evaluation of Expression of Intracellular Markers

Besides surface expression, also the expression of antigens, which are located intracellular and are connected to stem cell features or used to evaluate EMT, was evaluated by intracellular staining and subsequent IFC measurement on PA cells and three different spheroid cell lines derived thereof (SP, CS1, CS7). The number of experiments performed for intracellular staining of antigens was limited compared to those for evaluation of surface expression. Also the results in those experiments showed higher variations, caused by the intracellular staining method, which resulted in relatively high unspecific staining, as was seen from the strong signals obtained with isotype control antibodies. Also, the cellular status regarding intracellular expression of the evaluated antigens was determined in less detail with respect to possible changes over time in culture or medium-dependent variation. An overview of the results is summarized in table 5.7.1. Since no significant differences between the two cell lines CS1 and CS7 were detected, results for both cell lines were summarized in this overview. The results are discussed below in detail with a focus on their normal expression pattern and function, as well as cancer and stem cell related aspects and especially their expression pattern reported in kidney and RCC (see also chapter 5.5 for TNAP).

Antigen	PA	SP	CS
Vimentin	+++	+++	+++
Pan-CK	+++	+++	+++
Snail1	++	++	++
CK19	++	++	++
CK8	++	+	+
TNAP	+	+	+
Oct4A	+	+	+
Sox2	+	+	+

+	low (slight population shift)
++	intermediate (clear population shift)
+++	high (strong population shift)

Table 5.7.1: Overview of Expression Levels of All Investigated Intracellular Antigens

Summary of results obtained for intracellular staining of different cell lines for expression of various intracellular expressed antigens. Expression level was graded according to criteria listed in the legend by visual inspection of the histograms of all experiments, since number of experiments and variations between single experiments were not suited for statistical analysis.
CK: cytokeratin, CS: clonally expanded spheroid cells derived from PA (CS1 and CS7), PA: parental cell line, Pan-CK: antibody detecting various isoforms of cytokeratin, SP: spheroid cells derived from PA, TNAP: tissue non-specific alkaline phosphatase

5.7.1 Cytoskeletal Components

5.7.1.1 Cytokeratins

Cytokeratins (CK) are intermediate filament proteins of which 20 isoforms (CK1-20) have been categorized according to their molecular weight and isoelectric point. Two CK isoforms (one acidic/low molecular weight/type I/CK9-20 and one basic/high molecular weight/type II/CK1-8) combine to form different heteropolymeric intermediate filaments. Their primary function is maintaining the mechanical stability of individual cells and epithelial tissues. CK isoform expression varies for different epithelial tissues, and with exception of CK8 and CK18, which are expressed in transformed fibroblasts and certain smooth muscle cells as well as on UCB-MSC [425], their expression is restricted to epithelial cells, and no expression on cells of mesenchymal origin (with exception of vascular epithelial cells) is normally detected. Cytokeratin 8 (CK8) is expressed in most simple epithelia and also in most carcinomas, therefore this molecule is also used for tumor classification in IHC. [426] [427] The cytokeratin 19 (CK19), which is expressed by simple epithelial cells and is an established tumor marker, has been shown to be associated with a progenitor like phenotype in hepatocellular carcinoma (HCC) and is associated with higher metastatic potential and poorer overall survival of patients. [399] TMA studies on expression of CK19 and EMT markers on HCC tumor specimen revealed increased expression of EMT markers (Snail1, Snail2, and Twist) in CK19 positive tumors. [428] Takano et al [429] also show that CK19 expression is linked to EMT: knocking down CK19 resulted in increased E-Cadherin expression, accompanied by raised invasion ability of HepG2 cells. Additionally, CK19 expression in HCC has been shown to be associated with worse patient prognosis. [399] In pancreatic endocrine tumors CK19 expression has also be linked to worse prognosis. [430]

In the kidney CK7 and CK19, which are normally not stained in renal tubules, have been found to mark progenitor cells, which were identified by Lindgren et al [74] in this region. Staining for CK7 and CK19 was also observed the parietal epithelial cells of the Bowman's capsule in combination with CD133 and vimentin positive staining, which marks progenitor cells in this region. Staining for CK7 and CK19 is also seen in hepatic stem cells. [69] In $CD133^+$ renal progenitors, isolated from the papillary region of adult kidney and assayed by CIFM, fibrils positive staining for cytokeratins using Pan-CK antibody, which recognize a set of cytokeratins (CK1, 2, 3, 4, 5, 6, 7, 10, 14, 15, 16 and 19) was observed. [71]

Most RCC stain positive for CK19. CK expression is used for differential diagnosis of renal carcinomas. Clear cell (conventional) RCCs show weak to moderate staining for CK8, CK18, CK19 as well as minor CK7 staining, which is strongly expressed in tubular epithelial cells. Staining with Pan-CK antibody also shows weak positive staining. In contrast, papillary RCC typically show strong positive staining for CK7, CK8, CK18, CK19 and Pan-CK antibody. Both tumor types show strong staining for vimentin, which is not seen in oncocytoma and chromophobe RCC. [431] [432] [410]

CK19 was not found to be expressed on putative $CD133^+/CD24^+$ CSC isolated by Galleggiante et al [202] from RCC tumors, which show expression of CK19 only after epithelial differentiation of the cells and besides this differentiating potential also have been shown to differentiate into adipogenic and osteogenic lineages. Similarly Hu et al [200] observed positive immunohistochemical staining for CK7 in $CD105^+$ sorted ACHN tumor xenografts, only after culturing cells in standard medium conditions,

whereas no staining was seen, when cells were cultured in expansion medium with low serum content and growth factor supplementation. This might imply that expression of cytokeratins is induced by the standard culture conditions used for propagation of cell lines.

As expected for RCC cell lines, the investigated cell lines in this work showed moderate positive staining for CK19 and weak to moderate staining for CK8 as well as higher staining intensities for staining with Pan-CK antibodies in IFC experiments. The higher staining intensity seen for of Pan-CK compared to those seen for CK19, implies that also some of the other cytokeratins detected by the antibodies might be present in the investigated cell lines. For all cytokeratins higher staining intensities were seen in PA cells compared to spheroid cell lines, which might indicate a shift toward mesenchymal phenotype of the latter. The results seen from IFC experiments of PA, SP and A-SP cell lines were confirmed by mRNA expression levels detected in RNA-Sequencing experiments.

Expression of CK20 is not typic for RCC, usually the expression is restricted to some tissue origins: especially over 90% of cases of colon carcinoma and 86% of Merkel cell tumor of the skin as well as about 50% of transitional cell carcinoma of the bladder, gastric carcinoma and pancreatic adenocarcinoma stain positive for CK20. Although, CK20 positive tumors have been reported for small numbers of other tumor entities including RCC. [426] The cell line investigated seems to be one of the rare cases, as expression of CK20 was detected on mRNA level repeatedly by K. Heinrich [433]. CK20 mRNA expression level in RNA-Sequencing experiments of this work was also found to be higher in spheroid derived cell lines (SP and A-SP) than that of PA cells.

5.7.1.2 Vimentin

Vimentin is a class-III intermediate filament, which is expressed in mesenchymal cells and is known to maintain cellular integrity and provide stress resistance. Vimentin expression has been described in fibroblasts, in vascular endothelial cells, macrophages, neutrophils and several precursor cells including MSC. In the kidney mesangial cells and renal stromal cells have been shown to express vimentin. Vimentin is a marker for EMT and over-expression, which has been found in several epithelial tumor types including breast, gastrointestinal, lung and prostate cancer as well as in melanoma is correlated with accelerated tumor growth, invasion and poor prognosis. [434]

Vimentin staining is used for differential diagnosis of RCC, since ccRCC and pRCC typically show strong positive staining for vimentin, which is not seen in oncocytoma and chromophobe RCC. [431] [432] [410] In the adult kidney vimentin expression is found in podocytes residing in the Bowman's capsule [74], as well as in the parietal layer, showing co-localization with CD133 staining, which is a marker for renal progenitor cells in this region. Renal progenitors isolated from adult glomeruli, show strong staining for vimentin, which is lost upon differentiation of the cells into MSC- and kidney-specific lineages. [78] Vimentin expression is also found in the renal progenitor cell population, which is located in a scattered distribution in renal tubules, whereas the bulk of tubular epithelial cells do not express vimentin. $CD133^+$ renal progenitors isolated from the papillary region of adult kidney were also shown to stain positive for vimentin. [71] Comparison of gene expression profiles of normal kidney to RCC samples performed by Chen et al [394] yielded a set of EMT genes enriched in RCC compared to normal tissue. A better outcome of patients with low-level expression of CXCR4, vimentin, fibronectin and

Twist1 was observed. High expression of CXCR4 and VIM could serve as independent prognostic markers for poor survival of patients.

The cell lines investigated in my work, showed similar high expression of vimentin in IFC experiments. No significant differences were seen between spheroid cell lines and parental cell line, nor with time of culture or spheroids re-grown under adherent conditions. Since expression of the intermediate filament is seen frequently up-regulated in ccRCC, this result is not unexpected and the use of vimentin expression for detection of variations of EMT-state might not seem to be a suitable marker for this tumor entity. Although, several reports found differences in vimentin expression upon EMT induction in RCC cell lines, thus the high and relatively constant expression of vimentin might also be a characteristic of the cell lines investigated in this work.

5.7.2 Stem Cell Pluripotency Transcription Factor Markers Oct4 and Sox2

Oct4 (POU5F1) is a transcription factor expressed by embryonic stem cells (ESC) and together with Sox2 and Nanog regulates self-renewal and differentiation of the cells. A delicate balance among these factors is needed to retain the balance between pluripotency and differentiation ability. Expression level of the three factors influences pluripotency and differentiation. Very high or low expression of Oct4 and Sox2 induces differentiation of the cells, self-renewal is maintained at low to moderate expression levels of Oct4, moderate expression of Sox2 and high expression of Nanog transcription factors. [45] Induction of these factors has been correlated with hypoxic condition in several cancer cell lines including 786-O and RCC4. [435] [198]

Several isoforms of the Oct4 (POU5F1) gene exist, of which only the long Oct4A isoform is responsible for the pluripotency properties of ES cells, whereas the short Oct4B seems to be expressed upon cell stress and does not sustain self-renewal of ESC. [436] Antibodies that specifically bind to Oct4A isoform should be raised against the N-terminus of the protein. Using Oct4A specific antibodies in parallel with RT-PCR, Mueller et al [437] were unable to detect Oct4 expression neither in MSC nor in several tested cell lines including A549 (lung carcinoma), MCF7 (breast carcinoma), PC3 (prostate carcinoma), HEK293T (embryonic kidney), rather expression was confined to embryonic cell lines. Therefore reports on Oct4 expression may vary, according to antibody or primer specificity used for detection.

Another transcription factor, which has been shown to be involved in and to be able to induce an ESC-like program, when up-regulated in normal and cancer cells, is c-Myc transcription factor, which has been shown to be up-regulated in several tumors. [95]

Ward et al [76] investigated differential mRNA expression of Oct4, Sox2 and Nanog in $CD133^+$ sorted renal progenitor cells isolated from adult human papillary and unsorted cells as well as papillary cells compared to cortical cells. They found significantly increased expression of Sox2 and Nanog in the $CD133^+$ sorted cells compared to unsorted papillary cells as well as higher expression of the two transcription factors in papillary cells compared to cortical cells, whereas expression level of Oct4 did not show any differences between the tested entities.

Bussolati et al [71] also observed differences in expression of Oct4 isoforms in $CD133^+$ sorted progenitor cells isolated either from the papillary or the cortical region of the kidney, with tubular cells showing low Oct4A levels in respect to papillary cells, whereas the Oct4B isoform, known to be associated with

stress response, was increased at protein level in tubular cells. $CD133^+$ renal progenitors, isolated from the papillary region of adult kidney showed expression of Oct4A and Oct4B isoforms at similar level, which was reduced upon differentiation of the cells to 1/3 to 1/5 of the level seen in undifferentiated cells and found to be up-regulated under hypoxic conditions 2-3 fold after 24 h. In this study Oct4 expression was assayed by RT-PCR, at protein level as well as by transfection of cells with a reporter construct for Oct4-specific expression of GFP. In contrast, Sox2 expression was found inconsistent among the different cell lines in this study, being either completely absent or highly variable. Renal progenitors from adult glomeruli, which had previously been isolated by the same group and were found to reside in the $CD133^-$ fraction of this cells, did not show expression of Oct4, albeit expressing stem cell markers Nestin and Musashi.[78]

Expression of Oct4 and Sox2 was also investigated by Galleggiante et al [202] on $CD133^+/CD24^+$ sorted normal renal progenitors as well as on tumor derived cells with the same characteristics from the same donors. Thereby expression of Oct3/4 was similar in both cell types, but was higher than in normal renal proximal tubular epithelial cells (RPTEC) and $CD133^-$ sorted tumor cells. In contrast, Sox2 was expressed at the highest level in cells isolated from the tumor tissue, whereas low expression was seen in normal renal progenitors and $CD133^-$ sorted tumor cells and the expression level in RPTC was between the two extremes. By applying differentiating culture conditions to $CD105^+$ sorted TIC from primary tissue Azzi et al [119] observed a gradual loss of expression not only of CD105 but also of stem cell markers POU5F1/Oct4, Nestin and Nanog within 4 weeks. Also in $CD133^+$ renal progenitor cells, expression of Oct4 isoforms was detected, which was significantly reduced after epithelial differentiation of the cells. [71]

Chen et al [206] investigated the association of Oct4, Sox2 and Nanog expression with clinical outcome in RCC in a database search and found higher levels of Oct4 and Nanog expression were associated with worse survival of patients, whereas the expression levels of Sox2 and CD133 showed no significant correlation to survival rate of the RCC patients.

Expression of pluripotency transcription factors (Oct4, Sox2, Nanog, Musashi), evaluated by RT-PCR or immune histology, was observed in $CD105^+$ sorted CSC, isolated from RCC cell lines Caki-2 [198] [199], ACHN [199] [200], A498, SK-RC-39 [201], as well as from primary tumors [371] [119], whereas no or strongly reduced expression was observed in the $CD105^-$, non-CSC cell population in these studies. Expression level of Oct4 and NANOG in RCC cell lines ACHN, Caki-1/2, 786-O and SMKT-R2 was evaluated by RT-PCR in the study performed by Khan et al [319]. Relative mRNA expression levels for Oct4 normalized to the reference gene were low in Caki-1 and SMKT-R2 (below 10^{-2}), higher in Caki-2 and 786-O ($2x10^{-2}$) and highest in ACHN ($1.2x10^{-1}$). The same applied to NANOG expression levels, which were lower compared to Oct4. This suggests different stem cell properties of the evaluated cell lines, but interestingly, expression of stem cell transcription factors in this study did not correlate with CD105 marker expression of the cell lines, which was highest in Caki-1.

Lichner et al [212] evaluated mRNA expression of Oct4, NANOG, LIN28 and KLF4 in ACHN and Caki-1 RCC cell lines grown either adherently or as spheroids. They observed similar low expression of all factors in adherent cell lines. With exception of Oct4, which showed increased expression compared

to adherently grown cells only in ACHN cell line, they found increased expression of the factors in both cell lines when grown as spheroids.

The results obtained in this work by IFC staining for Oct4A and Sox2 showed low to moderate and relatively uniform staining for both markers in all cell lines investigated. Thereby no significant changes were seen in spheroid cells compared to parental cell line. Determination of mRNA expression by mRNA-Sequencing experiments also did not show significant differences in expression of Oct4 and Sox2 mRNA in PA and SP cell lines, although expression of POU5F1 mRNA levels were slightly higher in spheroid derived cells compared to PA cell line. Whereas only low-level expression of NANOG mRNA was detected in all cell lines. Sox2 mRNA expression, in contrast to results obtained by IFC, was found to be lower than that of Oct4 mRNA and was markedly reduced in A-SP cell line compared to both other cell lines. The differences in results obtained by the two methods, are probably attributed to the different staining-characteristics of the antibodies used. In contrast to results obtained by other groups, here no significant up-regulation of Oct4 or Sox2 expression at either protein or mRNA level was detected in spheroid cell lines.

A marked difference in expression at mRNA level was seen for the transcription factor Klf4 between PA, SP and A-SP cell lines, with lowest levels of expression seen in PA cell line and highest expression seen in A-SP cell line. Since Klf4 on the one hand is involved in regulation of Nanog expression, which was found to be low in the investigated cell lines, and on the other hand overexpression of Klf4 in the absence of Nanog has been found to induce ESC differentiation and Klf4 has also been shown to be involved in adipogenesis, the increased expression in SP and A-SP cell lines might be associated rather in adipogenic differentiation processes than in maintenance of self-renewal of the cells. [438] [439]

At mRNA level c-Myc was also found to be expressed in the investigated cell lines (PA, SP and A-SP) at similar high levels, which might be an indicator, that c-Myc is predominantly involved in conferring stem cell features in the investigated cell lines.

5.8 EMT Marker Expression and Status of the Cell Lines

The trans-differentiation process from polarized epithelial cells to a mesenchymal stem cell like state, termed EMT has been found to be an important process involved in tumor metastasis, but probably also may play a role in the formation of CSC. Current knowledge of signal transduction pathways involved in EMT induction as well the role of EMT in tumor formation and metastasis, especially in RCC are discussed in more detail below to rank the data obtained in this work in the context of information based on the literature.

5.8.1 EMT Signaling

EMT can be induced by various external signals. Thereby the transcription factor Snail1 is central for promotion of EMT. It increases directly the transcription of vimentin, fibronectin and N-Cadherin, as well as other EMT inducing factors Twist and Zeb, and by binding to E-Cadherin promoter directly represses its expression. [440]

In figure 5.9.1 for better orientation an overview of several signaling pathways and molecules involved in EMT is given.

EGF, FGF, HGF and VEGF growth factor signaling as well as IGF1 signaling have been shown to induce EMT in cell culture of epithelial cells, via activation of PI3K/AKT and MAPK/ERK pathways, which induce expression of Snail and/or Twist transcription factors as well as vimentin (via activation of FOXA1/2, FOXO3A, SOX9 transcription factors) and Zeb on the one hand, and/or stabilize Snail1 and its nuclear localization by inactivating GSK3β as well as Twist by MAPK phosphorylation.

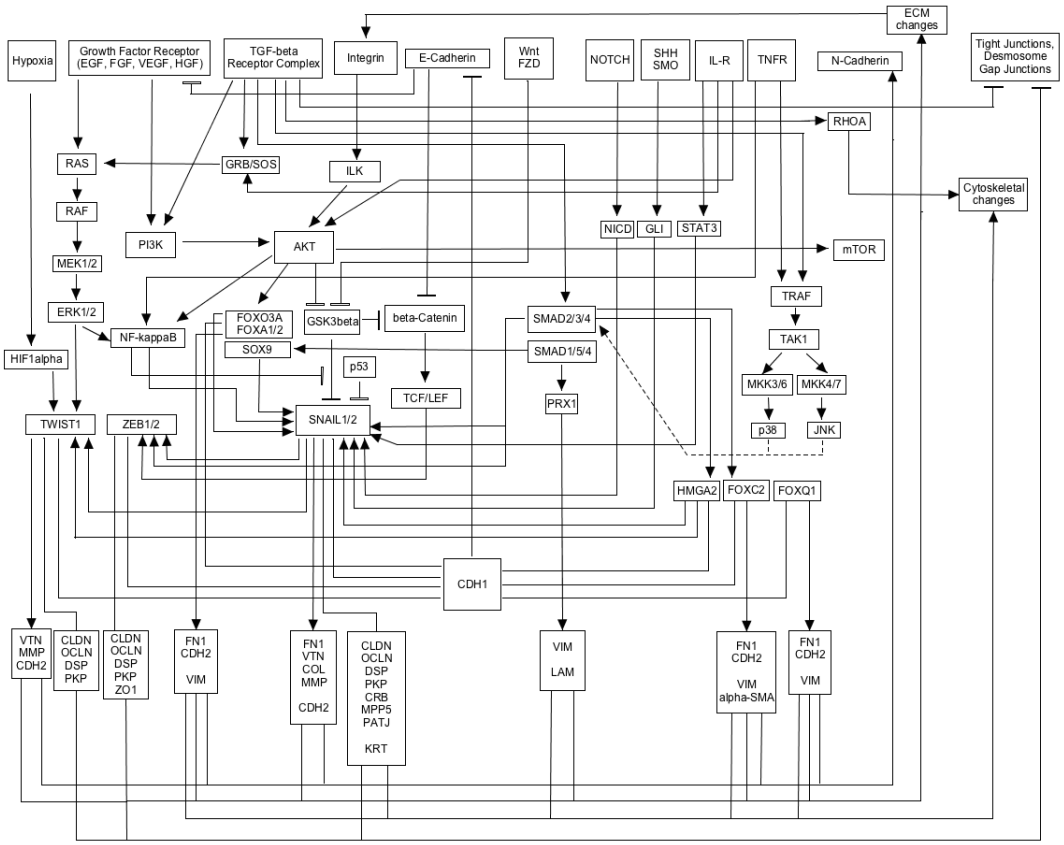

Figure 5.8.1: Overview of Signal Transduction Pathways Involved in EMT

Several signal transduction routes, leading to expression of the core EMT transcription factors Snail1/2, Zeb1/2 and Twist1 are depicted. The components are named according to their gene symbols. The figure was drawn according the information given in an overview article by Lamouille et al.[137]

The most prominent signaling pathway known to induce EMT in embryonic development and cancer is TGF-β signaling through SMAD2/3/4 (TGF-β) or SMAD1/5/4 (BMP) as well as non-SMAD pathways (PI3K/AKT, SHCA-GRB-SOS-RAS-RAF-MEK1/2-ERK1/2, TRAF6-TAK1-MKK3/6-p38 or MAPK4/7-JNK) induced by binding of different ligands (TGF-β1,2,3, BMP2/4/7). [137]

Also signaling by integrins via ILK-PI3K-AKT-GSK3β is involved in promoting EMT. [137]

Interleukin signaling, another microenvironmental signal, has also been shown to promote EMT, which, dependent on context and cell type might activate JAK/STAT pathway, via different adapters the SOS-RAS-RAF-MEK1/2-ERK1/2 pathway or PI3K-AKT pathway. [137] The dual role of interleukin 15 (IL-15) signaling for EMT has been shown for renal epithelial tubular cells and RCC. In normal renal epithelial cells autocrine IL-15 stimulation acts as homeostatic survival signal, which is mainly executed by JAK3/STAT5 signaling pathway and maintains E-Cadherin expression. In contrast, in the absence of JAK3/STAT5 activation due to the lack of CD132 (IL-15 receptor gamma chain) in RCC,

down-regulation of E-Cadherin and the commitment of the cells into the EMT process were observed. By ectopic expression of JAK and CD132 in these cells E-Cadherin expression could be rescued. [195] Besides these pathways EMT has also shown to be induced by hypoxia via HIF1α, which induces expression of Twist1. But also signaling induced by WNT via inactivation of GSK3β, Hedgehog via Gli1 mediated expression of Snail1, as well as Notch signaling via direct activation of expression of Snail2 may attenuate or promote EMT characteristics. [137]

5.8.2 Role of EMT in Kidney

In the kidney EMT contributes to establishment of fibrosis in chronic progressive kidney disease. The process has shown to be induced by hypoxia, reactive oxygen species (ROS) or inflammatory cytokines. Renal fibrosis is characterized by trans differentiation of proximal tubular epithelial cells (PTECs) into myofibroblasts, whereby expression of vimentin (VIM), α-smooth muscle actin (α-SMA), fibronectin (FN1) and matrix-metalloproteinase 9 (MMP-9) is up-regulated. It has been shown that the growth factor FGF-2 (bFGF) is capable of inducing EMT in PTECs. From the three signaling pathways primed by FGF-2 (PLCγ, MAPK(ERK1/2), PI3K/AKT) during induction of EMT the PI3K/AKT pathway has been observed to be rapidly and persistently activated. [441]

5.8.3 Role of EMT in RCC

Several studies investigated the role of EMT in RCC and revealed that this tumor type possess a high EMT status compared to normal tissue as well as to other tumor entities. Also correlation of EMT related gene expression with patient prognosis and survival were reported.

In a comprehensive study on gene expression in different cancer cell lines, 6/7 renal carcinoma cell lines highly expressed genes assigned to the mesenchymal gene cluster, containing the EMT markers N-Cadherin (CDH2) and fibronectin (FN1) as well as FGF-2/bFGF and the corresponding receptor BFGFR. [442] Also the EMT marker vimentin (VIM) is long been used to discriminate RCC subtypes (see chapter 5.7.1.2) [431], suggesting a principal role of EMT in RCC in general, which is different from carcinomas of other organ's origin. [443] This is in line also with results obtained by Tan et al [444] when comparing an EMT gene signature comprised of 314/218 weighted epithelial and mesenchymal specific genes to gene expression data from primary RCC and RCC cell lines. The signature revealed a predominant mesenchymal phenotype of this tumor type and a similar mesenchymal score was observed for germ cell tumors. From the analyzed tumor entities only melanoma, osteosarcoma and glioblastoma showed higher mesenchymal scores than RCC. Surprisingly, in their study the mesenchymal phenotype in RCC was correlated with higher disease free survival rate.

Comparison of gene expression profiles of normal kidney to RCC samples performed by Chen et al [394] yielded a set of EMT genes enriched in RCC compared to normal tissue. A better outcome of patients with low-level expression of CXCR4, vimentin, fibronectin and TWIST1 was observed. High expression of CXCR4 and VIM could serve as independent prognostic markers for poor survival of patients.

A comparison of gene expression by NGS in 26 patient matched normal and tumor samples was also done by Landolt et al [355] revealing an increased EMT score in ccRCC compared to normal tissue. They found MMP14, AXL, CAV1, ITGA5, VIM, IGFBP3, and ITGA1 among the top genes differentially

up-regulated in tumors compared to normal samples, whereas E-Cadherin (CDH1) and EpCAM, as well as growth factors EGF and FGF1 expression were down regulated in tumors. Of the identified genes MMP14 and AXL were correlated with worse patient prognosis. Comparison of tumor EMT expression pattern to classifiers of fibrosis revealed a tight link between EMT and fibrosis, since fibrosis markers could serve to discriminate tumors from normal samples.

Weygant et al [198] performed a comparison of „TCGA KIRC" RNA-Seq datasets and revealed that the mesenchymal markers vimentin (VIM) and N-Cadherin (CDH2) were overexpressed in RCC tumors compared to matched normal adjacent tissue, while E-Cadherin (CDH1) mRNA was significantly down regulated. Higher VIM expression was correlated with tumor stage and patients' median survival. Reduced CDH1 expression was also correlated with overall and median survival of the patients in the study. Similarly, the study of Boysen et al [378] found CDH2 among the top ranked pVHL-driven genes specific for ccRCC.

The connection between EMT marker expression in IHC staining of tumor samples and patient prognosis was investigated by Harada et al [445]. They also observed a correlation with strong vimentin and high Twist1, as well as low E-Cadherin expression as significant hazard markers for RCC. N-Cadherin and Snail1 expression did not show significance for prognosis. 70% of patient samples showed weak E-Cadherin staining. A high staining pattern for vimentin and N-Cadherin was observed in 50% of the samples, whereas 40% and 30% of the analyzed tissues showed strong expression of Twist and Snail respectively.

5.8.4 Induction of EMT by TNF-α in RCC cell lines

For ACHN and 786-O RCC-cell lines Zhang et al [446] were able to induce EMT by treatment with TNF-α for 7-14 days. They observed increased expression of VIM, SLUG (SNAI2), and ZEB1 at mRNA and protein level as well as decreased expression of E-Cadherin (CDH1) after TNF-α treatment. Changes in expression of mRNA for stem cell markers POU5F1/Oct4, NANOG and BMI1 were also reported. Additionally, they observed a 3- to 4-fold higher sphere-forming ability in both cell lines after EMT induction. For 786-O and A498 as well as for Caki-1 cell line, Ho et al [447] tested TNF-α induction of EMT and observed higher expression of vimentin and MMP9/2 in induced cells compared to uninduced cells, as well as a reduction in E-Cadherin expression. Sun et al [448] obtained similar results again with 786-O and A498 cell lines showing elevated expression of vimentin, Slug (Snail2) and Zeb1 as well as of chemokine receptors (CXCRs) and reduced expression of E-Cadherin (A498 cell seemed not to express E-Cadherin in this report) upon stimulation with TNF-α.

5.8.5 Investigation on EMT Induction by TGF-β in Tumor Cell Lines including RCC

In CRC cell lines TGF-β treatment induced EMT, indicated by increase of expression of N-Cadherin and vimentin and reduced expression of E-Cadherin. Besides these classical EMT markers also an increase in expression of NCAM and CD24 was observed after TGF-β treatment of the cells in the study performed by Okano et al [362]. Also in the ovarian cancer cell line Caov-3 EMT was induced by TGF-β, marked by reduced expression of E-Cadherin and induction of Snail1, as well as increased CD24 expression. In this study the same results were seen under hypoxic conditions. [358]

TGF-β stimulation of RCC cell lines A498 and 786-O enhanced their migratory ability in Matrigel™ via Smad/PAI-1 pathway, which has been shown to be significantly associated with tumor progression, metastasis, and survival in ccRCC. [449]

Bostrom et al [450] investigated the connection between EMT and sarcomatoid ccRCC, which account for approximately 8% ccRCC cases and are characterized by regions of radically different mesenchymal appearance, thereby histologically resembling sarcomas. Sarcomatoid ccRCC are associated with considerably worse prognosis due to higher metastatic potential. In 6 sarcomatoid RCC samples the authors found a higher portion of EMT markers in the sarcomatoid regions as well as high TGF-β expression. Evaluation of changes induced by exposure of RCC cell lines to TGF-β revealed changes in cell morphology similar to sarcomatoid ccRCC, accompanied by changes in RNA levels for key EMT markers. The results indicate a possible conversion of ccRCC by EMT to the more aggressive sarcomatoid subtype.

Expression of EMT markers was also evaluated by Hsieh et al [318] in the sarcomatoid RCC cell line RCC-52. Sorting of this cell line for $CD24^{Hi}$ and $CD24^{Low}$ cell populations, resulted in two clearly distinctive cell fractions, with epithelioid ($CD24^{Low}$) and fibroblastoid ($CD24^{Hi}$) phenotype respectively. Both cell fractions showed similar portions of N-Cadherin and vimentin positive staining cells, albeit the GM values measured for the fibroblastoid cell line were slightly higher. A clear difference was observed in E-Cadherin expression, which was seen in the epithelioid cell fraction only.

This might be an indicator, that N-Cadherin and vimentin are no suitable markers for EMT in cancer cell lines, since their variation upon mesenchymal transition seems to be only marginal.

The expression pattern of N-Cadherin and vimentin seen in the report of Hsieh et al [318] parallels the results obtained in my work. But regarding E-Cadherin and CD24 expression no difference was seen between the PA and spheroid cell lines, which when grown under ACC, similar to PA cell line showed epithelial morphology, though in contrast to the cell line investigated by Hsie et al [318] the expression of CD24 was constantly high in all investigated samples.

5.8.6 Expression of EMT Markers in Renal Progenitors and RCC Cell Lines

Expression of Snail1 and E-Cadherin was also investigated by Galleggiante et al [202] using protein array analysis on $CD133^{+}/CD24^{+}$ sorted adult normal renal progenitors (ARP) as well as of tumor derived cells with the same characteristics isolated from the same donors. The authors compared expression levels additionally to the $CD133^{-}$ tumor cell fraction as well as to normal renal proximal tubular epithelial cells (RPTEC). Thereby no significant changes in expression of E-Cadherin was found between all tested cells, with adult tubular progenitor cells showing slightly lower expression of E-Cadherin compared to tumor cells. Snail1 expression, albeit similar among ARPs and tumor derived cells, was markedly lower in the $CD133^{-}$ tumor cell fraction, but only slightly reduced in RPTECs compared to tumor cells, implying a connection between CD133 expression and Snail1 expression.

Lichner et al [212] evaluated mRNA expression of EMT markers ZEB1/2, Twist, N-Cadherin and vimentin in ACHN and Caki-1 RCC cell lines grown either adherently or as spheroids. They found up-regulated expression of the markers in spheroids compared to adherent cells, which was especially pronounced in ACHN cell line. Only ZEB1 was down regulated in spheroids from Caki-1 cell line, compared to adherent Caki-1 cells.

5.8.7 Results Obtained by Flow Cytometric Immunophenotyping (IFC)

For the investigated cell lines a hybrid EMT phenotype was observed, characterized by parallel expression of epithelial and mesenchymal markers. Although Snail1, which is known to suppress E-Cadherin expression, was clearly detected in the cell lines, E-Cadherin expression was relatively high. A possible explanation for this contradictory behavior seen in ccRCC was given by Sampson et al [451], who investigated WT1 influence on Snail1 and E-Cadherin expression in RCC cell lines ACHN and SN12C as well as in HEK293T and MDCK cells. WT1 is known to be up-regulated in RCC [355], while it is not expressed in adult kidneys (with exception of podocytes). The protein has been shown to regulate EMT and MET in different tissues. In their study the authors show that WT1 expression is up-regulated by VHL knockdown, a frequent mutation in RCC, in a HIF-dependent manner. In VHL knockdown cells, WT1 has been shown to induce expression of Snail1 on the one hand by binding to the WT1 binding sequence in the Snail1 promoter, as well as E-Cadherin expression on the other hand, which was shown by siRNA knockdown of WT1 in these cells. Experiments show that WT1 expression, which is induced by increased HIF activity in RCC may compete with Snail1 for E-Cadherin promoter binding and thus may relieve repressive effects of Snail1 on E-Cadherin expression. This results in epithelial morphology of the cells despite the hybrid EMT state. Interestingly, VHL knockdown cell lines expressed α-SMA, which was not seen in the more mesenchymal parental cell lines. Also epithelial marker ZO-1 (up-regulated) and NaK-β1 (down-regulated) were contrarily expressed upon VHL knockdown in the investigated cell lines. N-Cadherin was still expressed upon VHL knockdown, albeit at slightly lower level.

Co-expression of the mesenchymal marker vimentin with the epithelial cell marker Pan-CK, which was seen in my experiments, was also observed in renal progenitors isolated by CD133 positive sorting from human renal papillary tissue and from Bowman's capsule. [71] [73] Expression of CD24 in the investigated cell lines also is a strong indicator for the hybrid-EMT nature of the cell lines and implies a possible role of Notch signaling in the maintenance of this state. [360]

Surprisingly, no profound difference was seen in EMT status between the parental cell line and the spheroid cell lines in IFC analyses. Taking into account that two factors shown to induce EMT - growth factor signaling by bFGF and EGF as well as hypoxic conditions - applied to the latter, it was logical to assume that spheroid cells might show higher expression of mesenchymal markers compared to the parental cell line. This was true to some extent, when taking immunocytometric measured geo mean values for N-Cadherin staining into account, which were higher in spheres compared to PA cells. But for neither of the other measured EMT marker signals (E-Cadherin, vimentin, Snail1) significant differences were observed. Only a slightly higher expression of cytokeratins in PA cells compared to SP or CS cells could be detected.

Of note is that primary $CD105^+$ sorted, putative CSC from RCC were reported not to express E-Cadherin until they were differentiated by using standard media conditions. [119] Similarly, in the study by Hu et al [200] using xenograft tumors generated from $CD105^+$ sorted ACHN cells, staining for CK7 was absent in $CD105^+$ sorted xenograft tumors but was observed when the cells were cultured in standard RMPI-1640 medium instead of the expansion medium used by Bussolati [78]. In contrast, staining for the EMT marker vimentin was observed in $CD105^+$ sorted cells only but not in the parental

unsorted cells and the expression of vimentin was lost upon standard RMPI-1640 culture of the cells. These results imply, that $CD105^+$ CSC in RCC are of mesenchymal phenotype and acquire expression of epithelial markers only after differentiation under standard conditions.

This is interesting in two regards, on the one hand expression of CDH1 on PA cells, which are positive for CD105, may also have been induced by culturing the tumor cells under standard conditions. On the other hand an opposite effect concerning CDH1 expression in PA cell line was observed, namely a reduction of CDH1 expression and gradual evolvement of E-Cadherin negative cell fractions during prolonged culturing of the cells. This might have been due to selection of long-living stem-like cells over time in culture, as the same effect was observed for cells cultured as spheroids.

Interestingly, when re-growing spheroid cells containing E-Cadherin-negative cell fractions under ACC, E-Cadherin was again expressed on all cells in the culture. More detailed studies on the time course of this change, together with expression patterns of other markers in the cells lines used in this work might shed light on the nature of this process.

5.8.8 Results Obtained by mRNA Expression Analysis

Results obtained for mRNA expression of several EMT markers from RNA-Sequencing experiments of PA, SP and A-SP cells confirmed similar high expression of CDH1, CDH2 and vimentin in all cell lines. Similar to results obtained by IFC, PA cell line was found to show higher expression of keratins, compared to spheroid-derived cell lines. Surprisingly, SNAI1, TWIST1 and ZEB2 mRNA levels seemed to be reduced in SP cells compared to adherently grown cells, which might be attributed to different EMT inducing signals such as TGF-β and TNF-α signaling being present under the serum-containing culture conditions. In contrast to other EMT inducing transcription factors, expression levels of ZEB1 mRNA were found to be similar in the three investigated cell lines. An interesting result is the markedly higher expression of SNAI2 mRNA in PA cell line compared to spheroid derived cell lines. The mRNA expression pattern for EMT markers observed for the cell lines investigated in my work, thus differs in various aspects from reports for other RCC cell lines and further substantiates the complex nature of this multifactorial process that involves several pathways. [214 212 447 440]

Although the process of EMT was not investigated in very detail in this work, the results obtained concerning expression of EMT markers might be used as a basis for further detailed investigations of this complex process in RCC and also for further investigations of implications of transcription factors being associated not only with EMT but also with other functions in survival and promotion of tumor formation. [452] For example the transcription factor FOXQ1, which has been shown to be involved in EMT promotion of breast cancer cells [453], was among the top up-regulated genes in spheroid cells compared to PA cell line. Since pathways leading to activation of this transcription factor are not well known, the cell line might be a suitable tool for further investigation of the role of this factor in tumor formation and metastasis. It would also be interesting to investigate the influences of EMT inducing agents such as TNF-α or TGF-β on the cell lines established in this work.

5.9 Differential Gene Expression in PA, SP and A-SP Cell Lines

RNA-Sequencing analysis for differentially expressed genes between PA, SP and A-SP cell lines further substantiated expected enrichment of CSC characteristics in SP cell line compared to PA cell line, which were partially retained in adherently cultured cells. Among differentially expressed genes between spheroid-derived cells and PA cells were such involved in kidney development (PAX2, WT1, HNF1A, HNF4A, POU3F3, BMP2/4, SALL1), metabolism (MLXIPL, HMGCS, MAOA/B), oxygen status/HIF transcription factor network (EGLN3, NDRG1, EGR1), but also in several signal transduction pathways known to be active in tumor and stem cells and differentiation (RARRES2, PRKAA2, SHC3, EZH2, LRP2, SPOCK1, BMP2, BMP4) and signaling components of WNT, SHH, and MAPK pathways. Compared to spheroid cell lines, genes up-regulated under serum-containing medium conditions in contrast showed up-regulation of pathways predominantly involved in immune-regulation.

The high number of brain- or neuron-associated terms, which were found among the top listed entities for all datasets is in accordance with results obtained by Ross et al [442], who investigated gene signatures of cancer cell lines from different organs' origins by microarray analysis and identified a mesenchymal gene cluster to be up-regulated in RCC cell lines, which was also seen in CNS tumors and to a lesser extent in ovarian carcinomas. Also in two-dimensional hierarchical cluster analysis of expression data from the investigated cell lines RCC tumor cell lines grouped next to tumor cell lines derived from CNS.

Among top-ranked terms found for differentially expressed genes were various cancerous diseases, especially different histological subtypes of RCC. Also several genes that have been shown to be involved in RCC tumor formation or CSC from RCC for example KISS1R, MMP14, NDRG1, PRODH2, SELENBP1 and HOTAIR, IGFBP3, DNMT1, HDAC4, CAMK1 [192] [454] were found to be up-regulated in spheroid-derived cell lines. In contrast, no significant difference in mRNA expression levels of CBFA2T2, SIRT2, HIF1A, VHL, SETD2, DNAJB8, and c-MYC have been observed.

5.10 Tumor Formation Assay - Xenotransplantation

It was very disappointing to see, that no cell growth, even at a relative high cell numbers of 10^6 applied cells, was observed in the tumor formation assay. Taking into account the *in vitro* characteristics of the cells, which in many aspects (expression of CSC markers CD105, CD73, sphere-forming ability, high expression of ALDH, $Rho123^{high}$ side-population, colony growth in soft agar) resembled those of CSC from other RCC (primary and cell lines) and the applied cell numbers of 10^4-10^6 cells were relatively high, the results are very unexpected. The high cell numbers were actually chosen to gain xenograft material for further analysis, since in the NSG strain usually lower cell numbers have to be injected to see differences in tumor growth. For example a difference in tumorigenicity between different cell populations of DU145 prostate cancer cell line was seen only at small cell numbers of $3x10^3$ injected cells, whereas with $5x10^4$ injected cells tumors grew from all fractions. [455]

Compared to other tumor entities RCC are known to have reduced growth potential. But at similar cell numbers as were used in my experiment unsorted RCC cell lines ACHN (10^6 cells [456]), $2x10^6$ cells [457]), A498 ($2x10^6$ [457]), or HEK293T ($2x10^6$ cells [458]) were used to test for tumor growth inhibition or tumor

characterization studies in different mouse strains from “nude” or “SCID” background, which are less permissive for tumor growth than NSG mice. Another study reports that Caki-1 or ACHN cell lines were able to form tumors in 6/6 mice of the NOD/SCID type at a number of $1x10^5$ injected cells [203], and Song et al [210] report that $5x10^3$ adherently grown 768-O cells were able to induce tumor growth in 3/4 NOD/SCID mice whereas 10^6 injected cells formed tumors in 5/5 tested animals. In the NSG mouse strain Caki-1 cell line formed tumors in 4/4 mice with $1x10^6$ injected cells and 3/4 mice with 10^4 injected cells. [212] On the other hand subcutaneous application of the cells was heterotopic with respect to the tumor of origin and for some cell lines orthotopic transplantation is needed for cells to grow in xenografts. There are several RCC cell lines for which no tumor growth in mouse models was observed (see table 1.5.1). [193] This might be due for example to the different growth factor milieu in the recipient animals as some murine growth factors (e.g. TNF) are not cross-species reactive.

A general problem with cell preparations can be excluded, since growth assays performed with aliquots of the respective cell suspensions after injection did not show any irregularities. The SP cell line in high passage was chosen because of increased growth potential and CSC marker expression in higher spheroid passage numbers. In addition to growth characteristics, the cell line used for the assay showed also the expected expression pattern of these markers according to passage number.

One suspect reason for the lacking cell growth is the use of Matrigel™ as growth matrix for injection. In most published reports on RCC cell xenotransplantation cells are applied in PBS. Experiments performed to evaluate optimal transport conditions revealed, that the cells show sensitivity to low temperatures. Although no difference between different samples (medium, DPBS/ 4°C, RT) could be seen in IFC measurements using a viability stain (which is comparable to the trypanblue detection method of dead cells used for determination of implanted live cell content), in growth assays performed in parallel, a strongly reduced growth rate was observed, when cells were kept for the test period of 4 h at 4°C. Since Matrigel™ is liquid only at low temperatures and forms a gel at room temperature, the suspension of cells has to be done on ice. Although in cell culture experiments, when the chilling time was held short, the cells were able to grow in the matrix.

Finally, all speculations cannot substitute experimental results. A repetition of the experiment is needed to get clarity.

5.11 Summary of Results

A summarizing overview of results obtained for stem cell features investigated in this work for different cell lines is given in table 5.12.1. The comparison with expression patterns observed for investigated marker antigens, which is shown in table 5.6.1, reveals that no investigated marker was found to be well correlated with the observed spheroid growth characteristics or growth in soft agar assay experiments.

Feature	PA	Time	SP	Time	CS7	Time	CS1	Time	A-SP	Time
Unrestricted Growth Potential	+		+		+		+		ND	
Growth Rate	moderate	↑	low	↑	low-high	↑	low	↑	moderate	→
CSFE	8±4% to 0%	↓	5±1% to 68±8%	↑	4±4% to 38±10%	↑	7±3% to 77±7%	↑	similar to spheroids	
Adipogenic Differentiation Potential	+	→	++	→	o	→	+	→	similar to spheroids	
Osteogenic Differentiation Potential	+	→	++	→	+	→	o	→	similar to spheroids	
EMT-Status	intermediate	↑	intermediate	↑	intermediate	→	intermediate	↑	intermediate	↓
Specific Markers	CD106 CD243	≈±	CD10 SSEA-1^{low} TNAP CD73 high	≈± ↓ ≈± →	CXCR7 (CD184) (CD133)	↑	(CD133) (CD44) (EpCAM)	≈± ↓ ↓		
Spheroid Markers			CD184 CD56 CD271	↑ ↑ →	CD184 CD56 CD271	↑ ↑ →	CD184 CD271	≈± →	CD271	→
Soft Agar Serum	1±1.5%, 169±101 µm		14±7.9%, 263±185 µm		1±1.3%, 153±113 µm				12±7.1%, 210±112 µm	
Soft Agar NCFCA	0.4±0.4%, 176±118 µm		3.6±2.4%, 315±245 µm		0.6±0.9%, 413±408 µm				4.8±3.1%, 306±261 µm	
ALDH Expression	moderate to high		high		high		NA		NA	
Rhodamine 123 SP	Rho^{low}		Rho^{high}		Rho^{high}		Rho^{high}		Rho^{high} and Rho^{low}	
Tumor Formation	0/5		0/5		NA		NA		NA	

Symbol	Description
o	low or not detected
++	high
+	present
≈±	variable
↑	up
↓	down
→	no difference
NA	not determined

Table 5.11.1: Overview Results Obtained for Stem Cell Features Investigated on Different Cell Lines

Features were graded according to criteria listed in the legend using mean values of all performed measurements, when applicable. Variations seen over time of culture are indicated in the "Time" column as symbols. For CSFE minimal and maximal values are indicated. Change of EMT status to more mesenchymal phenotype is indicated as increase, whereas more epithelial state is indicated as decrease.
Markers expressed predominantly on one of the cell lines are indicated as "Specific Marker"; thereby brackets mark specific expression patterns in a cell line. Markers expressed predominantly on spheroid cell lines are indicated. For soft agar assay results, CFE values as well as mean diameter of colonies are indicated. NCSFC indicates growth in soft agar assay under SCC.
ALDH expression as evaluated by ALDEFLUOR^{TM} assay, high indicates more than 60%, moderate indicates more than 40% positive staining cells, thereby high variation of results was seen for PA cell line.
Capacity of pumping out dye in the Rhodamine 123 side population assay, which was shown to be correlated with CD243/MDR1 expression is indicated as follows: Rho$^{high/low}$: high/low dye retention of Rhodamine 123.
Tumor formation is indicted as number of tumors grown from 10^6 injected cells/number of mice injected.
ACC: adherent culture conditions, A-SP: SP cells cultured under ACC, CFE: colony-forming efficiency, CS: clonally expanded spheroid cells derived from PA (CS1 and CS7), CSFE: clonal spheroid-forming efficiency, PA: parental cell line, NCFCA: neural colony-forming cell assay, Rho: Rhodamine 123, SCC: spheroid culture conditions, SP: spheroid cells derived from PA

5.11.1 Differences between Spheroid Cell Lines and Parental Cell Line

PA cell line differed form spheroid cell lines in expression of several marker antigens as well as in spheroid and soft agar growth characteristics, both of which were reduced in PA cells compared to SP and CS cell lines. The spheroid-forming efficiency of PA cell line was rapidly reduced with prolonged culturing of the cells. A marked difference was also seen in Rhodamine 123 side population assay, where the dye was effectively pumped out in the PA cell line only, resulting in a relatively high Rho^{low} cell populations, which according to results obtained by Lu et al [209] and Song et al [210], seem to mark the non-CSC population of RCC in this assay.

5.11.2 Differences between Spheroid Cell Lines

The two different methods applied to generate spheroids yielded two clearly phenotypically distinguishable cell line entities. The clonally amplified CS cell lines were smaller in size and showed higher growth rates in long-term culture. In contrast, the ability to grow in serum-containing soft agar assay in both colony number, as well as colony size was reduced compared to spheroid cell lines that were grown as bulk culture. In contrast in soft agar assay using SCC, only the CFE, but not the colony size was reduced in CS cell lines compared to bulk cultured spheroids, indicating that both spheroid cell lines contained cells with stem cell characteristic growth potential, albeit at varying numbers.

Although CS cells morphologically appeared more homogenous than PA and SC cells, they showed higher heterogeneity in expression of investigated antigens. Detailed comparison of two CS cell lines (CS1 and CS7) revealed several differences between them (see table 5.6.1), whereas SP cell lines showed relatively constant characteristics in the three independently generated cell lines, of which two were characterized in more detail.

CS cell lines in contrast to SP and PA cells expressed CD133 at significant cell numbers, which has been shown to be a marker for high proliferative cells, and is used for isolation of renal progenitor cells but seems not to be a marker for CSC in RCC, when used not in combination with CD24 expression. The IFC profile for SSEA-4 expression compared to PA and SP cells showed a broader distribution in CS cell lines, indicating several populations with different grade of expression of the stem cell marker. In contrast to SP cells, expression of SSEA-1, at the beginning of spheroid culture was similar to that of PA cells, indicating a more mature phenotype of the cells, which was reduced upon long-term culture as spheroids. A common feature seen in the two CS cell lines was the fraction of CD105 negative cells, which evolved over time under SCC.

Also the differentiation abilities of CS cells were reduced compared to PA and especially to SP cells, since they were not able to differentiate into both cell types tested, rather CS1 showed only adipogenic and CS7 only osteogenic potential.

The cell line CS7 in contrast to all other tested cell lines did not change EMT status over time in culture, seeming to be locked in intermediate mesenchymal state. This cell line also showed markedly higher expression of the markers found to be predominantly expressed on spheroid cells, namely CD56, CXCR4 (CD184), CXCR7 and CD133, which were also found to increase with time culture under SCC. Variations in expression of EpCAM and CD44 with time of spheroid culture were observed in CS1 cell line exclusively and expression of spheroid-specific markers was less pronounced or

variable compared to CS7 cell line. In contrast to SP and CS7 cell lines, no expression of CD56 was observed.

CD10 positive staining as well as TNAP positive staining cell populations were found only in SP cell lines. This cell line also showed higher expression levels of CD73 compared to all other cell lines and was found to possess the highest differentiating potential.

Taken all this together the clonal sphere generation method seems to enrich for more mature progenitor cells as proposed in the model of Liu et al [321], probably due to the disturbance of equilibrium between stem cell and non stem cell compartment at the beginning of the culture. Whereas in "bulk" culture these disturbances are less pronounced and therefore no such enrichment occurs.

5.11.3 Spheroid Cell Lines Re-grown under Adherent Serum-Containing Culture Conditions

An important result of this work is the observation, that spheroids grown for longer periods under serum-containing adherent growth conditions retained the growth potential of their parental spheroid cell lines in NSA and SAA. This is in strong contrast to several reports, describing differentiation of spheroid-derived cells under these growth conditions, which was accompanied by loss of stem-cell characteristics. [459] [119] Similar results were reported by Song et al [210] for spheroids from primary RCC tissues and the 786-O RCC cell line. This growth potential was not reflected by expression of several markers, which were shown to enrich for CSC (CD56, CD184, CXCR7, CD133), since a reduction of expression of these markers on A-SP or A-CS cell lines was observed. Adherently grown spheroid cell lines also retained a substantial fraction of the Rho^{high} cell population, shown to mark cells with CSC in RCC. Also no differences in differentiation potential was observed in these cells, compared to parental spheroid cell lines. mRNA-Sequencing results also revealed up-regulated expression genes expressed at higher level in spheroid cell lines compared to PA cell line.

5.11.4 Plasticity and Heterogeneity

In accordance with the literature, the results obtained in this work did not fit a simple straightforward model. Instead, a high degree of heterogeneity and plasticity of the investigated cell line was observed, which became obvious by using different culture conditions, which in case of SP and CS cells varied only slightly. Some aspects were very similar among the spheroid cell lines, whereas others, which were described in the literature as probable markers for CSC, showed high variations. These were even more pronounced in the CS cell lines, which had passed a narrower bottleneck of selection. Similar results were seen for example also for clonally expanded MSCA-1^+/$CD56^+$ and MSCA-1^+/$CD56^-$ sorted MSC, which independently of CD56 expression, were shown to possess different phenotypes, proliferation rates, and differentiation capacity. [340] Surprisingly, spheroid cells cultured as "bulk" cells (SP) seemed to be less heterogeneous than the CS cell lines, possibly reflecting cell interactions needed to sustain a balance between stem and non-stem cell compartments.

Thus, the *in vitro* studies done here with an RCC cell line were also reflecting the results obtained *in vivo* in a study of Hasmin et al [356], who used xenograft propagation of primary ccRCC tumor cells. This study revealed that heterogeneous tumors arise from a single cell line, when transplanted in NOD/SICD mice. The xenografts differed from the parental tumor in reduced expression of CD133 and

a loss of CD105 expressing cells. The sorted cell populations from primary xenografts, resulted in secondary xenografts with further variations in cellular composition, indicated by increased expression of EpCAM in $CD132^+$ and $CD133^+$ sorted cells, and varying expression of CD133. This implies that several CSC subsets in the primary tumor may exist, which in the foreign environment further evolve. Comparing the observed stem cell features in the cell lines investigated in this work to other RCC cell lines shows, that only single aspects were found to be similar to a given cell line, whereas other aspects observed were found to be stamped quite differently. This observation further highlights the existence of several CSC sub-populations in RCC, which employ different possible pathways, resulting in specific signatures. These results weaken the hope for possible identification of single markers for targeting CSC for cancer therapy. Rather approaches targeting the plasticity of the cells directly, such as differentiation therapies using IL-15 [195] [119] for or BMP2 [207], which have been proposed for RCC might be promising directions in this field. Though, differentiation potential of CSC, especially to other than epithelial lineages, was investigated only in few reports. Here I show, that, besides other characteristics, also differentiation potential varied between the different spheroid-cell lines although all cell lines showed differentiation potential to adipogenic and/or osteogenic lineages, similar to the situation reported for sub-populations of MSC.

6 Conclusion

In my thesis, a clear cell renal cell carcinoma (ccRCC) cell line, of which a fourfold gene-modified derivative was already used in oncological clinical trials, served as the parent cell line (PA) for the generation of cell lines with cancer stem cell (CSC) characters. Isolation and enrichment of such CSC through cultivation of spheroids was evaluated.

Spheroids were generated using two cell culture methods. Spheroid yielding cell lines termed SP were cultured as bulk cultures directly from PA with regular disaggregation. Spheroids that lead to cell lines termed CS (for clonally derived spheroids) were cultivated at clonal densities, with longer cultivation periods under spheroid growth conditions and without disaggregation. The two methods resulted in clearly distinctive spheroid subtypes, differing in morphology, growth characteristics, marker expression, and differentiation potential.

Their long-term proliferative potential, a defining feature of stem cells, was assayed by long-term cultures of SP and CS. All cell lines derived by the two spheroid culture conditions were found to possess similar unrestricted proliferative potential without signs of senescence or reduction of growth rates in long-term cultures. Rather growth rates increased and cell sized decreased in SP and CS with time of culture.

The self-renewal abilities of SP and CS were assayed using the „Neurosphere Assay“ (NSA) in long-term passaging up to 60 weeks and 200 cell generations. Profound increases in spheroid-forming efficiency (CSFE) with time of culture were observed for SP and CS, as highly significant indicators for the enrichment of cells with stem cell characteristics. In contrast, CSFE of the PA parent cell line dropped dramatically to almost zero after about five weeks of culture, indicating loss of stem cell characteristics during long-term adherent culture.

In vitro tumorigenicity was assayed using the soft agar assay (SAA). Quantitative and qualitative differences between assayed cell lines were observed. The highest growth potential in soft agar was found for SP with a colony-forming capacity of 12% and larger colonies formed compared to CS and parent cell line PA. No significant differences in colony-forming capacity between PA and CS were observed. Both cell lines have colony-forming capacities in the range of 1% and display similar colony sizes. If assayed in soft agar under the same serum-free medium composition as used for spheroid culture, CFE dropped two- to threefold in all cell lines, but also led to an increase of colony sizes in SP and CS. Since larger colonies correlate with enhanced “stemness”, the respective stem cell character is highest in SP, lower in CS, and lowest in PA.

Most important for the subjects of my thesis, the growth potentials of spheroid cells observed in NSA and SAA was retained even after long culturing periods under conditions of adherent growth in cell monolayers (these derivatives of SP and CS were termed A-SP and A-CS). This is a strong indicator for enrichment of stem cells under spheroid culture conditions, either by selection or through epigenetic programing.

Another hallmark of stem cells, namely the generation of differentiated progeny, was assayed by *in vitro* differentiation of the cells towards adipogenic or osteogenic mesenchymal linages. Here, the highest differentiation potential towards both lineages was observed for SP. PA is also able to differentiate into both lineages, albeit at a much reduced level of efficacy. The two CS cell lines investigated (CS1 and CS7) differentiate into one of the lineages only (either adipogenic, or osteogenic) at similar efficacy levels to PA. This may indicate the generation of CSC already committed to differentiation by the initial CS spheroid culture conditions. All cell lines, PA, SP, and CS, maintained their differentiation potential even at high passage numbers, and SP and CS also after longer periods in adherent growth in monolayer culture.

As functional assays for CSC and stem cell characteristics the activities of ALDH and the ABC-transporter MDR1/CD243 were analyzed, using the ALDEFLUOR^{TM} assay and the Side Population assay, respectively.

ALDH activity is high in PA, SP, and CS, but highly variable results were obtained, which with the low number of repeated experiments did not allow for statistically significant conclusions. Thus, in our hands ALDH activity was of no use in analyzing CSC enrichment in SP and CS compared to PA. However, the Side Population assay using Rhodamine 123 was found suitable to quantify CSC enrichment. A clear difference was seen between the spheroid cell lines, SP and CS, and the parent cell line PA. Differences correlate well with the different expression patterns of MDR1/CD243 in the respective cell lines. PA cells are able to pump out the dye almost completely (Rho^{low}), whereas the dye is retained by SP and CS (Rho^{high}), which show reduced or lack of expression of the transporter. Importantly, other than published for CSC from different tumor sources, in RCC the dye-retaining cells (Rho^{high}) are those with stem cell characteristics, i.e. SP and CS, whereas the cells pumping out the dye (Rho^{low}) were found in PA. [209] [210] These results further support enrichment of CSC in the spheroid-derived cell lines. Again and of great importance, the dye-retaining property was maintained also in spheroid cell lines A-SP cultured as adherent monolayers. Of note, PA cells display a Rho^{high} fraction only at low passage numbers. This correlates nicely with their spheroid-forming ability, which is correspondingly found at low passage numbers of PA, only.

Expression of a plethora of markers, known to be expressed by CSC or adult progenitor cells, was evaluated by flow cytometric immunophenotyping. The expression of CD105, CD24, CD73, CD44, CD29, SSEA3/4 and EpCAM expression is relatively high and homogenously distributed in PA, SP, and CS, CD49f is expressed at similar low levels in all cell lines and expression of CD90 was not detected. CD106, MDR/CD243, and CD146 are expressed on PA at higher levels or exclusively. None of the investigated markers reflects the observed growth characteristics of the cell lines. Therefore, all these markers are not applicable for enrichment or characterization of CSC.

In contrast, CD133, CD56, CXCR4/CD184, CD10, and CD271 are expressed on SP and CS, only. Expression of CD133, CD56, CXCR4/CD184, CD106, CD243 and CD146 depends on culture condition of SP and CS. For example, CD133, CD56, CXCR4/CD184 increase with time of culture, but decrease when SP and CS are cultured under adherent growth conditions. Also, differences in CD expression patterns between CS subtypes, like CS1 and CS7, were observed.

Besides cell surface markers, also intracellular correlates of “stemness” or pluripotency, like transcription factors of the iPSC-programing set found my Takahashi and Yamanaka, were measured. Oct4 and Sox2, are found uniformly expressed at low levels in PA, SP, and CS, in flow cytometric immunophenotyping experiments. When analyzed by RNA-Seq c-Myc was found at high levels in PA, SP, and A-SP. Marked differences were seen for Klf4 with lowest amounts in PA and highest in A-SP.

The process of epithelial-to-mesenchymal-transition (EMT), which is a hallmark of cells when acquiring stem cell properties, was analyzed through expression of EMT markers E-Cadherin, N-Cadherin, Snail1, vimentin, and cytokeratin, again by flow cytometric immunophenotyping. No significant differences were found between PA, SP, and CS. However, similarly high levels of mesenchymal and epithelial markers indicate an intermediate EMT phenotype of the cell lines. This is a lead characteristic of RCC-derived cells. In long-term culture fractions with reduced E-Cadherin expression were seen, indicating a gradual reprogramming towards a more mesenchymal phenotype. This phenotype is maintained in PA, SP, and CS at high passage numbers, but lost upon adherent growth culture of spheroid cells.

While so many lines of evidence strongly support the CSC character of SP and CS as well as the presence of low amounts of CSC already in PA, one crucial experiment failed. Xenotransplantation of PA and SP into severely immunocompromised (NSG) mice did not induce tumors, even at high numbers of cells injected. Most certainly, failure was due to technical problems, but so far the single experiment could neither be repeated nor optimized for reasons not related to science.

In bioinformatic terms, the variety of assays described above are based on a trained set of tools, i.e. leading to pre-filtering in experimental design and results obtained by established knowledge. For a more neutral view, whole transcriptome shotgun sequencing of mRNA (RNA-Seq) from PA, SP, and A-SP was performed. Differentially expressed genes (DEG) were identified in PA, SP, and A-SP.

The most prominent mRNA in PA is coding for angiotensin-converting enzyme (ACE2); no ACE2 mRNA was found in SP and A-SP. In SP, mRNA for the urea transporter SLC14A1 and the nicotinamide riboside kinase NMRK2 are on top of the list of differentially expressed genes. In A-SP, it is the mRNA for one of the early response transcription factor, FOS. The differentially expressed genes were subjected to gene set enrichment analysis (GSEA). Results of GSEA revealed strong support for the CSC characteristics found in PA, SP, and A-SP. GSEA results nicely match the results found by the variety of assays above.

In the spheroid-derived cell lines (SP, A-SP) their cancer stem cell properties are elicited through up-regulated signaling by ERK and AKT, CREB, HIF-1α, Wnt/Hedgehog/Notch, EGFR (ERBB, HER1), and PAK. In the adherently growing parental cell line (PA) cell adhesion and angiogenic pathways as well as S1P and NF-kB signaling prevail. If SP cells are kept under non CSC-selecting conditions for adherent growth in monolayer cultures (A-SP), they retain their up-regulated CSC signaling, but re-activate cell adhesion pathways comparable to PA. In more general terms, SP is optimized for survival and proliferation under metabolic conditions of low oxygen, and when nutrition supply (sugars and amino acids) is low – the typical situation in a tumor microenvironment (TME). In A-SP these properties essential for CSC are kept, but those for cell adhesion and immune signatures to establish cell localization and cell identity are regained.

The results obtained in this work do not fit a simple straightforward model, and it will take complex algorithms to reach deeper into the understanding of the complex phenomena involved. Nonetheless, the heterogeneity and plasticity observed in SP, CS, and A-SP, fits the current view on CSC. [84 126 460]
The combination of the two conflicting models of tumor development, as outlined in Figure 1.3.1 of the Introduction, already predicts the quality of characteristics, now demonstrated in my thesis. The clonal evolution model can be seen a guardian of stability, whereas the cancer stem cell model is the source of heterogeneity and plasticity.
Due to their reflection of different aspects of CSC, such as expression of surface markers, EMT status, differentiation potential, and growth characteristics, the cell lines obtained and characterized in my thesis may serve as valuable sources to unravel the basic mechanisms in RCC tumors. The stability, especially of SP, against differentiation makes the SP cancer stem cell line an ideal candidate for the development of novel cell-based therapies and their clinical applications.

7 References

1. Singh, V. K., Saini, A., Kalsan, M., Kumar, N. & Chandra, R. Describing the Stem Cell Potency: The Various Methods of Functional Assessment and In silico Diagnostics. *Front. Cell Dev. Biol.* **4,** (2016).
2. Simerman, A. A., Perone, M. J., Gimeno, M. L., Dumesic, D. A. & Chazenbalk, G. D. A mystery unraveled: nontumorigenic pluripotent stem cells in human adult tissues. *Expert Opin. Biol. Ther.* **14,** 917–29 (2014).
3. Nieto, M. A. Epithelial Plasticity: A Common Theme in Embryonic and Cancer Cells. *Science (80-.).* **342,** 1234850–1234850 (2013).
4. Kirschstein, R. Stem cells: scientific progress and future directions. *National Institutes of Health Report* 1–222 (2001).
5. Wu, J. & Izpisua Belmonte, J. C. Stem Cells: A Renaissance in Human Biology Research. *Cell* **165,** 1572–1585 (2016).
6. Chen, X., Ye, S. & Ying, Q.-L. Stem cell maintenance by manipulating signaling pathways: past, current and future. *BMB Rep.* **48,** 668–76 (2015).
7. Murry, C. E. & Keller, G. Differentiation of Embryonic Stem Cells to Clinically Relevant Populations: Lessons from Embryonic Development. *Cell* **132,** 661–680 (2008).
8. Rossant, J. & Tam, P. P. L. New Insights into Early Human Development: Lessons for Stem Cell Derivation and Differentiation. *Cell Stem Cell* **20,** 18–28 (2017).
9. Hombach-Klonisch, S., Alberti, E. & Pocar, P. Adult stem cells and their trans-differentiation potential perspectives and therapeutic applications. *J Mol Med* **86,** 1301–1314 (2010).
10. Clevers, H. & Watt, F. M. Defining Adult Stem Cells by Function, Not by Phenotype. *Annu. Rev. Biochem.* **87,** annurev-biochem-062917-012341 (2018).
11. Colom, B. & Jones, P. H. Clonal analysis of stem cells in differentiation and disease. *Curr. Opin. Cell Biol.* **43,** 14–21 (2016).
12. Goodell, M. A., Nguyen, H. & Shroyer, N. Somatic stem cell heterogeneity: Diversity in the blood, skin and intestinal stem cell compartments. *Nat. Rev. Mol. Cell Biol.* **16,** 299–309 (2015).
13. Bhartiya, D. Pluripotent Stem Cells in Adult Tissues: Struggling To Be Acknowledged Over Two Decades. *Stem Cell Rev. Reports* **0,** 1–12 (2017).
14. Friedenstein, A., Chailakhjan, R. & Lalykina, K. The development of fibroblast colonies in monolayer cultures of guinea pig bone marrow and spleen cells. *Cell Tissue Kinet.* **3,** 393–403 (1970).
15. Caplan, A. I. *The mesengenic process. Clinics in plastic surgery* **21,** 429–35 (1994).
16. Pittenger, M. F. *et al.* Multilineage potential of adult human mesenchymal stem cells. *Science* **284,** 143–7 (1999).
17. Erices, a, Conget, P. & Minguell, J. J. Mesenchymal progenitor cells in human umbilical cord blood. *Br. J. Haematol.* **109,** 235–242 (2000).
18. Zuk, P. A. *et al.* Human Adipose Tissue Is a Source of Multipotent Stem Cells. *Mol. Biol. Cell* **13,** 4279–4295 (2002).
19. De Bari, C., Dell'Accio, F., Tylzanowski, P. & Luyten, F. P. Multipotent mesenchymal stem cells from adult human synovial membrane. *Arthritis Rheum* **44,** 1928–1942 (2001).
20. S. Gronthos, M. Mankani, J. Brahim, P. Gehron Robey, and S. S. Postnatal human dental pulp stem cells (DPSCs) in vitro and in vivo. *Proc. Natl. Acad. Sci.* **97,** 13625–13630 (2000).
21. Fukuchi, Y. *et al.* Human Placenta-Derived Cells Have Mesenchymal Stem/Progenitor Cell Potential. *Stem Cells* **22,** 649–658 (2004).
22. Chamberlain, G., Fox, J., Ashton, B. & Middleton, J. Concise Review: Mesenchymal Stem Cells: Their Phenotype, Differentiation Capacity, Immunological Features, and Potential for Homing. *Stem Cells* **25,** 2739–2749 (2007).
23. Shang, Y. *et al.* Wnt3a signaling promotes proliferation, myogenic differentiation, and migration of rat bone marrow mesenchymal stem cells 1. *Acta Pharmacol Sin* **28,** 1761–1774 (2007).
24. Tondreau, T. *et al.* Gene expression pattern of functional neuronal cells derived from human bone marrow mesenchymal stromal cells. *BMC Genomics* **9,** 166 (2008).

25. Dominici, M. *et al.* Minimal criteria for defining multipotent mesenchymal stromal cells. The International Society for Cellular Therapy position statement. *Cytotherapy* **8,** 315–7 (2006).
26. Rojewski, M. T., Weber, B. M. & Schrezenmeier, H. Phenotypic characterization of mesenchymal stem cells from various tissues. *Transfus. Med. Hemotherapy* **35,** 168–184 (2008).
27. da Silva Meirelles, L., Chagastelles, P. C. & Nardi, N. B. Mesenchymal stem cells reside in virtually all post-natal organs and tissues. *J. Cell Sci.* **119,** 2204–13 (2006).
28. Lv, F.-J., Tuan, R. S., Cheung, K. M. C. & Leung, V. Y. L. Concise Review: The Surface Markers and Identity of Human Mesenchymal Stem Cells. *Stem Cells* **32,** 1408–1419 (2014).
29. Cappellesso-Fleury, S. *et al.* Human Fibroblasts Share Immunosuppressive Properties with Bone Marrow Mesenchymal Stem Cells. *J. Clin. Immunol.* **30,** 607–619 (2010).
30. Kundrotas, G. Surface markers distinguishing mesenchymal stem cells from fibroblasts. *Acta medica Litu.* **19,** 75–79 (2012).
31. Tajbakhsh, S., Rocheteau, P. & Le Roux, I. Asymmetric Cell Divisions and Asymmetric Cell Fates. *Annu. Rev. Cell Dev. Biol.* **25,** 671–699 (2009).
32. Shenghui, H., Nakada, D. & Morrison, S. J. Mechanisms of Stem Cell Self-Renewal. *Annu. Rev. Cell Dev. Biol.* **25,** 377–406 (2009).
33. Chen, C., Fingerhut, J. M. & Yamashita, Y. M. The ins(ide) and outs(ide) of asymmetric stem cell division. *Curr. Opin. Cell Biol.* **43,** 1–6 (2016).
34. Daynac, M. & Petritsch, C. K. Asymmetric Cell Division in Development, Differentiation and Cancer. in *Results and Problems in Cell Differentiation 61* **61,** 375–399 (2017).
35. Mukherjee, S., Kong, J. & Brat, D. J. Cancer Stem Cell Division: When the Rules of Asymmetry Are Broken. *Stem Cells Dev.* **24,** 405–416 (2015).
36. Xie, J., Wooten, M., Tran, V. & Chen, X. Breaking Symmetry − Asymmetric Histone Inheritance in Stem Cells. *Trends Cell Biol.* **27,** 527–540 (2017).
37. Moorhead, L. H. and P. S. The Serial Cultivation of Human Diploid Cell Strains - Heyflick-Limit. *Exp. Cell Res.* **1,** 585–621 (1961).
38. Campisi, J. & d'Adda di Fagagna, F. Cellular senescence: when bad things happen to good cells. *Nat. Rev. Mol. Cell Biol.* **8,** 729–740 (2007).
39. Thomson, J. A. *et al.* Embryonic Stem Cell Lines Derived from Human Blastocysts. *Science (80-.).* **282,** 1145–1147 (1998).
40. Ćukušić, A., Škrobot Vidaček, N., Sopta, M. & Rubelj, I. Telomerase regulation at the crossroads of cell fate. *Cytogenet. Genome Res.* **122,** 263–272 (2009).
41. Kuhn, N. Z. & Tuan, R. S. Regulation of stemness and stem cell niche of mesenchymal stem cells: Implications in tumorigenesis and metastasis. *J. Cell. Physiol.* **222,** 268–277 (2010).
42. Morrison, S. J. & Spradling, A. C. Stem Cells and Niches: Mechanisms That Promote Stem Cell Maintenance throughout Life. *Cell* **132,** 598–611 (2008).
43. Li, L. & Xie, T. Stem Cell Niche: Structure and Function. *Annu. Rev. Cell Dev. Biol.* **21,** 605–631 (2005).
44. Rojas-Ríos, P. & González-Reyes, A. Concise review: The plasticity of stem cell niches: A general property behind tissue homeostasis and repair. *Stem Cells* **32,** 852–859 (2014).
45. Rizzino, A. & Wuebben, E. L. Sox2/Oct4: A delicately balanced partnership in pluripotent stem cells and embryogenesis. *Biochim. Biophys. Acta - Gene Regul. Mech.* **1859,** 780–791 (2016).
46. Jaenisch, R. & Young, R. Stem Cells, the Molecular Circuitry of Pluripotency and Nuclear Reprogramming. *Cell* **132,** 567–582 (2008).
47. Ng, H.-H. & Surani, M. A. The transcriptional and signalling networks of pluripotency. *Nat. Cell Biol.* **13,** 490–496 (2011).
48. Zhao, H. & Jin, Y. Signaling networks in the control of pluripotency. *Curr. Opin. Genet. Dev.* **46,** 141–148 (2017).
49. Yamanaka, K. T. and S. Induction of Pluripotent Stem Cells from Mouse Embryonic and Adult Fibroblast Cultures by Defined Factors. *Cell* **126,** 663–676 (2006).
50. Takahashi, K. *et al.* Induction of Pluripotent Stem Cells from Adult Human Fibroblasts by Defined Factors. *Cell* **131,** 861–872 (2007).

51. O'Connor, M. D. *et al.* Alkaline Phosphatase-Positive Colony Formation Is a Sensitive, Specific, and Quantitative Indicator of Undifferentiated Human Embryonic Stem Cells. *Stem Cells* **26,** 1109–1116 (2008).
52. Lanza R (Ed), Gearhart J, Hogan B, Melton D, Pedersen R. Thomas ED, Thomson J, Sir, W. I. *Essentials of Stem Cell Biology*. (Elsevier Inc., 2009). doi:10.1016/B978-0-12-374729-7.00026-3
53. Štefková, K. *et al.* Alkaline Phosphatase in Stem Cells. *Stem Cells Int.* **2015,** 1–11 (2015).
54. Schopperle, W. M. & DeWolf, W. C. The TRA-1-60 and TRA-1-81 Human Pluripotent Stem Cell Markers Are Expressed on Podocalyxin in Embryonal Carcinoma. *Stem Cells* **25,** 723–730 (2006).
55. Toyoda, H., Nagai, Y., Kojima, A. & Kinoshita-Toyoda, A. Podocalyxin as a major pluripotent marker and novel keratan sulfate proteoglycan in human embryonic and induced pluripotent stem cells. *Glycoconj. J.* **34,** 817–823 (2017).
56. Ginis, I. *et al.* Differences between human and mouse embryonic stem cells. *Dev. Biol.* **269,** 360–380 (2004).
57. Yanagisawa, M. Stem cell glycolipids. *Neurochem. Res.* **36,** 1623–1635 (2011).
58. Trusler, O., Huang, Z., Goodwin, J. & Laslett, A. L. Cell surface markers for the identification and study of human naive pluripotent stem cells. *Stem Cell Res.* **26,** 36–43 (2018).
59. Sivasubramaniyan, K. *et al.* Phenotypic and functional heterogeneity of human bone marrow- and amnion-derived MSC subsets. *Ann. N. Y. Acad. Sci.* **1266,** 94–106 (2012).
60. Kim, W.-T. & Ryu, C. J. Cancer stem cell surface markers on normal stem cells. *BMB Rep.* **50,** 285–298 (2017).
61. Young, R. A. Control of the embryonic stem cell state. *Cell* **144,** 940–954 (2011).
62. Spornitz, U. M. *Anatomie und Phyisologie*. (Springer Berlin Heidelberg, 2010).
63. Kriz, W. & Kaissling, B. *Structural Organization of the Mammalian Kidney*. *Seldin and Geibisch's The Kidney* **1,** (2013).
64. Schell, C., Wanner, N. & Huber, T. B. Glomerular development - Shaping the multi-cellular filtration unit. *Semin. Cell Dev. Biol.* **36,** 39–49 (2014).
65. McCampbell, K. K. & Wingert, R. A. Renal stem cells: fact or science fiction? *Biochem. J.* **444,** 153–168 (2012).
66. Pleniceanu, O., Harari-Steinberg, O. & Dekel, B. Concise review: Kidney stem/progenitor cells: Differentiate, sort out, or reprogram? *Stem Cells* **28,** 1649–1659 (2010).
67. O'Brien, L. L. & McMahon, A. P. Induction and patterning of the metanephric nephron. *Semin. Cell Dev. Biol.* **36,** 31–38 (2014).
68. Costantini, F. & Kopan, R. Patterning a complex organ: Branching morphogenesis and nephron segmentation in kidney development. *Dev. Cell* **18,** 698–712 (2010).
69. Axelson, H. & Johansson, M. E. Renal stem cells and their implications for kidney cancer. *Semin. Cancer Biol.* **23,** 56–61 (2013).
70. Oliver, J. A. & Al-Awqati, Q. *Stem Cells and Generation of New Cells in the Adult Kidney*. *Seldin and Geibisch's The Kidney* **1,** (Elsevier Inc., 2013).
71. Bussolati, B. *et al.* Hypoxia modulates the undifferentiated phenotype of human renal inner medullary CD133+ progenitors through Oct4/miR-145 balance. *AJP Ren. Physiol.* **302,** F116–F128 (2012).
72. Bussolati, B. *et al.* Isolation of Renal Progenitor Cells from Adult Human Kidney. *Am. J. Pathol.* **166,** 545–555 (2005).
73. Sagrinati, C., Netti GS, Mazzinghi B, Lazzeri E, Liotta F, Frosali F, Ronconi E, Meini C, Gacci M, Squecco R, Crini M, Gesuado L, Francini F, Maggi E, Annunziato F, Lasagni L, Serio M, Romagnani S, R. P. Isolation and Characterization of Multipotent Progenitor Cells from the Bowman's Capsule of Adult Human Kidneys. *J. Am. Soc. Nephrol.* **17,** 2443–2456 (2006).
74. Lindgren, D. *et al.* Isolation and Characterization of Progenitor-Like Cells from Human Renal Proximal Tubules. *Am. J. Pathol.* **178,** 828–837 (2011).
75. Angelotti, M. L. *et al.* Characterization of renal progenitors committed toward tubular lineage and their regenerative potential in renal tubular injury. *Stem Cells* **30,** 1714–1725 (2012).

76. Ward, H. H. *et al.* Adult human CD133/1+ kidney cells isolated from papilla integrate into developing kidney tubules. *Biochim. Biophys. Acta - Mol. Basis Dis.* **1812,** 1344–1357 (2011).
77. Ronconi, E. *et al.* Regeneration of Glomerular Podocytes by Human Renal Progenitors. *J. Am. Soc. Nephrol.* **20,** 322–332 (2009).
78. Bussolati, B., Bruno, S., Grange, C., Ferrando, U. & Camussi, G. Identification of a tumor-initiating stem cell population in human renal carcinomas. *FASEB J.* **22,** 3696–705 (2008).
79. Shen, W. C., Chou, Y. H. & Lin, S. L. Enthusiasm for induced pluripotent stem cell-based therapies in kidney regeneration. *J. Formos. Med. Assoc.* **115,** 593–594 (2016).
80. Hanahan, D. & Weinberg, R. A. The hallmarks of cancer. *Cell* **100,** 57–70 (2000).
81. Hanahan, D. & Weinberg, R. A. Hallmarks of cancer: The next generation. *Cell* **144,** 646–674 (2011).
82. Bernheim, A. Cytogenomics of cancers: From chromosome to sequence. *Mol. Oncol.* **4,** 309–322 (2010).
83. McGranahan, N. & Swanton, C. Biological and therapeutic impact of intratumor heterogeneity in cancer evolution. *Cancer Cell* **27,** 15–26 (2015).
84. Eun, K., Ham, S. W. & Kim, H. Cancer stem cell heterogeneity: Origin and new perspectives on CSC targeting. *BMB Rep.* **50,** 117–125 (2017).
85. Mazor, T., Pankov, A., Song, J. S. & Costello, J. F. Intratumoral Heterogeneity of the Epigenome. *Cancer Cell* **29,** 440–451 (2016).
86. Beksac, A. T. *et al.* Heterogeneity in renal cell carcinoma. *Urol. Oncol. Semin. Orig. Investig.* **35,** 507–515 (2017).
87. Hammerlindl, H. & Schaider, H. Tumor cell-intrinsic phenotypic plasticity facilitates adaptive cellular reprogramming driving acquired drug resistance. *J. Cell Commun. Signal.* **12,** 133–141 (2018).
88. Marjanovic, N. D., Weinberg, R. A. & Chaffer, C. L. Cell plasticity and heterogeneity in cancer. *Clin. Chem.* **59,** 168–179 (2013).
89. Huntly, B. J. P. & Gilliland, D. G. Timeline: Leukaemia stem cells and the evolution of cancer-stem-cell research. *Nat. Rev. Cancer* **5,** 311–321 (2005).
90. Tannishtha, R., Morrison, S. J., Clarke, M. F. & Weissman, I. L. Stem Cells, Cancer, and Cancer Stem Cells. *Nature* **414,** 105–111 (2001).
91. Pardal, R., Clarke, M. F. & Morrison, S. J. Applying the principles of stem-cell biology to cancer. *Nat. Rev. Cancer* **3,** 895–902 (2003).
92. Ward, R. J. & Dirks, P. B. Cancer Stem Cells: At the Headwaters of Tumor Development. *Annu. Rev. Pathol. Mech. Dis.* **2,** 175–189 (2007).
93. Dalerba, P., Cho, R. W. & Clarke, M. F. Cancer Stem Cells: Models and Concepts. *Annu. Rev. Med.* **58,** 267–284 (2007).
94. Lobo, N. A., Shimono, Y., Qian, D. & Clarke, M. F. The Biology of Cancer Stem Cells. *Annu. Rev. Cell Dev. Biol.* **23,** 675–699 (2007).
95. Wong, D. J. *et al.* Module map of stem cell genes guides creation of epithelial cancer stem cells. *Cell Stem Cell* **2,** 333–344 (2008).
96. Bonnet, D. & Dick, J. E. Human acute myeloid leukemia is organized as a hierarchy that originates from a primitive hematopoietic cell. *Nat. Med.* **3,** 730–737 (1997).
97. Al-Hajj, M., Wicha, M. S., Benito-Hernandez, A., Morrison, S. J. & Clarke, M. F. Prospective identification of tumorigenic breast cancer cells. *Proc. Natl. Acad. Sci.* **100,** 3983–3988 (2003).
98. Singh, S. K. *et al.* Identification of human brain tumour initiating cells. *Nature* **432,** 396–401 (2004).
99. Collins, A. T., Berry, P. A., Hyde, C., Stower, M. J. & Maitland, N. J. Prospective identification of tumorigenic prostate cancer stem cells. *Cancer Res.* **65,** 10946–10951 (2005).
100. Bapat, S., Mali, A., Koppikar, C. & Kurrey, N. Stem and progenitor-like cells contribute to the aggressive behavior of human epithelial ovarian cancer. *Cancer Res.* **65,** 3025–9 (2005).
101. Fang, D. *et al.* A tumorigenic subpopulation with stem cell properties in melanomas. *Cancer Res.* **65,** 9328–9337 (2005).
102. Ricci-Vitiani, L. *et al.* Identification and expansion of human colon-cancer-initiating cells. *Nature* **445,** 111–115 (2007).

103. Hermann, P. C. *et al.* Distinct Populations of Cancer Stem Cells Determine Tumor Growth and Metastatic Activity in Human Pancreatic Cancer. *Cell Stem Cell* **1,** 313–323 (2007).
104. Ma, S. *et al.* Identification and Characterization of Tumorigenic Liver Cancer Stem/Progenitor Cells. *Gastroenterology* **132,** 2542–2556 (2007).
105. Ho, M. M., Ng, A. V., Lam, S. & Hung, J. Y. Side population in human lung cancer cell lines and tumors is enriched with stem-like cancer cells. *Cancer Res.* **67,** 4827–4833 (2007).
106. Eramo, A. *et al.* Identification and expansion of the tumorigenic lung cancer stem cell population. *Cell Death Differ.* **15,** 504–514 (2008).
107. Visvader, J. E. & Lindeman, G. J. Cancer stem cells in solid tumours: accumulating evidence and unresolved questions. *Nat. Rev. Cancer* **8,** 755–68 (2008).
108. Visvader, J. E. Cells of origin in cancer. *Nature* **469,** 314–322 (2011).
109. Song, Y. *et al.* A unified model of the hierarchical and stochastic theories of gastric cancer. *Br. J. Cancer* **116,** 973–989 (2017).
110. Corrò, C. & Moch, H. Biomarker discovery for renal cancer stem cells. *J. Pathol. Clin. Res.* 3–16 (2017). doi:10.1002/cjp2.91
111. Kreso, A. & Dick, J. E. Evolution of the cancer stem cell model. *Cell Stem Cell* **14,** 275–291 (2014).
112. Papaccio, F. *et al.* Concise Review: Cancer Cells, Cancer Stem Cells, and Mesenchymal Stem Cells: Influence in Cancer Development. *Stem Cells Transl. Med.* **6,** 2115–2125 (2017).
113. Medema, J. P. Cancer stem cells: The challenges ahead. *Nat. Cell Biol.* **15,** 338–344 (2013).
114. Hombach-Klonisch, S. *et al.* Cancer stem cells as targets for cancer therapy: Selected cancers as examples. *Arch. Immunol. Ther. Exp. (Warsz).* **56,** 165–180 (2008).
115. Klonisch, T. *et al.* Cancer stem cell markers in common cancers - therapeutic implications. *Trends Mol. Med.* **14,** 450–460 (2008).
116. Chen, W., Dong, J., Haiech, J., Kilhoffer, M. C. & Zeniou, M. Cancer stem cell quiescence and plasticity as major challenges in cancer therapy. *Stem Cells Int.* **2016,** (2016).
117. Batlle, E. & Clevers, H. Cancer stem cells revisited. *Nat. Med.* **23,** 1124–1134 (2017).
118. Pützer, B. M., Solanki, M. & Herchenröder, O. Advances in cancer stem cell targeting: How to strike the evil at its root. *Adv. Drug Deliv. Rev.* **120,** 89–107 (2017).
119. Azzi, S. *et al.* Differentiation therapy: targeting human renal cancer stem cells with interleukin 15. *J Natl Cancer Inst* **103,** 1884–1898 (2011).
120. de Thé, H. Differentiation therapy revisited. *Nat. Rev. Cancer* (2017). doi:10.1038/nrc.2017.103
121. Jin Xiong, Jin Xun, K. H. Cancer stem cells and differentiation therapy. *Tumor Biol.* 1–11 (2017). doi:10.1159/000092323
122. Agliano, A., Calvo, A. & Box, C. The challenge of targeting cancer stem cells to halt metastasis. *Semin. Cancer Biol.* **44,** 25–42 (2017).
123. Fiori, M. E., Villanova, L. & De Maria, R. Cancer stem cells: at the forefront of personalized medicine and immunotherapy. *Curr. Opin. Pharmacol.* **35,** 1–11 (2017).
124. Islam, F., Gopalan, V., Smith, R. A. & Lam, A. K. Y. Translational potential of cancer stem cells: A review of the detection of cancer stem cells and their roles in cancer recurrence and cancer treatment. *Exp. Cell Res.* **335,** 135–147 (2015).
125. Ahmed M, Chaudhari K, Babaei-Jadidi R, Dekker L, S. N. A. Concise Review: Emerging Drugs Targeting Epithelial Cancer Stem-Like Cells. *Stem Cells* **35,** 839–850 (2017).
126. Gupta, P. B., Chaffer, C. L. & Weinberg, R. A. Cancer stem cells: mirage or reality? *Nat. Med.* **15,** 1010–1012 (2009).
127. Kalluri, R. & Weinberg, R. a. The basics of epithelial-mesenchymal transition. *J. Clin. Invest.* **119,** 1420–1428 (2009).
128. Scheel, C. & Weinberg, R. A. Cancer stem cells and epithelial-mesenchymal transition: Concepts and molecular links. *Semin. Cancer Biol.* **22,** 396–403 (2012).
129. Chaffer, C. L. *et al.* Normal and neoplastic nonstem cells can spontaneously convert to a stem-like state. *Proc. Natl. Acad. Sci.* **108,** 7950–7955 (2011).
130. Mani, S. A. *et al.* The Epithelial-Mesenchymal Transition Generates Cells with Properties of Stem Cells. *Cell* **133,** 704–715 (2008).

131. Thiery, J. P., Acloque, H., Huang, R. Y. J. & Nieto, M. A. Epithelial-Mesenchymal Transitions in Development and Disease. *Cell* **139,** 871–890 (2009).
132. Polyak, K. & Weinberg, R. A. Transitions between epithelial and mesenchymal states: acquisition of malignant and stem cell traits. *Nat. Rev. Cancer* **9,** 265–273 (2009).
133. Yang, J. & Weinberg, R. A. Epithelial-Mesenchymal Transition: At the Crossroads of Development and Tumor Metastasis. *Dev. Cell* **14,** 818–829 (2008).
134. Singh, M., Yelle, N., Venugopal, C. & Singh, S. K. EMT: Mechanisms and therapeutic implications. *Pharmacol. Ther.* **182,** 80–94 (2018).
135. Forte, E. *et al.* EMT/MET at the crossroad of stemness, regeneration and oncogenesis: The Ying-Yang equilibrium recapitulated in cell spheroids. *Cancers (Basel).* **9,** 1–15 (2017).
136. O'Brien-Ball, C. & Biddle, A. Reprogramming to developmental plasticity in cancer stem cells. *Dev. Biol.* **430,** 266–274 (2017).
137. Lamouille, S., Xu, J. & Derynck, R. Molecular mechanisms of epithelial–mesenchymal transition. *Nat. Rev. Mol. Cell Biol.* **15,** 178–196 (2014).
138. Baiocchi, M., Biffoni, M., Ricci-Vitiani, L., Pilozzi, E. & De Maria, R. New models for cancer research: Human cancer stem cell xenografts. *Curr. Opin. Pharmacol.* **10,** 380–384 (2010).
139. Day, C. P., Merlino, G. & Van Dyke, T. Preclinical Mouse Cancer Models: A Maze of Opportunities and Challenges. *Cell* **163,** 39–53 (2015).
140. Rongvaux, A. *et al. Human Hemato-Lymphoid System Mice: Current Use and Future Potential for Medicine*. *Annual Review of Immunology* **31,** (2013).
141. Gengenbacher, N., Singhal, M. & Augustin, H. G. Preclinical mouse solid tumour models: Status quo, challenges and perspectives. *Nat. Rev. Cancer* **17,** 751–765 (2017).
142. Rappa, G., Mercapide, J., Anzanello, F., Prasmickaite, L. & Xi, Y. Growth of cancer cell lines under stem cell-like conditions has the potential to unveil therapeutic targets Germana. **314,** 2110–2122 (2009).
143. van Staveren, W. C. G. *et al.* Human cancer cell lines: Experimental models for cancer cells in situ? For cancer stem cells? *Biochim. Biophys. Acta - Rev. Cancer* **1795,** 92–103 (2009).
144. Taub, M. The use of defined media in cell and tissue culture. *Toxicol. Vitr.* **4,** 213–225 (1990).
145. Ravi, M., Ramesh, A. & Pattabhi, A. Contributions of 3D Cell Cultures for Cancer Research. *J. Cell. Physiol.* **232,** 2679–2697 (2017).
146. Weiswald, L. B., Bellet, D. & Dangles-Marie, V. Spherical cancer models in tumor biology. *Neoplasia (New York, N.Y.)* **17,** 1–15 (2015).
147. Xia, P. Surface Markers of Cancer Stem Cells in Solid Tumors. *Curr. Stem Cell Res. Ther.* **9,** 102–111 (2014).
148. Abbaszadegan, M. R. *et al.* Isolation, identification, and characterization of cancer stem cells: A review. *J. Cell. Physiol.* **232,** 2008–2018 (2017).
149. Kastan, M. B. *et al.* Direct demonstration of elevated aldehyde dehydrogenase in human hematopoietic progenitor cells. *Blood* **75,** 1947–1950 (1990).
150. Ma, I. & Allan, A. L. The Role of Human Aldehyde Dehydrogenase in Normal and Cancer Stem Cells. *Stem Cell Rev. Reports* **7,** 292–306 (2011).
151. Tomita, H., Tanaka, K., Tanaka, T. & Hara, A. Aldehyde dehydrogenase 1A1 in stem cells and cancer. *Oncotarget* **7,** (2016).
152. Lorico, A. & Rappa, G. Phenotypic heterogeneity of breast cancer stem cells. *J. Oncol.* **2011,** (2011).
153. Wolf, N. S., Kone, A., Priestley, G. V & Bartelmez, S. H. In vivo and in vitro characterization of long-term repopulating primitive hematopoietic cells isolated by sequential Hoechst 33342-rhodamine 123 FACS selection. *Exp Hematol* **21,** 614–622 (1993).
154. Ding, X., Wu, J. & Jiang, C. ABCG2: A potential marker of stem cells and novel target in stem cell and cancer therapy. *Life Sci.* **86,** 631–637 (2010).
155. Zhou, S. *et al.* The ABC transporter Bcrp1/ABCG2 is expressed in a wide variety of stem cells and is a molecular determinant of the side-population phenotype. *Nat. Med.* **7,** 1028–1034 (2001).

156. Scharenberg, C. W. *et al.* The ABCG2 transporter is an efficient Hoechst 33342 efflux pump and is preferentially expressed by immature human hematopoietic progenitors The ABCG2 transporter is an efficient Hoechst 33342 efflux pump and is preferentially expressed by immature human h. *Blood* **99,** 507–512 (2013).
157. Jonker, J. W. *et al.* Contribution of the ABC transporters Bcrp1 and Mdr1a/1b to the side population phenotype in mammary gland and bone marrow of mice. *Stem Cells* **23,** 1059–1065 (2005).
158. Challen, G. A. & Little, M. H. A Side Order of Stem Cells: The SP Phenotype. *Stem Cells* **24,** 3–12 (2006).
159. Vasiliou, V., Vasiliou, K. & Nebert, D. W. Human ATP-binding cassette (ABC) transporter family. *Hum. Genomics* **3,** 281–90 (2009).
160. Huls, M. *et al.* The breast cancer resistance protein transporter ABCG2 is expressed in the human kidney proximal tubule apical membrane. *Kidney Int.* **73,** 220–225 (2008).
161. Hadnagy, A., Gaboury, L., Beaulieu, R. & Balicki, D. SP analysis may be used to identify cancer stem cell populations. *Exp. Cell Res.* **312,** 3701–3710 (2006).
162. Begicevic, R.-R. & Falasca, M. ABC Transporters in Cancer Stem Cells: Beyond Chemoresistance. *Int. J. Mol. Sci.* **18,** 2362 (2017).
163. Dean, M. ABC transporters, drug resistance, and cancer stem cells. *J. Mammary Gland Biol. Neoplasia* **14,** 3–9 (2009).
164. Reynolds, B. A. & Weiss, S. Nervous System Generation of Neurons and Astrocytes from Isolated Cells of the Adult Mammalian Central Nervous System. *Science (80-.).* **255,** 1707–1710 (1992).
165. Ishiguro, T. *et al.* Tumor-derived spheroids: Relevance to cancer stem cells and clinical applications. *Cancer Sci.* **108,** 283–289 (2017).
166. Ponti, D. *et al.* Isolation and In vitro Propagation of Tumorigenic Breast Cancer Cells with Stem/Progenitor Cell Properties. *Cancer Res* **65,** 5506–11 (2005).
167. Hirschhaeuser, F. *et al.* Multicellular tumor spheroids: An underestimated tool is catching up again. *J. Biotechnol.* **148,** 3–15 (2010).
168. Dontu, G. *et al.* In vitro propagation and transcriptional profiling of human mammary stem / progenitor cells. *Genes Dev.* **17,** 1253–1270 (2003).
169. Cao, L. *et al.* Sphere-forming cell subpopulations with cancer stem cell properties in human hepatoma cell lines. *BMC Gastroenterol.* **11,** 71 (2011).
170. Reynolds, B. A. & Rietze, R. L. Neural stem cells and neurospheres—re-evaluating the relationship. *Nat. Methods* **2,** 333–336 (2005).
171. Pastrana, E., Silva-Vargas, V. & Doetsch, F. Eyes wide open: A critical review of sphere-formation as an assay for stem cells. *Cell Stem Cell* **8,** 486–498 (2011).
172. Lindgren, D. *et al.* Cell-Type-Specific Gene Programs of the Normal Human Nephron Define Kidney Cancer Subtypes. *Cell Rep.* **20,** 1476–1489 (2017).
173. Kaphingst, K. A., Persky, S. & Lachance, C. Recent Updates in Renal Cell Carcinoma W. *Curr Opin Oncol.* **22,** 250–56 (2010).
174. Haynes, M. Renal cancer. *Surg. (United Kingdom)* **31,** 530–534 (2013).
175. Zhou M, H. H. Renal Cell Carcinoma. in *Renal Cell Carcinoma: Clinical Management, Current Clinical Urology* (eds. Zhou, M. & He, H.) (Humana Press, Springer, 2013). doi:10.1007/978-1-62703-062-5
176. Yuan, Z. X. *et al.* Targeting Strategies for Renal Cell Carcinoma: From Renal Cancer Cells to Renal Cancer Stem Cells. *Front Pharmacol* **7,** 423 (2016).
177. Grange, C., Collino, F., Tapparo, M. & Camussi, G. Oncogenic micro-RNAs and Renal Cell Carcinoma. *Front. Oncol.* **4,** 49 (2014).
178. Marmarelis, M. E. *et al.* Tumor control with PD-1 inhibition in a patient with concurrent metastatic melanoma and renal cell carcinoma. *J. Immunother. Cancer* **4,** 1–5 (2016).
179. ASCO 2018, annual meeting of the American Society of Clinical Oncology. (2018).
180. Jung, N.-C., Lee, J.-H., Chung, K.-H., Kwak, Y. S. & Lim, D.-S. Dendritic Cell-Based Immunotherapy for Solid Tumors. *Transl. Oncol.* **11,** 686–690 (2018).

181. Hirbod-Mobarakeh, A. *et al.* Specific immunotherapy in renal cancer: A systematic review. *Ther. Adv. Urol.* **9,** 45–58 (2017).
182. Volz, B. *et al.* Design and characterization of the tumor vaccine MGN1601, allogeneic fourfold gene-modified vaccine cells combined with a TLR-9 agonist. *Mol. Ther. — Oncolytics* **3,** 15023 (2016).
183. Grunwald, V. *et al.* Final results of patients with metastatic renal cell carcinoma treated with MGN1601 in the ASET study. *J. Clin. Oncol. Conf.* **32,** (2014).
184. Gudas, L. J., Fu, L., Minton, D. R., Mongan, N. P. & Nanus, D. M. The role of HIF1α in renal cell carcinoma tumorigenesis. *J. Mol. Med.* **92,** 825–836 (2014).
185. Ayerbes, M. V. *et al.* Origin of renal cell carcinomas. *Clin. Transl. Oncol.* **10,** 697–712 (2008).
186. Myszczyszyn, A. *et al.* The Role of Hypoxia and Cancer Stem Cells in Renal Cell Carcinoma Pathogenesis. *Stem Cell Rev. Reports* **11,** 919–943 (2015).
187. Shen, C. & Kaelin, W. G. The VHL/HIF axis in clear cell renal carcinoma. *Semin. Cancer Biol.* **23,** 18–25 (2013).
188. Gerlinger, M. *et al.* Genomic architecture and evolution of clear cell renal cell carcinomas defined by multiregion sequencing. *Nat. Genet.* **46,** 225–233 (2014).
189. Koul, H. *et al.* Molecular aspects of renal cell carcinoma: a review. *American journal of cancer research* **1,** 240–254 (2011).
190. Shuch, B. *et al.* Understanding pathologic variants of renal cell carcinoma: Distilling therapeutic opportunities from biologic complexity. *Eur. Urol.* **67,** 85–97 (2015).
191. Chen, F. *et al.* Multilevel Genomics-Based Taxonomy of Renal Cell Carcinoma. *Cell Rep.* **14,** 2476–2489 (2016).
192. Von Roemeling, C. A. *et al.* Functional genomics identifies novel genes essential for clear cell renal cell carcinoma tumor cell proliferation and migration. *Oncotarget* **5,** 5320–34 (2014).
193. Klaudia K. Brodaczewska, Cezary Szczylik, Michal Fiedorowicz, Camillo Porta, A. M. C. Choosing the right cell line for renal cell cancer research. *Mol. Cancer* (2016). doi:10.1186/s12943-016-0565-8
194. Grange, C. *et al.* Microvesicles released from human renal cancer stem cells stimulate angiogenesis and formation of lung premetastatic niche. *Cancer Res.* **71,** 5346–5356 (2011).
195. Giron-Michel, J. *et al.* Interleukin-15 is a major regulator of the cell-microenvironment interactions in human renal homeostasis. *Cytokine Growth Factor Rev.* **24,** 13–22 (2013).
196. Azzi, S. *et al.* Human renal normal, tumoral, and cancer stem cells express membrane-bound interleukin-15 isoforms displaying different functions. *Neoplasia* **17,** 509–517 (2015).
197. D'Amico, L. *et al.* C-met inhibition blocks bone metastasis development induced by renal cancer stem cells. *Oncotarget* **5,** (2014).
198. Weygant, N. *et al.* DCLK1 is a broadly dysregulated target against epithelial-mesenchymal transition, focal adhesion, and stemness in clear cell renal carcinoma. *Oncotarget* **6,** 2193–2205 (2015).
199. Matak, D. *et al.* Functional significance of CD105-positive cells in papillary renal cell carcinoma. *BMC Cancer* **17,** 21 (2017).
200. Hu, J. *et al.* Endoglin Is Essential for the Maintenance of Self-Renewal and Chemoresistance in Renal Cancer Stem Cells. *Stem Cell Reports* **9,** 464–477 (2017).
201. Zhang, X.-F. *et al.* Dendritic-cell-based immunotherapy evokes potent anti-tumor immune responses in CD105+ human renal cancer stem cells. *Mol. Carcinog.* 2499–2511 (2017). doi:10.1002/mc.22697
202. Galleggiante, V. *et al.* CTR2 Identifies a Population of Cancer Cells with Stem Cell-like Features in Patients with Clear Cell Renal Cell Carcinoma CTR2 Identifies a Population of Cancer Cells with Stem-Like Features in Patients with Clear Cell Renal Cell Carcinoma. *J. Urol.* **192,** 1831–41 (2014).
203. Xiao, W., Gao, Z., Duan, Y., Yuan, W. & Ke, Y. Notch signaling plays a crucial role in cancer stem-like cells maintaining stemness and mediating chemotaxis in renal cell carcinoma. *J. Exp. Clin. Cancer Res.* **36,** 41 (2017).
204. Gassenmaier, M. *et al.* CXC chemokine receptor 4 is essential for maintenance of renal cell carcinoma-initiating cells and predicts metastasis. *Stem Cells* **31,** 1467–1476 (2013).

205. Ueda, K. *et al.* Aldehyde Dehydrogenase 1 Identifies Cells with Cancer Stem Cell-Like Properties in a Human Renal Cell Carcinoma Cell Line. *PLoS One* **8,** (2013).
206. Chen, D.-C. *et al.* CBFA2T2 is associated with a cancer stem cell state in renal cell carcinoma. *Cancer Cell Int.* **17,** 103 (2017).
207. Wang, L., Park, P., La Marca, F., Than, K. D. & Lin, C. Y. BMP-2 inhibits tumor-initiating ability in human renal cancer stem cells and induces bone formation. *J. Cancer Res. Clin. Oncol.* **141,** 1013–1024 (2015).
208. Huang, B. *et al.* Cancer Stem Cell-Like Side Population Cells in Clear Cell Renal Cell Carcinoma Cell Line 769P. *PLoS One* **8,** (2013).
209. Lu, J. *et al.* Biological characteristics of Rh123high stem-like cells in a side population of 786-O renal carcinoma cells. *Oncol. Lett.* **5,** 1903–1908 (2013).
210. Song, L., Ye, W., Cui, Y., Lu, J. & Zhang, Y. Ecto-5 ′-nucleotidase (CD73) is a biomarker for clear cell renal carcinoma stem-like cells. *Oncotarget* **8,** 31977–31992 (2017).
211. Zhong, Y. *et al.* Spheres derived from the human SK-RC-42 renal cell carcinoma cell line are enriched in cancer stem cells. *Cancer Lett.* **299,** 150–160 (2010).
212. Lichner, Z. *et al.* miR-17 inhibition enhances the formation of kidney cancer spheres with stem cell/ tumor initiating cell properties. *Oncotarget* **6,** 5567–81 (2015).
213. Micucci, C., Matacchione, G., Valli, D., Orciari, S. & Catalano, A. HIF2α is involved in the expansion of CXCR4-positive cancer stem-like cells in renal cell carcinoma. *Br. J. Cancer* **113,** 1178–1185 (2015).
214. Debeb, B. G. *et al.* Characterizing cancer cells with cancer stem cell-like features in 293T human embryonic kidney cells. *Mol Cancer* **9,** 180 (2010).
215. Peired, A. J., Sisti, A. & Romagnani, P. Renal Cancer Stem Cells: Characterization and Targeted Therapies. *Stem Cells Int.* **2016,** (2016).
216. Welte, Y. Identification and characterization of cancer stem cells in cutaneous malignant melanoma. (Fachbereich Biologie, Chemie, Pharmazie, Freie Universität Berlin, 2012).
217. De Francesco, F. *et al.* Human CD34+/CD90+ ASCs are capable of growing as sphere clusters, producing high levels of VEGF and forming capillaries. *PLoS One* **4,** 1–13 (2009).
218. Martin, M. Cutadapt removes adapter sequences from high-throughput sequencing reads. *EMBnet.journal* **17,** 10 (2011).
219. Love, M. I., Anders, S., Kim, V. & Huber, W. RNA-Seq workflow: gene-level exploratory analysis and differential expression. *F1000Research* **4,** 1070 (2015).
220. Kim, D., Langmead, B. & Salzberg, S. L. HISAT: a fast spliced aligner with low memory requirements. *Nat. Methods* **12,** 357–60 (2015).
221. Kim, D. *et al.* Transcript-level expression analysis of RNA- seq experiments with HISAT , StringTie and Transcript-level expression analysis of RNA-seq experiments with HISAT , StringTie and Ballgown. *Nat. Protoc.* **11,** 1650–1667 (2016).
222. Li, H. *et al.* The Sequence Alignment/Map format and SAMtools. *Bioinformatics* **25,** 2078–2079 (2009).
223. Kamburov, A., Wierling, C., Lehrach, H. & Herwig, R. ConsensusPathDB - A database for integrating human functional interaction networks. *Nucleic Acids Res.* **37,** (2009).
224. Kamburov, A. *et al.* ConsensusPathDB: Toward a more complete picture of cell biology. *Nucleic Acids Res.* **39,** (2011).
225. Huang, D. W., Lempicki, R. a & Sherman, B. T. Systematic and integrative analysis of large gene lists using DAVID bioinformatics resources. *Nat. Protoc.* **4,** 44–57 (2009).
226. Huang, D. W., Sherman, B. T. & Lempicki, R. A. Bioinformatics enrichment tools: Paths toward the comprehensive functional analysis of large gene lists. *Nucleic Acids Res.* **37,** 1–13 (2009).
227. Rouillard, A. D. *et al.* The harmonizome: a collection of processed datasets gathered to serve and mine knowledge about genes and proteins. *Database (Oxford).* **2016,** 1–16 (2016).
228. Rouillard, A. D., Hurle, M. R. & Agarwal, P. Systematic interrogation of diverse Omic data reveals interpretable, robust, and generalizable transcriptomic features of clinically successful therapeutic targets. *PLoS Comput. Biol.* **14,** (2018).
229. Koressaar, T. & Remm, M. Enhancements and modifications of primer design program Primer3. *Bioinformatics* **23,** 1289–1291 (2007).

230. Untergasser, A. *et al.* Primer3-new capabilities and interfaces. *Nucleic Acids Res.* **40,** 1–12 (2012).
231. Curtis, A. S. G., Forrester, J. V., McInnes, C. & Lawrie, F. Adhesion of cells to polystyrene surfaces. *J. Cell Biol.* **97,** 1500–1506 (1983).
232. Ryan, J. A. Evolution of Cell Culture Surfaces. *BioFiles* 8–11 (2008).
233. Freshney, R. I. *Culture of Animal Cells: A Manual of Basic Technique and Specialized Applications: Sixth Edition*. *Culture of Animal Cells: A Manual of Basic Technique and Specialized Applications: Sixth Edition* (2011). doi:10.1002/9780470649367
234. Vescovi, A., Reynolds, B. A., Fraser, D. D. & Weiss, S. bFCF Regulates the Proliferative Fate of Unipotent (Neuronal) and Bipotent (NeuronallAstroglial) EGF-Generated CNS Progenitor Cells. *Neuron* **11,** 951–966 (1993).
235. Weiss, S. *et al.* Multipotent CNS stem cells are present in the adult mammalian spinal cord and ventricular neuroaxis. *J. Neurosci.* **16,** 7599–609 (1996).
236. Erickson, R. I., Paucar, A. A., Jackson, R. L., Visnyei, K. & Kornblum, H. Roles of insulin and transferrin in neural progenitor survival and proliferation. *J. Neurosci. Res.* **86,** 1884–1894 (2008).
237. Deleyrolle, L. P. & Reynolds, B. A. Isolation, Expansion and Differentiation of Adult Mammalian Neural Stem and Progenitor Cells Using the Neurosphere Assay. in *Methods in Molecular Biology* **549,** 91–101 (2009).
238. Wachs, F.-P. *et al.* High Efficacy of Clonal Growth and Expansion of Adult Neural Stem Cells. *Lab. Investig.* **83,** 949–962 (2003).
239. Louis, S. A., Mak, C. K. H. & Reynolds, B. A. Basic Cell Culture Protocols. *Methods Mol. Biol.* **946,** 479–506 (2013).
240. Toma, J. G., McKenzie, I. A., Bagli, D. & Miller, F. D. Isolation and characterization of multipotent skin-derived precursors from human skin. *Stem Cells* **23,** 727–37 (2013).
241. Singec, I. *et al.* Defining the actual sensitivity and specificity of the neurosphere assay in stem cell biology. *Nat. Methods* **3,** 801–806 (2006).
242. Wang, T. Y., Sen, A., Behie, L. A. & Kallos, M. S. Dynamic behavior of cells within neurospheres in expanding populations of neural precursors. *Brain Res.* **1107,** 82–96 (2006).
243. Coles-Takabe, B. L. K. *et al.* Don't Look: Growing Clonal Versus Nonclonal Neural Stem Cell Colonies. *Stem Cells* **26,** 2938–2944 (2008).
244. Louis, S. A. *et al.* Enumeration of Neural Stem and Progenitor Cells in the Neural Colony-Forming Cell Assay. *Stem Cells* **26,** 988–996 (2008).
245. Page, B., Page, M. & Noel, C. A new fluorometric assay for cytotoxicity measurements in vitro. *Int. J. Oncol.* **3,** 473–476 (1993).
246. Longo-Sorbello, G. S. A., Saydam, G., Banerjee, D. & Bertino, J. R. Cytotoxicity and cell growth assays. in *Cell Biology, Four-Volume Set* **1,** 315–324 (2006).
247. Hamburger, A. & Salmon, S. Primary bioassay of human tumor stem cells. *Science (80-.).* **197,** 461–463 (1977).
248. Fiebig, H. H., Maier, A. & Burger, A. M. Clonogenic assay with established human tumour xenografts: Correlation of in vitro to in vivo activity as a basis for anticancer drug discovery. *Eur. J. Cancer* **40,** 802–820 (2004).
249. Dodson, M. G., Slota, J., Lange, C. & Major, E. Distinction of the phenotypes of in vitro anchorage-independent soft-agar growth and in vivo tumorigenicity in the nude mouse. *Cancer Res.* **41,** 1441–1446 (1981).
250. Styner, M., Sen, B., Xie, Z., Case, N. & Rubin, J. Indomethacin promotes adipogenesis of mesenchymal stem cells through a cyclooxygenase independent mechanism. *J. Cell. Biochem.* **111,** 1042–1050 (2010).
251. Gregoire, F. M., Smas, C. M. & Sul, H. S. Understanding adipocyte differentiation. *Physiol. Rev.* **78,** 783–809 (1998).
252. Scott, M. A., Nguyen, V. T., Levi, B. & James, A. W. Current Methods of Adipogenic Differentiation of Mesenchymal Stem Cells. *Stem Cells Dev.* **20,** 1793–1804 (2011).
253. Green, H. & Meuth, M. An established pre-adipose cell line and its differentation in culture. *Cell* **3,** 127–133 (1974).

254. Langenbach, F. & Handschel, J. Effects of dexamethasone, ascorbic acid and β-glycerophosphate on the osteogenic differentiation of stem cells in vitro. *Stem Cell Res. Ther.* **4,** 117 (2013).
255. Cavallo, C. *et al.* Comparison of alternative mesenchymal stem cell sources for cell banking and musculoskeletal advanced therapies. *J. Cell. Biochem.* **112,** 1418–1430 (2011).
256. Köllmer, M., Buhrman, J. S., Zhang, Y. & Gemeinhart, R. A. Markers are shared between adipogenic and osteogenic differentiated mesenchymal stem cells. *J. Dev. Biol. Tissue Eng.* **5,** 18–25 (2013).
257. Kaltz, N. *et al.* Novel markers of mesenchymal stem cells defined by genome-wide gene expression analysis of stromal cells from different sources. *Exp. Cell Res.* **316,** 2609–2617 (2010).
258. Adriane Menssen, Thomas Häupl, Michael Sittinger, Bruno Delorme, Pierre Charbord, J. R. Differential gene expression profiling of human bone marrow-derived mesenchymal stem cells during adipogenic development-SupMat Genes with increased expression values during adipogenesis of human MSC - Sup Material. *BMC Genomics* 3–9 (2011).
259. Zhang, X. *et al.* Isolation and characterization of mesenchymal stem cells from human umbilical cord blood: Reevaluation of critical factors for successful isolation and high ability to proliferate and differentiate to chondrocytes as compared to mesenchymal stem cells fro. *J. Cell. Biochem.* **112,** 1206–1218 (2011).
260. Ramírez-Zacarías, J. L., Castro-Muñozledo, F. & Kuri-Harcuch, W. Quantitation of adipose conversion and triglycerides by staining intracytoplasmic lipids with oil red O. *Histochemistry* **97,** 493–497 (1992).
261. Gregory, C. A., Gunn, W. G., Peister, A. & Prockop, D. J. An Alizarin red-based assay of mineralization by adherent cells in culture: Comparison with cetylpyridinium chloride extraction. *Anal. Biochem.* **329,** 77–84 (2004).
262. Duplomb, L., Dagouassat, M., Jourdon, P. & Heymann, D. Concise Review: Embryonic Stem Cells: A New Tool to Study Osteoblast and Osteoclast Differentiation. *Stem Cells* **25,** 544–552 (2006).
263. Hatch, N. E. & Franceschi, R. T. Osteoblast differentiation stage-specific expression of the pyrophosphate-generating enzyme PC-1. *Cells Tissues Organs* **189,** 65–69 (2008).
264. Ali, A. T. *et al.* The relationship between alkaline phosphatase activity and intracellular lipid accumulation in murine 3T3-L1 cells and human preadipocytes. *Anal. Biochem.* **354,** 247–254 (2006).
265. Chirambo, G. M., van Niekerk, C. & Crowther, N. J. The role of alkaline phosphatase in intracellular lipid accumulation in the human hepatocarcinoma cell line, HepG2. *Exp. Mol. Pathol.* **102,** 224–229 (2017).
266. Lang, G. Histotechnik - Praxislehrbuch für die Biomedizinische Analytik. in *Histotechnik* 39–65 (2006). doi:10.1007/3-211-33142-5_5
267. Adan, A., Alizada, G., Kiraz, Y., Baran, Y. & Nalbant, A. Flow cytometry: basic principles and applications. *Crit. Rev. Biotechnol.* **37,** 163–176 (2017).
268. Moskalensky, A. E., Chernyshev, A. V, Yurkin, M. A., Nekrasov, V. M. & Polshchitsin, A. A. Dynamic quanti fi cation of antigen molecules with fl ow cytometry. *J. Immunol. Methods* **418,** 66–74 (2015).
269. Zhou, S. *et al.* Bcrp1 gene expression is required for normal numbers of side population stem cells in mice, and confers relative protection to mitoxantrone in hematopoietic cells in vivo. *Proc. Natl. Acad. Sci. U. S. A.* **99,** 12339–44 (2002).
270. Cabana, R. *et al.* The Minimal Instrumentation Requirements for Hoechst Side Population Analysis: Stem Cell Analysis on Low-Cost Flow Cytometry Platforms. *Stem Cells* **24,** 2573–2581 (2006).
271. Ferlini, C. & Scambia, G. Assay for apoptosis using the mitochondrial probes, Rhodamine123 and 10-N-nonyl acridine orange. *Nat. Protoc.* **2,** 3111–3114 (2007).
272. Darzynkiewicz, Z., Traganos, F., Kapuscinski, J. & Melamed, M. R. Interactionsof Rhodamine 123 with LivingCells Studied by Flow Cytometry1. *Cancer Res.* **42,** 799–806 (1982).

273. McKenzie, J. L., Takenaka, K., Gan, O. I., Doedens, M. & Dick, J. E. Low rhodamine 123 retention identifies long-term human hematopoietic stem cells within the Lin-CD34+CD38- population. *Blood* **109,** 543–545 (2007).
274. Gevensleben, H. *et al.* Rhodamine 123 efflux in human subpopulations of hematopoietic stem cells: comparison between bone marrow, umbilical cord blood and mobilized peripheral blood CD34+ cells. *Int. J. Mol. Med.* **22,** 237–243 (2008).
275. Liu, W. hui, Qian, N. song, Li, R. & Dou, K. feng. Replacing Hoechst33342 with Rhodamine123 in isolation of cancer stem-like cells from the MHCC97 cell line. *Toxicol. Vitr.* **24,** 538–545 (2010).
276. Golebiewska, A., Brons, N. H. C., Bjerkvig, R. & Niclou, S. P. Critical appraisal of the side population assay in stem cell and cancer stem cell research. *Cell Stem Cell* **8,** 136–147 (2011).
277. Ito, M. *et al.* Nod/scid/γ. *Bone* **100,** 3175–3182 (2002).
278. Fridman, R., Benton, G., Aranoutova, I., Kleinman, H. K. & Bonfil, R. D. Increased initiation and growth of tumor cell lines, cancer stem cells and biopsy material in mice using basement membrane matrix protein (Cultrex or Matrigel) co-injection. *Nat. Protoc.* **7,** 1138–1144 (2012).
279. Mühlhardt, C. *Der Experimentator: Molekularbiologie/Genomics*. (Spektrum Akademischer Verlag, 2003).
280. Fleige, S. & Pfaffl, M. W. RNA integrity and the effect on the real-time qRT-PCR performance. *Mol. Aspects Med.* **27,** 126–139 (2006).
281. Gallego Romero, I., Pai, A. A., Tung, J. & Gilad, Y. RNA-seq: Impact of RNA degradation on transcript quantification. *BMC Biol.* **12,** 1–13 (2014).
282. *Bioanalytik*. (Spektrum Akademischer Verlag, 1998).
283. Auer, H. & Lyianarachchi, S. Chipping away at the chip bias:RNA degradation in microarray analysis. *Nat. Genet.* **35,** 293 (2003).
284. Schroeder, A. *et al.* The RIN: An RNA integrity number for assigning integrity values to RNA measurements. *BMC Mol. Biol.* **7,** 1–14 (2006).
285. Mueller, O. & Schroeder, A. RNA Integrity Number (RIN) – Standardization of RNA Quality Control Application. *Agil. Technol. Appl. Notes* 1–8 (2016). doi:10.1101/gr.189621.115.7
286. AgilentTechnologies. Comparison of RIN and RIN e algorithms for the Agilent 2100 Bioanalyzer and the Agilent 2200 TapeStation systems. *Tech. Overv.* **Publicatio,** 1–4 (2016).
287. Metzker, M. L. Sequencing technologies the next generation. *Nat. Rev. Genet.* **11,** 31–46 (2010).
288. Mardis, E. R. Next-Generation Sequencing Platforms. *Annu. Rev. Anal. Chem.* **6,** 287–303 (2013).
289. Milos, F. O. and P. M. & Abstract. RNA sequencing: advances, challenges and opportunities. *Nat. Rev. Genet.* **12,** 87–89 (2011).
290. Goodwin, S., McPherson, J. D. & McCombie, W. R. Coming of age: Ten years of next-generation sequencing technologies. *Nat. Rev. Genet.* **17,** 333–351 (2016).
291. Cui, P. *et al.* A comparison between ribo-minus RNA-sequencing and polyA-selected RNA-sequencing. *Genomics* **96,** 259–265 (2010).
292. Levin, J. Z. *et al.* Comprehensive comparative analysis of strand-specific RNA sequencing methods. *Nat. Methods* **7,** 709–715 (2010).
293. Robasky, K., Lewis, N. E. & Church, G. M. The role of replicates for error mitigation in next-generation sequencing. *Nat. Rev. Genet.* **15,** 56–62 (2014).
294. Liu, Y., Zhou, J. & White, K. P. RNA-seq differential expression studies: More sequence or more replication? *Bioinformatics* **30,** 301–304 (2014).
295. Cock, P. J. A., Fields, C. J., Goto, N., Heuer, M. L. & Rice, P. M. The Sanger FASTQ file format for sequences with quality scores, and the Solexa/Illumina FASTQ variants. *Nucleic Acids Res.* **38,** 1767–1771 (2009).
296. Illumina. Quality Scores for Next-Generation Sequencing. *Illumina Technote Q-Scores* 1–2 (2011).
297. Hansen, K. D., Brenner, S. E. & Dudoit, S. Biases in Illumina transcriptome sequencing caused by random hexamer priming. *Nucleic Acids Res.* **38,** 1–7 (2010).

298. Bansal, V. A computational method for estimating the PCR duplication rate in DNA and RNA-seq experiments. *BMC Bioinformatics* **18,** (2017).
299. Delhomme, N., Mähler, N., Schiffthaler, B. & Sundell, D. Guidelines for RNA-Seq data analysis. *Epigenesys Protoc.* 1–24 (2014).
300. Love, M. I., Huber, W. & Anders, S. Moderated estimation of fold change and dispersion for RNA-seq data with DESeq2. *Genome Biol.* **15,** 1–21 (2014).
301. Chu, M.-K. M. Statistical methods for the analysis of RNA sequencing data. *Univ. West. Ontario - Electron. Thesis Diss. Repos.* (2014).
302. Mortazavi, A., Williams, B. A., McCue, K., Schaeffer, L. & Wold, B. Mapping and quantifying mammalian transcriptomes by RNA-Seq. *Nat. Methods* **5,** 621–628 (2008).
303. Wagner, G. P., Kin, K. & Lynch, V. J. Measurement of mRNA abundance using RNA-seq data: RPKM measure is inconsistent among samples. *Theory Biosci.* **131,** 281–285 (2012).
304. Abourbih, S. *et al.* Aldehyde dehydrogenase 1 expression in primary and metastatic renal cell carcinoma: an immunohistochemistry study. *World J. Surg. Oncol.* **11,** 298 (2013).
305. Rodier, F. & Campisi, J. Four faces of cellular senescence. *J. Cell Biol.* **192,** 547–556 (2011).
306. Biran, A. *et al.* Quantitative identification of senescent cells in aging and disease. *Aging Cell* **16,** 661–671 (2017).
307. Li, Q., Rycaj, K., Chen, X. & Tang, D. G. Cancer stem cells and cell size: A causal link? *Semin. Cancer Biol.* **35,** 191–199 (2015).
308. Zanoni, M. *et al.* 3D tumor spheroid models for in vitro therapeutic screening: A systematic approach to enhance the biological relevance of data obtained. *Sci. Rep.* **6,** 1–11 (2016).
309. Fennema, E., Rivron, N., Rouwkema, J., van Blitterswijk, C. & De Boer, J. Spheroid culture as a tool for creating 3D complex tissues. *Trends Biotechnol.* **31,** 108–115 (2013).
310. Qureshi-Baig, K. *et al.* What Do We Learn from Spheroid Culture Systems? Insights from Tumorspheres Derived from Primary Colon Cancer Tissue. *PLoS One* **11,** e0146052 (2016).
311. Rybak, A. P., He, L., Kapoor, A., Cutz, J. C. & Tang, D. Characterization of sphere-propagating cells with stem-like properties from DU145 prostate cancer cells. *Biochim. Biophys. Acta - Mol. Cell Res.* **1813,** 683–694 (2011).
312. Santini, R. *et al.* SOX2 regulates self-renewal and tumorigenicity of human melanoma-initiating cells. *Oncogene* **33,** 4697–4708 (2014).
313. Buzhor, E. *et al.* Kidney Spheroids Recapitulate Tubular Organoids Leading to Enhanced Tubulogenic Potency of Human Kidney-Derived Cells. *Tissue Eng. Part A* **17,** 2305–2319 (2011).
314. Peng, L., Hu, Y., Chen, D., Jiao, S. & Sun, S. Ubiquitin specific peptidase 21 regulates interleukin-8 expression, stem-cell like property of human renal cell carcinoma. *Oncotarget* **7,** 42007–42016 (2016).
315. Yun, E., Zhou, J., Lin, C., Xu, S. & Santoyo, J. The network of DAB2IP-miR-138 in regulating drug resistance of renal cell carcinoma associated with stem-like phenotypes. *Oncotarget* **8,** 66975–66986 (2017).
316. Li, W. *et al.* Honokiol suppresses renal cancer cells' metastasis via dual-blocking epithelial-mesenchymal transition and cancer stem cell properties through modulating miR-141/ZEB2 signaling. *Mol. Cells* **37,** 383–8 (2014).
317. Pode-Shakked, N. *et al.* Developmental tumourigenesis: NCAM as a putative marker for the malignant renal stem/progenitor cell population. *J. Cell. Mol. Med.* **13,** 1792–1808 (2009).
318. Hsieh, C., Hsiung, S., Yeh, C. & Yen, C. Differential expression of CD44 and CD24 markers discriminates the epitheliod from the fibroblastoid subset in a sarcomatoid renal carcinoma cell line : evidence suggesting the existence of cancer stem cells in both subsets as studied with sorted cells. *Oncotraget* **8,** 15593–15609 (2017).
319. Khan, M. I. *et al.* Comparative gene expression profiling of primary and metastatic renal cell carcinoma stem cell-like cancer cells. *PLoS One* **11,** 1–37 (2016).
320. Deleyrolle, L. P. *et al.* Determination of somatic and cancer stem cell self-renewing symmetric division rate using sphere assays. *PLoS One* **6,** (2011).
321. Liu, X. *et al.* Nonlinear Growth Kinetics of Breast Cancer Stem Cells: Implications for Cancer Stem Cell Targeted Therapy. *Sci. Rep.* **3,** 1–10 (2013).

322. Bruno, S. *et al.* Isolation and Characterization of Resident Mesenchymal Stem Cells in Human Glomeruli. *Stem Cells Dev.* **18,** 867–880 (2009).
323. Tun, H. W. *et al.* Pathway signature and cellular differentiation in clear cell renal cell carcinoma. *PLoS One* **5,** (2010).
324. Challen, G. A. Kidney Side Population Reveals Multilineage Potential and Renal Functional Capacity but also Cellular Heterogeneity. *J. Am. Soc. Nephrol.* **17,** 1896–1912 (2006).
325. Tang, Q. Q. & Lane, M. D. Adipogenesis: From Stem Cell to Adipocyte. *Annu. Rev. Biochem.* **81,** 715–736 (2012).
326. Dingwall, M., Marchildon, F., Gunanayagam, A., Louis, C. S. & Wiper-Bergeron, N. Retinoic acid-induced Smad3 expression is required for the induction of osteoblastogenesis of mesenchymal stem cells. *Differentiation* **82,** 57–65 (2011).
327. Ayala-Sumuano, J.-T. *et al.* Srebf1a is a key regulator of transcriptional control for adipogenesis. *Sci. Rep.* **1,** 178 (2011).
328. Rosen, E. D., Walkey, C. J., Puigserver, P. & Spiegelman, B. M. Transcriptional regulation of adipogenesis Transcriptional regulation of adipogenesis. *Genes Dev.* **14,** 1293–1307 (2000).
329. Gharibi, B. & Hughes, F. J. Effects of Medium Supplements on Proliferation, Differentiation Potential, and In Vitro Expansion of Mesenchymal Stem Cells. *Stem Cells Transl. Med.* **1,** 771–782 (2012).
330. Addla, S. K., Brown, M. D., Hart, C. A., Ramani, V. A. C. & Clarke, N. W. Characterization of the Hoechst 33342 side population from normal and malignant human renal epithelial cells - Table. *AJP Ren. Physiol.* **295,** F680–F687 (2008).
331. Huang, B. *et al.* PKCε inhibits isolation and stemness of side population cells via the suppression of ABCB1 transporter and PI3K / Akt , MAPK / ERK signaling in renal cell carcinoma cell line 769P. *Cancer Lett.* **376,** 148–154 (2016).
332. Lynn M. Opdenaker, Shirin R. Modarai, and B. M. B. The Proportion of ALDEFLUOR-Positive Cancer Stem Cells Changes with Cell Culture Density Due to the Expression of Different ALDH Isoforms Lynn. *CAncer Stud Mol Med* **2,** 87–95 (2015).
333. Suzuki, Y. *et al.* SSEA-3 as a novel amplifying cancer cell surface marker in colorectal cancers. *Int. J. Oncol.* **42,** 161–167 (2013).
334. Charafe-Jauffret, E. *et al.* Breast cancer cell lines contain funtional cancer stem cells with metastatic capacity and distinct molecular signature. *Cancer Res.* **69,** 1302–1313 (2009).
335. Ginestier, C. *et al.* ALDH1 Is a Marker of Normal and Malignant Human Mammary Stem Cells and a Predictor of Poor Clinical Outcome. *Cell Stem Cell* **1,** 555–567 (2007).
336. Wang, K. *et al.* Increased expression of ALDH1A1 protein is associated with poor prognosis in clear cell renal cell carcinoma. *Med. Oncol.* **30,** (2013).
337. Ozbek, E. *et al.* Stem cell markers aldehyde dehydrogenase type 1 and nestin expressions in renal cell cancer. *Arch. Ital. Urol. Androl.* **84,** 7–11 (2012).
338. Abdulrahman, M. *et al.* Identification of novel VHL targets that are associated with the development of renal cell carcinoma. *Oncogene* **26,** 1661–1672 (2007).
339. Sobiesiak, M. *et al.* The Mesenchymal Stem Cell Antigen MSCA-1 is Identical to Tissue Non-specific Alkaline Phosphatase. *Stem Cells Dev.* **19,** 669–677 (2010).
340. Battula, V. L. *et al.* Isolation of functionally distinct mesenchymal stem cell subsets using antibodies against CD56, CD271, and mesenchymal stem cell antigen-1. *Haematologica* **94,** 173–184 (2009).
341. Kim, Y. H., Yoon, D. S., Kim, H. O. & Lee, J. W. Characterization of Different Subpopulations from Bone Marrow-Derived Mesenchymal Stromal Cells by Alkaline Phosphatase Expression. *Stem Cells Dev.* **21,** 2958–2968 (2012).
342. Rao, S. R. *et al.* Tumour-derived alkaline phosphatase regulates tumour growth, epithelial plasticity and disease-free survival in metastatic prostate cancer. *Br. J. Cancer* **116,** 227–236 (2017).
343. Nouwen, E. J. & De Broe, M. E. Human intestinal versus tissue-nonspecific alkaline phosphatase as complementary urinary markers for the proximal tubule. *Kidney Int. Suppl.* **47,** S43–S51 (1994).
344. Trzpis, M., McLaughlin, P. M. J., de Leij, L. M. F. H. & Harmsen, M. C. Epithelial Cell Adhesion Molecule. *Am. J. Pathol.* **171,** 386–395 (2007).

345. van der Gun, B. T. F. *et al.* EpCAM in carcinogenesis: The good, the bad or the ugly. *Carcinogenesis* **31,** 1913–1921 (2010).
346. Schnell, U., Cirulli, V. & Giepmans, B. N. G. EpCAM: Structure and function in health and disease. *Biochim. Biophys. Acta - Biomembr.* **1828,** 1989–2001 (2013).
347. Visvader, J. E. Keeping abreast of the mammary epithelial hierarchy and breast tumorigenesis. *Genes Dev.* **23,** 2563–2577 (2009).
348. Liu, S. *et al.* Breast cancer stem cells transition between epithelial and mesenchymal states reflective of their normal counterparts. *Stem Cell Reports* **2,** 78–91 (2014).
349. Keller, P. J. *et al.* Defining the cellular precursors to human breast cancer. *Proc. Natl. Acad. Sci.* **109,** 2772–2777 (2011).
350. Bachelard-Cascales, E. *et al.* The CD10 enzyme is a key player to identify and regulate human mammary stem cells. *Stem Cells* **28,** 1081–1088 (2010).
351. Metsuyanim, S. *et al.* Expression of stem cell markers in the human fetal kidney. *PLoS One* **4,** (2009).
352. Seligson, D. B. *et al.* Epithelial cell adhesion molecule (KSA) expression: pathobiology and its role as an independent predictor of survival in renal cell carcinoma. *Clin Cancer Res* **10,** 2659–2669 (2004).
353. Zimpfer, A. *et al.* Prognostic and diagnostic implications of epithelial cell adhesion/activating molecule (EpCAM) expression in renal tumours: A retrospective clinicopathological study of 948 cases using tissue microarrays. *BJU Int.* **114,** 296–302 (2014).
354. Liu, L. *et al.* Immunohistochemical analysis of chromophobe renal cell carcinoma, renal oncocytoma, and clear cell carcinoma: an optimal and practical panel for differential diagnosis. *Arch. Pathol. Lab. Med.* **131,** 1290–1297 (2007).
355. Landolt, L. *et al.* Clear Cell Renal Cell Carcinoma is linked to Epithelial-to-Mesenchymal Transition and to Fibrosis. *Physiol. Rep.* **5,** 1–18 (2017).
356. Hasmim, M. *et al.* Isolation and characterization of renal cancer stem cells from patient-derived xenografts. *Oncotarget* **7,** 15507–15524 (2015).
357. Jaggupilli, A. & Elkord, E. Significance of CD44 and CD24 as cancer stem cell markers: An enduring ambiguity. *Clin. Dev. Immunol.* **2012,** (2012).
358. Nakamura, K. *et al.* CD24 expression is a marker for predicting clinical outcome and regulates the epithelial-mesenchymal transition in ovarian cancer via both the Akt and ERK pathways. *Oncol. Rep.* **37,** 3189–3200 (2017).
359. Keysar, S. B. & Jimeno, A. More than Markers: Biological Significance of Cancer Stem Cell-Defining Molecules. *Mol. Cancer Ther.* **9,** 2450–2457 (2010).
360. Boareto, M. *et al.* Notch-Jagged signalling can give rise to clusters of cells exhibiting a hybrid epithelial/mesenchymal phenotype. *J. R. Soc. Interface* **13,** (2016).
361. Gracz AD, Fuller MK, Wang F, Li L, Stelzner M, Dunn JCY, Martin MG, M. S. CD24 and CD44 mark human intestinal epithelial cell populations with characteristics of active and facultative stem cells. *Stem Cells* **31,** 2024–2030 (2013).
362. Okano, M. *et al.* Human colorectal CD24+ cancer stem cells are susceptible to epithelial-mesenchymal transition. *Int. J. Oncol.* **45,** 575–580 (2014).
363. Challen, G. A. Identifying the Molecular Phenotype of Renal Progenitor Cells. *J. Am. Soc. Nephrol.* **15,** 2344–2357 (2004).
364. Senbanjo, L. T. & Chellaiah, M. A. CD44: A Multifunctional Cell Surface Adhesion Receptor Is a Regulator of Progression and Metastasis of Cancer Cells. *Front. Cell Dev. Biol.* **5,** (2017).
365. Cheng, B. *et al.* Cancer stem cell markers predict a poor prognosis in renal cell carcinoma: a meta-analysis. *Oncotarget* **7,** (2016).
366. Quintanilla, R. H., Asprer, J. S. T., Vaz, C., Tanavde, V. & Lakshmipathy, U. CD44 is a negative cell surface marker for pluripotent stem cell identification during human fibroblast reprogramming. *PLoS One* **9,** (2014).
367. Sivasubramaniyan, K. *et al.* Expression of stage-specific embryonic antigen-4 (SSEA-4) defines spontaneous loss of epithelial phenotype in human solid tumor cells. *Glycobiology* **25,** 902–917 (2015).

368. Qian, H., Le Blanc, K. & Sigvardsson, M. Primary mesenchymal stem and progenitor cells from bone marrow lack expression of CD44 protein. *J. Biol. Chem.* **287,** 25795–25807 (2012).
369. Gao, Z. W., Dong, K. & Zhang, H. Z. The roles of CD73 in cancer. *Biomed Res. Int.* **2014,** (2014).
370. Zhang, B. CD73: A Novel Target for Cancer Immunotherapy. *Cancer Res* **70,** 6407–6411 (2010).
371. Fonsatti, E. & Maio, M. Highlights on endoglin (CD105): From basic findings towards clinical applications in human cancer. *J. Transl. Med.* **2,** 1–7 (2004).
372. Sánchez-Elsner, T., Botella, L. M., Velasco, B., Langa, C. & Bernabéu, C. Endoglin expression is regulated by transcriptional cooperation between the hypoxia and transforming growth factor-β pathways. *J. Biol. Chem.* **277,** 43799–43808 (2002).
373. Pérez-Gómez, E. *et al.* The Role of the TGF-β Coreceptor Endoglin in Cancer. *Sci. World J.* **10,** 2367–2384 (2010).
374. Boxall, S. A. & Jones, E. Markers for characterization of bone marrow multipotential stromal cells. *Stem Cells Int.* **2012,** (2012).
375. Sandlund, J. *et al.* Endoglin (CD105) expression in human renal cell carcinoma. *BJU Int.* **97,** 706–710 (2006).
376. Zanjani, L. S. *et al.* Expression of CD105 cancer stem cell marker in three subtypes of renal cell carcinoma. *Cancer Biomarkers -1* **21,** 1–17 (2017).
377. Masereeuw, R. *et al.* Regulation of P-glycoprotein in renal proximal tubule epithelial cells by LPS and TNF-α. *J. Biomed. Biotechnol.* **2010,** (2010).
378. Boysen, G. *et al.* Identification and Functional Characterization of pVHL-Dependent Cell Surface Proteins in Renal Cell Carcinoma. *Neoplasia* **14,** 535–IN17 (2012).
379. Shih, I.-M. THE ROLE OF CD146 (Mel-CAM) IN BIOLOGY AND PATHOLOGY. *J. Pathol.* **189,** 4–11 (1999).
380. Halfon, S., Abramov, N., Grinblat, B. & Ginis, I. Markers Distinguishing Mesenchymal Stem Cells from Fibroblasts Are Downregulated with Passaging. *Stem Cells Dev.* **20,** 53–66 (2011).
381. Bradley, J. E., Ramirez, G. & Hagood, J. S. Roles and regulation of Thy-1 , a context-dependent modulator of cell phenotype. *BioFactors* 258–265 (2009). doi:10.1002/biof.41
382. Yang, Z. F. *et al.* Significance of CD90+ Cancer Stem Cells in Human Liver Cancer. *Cancer Cell* **13,** 153–166 (2008).
383. Shaikh, M. V., Kala, M. & Nivsarkar, M. CD90 a potential cancer stem cell marker and a therapeutic target. *Cancer Biomarkers* **16,** 301–307 (2016).
384. Chosa, N. & Ishisaki, A. Two novel mechanisms for maintenance of stemness in mesenchymal stem cells: SCRG1/BST1 axis and cell–cell adhesion through N-cadherin. *Jpn. Dent. Sci. Rev.* **54,** 37–44 (2018).
385. Cruz-Morcillo, M. A. D. la *et al.* p75 neurotrophin receptor and pro-BDNF promote cell survival and migration in clear cell renal cell carcinoma. *Oncotarget* **5,** 34480–34497 (2016).
386. Büuhring, H. J. *et al.* Novel markers for the prospective isolation of human MSC. *Ann. N. Y. Acad. Sci.* **1106,** 262–271 (2007).
387. Ostyn, P. *et al.* Transient TNF regulates the self-renewing capacity of stem-like label-retaining cells in sphere and skin equivalent models of melanoma. *Cell Commun. Signal.* **12,** 52 (2014).
388. Menon, D. R. *et al.* A stress-induced early innate response causes multidrug tolerance in melanoma. *Oncogene* **34,** 4448–4459 (2015).
389. Redmer, T. *et al.* The role of the cancer stem cell marker CD271 in DNA damage response and drug resistance of melanoma cells. *Oncogenesis* **6,** 1–13 (2017).
390. Tomellini, E., Lagadec, C., Polakowska, R. & Le Bourhis, X. Role of p75 neurotrophin receptor in stem cell biology: More than just a marker. *Cell. Mol. Life Sci.* **71,** 2467–2481 (2014).
391. Chatterjee Samit, Azad Babak Behnam, N. S. The Intricate Role of CXCR4 in Cancer. *Adv Cancer Res.* 31–82 (2014). doi:10.3174/ajnr.A1256.Functional
392. Sun, X., Cheng, G., Hao, M., Zheng, J. & Zhou, X. CXCL12/CXCR4/CXCR7 Chemokine Axis and Cancer Progression. *Cancer Metastasis Rev.* **29,** 709–722 (2010).
393. Liu, Y., Carson-Walter, E. & Walter, K. A. Chemokine receptor CXCR7 is a functional receptor for CXCL12 in brain endothelial cells. *PLoS One* **9,** 4–12 (2014).

394. Chen, D. *et al.* Expression and Prognostic Significance of a Comprehensive Epithelial-Mesenchymal Transition Gene Set in Renal Cell Carcinoma. *J. Urol.* **191,** 479–486 (2014).
395. K Struckmann, KD Mertz, S Steu,M Storz, P Staller, W Krek, P. S. and H. M. pVHL co-ordinately regulates CXCR4/CXCL12 and MMP2/MMP9 expression in human clear-cell renal cell carcinoma. *J. Pathol.* **214,** 464–471 (2008).
396. Walsh, F. S. & Doherty, P. Neural Cell Adhesion Molecules Of The Immunoglobulin Superfamily: Role in Axon Growth and Guidance. *Annu. Rev. Cell Dev. Biol.* **13,** 425–456 (1997).
397. Van Acker, H. H., Capsomidis, A., Smits, E. L. & Van Tendeloo, V. F. CD56 in the immune system: More than a marker for cytotoxicity? *Front. Immunol.* **8,** 1–9 (2017).
398. Ditlevsen, D. K., Povlsen, G. K., Berezin, V. & Bock, E. NCAM-induced intracellular signaling revisited. *J. Neurosci. Res.* **86,** 727–743 (2008).
399. Chan, A. W. H., Tong, J. H. M., Chan, S. L., Lai, P. B. S. & To, K. F. Expression of stemness markers (CD133 and EpCAM) in prognostication of hepatocellular carcinoma. *Histopathology* **64,** 935–950 (2014).
400. Bösmüller, H.-C. *et al.* CD56 (Neural Cell Adhesion Molecule) Expression in Ovarian Carcinomas: Association with High-Grade and Advanced Stage but Not with Neuroendocrine Differentiation. *Int. J. Gynecol. Cancer* **27,** (2017).
401. Yun, J.-P., Xiang, J., Hou, J.-H., Tian, Q.-H. & Fu, J. Expression of CD56, as a potential diagnostic marker, in small cell carcinoma. *Ai Zheng* **24,** 1140–1143 (2005).
402. Zecchini, S. *et al.* The adhesion molecule NCAM promotes ovarian cancer progression via FGFR signalling. *EMBO Mol. Med.* **3,** 480–494 (2011).
403. Buzhor, E. *et al.* Reactivation of NCAM1 defines a subpopulation of human adult kidney epithelial cells with clonogenic and stem/progenitor properties. *Am. J. Pathol.* **183,** 1621–1633 (2013).
404. Daniel, L. *et al.* Neural cell adhesion molecule expression in renal cell carcinomas: Relation to metastatic behavior. *Hum. Pathol.* **34,** 528–532 (2003).
405. Maguer-Satta, V., Besançon, R. & Bachelard-Cascales, E. Concise review: Neutral endopeptidase (CD10): A multifaceted environment actor in stem cells, physiological mechanisms, and cancer. *Stem Cells* **29,** 389–396 (2011).
406. Granéli, C. *et al.* Novel markers of osteogenic and adipogenic differentiation of human bone marrow stromal cells identified using a quantitative proteomics approach. *Stem Cell Res.* **12,** 153–165 (2014).
407. Oba, J. *et al.* CD10-equipped melanoma cells acquire highly potent tumorigenic activity: A plausible explanation of their significance for a poor prognosis. *PLoS One* **11,** 1–16 (2016).
408. Lee, K. W. *et al.* CD10 expression is enhanced by Twist1 and associated with poor prognosis in esophageal squamous cell carcinoma with facilitating tumorigenicity in vitro and in vivo. *Int. J. Cancer* **136,** 310–321 (2015).
409. Mazal, P. R. *et al.* Expression of aquaporins and PAX-2 compared to CD10 and cytokeratin 7 in renal neoplasms: A tissue microarray study. *Mod. Pathol.* **18,** 535–540 (2005).
410. Shen, S. S., Truong, L. D., Scarpelli, M. & Lopez-Beltran, A. Role of immunohistochemistry in diagnosing renal neoplasms when is it really useful? *Arch. Pathol. Lab. Med.* **136,** 410–417 (2012).
411. Mitra, R., Chao, O. S., Nanus, D. M. & Goodman, O. B. Negative regulation of NEP expression by hypoxia. *Prostate* **73,** 706–714 (2013).
412. Dall'Era, M. A. *et al.* Differential expression of CD10 in prostate cancer and its clinical implication. *BMC Urol.* **7,** 3 (2007).
413. Grosse-Gehling, P. *et al.* CD133 as a biomarker for putative cancer stem cells in solid tumours: Limitations, problems and challenges. *J. Pathol.* **229,** 355–378 (2013).
414. Bruno, S. *et al.* CD133+ Renal Progenitor Cells Contribute to Tumor Angiogenesis. *Am. J. Pathol.* **169,** 2223–2235 (2006).
415. Saeednejad Zanjani, L. *et al.* Cytoplasmic expression of CD133 stemness marker is associated with tumor aggressiveness in clear cell renal cell carcinoma. *Exp. Mol. Pathol.* **103,** 218–228 (2017).

416. Li, Z. CD133: A stem cell biomarker and beyond. *Exp. Hematol. Oncol.* **2,** 1 (2013).
417. Giancotti, F. G. & Ruoslahti, E. Integrin signaling. *Science (80-.).* **285,** 1028–1032 (1999).
418. Harburger, D. S. & Calderwood, D. A. Integrin signalling at a glance. *J. Cell Sci.* **122,** 1472–1472 (2009).
419. Das, V., Kalyan, G., Hazra, S. & Pal, M. Understanding the role of structural integrity and differential expression of integrin profiling to identify potential therapeutic targets in breast cancer. *J. Cell. Physiol.* **233,** 168–185 (2018).
420. Zwolanek, D. *et al.* β1 Integrins Mediate Attachment of Mesenchymal Stem Cells to Cartilage Lesions. *Biores. Open Access* **4,** 39–53 (2015).
421. Ju, J. A. *et al.* Hypoxia Selectively Enhances Integrin α 5 β 1 Receptor Expression in Breast Cancer to Promote Metastasis. *Mol. Cancer Res.* **15,** 723–734 (2017).
422. Haraguchi, N. *et al.* CD49f-positive cell population efficiently enriches colon cancer-initiating cells. *Int. J. Oncol.* **43,** 425–430 (2013).
423. Korhonen, M., Sariola, H., Gould, V. E., Kangas, L. & Virtanen, I. Integrins and laminins in human renal carcinoma cells and tumors grown in nude mice. *Cancer Res.* **54,** 4532–4538 (1994).
424. Ming Zhou, C. M.-G. Immunohistochemical Markers in the Differential Diagnosis of Renal Neoplasms. *Patholoty Res. - Clin. Transl. -A Publ. Div. Pathol. Lab. Med. Clevel. Clin.* **1,** 4–6 (2005).
425. Rosada, C., Justesen, J., Melsvik, D., Ebbesen, P. & Kassem, M. The human umbilical cord blood: A potential source for osteoblast progenitor cells. *Calcif. Tissue Int.* **72,** 135–142 (2003).
426. Chu, PG and Weiss, L. Keratin expresssion in human tissues and neoplasms. *Histopathology* **40,** 403–439 (2002).
427. Karantza, V. Keratins in health and cancer: more than mere epithelial cell markers. *Oncogene* **30,** 127–138 (2011).
428. Kim, H. *et al.* Human hepatocellular carcinomas with 'Stemness'-related marker expression: Keratin 19 expression and a poor prognosis. *Hepatology* **54,** 1707–1717 (2011).
429. Takano, M. *et al.* Keratin 19 as a key molecule in progression of human hepatocellular carcinomas through invasion and angiogenesis. *BMC Cancer* **16,** 1–9 (2016).
430. Deshpande, V. *et al.* Cytokeratin 19 is a powerful predictor of survival in pancreatic endocrine tumors. *Am. J. Surg. Pathol.* **28,** 1145–1153 (2004).
431. Skinnider, B. F. *et al.* Distribution of cytokeratins and vimentin in adult renal neoplasms and normal renal tissue: Potential utility of a cytokeratin antibody panel in the differential diagnosis of renal tumors. *Am. J. Surg. Pathol.* **29,** 747–754 (2005).
432. Alexa A, Baderca F, Lighezan R, Izvernariu D, R. M. The diagnostic value of cytokeratins expression in the renal parenchyma tumors. *Rom. J. Morphol. Embryol.* **51,** 27–35 (2010).
433. Heinrich, K. Genexpressionsprofil einer vierfach transient genmodifizierten Nierenkarzinomzelllinie. (2015).
434. Satelli, A. & Li, S. Vimentin in cancer and its potential as a molecular target for cancer therapy. *Cell. Mol. Life Sci.* **68,** 3033–3046 (2011).
435. Mathieu, J. *et al.* HIF induces human embryonic stem cell markers in cancer cells. *Cancer Res.* **71,** 4640–4652 (2011).
436. Wang, X. & Dai, J. Concise review: Isoforms of OCT4 contribute to the confusing diversity in stem cell biology. *Stem Cells* **28,** 885–893 (2010).
437. Mueller, T., Luetzkendorf, J., Nerger, K., Schmoll, H. J. & Mueller, L. P. Analysis of OCT4 expression in an extended panel of human tumor cell lines from multiple entities and in human mesenchymal stem cells. *Cell. Mol. Life Sci.* **66,** 495–503 (2009).
438. Zhang, P., Andrianakos, R., Yang, Y., Liu, C. & Lu, W. Kruppel-like factor 4 (Klf4) prevents embryonic stem (ES) cell differentiation by regulating Nanog gene expression. *J. Biol. Chem.* **285,** 9180–9189 (2010).
439. Birsoy K, Chen Z, F. F. Transcriptional Regulation of Adipogenesis by KLF4. *Cell Matab* **7,** 339–347 (2008).

440. Piva, F. *et al.* Epithelial to Mesenchymal Transition in Renal Cell Carcinoma: Implications for Cancer Therapy. *Mol. Diagn. Ther.* **20,** 111–117 (2016).
441. Masola, V. *et al.* Heparanase and syndecan-1 interplay orchestrates fibroblast growth factor-2-induced epithelial-mesenchymal transition in renal tubular cells. *J. Biol. Chem.* **287,** 1478–1488 (2012).
442. Ross, D. T. *et al.* Systematic variation in gene expression patterns in human cancer cell lines. *Nat. Genet.* **24,** 227–35 (2000).
443. Young, A. N. *et al.* Expression profiling of renal epithelial neoplasms: A method for tumor classification and discovery of diagnostic molecular markers. *Am. J. Pathol.* **158,** 1639–1651 (2001).
444. Tan, T. Z. *et al.* Epithelial-mesenchymal transition spectrum quantification and its efficacy in deciphering survival and drug responses of cancer patients. *EMBO Mol. Med.* **6,** 1279–1293 (2014).
445. Harada, K. I., Miyake, H., Kusuda, Y. & Fujisawa, M. Expression of epithelial-mesenchymal transition markers in renal cell carcinoma: Impact on prognostic outcomes in patients undergoing radical nephrectomy. *BJU Int.* **110,** (2012).
446. Zhang, L. *et al.* TNF-α induced epithelial mesenchymal transition increases stemness properties in renal cell carcinoma cells. *Int. J. Clin. Exp. Med.* **7,** 4951–4958 (2014).
447. Ho, M.-Y. *et al.* TNF- Induces Epithelial-Mesenchymal Transition of Renal Cell Carcinoma Cells via a GSK3 -Dependent Mechanism. *Mol. Cancer Res.* **10,** 1109–1119 (2012).
448. Sun, K. H. *et al.* TNF-α augments CXCR2 and CXCR3 to promote progression of renal cell carcinoma. *J. Cell. Mol. Med.* **20,** 2020–2028 (2016).
449. Sitaram, R. T., Mallikarjuna, P. & Landström, M. Transforming growth factor-β promotes aggressiveness and invasion of clear cell renal cell carcinoma. *Oncotarget* **7,** (2016).
450. Bostrom, A.-K. *et al.* Sarcomatoid conversion of clear cell renal cell carcinoma in relation to epithelial-to-mesenchymal transition. *Hum. Pathol.* **43,** 708–719 (2012).
451. Sampson, V. B. *et al.* Wilms' tumor protein induces an epithelial-mesenchymal hybrid differentiation state in clear cell renal cell carcinoma. *PLoS One* **9,** (2014).
452. Goossens, S., Vandamme, N., Van Vlierberghe, P. & Berx, G. EMT transcription factors in cancer development re-evaluated: Beyond EMT and MET. *Biochim. Biophys. Acta - Rev. Cancer* **1868,** 584–591 (2017).
453. Zhang, H. *et al.* Forkhead transcription factor Foxq1 promotes epithelial-mesenchymal transition and breast cancer metastasis. *Cancer Res.* **71,** 1292–1301 (2011).
454. Chan, C. W. & Housseau, F. The 'kiss of death' by dendritic cells to cancer cells. *Cell Death Differ.* **15,** 58–69 (2008).
455. Sivasubramaniyan, K. *et al.* SuppExpression of Stage Specific Embryonic Antigen-4 (SSEA-4) defines spontaneous loss of epithelial phenotype in human solid tumor cells Running title : SSEA-4 defines changes in epithelial phenotype of solid tumors University Clinic of Tübingen , Depa. **4,** 1–48 (2015).
456. Teng, B. L., Hacker, K. E., Chen, S., Means, A. R. & Rathmell, W. K. Tumor suppressive activity of prolyl isomerase Pin1 in renal cell carcinoma. *Mol. Oncol.* **5,** 465–474 (2011).
457. Huang, D. *et al.* Inhibition of MAPK Kinase Signaling Pathways Suppressed Renal Cell Carcinoma Growth and Angiogenesis In vivo. *Cancer Res.* **68,** 81–88 (2008).
458. Jo, H. *et al.* Deactivation of Akt by a small molecule inhibitor targeting pleckstrin homology domain and facilitating Akt ubiquitination. *Proc. Natl. Acad. Sci.* **108,** 6486–6491 (2011).
459. Bussolati, B., Grange, C., Sapino, A. & Camussi, G. Endothelial cell differentiation of human breast tumour stem/progenitor cells. *J. Cell. Mol. Med.* **13,** 309–319 (2009).
460. Lenos, K. J. *et al.* Stem cell functionality is microenvironmentally defined during tumour expansion and therapy response in colon cancer. *Nat. Cell Biol.* **20,** 1 (2018).

8 Indices

8.1 Index of Figures

8.2 Index of Tables